Technical Report Documentation Page

1. Report No. FHWA/TX-09/0-5253-1	2. Government Accession No.	3. Recipient's Catalog No.
4. Title and Subtitle Strength and Serviceability Design of Reinforced Concrete Deep Beams		5. Report Date December 2008, Rev. 2009: March, April 6. Performing Organization Code
7. Author(s) David Birrcher, Robin Tuchscherer, Matt Huizinga, Oguzhan Bayrak, Sharon Wood, and James Jirsa		8. Performing Organization Report No. 0-5253-1
9. Performing Organization Name and Address Center for Transportation Research The University of Texas at Austin 3208 Red River, Suite 200 Austin, TX 78705-2650		10. Work Unit No. (TRAIS) 11. Contract or Grant No. 0-5253
12. Sponsoring Agency Name and Address Texas Department of Transportation Research and Technology Implementation Office P.O. Box 5080 Austin, TX 78763-5080		13. Type of Report and Period Covered Technical Report 9/1/2005 – 8/31/2008 14. Sponsoring Agency Code

15. Supplementary Notes
Project performed in cooperation with the Texas Department of Transportation and the Federal Highway Administration.

16. Abstract

An experimental study was conducted in which 37 reinforced concrete deep beam specimens were tested. The specimens are some of the largest deep beams ever tested in the history of shear research. The data from the experimental program and from a database of 179 deep beam tests in the literature were used to address eight tasks associated with the strength and serviceability design and performance of deep beams. The effects of the following variables were evaluated: distribution of stirrup legs transversely through the web, triaxial confinement via concrete of CCC and CCT nodal faces, quantity of web reinforcement, member depth, and a/d ratio. A new strut-and-tie design method was proposed that is simpler and significantly more accurate than the provisions in AASHTO LRFD (2008) and ACI 318-08, yet just as conservative. Also, it was shown that the discrepancy in shear strength calculated using STM and sectional shear provisions in AASHTO LRFD (2008) at an a/d ratio of 2 is greatly reduced with the use of the proposed STM procedure. A recommendation was made on the amount of minimum web reinforcement needed for strength and serviceability considerations. A simple service-load check was proposed for the purpose of limiting diagonal cracking under service loads. Lastly, a chart was created to aid in the distress evaluation of a diagonally-cracked bent cap in the field.

17. Key Words Bent Caps, Deep Beams, Strut-and-Tie Modeling, Crack Widths, Diagonal Cracking, Serviceability	18. Distribution Statement No restrictions. This document is available to the public through the National Technical Information Service, Springfield, Virginia 22161; www.ntis.gov.

19. Security Classif. (of report) Unclassified	20. Security Classif. (of this page) Unclassified	21. No. of pages 400	22. Price

Form DOT F 1700.7 (8-72) Reproduction of completed page authorized

STRENGTH AND SERVICEABILITY DESIGN OF REINFORCED CONCRETE DEEP BEAMS

David Birrcher
Robin Tuchscherer
Matt Huizinga
Oguzhan Bayrak
Sharon Wood
James Jirsa

CTR Technical Report:	0-5253-1
Report Date:	December 2008, Rev. March 2009, April 2009
Project:	0-5253
Project Title:	Strength and Serviceability Design of Reinforced Concrete Deep Beams
Sponsoring Agency:	Texas Department of Transportation
Performing Agency:	Center for Transportation Research at The University of Texas at Austin

Project performed in cooperation with the Texas Department of Transportation and the Federal Highway Administration.

Center for Transportation Research
The University of Texas at Austin
3208 Red River
Austin, TX 78705

www.utexas.edu/research/ctr

Disclaimers

Author's Disclaimer: The contents of this report reflect the views of the authors, who are responsible for the facts and the accuracy of the data presented herein. The contents do not necessarily reflect the official view or policies of the Federal Highway Administration or the Texas Department of Transportation (TxDOT). This report does not constitute a standard, specification, or regulation.

Patent Disclaimer: There was no invention or discovery conceived or first actually reduced to practice in the course of or under this contract, including any art, method, process, machine manufacture, design or composition of matter, or any new useful improvement thereof, or any variety of plant, which is or may be patentable under the patent laws of the United States of America or any foreign country.

Engineering Disclaimer

NOT INTENDED FOR CONSTRUCTION, BIDDING, OR PERMIT PURPOSES.

O. Bayrak

Research Supervisor

Acknowledgments

The authors are sincerely grateful to the Texas Department of Transportation (TxDOT) for providing the funds to conduct this research study. The contributions of the project director Dean Van Landuyt (Bridge Division) and other members of TxDOT including John Vogel (Houston District) and David Hohmann (Bridge Division) are deeply appreciated. Also, the recommendations of Dr. John Breen greatly improved the quality of this report, and thus, are greatly valued.

Table of Contents

Chapter 1. Introduction 1
1.1 Overview 1
1.2 Project Objective 2
1.3 Project Scope 2
1.4 Organization 3

Chapter 2. Background of Strut-and-Tie Modeling of Deep Beams 5
2.1 Overview 5
2.2 Deep Beam vs. Sectional Behavior 5
2.3 Theoretical Background of Strut-and-Tie Modeling 6
2.3.1 Struts 10
2.3.2 Ties 11
2.3.3 Nodal Zones 11
2.4 Proportioning STM Elements using Non-Hydrostatic Nodes 14
2.4.1 Proportioning a CCC Node 14
2.4.2 Proportioning a CCT Node 15
2.4.3 Proportioning a CTT Node 16
2.4.4 Proportioning a Strut 17
2.4.5 Proportions and Placement of Tie Reinforcement 17
2.5 Deep Beam Database 18
2.5.1 Filtered Database 19
2.5.2 Evaluation Database 19
2.6 Summary 20

Chapter 3. Experimental Program 23
3.1 Overview 23
3.2 Testing Program 23
3.2.1 Series I: Distribution of Stirrups across Beam Web 26
3.2.2 Series II: Triaxially Confined Nodal Regions 27
3.2.3 Series III: Minimum Web Reinforcement 29
3.2.4 Series IV: Depth Effect 31
3.2.5 Series M: Multiple Purpose 33
3.2.6 Summary of Test Specimen Details 34
3.3 Testing Frame 39
3.4 Fabrication of Specimens 42
3.4.1 Steel Reinforcement 42
3.4.2 Concrete Mixture Design 42
3.4.3 Construction of Specimens 43
3.5 Instrumentation 46
3.5.1 Strain Measurements: Reinforcing Bars 46
3.5.2 Strain Measurements: Concrete Surface 48
3.5.3 Load and Displacement Measurements 49
3.5.4 Crack Width Measurements 51
3.6 Test Procedure 52
3.7 Summary 55

Chapter 4. Experimental Results 57
4.1 Overview 57
4.2 Summary of Experimental Results 57
4.2.1 Evaluation of Strength Data 60
4.2.2 Evaluation of Serviceability Data 61
4.3 Distribution of Stirrups across the Web 65
4.3.1 Background 65
4.3.2 Strength Results 70
4.3.3 Serviceability Results 76
4.3.4 Evaluation of Specimens with Current Code Expressions 80
4.3.5 Summary 81
4.4 Triaxially Confined Nodal Zones 83
4.4.1 Background 83
4.4.2 Overview of Testing: Series II and Series M 89
4.4.3 Strength Results 93
4.4.4 Serviceability Results 97
4.4.5 Evaluation of Specimens with Current Code Expressions 102
4.4.6 Summary 106
4.5 Minimum Web Reinforcement 107
4.5.1 Background 107
4.5.2 Strength Results 114
4.5.3 Serviceability Results 127
4.5.4 Design Recommendations 142
4.5.5 Summary 142
4.6 Effect of Member Depth 143
4.6.1 Background 143
4.6.2 Strength Results 144
4.6.3 Serviceability Results 163
4.6.4 Design Recommendations 172
4.6.5 Summary 172
4.7 Summary 173

Chapter 5. Analysis of Results 175
5.1 Overview 175
5.2 Proposed STM Design Provisions 175
5.2.1 Current Code Provisions for STM 175
5.2.2 Historic Development of Empirical Shear Provisions 181
5.2.3 Historic Development of Strut-and-Tie Model Provisions 183
5.2.4 Overview of Proposed STM Design Method 192
5.2.5 Selection of Strut-and-Tie Model 192
5.2.6 Evaluation of Current Design Provisions 198
5.2.7 Proposed method 203
5.2.8 Assessment of Proposed Method 218
5.2.9 Outline of Proposed Strut-and-Tie Modeling Procedure 225
5.2.10 Proposed STM Procedure: Summary 227

5.3 Discrepancy in Calculated Shear Strength at a/d Ratio of 2.0 229
5.3.1 Background 229
5.3.2 Effect of a/d ratio on Shear Behavior 230
5.3.3 Reducing Discrepancy between Shear Models at a/d ratio of 2.0 244
5.3.4 Design Implications 250
5.3.5 Summary and Conclusions 251
5.4 Diagonal Cracking under Service Loads 253
5.4.1 Background 253
5.4.2 Approach 254
5.4.3 Results 255
5.4.4 Design Implications 269
5.4.5 Summary and Conclusions 270
5.5 Correlation of Maximum Diagonal Crack Width to Capacity 272
5.5.1 Background 272
5.5.2 Approach 278
5.5.3 Results 280
5.5.4 Summary and Conclusions 294
5.6 Summary 294

Chapter 6. Summary and Conclusions 295
6.1 Summary 295
6.2 Conclusions 296
6.2.1 Distribution of Stirrups across the Width of a Beam Web 296
6.2.2 Triaxial Confinement of Load and Support Plates (CCC and CCT Nodes) 297
6.2.3 Minimum Web Reinforcement 297
6.2.4 Effect of Member Depth 298
6.2.5 Proposed STM Design Provisions 298
6.2.6 Discrepancy in Calculated Shear Strength at a/d Ratio of 2 299
6.2.7 Limiting Diagonal Cracking under Service Loads 300
6.2.8 Correlation of Maximum Diagonal Crack Width to Capacity 300
6.3 Concluding Remarks 300

References 303

APPENDIX A: Proposed Changes to the AASHTO LRFD (2008) Bridge Design Specifications 311
A.1.1 Introduction 311
A.1.2 Proposed Changes to AASHTO LRFD Bridge Design Specifications 312
A.1.3 Explanation for Proposed Changes 320
A.1.4 Summary 320

APPENDIX B: Design Example 321
B.1 Overview 321
B.2 Deep Beam Design 324
B.2.1 Determination of Preliminary Truss Model 324
B.2.2 Shear Region with an a/d Ratio Equal to 0.85 325

B.2.3 Shear Region with an a/d Ratio Equal to 2.05 334
B.3 Sectional Shear Design 346
B.3.1 Shear Region with a/d Ratio Equal to 2.05 346
B.3.2 Comparison of Deep Beam and Sectional Shear Provisions 348
B.4 Summary 349
APPENDIX C: Collection Database 351
C.1 References 351
APPENDIX D: Evaluation Database 357
D.1 Overview 357
APPENDIX E. Outline of STM Calculations 369
E.1 Overview 369
E.1.1 Known STM Truss Geometries 369
E.2 Determination of Experimental/Calculated Ratio 371

List of Figures

Figure 1.1: (a) I-45 bent cap in Houston, Texas with several diagonal cracks in service. (b) The bent cap after repair 2
Figure 2.1: Stress trajectories in B-regions and near discontinuities (D-regions). 5
Figure 2.2: Strut-and-tie model: Simply supported beam supporting concentrated load. 7
Figure 2.3: Strut-and-tie model with truss elements drawn to scale. 7
Figure 2.4: Step 1 for STM is calculation of support reactions. 8
Figure 2.5: STM: (a) One-panel and (b) two-panel. 8
Figure 2.6: Direct strut or one-panel shear failure (a/d = 1.2). 9
Figure 2.7: Sectional or two-panel shear failure (a/d = 2.5). 9
Figure 2.8: Combination of one and two-panel behavior (a/d = 1.85). 10
Figure 2.9: STM containing prismatic and bottle-shaped struts. 11
Figure 2.10: Nodal zones typically employed in STMs. 11
Figure 2.11: Stresses on hydrostatic and non-hydrostatic nodes (Brown et al. 2006). 12
Figure 2.12: Difference between hydrostatic and non-hydrostatic nodes as the strut angle decreases. 13
Figure 2.13: CCC Node. 14
Figure 2.14: CCT Node 15
Figure 2.15: CTT Node. 16
Figure 2.16: Determination of CTT vertical tie (Wight and Parra-Montesinos, 2003) 16
Figure 2.17: Development length of a tie. 17
Figure 2.18: Summary of beam proportions in filtered database (N=607). 19
Figure 3.1: Scaled comparison between actual bent caps and beams included in past research programs. 24
Figure 3.2: Effective width of strut anchored by reinforcement at the CCT node. 26
Figure 3.3: Series I: description of nomenclature used for Specimen I.D. 27
Figure 3.4: Series I beam details. 27
Figure 3.5: Plate sizes investigated within Series II. 28
Figure 3.6: Series II: Description of nomenclature used for Specimen I.D. 29
Figure 3.7: Series II beam details. 29
Figure 3.8: Definition for vertical and horizontal web reinforcement ratios 30
Figure 3.9: Series III: Description of nomenclature used for Specimen I.D. 31

Figure 3.10: Series III beam details. 31
Figure 3.11: Series IV - Description of nomenclature used for Specimen I.D. 32
Figure 3.12: Series IV beam details. 33
Figure 3.13: Series M - description of nomenclature used for Specimen I.D. 34
Figure 3.14: Series M beam details 34
Figure 3.15: Comparison of beams sizes between current and past studies. 35
Figure 3.16: Scaled comparison of actual bent caps and beams included in current and past research programs. 35
Figure 3.17: Elevation view of test setup 39
Figure 3.18: Section view of test setup 40
Figure 3.19: Installation of strong floor: (a) steel platen (b) floor excavation (c) fabrication of platen support (d) lowering of platen into position, and (e) test setup. 41
Figure 3.20: Fabrication of a typical beam: (a) assembly of reinforcement cage (b) placement of cage in formwork (c) forms in place prior to concrete placement (d) placement of concrete (e) beam curing (f) test specimen after the removal of forms. 44
Figure 3.21: Fabrication of a 21”x75” beam: (a) movement of reinforcement cage into formwork (b) placement of concrete into steel formwork 45
Figure 3.22: Fabrication of a 36”x48” beam: (a) tied reinforcement cage (b) placement of concrete into wooden formwork 45
Figure 3.23: Installation of strain gauge for measuring steel strains. 46
Figure 3.24: Typical internal strain gauge locations for each series 47
Figure 3.25: Installation of a concrete surface gauge for measuring concrete strains. 48
Figure 3.26: Concrete strain gauge locations 49
Figure 3.27: Load cells measure the reaction in each rod 49
Figure 3.28: Linear potentiometer locations. 50
Figure 3.29: Linear potentiometer used to measure the displacement at the load point 50
Figure 3.30: Diagram of beam displacements due to rigid body motion and flexural and shear deformations early in the test 51
Figure 3.31: Diagram of beam displacements due to rigid body motion and flexural and shear deformations after all reaction nuts are engaged 51
Figure 3.32: Example of crack width measurement technique 52
Figure 3.33: Each end of a beam is loaded to failure resulting in two tests: (a) shear failure in Test Region A (b) and shear failure in Test Region B with external post-tensioned clamps in Test Region A 53

Figure 3.34: Hydraulic ram was not moved for 75-inch specimens: (a) shear failure in Test Region A (b) shear failure in Test Region B with external post-tensioned clamps in Test Region A 54
Figure 3.35: (a) Photographs are orientated upside-down in order to present test results in conventional manner; (b) actual picture location 55
Figure 4.1: Force and shear force diagram for typical beam test 60
Figure 4.2: Visual and experimental determination of first cracking load. 62
Figure 4.3: Sample crack width data for all series 63
Figure 4.4: Estimate of service load as a function of experimental capacity 64
Figure 4.5: AASHTO LRFD requirement for a strut anchored by reinforcement (AASHTO LRFD, 2008 and Brown et al. 2006). 66
Figure 4.6: The oblique strut supported by vertical stirrup legs (taken from Leonhardt and Walther, 1961). 67
Figure 4.7: Details of specimens tested by Hsuing and Frantz (1985). 67
Figure 4.8: Details of specimens tested by Anderson and Ramirez (1989). 68
Figure 4.9: Effective strut width of specimens tested by Anderson and Ramirez (1989). 69
Figure 4.10: Summary of tests studying distribution of stirrups across web. 70
Figure 4.11: Effective strut widths at CTT nodes for specimens with 2-leg and 4-leg stirrups 71
Figure 4.12: Series I test specimens at failure. 73
Figure 4.13: Measured longitudinal strains within the outermost layer of tension reinforcement. 75
Figure 4.14: Crack pattern at approximately 90% of capacity and crack width behavior: 0.3% transverse reinforcement in each direction. 77
Figure 4.15: Crack pattern at approximately 90% of capacity and crack width behavior: 0.2% transverse reinforcement in each direction. 78
Figure 4-16. Shear carried in a test specimen versus the corresponding maximum diagonal crack width. 79
Figure 4.17: Comparison of experimental capacity with ACI 318 and AASHTO LRFD one and two-panel STM calculations. 80
Figure 4.18: Comparison between one and two-panel STM: per ACI 318. 81
Figure 4.19: Stress-strain curve for concrete cylinder under triaxial compression (MacGregor and Wight, 2005). 83
Figure 4.20: Bearing load under (a) triaxial (b) biaxial confinement. 84
Figure 4.21. Application of frustum to find A_2 in stepped or sloped supports (taken from ACI 318-08). 85

Figure 4.22: Definition of triaxial confinement geometries used in fib (1999). 86
Figure 4.23: Detail of Leonhardt and Walter (1961) and Furuuchi et al. (1998) test specimens. 86
Figure 4.24: Detail of the specimens tested by Adebar and Zhou (1993) 88
Figure 4.25: Detail of specimens tested by Brown et al. (2006). 89
Figure 4.26: Summary of tests within Series II: 21”x42” specimens. 91
Figure 4.27: Summary of tests within Series M: 36”x48” specimens. 92
Figure 4.28: Series II specimens with various bearing plate sizes at the CCC node at failure. 94
Figure 4.29: Series II specimens with various bearing plate sizes at the CCT node at failure. 95
Figure 4.30: Serviceability data for triaxially confined CCC nodes: Crack patterns and widths at approximately 90% of capacity; 0.3% transverse reinforcement in each direction. 98
Figure 4.31: Serviceability data for triaxially confined CCT nodes: Crack patterns and widths at approximately 90% of capacity; 0.3% transverse reinforcement in each direction. 99
Figure 4.32: Serviceability data for triaxially confined CCC nodes: Crack patterns and widths at approximately 90% of capacity; 0.2% transverse reinforcement in each direction. 100
Figure 4.33: Serviceability data for triaxially confined CCT nodes: Crack patterns and widths at approximately 90% of capacity; 0.2% transverse reinforcement in each direction. 101
Figure 4.34: Comparison of experimental capacity with ACI 318-08 and AASHTO LRFD (2008) one-panel STM calculations: CCC specimens. 102
Figure 4.35: Comparison of experimental capacity with ACI 318-08 and AASHTO LRFD (2008) one-panel STM calculations: CCT specimens. 103
Figure 4.36: Conservatism of ACI 318 STM calculation with and without an increase in capacity due to triaxial confinement. 104
Figure 4.37: Conservatism of AASHTO LRFD STM calculation with and without an increase in capacity due to triaxial confinement. 104
Figure 4.38: ACI 318-08 STM calculations for all beams in database that contain triaxially confined nodal regions. 105
Figure 4.39: AASHTO LRFD (2008) STM calculations for all beams in database that contain triaxially confined nodal regions. 105
Figure 4.40: Deep beam showing nomenclature for Equation 4.7 109
Figure 4.41: Minimum horizontal reinforcement for deep beams in several specifications 112
Figure 4.42: Minimum vertical reinforcement for deep beams in several specifications 112

Figure 4.43: Effect of horizontal reinforcement on strength of beams in evaluation database 114
Figure 4.44: Effect of vertical reinforcement on strength of beams in evaluation database 115
Figure 4.45: Effect of vertical web reinforcement on strength after first cracking 116
Figure 4.46: Effect of horizontal web reinforcement on strength after first cracking 117
Figure 4.47: Crack development in specimen without web reinforcement, III-1.85-0..... 119
Figure 4.48: Crack development in specimen with 0.3% in each direction, III-1.85-03b..... 120
Figure 4.49: Strength results of Series III and IV specimens at a/d ratio of 1.85..... 121
Figure 4.50: Strength results comparison of III-1.85-01 and III-1.85-03 122
Figure 4.51: Applicable strength results from Series M 123
Figure 4.52: Applicable strength results from Series I 124
Figure 4.53: Strength results from specimens tested at a/d ratio of 1.2..... 125
Figure 4.54: Crack development in III-2.5-0 126
Figure 4.55: Strength results from specimens tested at an a/d ratio of 2.5 126
Figure 4.56: Effect of vertical reinforcement on the diagonal cracking load 127
Figure 4.57: Effect of horizontal reinforcement on the diagonal cracking load..... 128
Figure 4.58: Diagonal cracking loads of specimens in current task 130
Figure 4.59: Diagonal crack widths for 6 - 21”x42” specimens tested at a/d of 1.85 131
Figure 4.60: Crack patterns of four specimens at approximately 90% of capacity 133
Figure 4.61: Diagonal crack widths for 8 – 21”x42” specimens tested at a/d of 1.85..... 134
Figure 4.62: Diagonal crack widths of 8 – 21”x42” specimens versus applied shear 135
Figure 4.63: Diagonal crack widths for 21”x75” specimens with 0.2% and 0.3% reinforcement 136
Figure 4.64: Diagonal crack widths for 36”x48” specimens with 0.2% and 0.3% reinforcement 136
Figure 4.65: Diagonal crack widths for 21”x44” specimens with 0.2% or 0.3% 2-legged reinforcement 137
Figure 4.66: Diagonal crack widths for 21”x44” specimens with 0.2% or 0.3% 4-legged reinforcement 137
Figure 4.67: Diagonal crack width data for all comparable specimens at a/d of 1.85..... 138
Figure 4.68: Diagonal crack widths of specimens tested at an a/d ratio of 1.2 139
Figure 4.69: Diagonal crack widths of specimens tested at an a/d ratio of 2.5 140
Figure 4.70: Effect of stirrup spacing on crack width for specimens with 0.2% web reinforcement 141

Figure 4.71: Effect of stirrup spacing on crack width for specimens with 0.3% web reinforcement 141
Figure 4.72: Size effect strength results from Walraven and Lehwalter (1994) 145
Figure 4.73: Size effect strength results from Tan and Lu (1999) 146
Figure 4.74: Size effect strength results from Matsuo et al. (2001) 147
Figure 4.75: Size effect strength results from Zhang and Tan (2007) 148
Figure 4.76: FEM results in which bearing plate sizes increased with increasing member depth (Zhang and Tan, 2007) 149
Figure 4.77: FEM results in which bearing plate sizes were constant with increasing member depth (Zhang and Tan, 2007) 149
Figure 4.78: Bearing plate dimensions in several TxDOT bent caps (TxDOT, 2008) 151
Figure 4.79: Relative size of nodal regions for depth effect specimens 152
Figure 4.80: Relative size of nodal regions in depth effect specimens (2) 152
Figure 4.81: Strength results of depth effect specimens at a/d of 1.85 155
Figure 4.82: Failure photographs for depth effect specimens with a/d of 1.85 and 0.2% reinforcement 156
Figure 4.83: Strength results of all depth effect specimens 157
Figure 4.84: Failure photographs of depth effect specimens with a/d of 1.2 158
Figure 4.85: Failure photographs of depth effect specimens with a/d of 2.5 159
Figure 4.86: Experimental strength of depth effect specimens normalized by calculated strength 160
Figure 4.87: Strength results of size effect specimens with a/d of 2.5 161
Figure 4.88: Level of conservatism in sectional shear provisions for specimens with a/d of 2.5 162
Figure 4.89: Ultimate shear capacity (kips) of size effect speicmens 163
Figure 4.90: Diagonal cracking loads of size effect specimens in literature 164
Figure 4.91: Diagonal cracking loads of size effect specimens in literature (function of ultimate) 165
Figure 4.92: Service loads (diagonal crack width = 0.012-inches) as function of ultimate of size effect specimens in literature 166
Figure 4.93: Normalized diagonal cracking loads for the depth effect specimens 168
Figure 4.94: Diagonal cracking loads normalized by ultimate strength for depth effect tests 169
Figure 4.95: Diagonal crack widths for depth effect specimens with an a/d ratio of 1.2 170
Figure 4.96: Diagonal crack widths for depth effect specimens with an a/d ratio of 1.85 and 0.2% web reinforcement 170

Figure 4.97: Diagonal crack widths for depth effect specimens with an a/d ratio of 1.85 and 0.3% web reinforcement 171
Figure 4.98: Diagonal crack widths for depth effect specimens with an a/d ratio of 2.5 171
Figure 5-1. Stress condition at the back face of a CCT node: (a) bonding stress; (b) bearing of an anchor plate; (c) interior node over a continuous support. 179
Figure 5.2: Comparison of strut efficiency factors: ACI 318-08 186
Figure 5.3: Details of Isolated Node Specimens. 189
Figure 5.4: Comparison of nodal efficiency factors: fib (1999) 190
Figure 5.5: Examples of D-regions. 193
Figure 5.6: Non-hydrostatic single-panel strut-and-tie model. 194
Figure 5.7: Definition of the geometry of a (a) CCC Node (b) CCT Node 195
Figure 5.8: Difference between hydrostatic and non-hydrostatic nodes as a/d ratio increases. 197
Figure 5.9: Typical difference in node dimensions between an a/d ratio of one and two. 198
Figure 5.10: Seven stress checks used to evaluate STM procedures. 199
Figure 5.11: Primary attributes of the specimens in the evaluation database (N = 179). 200
Figure 5.12: Range of experimental/calculated values determined using evaluation database (179 data points). 201
Figure 5.13: Application of frustum to find A_2 in stepped or sloped supports (ACI 318-08). 204
Figure 5.14: The effect of triaxial confinement: Experimental capacity/Estimated capacity (ACI 318-08). 205
Figure 5.15: Back face of a CCT node. 206
Figure 5.16: Governing node face with and without a stress check at the back face of the CCT node: ACI 318. 207
Figure 5.17: Assumed nodal dimensions and allowable stress distribution at back face of CCT node. 208
Figure 5.18: Strain distribution measured behind the support plate at 90% of ultimate capacity. 208
Figure 5.19: Bearing and back face of a CCC node. 210
Figure 5.20: CCC back (N=19) and bearing face (N=6) efficiency factor: Proposed Method. 211
Figure 5.21: Bearing face of a CCT node. 211
Figure 5.22: CCT bearing face efficiency factor (N = 5): Proposed Method. 212
Figure 5.23: CCC and CCT strut-to-node interface. 212

Figure 5.24: Experimental efficiency vs. ACI 318-08 at the CCC and CCT strut-to-node interface..... 213
Figure 5.25: Experimental efficiency vs. AASHTO LRFD (2007) at the CCC and CCT strut-to-node interface..... 214
Figure 5-26. Experimental efficiency vs. fib (1999) recommendations at the CCC and CCT strut-to-node interface..... 215
Figure 5.27: Experimental vs. proposed efficiency at the CCC and CCT strut-to-node interface..... 216
Figure 5-28. Proposed STM design provisions..... 218
Figure 5.29: Comparison of proposed STM provisions with other design provisions (Evaluation Database = 179 data points)..... 220
Figure 5-30. Comparison of proposed STM provisions with other design provisions (Filter Database with $\rho_{\perp} > 0.1\% =$ 381 data points)..... 222
Figure 5.31: Influence that transverse reinforcement ratio has on the COV of various STM provisions..... 224
Figure 5.32: (a) Single-panel STM (b) CCC Node (c) CCT Node..... 226
Figure 5.33: Application of frustum to find A_2 in stepped or sloped supports (ACI 318-08)..... 227
Figure 5.34: Stress trajectories in an asymmetrically-loaded beam..... 229
Figure 5.35: Discontinuity in calculated shear capacity in AASHTO LRFD 2008 at a/d ratio of 2..... 230
Figure 5.36: Proposed shear-strength envelope by Kani (Kani et al., 1979)..... 232
Figure 5.37: Effect of a/d ratio on experimental strength of test specimens..... 234
Figure 5.38: Failure pictures of test specimens with 0.2-percent reinforcement and variable a/d..... 235
Figure 5.39: Failure pictures of test specimens with 0.3-percent reinforcement and variable a/d..... 236
Figure 5.40: Distribution of force in longitudinal tension steel along length of beam according to different shear models..... 237
Figure 5.41: Comparison of measured and calculated strain along the length of specimen with a/d of 1.85..... 239
Figure 5.42: Comparison of measured and calculated strain along length of specimen with a/d of 1.2 and 2.5..... 241
Figure 5.43: Experimental strength divided by calculated strength for depth effect specimens..... 243
Figure 5.44: Difference in node geometry with increasing a/d ratio for single-panel STM..... 244
Figure 5.45: Level of conservatism in STM provisions with increasing a/d ratio..... 245

Figure 5.46: Free-body diagram used as basis for sectional shear model 246
Figure 5.47: Level of conservatism in sectional shear provisions with increasing a/d ratio 248
Figure 5.48: Level of conservatism in sectional shear provisions for a/d ratios between 2 and 2.5 249
Figure 5.49: Comparison of calculated capacity: Project 5253 STM vs. sectional shear 250
Figure 5.50: Reduction in discrepancy in shear capacity at a/d ratio of 2 with the proposed STM provisions 252
Figure 5.51: Types of cracks in reinforced concrete deep beams 253
Figure 5.52: First pictures taken after the formation of first diagonal crack in several tests 254
Figure 5.53: Stress trajectories in B-regions (Bernoulli) and in D-regions (discontinuity) 255
Figure 5.54: Effect of shear area on the diagonal cracking load of beams in evaluation database 257
Figure 5.55: Effect of tensile strength on diagonal cracking load of deep beams in database 258
Figure 5.56: Effect of a/d ratio on diagonal cracking load of deep beams in database 259
Figure 5.57: Effect of longitudinal reinforcement ratio on diagonal cracking load of beams in the database 260
Figure 5.58: Effect of longitudinal reinforcement ratio on diagonal cracking load of beams with the same a/d ratio 260
Figure 5.59: Effect of depth on the diagonal cracking load of beams in the evaluation database 261
Figure 5.60: Effect of depth on the diagonal cracking load of deep beams in testing program 262
Figure 5.61: Effect of web reinforcement on the diagonal cracking load of similarly sized deep beams 263
Figure 5.62: Comparison of measured and estimated diagonal cracking loads – ACI Eq. 11-5 264
Figure 5.63: Comparison of measured and estimated diagonal cracking loads – Zsutty Equation 265
Figure 5.64: Comparison of measured and estimated cracking loads – Shin et al. Eq. 267
Figure 5.65: Diagonal cracking loads for nominally-identical specimens 268
Figure 5.66: Development of proposed equation for a reasonably conservative estimate of diagonal cracking 269
Figure 5.67: Types of cracks in reinforced concrete deep beams 273
Figure 5.68: Effect of transverse reinforcement on width of diagonal cracks (Bracci et al., 2000) 275

Figure 5.69: Effect of a/d ratio on width of diagonal cracks (Kong et al., 1970) 276
Figure 5.70: Effect of a/d ratio on diagonal crack width (Smith and Vantsiotis, 1982) 277
Figure 5.71: Preliminary analytical model for estimating diagonal crack widths 279
Figure 5.72: Effect of web reinforcement on diagonal crack widths of test specimens 284
Figure 5.73: Effect of a/d ratio on diagonal cracking widths, 3 specimens, 0.3% reinf. 285
Figure 5.74: Effect of a/d ratio on diagonal crack widths, 9 specimens, 0.3% reinf. 286
Figure 5.75: Effect of a/d ratio on diagonal crack widths, 2 specimens, 0.2% reinf. 287
Figure 5.76: Effect of a/d ratio on diagonal crack widths, 11 specimens, 0.2% reinf. 287
Figure 5.77: Effect of longitudinal reinforcement on diagonal cracks in shear-critical members 288
Figure 5.78: All crack width data at a/d ratio of 1.85 used in this task with trend lines 290
Figure 5.79: All crack width data at a/d ratio used in this task with straight line approximations 290
Figure 5.80: Proposed chart that links diagonal crack width to percent of ultimate capacity of RC deep beams 291
Figure 5.81: Comparison of crack width data from Bracci et al. (2000) and chart estimates 292
Figure 5.82: Comparison of data from specimens tested at a/d of 1.2 and chart estimates 293
Figure B.1: I-45 over Greens Road Bent Cap 321
Figure B.2: Preliminary plan; elevation; and cross-sectional details at critical shear regions. 322
Figure B.3: Strut-and-tie model with AASHTO LRFD (2008) factored loads. 324
Figure B.4: Critical strut in region with a/d equal to 0.85 (AASHTO LRFD factored loads). 325
Figure B.5: Determination of Triaxial Confinement Factor 326
Figure B-6. Strut proportions associated with an increase in overall depth of 18-inches and increase in back face of Node A of 2.5-inches (ACI 318-08 load factors) 330
Figure B.7: Comparison of required cross-section per the proposed method, ACI 318-08, and AASHTO LRFD: a/d ratio = 0.85. 333
Figure B-8. Critical strut in region with a/d = 2.05. 335
Figure B-9: Strut proportions and forces associated with a 6-inch increase in depth of bent. 337
Figure B.10: Strut proportions and forces associated with a 25-inch increase in bent height and 6-inch increase in depth of Node E (ACI 318 factored loads) 339
Figure B.11: Strut proportions and forces associated with a 35-inch increase in bent depth and 10.5-inch increase in depth of Node E (AASHTO LRFD factored loads). 342

Figure B.12: Comparison of required cross-section per the proposed method, ACI 318-08, and AASHTO LRFD (2007): a/d ratio = 2.05. 344
Figure E.1: Truss model. 369
Figure E.2: CCC and CCT nodes. 369

List of Tables

Table 2.1: Filtering of the deep beam (a/d ≤ 2.5) database 18
Table 3.1: Variables in Testing Program. 25
Table 3.2: Summary of all beam details. 37
Table 3.3: Concrete mixture proportions 43
Table 4.1: Summary of experimental results. 58
Table 4.2: Tolerable widths of flexural cracks 64
Table 4.3: Test Results: Series I 72
Table 4.4: Test Results: Series II 93
Table 4.5. Effect of Triaxial Confinement for CCC Specimens. 96
Table 4.6: Assumptions made to plot minimum web reinforcement provisions 113
Table 4.7: Summary of strength results for specimens in minimum reinforcement task 118
Table 4.8: Amount of web reinforcement from several provisions used in current task 121
Table 4.9: Summary of serviceability results for specimens in minimum reinforcement task 129
Table 4.10: Strength results for depth effect specimens 154
Table 4.11: Diagonal cracking loads of depth effect specimens 167
Table 5.1: Allowable Stresses for a CCC Node. 177
Table 5.2: Allowable Stresses for a CCT Node. 178
Table 5.3: Allowable Stresses for a CTT Node. 180
Table 5.4. STM Provisions: Evaluation Database 202
Table 5.5. STM Provisions: Evaluation Database 219
Table 5.6. Influence that Transverse Reinforcement Ratio has on Accuracy of STM Provision 224
Table 5.7: Specimens used in correlating crack width-to-capacity (shaded tests not used) 282
Table 5.8: Summary of beam details for two specimens tested by Deschenes (2009) 283
Table 5.9: Summary of test results for two specimens tested by Deschenes (2009) 283
Table B.1. Shear Capacity of Original Cross-Section B (a/d = 2.05) 348
Table D.1. Evaluation Database 358

Chapter 1. Introduction

1.1 Overview

A *deep beam* is a structural member whose behavior is dominated by shear deformations. In practice, engineers typically encounter deep beams when designing transfer girders, pile supported foundations, or bridge bents. Until recently, the design of deep beams per U.S. design standards was based on empirically derived expressions and *rules of thumb*. The structural design standards, AASHTO LRFD (2008) and ACI 318-08, adopted the use of strut-and-tie modeling (STM) for the strength design of deep beams or other regions of discontinuity in 1994 and 2002, respectively. Based on the theory of plasticity, STM is a design method that idealizes stress fields as axial members of a truss. The primary advantage of STM is its versatility. It is valid for any given loading or geometry. However, the primary weakness of STM is also its versatility. The freedom associated with the method results in a vague and inconsistently defined set of guidelines. Because of the lack of a well-ordered design process, many practitioners are reluctant to use STM. A goal of the current research program is to overcome this ambiguity through the development of simple and safe STM provisions.

For structural members exposed to public view or environmental elements, the serviceability performance of the structure is arguably as significant as its strength. Typically, the serviceability performance of reinforced concrete deep beams is quantified by the width and spacing of diagonal cracks that form under the application of service loads. In design, diagonal cracking in service can be limited by comparing the cracking load to the service load and adjusting the section as necessary. Also, web reinforcement can be provided to restrain the width of diagonal cracks if they do happen to form in service. Currently, the minimum web reinforcement provisions in various design specifications are inconsistent and in general, do not address whether the required reinforcement considers serviceability demand as well as strength demand. Hence, another goal of the current research project is to improve the serviceability design provisions for deep beams by recommending an appropriate amount of minimum web reinforcement and by outlining a service-load check to assess the likelihood of diagonal cracking.

As part of the current research program, approximately 250 deep beam specimens were added to a database originally compiled by Brown et al. (2006). In total, the test results of 868 deep beam specimens (shear-span-to-depth ratio, $a/d \leq 2.5$) were collected from the literature. These test data represent the current state of knowledge of deep beam shear. The majority of the specimens in the database are significantly smaller than actual beams designed in practice. A typical test specimen may have an area of 100-in^2 whereas a typical bridge bent or transfer girder can have an area that is ten to twenty times larger. In the current research project, it was determined that the best means to improve the design and performance of actual bent caps was to examine specimens that were as representative as possible. As a result, filtering criteria were established based primarily off of cross-sectional dimensions, quantity of web reinforcement, and sufficient bearing plate details to remove specimens from the database that were exceptionally un-representative of actual members.

In addition, 37 specimens were fabricated and tested as part of the current research program. The cross-sectional dimensions of the test specimens more closely matched the sizes

of typical bent caps in Texas. These test specimens are some of the largest deep beams ever tested in the history of shear research.

1.2 Project Objective

This research project was funded by the Texas Department of Transportation (TxDOT). Since the inclusion of Strut-and-Tie Modeling (STM) provisions in the AASHTO LRFD specifications in 1994, TxDOT engineers have been examining the impact that the provisions have on the design of their bent caps. In general, it has been difficult to implement the STM provisions due to their seemingly complicated nature. In addition, bent caps in the State of Texas are experiencing diagonal cracking problems with increasing frequency. An example of a bent cap that developed a significant number of diagonal cracks in service is shown in Figure 1.1(a) and 1.1(b). This structure is one of several bent caps that support I-45 in Houston, Texas at the intersection with Greens Road. Due to the width and number of diagonal cracks in the bent caps throughout the interchange (maximum diagonal crack width ≈ 0.035-inches), the retrofit shown in Figure 1.1(b) was performed on each bent cap. At the time of the retrofit, the structure was approximately 10-years old.

(a) (b)

Figure 1.1: (a) I-45 bent cap in Houston, Texas with several diagonal cracks in service. (b) The bent cap after repair

Field-related issues, such as the diagonal cracking problem shown above, and the difficulty in implementing the AASHTO LRFD provisions in their design practice were the impetus for TxDOT to fund the current project. The overall objective for the project was to develop safe and consistent design guidelines in regards to both strength and serviceability of bent caps and other deep beams.

1.3 Project Scope

To develop strength and serviceability guidelines for bent caps and other deep beams, the following eight tasks were addressed:

1. Determine the influence that the distribution of stirrups across the width of a beam web has on the strength and serviceability behavior of a deep beam.

2. Determine the influence that triaxially confined nodes forming under bearing plates has on the strength and serviceability behavior of a deep beam.
3. Determine the influence that the amount of web reinforcement (stirrups and longitudinal side face reinforcement) has on the strength and serviceability behavior of a deep beam.
4. Determine the influence that member depth has on the strength and serviceability behavior of a deep beam.
5. Propose a simple STM design methodology for the design of deep beams.
6. Make a recommendation to reduce the discrepancy between shear strength calculated using STM and sectional shear provisions at an a/d ratio of 2.
7. Make a recommendation on the feasibility of limiting diagonal cracking under service loads.
8. Make a recommendation on a methodology for relating the maximum diagonal crack width of a deep beam to its residual capacity.

Data from the experimental program and from the database were used to accomplish the stated tasks. The first four tasks (1 through 4) were addressed specifically with the tests in the experimental program. For each task, a series of specimens were tested and numbered accordingly (Series I through IV). A fifth series of tests (Series M) was conducted in which multiple objectives were evaluated. To accomplish the last four tasks (5 though 8), data from the experimental program and from the database were analyzed. Specifics of the organization of this document are presented in the following section.

1.4 Organization

A background of strut-and-tie modeling concepts as they apply to deep beams is provided in Chapter 2. The theory supporting strut-and-tie modeling and the techniques required to proportion all of the elements in a model is discussed. At the end of Chapter 2, the criteria used to filter the database are presented. In Chapter 3, an overview of the experimental program including the design, fabrication, instrumentation, and testing of the specimens is provided. Also, a summary of the beam details for all of the test specimens is included. In Chapter 4, the results of the experimental program are presented. A summary of the results from all of the tests is presented in Section 4.2. Tasks 1 through 4 of the project are addressed individually in Sections 4.3 through 4.6. In Chapter 5, the findings associated with tasks 5 through 8 are provided individually (Sections 5.2 through 5.5). In general, each task was addressed with data from the experimental program and the database. All the findings and conclusions of the research program are summarized in Chapter 6. In Appendix A, proposed revisions to the AASHTO LRFD (2008) specifications are presented. In Appendix B, a case study, that may be viewed as multiple examples combined in a comprehensive field problem, is presented to highlight the differences between the proposed provisions and the AASHTO LRFD (2008) specifications. For the case study, one of the Greens Road bent caps in Houston, Texas that developed a significant number of diagonal cracks in service was analyzed. In Appendix C, the references used to collect test results for the database are listed. The pertinent beam details of the test specimens in the evaluation database are presented in Appendix D. Lastly, in Appendix E, an outline of calculations used in the evaluation of the strut-and-tie provisions of various design specifications is given.

Chapter 2. Background of Strut-and-Tie Modeling of Deep Beams

2.1 Overview

Included in this Chapter is an overview of the theoretical background of deep beam shear behavior and strut-and-tie modeling. The basic concepts of deep beam shear behavior are introduced. Then, the theoretical background of strut-and-tie modeling and a summary of commonly employed modeling techniques are provided. Lastly, the deep beam database is presented; and the process of filtering the database to remove specimens that were considered un-representative of actual structures is provided. A review of the literature pertaining to each specific task addressed in the current project is presented in each respective section.

2.2 Deep Beam vs. Sectional Behavior

Typically, reinforced concrete members are designed to resist shear and flexural forces based on the assumption that strains vary linearly at a section. Referred to as the *Bernoulli hypothesis* or *beam theory*, the mechanical behavior of a beam is commonly defined by assuming that *plane sections remain plane*. The region of a structure where the Bernoulli hypothesis is valid is referred to as a *B-region* (B standing for *beam* or *Bernoulli*). In B-regions, the internal state of stress can be derived from the sectional forces before and after the concrete cracks. Therefore, the design of these regions is often referred to as a *sectional design*.

A *deep beam design* must be treated differently than a sectional design because the assumptions used to derive the sectional theory are no longer valid. A deep beam is a member whose shear span-to-depth, *a/d*, ratio is relatively small such that nonlinear shearing strains dominate the behavior. Typically, a region of a beam with an a/d ratio less than 2.0 to 2.5 is considered to behave as a deep beam; whereas, a region of a beam with a greater a/d ratio is assumed to behave according to sectional principles. For example, the beam shown in Figure 2.1 has an a/d ratio of approximately two to the right of the concentrated load and five to the left of the load. The left side of the beam (Section A-A) contains a B-region and stresses can be determined according to sectional methods. The right side of the beam (Section B-B) is considered a deep beam region. Shear strains dominate the behavior and beam theory cannot be used to determine the internal state of stress.

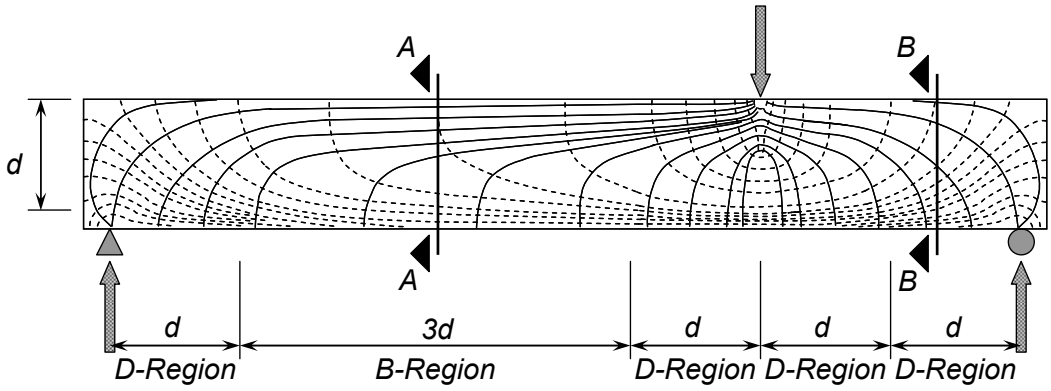

Figure 2.1: Stress trajectories in B-regions and near discontinuities (D-regions).

Nonlinear strain distributions are often caused either by abrupt changes in geometry or abrupt changes in loading. These regions of discontinuity are referred to as *D-regions* (D standing for *discontinuity* or *disturbance*). An elastic stress analysis suggests that the localized effect of a concentrated load or geometric discontinuity will attenuate about one member depth away from the discontinuity (St. Venant's Principle). For this reason, D-Regions are assumed to extend one member depth from the load or discontinuity. Figure 2.1 illustrates the location of B-regions and D-regions in a typical simply supported beam loaded at a single point.

Due to the nonlinearity of strains and inelasticity of concrete, a general theory of behavior is complicated to derive in a D-region. As a result, designers typically employ either empirically derived design methods or a hypothetical truss model such as a *strut-and-tie model* (STM).

The theoretical background of STM is presented in Section 2.3. Specific details related to the elements that form a truss model are presented in Section 2.3. Next, a summary of current code provisions is presented in Section 2.4. A historical background of the current design provisions is presented in Sections 5.2.

2.3 Theoretical Background of Strut-and-Tie Modeling

A strut-and-tie model idealizes the complex flow of stresses in a structural member as axial elements in a truss member. The compressive stress fields are resisted by concrete *struts* and the tensile stress fields are resisted by reinforcing steel *ties*. Struts and ties intersect at regions called *nodes*. Struts, ties, and nodes are the three elements that comprise a STM and they must be proportioned to resist the applied forces. According to the *lower bound theory of plasticity*, the capacity of a STM is always less than the structure's actual capacity provided the truss is in equilibrium and *safe*. A safe STM must have sufficient deformation capacity to redistribute forces into the assumed truss elements, and the stresses applied to the elements must not exceed their *yield* or *plastic flow* capacity. Failure of a STM can be attributed to crushing of the struts, crushing of concrete at the face of a node, yielding of the ties, or anchorage failure of the ties.

As an example, the loads supported by the beam shown in Figure 2.1 can be supported by the determinate truss shown in Figure 2.2. The same truss model is shown in Figure 2.3 with the concrete struts, nodes, and reinforcement drawn to scale. In Figure 2.3, the portions of the beam not considered in the truss model have been removed in order to illustrate the concept of a lower-bound solution. For this particular example, a fraction of the original beam is considered to resist the applied forces. If the laws of statics are satisfied and the materials do not exceed their yield capacity, then the estimated strength of the STM is less than or equal to the actual capacity of the beam.

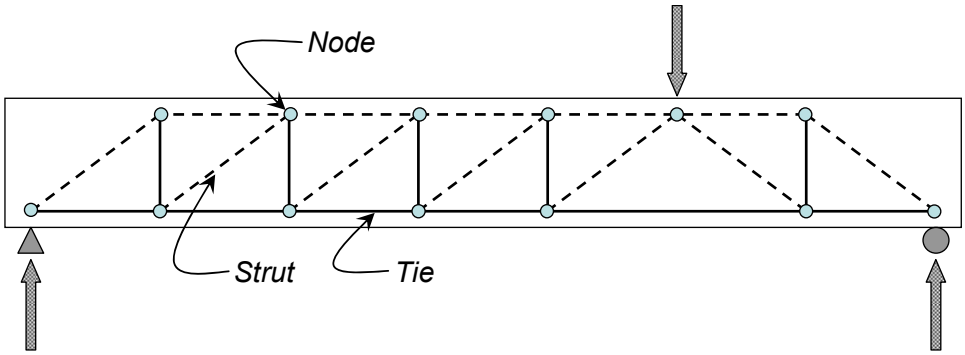

Figure 2.2: Strut-and-tie model: Simply supported beam supporting concentrated load.

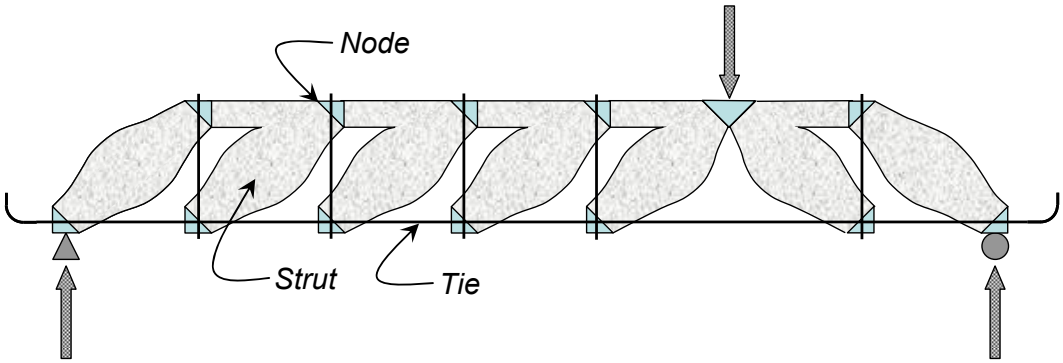

Figure 2.3: Strut-and-tie model with truss elements drawn to scale.

A STM is a powerful design tool as it is valid for any stable truss configuration a designer chooses. However, the downfall of an STM can also be attributed to its adaptability. There are no right or wrong solutions, but there are good and bad choices that can be made in developing a solution. For example, if the selected model varies substantially from the actual stress field, then the structure must undergo substantial deformation in order to develop the poorly assumed model. As a result, there is an increased chance that wide cracks could form. According to Schlaich et al. (1987):

Doubts could arise as to whether the correct model has been chosen out of several possible ones. In selecting the model, it is helpful to realize that loads try to use the path with the least forces and deformations. Since reinforced ties are much more deformable than concrete struts, the model with the least ties is the best. Of course, it should be understood that there are no unique or optimum solutions. Replacing a continuous set of smooth curves by individual polygonal lines is an approximation and leaves ample room for subjective decisions.

In developing a strut-and-tie model for a structure, the first step is to calculate the reactions supporting the applied loads. For example, consider the right side (deep beam portion) of the beam shown in Figure 2.1. Assume that the point load is 100-kips and ignore the self-weight of the beam. According to statics, 71-kips will flow to the right support and 29-kips to the left (i.e. $100 \cdot {}^{5}\!/_{7} = 71$). The right portion (i.e. deep beam portion) is illustrated in Figure 2.4.

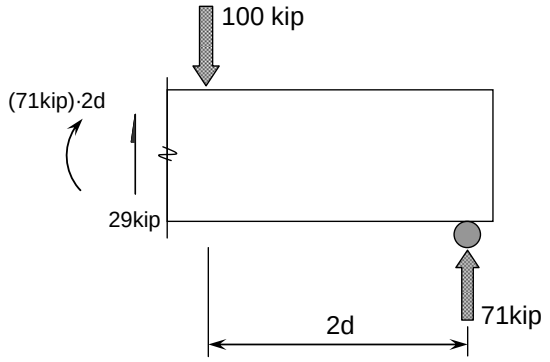

Figure 2.4: Step 1 for STM is calculation of support reactions.

For the next step, it is common to employ some type of linear elastic analysis in order to visualize the flow of forces within the member; and align the struts and ties according to the stress trajectories. Schlaich et al. (1987) recommend aligning struts within ±15° of the stress trajectories. In order to ensure adequate deformation capacity to develop the steel stresses, the orientation of the struts should not be excessively shallow. According to Ramirez and Breen (1991):

Large deviations from 45-degrees of the angle of inclination will demand excessive strains in the reinforcement together with extremely wide crack openings at failure. These diagonals must be [less than 65-degrees and greater than 30-degrees].

Also, if pictures of the cracking pattern in a similar structure are available, the location of the struts and ties can be arranged within the structure such that struts follow the known crack patterns (MacGregor 2005).

Based on the aforementioned guidelines for laying out a truss model and the stress trajectories shown in Figure 2.1, either a *one-panel* or *two-panel* truss is an appropriate solution. These two options are presented in Figure 2.5. Note, the point load is divided into 71 and 29-kips for the sake of convenience; it does not change the equilibrium of the model.

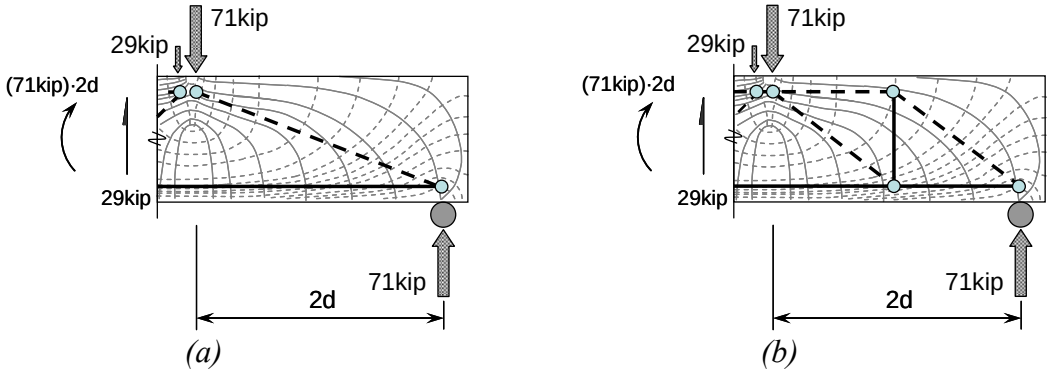

Figure 2.5: STM: (a) One-panel and (b) two-panel.

For an a/d ratio less than two, the transfer of shear predominantly results from compressive stresses flowing directly from the load to the support (i.e. one-panel truss model). For this type of behavior, the capacity of the beam is primarily dependent on the compressive strength of concrete in the direct strut. The transverse reinforcement (i.e. stirrups) has little

influence on the shear strength. A one-panel shear failure is illustrated in Figure 2.6 for a deep beam with an a/d ratio equal to 1.2.

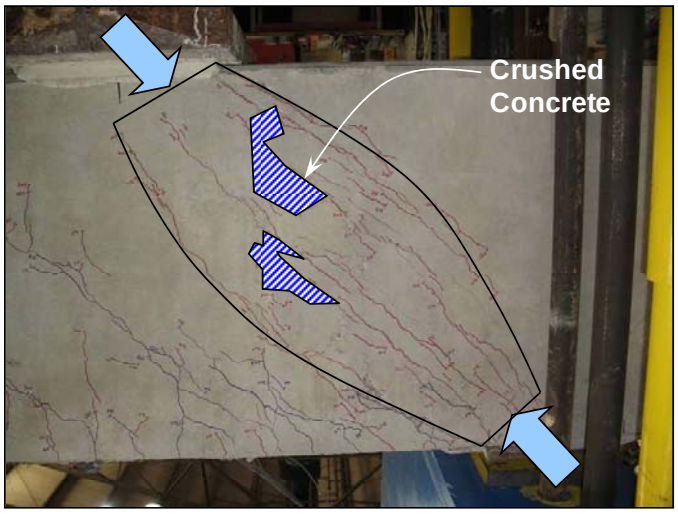

Figure 2.6: Direct strut or one-panel shear failure (a/d = 1.2).

If the a/d ratio exceeds a value of two, the mechanism of shear failure is better characterized as sectional shear rather than deep beam shear. The ability of a structure to resist sectional shear is due to many attributes of the cross-section including: the friction force along the inclined crack due to aggregate interlock; the increased shear capacity of the confined compression region; dowel-action of the horizontal reinforcement; and the tensile resistance of the vertical reinforcement. The web reinforcement is a main component that is used to determine the sectional shear resistance of a beam. After a diagonal crack has formed, the web reinforcement is the primary mechanism with which the structure transfers shear stresses across the crack and to the support. Failure is typically preceded by the yielding of the stirrups. A two-panel strut-and-tie model is akin to sectional shear behavior as both are largely influenced by the yielding of the vertical web reinforcement. A two-panel truss failure is illustrated in Figure 2.7 for a deep beam with an a/d ratio equal to 2.5.

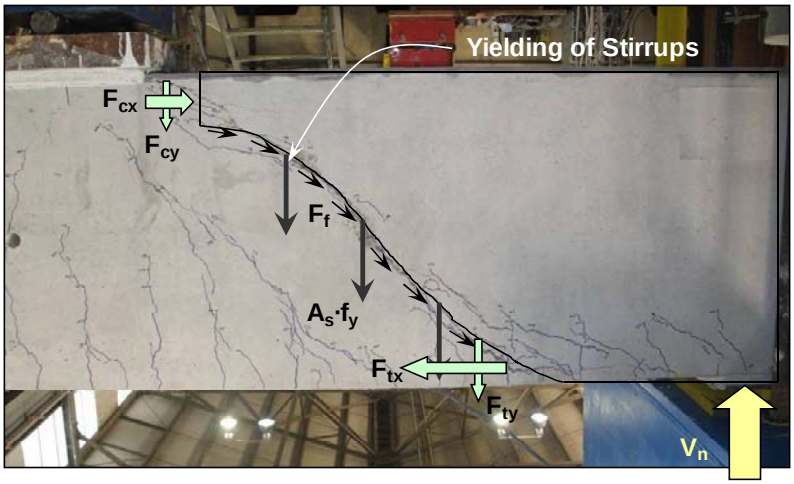

Figure 2.7: Sectional or two-panel shear failure (a/d = 2.5).

When the a/d ratio is near two, the shear mechanism may be attributed to a combination of both one and two-panel behavior. For example, consider the beam with an a/d ratio equal to 1.85 presented in Figure 2.8.

Figure 2.8: Combination of one and two-panel behavior (a/d = 1.85).

Upon examination of the cracking pattern, a combination of a one and two-panel model may be the most accurate. However, additional accuracy may not necessarily benefit the designer given the additional complication. Ultimately, the decision on which model to use is left to the discretion of the designer. According to the principles of STM, either model will result in a safe solution.

According to Kani et al. (1979), the transition in shear behavior between a direct strut (one-panel) and sectional shear (two-panel) occurs at an a/d ratio of 2.5:

The graphs of the [shear capacity versus a/d ratio] results seem to be made up of two different functions of which a/d = 2.5 is the point of intersection. There should be two totally different laws of failure governing each region.

Therefore, a one-panel strut-and-tie model is used to evaluate all beams tested as part of current and past experimental programs where a/d $\leq$ 2.5. The implication of using a one-panel model for a/d ratios up to 2.5 is discussed in Section 5.2 and 5.3.

Once a truss model has been selected, the next step is to proportion its elements (struts, ties, and nodes) accordingly; details on these elements are presented as follows.

2.3.1 Struts

Struts vary in shape depending on their location within a structure. Most struts in a two dimensional STM are *bottle-shaped*; that is, they spread laterally along their length. The lateral spreading of a bottle-shaped strut introduces tensile stresses transverse to the strut. These tensile stresses could potentially cause cracking along the length of the strut resulting in premature failure; hence, transverse reinforcement should be provided in order to control the cracking. Often, bottle-shaped struts in an STM are idealized as *prismatic*. However, this simplification does not eliminate the fact that the strut is, in actuality, still bottle-shaped and at a risk of splitting longitudinally; transverse reinforcement must be provided. Prismatic struts exist in the compression zone of a beam's flexural region. Figure 2.9 illustrates bottle-shaped, prismatic, and

idealized prismatic struts found in a typical STM. Design guidelines for the proportioning of struts are discussed in Section 2.4.4.

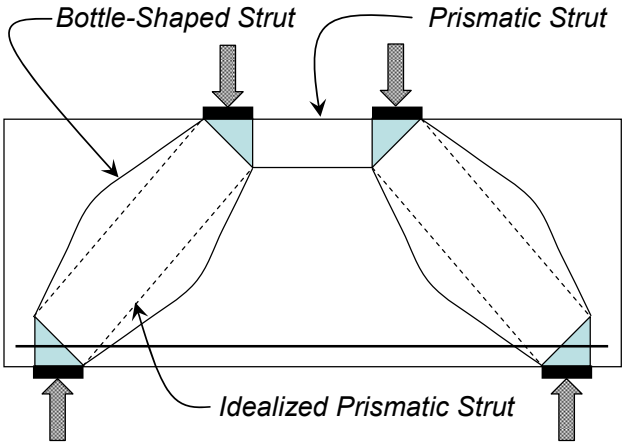

Figure 2.9: STM containing prismatic and bottle-shaped struts.

2.3.2 Ties

In general, reinforcing steel is placed at tie locations in an STM. The reinforcement should be distributed so that its centroid coincides with the tie location. Selection and placement of reinforcement for strength of a STM is fairly straight forward; details such as bar spacing, distribution, and anchorage are factors that deserve the most consideration when selecting and placing the reinforcement. Design guidelines for proportioning and placing tie reinforcement are presented in Section 2.4.5.

2.3.3 Nodal Zones

Nodes are named based on the nature of the elements that frame into them. For example, the nodal zone where two struts and a tie intersect is referred to as a *CCT* node (*C* stands for *compression* and *T* stands for *tension*). If more than three forces intersect at a node, it is often necessary to resolve some of the forces to end up with three resulting forces. The three types of nodes commonly used in a STM are shown in Figure 2.10.

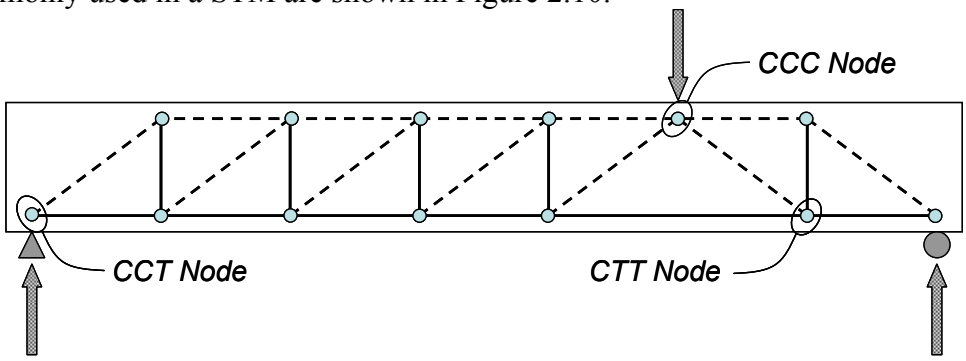

Figure 2.10: Nodal zones typically employed in STMs.

Ideally, nodes may be proportioned so that the stresses on all faces are equal. If the stresses are equal on all faces, the ratio of the area of the side face is proportional to the applied force. In this case, the node is called a *hydrostatic node*. Principal stresses are equal on all sides of a hydrostatic node; thus, shear stresses do not exist within the node. The absence of shear in the node and the simplicity of dimensioning hydrostatic nodes are their primary advantages.

If a node is proportioned such that unequal stresses exist on each face, then it is termed *non-hydrostatic*. Figure 2.11 illustrates the states of stress associated with hydrostatic and non-hydrostatic nodes.

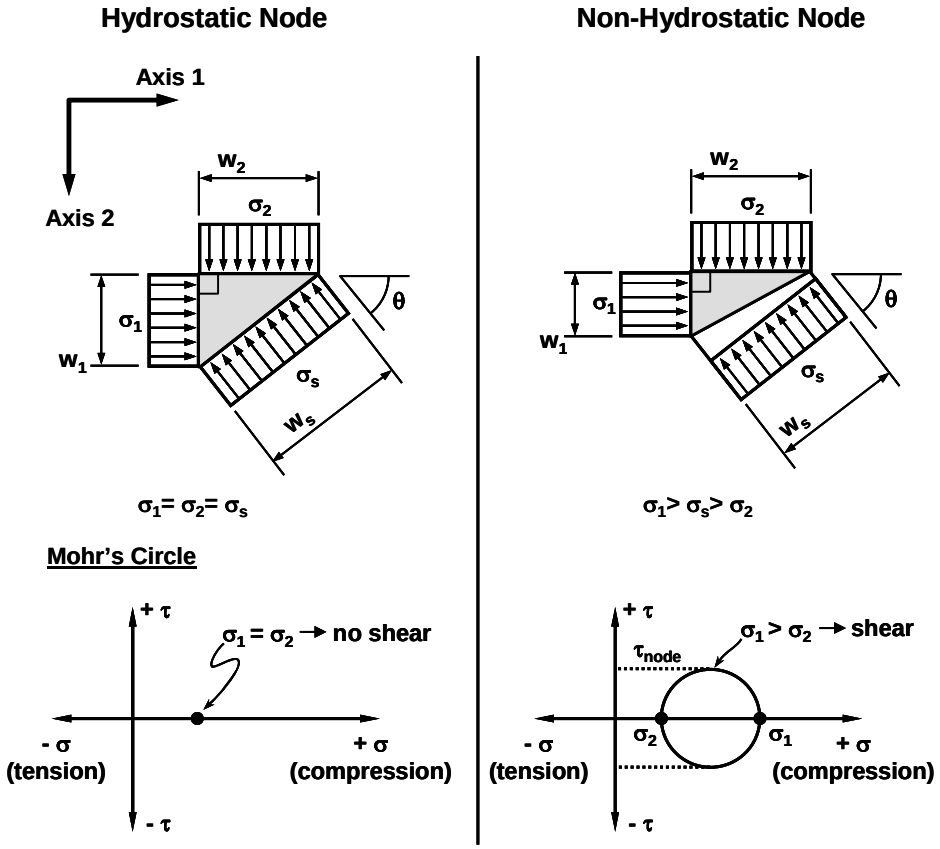

Figure 2.11: Stresses on hydrostatic and non-hydrostatic nodes (Brown et al. 2006).

It is important to note that both hydrostatic and non-hydrostatic nodes are idealizations of reality. They are proportioning techniques that have been established to create a strut-and-tie model. The influence that node type has on a strut-and-tie model of a deep beam is illustrated in Figure 2.12.

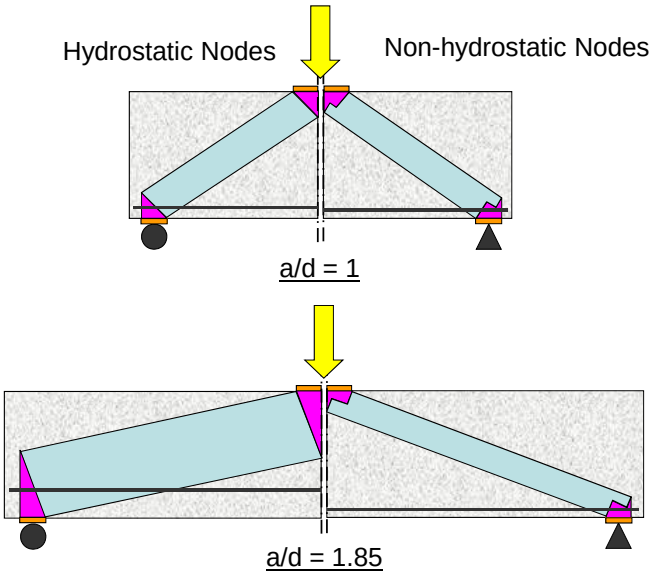

Figure 2.12: Difference between hydrostatic and non-hydrostatic nodes as the strut angle decreases.

Proportioning a hydrostatic node is a relatively straightforward procedure. The stress beneath the bearing plate is calculated with the applied force and the size of the bearing plate. Using this stress, the other dimensions of the hydrostatic node are determined so that equal stresses exist on all faces. Thus, the dimensions of the vertical back face (w_1 in Figure 2.11) and the node-to-strut interface (w_s in Figure 2.11) of hydrostatic nodes are based on the bearing stress. By geometry, each face of the node is perpendicular to the stress acting on it. In other words, the size of hydrostatic nodes is a function of the bearing plate length and the strut inclination (i.e. a/d ratio). As shown in the left side of Figure 2.12, this procedure can result in an unrealistically large strut and an impractical layout of longitudinal tie reinforcement as the strut angle becomes shallower.

Non-hydrostatic nodes are proportioned differently. The dimension of the bearing face of the node is determined by the length of the bearing plate as in the case of hydrostatic nodes. The back face of non-hydrostatic nodes, however, is proportioned by considering the origin of the applied stress. In the case of CCC nodes, the back face dimension is taken as the effective depth of the compression block as determined by a flexural analysis. In the case of CCT nodes, the back face dimension is taken as twice the distance from the centroid of the longitudinal reinforcement to the extreme tension fiber of the beam. The purpose of these proportioning techniques is for the assumed nodal geometry to more closely match the actual stress concentrations in these nodal regions. This is the primary advantage of non-hydrostatic nodes and the reason that they are preferred in design. The node-to-strut interface of non-hydrostatic nodes is determined by connecting the edges of the bearing and the back face. As shown in the right side of Figure 2.12, the node-strut interface is "stepped" so that it is perpendicular to the direction of the applied stress.

It is well documented that the shear capacity of a deep beam decreases as the a/d ratio increases. When hydrostatic nodes are used in a direct-strut model (Figure 2.12), the strength of a strut must be proportionally reduced as the a/d ratio increases in order to counteract the increasing size of the strut. Contrarily, when non-hydrostatic nodes are used, the dimension of

the strut-to-node interface decreases slightly as the a/d ratio increases, thereby accounting for the reduction in shear strength. This is another advantage of non-hydrostatic nodes.

2.4 Proportioning STM Elements using Non-Hydrostatic Nodes

The capacity of a beam as determined from a STM is inherently connected to the proportions of the nodal regions. Procedures for proportioning nodes have been well established by past researchers. This established set of guidelines is presented in Sections 2.4.1 through 2.4.3. For the sake of consistency, the following proportioning techniques are used to evaluate all of the beams contained in past and current experimental programs.

2.4.1 Proportioning a CCC Node

Refer to the CCC node shown in Figure 2.10. It has been magnified and is presented approximately to scale in Figure 2.13.

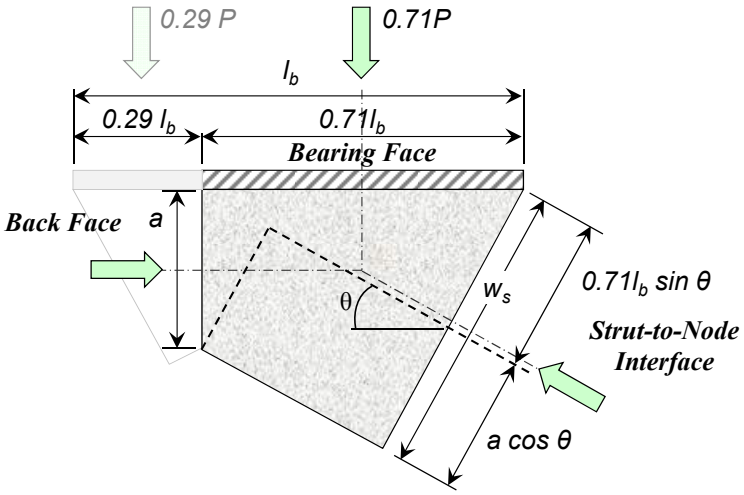

Figure 2.13: CCC Node.

For the beam shown in Figure 2.10, 71% of the applied load flows into the right support and the other 29% is transferred to the left support. Therefore, when proportioning the node, the length of the bearing face is set equal to 71% of the bearing plate length, l_b. The height of the back face, a, is assumed to be equivalent to the depth of the equivalent flexural stress block obtained from a typical flexural analysis. Admittedly, assumptions used in a flexural analysis are not valid within a D-region; especially for very low a/d ratios. However, the proportioning procedure is well-established in practice, and it is conservative. For a rectangular beam, a is calculated according to Equation 2.1.

$$a = \frac{\left(A_s \cdot f_s - A_s' \cdot f_s'\right)}{0.85 f_c' \cdot b_w} \tag{2.1}$$

Where,

A_s = Area of tension reinforcement, in^2
A_s' = Area of compression reinforcement, in^2
b_w = Web width, in.

f_c' = Specified concrete compressive strength, psi
f_s = Stress in tension reinforcement, psi
f_s' = Stress in compression reinforcement, psi

The angle of the strut abutting the strut-to-node interface, θ, depends on the truss configuration. Based on the length of the bearing plate and height of the back face, a, the width of the strut-to-node interface, w_s, is determined according to the following equation:

$$w_s = l_b \cdot \sin\theta + a \cdot \cos\theta \tag{2.2}$$

Where,

l_b = Length of bearing plate, in.
a = Height of back face of node, in.
θ = Angle of strut measured from the horizontal axis

Equation 2.2 is included in a figure of the ACI 318-08 code (ACI Figure RA.1.6), but not in the body of the code itself. According to MacGregor (2002), *future code committees should consider adding such equations to the Commentary.*

2.4.2 Proportioning a CCT Node

Refer to the CCT node shown in Figure 2.10. It has been magnified and is presented approximately to scale in Figure 2.14.

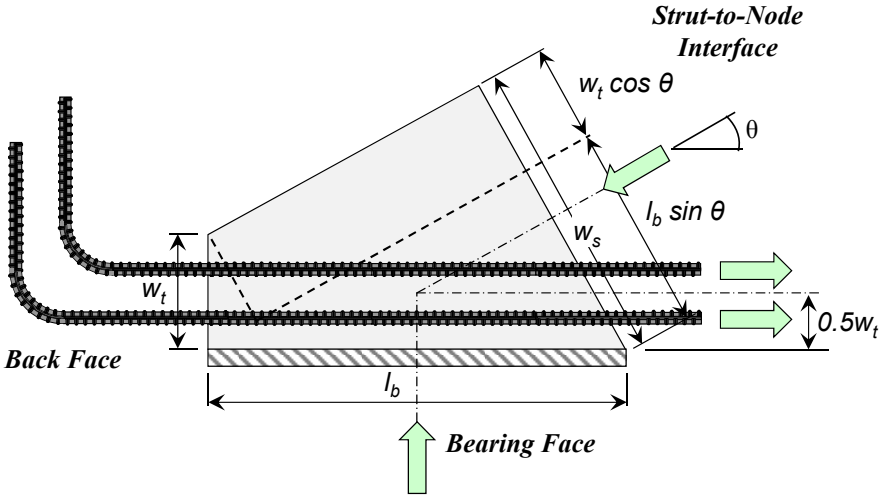

Figure 2.14: CCT Node.

The bearing face of a CCT node has the same dimensions as the bearing plate, l_b. The height of the back face, w_t, is taken as twice the distance from the near face of the beam to the centroid of the tension reinforcement. Finally, the angle of the strut abutting the strut-to-node interface depends on the truss configuration. Based on the given dimensions, the width of the strut-to-node interface, w_s, is determined the same as it is for a CCC node (Equation 2.2).

2.4.3 Proportioning a CTT Node

Refer to the CTT node shown in Figure 2.10. It has been magnified and is presented approximately to scale in Figure 2.15.

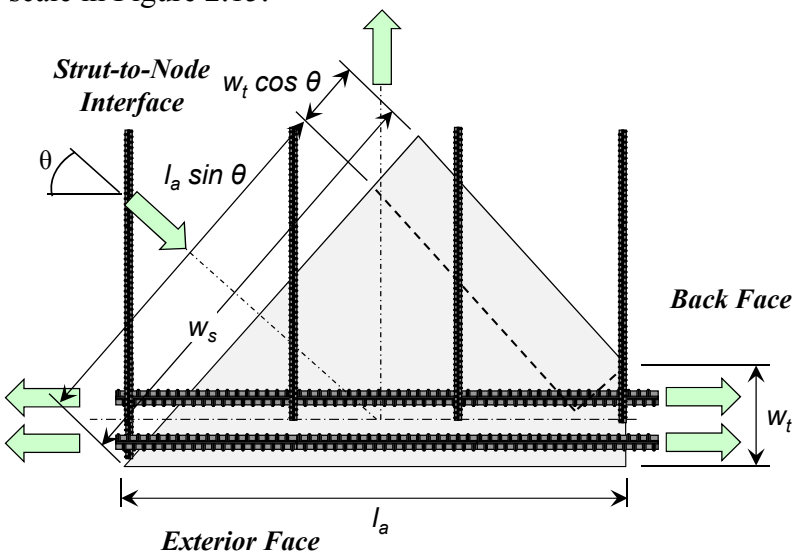

Figure 2.15: CTT Node.

Interior nodes, which are not bounded by a bearing plate, are often referred to as *smeared* nodes. Forces from compressive struts spread, or smear, and are equilibrated by multiple stirrups, or ties. Because a bearing plate does not abut the node, a proportioning technique must be employed to determine the extents of the exterior face, l_a. The method that is employed for the current project (TxDOT project 5253) is that recommended by Wight and Parra-Montesinos (2003). They propose that any stirrup that intersects an adjacent strut at an angle greater than 25-degrees be engaged as part of the vertical tie of the CTT node (Figure 2.16).

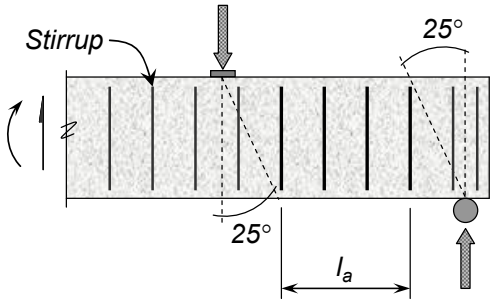

Figure 2.16: Determination of CTT vertical tie (Wight and Parra-Montesinos, 2003)

According to Wight and Parra-Montesinos (2003), it is conservative to assume that the exterior face, l_a, of the CTT node is as wide as the distance between the outermost stirrups included in the vertical tie.

The back face, w_t, of the node is calculated the same way as for a CCT node; twice the distance to the centroid of the tension steel, measured from the near face of the beam. Finally, the angle of the strut coming into the strut-to-node interface is based on the truss geometries. Based

on the given dimensions, the width of the strut-to-node interface, w_s, is determined the same as the CCC and CCT nodes (Equation 2.2).

2.4.4 Proportioning a Strut

Struts can be prismatic or bottle-shaped (Figure 2.9). A prismatic strut occurs within the compression zone of a beam's flexure region and is designed accordingly. Most struts are bottle-shaped and concentrate into the nodal regions. So, the highest stress that a strut must resist occurs at the location where the strut and node abut one another, or the strut-to-node interface. Even if a strut is idealized as prismatic, the highest stress occurs at the strut to node interface. Therefore, the critical proportions of a strut are based on the nodal proportions, specifically the width of the node-to-strut interface (w_s). The critical capacity of a strut is taken to be identical to the capacity of the node-to-strut interface.

2.4.5 Proportions and Placement of Tie Reinforcement

Ties shown in a strut-and-tie model are simple representations of tensile forces within a D-region. Proper placement of tie reinforcement is accomplished by matching the centroid and direction of the reinforcement with the axis of the tie in the truss model.

Tie details that deserve the most consideration are proper bar distribution, spacing, and development. In order to develop the reinforcing steel, ties must be properly anchored behind the front of the nodal zones. Figure 2.17 illustrates the development length of a typical tie.

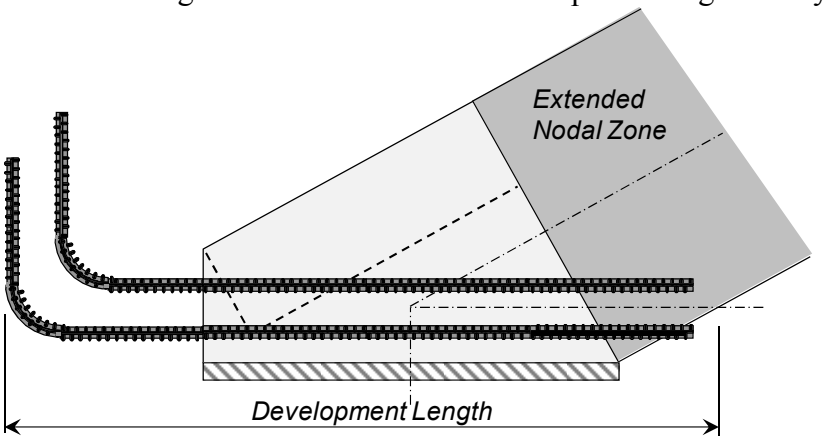

Figure 2.17: Development length of a tie.

ACI 318 allows the development length to be measured from the intersection of the extended nodal zone and the centroid of the bars, as shown in Figure 2.17. For the sake of simplicity, the development length can conservatively be taken from the edge of the bearing plate.

Proportioning nodes can be an iterative process. The size of the node is dependent on beam details such as bearing plate size and reinforcement location. Therefore, it may be necessary to adjust beam geometry, reinforcement location, and bearing plate size after the initial design iteration so that the stress applied to a nodal region is less than its nominal capacity.

In the previous two sections (2.3 and 2.4), the basic theory behind strut-and-tie modeling and typical proportioning techniques of struts, ties, and non-hydrostatic nodes were presented. This review was intended to provide the reader with a basic foundation of knowledge for the

material in the remainder of the report. Additional background information with regard to each project task is presented at the beginning of the results section for each task. In the next section (2.5), background information regarding the deep beam database that was compiled in this project is discussed.

2.5 Deep Beam Database

In addition to the experimental portion of the current research program, a database of deep beam shear tests ($a/d \leq 2.5$) has been compiled. The purpose of the database is to supplement the experimental program and provide an additional means of examining design provisions. The database is an expansion of a database originally compiled by Brown et al. (2006). All of the tests from the Brown et al. (2006) database with an a/d ratio greater than 2.5 have been removed; the remaining dataset has been rechecked and additional deep beam tests have been added. The total number of deep beam shear tests is 905 (including the 37 tests conducted in the current project). This database will subsequently be referred to as the *collection database*. The collection database was compiled based on the research papers cited in Appendix C and the experimental work in the current project.

The collection database was filtered in two stages (Table 2.1). In the first stage, test results were removed, for the most part, due to a lack of sufficient details to perform a strut-and-tie analysis. The resulting database is referred to as the *filtered database*. In the second stage, additional test results were removed in which the specimens were considered "less-representative" of field members. The resulting database is referred to as the *evaluation database.* An overview of the number of specimens that were removed from the database in each stage is provided in Table 2.1. Explanations for the removal of these test results are provided in the next two sections.

Table 2.1: Filtering of the deep beam ($a/d \leq 2.5$) database

Collection Database		***905 tests***
Stage 1 filtering	- incomplete plate size information	- 284 tests
	- subjected to uniform loads	- 7 tests
	- stub column failure	- 3 tests
	- $f'_c < 2{,}000$ psi	- 4 tests
Filtered Database		***607 tests***
Stage 2 filtering	- $b_w < 4.5$ in.	- 222 tests
	- $b_w d < 100$ in.^{2}	- 73 tests
	- $d < 12$ in.	- 13 tests
	- $\sum \rho_\perp < 0.001^*$	- 120 tests
Evaluation Database		***179 tests***

$^*\rho_\perp$ is defined in Equation 4.7

2.5.1 Filtered Database

Complete test results were desired in the filtered database. A large number of specimens in the collection database (284) did not contain adequate or verifiable bearing plate dimensions. This information was required to perform a strut-and-tie analysis on the specimens. As such, the results from these 284 tests were removed.

Only beams that were tested with one or two point loads were considered; thus, uniformly loaded beams were filtered from the database (7). The definition of the a/d ratio for a uniformly loaded beam is not straightforward. Also, determination of a truss model is slightly more complicated.

Of the remaining specimens, three failed due to crushing of their stub columns rather than failure of the beam. For these tests, stub columns were used at the bearing points to support the beam and apply the load. The details in the stub column were not the same as in the beam; and as a result, these test results were filtered from the database as well.

Finally, four specimens were removed from the remaining dataset due to the fact that the compressive strength of concrete at the time of testing was less than 2,000-psi. For concrete to be considered *structural*, it must have a compressive strength greater than or equal to 2,000-psi.

In summary, the filtered database contains 607 test results. The specimens in the filtered database have adequate details necessary to perform strut-and-tie analyses with reliability and relative ease.

2.5.2 Evaluation Database

Due to the limitations of testing capacity and/or research budgets, most of the specimens in the filtered database are unrealistically proportioned. In order to illustrate this point, the specimens in the filtered database are plotted in Figure 2.18 by their shear area ($b_w \cdot d$) along the vertical axis and aspect ratio of their cross-section (d/b_w) along the horizontal axis.

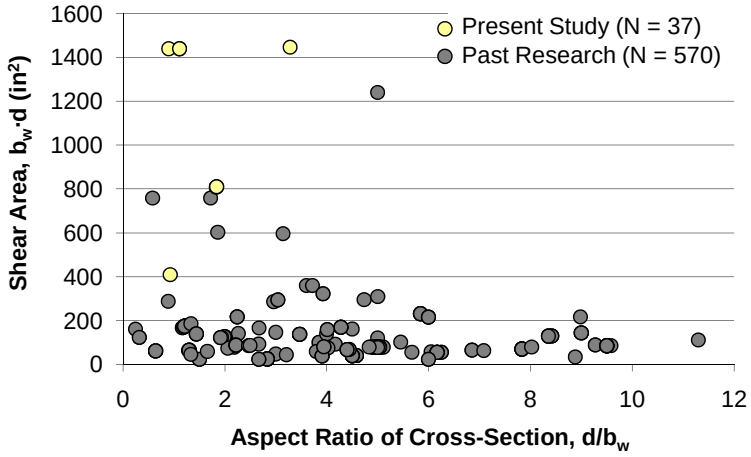

Figure 2.18: Summary of beam proportions in filtered database (N=607).

The majority of the specimens in the filtered database have an area less than 200-in^2. Yet, bent caps in the State of Texas are typically on the order of 1200-in^2 and greater. Also, a significant number of beams in the filtered database have an aspect ratio greater than four – some

have a depth over 8 times greater than their width. Such a high aspect ratio is unrealistic. Conventional beams have an aspect ratio of approximately one to three.

In addition to specimen size, a significant number of the beams in the filtered database do not have any or contain unrealistically low amounts of transverse reinforcement. Although testing specimens without any transverse reinforcement may be interesting from an academic standpoint, most beams in the field, particularly deep beam regions, contain a minimum amount of transverse reinforcement. Therefore, it was determined that unreinforced beams should not used to evaluate STM provisions. However, it is of interest to evaluate specimens that have less transverse reinforcement than the minimum required by design specifications. By examining the trends of *lightly reinforced* specimens, a determination can be made as to an adequate amount of reinforcement necessary to maintain the integrity or strength of a D-region.

As stated, it is the goal of the research program to only consider those beams that better represent actual bent caps. This criterion was given the most weight when forming the evaluation database. In addition, it was necessary that the number of remaining beams in the evaluation database was statistically significant. Accordingly, the following criteria were used to remove 428 of the *less representative* specimens from the filtered database (Table 2.1):

- **Beam width, b_w, greater than 4.5-inches:** 222 specimens had a width less than 4.5-inches.
- **Shear area, $b_w \cdot d$, greater than or equal to 100-in^2:** of the remaining dataset, 73 specimens had a shear area less than 100-in^2.
- **Depth, d, greater than or equal to 12-inches**: of the remaining dataset, 13 specimens had a depth less than 12-inches.
- **Transverse reinforcement ratio, $\Sigma\rho_\perp$, greater than 0.1%** (ACI 318 definition, Equation 4.7): of the remaining dataset, 120 specimens had $\Sigma\rho_\perp$ less than 0.1%.

The remaining database is referred to as the *evaluation database* and contains 179 specimens; 35 of which have been tested as part of the current research program (2 specimens from this study were filtered out of the evaluation database because they did not contain sufficient transverse reinforcement). Specimens in the evaluation database are considered to be more representative of deep beams in the field than those that were filtered out. The data from the tests in the evaluation database were used throughout the remainder of the current research program in evaluating and formulating STM design provisions. The complete details of the beams in the evaluation database are presented in Appendix D.

It is important to note that specimens that failed in shear and in flexure, as reported by the researcher, were both included in the evaluation database. Since strut-and-tie modeling is a general procedure that accounts for both shear and flexure through the numerous design checks of each nodal face and tension tie, it is appropriate to evaluate both failure modes.

2.6 Summary

Deep beam shear behavior is typically analyzed using an empirically derived equation or a strut-and-tie model. Strut-and-tie modeling is a simple method that can be used to determine the capacity of a complex D-region. The method conforms to the lower bound theory of plasticity. Thus, it is inherently conservative. A strut-and-tie model is a truss composed of struts and ties interconnected by nodes. To design or analyze a deep beam or D-region with strut-and-tie models, it is necessary to proportion the nodal regions. Typically, designers proportion *non-hydrostatic nodes* to more closely match the assumed nodal geometry with the actual stress

concentrations in the member. Proportioning the node-to-strut interface determines the narrowest and most highly-stressed portion of a strut. Tensile reinforcement is placed to coincide with the centroid of the tie in the strut-and-tie model. The purpose of presenting the background information for deep beam shear behavior and strut-and-tie modeling is to provide a foundation to the reader to better understand the project objectives, development of the experimental program, and implications of the findings. Additional background information related to each project objective is presented with the results of each objective.

In Section 2.5, information regarding the development and filtering of a deep beam database used in the current project was provided. After the test results of specimens that lacked sufficient details or that were considered grossly unrepresentative of deep beams in the field were removed, an *evaluation database* of 179 test results remained. This database is used throughout the report to supplement the findings of the current project. Information regarding the experimental program is presented in Chapter 3.

Chapter 3. Experimental Program

3.1 Overview

In this chapter, details of the design, fabrication, and testing of the specimens in the experimental program are provided. Thirty-seven tests were conducted on beams with various section sizes, web reinforcement details, bearing plate details, and a/d ratios.

3.2 Testing Program

In the experimental research program, eight individual objectives were addressed (Section 1.3). All of the objectives were associated with the design or performance of reinforced concrete deep beams. The effects of the following variables on the strength and serviceability performance of deep beams were specifically addressed with the experimental program:

1. The distribution of stirrups across the web of the beam (2 legs vs. 4 legs)
2. Triaxial confinement (via concrete) of nodal regions
3. The amount of minimum web reinforcement (transverse and longitudinal)
4. The depth of the member

The results of these four tasks are presented individually in Chapter 4. The four remaining objectives of the project were addressed with the analysis of the results from the experimental program and the evaluation database. They included:

5. Improvement of strut-and-tie design method for deep beams
6. Improvement of the discrepancy in shear design models at the transition from deep beam to sectional behavior at an a/d ratio of 2.
7. Recommendation for limiting diagonal cracking under service loads
8. Method to correlate maximum width of diagonal cracks to residual capacity of in-service bent caps

The results of these four tasks are presented individually in Chapter 5.

To accomplish the objectives of the current project, it was necessary to develop an extensive testing program. Data in the literature was generally insufficient to address the tasks of the project for two reasons. First, very little serviceability information, primarily diagonal crack width data, exists in the literature. With the exception of task 6, all of the project objectives required the evaluation of the serviceability performance of deep beams. Second, the cross-sectional dimensions of deep beams, particularly the beam width, tested in the past are drastically smaller than those of members in service. Two of the aforementioned tasks required data from specimens with widths of realistic size (tasks 1 and 2). Task 8 was aimed at the specific performance of in-service bent caps and thus, benefitted from data from beams of comparable size. As a whole, it was determined that testing specimens of comparable size to that of members in service provided the best means to improve their design and performance.

A comparison between the cross-sectional dimensions of several bent caps in Texas to those of test specimens in the literature is made in Figure 3.1. The cross-sections of two bent caps that experienced significant diagonal cracking problems in service are shown at the far left. The cracking problem and required retrofit of the I-45 bent cap in Houston was discussed in Section 1.2. The cross sections of two standard bent caps used by TxDOT to support Type IV and Type C prestressed girders are also shown in Figure 3.1. The cross-sections used in several

testing programs that provided the basis for much of the current deep beam design provisions are illustrated at the far right of Figure 3.1. It is clear that the sizes of bent caps in service are significantly different from that of the deep-beam specimens tested previously.

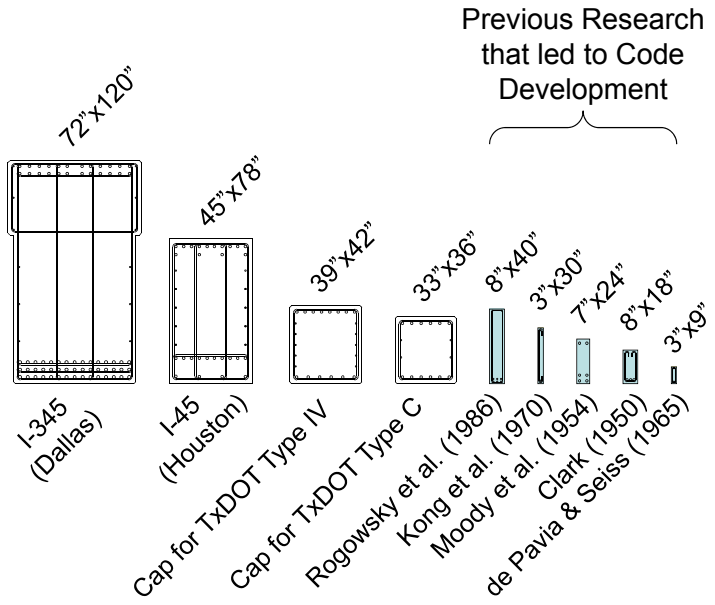

Figure 3.1: Scaled comparison between actual bent caps and beams included in past research programs.

The testing program was divided into five series to isolate the primary objectives of the research project. The purpose of Series I through IV was to address tasks 1 through 4 of the current project. Series M consisted of five tests on 36"x48" specimens in which multiple objectives were evaluated. The specimens in Series III and IV were tested at three different a/d ratios to specifically address task 6. All of the specimens in the experimental program were used to address tasks 5, 7, and 8. The titles of each series are as follows:

- Series I: Distribution of Stirrups across the Beam Web (2 legs vs. 4 legs)
- Series II: Triaxially Confined Nodal Regions
- Series III: Minimum Web Reinforcement (see Figure 3.8 for definition)
- Series IV: Depth Effect
- Series M: Multiple Purpose

An overview of the variables used in each test series is provided in Table 3.1. A brief description of each testing series and the details of the test specimens used in each series are provided in Sections 3.2.1 to 3.2.5.

Table 3.1: Variables in Testing Program.

Testing Series	b in.	d in.	Support Plate†	Load Plate†	No. of Stirrup Legs	ρ_v*	ρ_h*	a/d ratio
Series I Dist. of Stirrups across Web	21	38.5	16”x21”	20”x21”	2	0.003	0.003	1.84
					4			
					2	0.002	0.002	
					4			
Series II Triaxially Confined Nodal Regions	21	38.6	10”x21”	20”x21”	2	0.003	0.003	1.84
			10”x21”	10”x7”				
			10”x21”	36”x21”				
			5”x7”	36”x21”				
			5”x7”	36”x21”		0.002	0.002	
			10”x21”	10”x7”				
			10”x21”	10”x21”				
			5”x21”	20”x21”				
Series III Minimum Web Reinforcement	21	38.6	16”x21”	20”x21”	-	0.000	0.000	1.84
								2.47
					2	0.002	0.002	1.84
						0.0025	0.0015	
						0.003	0.003	
						0.001	0.001	
						0.003	0.003	
						0.002	0.002	
						0.002	0.002	1.20
						0.003	0.003	
						0.002	0.002	2.49
						0.003	0.003	
Series IV Depth Effect	21	68.9	16”x21”	29”x21”	2	0.002	0.002	1.85
						0.003	0.003	
				24”x21”		0.002	0.002	2.50
						0.002	0.002	1.20
		19.5		16.5”x21”		0.003	0.003	1.85
						0.002	0.002	
				15.5”x21”		0.002	0.002	2.50
				18”x21”		0.002	0.002	1.20
Series M Multiple Purpose	36	40	16”x36”	24”x36”	4	0.003	0.003	1.85
				8”x12”		0.003	0.003	
				24”x36”		0.009	0.003	
				24”x36”		0.002	0.002	
				24”x36”	2	0.003	0.003	

† Load plate dimensions: [in direction of span] x [transverse to direction of span]

*Actual reinforcement ratios differed slightly from targeted values

3.2.1 Series I: Distribution of Stirrups across Beam Web

For the design of CTT nodes, AASHTO LRFD (2008) requires the use of multiple stirrup legs in order to utilize the entire width of a beam in determining available strut width (as shown in AASHTO LRFD 2008 Figure 5.6.3.3.2-1 (a)). ACI 318-08 recommends additional stirrup legs across the width of wide beams for sectional shear. In order to investigate these provisions, four tests were conducted on specimens with a 21"x44" cross-section. Additional background information regarding this issue and the results of the four Series I tests are provided in Section 4.3.

According to AASHTO LRFD (2008), the width of a strut anchored by stirrups is limited to a distance equal to six longitudinal bar diameters from the centroid of the stirrups. Therefore, multiple stirrup legs must be provided in order to fully utilize the section. The reinforcement for the Series I specimens was configured in order to specifically evaluate this AASHTO LRFD effective strut width provision. An overview of the effective strut widths of the Series I specimens is shown in Figure 3.2. The difference between the effective widths of the struts supported by two and four stirrup legs was 11.3 and 21-inches respectively (Figure 3.2), a 46-percent difference.

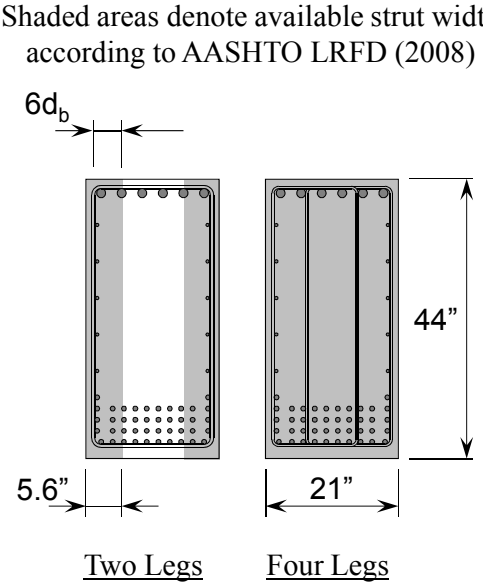

Figure 3.2: Effective width of strut anchored by reinforcement at the CCT node.

The 21"x44" test specimens were designed such that shear was the critical mode of failure. The width was proportioned in order to maximize the width of the specimen, while keeping it narrow enough to ease installation to and removal from the test setup. Two distributions of web reinforcement were evaluated: 0.2% and 0.3% reinforcement in each direction. The spacing of the reinforcement was kept relatively constant so that the only variable between companion tests was the number of stirrups distributed across the web. Additional details of the Series I specimens are provided in Section 3.2.6 in Table 3.2.

Series I: Beam Details

In order to distinguish Series I specimens from one another, the nomenclature presented in Figure 3.3 was developed. Each numeral is a variable within the testing series. Beam details other than those shown in the specimen I.D. (Figure 3.3) remained constant and are presented in Table 3.2.

.

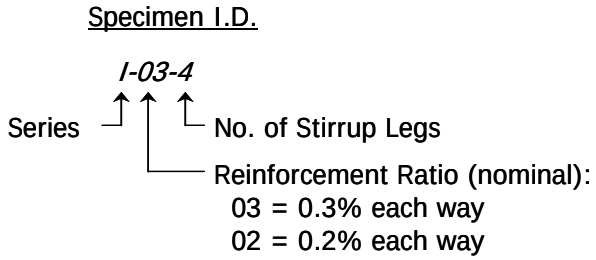

Figure 3.3: Series I: description of nomenclature used for Specimen I.D.

Geometric and reinforcement details for all the Series I beams are presented in Figure 3.4 and Table 3.2. The position of the longitudinal reinforcement in the section was controlled with steel chairs. The clear cover was relatively small (¾" side cover and 1" top and bottom cover) for all of the 21" wide specimens when compared with standard TxDOT members. These values were selected due to their agreement with the reinforcement layout and overall width restriction of the test specimens. They match minimum cover for precast conditions which seemed appropriate since the specimens were cast in a laboratory with steel formwork and the use of form-attached vibrators. No problems with consolidation were noticed in any of the specimens. Durability implications were not a concern for the test specimens.

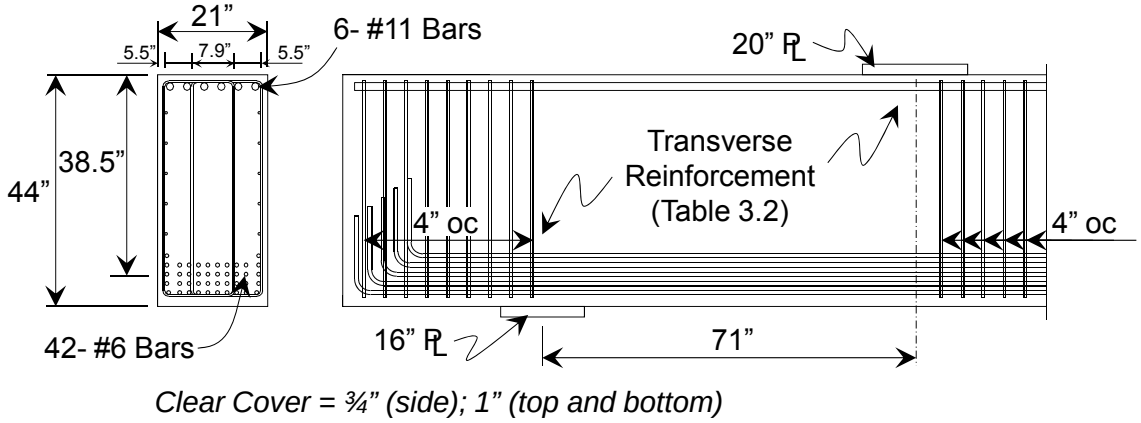

Figure 3.4: Series I beam details.

3.2.2 Series II: Triaxially Confined Nodal Regions

Researchers (Hawkins, 1968; Adebar and Zhou, 1993; and MacGregor and Wight, 2005) agree that triaxial confinement from surrounding concrete can increase its compressive strength.

However, there is not a code provision in place allowing an increase in the strength of a triaxially confined nodal zone in ACI 318-08 or AASHTO LRFD (2008). Triaxial confinement within nodal zones is an important issue as the size of a bearing plate can have a pronounced effect on the capacity predicted from a STM. Additional background information regarding this issue and the results of the Series II specimens are presented in Section 4.4.

In order to investigate the effect of triaxial confinement within a deep beam nodal region, identical tests were conducted in which the only variable was the size of the bearing plate. For a plate to be triaxially confined by surrounding concrete, its width must be substantially less than that of the beam. Concurrently, it was important that the width of the test specimen was large enough such that there was a significant difference between a reduced and full size bearing plate. For the specimens tested in Series II, the width of the bearing plates used to achieve triaxially confined nodes was three times narrower than the width of the beam (e.g. from 21-inches to 7-inches). Triaxial confinement was investigated at both the load (CCC node) and support (CCT node) bearing plates. The plate sizes used for the eight tests conducted in Series II are illustrated in Figure 3.5. All of the specimens had a 21"x42" cross-section.

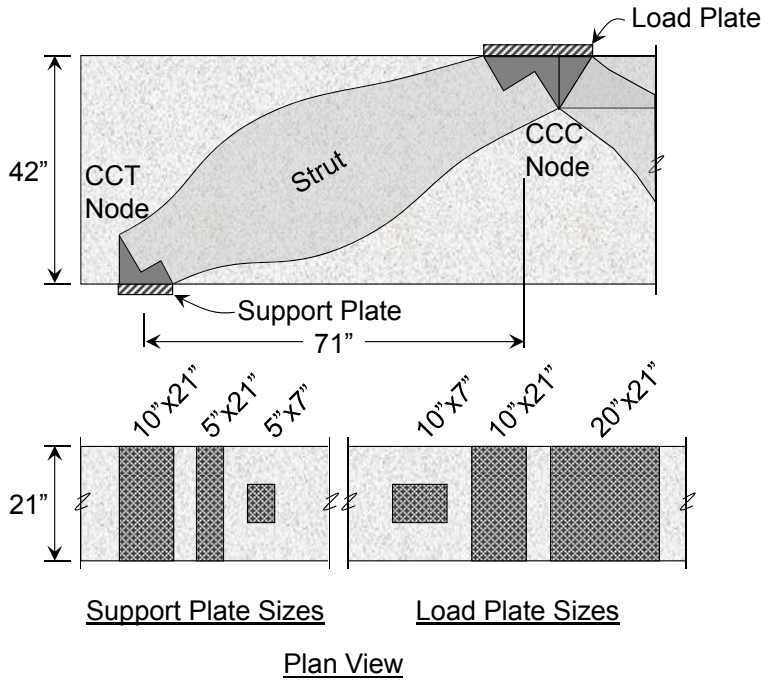

Figure 3.5: Plate sizes investigated within Series II.

The 21-inch wide specimens were designed in the same manner as the Series I specimens; i.e. so that shear would be the dominant mode of failure. Two different quantities of web reinforcement were evaluated in Series II to evaluate its effect, if any, on triaxial confinement. Additional details of the Series II specimens are provided in Table 3.2.

Series II: Beam Details

In order to distinguish Series II beams from one another, the nomenclature presented in Figure 3.6 was developed. Each numeral is a variable within the testing series. Beam details other than those shown in the specimen I.D. remained constant and are presented in Table 3.2.

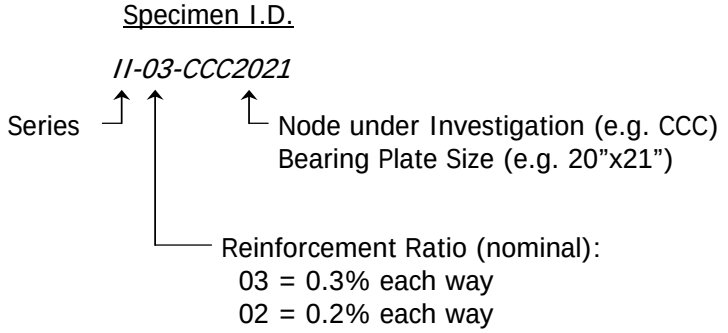

Figure 3.6: Series II: Description of nomenclature used for Specimen I.D.

Geometric and reinforcement details for the Series II beams are presented in Figure 3.7.

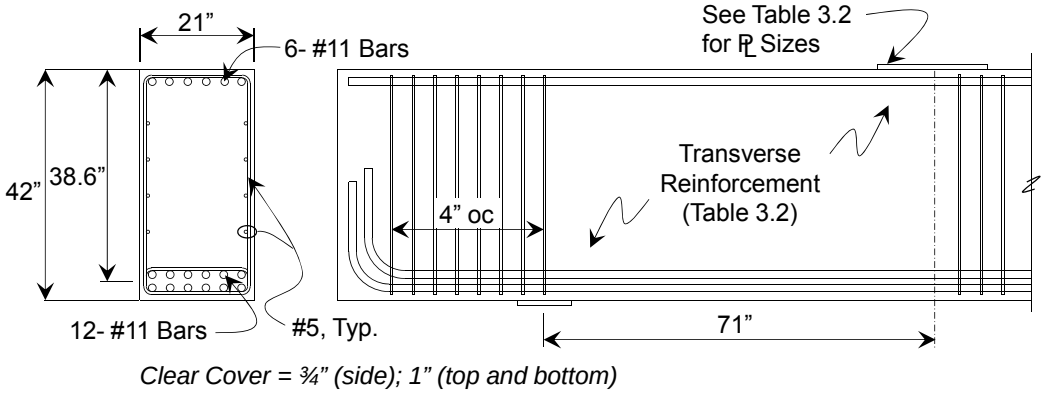

Figure 3.7: Series II beam details.

3.2.3 Series III: Minimum Web Reinforcement

The purpose of the Series III specimens was to determine the appropriate amount of minimum reinforcement considering both the strength and serviceability performance of deep beams. In current design provisions, several different recommendations exist for minimum web reinforcement. There is little consensus regarding whether minimum reinforcement should address both strength and serviceability considerations. The results of the specimens tested in Series III are provided in Section 4.5.

Twelve tests were conducted in Series III on 21"x42" specimens. The specimens were tested at three different a/d ratios: 1.2, 1.85, and 2.5. At an a/d ratio of 1.85, several specimens were tested in which the only variable was the quantity of vertical and horizontal web reinforcement. At a/d ratios of 1.2 and 2.5, reinforcement corresponding to 0.2% and 0.3% in each orthogonal direction was placed in companion specimens.

The amount of web reinforcement in the test specimens was categorized by the reinforcement ratio definitions given in Figure 3.8. The vertical and horizontal reinforcement was placed evenly throughout the shear span and the strut area, respectively. The height of the strut was estimated by subtracting twice the distance from the extreme tension fiber to the

centroid of the tension reinforcement and twice the distance from the extreme compression fiber to the centroid of the compression reinforcement from the total height of the section (Van Landuyt, 2006). This definition differed from the minimum reinforcement provisions in the STM section of AASHTO LRFD (2008) which bases the total amount of horizontal reinforcement on the gross concrete section (b_w*h). Since this reinforcement is intended primarily to reinforce bottle-shaped struts, it is appropriate to base the amount of reinforcement on the area of the bottle-shaped strut.

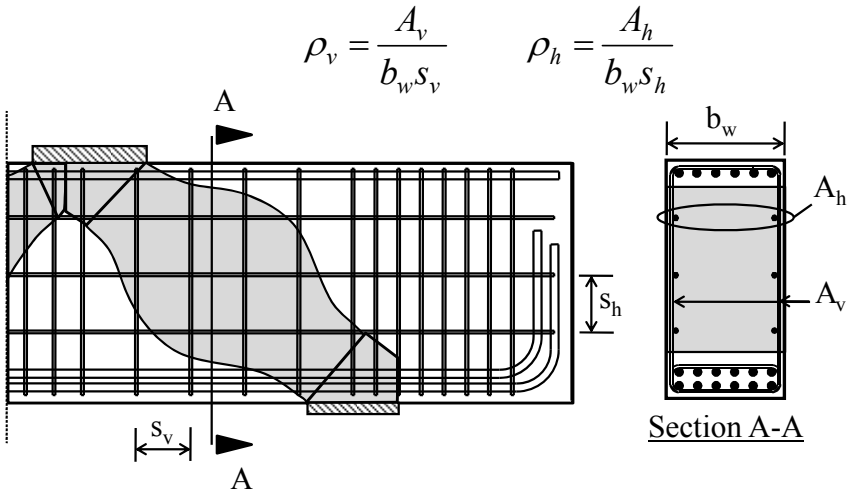

Figure 3.8: Definition for vertical and horizontal web reinforcement ratios

As in Series I and II, the specimens in Series III were designed such that shear was the critical failure mode. Thus, the same longitudinal reinforcement (2.3%) was used which enabled the comparison of several tests across series. The primary variables in Series III were the quantity of web reinforcement and the a/d ratio. The spacing of the web reinforcement was not directly studied although some comparisons were made possible through the testing program. Other variables such as the size of the bearing plates were kept constant. Complete details are summarized in Table 3.2.

Series III: Beam Details

In order to distinguish Series III beams from one another, the nomenclature presented in Figure 3.9 was developed. Each numeral is a variable within the testing series. Beam details other than those shown in the specimen I.D. remained constant and are presented in Table 3.2.

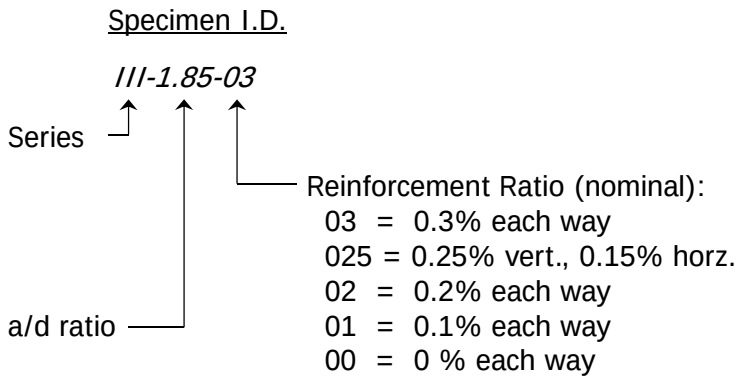

Figure 3.9: Series III: Description of nomenclature used for Specimen I.D.

Geometric and reinforcement details for the Series III beams are presented in Figure 3.10. Similar detailing was used in the Series II and III specimens.

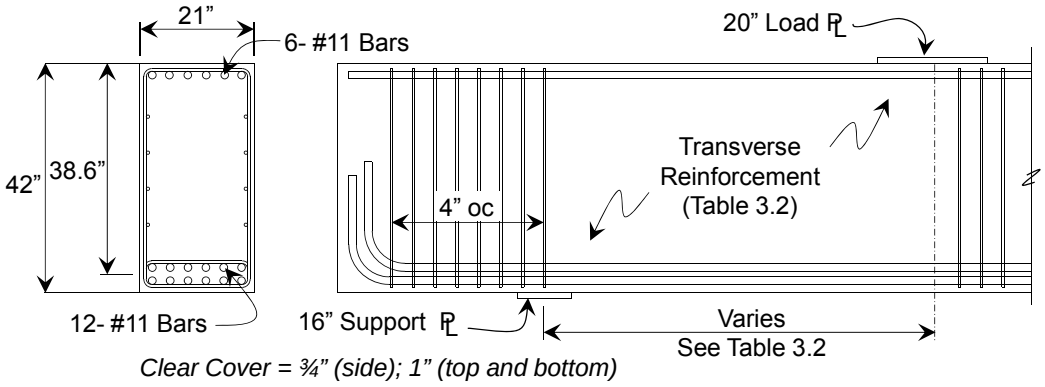

Figure 3.10: Series III beam details.

3.2.4 Series IV: Depth Effect

The purpose of the Series IV specimens was to investigate the effect of member depth on the strength and serviceability performance of reinforced concrete deep beams. Most of the bent caps in service in Texas are considerably larger (in width and in depth) than those in the literature (Figure 3.1). It is necessary to understand the effect that member depth may have on the performance of deep beams to improve the design of actual structures. Other researchers have concluded that the width of deep beams does not affect their performance provided that the beam is laterally stable and can be properly detailed (Kani et al., 1979).

In Series IV, four tests were conducted on beams with a 21"x75" cross-section. Four tests were conducted on beams with a 21"x23" cross-section. At an a/d ratio of 1.85, a specimen was tested at each depth with 0.2% and 0.3% web reinforcement in each direction. At a/d ratios of 1.2 and 2.5, specimens were tested at each depth with 0.2-percent web reinforcement. The specimens were designed such that they could be directly compared with the 21"x42" specimens tested in Series III. Complete details of the Series IV specimens are summarized in Table 3.2.

The size of the nodal regions (CCC and CCT) was kept relatively constant for the specimens with different depths that were tested at the same a/d ratio. This decision was made to evaluate the effect of changing the depth of the member without proportionately changing the size of the nodal regions. In this way, the depth of the member was the only variable between each test. Additional discussion regarding the Series IV specimens and their test results is provided in Section 4.6.

Series IV: Beam Details

In order to distinguish Series IV beams from one another, the nomenclature presented in Figure 3.11 was developed. Each numeral is a variable within the testing series. Beam details other than those shown in the specimen I.D. remained constant and are presented in Table 3.2.

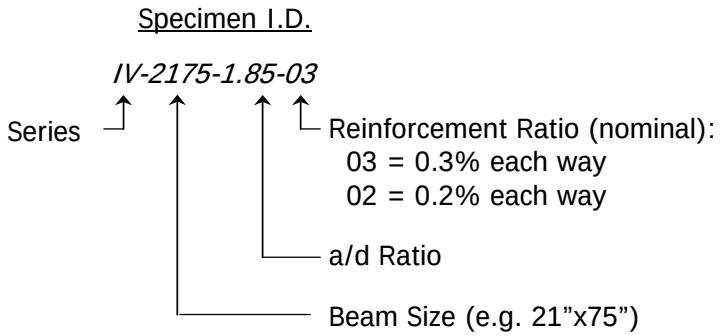

Figure 3.11: Series IV - Description of nomenclature used for Specimen I.D.

Geometric and reinforcement details for the Series IV beams are presented in Figure 3.12. Similar beam parameters were used in the Series IV and Series III specimens to permit their direct comparison (Table 3.2).

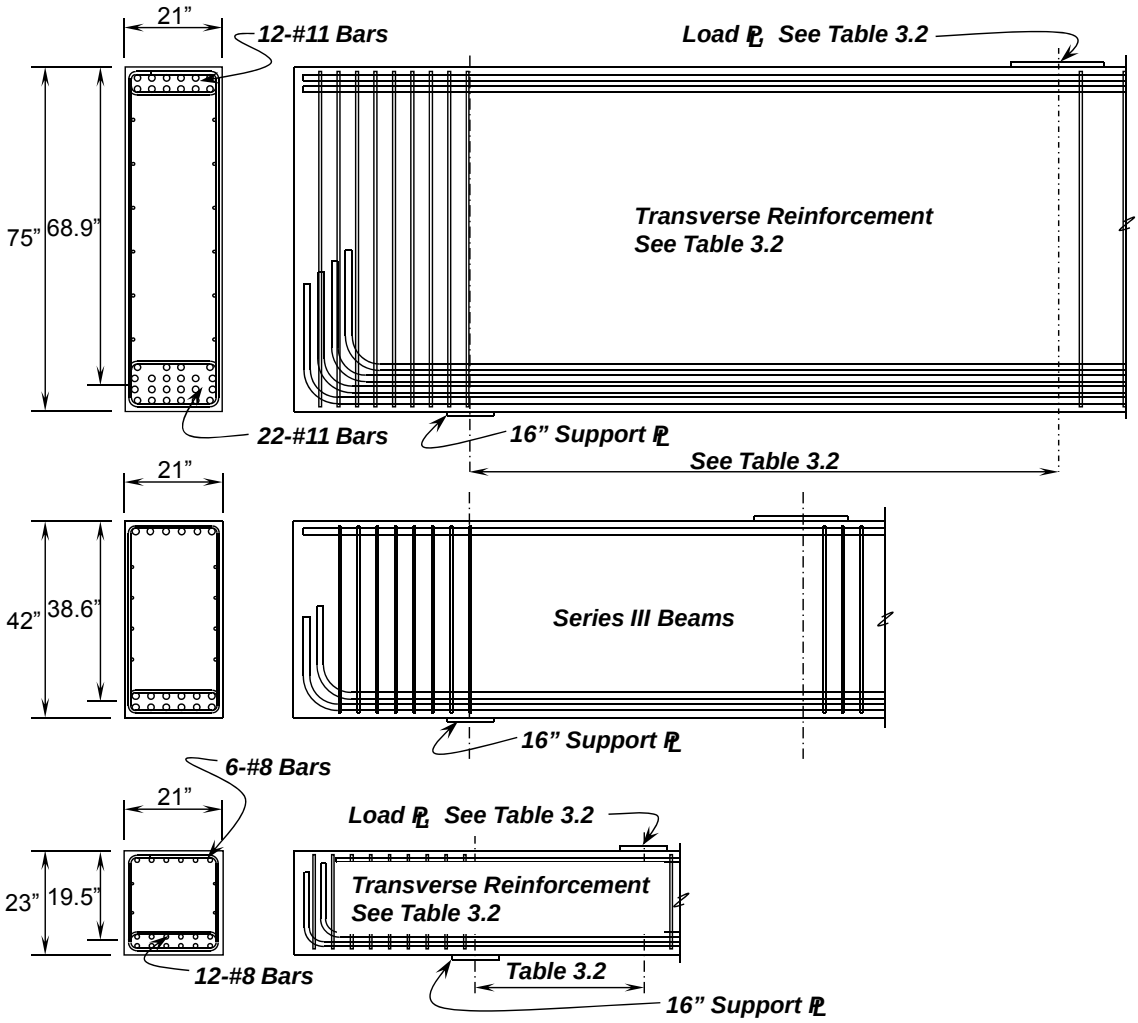

Figure 3.12: Series IV beam details.

3.2.5 Series M: Multiple Purpose

The Series M specimens were the first specimens fabricated and tested in the current project. All of the Series M specimens had a 36" x 48" cross-section. The primary variables in Series M were the amount of web reinforcement, the distribution of stirrups across the web, and the size of the load plate. Five tests were conducted. The results of these tests were used to design the rest of the experimental program (Series I through IV) and are included with the results of the other Series that addressed a similar objective. The results from the Series M specimens were exceptionally valuable due to the size of the cross-section.

The Series M specimens were also designed such that shear was the critical failure mode. There were some differences between the Series M specimens and those in the other series such as the beam width, the ratio of the longitudinal compression reinforcement to the effective area, the ratio of the longitudinal tension reinforcement to the effective area, and the concrete cover. A larger cover (2" all sides) was used in the Series M specimens as compared to those in Series I

through IV since these members were cast with wood formwork and without the benefit of form vibrators (Section 3.4.3). Complete beam details for the Series M specimens are summarized in Table 3.2.

Series M: Beam Details

In order to distinguish Series M beams from one another, the nomenclature presented in Figure 3.13 was developed. Each numeral is a variable within the testing series. Beam details other than those shown in the specimen I.D. remained constant and are presented in Table 3.2.

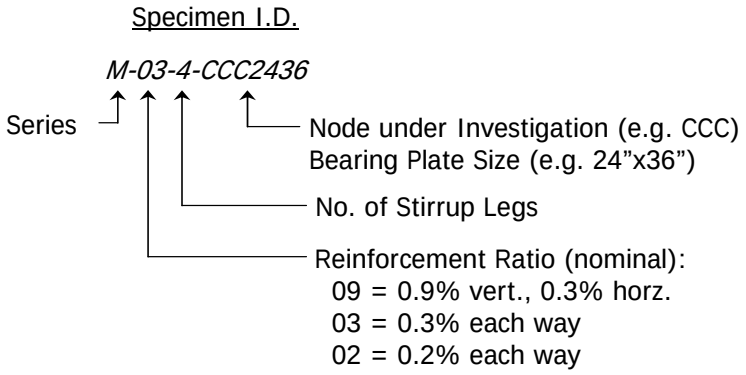

Figure 3.13: Series M - description of nomenclature used for Specimen I.D.

Geometric and reinforcement details for the Series M beams are presented in Figure 3.14.

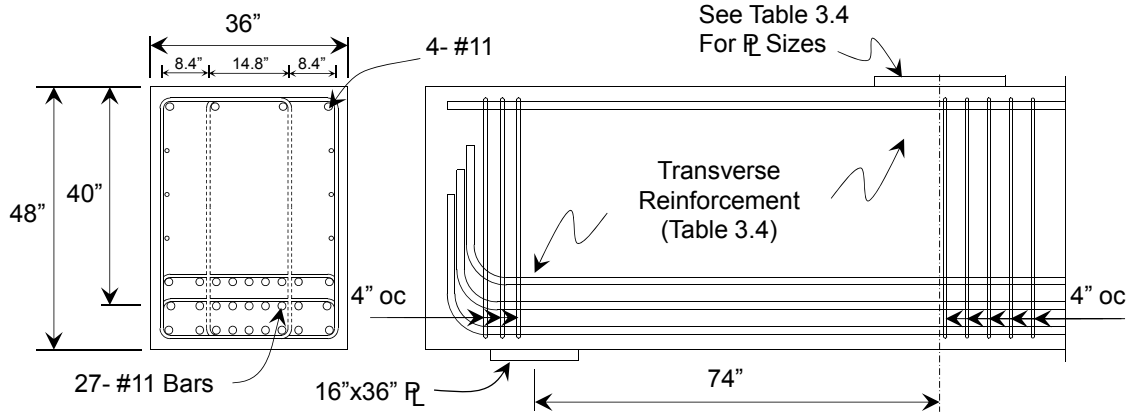

Figure 3.14: Series M beam details.

3.2.6 Summary of Test Specimen Details

Thirty-seven beam tests were conducted in the current experimental program. The deep beams tested represent some of the largest deep beam shear tests available in the literature. As seen in Figure 3.15, the specimens from the current study populate the upper bound of the deep beam data in the literature as measured by the shear area of the beam ($b_w d$). As previously noted, the objectives of the current study necessitated the testing of specimens of comparable

size to field members. A comparison between bent caps used in the State of Texas, the beams in the current study, and beams from previous research projects is provided in Figure 3.16.

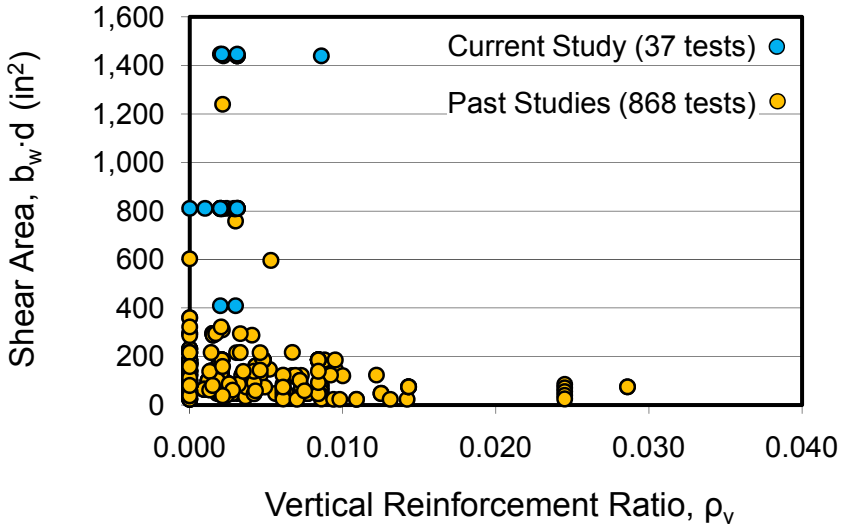

Figure 3.15: Comparison of beams sizes between current and past studies.

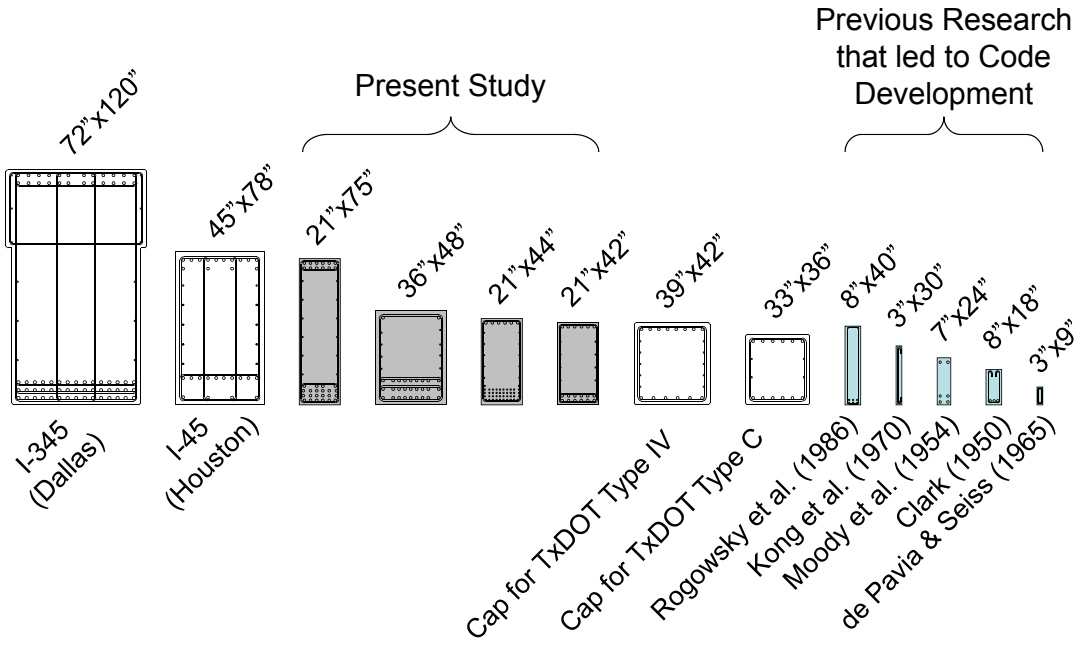

Figure 3.16: Scaled comparison of actual bent caps and beams included in current and past research programs.

A summary of the details for the 37 tests in the experimental program is presented in Table 3.2. The experimental results for the test specimens are provided and discussed in Chapter 4. The variables used in Table 3.2 are defined as follows:

b_w = beam width, in.
h = beam height, in.
d = distance form extreme compression fiber to centroid of tensile reinforcement, in.
ρ_l = ratio of longitudinal tensile reinforcement to effective area (A_s / b_wd)
ρ_l' = ratio of longitudinal compression reinforcement to effective area (A'_s / b_wd)
ρ_v = ratio of vertical web reinforcement to effective area (A_v / $b_w s_v$)
s_v = spacing of vertical web reinforcement, in.
ρ_h = ratio of horizontal web reinforcement to effective area (A_h / $b_w s_h$)
s_h = spacing of horizontal web reinforcement, in.
Load Plate = dimensions of the load bearing plate measured in the longitudinal and transverse direction of the beam (*l x w*), in.
Support Plate = dimensions of the support bearing plate measured in the longitudinal and transverse direction of the beam (*l x w*), in.
a/d ratio = shear span-to-depth ratio

Table 3.2: Summary of all beam details.

Beam I.D.	b_w in.	h in.	d in.	ρ_l	ρ_l'	ρ_v	Size and Spacing (s_v)	ρ_h	Size and Spacing (s_h)	Support Plate in.	Load Plate in.	a/d ratio
I-03-2	21	44	38.5	0.0229	0.0116	0.0029	#4 @ 6.5”	0.0033	#4 @ 5.75”	16x21	20x21	1.84
I-03-4	21	44	38.5	0.0229	0.0116	0.0030	#3 @ 7.0”	0.0033	#4 @ 5.75”	16x21	20x21	1.84
I-02-2	21	44	38.5	0.0229	0.0116	0.0020	#4 @ 9.5”	0.0020	#4 @ 9.5”	16x21	20x21	1.84
I-02-4	21	44	38.5	0.0229	0.0116	0.0021	#3 @ 10.0”	0.0020	#4 @ 9.5”	16x21	20x21	1.84
II-03-CCC2021	21	42	38.6	0.0231	0.0115	0.0031	#5 @ 9.5”	0.0045	#5 @ 6.6”	10x21	20x21	1.84
II-03-CCC1007	21	42	38.6	0.0231	0.0115	0.0031	#5 @ 9.5”	0.0045	#5 @ 6.6”	10x21	10x7	1.84
II-02-CCC1007	21	42	38.6	0.0231	0.0115	0.0020	#5 @ 15.0”	0.0019	#4 @ 10.1”	10x21	10x7	1.84
II-02-CCC1021	21	42	38.6	0.0231	0.0115	0.0020	#5 @ 15.0”	0.0019	#4 @ 10.1”	10x21	10x21	1.84
II-03-CCT1021	21	42	38.6	0.0231	0.0115	0.0031	#5 @ 9.5”	0.0045	#5 @ 6.6”	10x21	36x21	1.84
II-03-CCT0507	21	42	38.6	0.0231	0.0115	0.0031	#5 @ 9.5”	0.0045	#5 @ 6.6”	5x7	36x21	1.84
II-02-CCT0507	21	42	38.6	0.0231	0.0115	0.0020	#5 @ 15.0”	0.0019	#4 @ 10”	5x7	36x21	1.84
II-02-CCT0521	21	42	38.6	0.0231	0.0115	0.0020	#5 @ 15.0”	0.0019	#4 @ 10.1”	5x21	20x21	1.84
III-1.85-00	21	42	38.6	0.0231	0.0115	0.000	-	0.000	-	16x21	20x21	1.84
III-2.5-00	21	42	38.6	0.0231	0.0115	0.000	-	0.000	-	16x21	20x21	2.47
III-1.85-02	21	42	38.6	0.0231	0.0115	0.0020	#5 @ 14.5”	0.0019	#4 @ 10.1”	16x21	20x21	1.84
III-1.85-025	21	42	38.6	0.0231	0.0115	0.0024	#5 @ 12.0”	0.0014	#3 @ 7.6”	16x21	20x21	1.84
III-1.85-03	21	42	38.6	0.0231	0.0115	0.0029	#5 @ 10.0”	0.0029	#5 @ 10.1	16x21	20x21	1.84
III-1.85-01	21	42	38.6	0.0231	0.0115	0.0010	#4 @ 18.0”	0.0014	#3 @ 7.6”	16x21	20x21	1.84

Table 3.2 (cont.'d): Summary of all beam details

Beam I.D.	b_w in.	h in.	d in.	ρ_l	ρ_l'	ρ_v	Size and Spacing (s_v)	ρ_h	Size and Spacing (s_h)	Support Plate in.	Load Plate in.	a/d ratio
III-1.85-03b	21	42	38.6	0.0231	0.0115	0.0031	#4 @ 6.0"	0.0029	#5 @ 10.1"	16x21	20x21	1.84
III-1.85-02b	21	42	38.6	0.0231	0.0115	0.0020	#4 @ 9.5"	0.0019	#4 @ 10.1"	16x21	20x21	1.84
III-1.2-02	21	42	38.6	0.0231	0.0115	0.0020	#4 @ 9.5"	0.0019	#4 @ 10.1"	16x21	20x21	1.20
III-1.2-03	21	42	38.6	0.0231	0.0115	0.0031	#5 @ 9.5"	0.0029	#5 @ 10.1"	16x21	20x21	1.20
III-2.5-02	21	42	38.6	0.0231	0.0115	0.0020	#4 @ 9.5"	0.0019	#4 @ 10.1"	16x21	20x21	2.49
III-2.5-03	21	42	38.6	0.0231	0.0115	0.0031	#5 @ 9.5"	0.0029	#5 @ 10.1"	16x21	20x21	2.49
IV-2175-1.85-02	21	75	68.9	0.0237	0.0129	0.0021	#4 @ 9.5"	0.0019	#4 @ 10.1"	16x21	29x21	1.85
IV-2175-1.85-03	21	75	68.9	0.0237	0.0129	0.0031	#5 @ 9.5"	0.0029	#5 @ 10.1"	16x21	29x21	1.85
IV-2175-2.5-02	21	75	68.9	0.0237	0.0129	0.0021	#5 @ 14.25"	0.0021	#5 @ 14.25"	16x21	24x21	2.50
IV-2175-1.2-02	21	75	68.9	0.0237	0.0129	0.0021	#5 @ 14.25"	0.0021	#5 @ 14.25"	16x21	24x21	1.20
IV-2123-1.85-03	21	23	19.5	0.0232	0.0116	0.0030	#4 @ 6.25"	0.0030	#4 @ 6.25"	16x21	16.5x21	1.85
IV-2123-1.85-02	21	23	19.5	0.0232	0.0116	0.0020	#3 @ 5.25"	0.0017	#3 @ 6.25"	16x21	16.5x21	1.85
IV-2123-2.5-02	21	23	19.5	0.0232	0.0116	0.0020	#3 @ 5.25"	0.0017	#3 @ 6.25"	16x21	15.5x21	2.50
IV-2123-1.2-02	21	23	19.5	0.0232	0.0116	0.0020	#3 @ 5.25"	0.0017	#3 @ 6.25"	16x21	18x21	1.20
M-03-4-CCC2436	36	48	40	0.0293	0.0043	0.0031	#5 @ 11"	0.0027	#5 @ 6.5"	16x36	24x36	1.85
M-03-4-CCC0812	36	48	40	0.0293	0.0043	0.0031	#5 @ 11"	0.0027	#5 @ 6.5"	16x36	8x12	1.85
M-09-4-CCC2436	36	48	40	0.0293	0.0043	0.0086	#5 @ 4"	0.0027	#5 @ 6.5"	16x36	24x36	1.85
M-02-4-CCC2436	36	48	40	0.0293	0.0043	0.0022	#4 @ 10"	0.0022	#5 @ 8"	16x36	24x36	1.85
M-03-2-CCC2436	36	48	40	0.0293	0.0022	0.0031	#7 @ 11"	0.0027	#5 @ 6.5"	16x36	24x36	1.85

3.3 Testing Frame

A new test setup was designed and constructed in the Phil M. Ferguson Structural Engineering Laboratory to load the test specimens to failure. A key component of the new testing frame was a 96,000-pound steel platen or *strong floo*r. The strong floor was salvaged from a six-million pound capacity testing frame that had been decommissioned by the Navy and donated to the Ferguson Laboratory. Illustrations of the final test setup are presented in Figure 3.17 and Figure 3.18. The construction and installation of the strong floor is depicted in Figure 3.19. Also, a picture of the test setup immediately prior to a test is presented in Figure 3.19. For additional details on the design and construction of the testing frame, refer to Huizinga (2007).

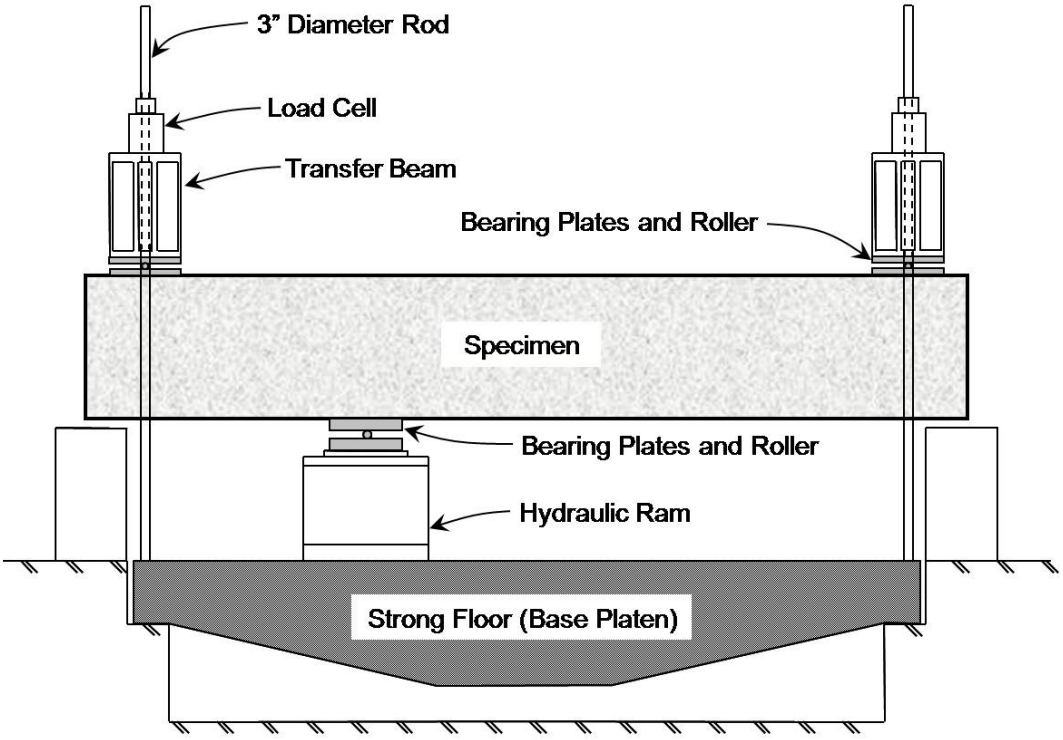

Figure 3.17: Elevation view of test setup

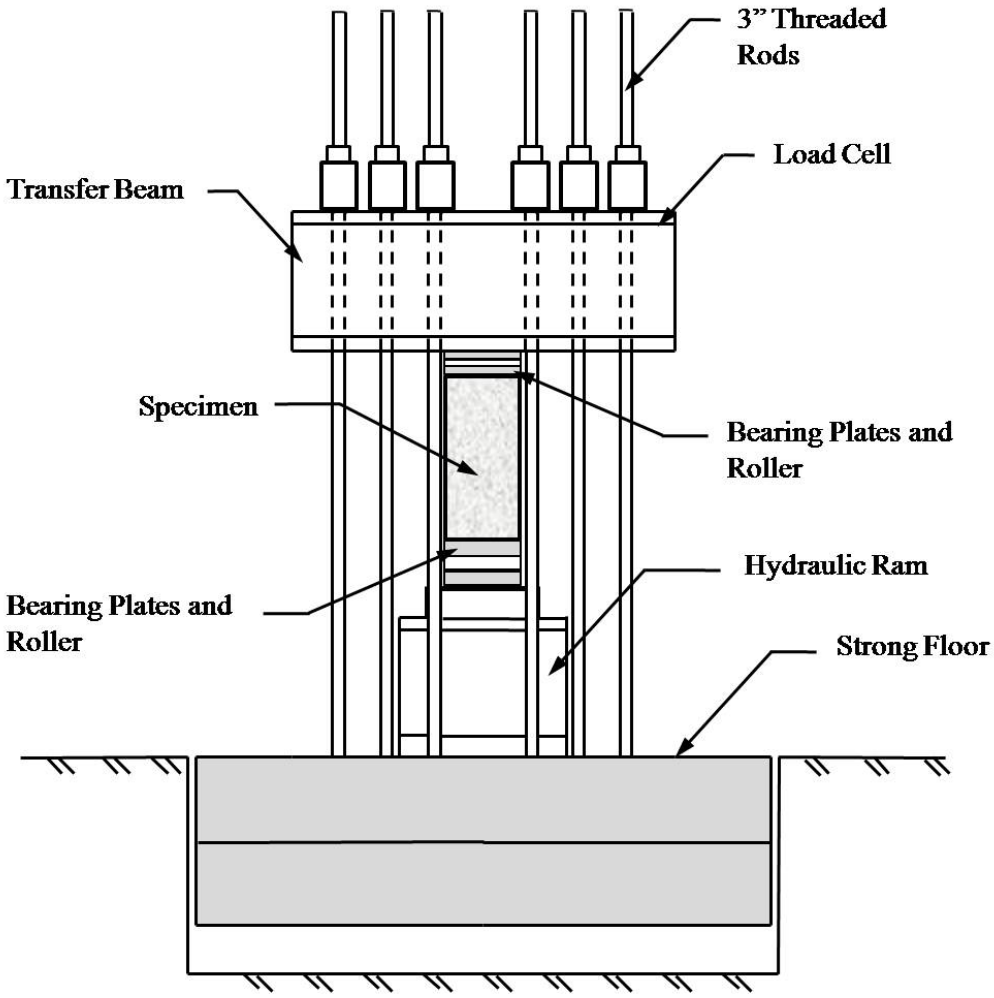

Figure 3.18: Section view of test setup

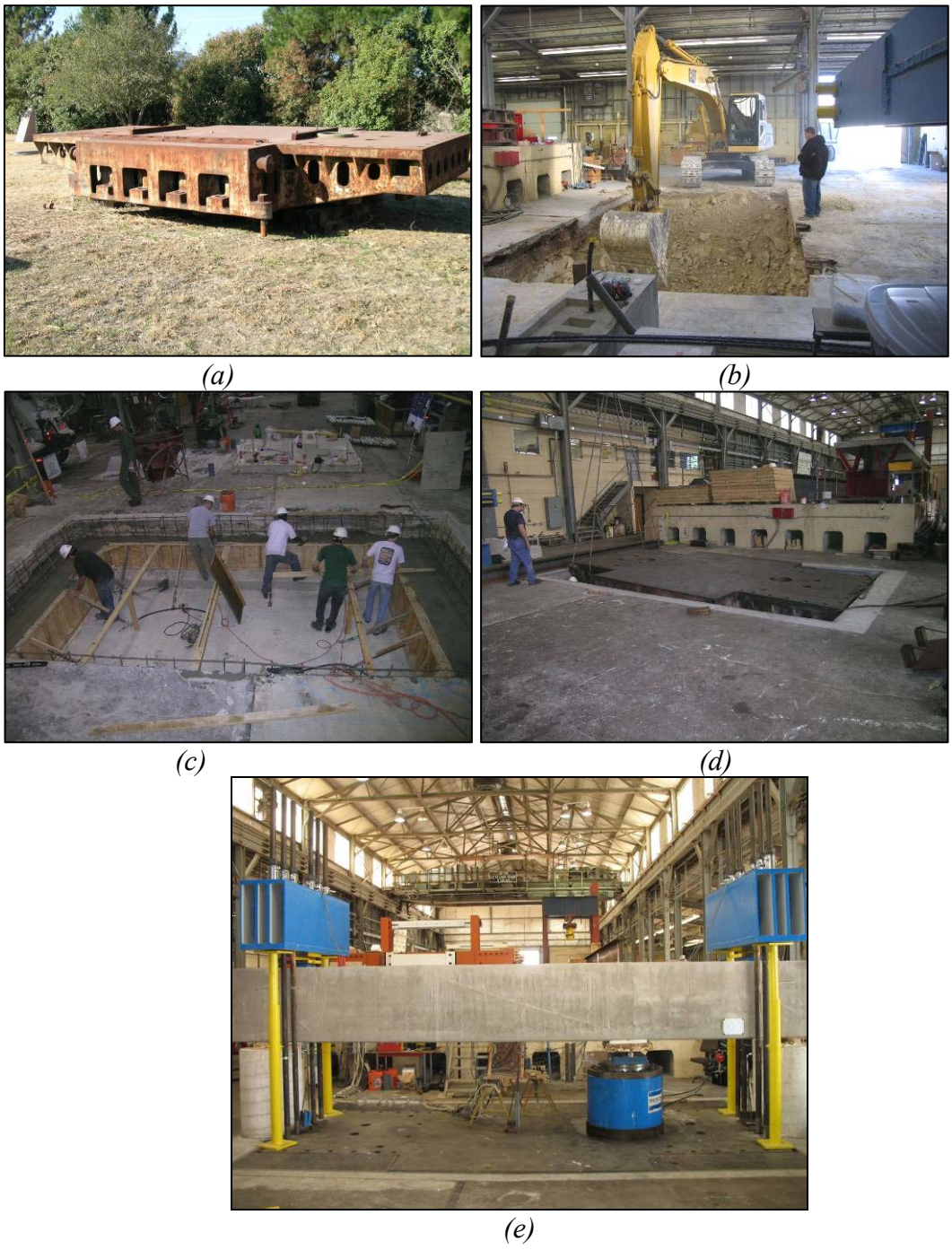

Figure 3.19: Installation of strong floor: (a) steel platen (b) floor excavation (c) fabrication of platen support (d) lowering of platen into position, and (e) test setup.

The test setup was designed for an upside-down simply-supported beam test. The load was applied via a 5 million pound capacity, double-acting hydraulic ram. At each support, 6 – 3-inch diameter, threaded rods resisted the applied load. In the current configuration, the test setup can resist a shear force of approximately 1.5 million pounds or an applied load at midspan of approximately 3 million pounds.

At each support, pin connections were created with two 2-inch steel plates sandwiching a two-inch diameter steel bar. The bar was welded to the bottom plate to simulate a pinned connection. Horizontal movement was permitted by the flexibility of the 6 threaded rods at each support. A thin layer of hydrostone was applied to the top surface of the test specimens at the location of the support plates to provide a planar reaction surface. At the applied load, rotation was permitted with a 3-inch diameter steel bar. The bar was allowed to roll freely between two four-inch thick steel plates. A smaller ½-inch thick steel plate was placed on top of the upper 4-inch plate to obtain the desired size of the load plate. Hydrostone was also placed between this plate and the bottom surface of the test specimen to obtain a planar bearing surface.

3.4 Fabrication of Specimens

Specimens were constructed using conventional materials. The use of steel formwork accelerated the fabrication process and provided dimensional accuracy. In general, the assembly of the reinforcement cage, installation of strain gauges, placement of concrete, and removal of formwork took about two weeks to complete per specimen. Beams were tested at a minimum of 28-days after concrete placement.

3.4.1 Steel Reinforcement

Steel reinforcement (rebar) was domestic Grade 60 deformed bars meeting the requirements of ASTM A615. Cross sectional dimensions of the bars complied with the nominal sizes given in ASTM A615.

Each rebar order delivered to the Ferguson Laboratory was accompanied with a set of four coupons of each bar size. The tensile strength of the coupons was measured in accordance with ASTM A370. At least three of the coupons were tested for each bar size. The tensile strength of the longitudinal and web reinforcement for Series I, II, III, IV and M test specimens are provided in Table 4.1.

3.4.2 Concrete Mixture Design

Typically, TxDOT engineers specify the compressive strength of concrete used for a bent cap to be between 3600 and 5000-psi. As a result, the specified compressive strength of concrete used for the experimental program was designed to be within the same range. The actual measured compressive strength of concrete ranged between 3120 and 5330-psi. Concurrent with the placement of concrete for each beam, standard 4”x8” cylinders were prepared in accordance with ASTM C31 and tested in accordance with ASTM C39. Proportions of the concrete mixture are presented in Table 3.3.

Table 3.3: Concrete mixture proportions

Material	Quantity
Type I Portland Cement	300 to 317 lb/cy
Fly Ash	79 to 83 lb/cy
CA: ¾" River Rock	1800 to 1850 lb/cy
FA: Sand	1370 to 1515 lb/cy
Water	29 to 31 gallons/cy
HRWR* Admixture	15 to 20 oz/cy
Set Retardant Admixture	6 oz/cy
Water/Cement Ratio	0.62 to 0.68
Slump	4 to 8 inches

**HRWR:* High Range Water Reducing (i.e. *Superplasticizer*)

3.4.3 Construction of Specimens

The reinforcing steel was supplied by a local steel manufacturer. All of the steel was delivered in the specified lengths and with the appropriate bends. The reinforcement cages were assembled in the laboratory and upon completion, were moved to the casting area. The specimens were cast in the same orientation as they were tested. Since the beams were loaded from beneath, the primary tension steel was located at the top of the section.

The concrete used to fabricate the specimens was provided from a local ready-mix supplier. Upon the arrival of concrete at the Ferguson Laboratory, a slump test was conducted according to ASTM C143. If necessary, additional water was added to increase the slump to approximately 6 ± 2-inches. In all cases where water was added, the additional amount did not exceed the amount of water that was held back at the batch plant (as indicated on the batch tickets). Twelve to twenty 4-inch diameter cylinders were prepared in accordance with ASTM C31. The cylinders were covered with a plastic sheet and cured under the same ambient conditions as the beam specimens.

For the 21"x75" and the 36"x48" specimens, two ready-mix trucks were required to supply enough concrete to cast each of the specimens. Each truck was filled with the same mixture design from the same batch plant. In every case, the second truck was scheduled to arrive approximately 30-minutes after the first truck. This schedule kept the idling time for the second truck at a minimum and eliminated the presence of a cold joint. Standard 4-inch diameter cylinders were prepared from the concrete in each truck. The concrete strength from one truck was generally within 20-percent of the concrete strength of the other. The compressive strength values reported for these large specimens were the weighted average of the results of three cylinders from each truck on the day of the test.

All specimens were fabricated relatively quickly and with accurate dimensional tolerances due to the use of steel formwork. External pneumatic vibrators attached to a bracket that moved along the length of the formwork and internal rod vibrators, or stingers, placed in the concrete from the top were used to help consolidate the concrete. After the placement of concrete, the beams were covered with a plastic sheet and cured under the ambient laboratory

conditions. An illustration of the fabrication procedure from assembly of reinforcing cages to removal of formwork for a 21”x42” specimen is presented in Figure 3.20.

Figure 3.20: Fabrication of a typical beam: (a) assembly of reinforcement cage (b) placement of cage in formwork (c) forms in place prior to concrete placement (d) placement of concrete (e) beam curing (f) test specimen after the removal of forms.

The fabrication of the 21”x23” and the 21”x75” specimens was carried out in a similar fashion to that of the standard 21”x42” specimens. The steel cages were tied in the laboratory and lifted with a spreader beam and crane to the casting area. For the 23-inch deep specimens, smaller 24-inch tall steel side forms were used to cast the beams. For the 75-inch specimens, the

24-inch side walls were bolted to the top of the original 52-inch tall side forms with 33 – 5/8-inch diameter bolts. A couple of pictures illustrating the fabrication of a 21"x75" specimen are provided in Figure 3.21.

(a)

(b)

Figure 3.21: Fabrication of a 21"x75" beam: (a) movement of reinforcement cage into formwork (b) placement of concrete into steel formwork

The fabrication of the 36"x48" specimens was accomplished with wooden formwork. Numerous crossties and wooden kickers were used to provide lateral stability to the formwork. Only internal rod vibrators were used to aid in the consolidation of the concrete. For this reason, a clear cover of 2-inches was provided for these specimens. A couple of pictures illustrating the fabrication of a 36"x48" specimen are provided in Figure 3.22.

(a)

(b)

Figure 3.22: Fabrication of a 36"x48" beam: (a) tied reinforcement cage (b) placement of concrete into wooden formwork

After casting, all of the specimens were moved into the test setup with an overhead crane. Two-inch diameter steel bars were inserted into PVC sleeves that were cast in the specimen. Large steel cables were looped around the steel bars immediately adjacent to the side of the specimen to prevent bending of the bars. The specimen was then lifted and placed in the test setup with an overhead, 25-ton capacity crane.

3.5 Instrumentation

Several different instruments were used to obtain data during the tests in the experimental program. The instruments included steel and concrete electrical strain gauges, linear potentiometers, load cells, and crack comparator cards. Details regarding each of these devices are provided in this section.

3.5.1 Strain Measurements: Reinforcing Bars

Strain gauges were affixed to the transverse and longitudinal reinforcement in order to measure the change in strain. The gauge type was *FLA-3-11-5LT* manufactured by Tokyo Sokki Kenkyujo Co. These gauges are intended for general purpose mild steel applications. The width and length of the gauges were 1.5- and 3-mm, respectively, with a resistance of 120-ohms (± 0.5) (Figure 3.23). The surface of the reinforcement was lightly sanded and polished to provide a relatively smooth surface for the application of the strain gauges. Care was taken not to significantly reduce the cross section of the reinforcement. The gauges were glued to the reinforcement, sealed with acrylic, protected with a neoprene pad, and taped to further isolate them from the water in the concrete.

Figure 3.23: Installation of strain gauge for measuring steel strains.

Typical locations of internal strain gauges for the Series I through IV specimens are illustrated in Figure 3.24. Only one test region is shown in each of the sketches in Figure 3.24. The 36”x48” Series M beams had internal gauges in a similar arrangement to the Series II specimens.

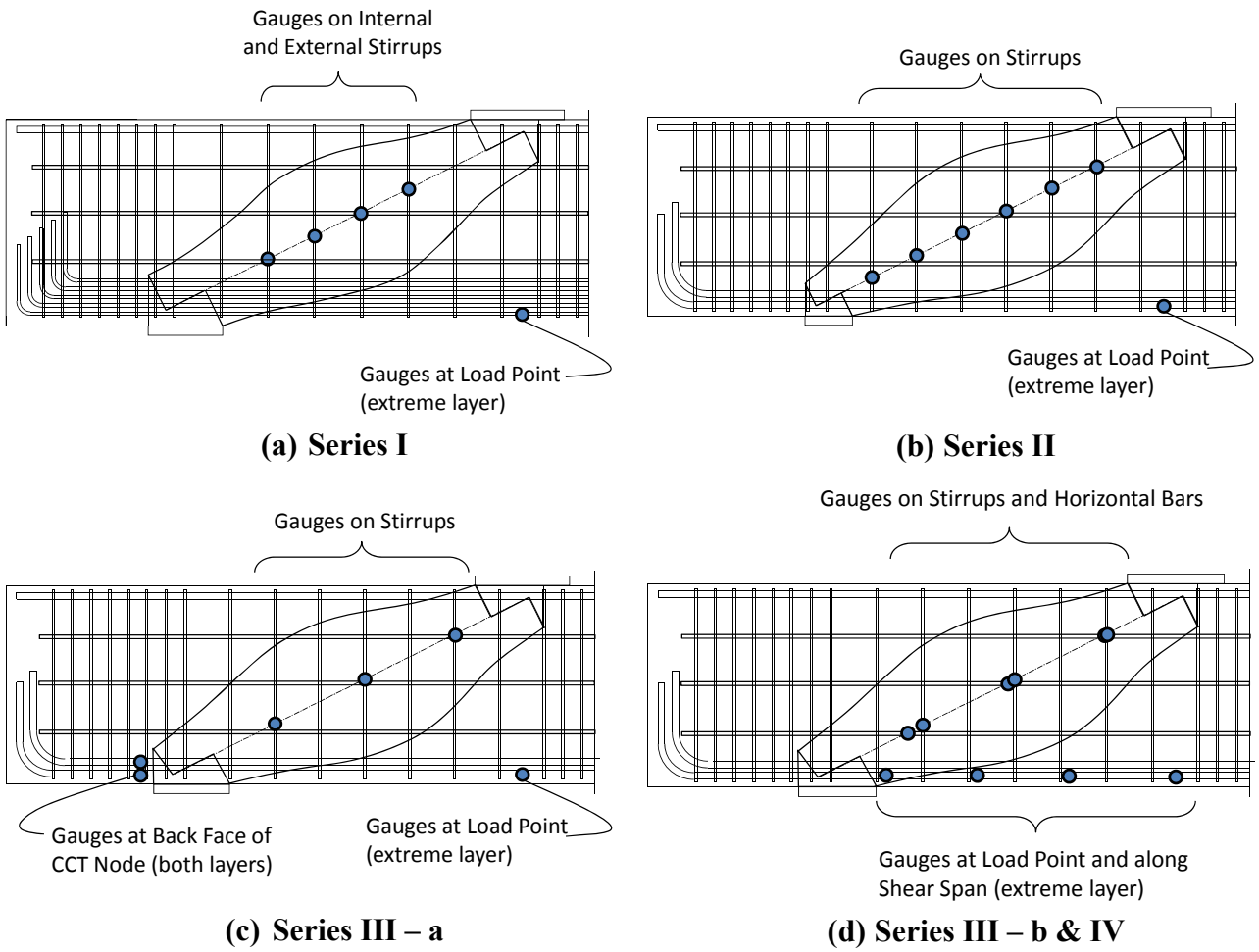

Figure 3.24: Typical internal strain gauge locations for each series

Strain gauges were attached to the stirrups along the assumed centerline of the inclined strut in all of the test specimens (Figure 3.24). The purpose of locating a gauge along the strut centerline was to measure steel strains at or close to the primary diagonal splitting crack. Four stirrups were instrumented within the test regions of the Series I beams (Figure 3.24(a)). In each of these locations, both external and internal stirrups legs were instrumented. None of the Series II, III, or IV beams contained internal stirrups. For those beams, both legs of each external stirrup shown in Figure 3.24 were instrumented. In addition, for most of the Series III and all of the Series IV specimens, the horizontal reinforcement was instrumented at the intersection with the assumed diagonal strut. An example of this arrangement is provided in Figure 3.24 (d).

The strain in the primary tension reinforcement was also monitored in each specimen. For the Series I through IV specimens, the longitudinal strain was measured in at least three of the bars in the outermost layer at the location of the applied load (Figure 3.24). The purpose of providing gauges at this location was to monitor the maximum strain in the reinforcement as the beam was loaded to failure.

Additional strain gauges were attached to the longitudinal reinforcement in the Series III and IV specimens. In most of the Series III specimens and in all of the Series IV specimens, strain gauges were applied to the longitudinal bars along the test region (Figure 3.24 (d)). The

purpose of these gauges was to monitor the strain in the primary tension tie throughout the shear span. Other researchers have monitored this strain to compare the behavior of the test specimen to an assumed strut-and-tie model (Rogowsky et al., 1986, Quintero-Febres et al., 2006, and Tan et al., 2007). In a single-panel strut-and-tie model, the force in the primary tension tie is constant throughout the shear span. Therefore, the data from this instrumentation in the Series III and IV beams was used to assess the applicability of a single-panel STM for several a/d ratios and specimen sizes.

In specimens III-1.85-02 and III-1.85-025, all twelve longitudinal bars were instrumented at the back face of the CCT node (Figure 3.24 (c)). The purpose of measuring the strain at the back face of the CCT node was to examine the accuracy and conservatism of the modeling assumptions typically made to determine the back face dimension. The depth of the back face of a CCT node is commonly assumed to be equal to twice the distance from the exterior of the beam to the centroid of the tension reinforcement (Section 2.3). Often times, the distance is quite small; resulting in a small area to resist the applied force assumed from a STM. By measuring the internal straining of the bars, the amount of stress applied to the back face of the CCT node could be quantified. Similar strain measurements were taken from strain gauges applied to the surface of the concrete (Section 3.5.2).

3.5.2 Strain Measurements: Concrete Surface

Strain gauges were affixed to the surface of the beam as well. The gauge type was *PL-60-11-5LT* manufactured by Tokyo Sokki Kenkyujo Co. These gauges are intended for general purpose concrete surface applications. The gauges have a width of 8-mm, a length of 60-mm and a resistance of 120-ohms (± 0.5) (Figure 3.25). The surface of the concrete was lightly sanded to remove the outer paste and expose any minor voids. Then, a thin coat of epoxy was applied to the cleaned surface. Care was taken to apply the epoxy as smooth as possible. After approximately 24-hours, the epoxy was sanded and cleaned with acid and base solutions provided by the manufacturer of the strain gauges. The gauges were then glued into place.

Figure 3.25: Installation of a concrete surface gauge for measuring concrete strains.

The back face of CCT nodes were instrumented with concrete surface strain gauges for all of the Series I specimens and the following specimens within Series II and III: II-03-CCT1021 and II-03-CCT0507; III-1.85-00, III-1.85-02, and III-1.85-025. The location of these concrete gauges is illustrated in Figure 3.26.

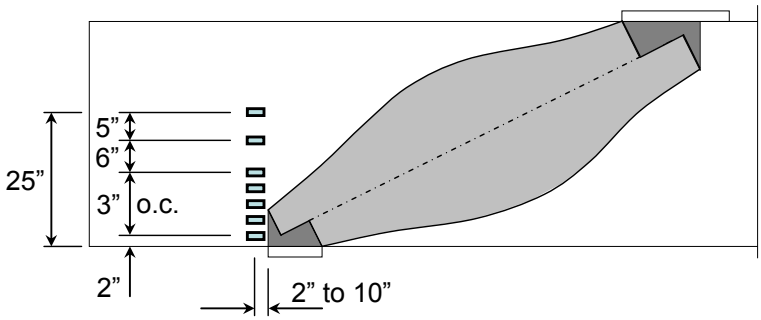

Figure 3.26: Concrete strain gauge locations

The purpose of measuring external strains was to verify the modeling assumption used to proportion the back face of a CCT node. By measuring the strain of the concrete, the accuracy and conservatism of hydrostatic and non-hydrostatic node geometry assumptions could be examined. The strain gauges affixed to the reinforcement at the CCT back face (Section 3.5.1) were located in the same plane as the surface gauges in order to compare the values from the two locations.

3.5.3 Load and Displacement Measurements

500-kip capacity load cells were placed between the transfer beam and the reaction nuts at all twelve rod locations, six at each support (Figure 3.27). Therefore, it was possible to directly measure the reaction at each support. The position of the load cells on top of the transfer beam is illustrated in Figure 3.27.

Figure 3.27: Load cells measure the reaction in each rod.

Four 6-inch linear potentiometers were used to measure the displacement of a beam during testing. Linear potentiometers were located at the supports, load point, and centerline of

the beam. The locations of the linear potentiometers are shown in Figure 3.28. A photograph of the linear potentiometer used to measure the load plate displacement is presented in Figure 3.29.

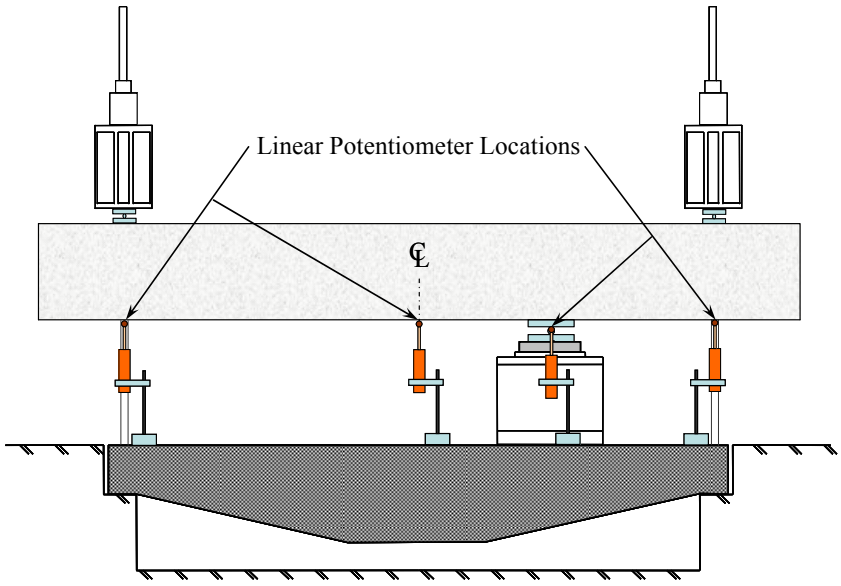

Figure 3.28: Linear potentiometer locations.

Figure 3.29: Linear potentiometer used to measure the displacement at the load point.

The purpose of the linear potentiometers was to measure the deflections of the beam throughout the test. The test specimens underwent rigid body motion as they were lifted off of their supports at the start of the test and as the 3-inch diameter support rods elongated. The displacement measured at the supports was used to subtract the rigid body motion from the beam deformations. An illustration of the rigid body motion and beam deformation early in the test is presented in Figure 3.30. An illustration of the rigid body motion and beam deformation after both transfer girders engaged the reaction nuts is presented in Figure 3.31. It is important to note that the shear in the test region was accurately measured throughout this loading history due to

the location of the load cells on each support rod. The beam displacement at the location of the load throughout the test, Δ_{BEAM}, was determined according to Equation 3-1.

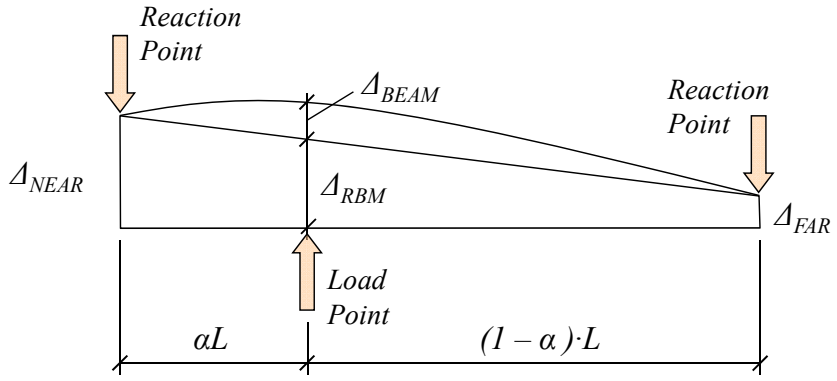

Figure 3.30: Diagram of beam displacements due to rigid body motion and flexural and shear deformations early in the test

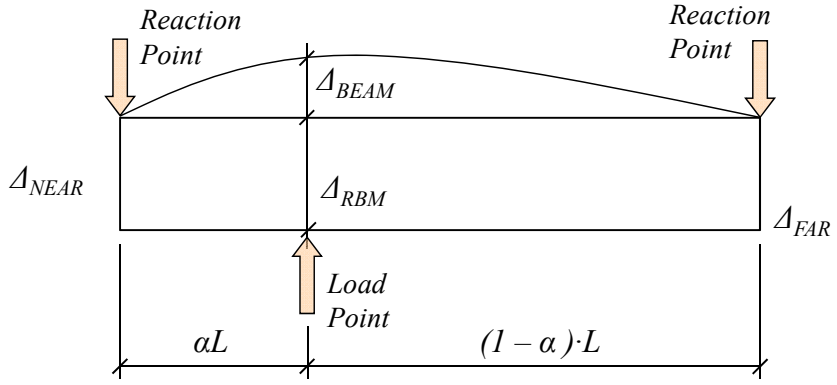

Figure 3.31: Diagram of beam displacements due to rigid body motion and flexural and shear deformations after all reaction nuts are engaged

$$\Delta_{RBM} = \Delta_{FAR} + (1-\alpha)\cdot(\Delta_{NEAR} - \Delta_{FAR}) \tag{3.1}$$
$$\Delta_{BEAM} = \Delta_{LOAD} - \Delta_{RBM}$$

Where,

Δ_{RBM} = Displacement due to rigid body motion
Δ_{NEAR} = Recorded displacement at near reaction point
Δ_{FAR} = Recorded displacement at far reaction point
Δ_{LOAD} = Recorded displacement at load point
Δ_{BEAM} = Displacement due to flexural and shear deformations

3.5.4 Crack Width Measurements

Diagonal crack width measurements were collected for the test specimens as part of the experimental program. At each load increment, the maximum width of any diagonal crack was

recorded on each face of the shear span under investigation. The measurements were obtained by graduate students with the use of a crack comparator card (Figure 3.32). The measurements from the two students were averaged producing diagonal crack width data at each load increment for each face of the test specimen. No distinction was made between flexure-shear cracks or web-shear cracks. As long as the crack formed a significant angle with respect to the vertical, it was considered a diagonal crack. In general, the maximum width of a diagonal crack was near the midheight of the member. A picture illustrating the crack width measurement for a 21"x75" test specimen is shown in Figure 3.32. Due to the size of these specimens, scaffolding was needed to access the specimen.

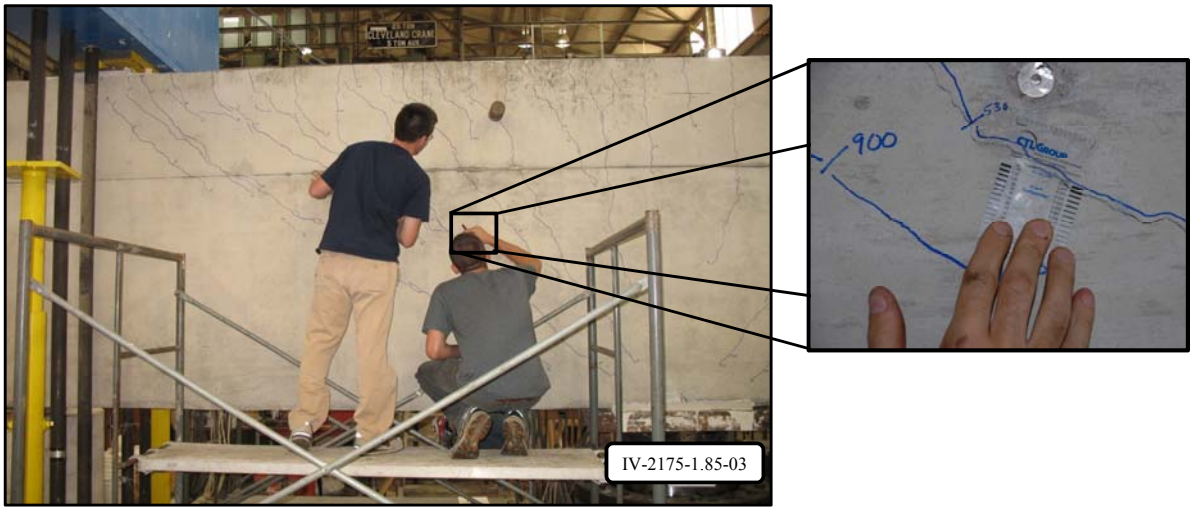

Figure 3.32: Example of crack width measurement technique

3.6 Test Procedure

Beams were loaded monotonically in 50 to 150-kip increments depending on the size of the specimen. Generally, the amount of load in each increment was taken as 10-percent of the expected ultimate capacity. After each load increment, cracks were marked and the width of the widest diagonal shear crack on each face of the beam was recorded by two graduate students. Photographs were taken after each load increment, and the entire test was recorded with a video camera.

Two tests were conducted on each beam. First, the beam was loaded near one support corresponding to the appropriate a/d ratio. The behavior of the specimen was monitored until a shear failure was reached in the test region. Then, external post-tensioned clamps were installed to strengthen the previously sheared portion of the beam. The hydraulic actuator was moved to the opposite end of the beam and positioned based on the appropriate a/d ratio. The beam was loaded again, and the behavior of the second test region was monitored. An illustration of the process of testing one side of a beam, securing the failure zone with clamps, and testing the other side is presented in Figure 3.33.

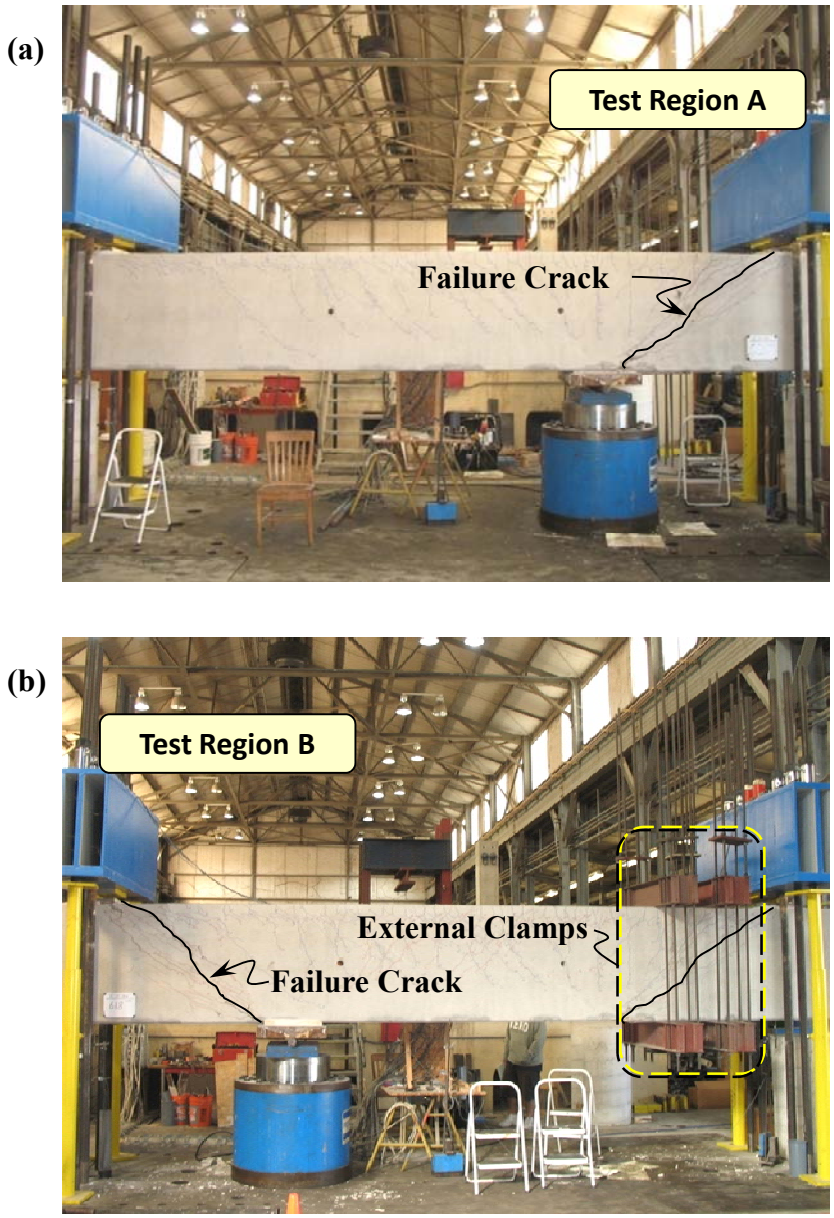

Figure 3.33: Each end of a beam is loaded to failure resulting in two tests: (a) shear failure in Test Region A (b) and shear failure in Test Region B with external post-tensioned clamps in Test Region A

During the first test of each 42-inch specimen, the low-shear span was subjected to shear up to 40-percent of its ultimate capacity. Under this amount of load and corresponding moment, the specimen generally cracked. Therefore, the second test of each 42-inch beam was conducted on a *pre-cracked* shear span. As a result, the load at first diagonal cracking was only obtained for the first test of each 42-inch specimen. For the 23-inch specimens, the region for the second test remained uncracked during the first test due to the low level of shear and moment in the region of the second test. For the two 75-inch specimens, the size of the specimen was chosen such that the resulting a/d ratios on each side of the beam matched the appropriate a/d ratios of the experimental program. Therefore, two tests were conducted simultaneously for these two

specimens. Both sides of the beam were monitored during the start of the test. After one side of the beam failed, the applied load was removed and external post-tensioned clamps were attached to the failed shear span as before. Then, the load was reapplied at the same location until the other side of the beam failed. In both cases, the external clamps provided enough additional shear strength to obtain a shear failure in the opposite span. Pictures illustrating the test sequence procedure for IV-2175-2.5-02 and IV-2175-1.2-02 are provided in Figure 3.34.

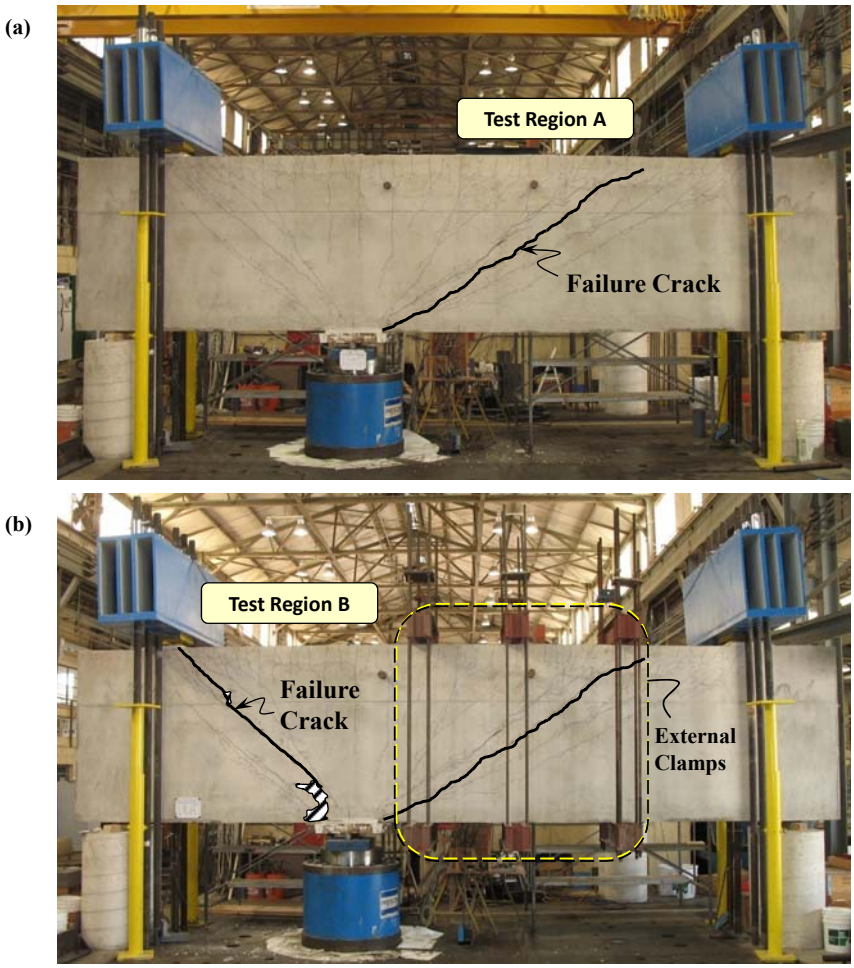

Figure 3.34: Hydraulic ram was not moved for 75-inch specimens: (a) shear failure in Test Region A (b) shear failure in Test Region B with external post-tensioned clamps in Test Region A

Nineteen (19) beams were tested in the aforementioned manners, i.e. two tests on each beam. One test on a 36"x48" specimen was a pilot test in which the size of the load plate was changed twice prior to reaching failure in the specimen. The results of this test are not included in this report since the bearing plate dimensions were not constant in the test. As such, 37 valid tests were conducted in the experimental program.

The photographs of the test regions in this report are generally flipped so that the shear region is viewed in a conventional manner; i.e. with the tension steel at the bottom of the beams, and the load applied from the top. A typical figure and corresponding photograph location are presented in Figure *3.35*.

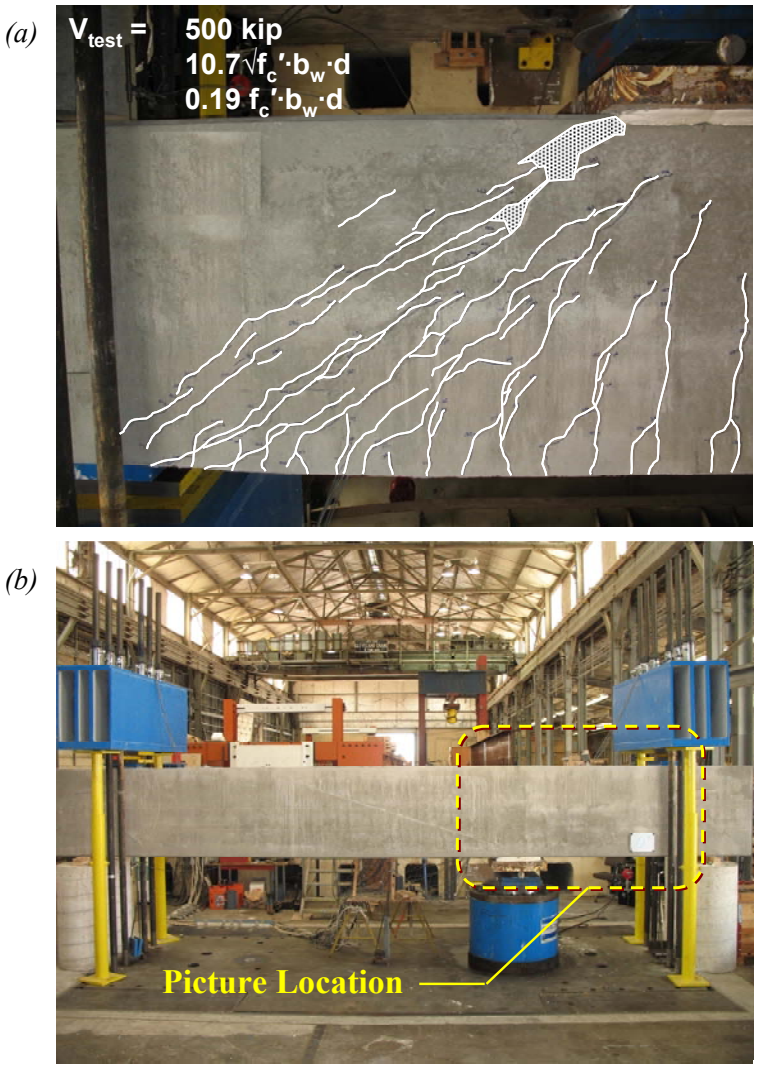

Figure 3.35: (a) Photographs are orientated upside-down in order to present test results in conventional manner; (b) actual picture location.

3.7 Summary

In this chapter, the details of the experimental program were provided. The experimental program was designed to address several objectives in the current project. Specifically, the test specimens were designed to evaluate the effect of (1) the distribution of stirrups across the beam web, (2) triaxially-confined nodal regions, (3) minimum web reinforcement, and (4) member depth on the strength and serviceability performance of reinforced concrete deep beams. Due to the nature of these objectives, specimens of comparable size to field members were designed and tested. Thirty-seven tests were conducted in all on beams with the following cross-sections: 21”x23”, 21”x42”, 21”x44”, 21”x75”, and 36”x48”. The sizes of the test specimens were shown to be among the largest deep beams available in the literature.

In addition, the details of the testing procedure were provided in this chapter. Two tests were conducted on each beam with the aid of external post-tensioned clamps. During each test, several instruments were monitored. They included 500-kip capacity load cells on each support

rod, numerous electrical strain gauges on the rebar and on the concrete surface, and linear potentiometers measuring the deflection of the beam. Also, the maximum width of diagonal cracks was recorded during each load increment on both sides of the test region.

The test results for the experimental program are presented in Chapter 4. Based on the data obtained from the experimental program and from the evaluation database, the results from additional objectives of the current project are presented in Chapter 5.

Chapter 4. Experimental Results

4.1 Overview

In this chapter, the experimental results of the testing program are presented in detail. Specifically, the following four tasks are addressed.

- Distribution of stirrups across the web (Section 4.3)
- Triaxially confined nodal zones (Section 4.4)
- Minimum web reinforcement (Section 4.5)
- Effect of member depth (Section 4.6)

Prior to the discussion of these individual tasks, a summary of the experimental results for all of the test specimens is provided for quick reference. In addition, important information regarding the evaluation of the strength and serviceability data is given to aid the reader.

4.2 Summary of Experimental Results

The experimental results for the 37 tests conducted in the experimental program are presented in Table 4.1. Other important details of the test specimens were provided previously in Table 3.2. The variables used in Table 4.1 are defined as follows:

b_w = beam width, in.

d = distance from extreme compression fiber to centroid of tensile reinforcement, in.

f_c' = compressive strength of concrete at the time of testing measured in accordance with ASTM C39 (Section 3.4.2), psi.

f_{yl} = yield strength of longitudinal reinforcement measured in accordance with ASTM A370 (Section 3.4.1), ksi.

f_{yv} = yield strength of vertical web reinforcement measured in accordance with ASTM A370 (Section 3.4.1), ksi.

f_{yh} = yield strength of horizontal web reinforcement measured in accordance with ASTM A370 (Section 3.4.1), ksi.

a/d ratio = shear span-to-depth ratio

V_{crack} = shear carried in the test region when the first diagonal crack formed, kip
Specific details regarding the determination of the diagonal cracking load are presented in Section 4.2.2

V_{test} = maximum shear carried in test region, including the estimated self weight of the specimen and transfer girders, kip
Specific details regarding the determination of the applied shear force are presented in Section 4.2.1

Table 4.1: Summary of experimental results.

Beam I.D.	b_w in.	**d** in.	f_c' psi	f_{yl} ksi	f_{yv} ksi	f_{yh} ksi	**a/d ratio**	V_{crack} kip	$\frac{V_{crack}}{\sqrt{f_c'} \cdot b_w d}$	V_{crack} / V_{test}	V_{test} kip	$\frac{V_{test}}{f_c' \cdot b_w d}$	$\frac{V_{test}}{\sqrt{f_c'} \cdot b_w d}$
I-03-2	21	38.5	5240	73	67	67	1.84	144	2.5	0.25	569	0.13	9.7
I-03-4	21	38.5	5330	73	73	67	1.84	-	-	-	657	0.15	11.1
I-02-2	21	38.5	3950	73	67	67	1.84	121	2.4	0.27	454	0.14	8.9
I-02-4	21	38.5	4160	73	73	67	1.84	-	-	-	528	0.16	10.1
II-03-CCC2021	21	38.6	3290	64	65	65	1.84	139	3.0	0.28	500	0.19	10.7
II-03-CCC1007	21	38.6	3480	64	65	65	1.84	-	-	-	478	0.17	10.0
II-02-CCC1007	21	38.6	3140	69	64	63	1.84	-	-	-	335	0.13	7.4
II-02-CCC1021	21	38.6	4620	69	67	62	1.84	132	2.4	0.40	329	0.09	6.0
II-03-CCT1021	21	38.6	4410	66	71	71	1.84	-	-	-	636	0.18	12.1
II-03-CCT0507	21	38.6	4210	66	71	71	1.84	146	2.7	0.24	598	0.18	11.1
II-02-CCT0507	21	38.6	3120	69	64	63	1.84	94	2.1	0.23	401	0.16	8.9
II-02-CCT0521	21	38.6	4740	69	67	62	1.84	-	-	-	568	0.15	10.2
III-1.85-00	21	38.6	3170	66	-	-	1.84	98	2.1	0.27	365	0.14	8.0
III-2.5-00	21	38.6	3200	66	-	-	2.47	-	-	-	82	0.03	1.8
III-1.85-02	21	38.6	4100	69	64	62	1.84	112	2.2	0.23	488	0.15	9.4
III-1.85-025	21	38.6	4100	69	64	73	1.84	-	-	-	516	0.16	9.9
III-1.85-03	21	38.6	4990	69	64	63	1.84	137	2.4	0.33	412	0.10	7.2
III-1.85-01	21	38.6	5010	69	63	73	1.84	-	-	-	273	0.07	4.8

Table 4.1 (cont.'d): Summary of experimental results.

Beam I.D.	b_w in.	d in.	f'_c psi	f_{yl} ksi	f_{yv} ksi	f_{yh} ksi	a/d ratio	V_{crack} kip	$\frac{V_{crack}}{\sqrt{f_c'} \cdot b_w d}$	$\frac{V_{crack}}{V_{test}}$	V_{test} kip	$\frac{V_{test}}{f_c' \cdot b_w d}$	$\frac{V_{test}}{\sqrt{f_c'} \cdot b_w d}$
III-1.85-03b	21	38.6	3300	69	62	67	1.84	114	2.4	0.24	471	0.18	10.1
III-1.85-02b	21	38.6	3300	69	62	62	1.84	-	-	-	468	0.17	10.1
III-1.2-02	21	38.6	4100	66	60	60	1.20	165	3.2	0.20	846	0.25	16.3
III-1.2-03	21	38.6	4220	66	68	68	1.20	-	-	-	829	0.24	15.7
III-2.5-02	21	38.6	4630	66	62	62	2.49	105	1.9	0.35	298	0.08	5.4
III-2.5-03	21	38.6	5030	66	65	65	2.49	-	-	-	516	0.13	9.0
IV-2175-1.85-02	21	68.9	4930	68	66	66	1.85	216	2.1	0.28	763	0.11	7.5
IV-2175-1.85-03	21	68.9	4930	68	66	66	1.85	218	2.1	0.26	842	0.12	8.3
IV-2175-2.5-02	21	68.9	5010	68	64	64	2.50	144	1.4	0.28	510	0.07	5.0
IV-2175-1.2-02	21	68.9	5010	68	64	64	1.20	262	2.6	0.21	1223	0.17	11.9
IV-2123-1.85-03	21	19.5	4160	66	66	66	1.85	60	2.3	0.18	329	0.19	12.5
IV-2123-1.85-02	21	19.5	4220	66	81	81	1.85	65	2.4	0.19	347	0.20	13.0
IV-2123-2.5-02	21	19.5	4570	65	58	64	2.50	51	1.8	0.32	161	0.09	5.8
IV-2123-1.2-02	21	19.5	4630	65	58	64	1.20	124	4.5	0.21	592(f)	0.31	21.2
M-03-4-CCC2436	36	40	4100	67	61	61	1.85	354	3.8	0.31	1128	0.19	12.2
M-03-4-CCC0812	36	40	3000	65	63	63	1.85	-	-	-	930	0.22	11.8
M-09-4-CCC2436	36	40	4100	67	61	61	1.85	-	-	-	1415(f)	0.24	15.3
M-02-4-CCC2436	36	40	2800	65	63	63	1.85	256	3.4	0.23	1102	0.27	14.5
M-03-2-CCC2436	36	40	4900	68	62	62	1.85	-	-	-	1096(i)	0.16	10.9

(f) *Maximum shear carried in specimen upon the occurrence of concrete crushing at the compression face.*

(i) *Test was stopped due to initiation of yielding of the tensile reinforcement and crushing of concrete at the compression face.*

4.2.1 Evaluation of Strength Data

The shear strength of the test specimens, V_{test} in Table 4.1, was the shear at the critical section at the maximum applied load. The critical section was defined as the point halfway between the support and the applied load in the test region of interest. At this location, a portion of the beam weight and the weight of one transfer girder was added to the load cell readings from the near support to obtain the appropriate shear. The location of and the calculations for V_{test} are provided in Figure 4.1. In Figure 4.1, R_A and R_B denoted the reactions measured by the load cells. P_{TR} represents the weight of each blue transfer girder (7.8-kips), and P_D represents the weight of the test specimen. For the 23-inch specimens, a spacer was provided between the transfer girder and the spacing that effectively increased P_{TR} from 7.8-kips to 8-kips.

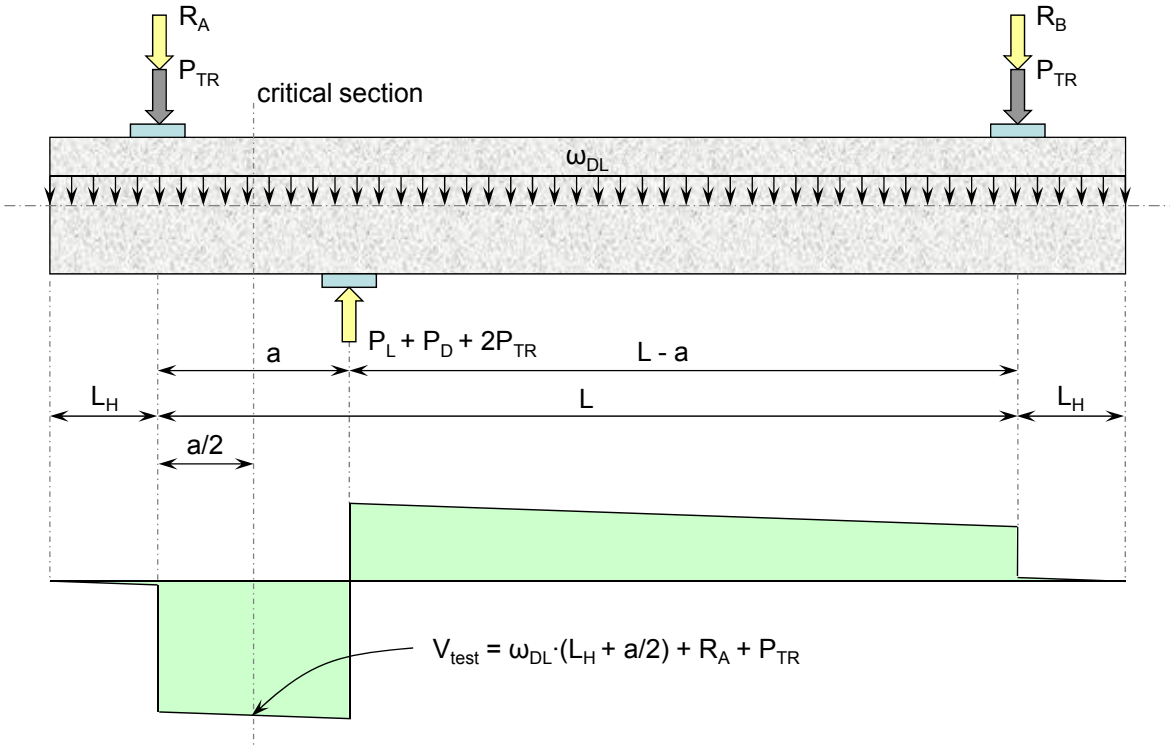

WHERE, $P_L = R_A + R_B$ | $P_D = \omega_{DL}\cdot(2L_H + L)$ | $L = 255.25$" | $L_H = 38.375$" | $P_{TR} = 7.8$ kip | $\omega_{21x23} = 0.49$ kip/ft | $\omega_{21x42} = 0.92$ kip/ft | $\omega_{21x44} = 0.96$ kip/ft | $\omega_{21x75} = 1.63$ kip/ft | $\omega_{36x48} = 1.80$ kip/ft

Figure 4.1: Force and shear force diagram for typical beam test.

It should be noted that three specimens in the experimental program failed in flexure. These specimens are denoted with an (f) or (i) in Table 4.1. The test results were considered

valid since a strut-and-tie analysis inherently considers both shear and flexural failures. Furthermore, beams are often designed such that flexure governs. For these reasons, it was determined that the results from these specimens should be included in all of the analyses. Where appropriate, a flexural failure note was attached to the data from these specimens. In general, the rest of the specimens in the experimental program failed in shear. For the beams loaded with an a/d ratio < 2, the failure was consistent with a direct-strut transfer mechanism. That is, failure ensued after crushing along the strut or at the nodal regions. For the beams loaded with an a/d ratio > 2, the failure was consistent with a sectional shear failure. The specific failure modes of many of the specimens are discussed in the individual sections of Chapter 4 and 5.

Traditionally, the shear capacity of test specimens is normalized by the cross-sectional dimensions and the strength of concrete to account for variations in section size and concrete strength. For experimental loads that are associated with the tensile strength of concrete, such as the diagonal cracking load or the sectional shear (diagonal tension) strength of a member, it is appropriate to normalize the value by $\sqrt{f_c'}$. For experimental loads that are associated with the compression strength of concrete, such as the ultimate capacity of a deep beam, it is appropriate to normalize the value by f_c'. In Table 4.1, the diagonal cracking loads of the test specimens are normalized by $\sqrt{f_c'}\, b_w d$, and the ultimate capacity of the test specimens are normalized by both $f_c' b_w d$ and $\sqrt{f_c'}\, b_w d$. Regarding the ultimate capacity, both normalization techniques were utilized since different modes of failures were observed in the test specimens. At low a/d ratios (< 2.0), the mode of failure was generally consistent with the crushing of a direct strut between the load and the support. Normalizing the capacity by $f_c' b_w d$ was appropriate for these specimens. At higher a/d ratios (> 2.0), the mode of failure was often consistent with a sectional shear (or diagonal tension) failure. Normalizing the capacity by $\sqrt{f_c'}\, b_w d$ was appropriate for these specimens. It should be noted that the only difference between these normalization techniques is the degree with which the strength of concrete is taken into account.

One exception to the aforementioned normalization techniques is for deep beams of significantly different depths. Normalizing the shear capacity of a deep beam by $f_c' b_w d$ suggests that the capacity of the member is a function of the section size. A strut-and-tie model analysis would suggest that the strength of a deep beam is a function of the nodes, struts, and ties, not the depth explicitly. As such, when comparing the strength of deep beams with significantly different depths, normalizing the capacity by $f_c' b_w d$ can impose unwanted errors. This issue is addressed clearly in Section 4.6. When comparing the strength of deep beams with similar depths however, normalizing the capacity by $f_c' b_w d$ is appropriate and is therefore used throughout this report.

4.2.2 Evaluation of Serviceability Data

In the experimental program, the maximum width of diagonal cracks and the diagonal cracking loads were obtained to measure serviceability performance.

The first cracking load was determined by a sudden increase in strain measured by gauges affixed to the stirrups and confirmed by visual observation. Upon examination of the

data, the magnitude of shear at which the stirrup strains increased substantially was considered to be the first cracking load. This load was confirmed with the diagonal cracking load obtained by visual inspection during each test. In all cases, the first diagonal crack extended beyond the mid-depth of the member. At each load increment, the beam was inspected and cracks were marked and measured. In general, the first diagonal crack formed at a 45-degree angle with respect to the load plate. It usually extended from a pre-existing flexural crack or formed simultaneously with a flexure crack. Regardless, any crack that formed at a considerable angle with respect to the vertical was considered a diagonal crack. An example of the determination of the first cracking load is presented in Figure 4.2. The 'E' and 'W' symbols in the figure represent the east and west side of the beam.

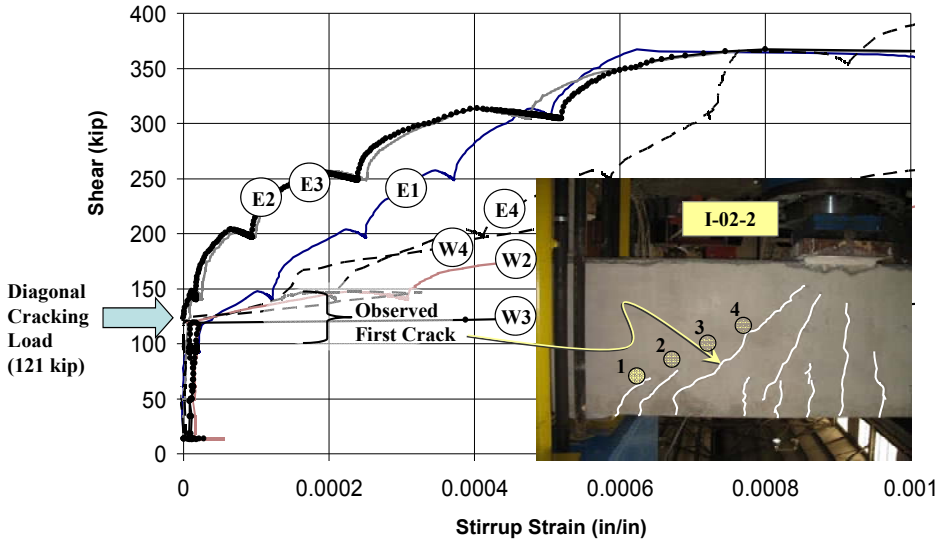

Figure 4.2: Visual and experimental determination of first cracking load.

As noted in Section 3.6, the diagonal cracking loads were only obtained for the first test of each 42-inch specimen. The region for the second test of each 42-inch specimen was cracked during the first test. Diagonal cracking loads were obtained for both tests on the 23- and 75-inch specimens due to the explanation provided in Section 3.6.

The maximum width of the diagonal cracks in each specimen was also monitored throughout the test to evaluate the serviceability performance of deep beams. In general, the maximum width of a diagonal crack was near the midheight of the member. As noted in Section 3.5.4, the maximum width of any diagonal crack was recorded at each load increment by graduate students using crack comparator cards. Measurements were obtained on each face by two students and were averaged. Therefore, in the presentation of crack width data, at a given load level, two crack width values generally exist. These values represent the crack width on each face of the test specimen as an average of two independent measurements. If two data points do not exist at a given load level, then the maximum width of the diagonal cracks were identical on both sides of the test region. An example of the presentation of crack width data is given in Figure 4.3. An approximate service load level and a benchmark crack width are presented with the crack width data. Explanations for these values are given later in this section.

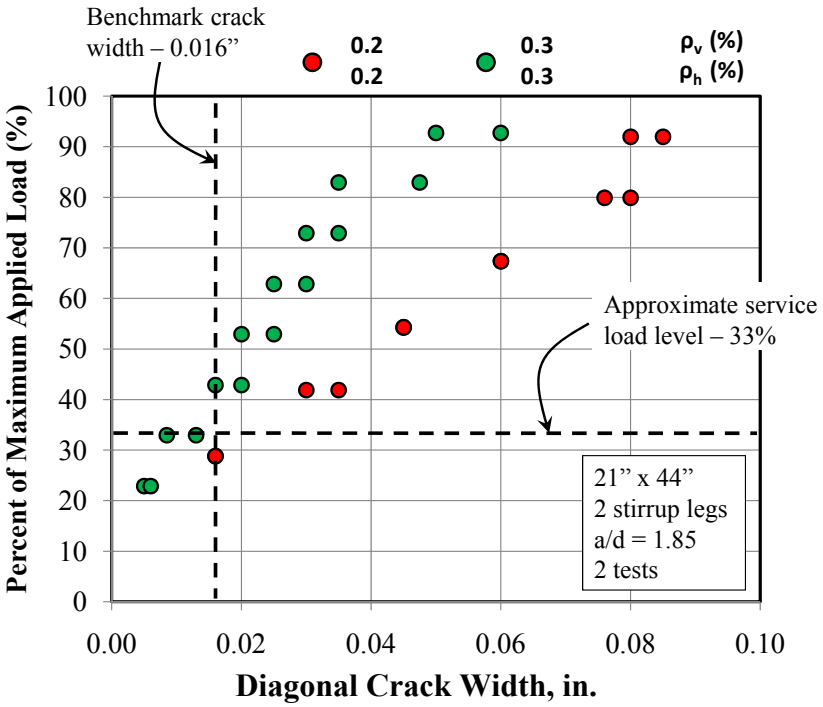

Figure 4.3: Sample crack width data for all series

In this report, the crack width data is plotted versus the percent of the maximum applied load. This method was chosen to be consistent with the *correlation of crack width to capacity* objective of the current project (Section 5.5). Also, it was evident from the trends in the data that the width of diagonal cracks was proportional to the percent of maximum applied load.

To evaluate the serviceability data obtained in the experimental program, criteria were needed. In ACI 318-95, spacing of flexural reinforcement was based off of limiting flexural crack widths for structures with exterior exposure to 0.013-inches and with interior exposure to 0.016-inches (ACI-318-95). In subsequent versions of ACI-318, the specific reference to these crack width limits were removed, primarily due to "the inherent variability in cracking" (ACI 318 Committee Closure, 1999). It was determined that specifying distinct limits for crack widths was impractical. Similar limits were found in ACI 224R-01: Control of Cracking in Concrete Structures (ACI 224R-01). A tolerable crack width of 0.012-inches was suggested for moist conditions; a tolerable crack width of 0.016-inches was suggested for dry conditions. These values are listed in Table 4.2.

In the concrete design recommendations developed by the fédération international du béton (*fib;* i.e. international concrete federation), the same tolerable crack widths that existed in ACI 224R-01 were provided. Again, they were a function of the exposure condition of the member. Even though these limits were intended for flexural crack widths, they provide the only available guidance for tolerable crack widths in reinforced concrete structures. The tolerable crack widths are shown in Table 4.2.

Table 4.2: Tolerable widths of flexural cracks

Exposure Condition	ACI 224R-01 (in.)	*fib* (1999) (in.)
Dry air, protective membrane, indoors	0.016	0.016
Humidity, moist air, soil, cyclic wet and dry	0.012	0.012

In addition, an internal discussion amongst the members of the project team determined that a crack width of 0.016-inches, in general, is the typical width at which attention is garnered in TxDOT (Vogel, 2008). Based on this discussion and the crack width limits set forth in ACI 318-95 and *fib*, a crack width of 0.016-inches was used as a benchmark to compare the serviceability performance of the specimens in the current project. It should be emphasized that since crack widths are highly variable, it is not appropriate to assess the data with a strict limit. The limit of 0.016-inches should be used as an approximate boundary between acceptable and unacceptable performance.

In conjunction with the tolerable crack width limit, an approximate service load as a function of the ultimate capacity of the test specimen was used to evaluate the crack width data. In a study by Tan and Lu (1999), the serviceability load was taken as the load at which the width of a diagonal crack reached a tolerable crack width limit, such as 0.016-inches. However, in the current project, it was determined that a service load independent of crack widths should be used. In a study by Grob and Thürlimann (1976), the service load was assumed to be equal to the theoretical capacity of the specimen divided by a global safety factor of 1.8. A similar approach to estimate the service load was used in the current study as detailed in Figure 4.4.

$$\varphi \text{ Nominal Capacity} \approx \eta \text{ Service Load}$$

$$\frac{\varphi}{\eta} \approx \frac{\text{Service Load}}{\text{Nominal Capacity}}$$

Assumptions:
1). Load Case: 1.25DL + 1.75LL
2). DL = 75% of Service Load
LL = 25% of Service Load
3). Nominal = 2/3 Experimental

} $\eta = 1.4$

$$2/3 \quad \frac{0.70}{1.4} = 0.33 \approx \frac{\text{Service Loads}}{\text{Experimental Capacity}}$$

φ = strength reduction factor, 0.70
η = load factor
DL = dead load
LL = live load

Figure 4.4: Estimate of service load as a function of experimental capacity

As shown in Figure 4.4, the LRFD strength equation can be re-written such that the ratio of the strength reduction factor (φ) to the load factor (η) is approximately equal to the ratio of the service load to the nominal capacity. The φ factor for compression elements in a strut-and-tie model is 0.70 in AASHTO LRFD (2008). The η factor is a function of the load case and the distribution of the loads for that particular case. If the following two assumptions are made, then η equals approximately 1.4:

- Strength I in AASHTO LRFD governs design, 1.25DL + 1.75LL.
- 75-percent of the service load is DL; 25-percent of the service load is LL.

Lastly, if it is assumed that the experimental capacity is approximately 1½ times the nominal capacity, then the service load should be about 1/3 of the experimental capacity. This final assumption was justified through the strut-and-tie analysis of the database discussed in Section 5.2. It is clear that several assumptions are needed to estimate the service load as a function of the ultimate capacity of deep beams. Error in any of these assumptions can shift the estimated service load up or down accordingly. As such, it is important to treat this value (0.33) as a general representation of the service load on a deep beam.

In the following four sections, the experimental results as they relate to the four distinct tasks listed in Section 4.1 are discussed in detail.

4.3 Distribution of Stirrups across the Web

4.3.1 Background

According to the Commentary of ACI 318-08 (§ R11.5.7):

Research has shown that shear behavior of wide beams with substantial flexural reinforcement is improved if the transverse spacing of stirrup legs across the section is reduced.

The preceding recommendation only appears in the Commentary of the ACI 318-08 specifications – within the portion that includes sectional shear design provisions. Within the main body of the code and in Appendix A, the distribution of transverse reinforcement across the web is not required. The research cited by ACI 318-08 is that conducted by Leonhardt and Walther (1961); and Anderson and Ramirez (1989) and is discussed later in this section.

According to Eurocode 2 (§ 9.3.2), the transverse spacing, s_{wt}, of shear reinforcement is limited to:

$s_{wt} \leq d \leq 31\text{-inches} \quad [V_u < 0.2\ V_n]$
$s_{wt} \leq 0.3 \cdot d \leq 8\text{-inches} \quad [V_u > 0.67\ V_n]$

This requirement is for a conventionally loaded beam. It is not referenced in the deep beam portion of Eurocode 2. The requirement is similar to the recommendation proposed by Leonhardt and Walther (1961). The background of this study is presented as follows.

AASHTO LRFD (2008) specifications contain a provision that directly penalizes a deep beam design if stirrups are not distributed across the web (AASHTO Article 5.6.3.3.2 and Figure 5.6.3.3.2-1 (a)). According to AASHTO LRFD (2008), the width of a strut framing into a CTT

node is reduced if stirrups are not distributed across the web. This requirement is illustrated in Figure 4.5. It is important to note that the requirement is only for a strut framing into a CTT node and only required in the STM section of the code.

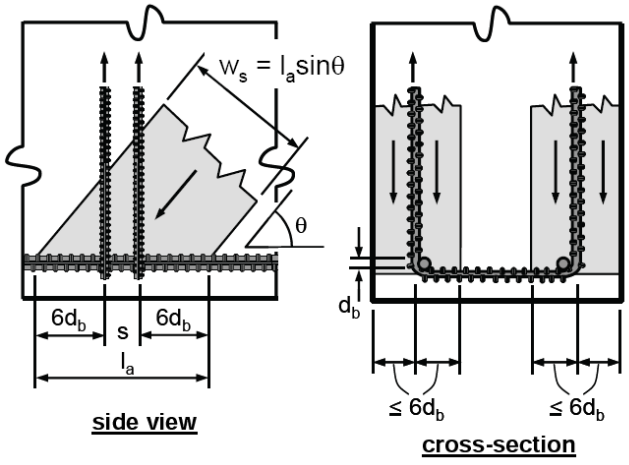

Figure 4.5: AASHTO LRFD requirement for a strut anchored by reinforcement (AASHTO LRFD, 2008 and Brown et al. 2006).

Limiting the width of a strut framing into a CTT node may be unnecessarily conservative given that, in practice, most CTT nodes are smeared (Section 2.4.3). Also, this AASHTO LRFD (2008) provision is only applicable when designing a D-region. Yet, when the a/d ratio is less than two, a direct strut is the predominant mechanism of shear transfer; the use of a CTT node is not necessary. The applicability of using a direct strut or multiple-panel model for the design of a D-region is an issue that is further addressed as part of this research project. One of the goals of the current research program is to investigate the AASHTO LRFD provision that limits the width of a strut framing into a CTT node. Previous research that has focused this issue is as follows.

Leonhardt and Walther (1961)

Leonhardt and Walther (1961) theorized that an oblique strut in a deep beam acts like a beam supported at the stirrup legs (Figure 4.6). As a result, the researchers theorized that more intermediate supports (i.e. stirrup legs) would have the effect of increasing the shear capacity of the beam.

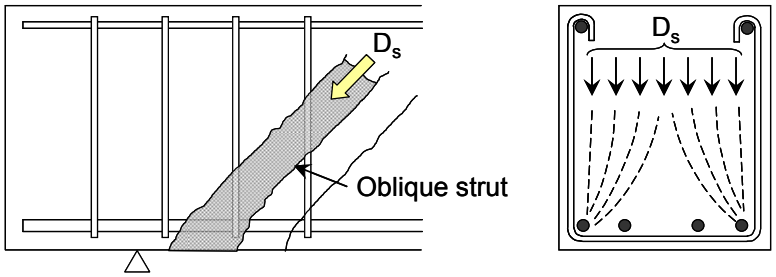

Figure 4.6: The oblique strut supported by vertical stirrup legs (taken from Leonhardt and Walther, 1961).

The researchers recommended spacing stirrups across the web at 20-cm (7.9-inches) for beams with high shear stresses and at 40-cm (15.7-inches) for beams with low shear stresses. Also, they recommended limiting the maximum spacing of stirrups across a beam web to a distance less than the beam's effective depth, *d*.

However, the widest beam that the researchers tested was 12-inches in sectional shear. Leonhardt and Walther (1961) admitted that their tests were not sufficient to make a determination on the effect of stirrup distribution across the web:

> *More attention in the future will have to be paid to the distribution of the stirrups. These tests were concerned with fairly narrow webs (up to 12-inches).*

Hsuing and Frantz (1985)

Hsuing and Frantz (1985) tested five beams with varying widths and stirrup distribution. Cross-sectional details of the beams are illustrated in Figure 4.7.

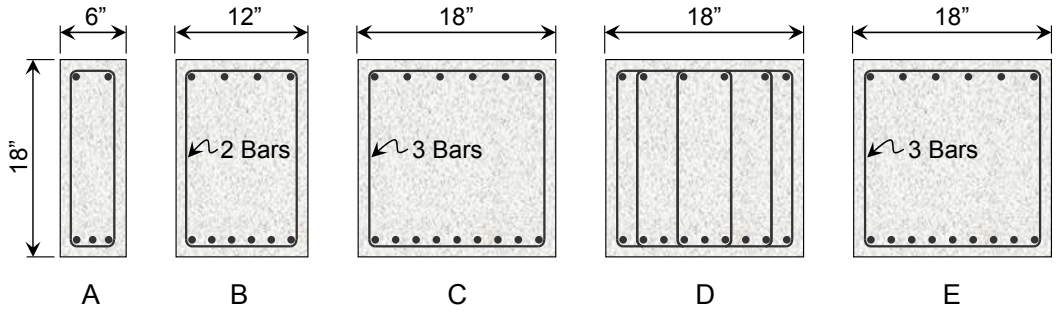

Figure 4.7: Details of specimens tested by Hsuing and Frantz (1985).

All of the specimens were tested with a shear span to depth ratio of 3.0. Each beam had identical longitudinal and transverse reinforcement ratios (1.8% tension, 0.2% compression, and 0.2% transversely).The stirrup spacing was held constant by bundling the stirrups for beams B, C, and E. The concrete strength was the same for all five specimens at the time of testing.

The ratio of measured to predicted capacities was 0.98, 0.89, 1.01, and 1.03 for beams A through D (Beam E was loaded to only 80% of its ultimate capacity). The researchers concluded that there was no significant influence on the relative shear strength caused by the beam width or distribution of stirrups.

Hsuing and Frantz (1985) noted that Beam C had narrower crack widths than Beam D up to 90% of their respective capacities. They suggested that this was due to the fact that Beam C contained more reinforcement than Beam D at the location of crack measurement (i.e. at the beam surface).

In order to investigate the difference in crack widths between Beams C and D, Beam E was fabricated and loaded to 80% of its capacity; the main shear crack was epoxy injected; and the load was sustained as the epoxy cured. After the epoxy had cured, the beam was unloaded and the web was cored at the location of the main shear crack. The variation in crack width through the web was examined in order to ascertain if a lack of distributed stirrups results in wider interior crack widths. The researchers found that:

> *Although the center region of the cores usually contained the larger crack widths, it was not possible to conclude that a significant variation in crack width existed along the core length in this beam that had stirrups located only along the edges*.

The fact that crack widths did not vary through the web is inconsistent with the previous suggestion that the crack widths in Beam C were narrower than those of Beam D because more reinforcement was located at the surface. The researchers did not provide an explanation for this discrepancy.

The beams tested by Hsuing and Frantz (1985) had an a/d ratio of 3.0. The current research program is focused on deep beams with an a/d ratio less than 2.5. Therefore, the research conducted by Hsuing and Frantz (1985) is significant but inconclusive in regards to the effect that stirrup distribution has on the strength and serviceability behavior of deep beams (a/d < 2.5).

Anderson and Ramirez (1989)

Anderson and Ramirez (1989) tested four 16-inch wide specimens with varying stirrup distribution. All of the specimens were tested with a shear span to depth ratio of 2.65. Each beam had identical longitudinal and transverse reinforcement ratios (2.3% tension, 1.0% compression, and 0.4% transversely). Cross sectional details of the beams are illustrated in Figure 4.8.

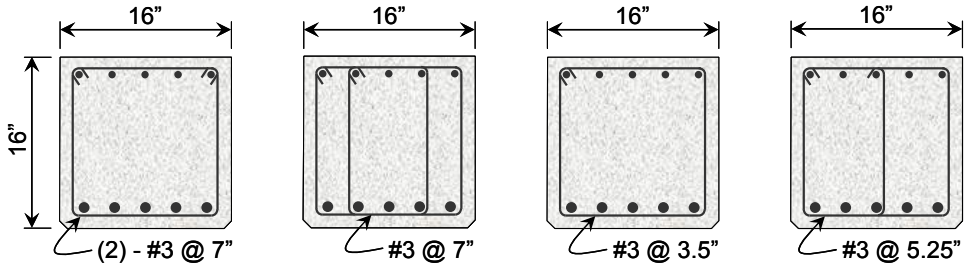

	W1	W2	W3	W4
V_{TEST}	103.4 kip	123.4 kip	113.4 kip	131.4 kip
V_{TEST} / V_{ACI}	1.05	1.23	1.13	1.30
f_c'	4230 psi	4670 psi	4690 psi	4900 psi

Figure 4.8: Details of specimens tested by Anderson and Ramirez (1989).

Anderson and Ramirez (1989) theorized that a lack of distributed stirrups across the width of the web could result in a concentration of compression stresses at the intersection between the stirrup and longitudinal tensile reinforcement. This situation could lead to premature failure due to the crushing of concrete within the nodal zone.

The beams tested by Anderson and Ramirez (1989) did not fail due to crushing in the CTT nodal zone. However, the researchers found that longitudinal bar strains were higher for interior bars when stirrups were distributed across the web; indicating that distributing the transverse reinforcement utilizes the interior longitudinal bars more effectively. As a result, the researchers concluded that stirrups should be distributed transversely across the web for wide beams with multiple longitudinal bars.

Upon examination of their data, the significance in the shear strength differences is found to be questionable (Figure 4.8). The ratio of measured to calculated capacities varied between 1.05 and 1.30 for beams W1 through W4. The multiple stirrup specimens (W2 and W4) had a relatively higher capacity beyond the nominal value; however, the compressive strength of concrete for these specimens was also relatively higher. If the beam capacities are normalized by their concrete compressive strength, the maximum difference in their normalized capacity is less than 8-percent (Figure 4.8); an insignificant amount given the degree of scatter associated with shear testing. In addition, all of the specimens carried more shear than predicted by ACI 318-08. Therefore, considering that the strength of all the specimens was safely estimated and given the nominal difference in strength, the benefit of providing multiple stirrup legs is questionable.

Anderson and Ramirez (1989) did not specifically evaluate the strut width limitation specified by AASHTO LRFD (2008). AASHTO LRFD (2008) limits the designer to use an effective strut width that extends at a maximum of six longitudinal bar diameters from the centroid of a stirrup (Figure 4.5). Under this provision, the full width of the beams with two-legged stirrups tested by Anderson and Ramirez could be utilized (Figure 4.9). The distance from the centroid of the stirrup to the center of the cross-section was only 5.6 longitudinal bar diameters. Therefore, since all of the specimens tested by Anderson and Ramirez satisfy the CTT strut width limitation in AASHTO LRFD (2008), they cannot be used to evaluate it.

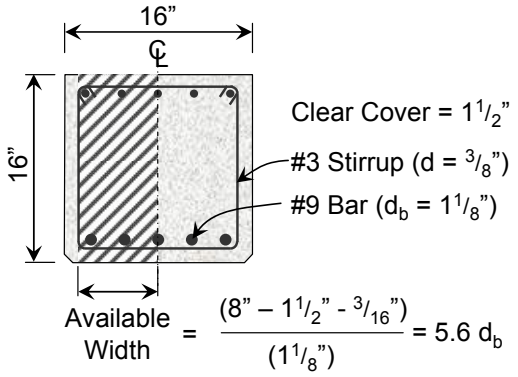

Figure 4.9: Effective strut width of specimens tested by Anderson and Ramirez (1989).

Finally, the specimens tested by Anderson and Ramirez (1989) had an a/d ratio of 2.65. These beams are not considered deep beams and would be designed using sectional methods. It

is not necessary to use STM to design these beams; therefore, an effective strut width limitation is not required according to AASHTO LRFD (2008). In summary, it can be concluded that the previous research did not evaluate the effects of distributing transverse reinforcement in deep beams; a topic of interest to the current research program.

4.3.2 Strength Results

The purpose of the Series I and M testing programs were to evaluate the benefit of distributing stirrups across the web for beams subjected to deep beam shear. In order to accomplish this objective, six tests were conducted on the three beams illustrated in Figure 4.10.

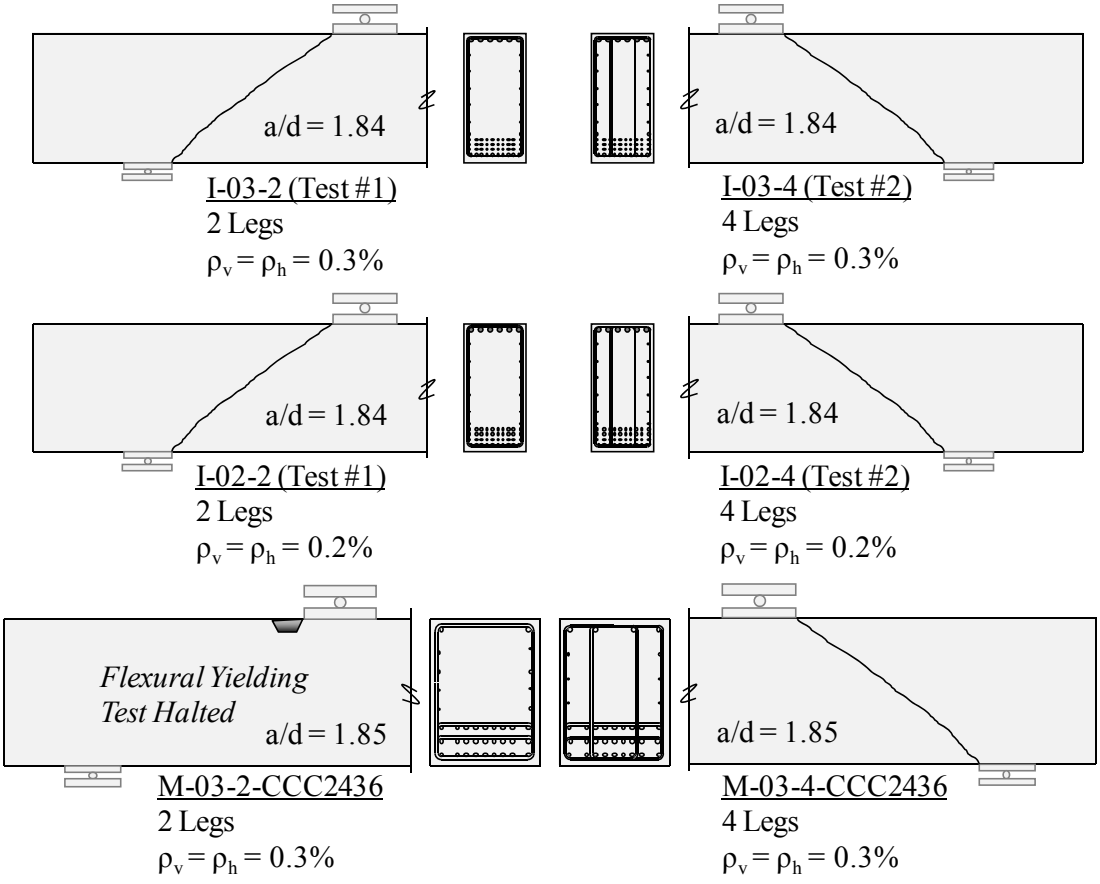

Figure 4.10: Summary of tests studying distribution of stirrups across web.

The test specimens illustrated in Figure 4.10 were designed and detailed such that a similar reinforcement ratio existed in companion tests but with a different number of stirrup legs, 2 or 4. The spacing of the stirrups was also kept reasonably similar between companion tests such that the size of the bars varied. Thus, the difference between concentrating stirrups near the member side face and distributing them across the web, while maintaining a similar reinforcement ratio, was directly evaluated in this task. Details on the design, fabrication and testing of the Series I and M test specimens are given in Chapter 3.

The stirrup configuration was selected in order to evaluate the AASHTO LRFD (2008) provision described in Figure 4.5. In summary, the provision limits the width of a strut framing into a CTT node to six times the diameter of the main longitudinal reinforcement on either side of the stirrup. Based on this requirement, Series I specimens that contain two stirrup legs have an effective strut width of 5.6-inches on each side of the beam (Figure 4.11). If a designer wishes to utilize the full beam width, then four stirrup legs must be provided. Cross sectional details of the specimens that contain stirrups with two and four legs are illustrated in Figure 4.11.

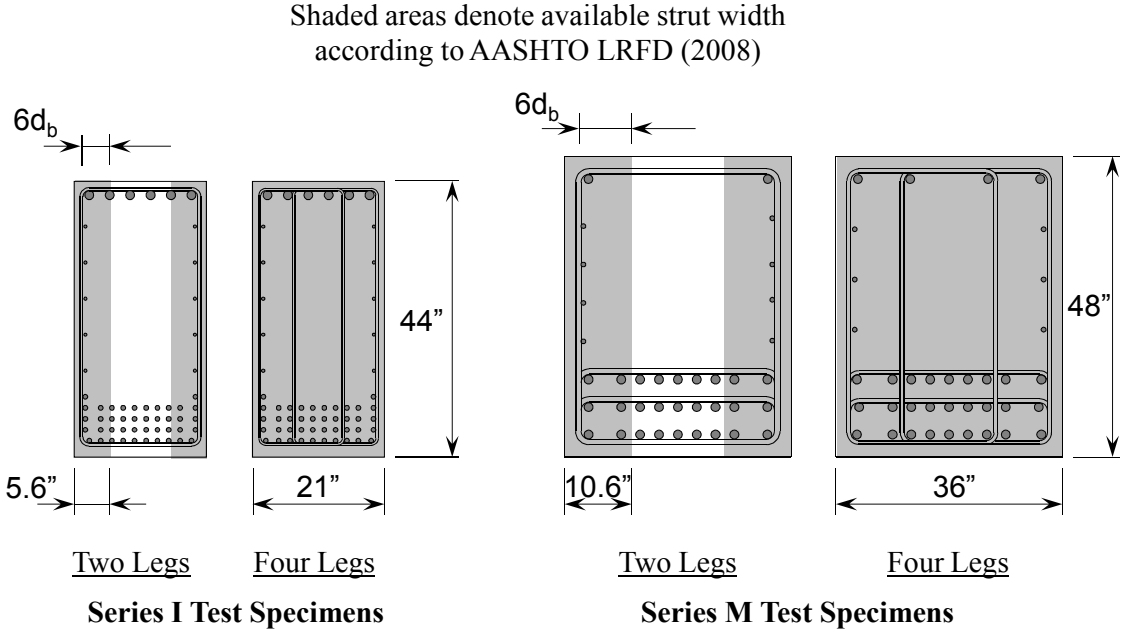

Figure 4.11: Effective strut widths at CTT nodes for specimens with 2-leg and 4-leg stirrups

The results of the six tests conducted in this task are provided in Table 4.3. The shear capacity of the four Series I specimens is presented with the final cracking patterns in Figure 4.12. The side of each beam with two stirrup legs was tested first; the side with four stirrup legs was tested second. Therefore, the specimens that contained four stirrup legs are denoted as *pre-cracked* to indicate that minor flexural cracks were present prior to testing.

Table 4.3: Test Results: Series I

Specimen I.D.	f_c' (psi)	V_{test} † (kip)	$\frac{V_{test}}{\sqrt{f'_c}\,b_w d}$	$\frac{V_{test}}{f'_c\,b_w d}$	V_{crack} (kip)	$\frac{V_{crack}}{\sqrt{f'_c}\,b_w d}$
I-03-2	5240	569	9.7	0.13	144	2.5
I-03-4	5330	657	11.1	0.15	-	-
I-02-2	3950	454	8.9	0.14	121	2.4
I-02-4	4160	528	10.1	0.16	-	-
M-03-4-CCC2436	4100	1128	12.2	0.19	354	3.8
M-03-2-CCC2436	4900	1096[f]	10.9	0.16	-	-

† See Section 4.2.1 for determination of critical shear value, V_{test}

f Test was stopped prior to failure of the specimen due to the onset of yielding of the tensile reinforcement and crushing of concrete in the compression zone

It is important to note that Specimen M-03-2-CCC2436 did not experience shear failure. The test was halted upon the onset of yielding of the flexural tensile reinforcement and crushing of the concrete in the compression region. As a result, the maximum shear value reported (V_{test}) in Table 4.3 is the amount of shear carried in the beam upon the onset of flexural failure. Nonetheless, results are reported for this specimen because they are note-worthy with regard to a 36-inch wide deep beam reinforced with two and four stirrup legs.

The crack patterns at failure for the Series I specimens (Figure 4.12) indicate that a direct strut or single-panel mechanism was the predominant mechanism for shear transfer and the mode of failure. Parallel cracks between the load point and support delineated the boundary of the strut. Crushing occurred in the compression region adjacent to the load point and along the strut. Subsequently, normalizing the capacity of a specimen by the compressive strength of concrete is more appropriate than the square root of the compressive strength as noted in Section 4.2.1.

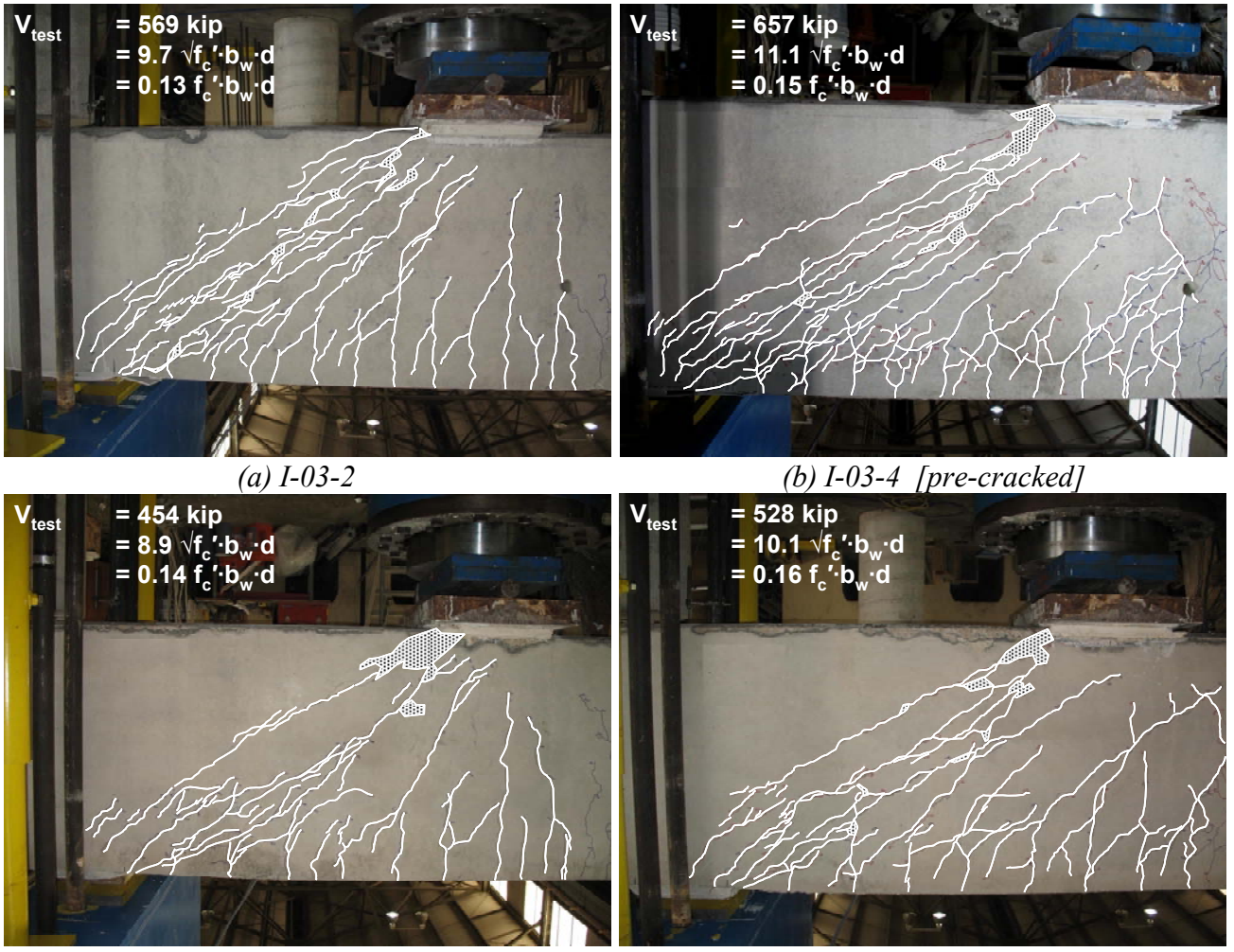

(a) I-03-2 *(b) I-03-4 [pre-cracked]*

(c) I-02-2 *(d) I-02-4 [pre-cracked]*

Figure 4.12: Series I test specimens at failure.

The normalized capacity of the Series I specimens varied between 0.13 and $0.16f_c' \cdot b_w \cdot d$ (Table 4.3). The specimens with 4 stirrup legs failed at approximately 15% higher normalized shear stress than the specimens with 2 stirrup legs. However, considering the well-documented variability in shear strength, a difference of 15% is not very significant. With additional testing, this trend may disappear.

A similar conclusion can be reached based on the examination of the two Series M test specimens. The test with four stirrup legs, M-03-4-CCC2436, had a normalized shear capacity of $0.19 \cdot f_c' \cdot b_w \cdot d$. The maximum shear carried for the beam with two stirrup legs, M-03-2-CCC2436, was $0.16 \cdot f_c' \cdot b_w \cdot d$. Again, considering the inherent variability in deep beam shear strength, the difference in shear capacity between the two 36"x48" specimens is largely trivial. As a result, stirrup distribution did not appear to have a significant influence on the capacity of a 36-inch wide deep beam.

Effectiveness of Longitudinal Tension Reinforcement

Anderson and Ramirez (1989) tested the effectiveness of distributing stirrups across a beam's web for 16"x16" specimens. The researchers concluded that stirrups should be distributed across the web. The main justification for their recommendation was the observation that strains on interior longitudinal bars were higher for beams with distributed stirrups than for those without. Note, the research conducted by Anderson and Ramirez (1989) investigated the effect of distributed reinforcement on the behavior of beams loaded in sectional shear (a/d = 2.65). Stirrups are more effective in a sectional shear region (i.e. multiple-panel truss model) than a deep beam region (i.e. single-panel truss model). Nonetheless, upon examination of their results, the difference in capacity between specimens is debatable (as previously discussed). Series I beams were loaded in deep beam shear (a/d = 1.85). Thus, stirrup distribution is expected to have an even lesser effect on the behavior of these specimens.

In concurrence with Anderson and Ramirez (1989), the magnitudes of the strains at the outer-most layer of the longitudinal bars were measured as part of the Series I program. The strain data is presented in Figure 4.13. Upon examination of the strain data presented in Figure 4.13, it can be concluded that the detailing of stirrups had no influence on the distribution of longitudinal strains for Series I test specimens.

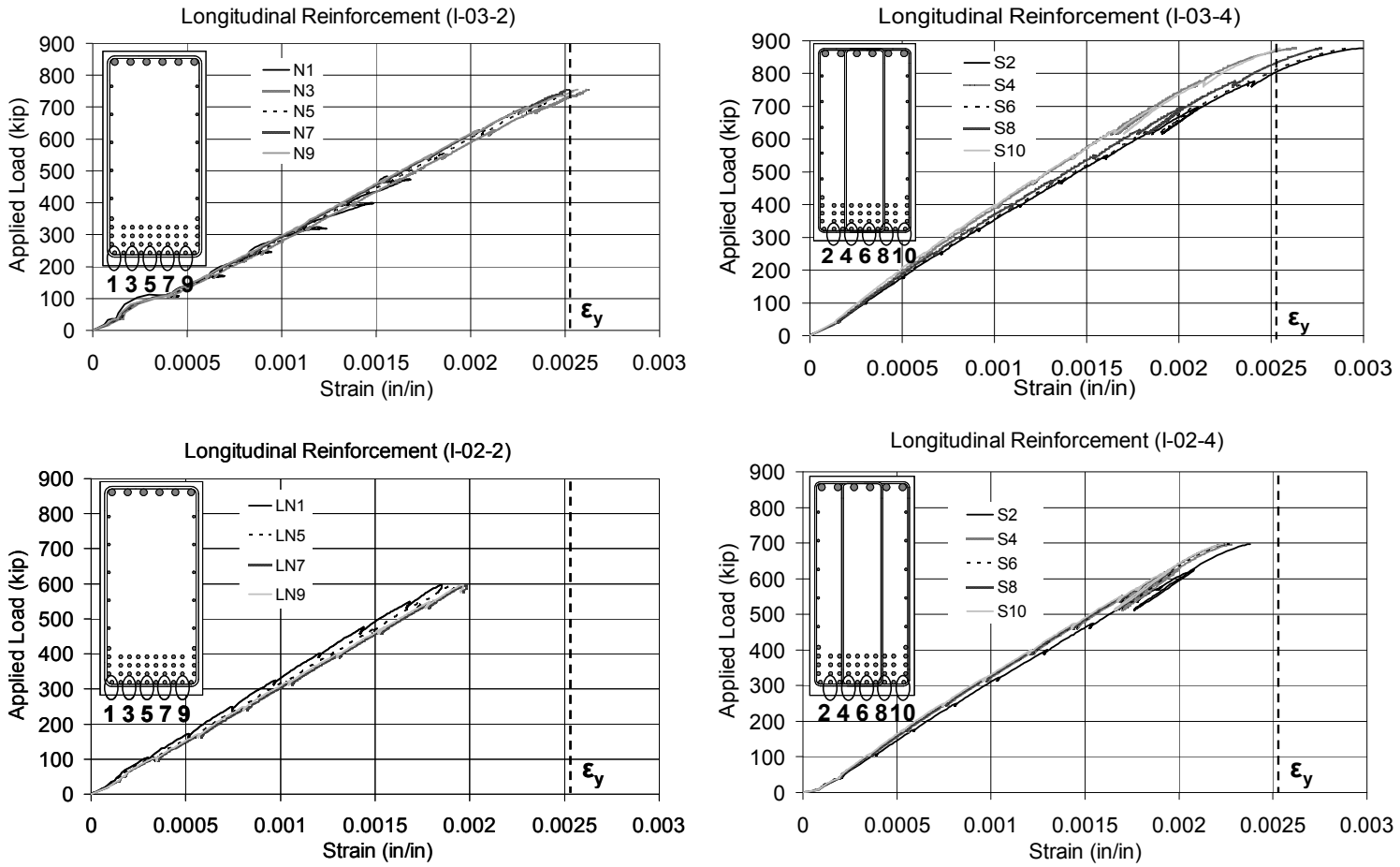

Figure 4.13: Measured longitudinal strains within the outermost layer of tension reinforcement.

4.3.3 Serviceability Results

In addition to the strength data, serviceability data were collected for each of the tests within Series I, including the first cracking load and crack widths at each load increment. As the first cracking load is associated with the tensile strength of concrete, values presented in Table 4.3 are normalized with respect to the square root of the compressive strength of concrete. Unfortunately, it was not possible to compare the first cracking load of specimens with two stirrup legs to those with four stirrup legs because both tests were conducted on opposite sides of the same beam. In other words, the second test region was pre-cracked during the first test. Therefore, the load at first diagonal cracking was determined for the specimens with two stirrup legs only (I-02-2 and I-03-2). The diagonal cracking loads of these specimens are evaluated with those of other beams with varying amounts of transverse reinforcement in Section 4.5.3. Based on similar findings in the current experimental program (Sections 4.4.3 and 4.5.3), it is unlikely that the transverse distribution of stirrups would affect the diagonal cracking load of deep beams. Prior to cracking, all deep beams regardless of the amount or distribution of transverse reinforcement behave elastically.

Crack patterns at approximately 90% of capacity and corresponding crack width data are presented in Figure 4.14 for specimens with 0.3% transverse reinforcement in each direction and in Figure 4.15 for specimens with 0.2% in each direction. The crack widths measured on each beam face are presented at individual load increments and normalized by the ultimate capacity of the specimen.

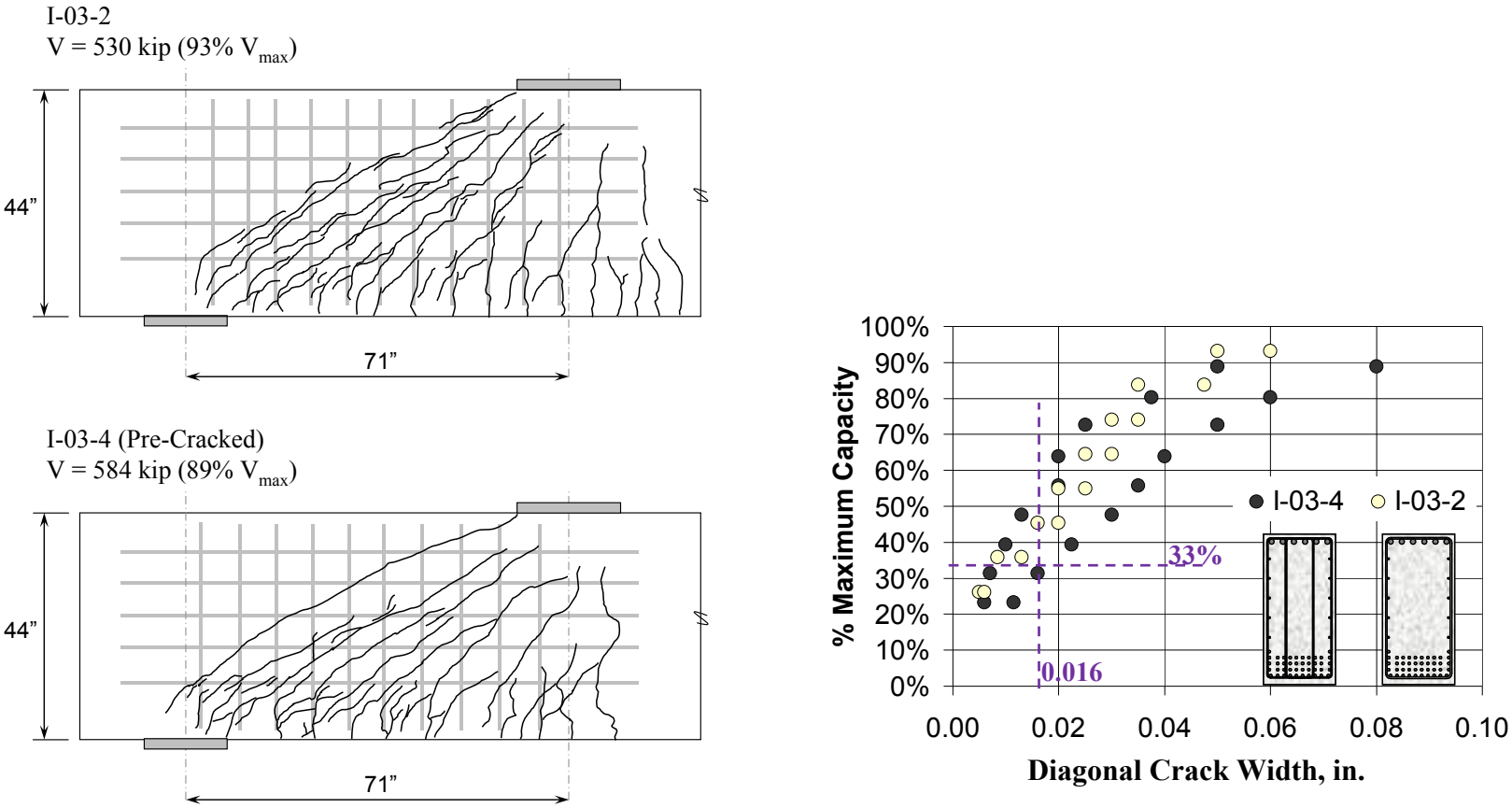

Figure 4.14: Crack pattern at approximately 90% of capacity and crack width behavior: 0.3% transverse reinforcement in each direction.

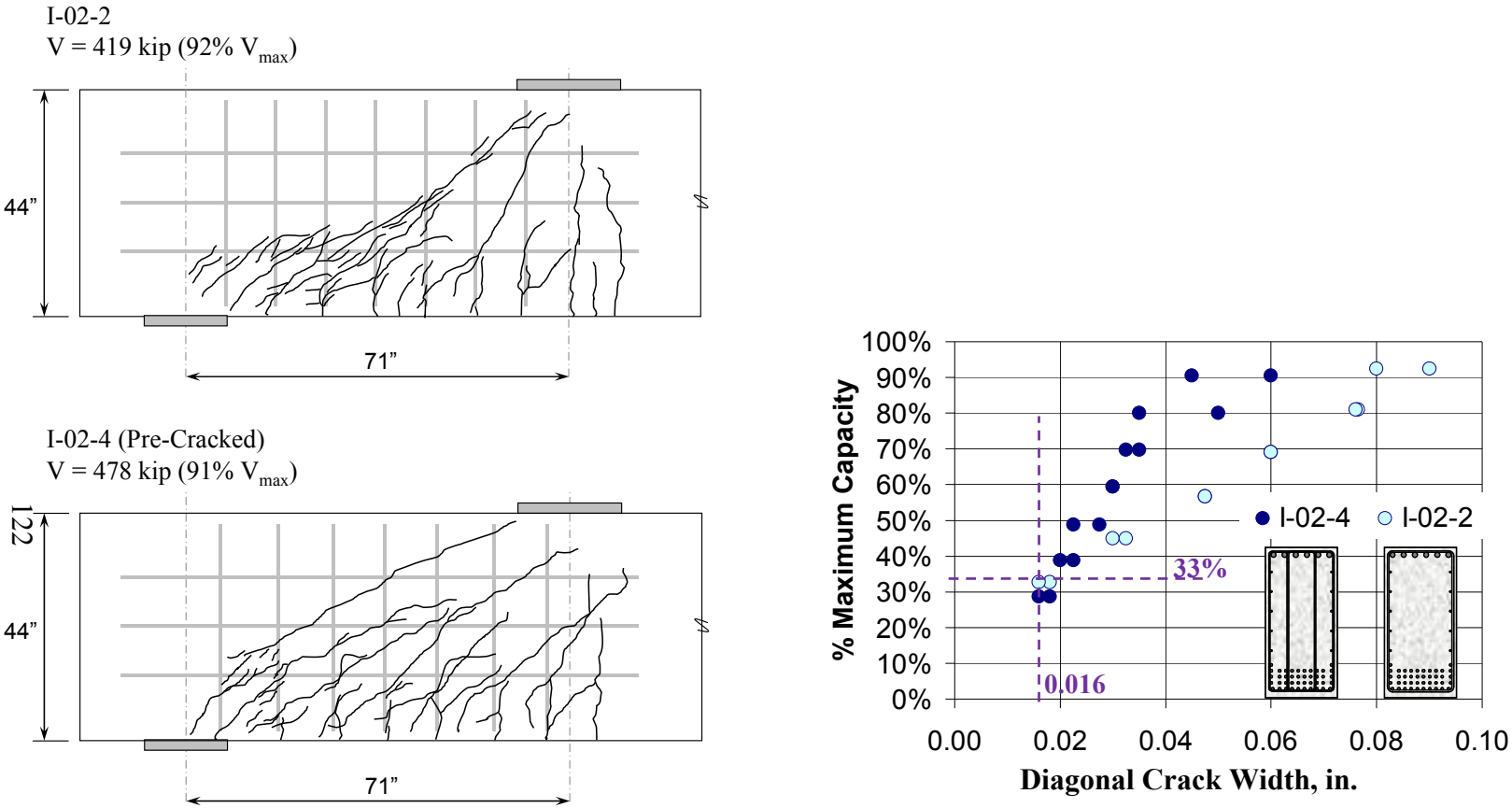

Figure 4.15: Crack pattern at approximately 90% of capacity and crack width behavior: 0.2% transverse reinforcement in each direction.

Upon a comparative examination of the crack width data and crack maps of specimens with 0.3% transverse reinforcement in the vertical and horizontal directions (Figure 4.14), the following conclusion can be reached: the serviceability performance of beams with two stirrup legs is equivalent to those with four stirrup legs. When the maximum diagonal crack widths are compared at an estimated service load of 33-percent of ultimate (Section 4.2.2), a negligible difference is observed on average.

Upon an examination of the crack width data and crack maps of specimens with 0.2% transverse reinforcement in the vertical and horizontal directions (Figure 4.15), the following conclusion can be reached: specimens detailed with four stirrup legs demonstrated narrower diagonal crack widths with more crack distribution compared to specimens detailed with two stirrup legs. However, the difference in crack width was most evident at loads higher than estimated service loads (33-percent). Also, it is interesting to note that the specimens with 0.2% web reinforcement had maximum diagonal crack widths at the first cracking equivalent to the tolerable crack width limit of 0.016-inches. On the contrary, the specimens with 0.3% web reinforcement had significantly narrower crack widths at first cracking (Figure 4.14). The effect of the quantity of transverse reinforcement on diagonal crack width is discussed in detail in Section 4.5.3.

Similarly, crack width data for the Series M specimens is presented in Figure 4-16. Cracking data for the specimens presented in Figure 4-16 is not normalized by their shear capacity, as Specimen M-03-2-CCC2436 did not experience a shear failure.

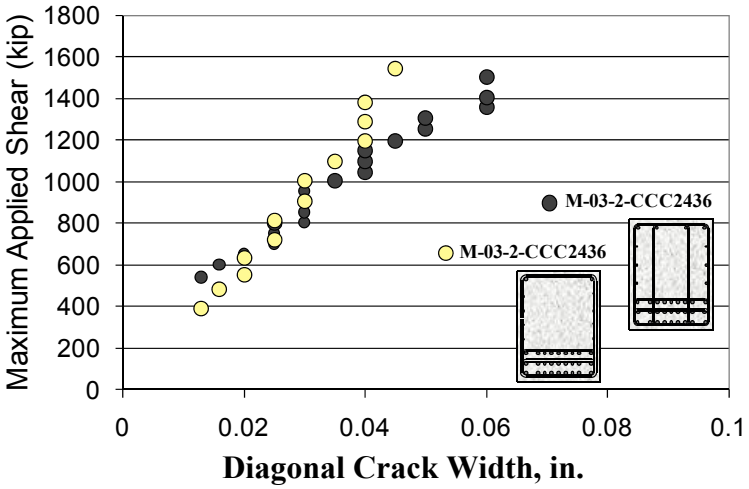

Figure 4-16. Shear carried in a test specimen versus the corresponding maximum diagonal crack width.

Upon examination of the crack width data presented in Figure 4-16 it can be concluded that the serviceability performance for these beams was not detrimentally affected by reducing the distribution of stirrups from four to two legs across the web.

The objective of the Series I and M testing programs were to investigate the strength and serviceability effects caused by the distribution of stirrups across the web. For additional information relating the quantity of transverse reinforcement to the corresponding serviceability behavior, refer to Section 4.5.3.

4.3.4 Evaluation of Specimens with Current Code Expressions

A comparison between the experimental shear strength and nominal capacity calculated per the ACI 318-08 and AASHTO LRFD (2008) STM provisions is illustrated in Figure 4.17 for both a one-panel and two-panel truss model. The values were normalized by the compressive strength of concrete at the time of testing. The difference in the estimations obtained from one-panel truss models is attributed to the different efficiency factors specified in the ACI 318-08 and AASHTO LRFD (2008) provisions. The strength estimations obtained through the use of a two-panel truss model were the same for the ACI 318-08 and AASHTO LRFD (2008) provisions as the estimate is governed by the yield capacity of the vertical tie (i.e. stirrups).

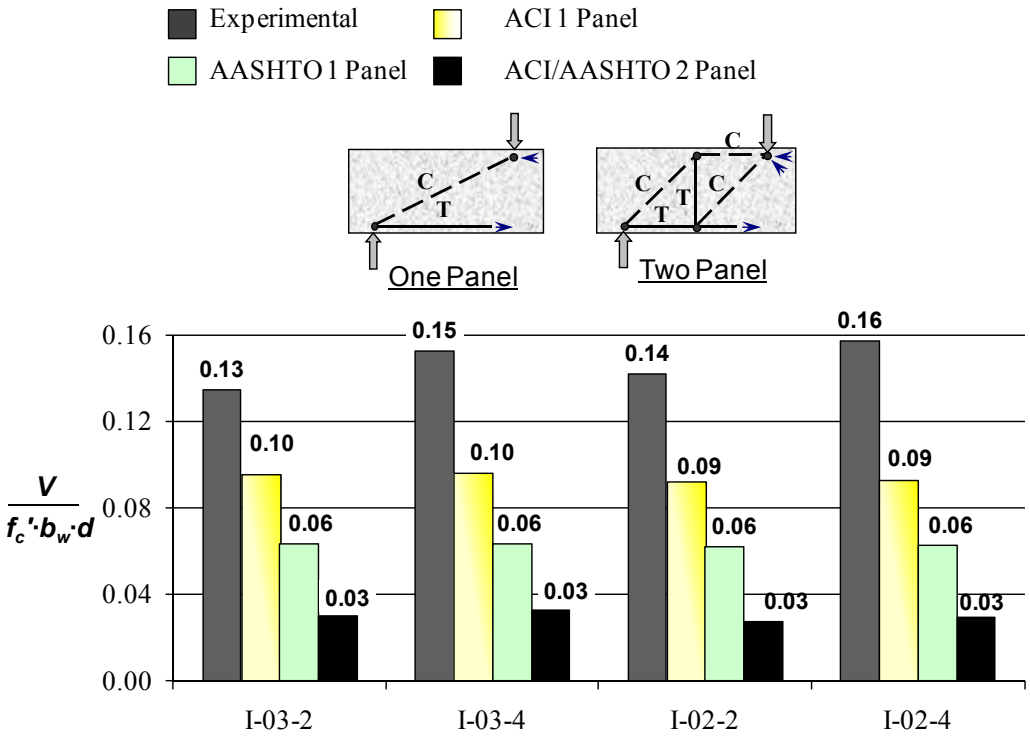

Figure 4.17: Comparison of experimental capacity with ACI 318 and AASHTO LRFD one and two-panel STM calculations.

Upon comparison of the experimental and estimated capacities presented in Figure 4.17, it can be concluded that the shear capacity estimated by the ACI 318-08 and AASHTO LRFD (2008) STM provisions was conservative for beams that contained 0.2% and 0.3% reinforcement. In addition, both provisions estimated similarly conservative capacities regardless of whether or not two or four stirrup legs were provided.

The difference between experimental and calculated shear capacities presented in Figure 4.17 illustrates the inappropriateness of using a two-panel truss model in a deep beam region. The nominal capacity calculated using a two-panel model was approximately five times less than the actual capacity. Also, the failure of the Series I specimens was preceded by the crushing of concrete near the load plate and along the strut (Figure 4.12). This type of behavior is better represented by a one-panel STM. As a result, the nominal capacity calculated using a one-panel model was more appropriate.

This point can be illustrated with the following example presented in Figure 4.18.

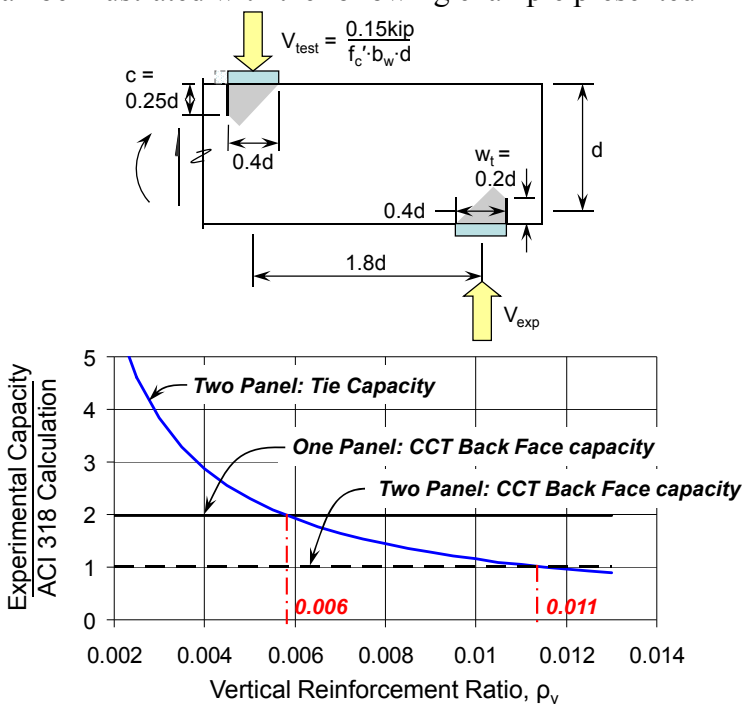

Figure 4.18: Comparison between one and two-panel STM: per ACI 318.

For the example shown, the capacity of a two-panel STM is controlled by the vertical tie if the transverse reinforcement ratio is less than 1.1%; an unrealistically high percentage. In other words, the capacity of the preceding D-region is usually controlled by the capacity of the vertical tie when modeled with a two-panel STM.

For this example, in order for the capacity calculated from a two-panel truss model to govern over that calculated from a one-panel truss model, a vertical reinforcement ratio of over 0.6% would have to be provided; a fairly large amount. In general, a one-panel truss is more appropriate than a two-panel truss when modeling a deep beam region (a/d < 2) with a STM. More information regarding the most appropriate model to use for beams loaded with an a/d ratio < 2, refer to Section 5.3.

4.3.5 Summary

In this task, the difference between concentrating stirrups near the member side face (2 legs) and distributing them across the web (4 legs), without changing the reinforcement ratio, was evaluated. Four tests were conducted on beams with a 21”x44” cross-section and a shear span-to-depth ratio of 1.85. Two tests were conducted on a 36”x48” cross-section and a shear span-to-depth ratio of 1.85. The strength and serviceability performance of members with 2- and 4-legged stirrups were compared. Transverse reinforcement ratios of 0.2% and 0.3% reinforcement were evaluated. Based on the test results, the following conclusions are reached:

- Distributing stirrup legs across the width of the web had a small, but insignificant influence on the strength of the specimen.
- Distributing stirrup legs across the width of the web did not have a significant influence on the maximum width of diagonal cracks for specimens with 0.3%

transverse reinforcement in both the horizontal and vertical directions at service loads or higher.

- Distributing stirrup legs across the width of the web reduced the maximum diagonal crack widths of beams reinforced with 0.2% transverse reinforcement in both the horizontal and vertical directions at loads greater than service (> 40% capacity). Near service loads, the width of diagonal cracks was similar for beams with 0.2% transverse reinforcement distributed in 2 or 4 legs.

The impetus for this research task was to evaluate the AASHTO provision that limits the width of the strut framing into a CCT node in a deep beam. Based on the findings of the experimental program, the AASHTO LRFD (2008) provision was found to be inappropriate. The provision only is applicable when a multiple panel truss model is used. It was determined that a single panel model is more appropriate when the a/d ratio is less than two (Section 5.3). Additionally, if a two-panel STM is used to model a D-region, the capacity of the interior vertical tie force is likely to govern. This further illustrates the inappropriateness of the provision. As such, the limitation on the width of a strut framing into a CTT node should be removed from the AASHTO LRFD Bridge Design Specifications (2008).

4.4 Triaxially Confined Nodal Zones

4.4.1 Background

Another objective of the current research program is to determine the effect of triaxially confined nodal regions on the strength and serviceability behavior of deep beams. It is a well known fact that the strength and ductility of concrete is higher under triaxial compression than it is under uniaxial compression (Figure 4.19).

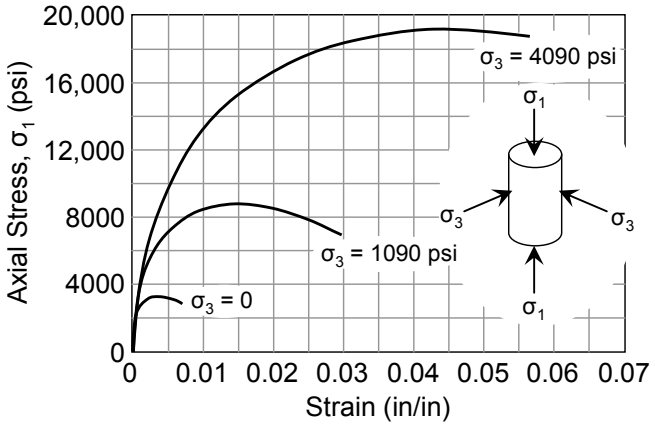

Figure 4.19: Stress-strain curve for concrete cylinder under triaxial compression (MacGregor and Wight, 2005).

In concrete structures, confining stresses are achieved with closely spaced hoops or spiral reinforcement, or additional concrete surrounding the loaded area. When concrete is loaded uniaxially, it expands in the transverse directions. If reinforcement or additional concrete is provided to confine the expansion, the offsetting transverse stresses provide triaxial confinement. As a result, the strength of the confined region is increased.

In STM, nodal zones are generally either biaxially or triaxially confined. Biaxial or two-dimensional confinement occurs when a load plate extends between opposite sides of a loaded area (Figure 4.20b). As a result, the lateral spread of compression is confined in two opposing planes. Triaxial confinement occurs when a load plate is surrounded by concrete on all sides. In this case, the lateral spread of compression is confined in all directions transverse to the loading direction. Figure 4.20 illustrates the differences between biaxial and triaxial confinement.

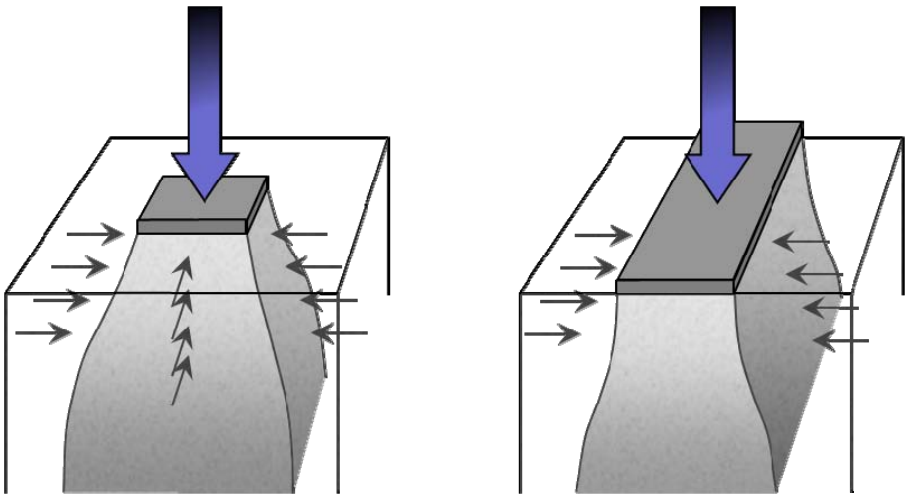

Figure 4.20: Bearing load under (a) triaxial (b) biaxial confinement.

Many researchers recognized the fact that the bearing capacity of triaxially confined concrete can be increased. ACI 318-08 and AASHTO LRFD (2008) contain provisions permitting an increase in the design bearing strength of concrete when the loaded area is smaller than the supporting area. The AASHTO LRFD (2008) specifications express the effective compressive strength of concrete in bearing, f_{cb}, as follows (the ACI 318-08 expression is essentially identical).

$$f_{cb} = 0.85 f'_c \cdot m \tag{4.1}$$

$$m = \sqrt{\frac{A_2}{A_1}} \leq 2$$

Where,

m = confinement modification factor
f_c' = specified compressive strength of concrete, psi

The definition of A_2 and A_1 is illustrated in Figure 4.21.

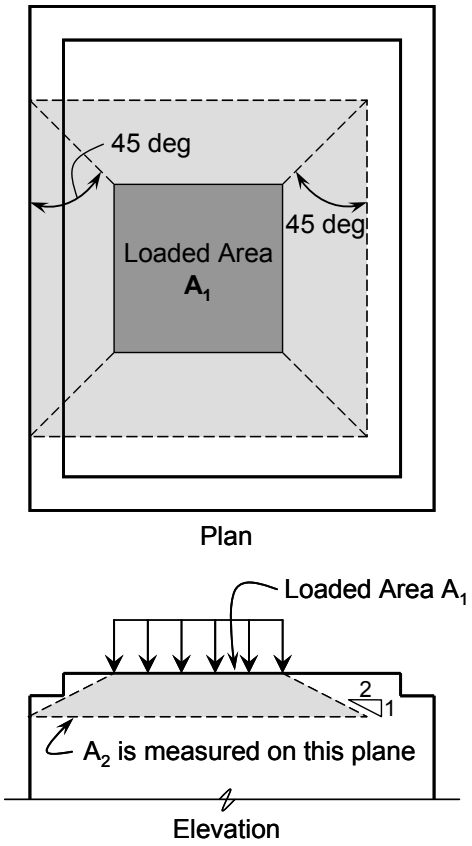

Figure 4.21. Application of frustum to find A_2 in stepped or sloped supports (taken from ACI 318-08).

The ACI 318-08 and AASHTO LRFD (2008) specifications allow the bearing capacity of concrete to be increased due to triaxial confinement. However, these design provisions do not explicitly allow a similar increase in the nodal regions of a strut-and-tie model. Both provisions contain the following note with regard to triaxial confinement:

> *Unless confining reinforcement is provided within the nodal zone and its effect is supported by tests and analysis, the calculated effective compressive stress… shall not exceed the value given…[in Table 5.1 and Table 5.2]*

The preceding provision is attributed to the research conducted by Bergmeister et al. (1993). The researchers made recommendations for the design of bursting reinforcement required around a post-tensioned anchorage zone. Their design expression allows an increase in the bearing capacity of an anchorage zone when closed stirrups and hoops are provided

In contrast to ACI 318 and AASHTO LRFD, *fib* (1999) contains the following provision allowing the designer to increase the effective strength of concrete at all nodal boundaries when triaxial confinement is present:

> *For nodes with secured triaxial compression due to local compression… the increased strength values for multiaxial states of stress may be applied to individual node surfaces…*

The confinement factor specified in *fib* (1999) is expressed in Equation 4.2 and illustrated Figure 4.22.

$$\beta = min\left(\frac{b}{b_1} \; or \; \frac{a}{a_1}\right) \leq 4 \tag{4.2}$$

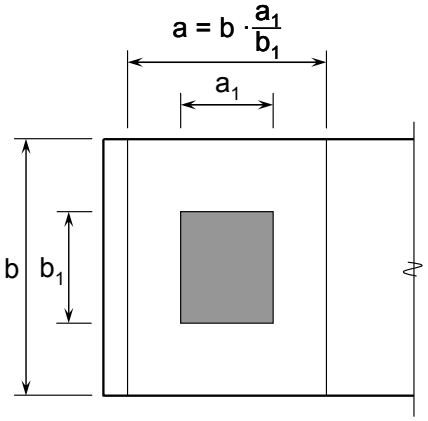

Figure 4.22: Definition of triaxial confinement geometries used in fib (1999).

Current STM efficiency factors have been mostly calibrated with beams whose bearing plates extended the full width of the beam; yet often times, in practice, bearing plates do not extend the full width. As a result, if a designer is using ACI 318-08 or AASHTO LRFD (2008) for a deep beam design, excessively large bearing plates may be necessary as provisions do not allow for an increase in nodal strength due to triaxial confinement. A goal of the current research program is to examine the influence that triaxial confinement has on the strength and serviceability behavior of deep beams. Past research related to this topic is presented as follows.

Leonhardt and Walther (1961), Furuuchi et al (1998)

Leonhardt and Walther (1961) and Furuuchi et al. (1998) investigated the effects of reduced load plate size on the shear strength of deep slab specimens. The cross-sectional dimensions of the test specimens were 8"x20" (Figure 4.23).

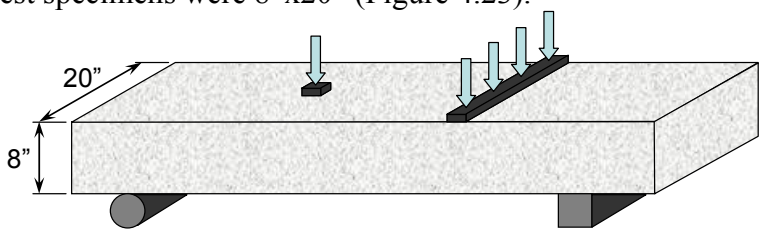

Figure 4.23: Detail of Leonhardt and Walter (1961) and Furuuchi et al. (1998) test specimens.

The specimens tested by Leonhardt and Walther (1961) contained longitudinal reinforcement in the tensile zone and were otherwise unreinforced. The a/d ratio varied between 2.5 and 4.4. The specimens tested by Furuuchi et al. (1998) contained longitudinal reinforcement in the top and bottom side of the beam, but did not contain any shear reinforcement. The a/d ratio varied between 1.25 and 2.25.

The specimens tested by Leonhardt and Walther (1961) failed at both the concentrated and line-load side. According to the researchers:

...since there appears to be no special reason for this different failure behavior... it must be assumed that the shear strength does not differ much for the two types of loading and that the occurrence of failure on the one or other side is probably decided by minor local differences in the quality of concrete.

Furuuchi et al. (1998) derived an expression for effectively increasing the load plate width. The researchers found that the effective width of the load or support plate could be increased by a factor of two to three, but not more than the beam width.

The specimens tested by Leonhardt and Walther (1961) and Furuuchi et al. (1998) can not be used to fully address one of the primary objectives of this research project; an examination of the effects of triaxially confined nodal regions. Specimens tested by Leonhardt and Walther (1961) were only tested under sectional shear forces; therefore, it is expected that the size of the plate would have little influence on the shear capacity. A goal of the current research program is to examine the effect of varying both the load plate and the support plate for deep beams. Furuuchi et al. (1998) tested beams with an a/d ratio less than 2.5 and varied both support and load plates; however his specimens were only 6-inches deep and did not contain transverse reinforcement. An objective of the current research program is to test large-scale specimens that are a realistic representation of deep beams used in practice.

Hawkins (1968)

Hawkins (1968) tested 230 concrete cubes in uniaxial compression and developed an expression to predict their capacity. The loading geometry, specimen size, and type and strength of concrete were varied. The majority of the specimens were 6-inch cubes. The cubes were loaded with a ¾-inch thick bearing plate with an area that was between one to thirty-six times smaller than the area of the cube face.

Based on the findings of the research program, Hawkins (1968) proposed an increase in the compressive strength of concrete according to the following expression.

$$1 + \frac{K}{\sqrt{f'_c}}\left(\sqrt{\frac{A_2}{A_1}} - 1\right) \tag{4.3}$$

Where,

K = constant depending on concrete characteristics

According to Hawkins (1968), the material constant, *K*, varies between 50 and 65. Accordingly, if the compressive strength of concrete is equal to 2500 to 4000-psi; then the $\frac{K}{\sqrt{f'_c}}$ term is essentially equal to 1.0 (i.e. $\sqrt{2500} = 50$ and $\sqrt{4000} = 63$). By setting the $\frac{K}{\sqrt{f'_c}}$ term equal to one, Equation 4.3 is simplified such that the bearing strength factor is equal to $\sqrt{\frac{A_2}{A_1}}$; which is the same factor adopted by the ACI 318-08 and AASHTO LRFD (2008) provisions for bearing (Equation 4.1).

Adebar and Zhou (1993)

Adebar and Zhou (1993) tested concrete cylinders of varying geometry and load plate dimensions in uniaxial compression in order to determine an effective increase in compressive strength resulting from triaxial confinement. The tests consisted of plain concrete cylinders that

were loaded in the axial direction to mimic an unreinforced strut. A detail of their test specimens is illustrated in Figure 4.24.

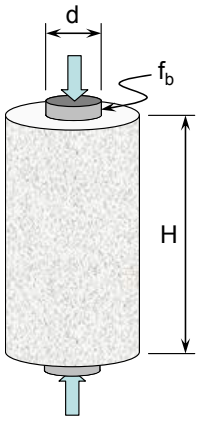

Figure 4.24: Detail of the specimens tested by Adebar and Zhou (1993)

The researchers varied the diameter of the load plate, cylinder, and height of the cylinder in order to derive an expression for a confined CCC node and strut. The recommendation made by Adebar and Zhou (1993) is as follows.

$$f_b \le 0.6 \cdot f'_c \cdot (1 + 2 \cdot \alpha \cdot \beta) \tag{4.4}$$

Where,

$$\alpha = 0.33 \cdot \left(\sqrt{\frac{A_2}{A_1}} - 1 \right) \le 1.0$$

$$\beta = 0.33 \cdot \left(\frac{H}{d} - 1 \right) \le 1.0$$

f_b = allowable bearing stress, psi
α = factor for confinement of surrounding concrete
β = factor for aspect ratio of strut
H = length of the strut from the face of the node, in.
d = width of strut, measured at the nodal interface, in.
A_1 = area of strut at nodal interface, in^2
A_2 = area of strut at point of maximum spreading, in^2

A lower bearing stress limit of $0.6f_c'$ was selected as an appropriate limit when there is a lack of confinement. The upper limit of $1.8\ f_c'$ was selected to correspond approximately to the ACI 318-08 bearing capacity limit (Equation 4.1).

The recommendation provided by Adebar and Zhou (1993) is based solely on isolated strut specimens. A goal of the current research program is to calibrate efficiency factors for actual beam specimens. Also, the researchers only considered struts bound by CCC nodes. In a truss model, struts are typically bounded by both CCC and CCT nodes. The current research program examines the effects of triaxial confinement at both the CCC and CCT nodal zones.

Brown et al. (2006)

Brown et al. (2006) conducted ten tests on seven specimens with reduced support plate widths. An illustration of the beams tested by the researchers is shown in Figure 4.25. The beam cross-sections were either 18”x18” or 30”x18”.

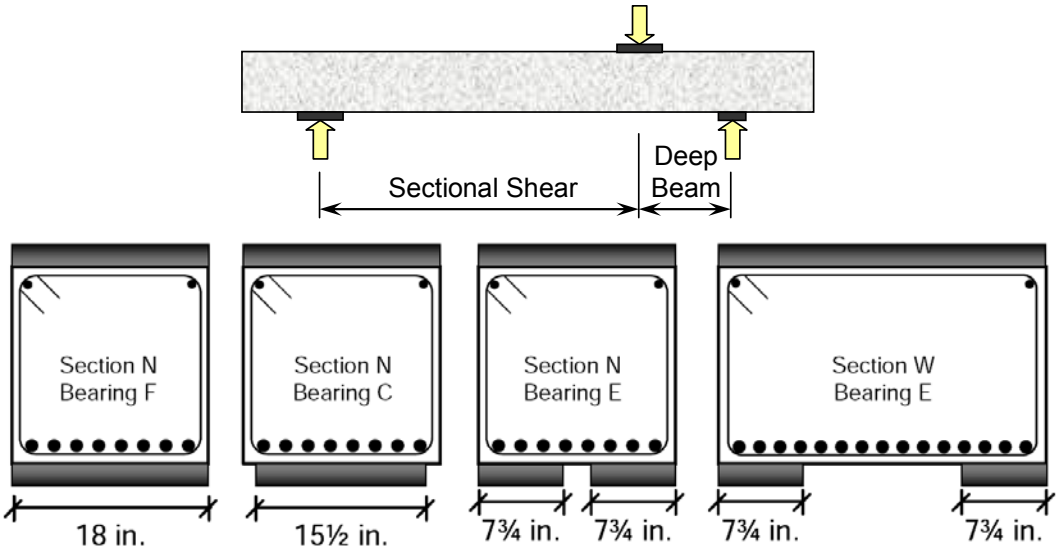

Figure 4.25: Detail of specimens tested by Brown et al. (2006).

The researchers varied the width of the beam specimens and kept the bearing plates the same size. According to the provisions of STM, if the strut width is kept constant, then the beams should have the same strength regardless of their width. This was not the case; the wider beam specimens carried almost twice the load. Unfortunately, all of the wide beam specimens failed in sectional shear in the *long span* (Figure 4.25); whereas the narrow beams failed in deep beam shear in the *short span* (Figure 4.25). The researchers addressed this discrepancy by demonstrating that the amount of shear force carried by the wide specimens in the deep beam side was more than twice shear carried by the narrow beams. Additionally, only the CCT node was investigated by Brown et al. (2006). Therefore, the results of their tests cannot be used to fully address the objectives of this research study.

In summary, previous research studying the effects of triaxial confinement on the behavior of deep beams is found to be inconclusive for the purpose of this research study. The current research program is designed to provide the necessary additional information. Also, very little information exists on the crack width or serviceability behavior of deep beams; another objective of the current project.

4.4.2 Overview of Testing: Series II and Series M

The purpose of the Series II testing program was to evaluate and quantify the benefits provided by triaxial confinement in the nodal regions of a beam subjected to deep beam shear. To achieve this goal, five beams were fabricated and tested in the Ferguson Structural Engineering Laboratory. Two ends of a beam were tested resulting in a total of ten tests. Eight tests were conducted on beam specimens with a 21”x42” cross-section. Two tests were conducted on larger beams with a 36”x48” cross-section (Series M). As explained earlier, Series M beam specimens were designed as multiple purpose test specimens. Two tests conducted on Series M test specimens relate to triaxially confined nodes. Therefore, the results of these tests are included in the comparative analysis presented in this chapter.

Within the Series II testing program, most of the details of the beam specimens were kept constant. The primary experimental variables were the size of the load and support plates and the amount of transverse reinforcement. The two transverse reinforcement ratios that were

investigated were 0.3% and 0.2% in the vertical and horizontal direction. For the experimental program, the *length* of a bearing plate is defined as the dimension of the plate measured along the span; the *width* of a bearing plate is defined as the dimension measured transverse to the span. All plate dimensions are reported with the length-dimension first, then the width-dimension (i.e. *length* x *width*). Details of the design of the Series II and Series M beams are included in Section 3.2. A summary of the ten tests is illustrated in Figure 4.26 and Figure 4.27.

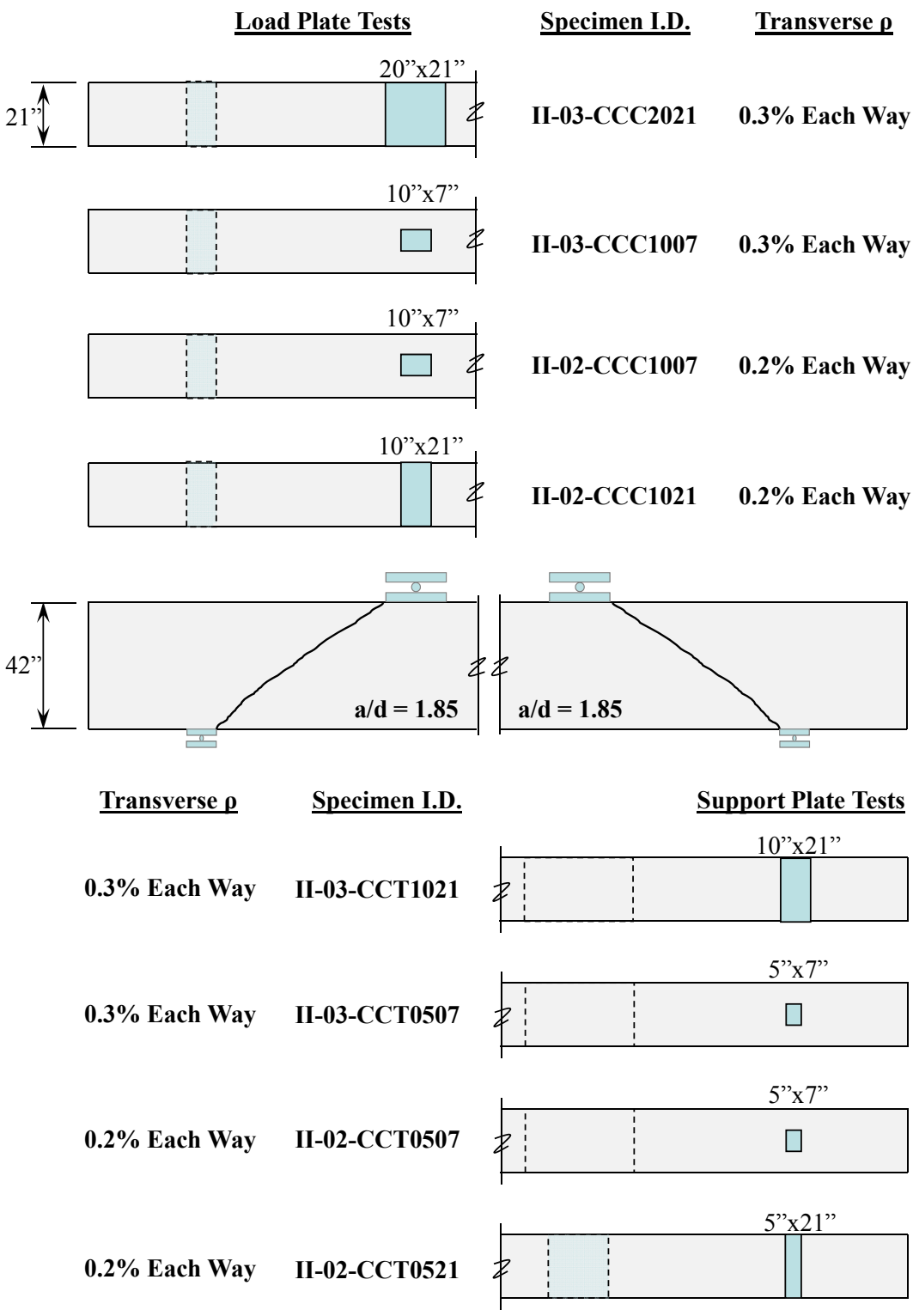

Figure 4.26: Summary of tests within Series II: 21”x42” specimens.

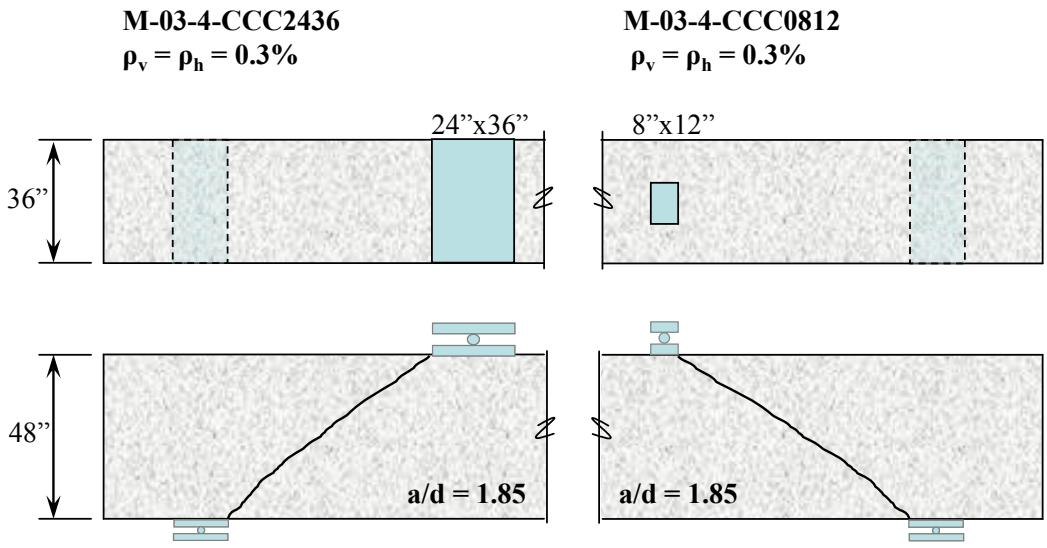

Figure 4.27: Summary of tests within Series M: 36"x48" specimens.

Note, for three of the CCT nodal tests shown in Figure 4.26, the size of the non-critical load plate (CCC node) was 36"x21". A very large load plate was purposely selected in order to ensure that the CCT nodal region would be critical. The non-critical load plate for specimen II-02-CCT0521 was smaller (20"x21"). However, it was large enough to ensure that the CCT nodal region was critical; as evident from the shear capacity and serviceability performance of these test specimens.

In order to address the research objective related to triaxially confined nodes, strength and serviceability data was collected for each test. A summary of the strength results and first diagonal cracking loads are presented for Series II and M beams in Table 4.4. Values are normalized by the compressive strength and square root of the compressive strength of concrete in the same manner as described in Section 4.2. First diagonal cracking loads are not presented for the second test conducted on each specimen.

Table 4.4: Test Results: Series II

Specimen I.D.	f_c' (psi)	V_{test} (kip)	$\frac{V_{test}}{f'_c b_w d}$	V_{crack} (kip)	$\frac{V_{crack}}{\sqrt{f'_c} b_w d}$	f_b / f_c' †
II-03-CCC2021	3290	500	0.19	139	3.0	0.50
II-03-CCC1007	3480	478	0.17	-	-	2.71
II-02-CCC1007	3140	335	0.13	-	-	2.11
II-02-CCC1021	4620	329	0.09	132	2.4	0.47
II-03-CCT1021	4410	636	0.18	-	-	0.69
II-03-CCT0507	4210	598	0.18	146	2.8	4.05
II-02-CCT0507	3120	401	0.16	94	2.1	3.68
II-02-CCT0521	4740	568	0.15	-	-	1.14
M-03-4-CCC2436	4100	1128	0.19	354	3.8	0.45
M-03-4-CCC0812	3000	930	0.22	-	-	4.55

† f_b/f_c' = maximum stress in bearing over specified concrete compressive strength

4.4.3 Strength Results

The shear capacity of the Series II specimens is presented with the cracking patterns at failure in Figure 4.28 and Figure 4.29. Recall, two tests were conducted on each beam specimen. The second test conducted on each specimen is marked as *pre-cracked* in Figure 4.28 and Figure 4.29 to indicate that some cracks were present prior to testing.

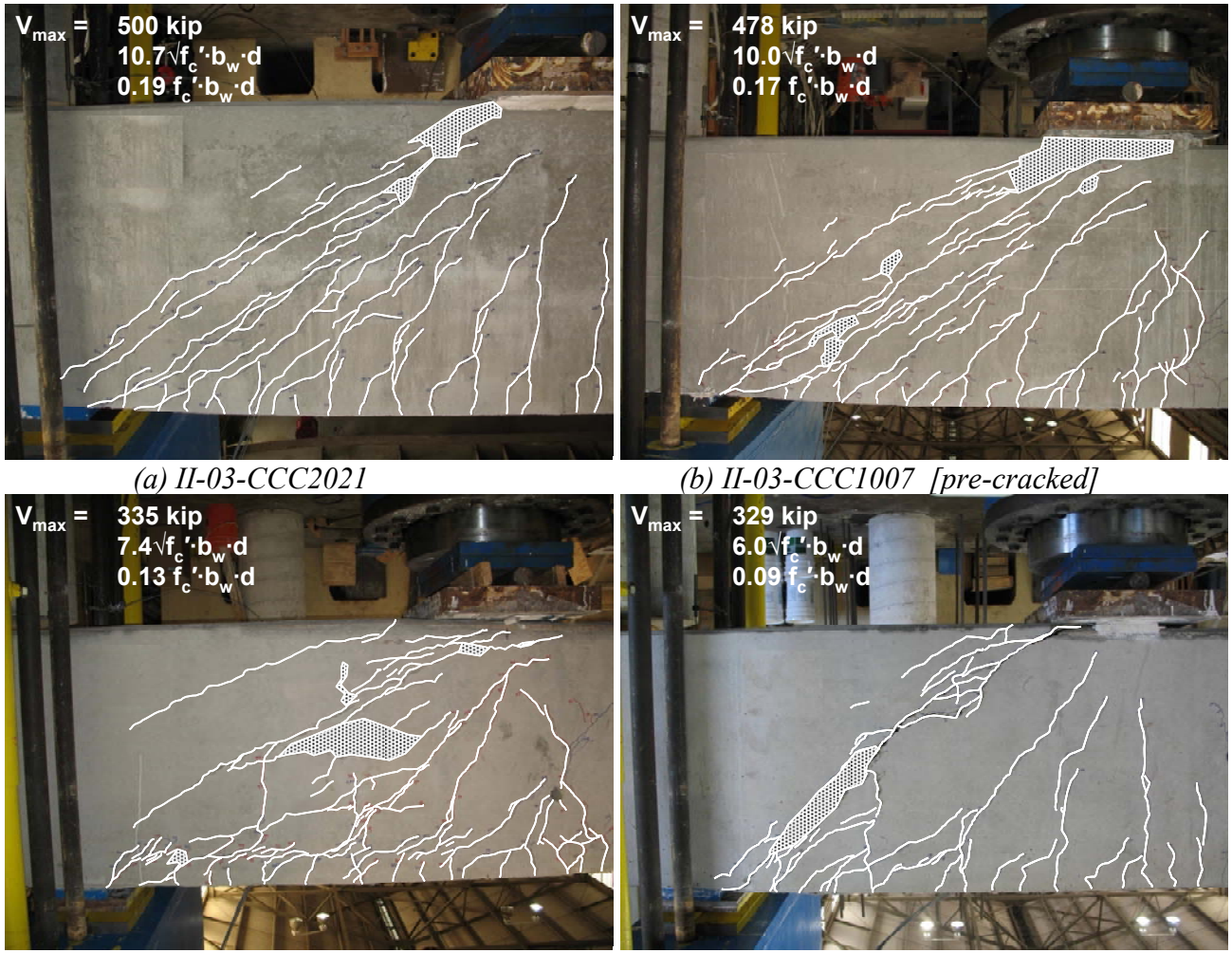

(a) II-03-CCC2021 *(b) II-03-CCC1007 [pre-cracked]*

(c) II-02-CCC1007 [pre-cracked] *(d) II-02-CCC1021*

Figure 4.28: Series II specimens with various bearing plate sizes at the CCC node at failure.

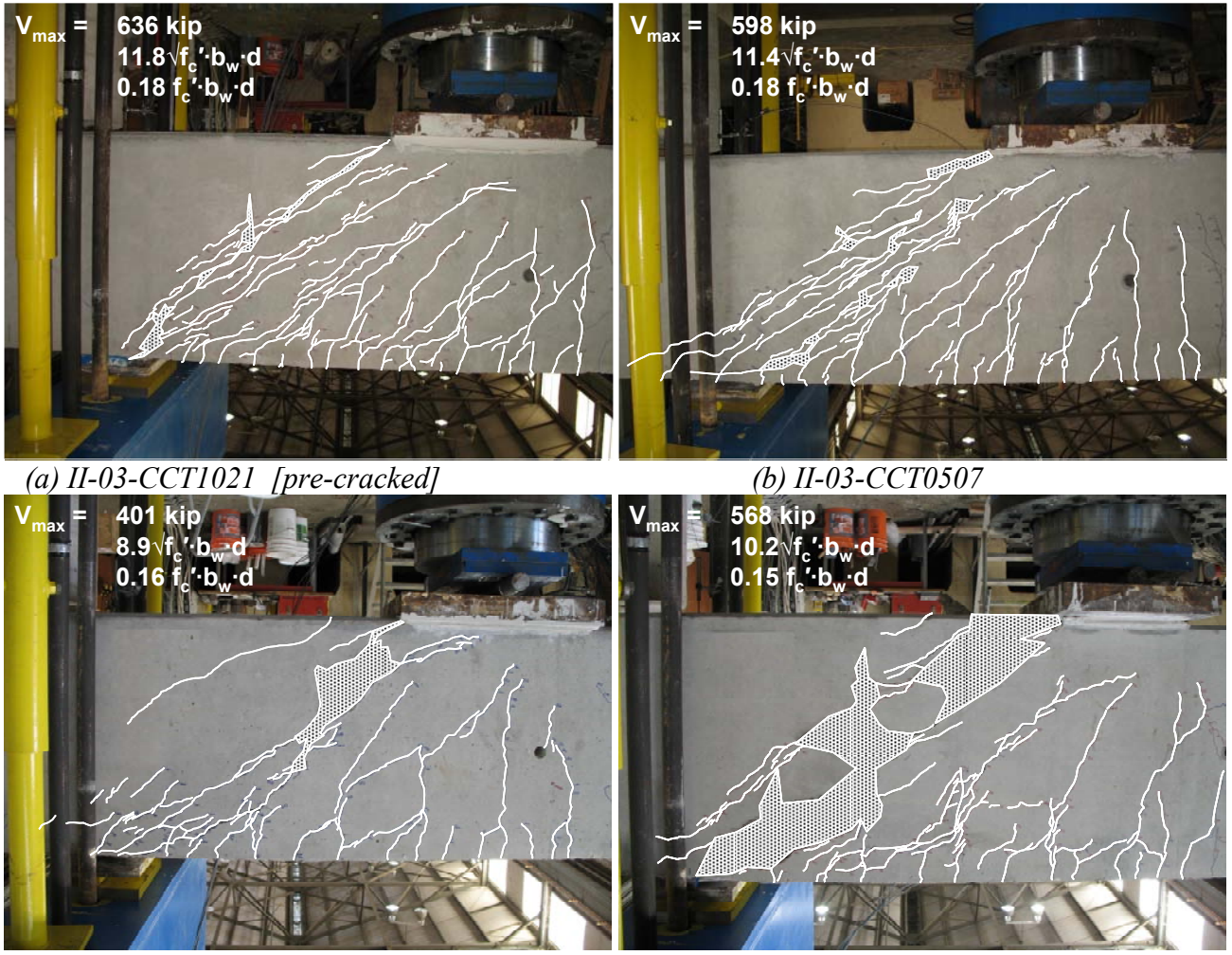

(a) II-03-CCT1021 [pre-cracked] *(b) II-03-CCT0507*

(c) II-02-CCT0507 *(d) II-02-CCT0521 [pre-cracked]*

Figure 4.29: Series II specimens with various bearing plate sizes at the CCT node at failure.

The crack patterns at failure (shown in Figure 4.28 and Figure 4.29) indicate that the formation of a direct strut was the predominant shear transfer mechanism. Parallel cracks between the load point and support delineate the approximate boundary of the strut. Crushing occurred in the compression region adjacent to the load point and along the strut. Therefore, normalizing the capacity values by the compressive strength of concrete is more appropriate than the square root of the compressive strength. Normalization is necessary to account for the unintended differences in the compressive strength of concrete of the specimens at the time of testing.

The normalized capacity of specimens with different support plate (CCT node) dimensions varied between $0.15 f_c' \cdot b_w \cdot d$ and $0.18 f_c' \cdot b_w \cdot d$ (Table 4.4). This difference is within the range of scatter expected with deep beam shear testing. At failure, the stress applied to the bearing plate ranged from 0.7 to $1.1 \cdot f_c'$ for cases in which the CCT nodes were unconfined, and 0.45 to $0.5 \cdot f_c'$ for cases in which the CCC nodes were unconfined. For cases in which confinement was provided at the CCT and CCC nodes, the applied bearing stress was as high as 4.1 and $4.6 \cdot f_c'$, respectively. Therefore, it can be concluded that triaxial confinement allowed the application of bearing stresses much higher than the compressive strength of concrete.

The normalized capacity of specimens with support plates of 10"x21" and 5"x21" was $0.18 f_c' \cdot b_w \cdot d$ and $0.15 f_c' \cdot b_w \cdot d$, respectively (Table 4.4). This difference is minimal considering the inherent scatter in deep beam shear testing. It is unclear why there was not a greater difference in capacity between these tests since the size of the support plate was reduced by a factor of 2 without the benefit of triaxial confinement. It is possible that despite efforts to the contrary, the stress conditions at the CCT node did not govern the behavior of these specimens. This topic may require future research.

The normalized capacity of specimens with different load plate (CCC node) dimensions varied between $0.09 f_c' \cdot b_w \cdot d$ and $0.19 f_c' \cdot b_w \cdot d$ (Table 4.4). Such a significant difference must be attributed to more than the scatter associated with shear testing. Both load plate dimensions and reinforcement details varied among these specimens; the influence of these variables is examined in further detail.

Upon further examination, it can be concluded that the shear capacity of the specimens where the CCC nodes were triaxially confined benefitted from this triaxial confinement. Table 4.5 presents pairs of specimens considered to be nominally identical to each other in all aspects other than the load plate size.

Table 4.5. Effect of Triaxial Confinement for CCC Specimens.

Specimen Comparison	**Load Plate Size *(l x w)***	$\frac{V_{test}}{f'_c \, b_w d}$	f_b / f_c' †
M-03-4-CCC2436	24"x36"	0.19	0.45
M-03-4-CCC0812	8"x12"	0.22	4.55
II-03-CCC2021	20"x21"	0.19	0.50
II-03-CCC1007	10"x7"	0.17	2.71
II-02-CCC1007	10"x7"	0.13	2.11
II-02-CCC1021	10"x21"	0.09	0.47

† f_b/f_c' = maximum stress in bearing over specified concrete compressive strength

An examination of the pairs of test results listed in Table 4.5 illustrates that triaxial confinement provided for bearing stresses higher than the compressive strength of concrete; thereby allowing beam specimens with less than full-width bearings to reach their full shear capacity.

The shear capacity was significantly influenced by the length of the load plate. Upon comparison of specimens II-03-CCC2021 and II-02-CCC1021, it is observed that a reduction in the length of an unconfined load plate from 20"x21" to 10"x21" significantly reduced the shear capacity. It must be noted that both of these specimens contained different amounts of transverse reinforcement (0.3% versus 0.2%). However, it is shown in Section 4.5.2 that the differences in shear capacity of specimens with either 0.3% or 0.2% transverse reinforcement are negligible at a/d ratios of 1.85. Reinforcement in excess of that required to maintain equilibrium of the direct, bottle-shaped strut does not significantly increase the capacity. Therefore, it can be concluded that the length of a load plate at a CCC node has a significant influence on the shear capacity of a deep beam.

4.4.4 Serviceability Results

First cracking loads and crack width data were collected from Series II test specimens. The initial diagonal cracking load was only recorded for the first test conducted on each beam specimen. No pair of first tests exists to isolate the effect of plate size on the diagonal cracking load of deep beams. Variables that affect the first diagonal cracking load are discussed in detail in Section 5.4.

Crack patterns at approximately 90% of capacity and corresponding crack width data are presented in Figure 4.30 through Figure 4.33. The crack widths measured on each face are presented at individual load increments and normalized by the ultimate capacity of the test specimen. The purpose of presenting the crack data in Figure 4.30 through Figure 4.33 is to present a relative comparison between specimens with confined and unconfined bearing plates. For information with regard to an acceptable crack width and corresponding serviceability load level, refer to Section 4.2.2.

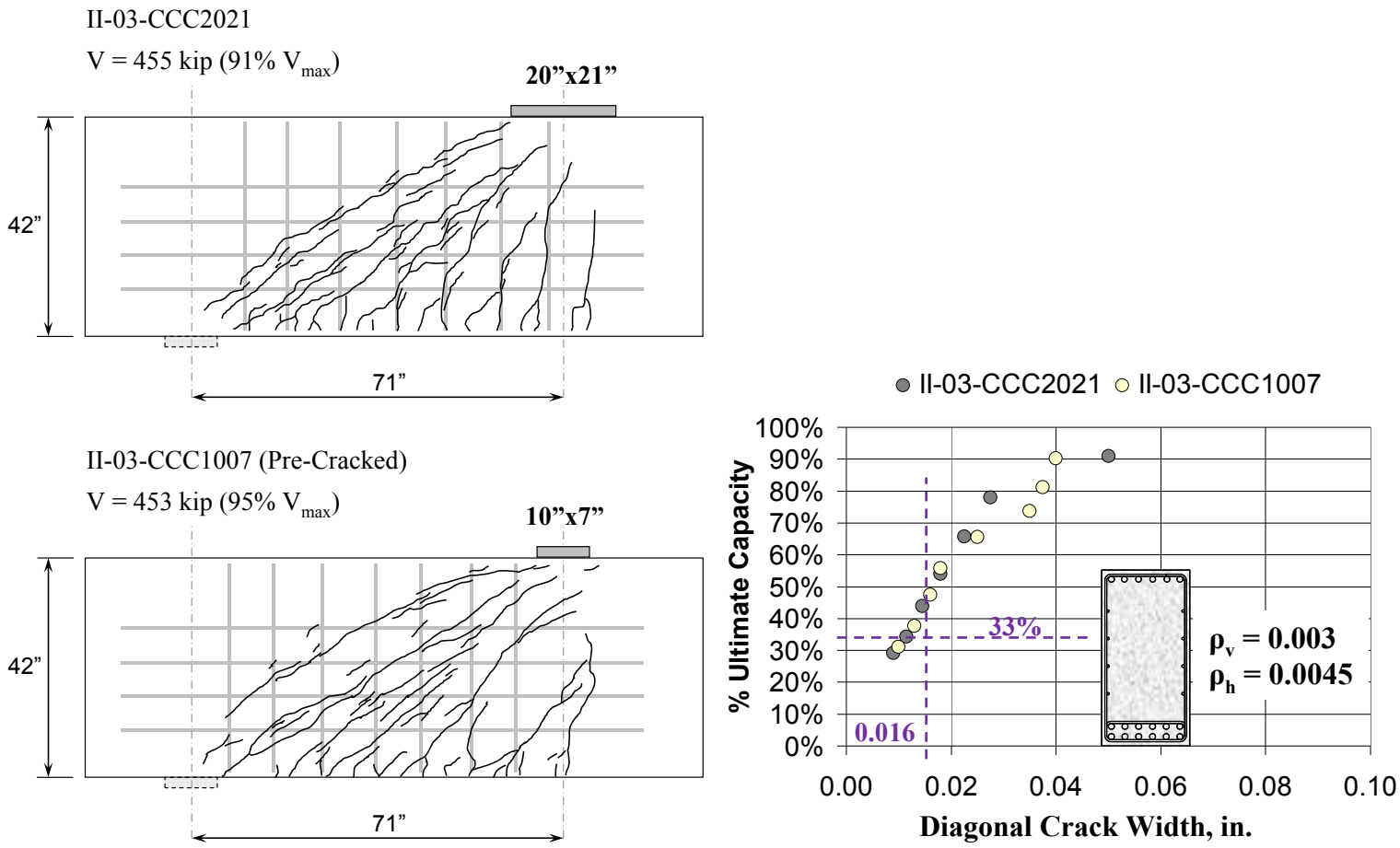

Figure 4.30: Serviceability data for triaxially confined CCC nodes: Crack patterns and widths at approximately 90% of capacity; 0.3% transverse reinforcement in each direction.

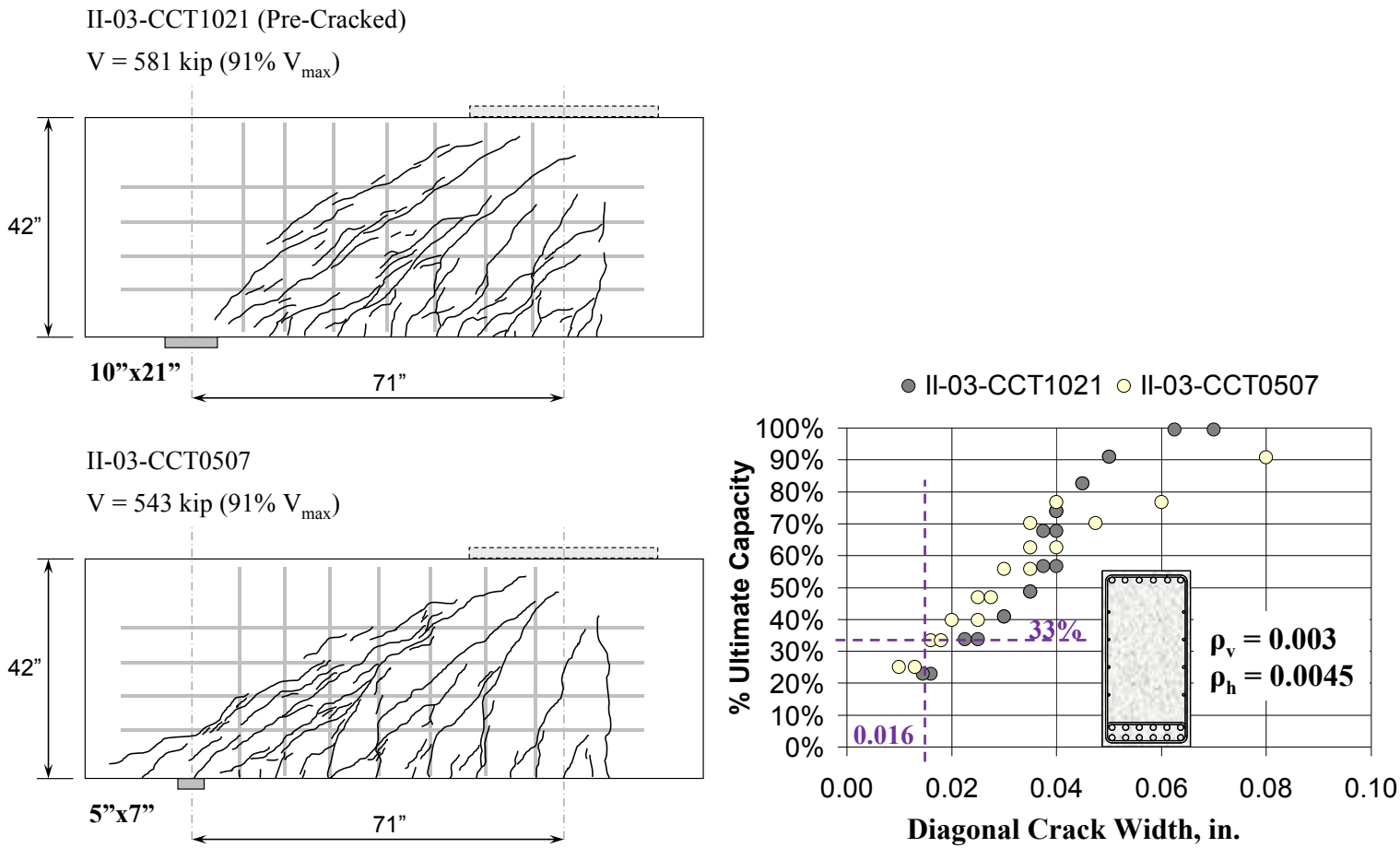

Figure 4.31: Serviceability data for triaxially confined CCT nodes: Crack patterns and widths at approximately 90% of capacity; 0.3% transverse reinforcement in each direction.

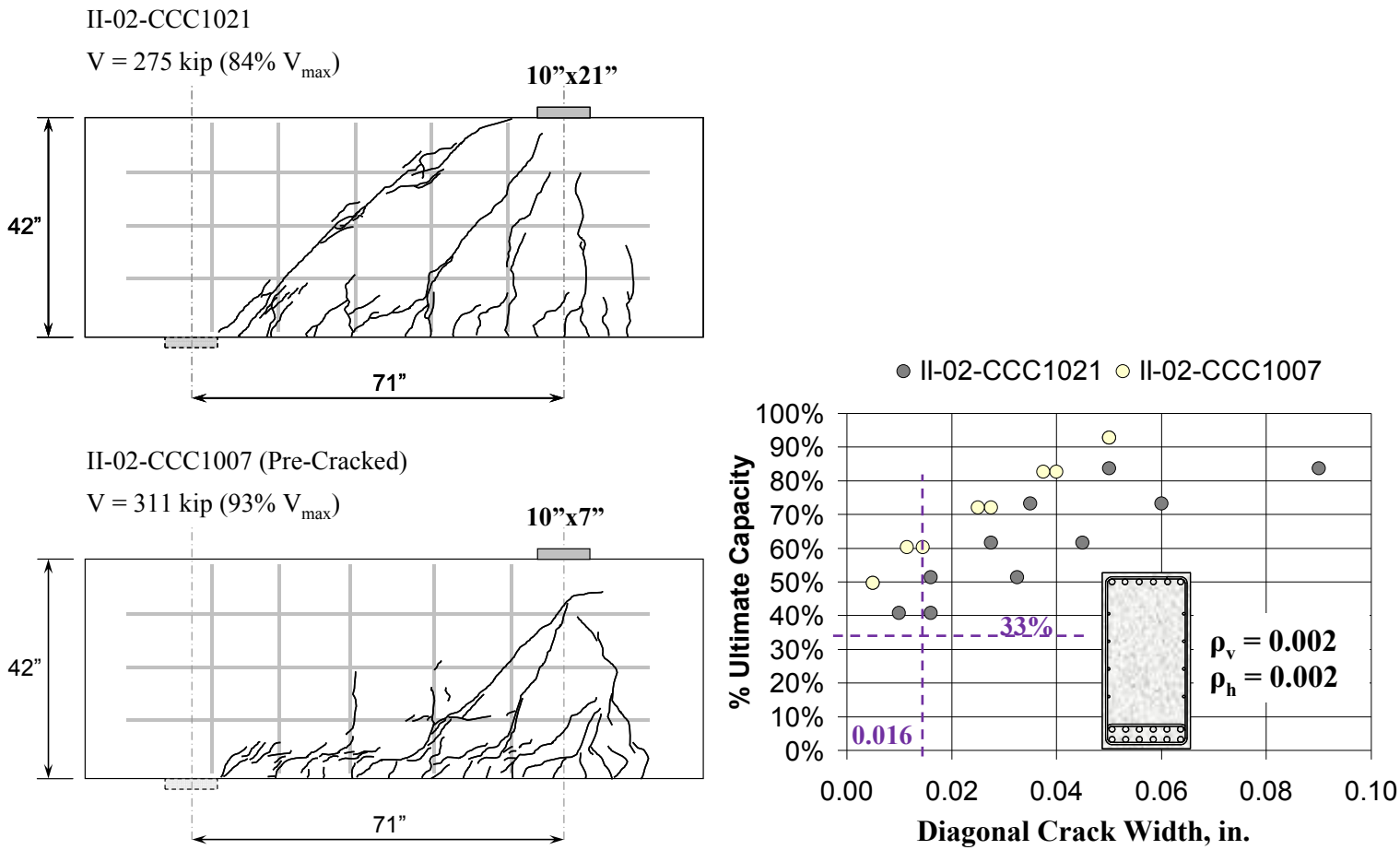

Figure 4.32: Serviceability data for triaxially confined CCC nodes: Crack patterns and widths at approximately 90% of capacity; 0.2% transverse reinforcement in each direction.

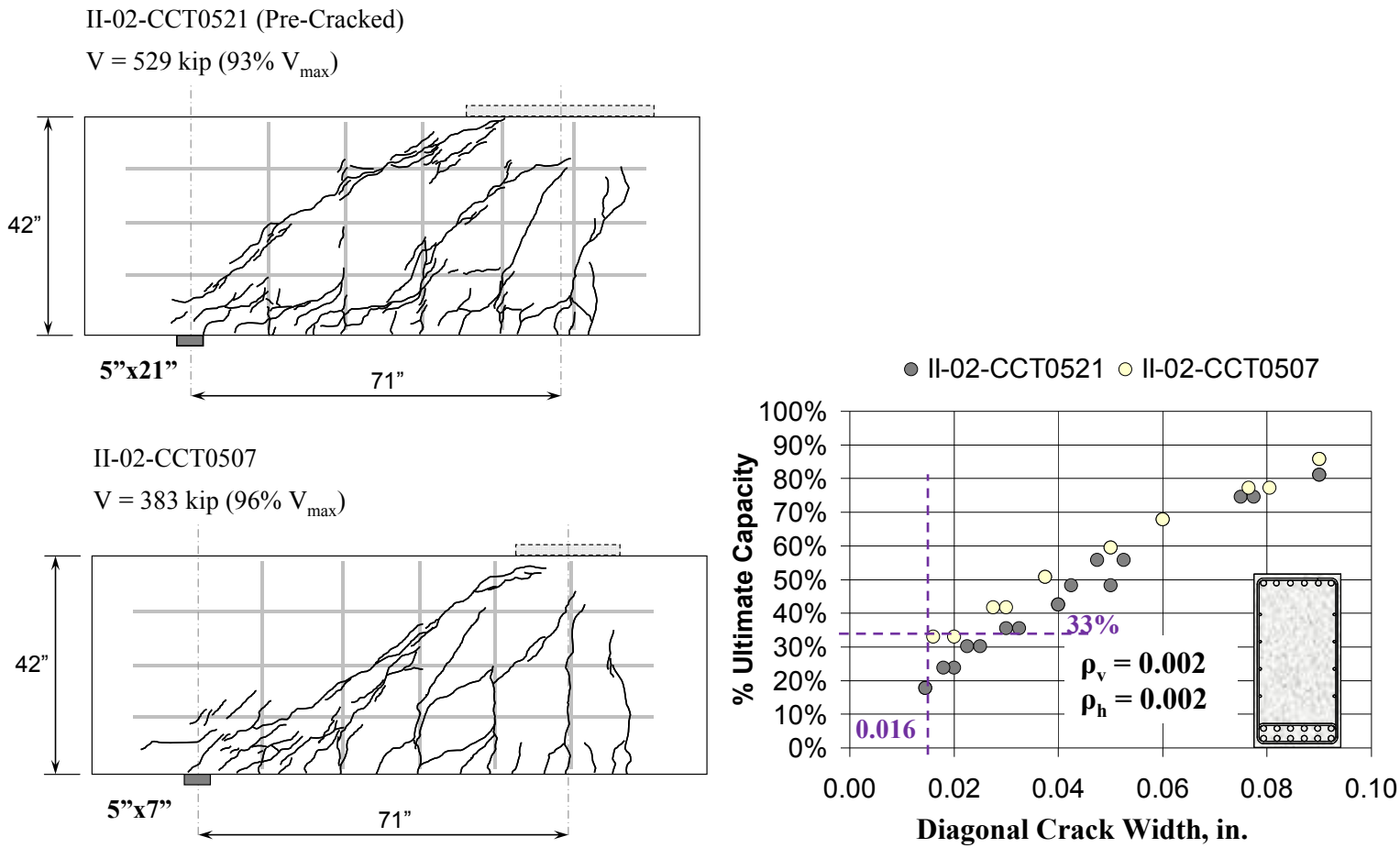

Figure 4.33: Serviceability data for triaxially confined CCT nodes: Crack patterns and widths at approximately 90% of capacity; 0.2% transverse reinforcement in each direction.

By examining the crack width data presented in Figure 4.30 through Figure 4.33, the following observations can be made. For specimens reinforced with a transverse reinforcement ratio of 0.3% in each direction, the size of the load or support plate – triaxially confined or not – did not have a significant influence on the serviceability behavior. For specimens reinforced with a transverse reinforcement ratio of 0.2% in each direction, the serviceability performance as quantified by crack patterns and widths was less regular or predictable. In fact, as shown in Figure 4.33, the maximum diagonal crack widths for the specimens with 0.2% reinforcement exceeding the tolerable crack width limit of 0.016-inches at the estimated service load (33% of ultimate). Therefore, from a serviceability standpoint, a transverse reinforcement ratio of 0.3% in each direction provided a more desirable and consistent performance. It should be noted that the effect of transverse reinforcement on the serviceability performance of deep beams is discussed in detail in Section 4.5.3.

4.4.5 Evaluation of Specimens with Current Code Expressions

A comparison between the experimental capacities and nominal capacities calculated per the ACI 318-08 and AASHTO LRFD (2008) provisions is illustrated in Figure 4.34 for the specimens with varying load plate dimensions at the CCC node; and in Figure 4.35 for the specimens with varying support plate dimensions at the CCT node. The values were normalized by the compressive strength of concrete at the time of testing. The difference in the capacities estimated by using the ACI 318-08 and AASHTO LRFD (2008) provisions is attributed to the different efficiency factors for a single-panel truss model.

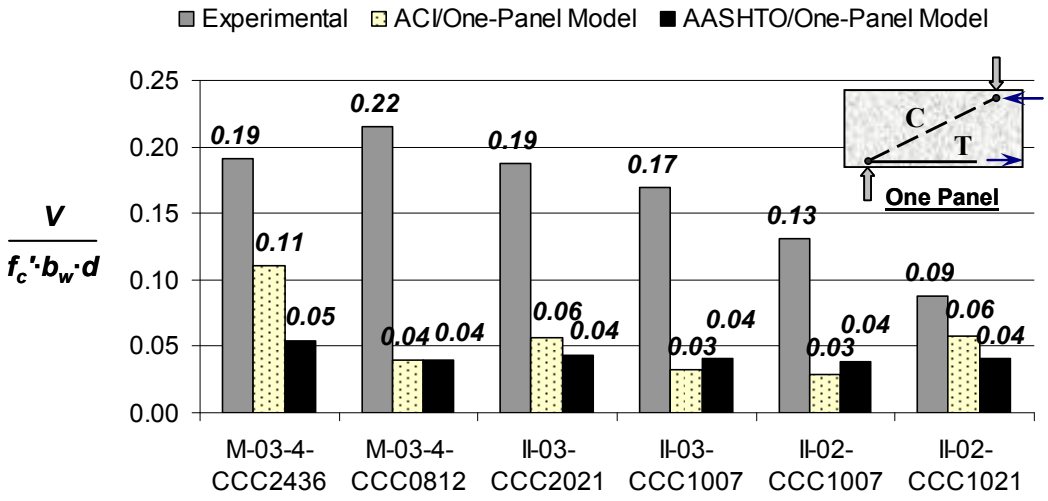

Figure 4.34: Comparison of experimental capacity with ACI 318-08 and AASHTO LRFD (2008) one-panel STM calculations: CCC specimens.

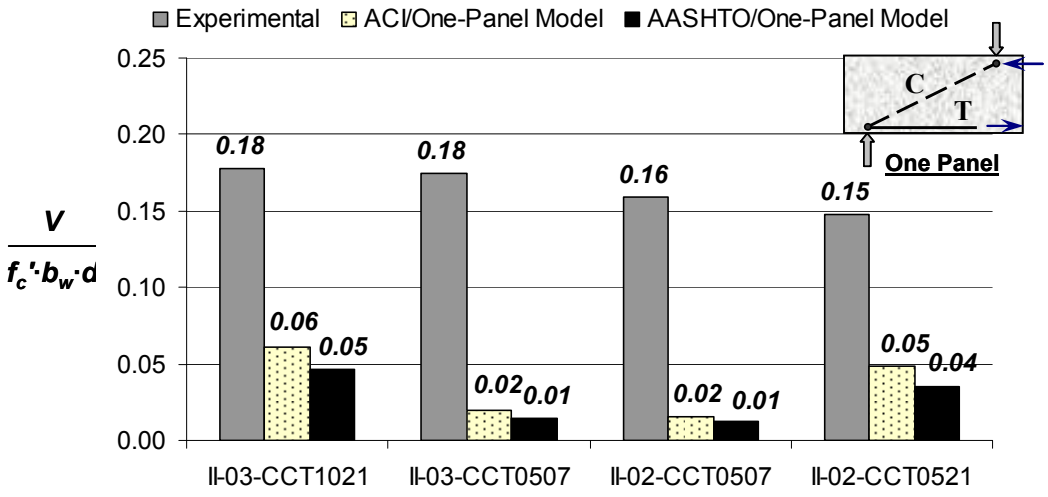

Figure 4.35: Comparison of experimental capacity with ACI 318-08 and AASHTO LRFD (2008) one-panel STM calculations: CCT specimens.

Upon examination of the experimental and calculated capacities presented in Figure 4.34 and Figure 4.35, the following observations can be made.

The AASHTO LRFD (2008) STM provisions are generally more conservative than ACI 318-08. This is likely a result of the fact that the AASHTO LRFD (2008) efficiency factor at the CCT strut-to-node interface reduces as the a/d ratio increases.

The calculated capacity of Specimen II-03-CCC1007 and II-02-CCC1007 was controlled by the efficiency of the strut-to-node interface at the CCC node. The efficiency factor at this boundary is 0.85 according to AASHTO LRFD (2008) and 0.64 according to ACI 318-08. Thus, for this case, ACI 318-08 is more conservative than AASHTO LRFD (2008).

The nominal capacity calculated per the ACI 318-08 and AASHTO LRFD (2008) provisions are overly conservative. The conservatism increases substantially when small bearing plates that triaxially confine the CCC or CCT nodes are provided. This is due to the fact that the capacity calculated by using a STM is directly related to the size of the nodal regions (i.e. size of the bearing plates). Based on these observations, it is proposed that the allowable stresses in triaxially confined nodal regions be increased according to Equation 4.5.

$$m = \sqrt{A_2 / A_1} \leq 2 \tag{4.5}$$

m = triaxial confinement modification factor

The definition of A_2 and A_1 is illustrated in Figure 4.21.

ACI 318-08 §10.14 and AASHTO LRFD (2008) Article 5.7.5 allow for an increase in the bearing capacity of concrete when triaxial confinement is present. However, there is not a provision in place within the STM provisions allowing for a similar increase in the capacity of all six nodal faces in a STM. Thus, it is proposed that the allowable stress at each face of a triaxially confined nodal region be increased by the factor specified in ACI 318-08 and AASHTO LRFD (2008) allowing an increase in the bearing capacity of concrete (Equation 4.5). The implications of increasing the capacity according to Equation 4.5 are presented in Figure 4.36 for ACI 318-08 and Figure 4.37 for AASHTO LRFD (2008).

The ratio of experimental to calculated capacities are presented for all beams within Series II and M whose bearing plates were narrower than the width of the beam (note, a value greater than one represents a beam whose nominal design strength was conservatively estimated).

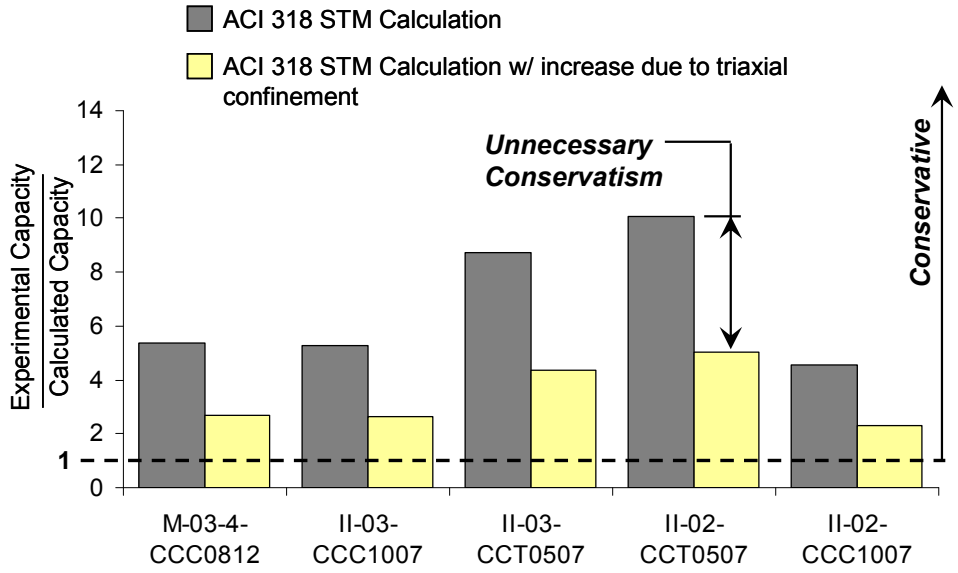

Figure 4.36: Conservatism of ACI 318 STM calculation with and without an increase in capacity due to triaxial confinement.

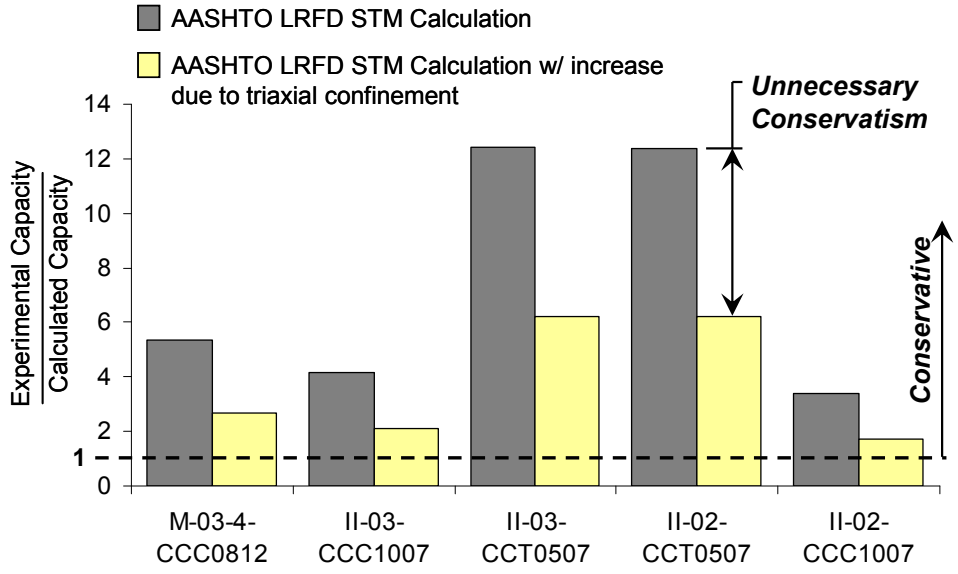

Figure 4.37: Conservatism of AASHTO LRFD STM calculation with and without an increase in capacity due to triaxial confinement.

Based on the data and results of calculations presented in Figure 4.36 and Figure 4.37, it can be concluded that the proposal of increasing the permissible capacity of triaxially confined

nodal regions results in more accurate estimations without compromising conservatism (all experimental / capacity > 1.0). A similar comparison is conducted for all the beams in the filtered database that have a bearing plate narrower than their width (i.e. specimens with triaxially confined nodes). The results from these specimens are illustrated in Figure 4.38 for ACI 318-08 and Figure 4.39 for AASHTO LRFD (2008). Once again, it can be concluded that calculations that allow for an increase in nodal capacity due to triaxial confinement are more accurate without compromising conservatism.

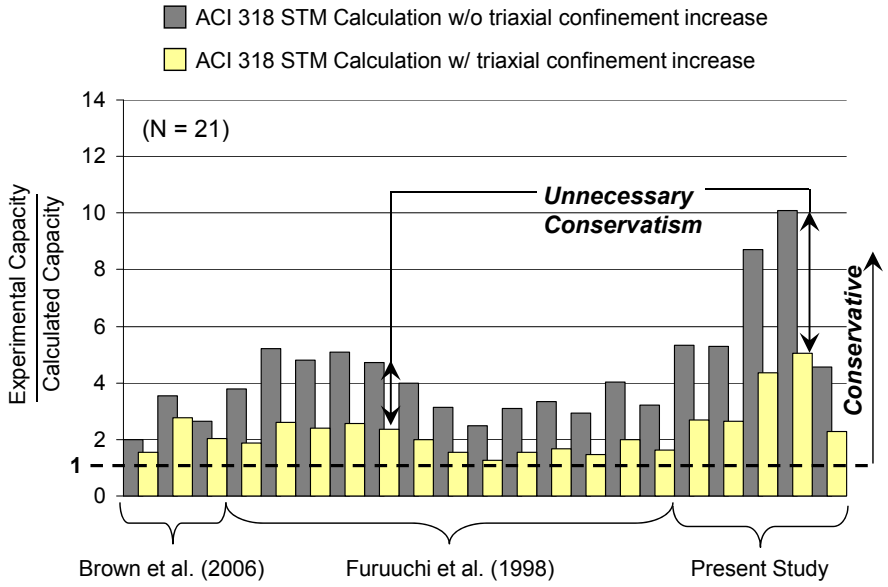

Figure 4.38: ACI 318-08 STM calculations for all beams in database that contain triaxially confined nodal regions.

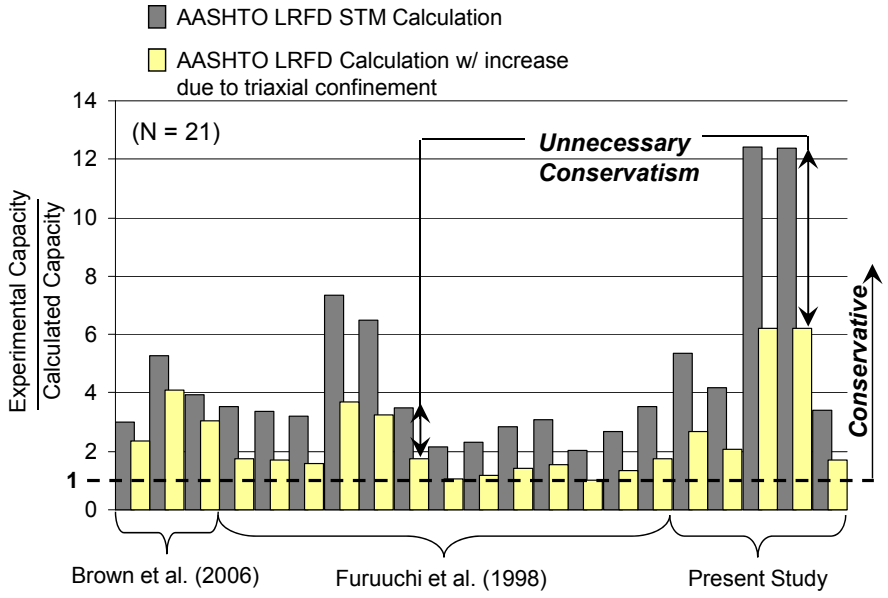

Figure 4.39: AASHTO LRFD (2008) STM calculations for all beams in database that contain triaxially confined nodal regions.

4.4.6 Summary

The purpose of the Series II testing program was to investigate the effects of triaxial confinement in CCC and CCT nodal regions. Two tests on a 36”x48” beam specimen and eight on 21”x42” specimens were conducted at a shear span-to-depth ratio of 1.85. Two transverse reinforcement ratios were investigated: 0.2% and 0.3% in the vertical and horizontal directions.

Based on the results of the testing program, the following conclusions are reached:

- A CCC or CCT node, triaxially confined by surrounding concrete, can achieve bearing stresses much higher than the compressive strength of concrete.
- Reducing the length of a full-width load plate at the CCC node significantly reduced the shear capacity.
- Reducing the length of a full-width support plate at the CCT node did not have a significant influence on the shear capacity. This finding was not expected. It is possible that the stress conditions at the CCT node did not govern for these tests despite efforts to the contrary.
- The serviceability performance (maximum diagonal crack widths) of a deep beam (a/d = 1.85) was not influenced by the size of the bearing plate at the CCC or CCT node, nor was it influenced by presence or absence of triaxial confinement of the bearing plate – provided that the beam contained a ratio of 0.3% transverse reinforcement in each direction.
- For specimens that contained a ratio of 0.2% transverse reinforcement in each direction, the serviceability behavior was more sensitive to the bearing plate configuration and reinforcement details.
- Increasing the ACI 318-08 or AASHTO LRFD (2008) efficiency factors prescribed at all nodal faces by the bearing capacity factor [i.e. triaxial confinement modification factor, *m,* (Equation 4.5)], results in more accurate STM calculations with less unnecessary conservatism (Figure 4.36 through Figure 4.39).

4.5 Minimum Web Reinforcement

In this task, the effect of web reinforcement on the strength and serviceability behavior of reinforced concrete deep beams was evaluated. The purpose of the task was to recommend minimum horizontal and vertical reinforcement that ensured adequate strength and serviceability performance.

4.5.1 Background

Minimum reinforcement provisions that pertain to deep beam design or strut-and-tie model design are compared for several different design specifications. For reference, two other provisions in AASHTO LRFD that specify web reinforcement are discussed as well.

AASHTO LRFD 2008 and CHBDC 2006

There are two different minimum horizontal and vertical reinforcement requirements for deep beam design in AASHTO LRFD 2008. The first requirement is in the strut-and-tie model section (5.6.3.6) of the specification. An orthogonal grid of reinforcement is required at each face such that the ratio of the total reinforcement to the gross concrete area is equal to 0.003 (0.3%). The spacing of the reinforcement is limited to 12-inches. In the commentary, the following excerpt is found:

> *This reinforcement is intended to control the width of cracks and to ensure a minimum ductility for the member so that, if required, significant redistribution of internal stresses is possible.*
>
> *(AASHTO C5.6.3.6, 2008)*

From this note in the commentary, it is evident that strength and serviceability were considered in this provision. The same minimum reinforcement is required in the Canadian Highway Bridge Design Code (CHBDC, 2006).

In Section 5.13.2.3, another minimum reinforcement provision for deep beams exists. Equation 5.13.2.3-2 in AASHTO LRFD is rewritten as Equation 4.6 in this report in terms of the reinforcement ratio.

$$\frac{A_s}{b_v s} \geq \frac{0.12}{\phi f_y} \tag{4.6}$$

with A_s = area of steel within a distance s (in.^{2})
b_v = width of web (in.)
s = spacing of reinforcement (in.)
φ = resistance factor, 1.0 for tension members in STM
f_y = yield strength of reinforcing steel (ksi.)

When f_y is equal to 60-ksi and φ is equal to 1.0 (Section 5.5.4.2), a minimum reinforcement ratio of 0.002 is required. Both vertical and horizontal reinforcement must meet Equation 4.6 and must be well distributed. Maximum spacing for the vertical reinforcement is d/4 or 12-inches; maximum spacing for horizontal reinforcement is d/3 or 12-inches, where d is

the effective depth of the section. There is no indication in AASHTO LRFD (2008) as to whether this provision was based on strength or serviceability requirements.

CSA A23.3-04 and fib (CEB-FIP) 1999

The same minimum reinforcement requirements for deep beams are listed in the Canadian Building code and the *fib* recommendations. An orthogonal grid of reinforcement is required at each face such that the ratio of the total reinforcement to the gross concrete area is equal to 0.002 (0.2%) (CSA A23.3-04 11.4.5, 2004 and *fib* 7.3.2, 1999). There is no indication in either document as to the specific purpose of the reinforcement, i.e. for strength or both strength and serviceability. Maximum spacing is restricted to 12-inches.

ACI 318-08

There are two minimum reinforcement provisions that pertain to deep beam design in ACI 318-08. If the deep beam design provisions in section 11.8 are used, then reinforcement ratios of 0.0025 and 0.0015 are required in the vertical and the horizontal directions, respectively. Maximum spacing of the reinforcement in both cases shall not exceed d/5 or 12-inches. It is interesting to note that 0.25% reinforcement was required in the horizontal direction and 0.15% reinforcement was required in the vertical direction for this provision in ACI 318-71 through ACI 318-95. Data obtained from research conducted by Rogowosky et al. in 1986 indicated that vertical reinforcement was more effective than horizontal reinforcement in terms of the shear strength of deep beams. As such, the provision was changed. No indication of serviceability performance was indicated in the paper by Rogowsky et al. (1986). In the commentary, however, it is stated that the maximum spacing was reduced to 12-inches from 18-inches because "the steel is provided to restrain the width of the cracks" (ACI 318-08 R11.8.4, 2008). Therefore, while this provision may not be based on serviceability considerations, ACI 318 acknowledges that the minimum reinforcement requirement should address serviceability.

If the strut-and-tie requirements of Appendix A are used in deep beam design, then the minimum reinforcement provisions for concrete struts apply. If a concrete strut efficiency factor, β_s, of 0.75 is used, then reinforcement satisfying Equation 4.7 must be provided. This reinforcement is "*related to the tension force in the concrete due to the spreading of the strut*" and is depicted in Figure 4.40 (ACI 318-08 RA.3.3). Due to the sin α_i term, this requirement favors the placement of reinforcement perpendicular to the axis of the strut, or the assumed inclination of the diagonal cracks. However, there is no requirement for a minimum amount of reinforcement in either the horizontal or vertical directions. It is up to the discretion of the designer. If the same amount of reinforcement is desired in both directions, then Equation 4.7 requires a reinforcement ratio of approximately 0.0022 in each direction for the range of applicable values of theta, i.e. between 25 and 65 degrees. If a more efficient placement of reinforcement is desired with a minimum of 0.0015 in each direction, the required reinforcement ratio in the horizontal and vertical directions are those depicted in Figure 4.41 and Figure 4.42, respectively.

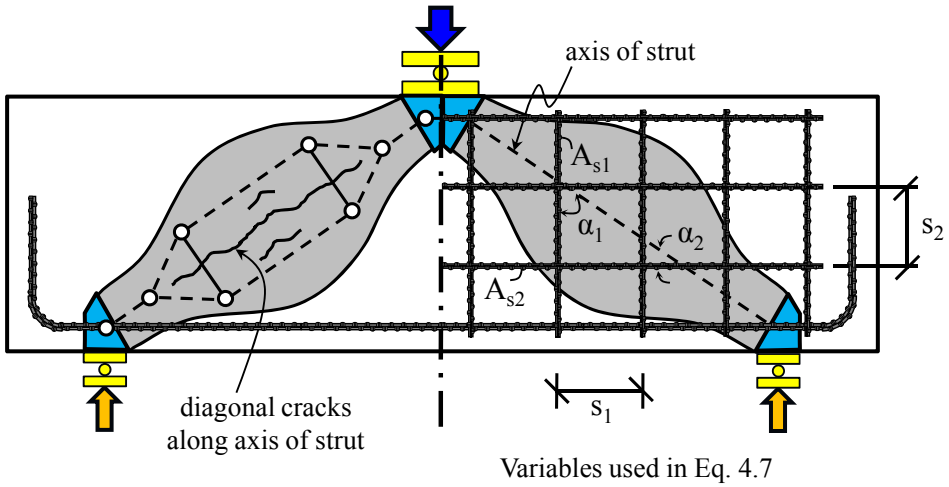

Figure 4.40: Deep beam showing nomenclature for Equation 4.7

$$\rho_{\perp} = \sum \frac{A_{si}}{b_s s_i} \sin \alpha_i \geq 0.003 \tag{4.7}$$

with A_s = area of reinforcement in the i-th later crossing strut (in.^{2})
b_s = width of strut perpendicular to the plane of reinforcement (in.)
s_i = spacing of reinforcement in i-th layer adjacent to surface of the member (in.)
α_i = angle between axis of strut and i-th layer of reinforcement

If a lower concrete strut efficiency factor, β_s, of 0.60 is used with the strut-and-tie method of ACI Appendix A, no minimum reinforcement is required. It is assumed that the tensile strength of the concrete can resist the transverse tension in the bottle-shaped struts depicted in Figure 4.40. With a lower efficiency factor, deep beams without transverse reinforcement can be designed according to ACI Appendix A. Relying on the tensile strength of concrete does not seem appropriate.

TxDOT 4371 Minimum Reinforcement Recommendations

In TxDOT Project 4371, an equation for minimum reinforcement was developed based on strength. Specifically, the reinforcement required to resist the transverse tension forces associated with spreading compressive stresses in a bottle-shaped strut is calculated with Equation 4.8 (Figure 4.40). The equation is a function of the force in the strut and the slope of the angle of dispersion of the compressive stresses in the strut, m. It was recommended that this slope be calculated with a variable angle of dispersion model developed by Schlaich and Weischede (1982). When applied to the database, an equivalent reinforcement ratio perpendicular to the strut axis of 0.0015 (0.15%) is required by Equation 4.8 on average. Therefore, in general, half as much reinforcement is required according to Equation 4.8 compared to Equation 4.7. This difference is primarily attributed to the variable angle of dispersion used in the 4371 approach as opposed to ACI which assumes that the slope of the angle of dispersion, m, is 2. In the project 4371 report, it was stated that the amount of reinforcement according to Equation 4.8 was intended for strength only; additional research was

recommended to determine the serviceability demand. More detailed information of the 4371 minimum reinforcement recommendation and the variable angle of dispersion model can be found elsewhere (Brown et al., 2006).

$$\rho_{\perp \min} = \frac{\nu_R f'_c A_c \sin\theta}{f_y b d m} \tag{4.8}$$

with ν_R = efficiency factor for reinforced struts developed in Project 4371
f'_c = compressive strength of the concrete (psi)
A_c = minimum cross-sectional area of the strut (in.^{2})
θ = angle of strut with respect to the horizontal
f_y = yield strength of web reinforcement (psi)
b = width of strut (in.)
d = effective depth of the strut (in.)
m = slope of the angle of dispersion

Other minimum reinforcement provisions in AASHTO LRFD

In addition to the aforementioned provisions for deep beams, there are other minimum web reinforcement requirements for reinforced concrete members. Two relevant provisions include minimum transverse reinforcement required for members analyzed with a sectional shear model (i.e. $V_c + V_s$) and minimum skin reinforcement required for the webs of members with large depths. For simplicity, only the AASHTO versions of these provisions are presented.

In the sectional shear design provisions of AASHTO LRFD 2008, Equation 4.9 is listed. With this equation, it is ensured that enough steel is present in the member to resist half of the concrete contribution to shear strength when performing a sectional analysis. When the compressive strength of the concrete is 4-ksi and the yield strength of the steel is 60-ksi, a reinforcement ratio of 0.001 (0.1%) is specified with Equation 4.9. This provision is solely based on strength considerations.

$$A_v \geq 0.0316\sqrt{f'_c}\,\frac{b_v s}{f_y} \tag{4.9}$$

with A_v = area of transverse reinforcement within a distance s (in.^{2})
f'_c = compressive strength of the concrete (ksi)
b_v = width of web (in.)
s = spacing of transverse reinforcement (in.)
f_y = yield strength of the reinforcement (ksi)

In Section 5.7.3.4 of AASHTO LRFD, another requirement for web reinforcement exists (2008). It is reproduced as Equation 4.10. This provision applies to members with depths greater than 36-inches. The reinforcement must be distributed within the distance $d_e/2$ from the tension face of the member at a spacing of $d_e/6$ or 12-inches, where d_e is the effective member depth. The purpose of this provision is to restrain flexural cracks throughout the tension region of members of large depth. As such, it is based on serviceability considerations. It is important

to note that the area of reinforcement calculated in Equation 4.10 is the amount per face and per foot of section height.

$$A_{sk} \geq 0.012(d_e - 30) \leq \frac{A_s + A_{ps}}{4} \tag{4.10}$$

with A_{sk} = area of skin reinforcement on each side face in in.^{2} / ft. of height
d_e = effective member depth (in.)
A_s = area of tension reinforcement (in.^{2})
A_{ps} = area of prestressed reinforcement (in.^{2})

Equation 4.10 can be rewritten in terms of the reinforcement ratio based off the full width of the section and the tension region of the member (d_e/2). In this way, it can be directly compared to the aforementioned minimum reinforcement requirements. The rewritten equation is presented as Equation 4.11. Values computed with Equation 4.11 are plotted with assumed values of b_w with respect to the effective depth of the member in Figure 4.41.

$$\rho_{g\_sk} \geq \frac{0.002(d_e - 30)}{b_w} \tag{4.11}$$

with ρ_{g_sk} = reinforcement ratio calculated from total web reinforcement according Equation 4.10 and distributed within half the member depth
b_w = width of web (in.)

Comparison of minimum reinforcement provisions

The aforementioned provisions for minimum reinforcement in the horizontal and vertical directions are compared in Figure 4.41 and Figure 4.42, respectively. The minimum reinforcement requirement of Project 4371 was omitted from the following plots due to the large number of variables that are required to plot it. For some of the other provisions, minor assumptions were necessary to plot the equations in each graph. These assumptions are listed in Table 4.6.

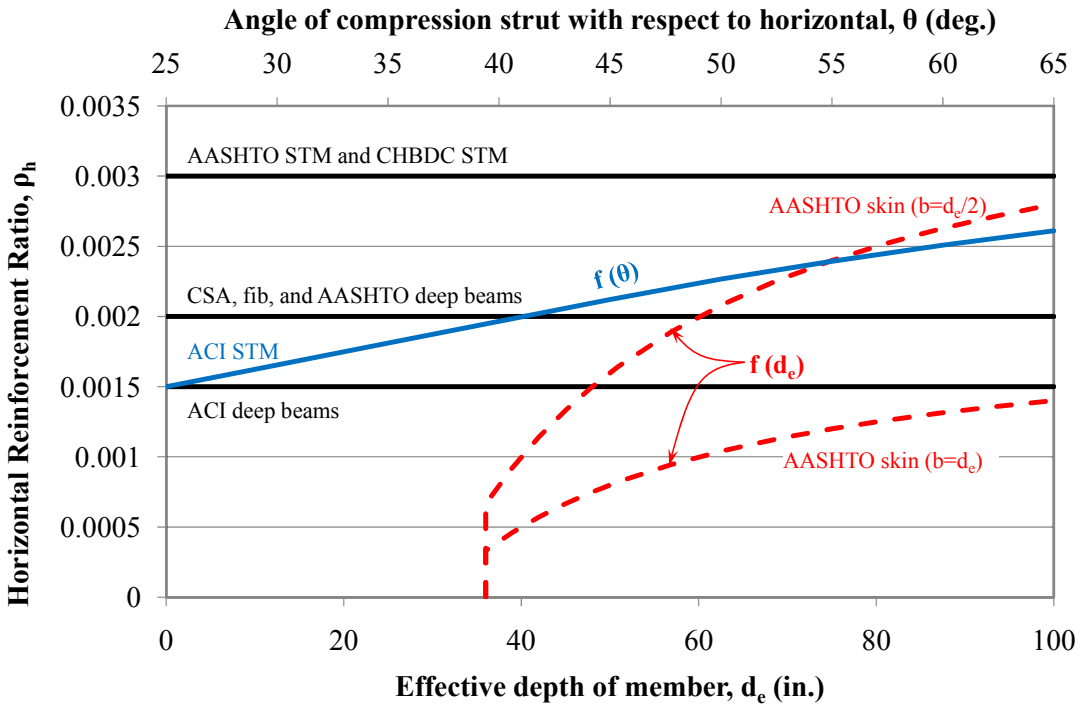

Figure 4.41: Minimum horizontal reinforcement for deep beams in several specifications

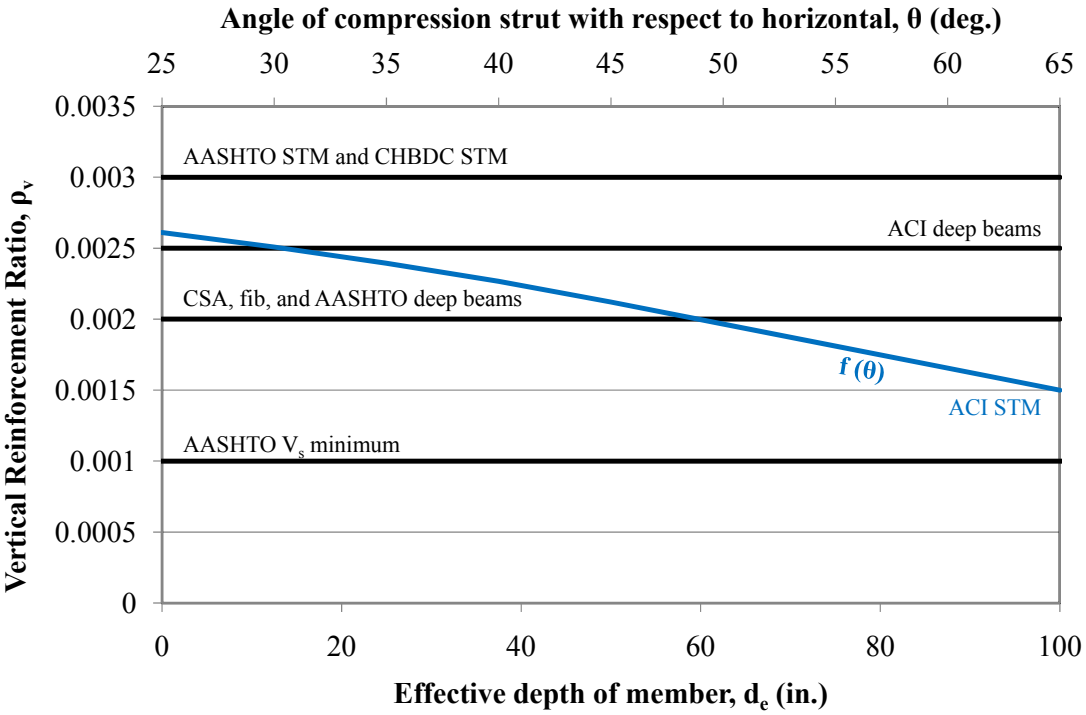

Figure 4.42: Minimum vertical reinforcement for deep beams in several specifications

Table 4.6: Assumptions made to plot minimum web reinforcement provisions

Use	Provision	ρ_h (%)	ρ_v (%)	Assumption for plotting
Deep Beams	AASHTO & CHBDC STM	0.3	0.3	N/A
	AASHTO Deep Beam	0.2	0.2	f_y = 60 ksi
	CSA / *fib*	0.2	0.2	N/A
	ACI Deep Beams	0.15	0.25	N/A
	ACI STM	function of θ		Minimum ρ_h & ρ_v = 0.0015
Other	AASHTO sectional	N/A	0.1	f'_c = 4 ksi & f_y = 60 ksi
	AASHTO skin	function of d_e	N/A	$b_w = d_e$ & $b_w = d_e/2$

In Figure 4.41 and Figure 4.42, it is evident that the minimum reinforcement provisions in several building and bridge design specifications differ for deep beams. The required minimum reinforcement in AASHTO LRFD 2008 and CHBDC 2006 corresponding to 0.003 in each direction is the most stringent requirement. In the commentary of AASHTO LRFD, it is stated that 0.003 in both directions is for both strength and serviceability considerations. The other minimum reinforcement requirements for deep beams plotted in Figure 4.41 and Figure 4.42 range from 17% to 50% lower. The minimum reinforcement provision in the ACI STM specification (Equation 4.7 and blue line in above figures) is a function of the axis of the diagonal strut, or the a/d ratio for single-panel models. When the angle of the strut with respect to the horizontal approaches the lower limit (a/d ≈ 2), the ACI STM reinforcement is very similar to those in the ACI deep beam section (ρ_v = 0.0025, ρ_h = 0.0015). At a/d ratios close to 1 (θ = 45-degrees), the ACI STM reinforcement approaches the minimum reinforcement provisions in the Canadian Building Code and *fib* (0.2% in each direction). Thus, these minimum reinforcement requirements do not differ greatly; they are similar to 0.2% in each direction. It is not clear in the commentary of these specifications if 0.2% is intended to address strength and serviceability requirements.

In Figure 4.41 and Figure 4.42, two other minimum reinforcement provisions that do not explicitly address deep beam behavior are plotted for reference. The AASHTO sectional shear requirement for minimum reinforcement (Equation 4.9) is considerably lower than those for deep beams (Figure 4.42). The reason for this discrepancy is that deep beams are strongly influenced by shear behavior whereas Bernoulli beams are often governed by flexure. The AASHTO skin reinforcement provision (Equation 4.11) is also compared to minimum reinforcement requirements for deep beams (Figure 4.41). It is clear that the quantity of required skin reinforcement increases with increasing depth of the member. For most applications, the reinforcement according to this provision will be less than or equal to a ρ_h of 0.002. It is important to note that this provision is intended to restrain the width of flexural cracks which are oriented perpendicular to the reinforcement.

In the current task, the strength and serviceability performance of deep beams with reinforcement corresponding to 0.2% in each direction, 0.3% in each direction, and several other distributions were compared.

4.5.2 Strength Results

The effect of web reinforcement on the strength of deep reinforced concrete members was determined with the evaluation database and through the current experimental program.

Strength Results from the Evaluation Database

The experimental strength of the 179 beams in the evaluation database was plotted versus the horizontal and vertical reinforcement ratio of the member in Figure 4.43 and Figure 4.44, respectively. The data was sorted into 5 groups by a/d ratio. All of the beams in the evaluation database have at least an angular summation of web reinforcement equal to or greater than 0.1%. Based on Brown et al., this amount of reinforcement was considered to be the minimum required to satisfy equilibrium in the bottle-shaped strut (2006). As such, the following plots were used to assess the effect of additional web reinforcement on the strength of deep beams.

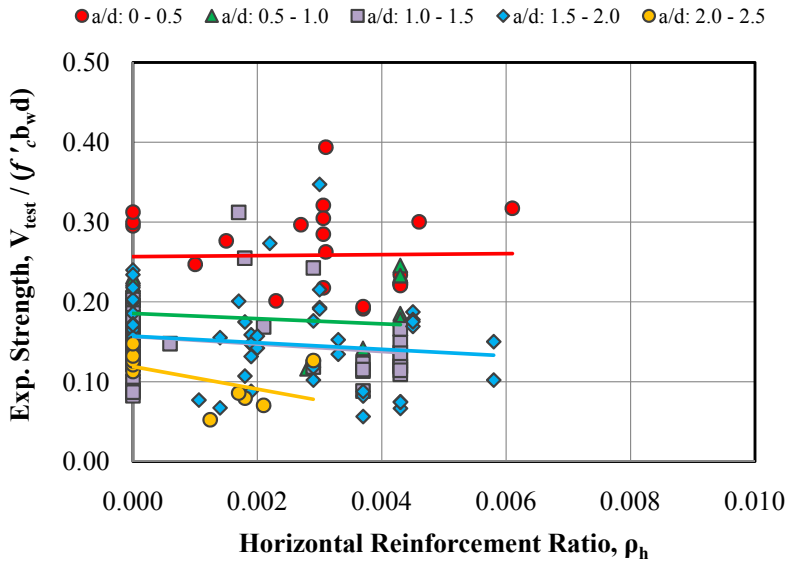

Figure 4.43: Effect of horizontal reinforcement on strength of beams in evaluation database

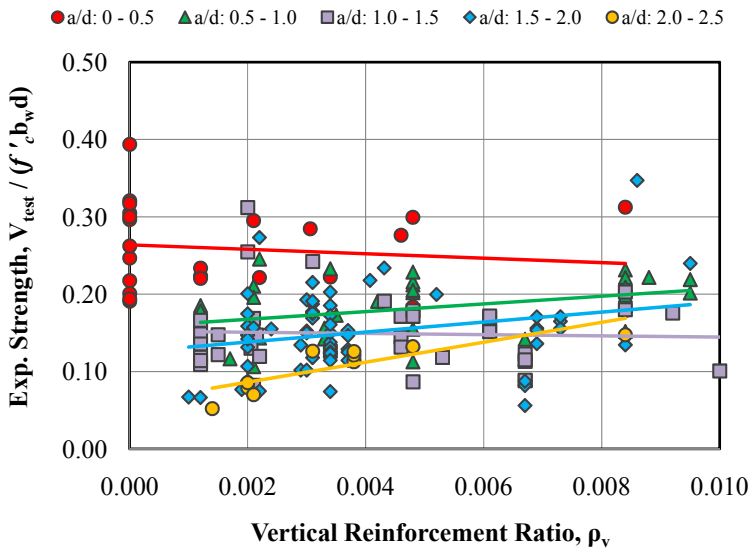

Figure 4.44: Effect of vertical reinforcement on strength of beams in evaluation database

In Figure 4.43, it is clear that horizontal reinforcement has little effect on the shear strength of deep beams. This conclusion was echoed by many previous researchers. Smith and Vantsiotis (1982), Rogowsky et al. (1986), Oh and Shin (2001), Tan et al. (1997), and Brown et al. (2006) concluded that horizontal reinforcement did not have an appreciable effect on the shear strength of deep beams, especially for a/d ratios exceeding 1.0. Kong et al. noted that horizontal reinforcement was only effective at low a/d ratios (0.35) and if it was spaced near the tension reinforcement (1970). With this arrangement, the horizontal reinforcement improves the distribution of the stresses in the primary tension tie, but does not reinforce the bottle-shaped strut.

In Figure 4.44, the effect of vertical reinforcement on the shear strength of deep beams is illustrated. For a/d ratios less than or equal to 1.5, a negligible increase in shear strength is seen for increasing amounts of vertical reinforcement. The same observation was made by De Paiva and Seiss (1965), Rogowsky et al. (1986), and Brown et al. (2006). For a/d ratios approaching and exceeding 2.0, a slight increase in shear strength is seen for increasing amounts of vertical reinforcement (Figure 4.44). This conclusion was reached by several researchers as well (Kong et al., 1970, Smith and Vantsiotis, 1982, Oh and Shin, 2001, and Tan et al., 1997). In short, the effect of web reinforcement on the shear strength of deep beams can be classified as nominal and is most evident at higher a/d ratios (a/d > 1.5).

It is clear that web reinforcement does not play the same role in deep beam behavior as it does in Bernoulli beam behavior. The purpose of web reinforcement, in terms of a single-panel strut-and-tie analysis, is to resist the transverse tensile forces developed in a bottle-shaped strut. Increasing the amount of web reinforcement above the amount required to resist these transverse stresses does not significantly improve the shear strength of the member. As the a/d ratio increases and the behavior of the beam transitions from a deep beam to a Bernoulli beam, the effectiveness of vertical reinforcement increases.

The effect of web reinforcement on the diagonal cracking load as a percentage of the ultimate strength was also assessed with the evaluation database. Normalizing the diagonal cracking load with the ultimate strength of the member quantifies the strength after first diagonal

cracking. The results are plotted in Figure 4.45 and Figure 4.46 versus the quantity of web reinforcement in each orthogonal direction. In Figure 4.45, a slight trend with ρ_v exists. With increasing amount of vertical reinforcement, the diagonal cracking load as a function of the ultimate strength slightly decreases. This trend indicates that vertical reinforcement in addition to that required for equilibrium does slightly affect the strength of deep beams by providing reserve strength after first cracking. Additional vertical reinforcement improves the distribution of stress in the deep beam leading to a more robust member. In Figure 4.46, a trend with the amount of horizontal reinforcement is not apparent for the data as a whole. However, the trend of the data from the current project suggests a similar, but reduced benefit with respect to ρ_h as to ρ_v. In both cases, it appears that additional reinforcement provides additional redistribution capacity in the member. For a handful of specimens with less crack control reinforcement than 0.2-% in each orthogonal direction, the reserve strength after first cracking was exceptionally small.

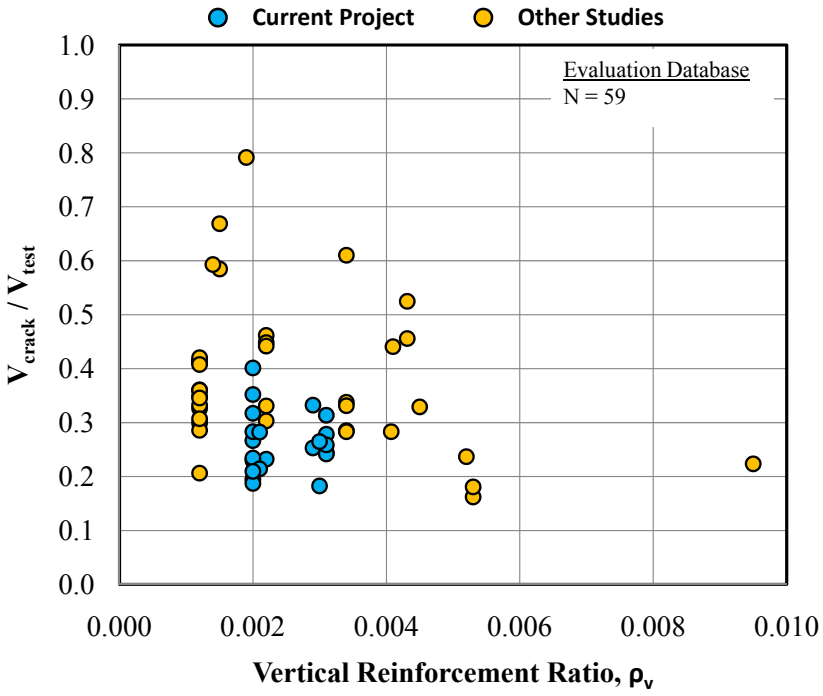

Figure 4.45: Effect of vertical web reinforcement on strength after first cracking

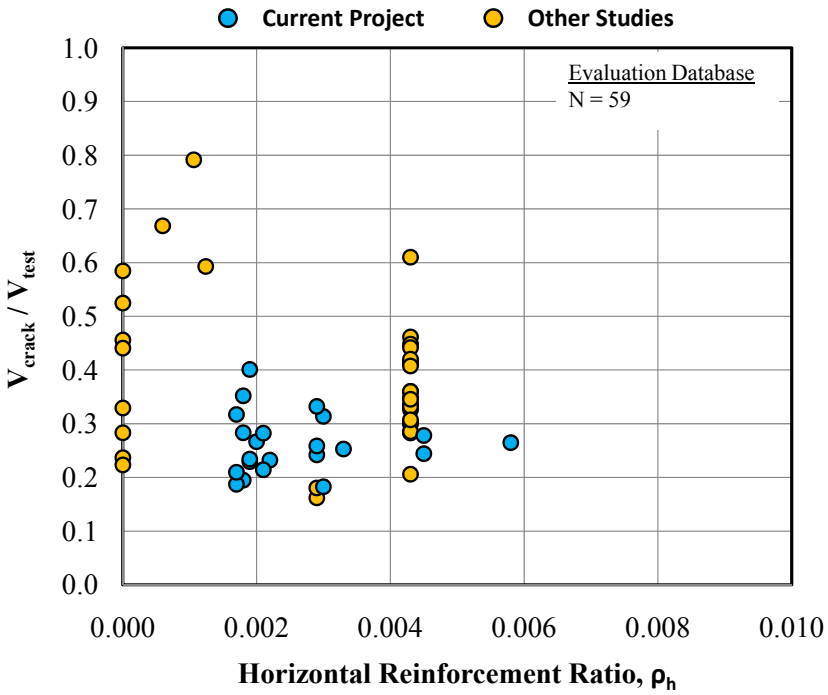

Figure 4.46: Effect of horizontal web reinforcement on strength after first cracking

Strength Results from the Experimental Program

In the current experimental program, numerous tests were conducted in which the amount of web reinforcement was the primary variable. Most of these tests were performed at a shear-span-to-depth (a/d) ratio of 1.85. Two specimens were tested at an a/d ratio of 1.2; three specimens were tested at an a/d ratio of 2.5. The majority of the testing for this task was performed within Series III in which different quantities of web reinforcement were provided in each test region. Tests conducted within other series in which the quantity of web reinforcement was the only variable were also used in the current task. All of the tests in the experimental program that were relevant to the minimum web reinforcement task are listed in Table 4.7. The experimental shear strength and the amount of web reinforcement for each specimen are provided. It should be noted that the reinforcement ratios were calculated using the equations provided in Section 3.2.3. The vertical reinforcement was spaced evenly throughout the test region. The horizontal reinforcement was placed evenly throughout the effective strut area. The horizontal and vertical spacing of the reinforcement was not a primary variable in the testing program.

Table 4.7: Summary of strength results for specimens in minimum reinforcement task

Beam I.D.	b_w in.	d in.	ρ_v	Bar size	s_v in.	ρ_h	Bar size	s_h in.	a/d ratio	V_{test} kip	$\frac{V_{test}}{f_c' \cdot b_w d}$	$\frac{V_{test}}{\sqrt{f_c'} \cdot b_w d}$
I-03-2	21	38.5	0.0029	#4	6.5	0.0033	#4	5.75	1.84	569	0.13	9.7
I-03-4	21	38.5	0.0030	#3	7.0	0.0033	#4	5.75	1.84	657	0.15	11.1
I-02-2	21	38.5	0.0020	#4	9.5	0.0020	#4	9.5	1.84	454	0.14	8.9
I-02-4	21	38.5	0.0021	#3	10	0.0020	#4	9.5	1.84	528	0.16	10.1
II-03-CCC2021	21	38.6	0.0031	#5	9.5	0.0045	#5	6.6	1.84	500	0.19	10.7
III-1.85-00	21	38.6	0	-	-	0	-	-	1.84	365	0.14	8.0
III-2.5-00	21	38.6	0	-	-	0	-	-	2.47	82	0.03	1.8
III-1.85-02	21	38.6	0.0020	#5	14.5	0.0019	#4	10.1	1.84	488	0.15	9.4
III-1.85-025	21	38.6	0.0024	#5	12	0.0014	#3	7.6	1.84	516	0.16	9.9
III-1.85-03	21	38.6	0.0029	#5	10	0.0029	#5	10.1	1.84	412	0.10	7.2
III-1.85-01	21	38.6	0.0011	#4	18	0.0014	#3	7.6	1.84	273	0.07	4.8
III-1.85-03b	21	38.6	0.0032	#4	6	0.0029	#5	10.1	1.84	471	0.18	10.1
III-1.85-02b	21	38.6	0.0020	#4	9.5	0.0019	#4	10.1	1.84	468	0.17	10.1
III-1.2-02	21	38.6	0.0020	#4	9.5	0.0019	#4	10.1	1.20	846	0.25	16.3
III-1.2-03	21	38.6	0.0031	#5	9.5	0.0029	#5	10.1	1.20	829	0.24	15.7
III-2.5-02	21	38.6	0.0020	#4	9.5	0.0019	#4	10.1	2.49	298	0.08	5.4
III-2.5-03	21	38.6	0.0031	#5	9.5	0.0029	#5	10.1	2.49	516	0.13	9.0
IV-2175-1.85-02	21	68.9	0.0020	#4	9.5	0.0019	#4	10.1	1.85	763	0.11	7.5
IV-2175-1.85-03	21	68.9	0.0031	#5	9.5	0.0029	#5	10.1	1.85	842	0.12	8.3
IV-2175-2.5-02	21	68.8	0.0021	#5	14.25	0.0021	#5	14.25	2.5	510	0.07	5.0
IV-2175-1.2-02	21	68.9	0.0021	#5	14.25	0.0021	#5	14.25	1.2	1223	0.17	11.9
IV-2123-1.85-03	21	19.5	0.0030	#4	6.25	0.0030	#4	6.25	1.85	329	0.19	12.5
IV-2123-1.85-02	21	19.5	0.0020	#3	5.25	0.0017	#3	6.25	1.85	347	0.20	13.0
M-03-4-CCC2436	36	40	0.0031	#5	11	0.0027	#5	6.5	1.85	1128	0.19	12.2
M-09-4-CCC2436	36	40	0.0086	#5	4	0.0027	#5	6.5	1.85	1415(f)	0.24	15.3
M-02-4-CCC2436	36	40	0.0022	#4	10	0.0022	#5	8	1.85	1102	0.27	14.5

Specimens tested at a/d ratio of 1.85

To evaluate the behavior and strength of a beam without web reinforcement, test III-1.85-0 was conducted. Pictures from the test are shown in Figure 4.47. For the duration of the test, a single, diagonal (flexure-shear) crack that extended from the load to the support dominated the behavior of the specimen. The crack increased in length and width with increasing applied load. At the maximum applied load, a parallel shear crack formed accompanied with a loud popping sound (Figure 4.47 (d)). The formation of this crack represented the splitting of the compression strut due to transverse tensile stresses. Since there was not any web reinforcement to transfer stresses across this crack, the beam could not resist any additional load after the parallel crack formed. Failure occurred at an applied shear of 365-kips or $0.14f'_c b_w d$.

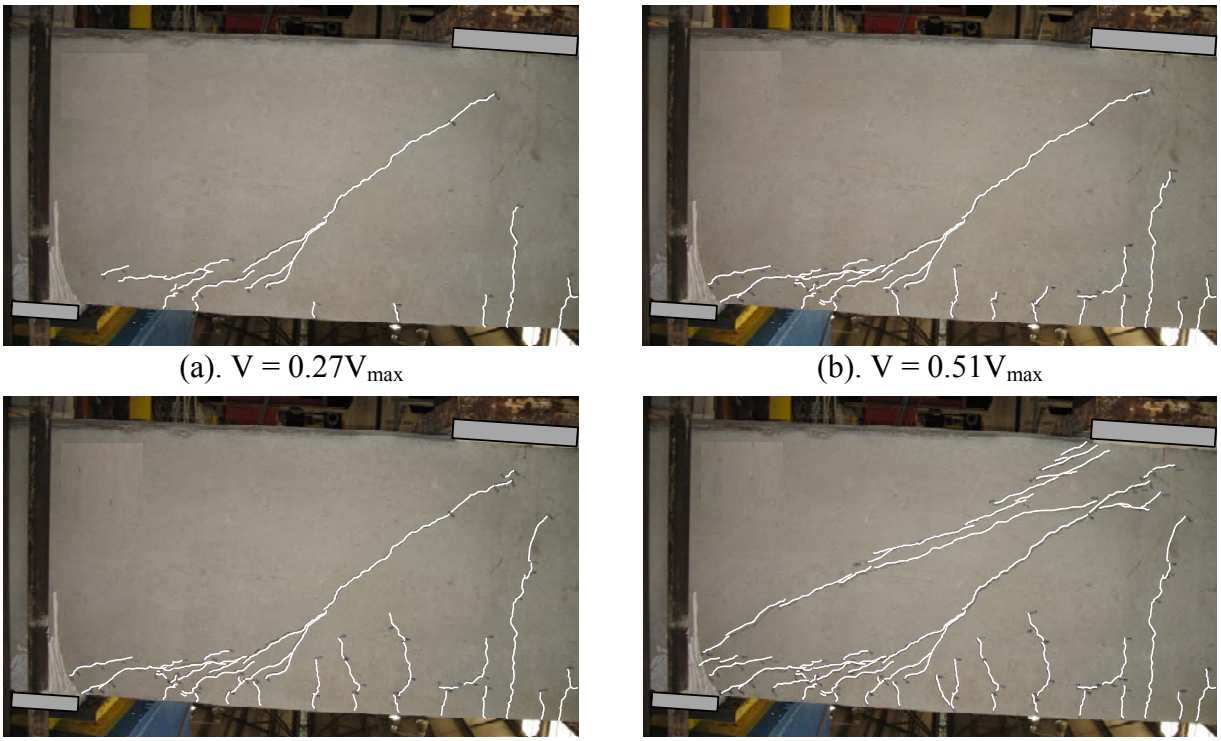

(a). $V = 0.27V_{max}$ (b). $V = 0.51V_{max}$

(c). $V = 0.71V_{max}$ (d). $V = V_{max}$

Figure 4.47: Crack development in specimen without web reinforcement, III-1.85-0

The behavior observed in test III-1.85-0 was consistent with a single-panel strut-and-tie model. The failure of the specimen was a result of the diagonal splitting of the compression strut. As such, the results of this test illustrated the primary role of web reinforcement in deep beams in regards to strength: to resist the transverse tensile stresses created in bottle-shaped struts. The shear strength of III-1.85-0 is compared to the shear strength of the other Series III beams in Figure 4.49.

In Figure 4.48, pictures of specimen III-1.85-03b are shown to illustrate the crack propagation in a typical test for a specimen with web reinforcement. At approximately 25-percent of the maximum applied load, the first diagonal shear crack formed in the test region. It

extended from the tip of a flexural crack. With additional applied load, parallel shear cracks developed and grew in length and width. The presence of web reinforcement in the member ($\rho_v = \rho_h = 0.003$) allowed for these parallel cracks to form. At the maximum applied load, extensive diagonal cracking was present in the deep beam region of the member. Crushing of the concrete occurred in several places along the strut and in the nodal regions. The effect of web reinforcement on the crack distribution and overall appearance of the member throughout its loading history is evident with the comparison of Figure 4.47 and Figure 4.48. Crack width information is discussed in detail in Section 4.5.3.

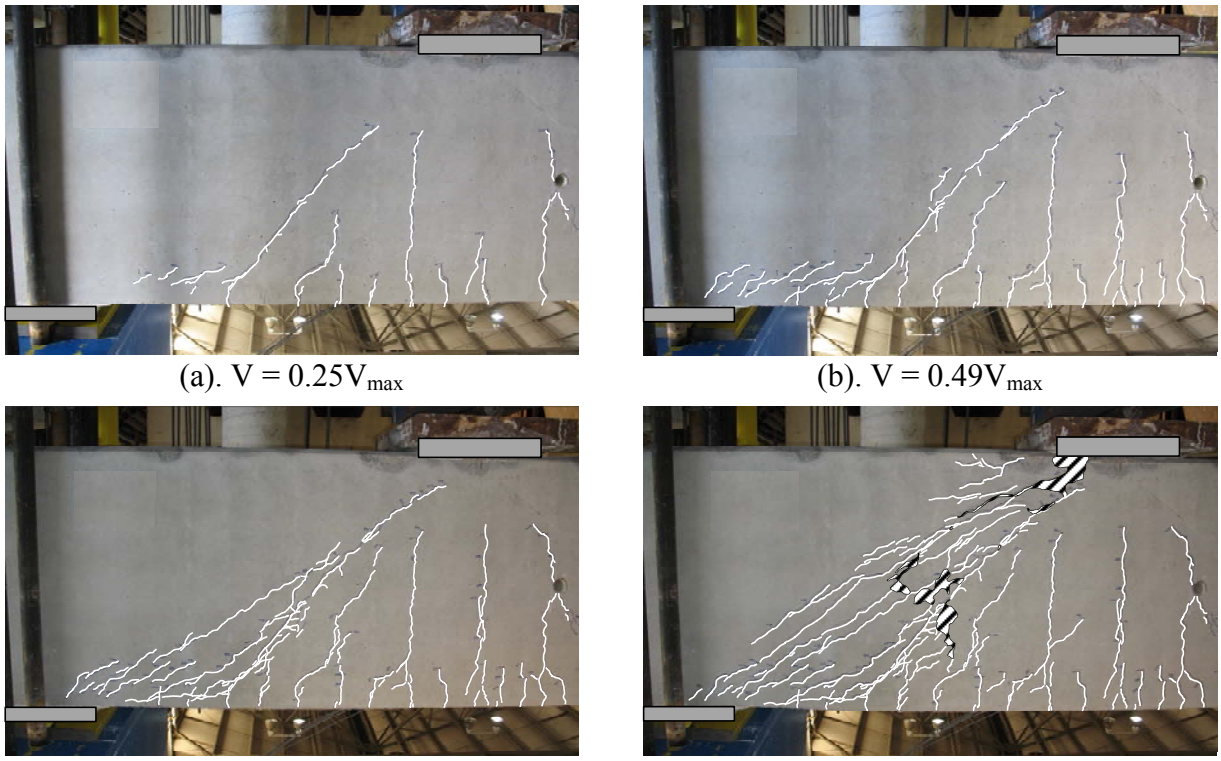

(a). $V = 0.25V_{max}$ (b). $V = 0.49V_{max}$

(c). $V = 0.73V_{max}$ (d). $V = V_{max}$

Figure 4.48: Crack development in specimen with 0.3% in each direction, III-1.85-03b

Several reinforcement arrangements were evaluated in the current task. Simplified versions of the minimum reinforcement provisions discussed in Section 4.5.1 were used specifically in the test specimens (Table 4.8). Note the two different horizontal reinforcement ratios according to the STM provisions of AASHTO LRFD (2008) and CHBDC (2006). These two ratios were the result of the literal interpretation of each provision and the revised interpretation discussed in Section 3.2.3. The literal interpretation consisted of a total amount of horizontal reinforcement equal to 0.003 times the gross concrete section. Distributing this amount of reinforcement within the effective strut area of the specimen produced a reinforcement ratio of 0.0045. The revised interpretation consisted of a total amount of horizontal reinforcement equal to 0.003 times the effective strut area. As such, both of these arrangements were evaluated in the current task. As noted in Table 4.7, a few other reinforcement distributions in addition to those listed in Table 4.8 were evaluated in this task as well.

Table 4.8: Amount of web reinforcement from several provisions used in current task

Minimum Reinforcement Provisions	ρ_v	ρ_h
TxDOT 4371	0.001	0.001
CSA, *fib*, AASHTO Deep Beam	0.002	0.002
ACI Deep Beam	0.0025	0.0015
AASHTO, CHBDC STM (Section 3.2.3)	0.003	0.003
AASHTO, CHBDC STM	0.003	0.0045

The strength results of several specimens with varying amounts of web reinforcement are provided in Figure 4.49. These tests were conducted in Series III and IV at an a/d ratio of 1.85. Specimens of the same size with different amounts of reinforcement failed at similar normalized shear stresses. Specifically, companion specimens of three different sizes (21"x23", 21"x42", and 21"x75") with reinforcement ratios corresponding to 0.2% or 0.3% in each direction failed at nearly identical levels of applied stress. In addition, the 21"x42" specimen with 0.25% reinforcement in the vertical direction and 0.15% reinforcement in the horizontal direction failed at a comparable shear stress as its companion specimen with 0.2% reinforcement in each direction. Since the mode of failure was generally the crushing of the direct strut between the load and the support, increasing the quantity of web reinforcement did not play an appreciable role in the capacity of the members. In general, the test results depicted in Figure 4.49 (at an a/d ratio of 1.85) agree favorably with those obtained from the database.

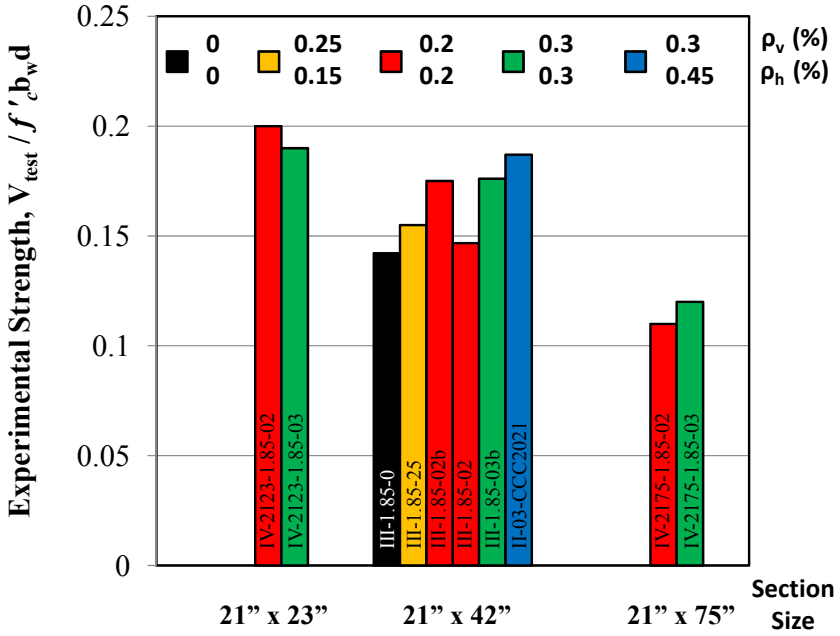

Figure 4.49: Strength results of Series III and IV specimens at a/d ratio of 1.85

The unreinforced specimen (III-1.85-0) failed at only a slightly smaller normalized shear stress than the reinforced beams. For this specimen, the tensile strength of the concrete was sufficient to resist the transverse tensile stresses in the bottle-shaped strut until an applied load comparable with that of the reinforced beams was placed on the member. However, relying on the tensile strength of concrete to consistently resist these tensile stresses is not advised.

The strength results from one beam consisting of tests III-1.85-01 and III-1.85-03 are provided in Figure 4.50. These results are discussed separately from those displayed in Figure 4.49 due to the unusually low experimental strength values for each test, particularly those of III-1.85-03. III-1.85-03 failed at a shear of $0.10f'_c b_w d$, while a nominally identical specimen, III-1.85-03b, failed at a shear of $0.18f'_c b_w d$. The reason for this discrepancy is unclear since a similar mix design, grade of steel, fabrication technique, and testing procedure was used in all tests. At the same time, there is no reason to discount the validity of this test. At a minimum, the range of potential scatter in shear strength is illustrated by test III-1.85-03.

Comparing the experimental strength to the calculated strength of test III-1.85-03 shows that the strength was conservatively calculated using the proposed STM provisions discussed in Section 5.2 (Figure 4.50). This was not true for test III-1.85-01. Since the calculated strength of each specimen was identical, the difference in conservatism between the two was the result of the low experimental strength of test III-1.85-01. The lower amount of web reinforcement was the primary reason for the reduction in shear strength. Unlike the previously-discussed tests, the amount of web reinforcement in III-1.85-01 ($\rho_v = \rho_h \approx 0.001$) significantly affected the experimental strength. The appearance of the beam at ultimate further supports this claim. As shown in the test pictures in Figure 4.50, the failure mode of III-1.85-03 was consistent with the crushing of a direct strut between the load and the support; whereas, the failure mode of III-1.85-01 had a sectional-shear appearance to it. There was not enough reinforcement to distribute the diagonal cracks within the test region. In general, a strut-crushing failure will occur at a higher applied stress than the stress corresponding to a sectional-shear failure.

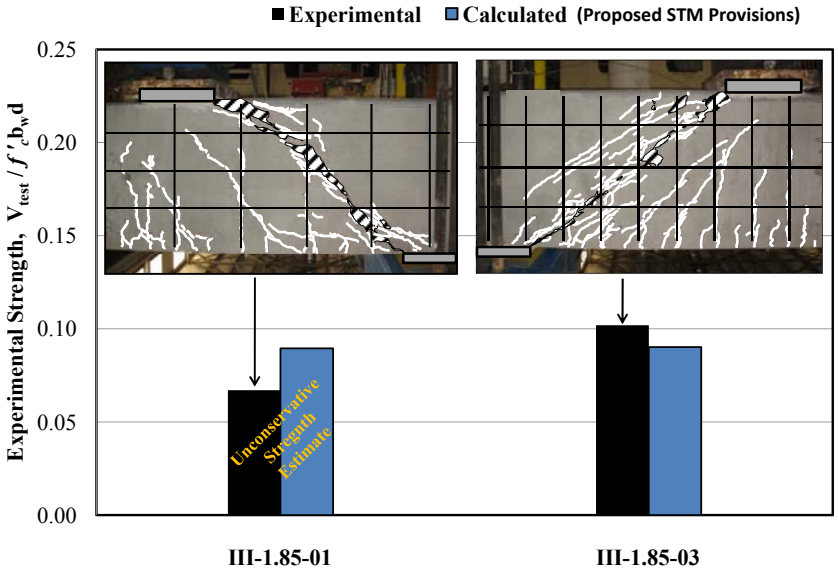

Figure 4.50: Strength results comparison of III-1.85-01 and III-1.85-03

In short, the results of tests III-1.85-01 and III-1.85-03 demonstrated two important points. First, significant scatter (50%) can exist for the experimental shear strength of deep beams. Second, while the amount of reinforcement does not generally affect the shear strength of deep beams, there may be cases where it can. If the quantity of web reinforcement is low ($\rho_v \approx \rho_h \approx 0.001$) and the transverse spacing is relatively high (s_v = 18-in. ≈ d/2), then the concrete strut may not be able to develop its full design strength. In the case of III-1.85-01, the strength was unconservatively estimated.

In Series M, three 36"x48" specimens were tested with different quantities of web reinforcement (Table 4.7). The results of these tests (Figure 4.51) were similar to those from Series III and IV depicted in Figure 4.49. The amount of web reinforcement did not play an appreciable role in the strength of the specimens. In fact, the specimen with 0.2% in each direction (M-02-4-CCC2436) failed at a higher normalized shear stress than the specimen with 0.3% in each direction (M-03-4-CCC2436). However, it should be noted that these tests were conducted on different beams where the compressive strength of the concrete, f'_c, was 2,800-psi and 4,100-psi, respectively. The shear force at ultimate was similar for the two tests: 1,102-kips for the beam with 0.2% steel, and 1,128-kips for the beam with 0.3% steel. Therefore, no discernible difference in strength was observed for the beams in Series M with either 0.2% or 0.3% web reinforcement in each direction.

M-03-4-CCC2436 and M-09-4-CCC2436 were companion tests conducted on the same beam. The only difference between the two tests was ρ_v equaled 0.003 and 0.009, in M-03-4-CCC2436 and M-09-4-CCC2436, respectively. Increasing the amount of web reinforcement by 300% altered the failure mode from shear to flexure, but only increased the capacity of the member by approximately 25%.

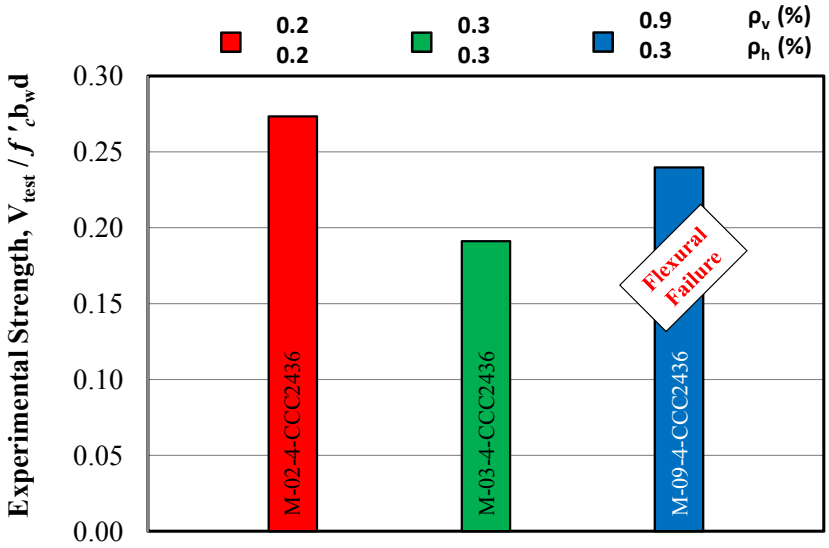

Figure 4.51: Applicable strength results from Series M

The quantity of web reinforcement was varied in Series I as well. The results from this series further supported the aforementioned findings in regards to the effect of web reinforcement on the strength of deep beams. The experimental strength results of the four beams in Series I are plotted in Figure 4.52. No discernible difference in strength was observed

for the beams with either 0.2% or 0.3% in each orthogonal direction and with either 2- or 4-legged stirrups.

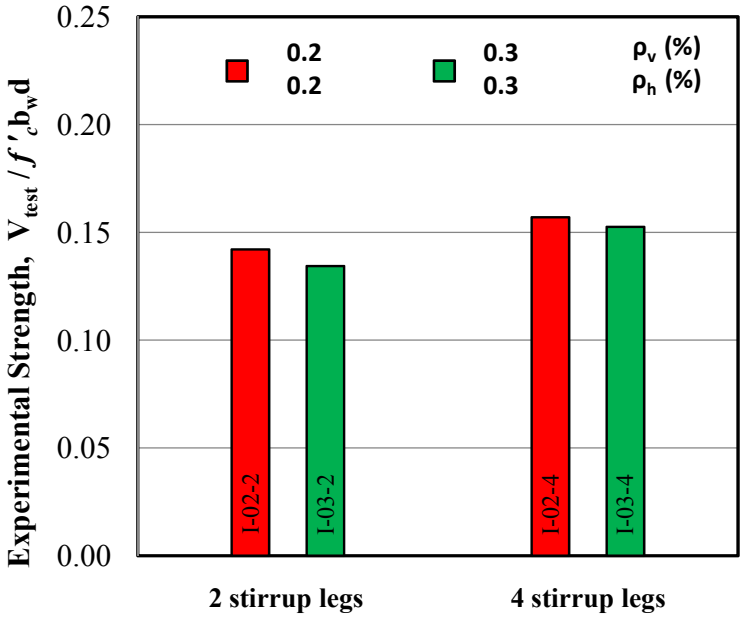

Figure 4.52: Applicable strength results from Series I

Specimens tested at other a/d ratios: 1.2 and 2.5

In addition to an a/d ratio of 1.85, the effect of web reinforcement on the strength of deep beams was also evaluated at other a/d ratios. In Series III, two spans were tested at an a/d ratio of 1.2; three spans were tested at an a/d ratio of 2.5.

The two beams tested at an a/d ratio of 1.2 provided very consistent results with those tested at an a/d ratio of 1.85. As seen in Figure 4.53, the failure mode of each beam was the crushing of the direct strut between the load and support. There was no difference in strength between the beams with 0.2% or 0.3% in each orthogonal direction.

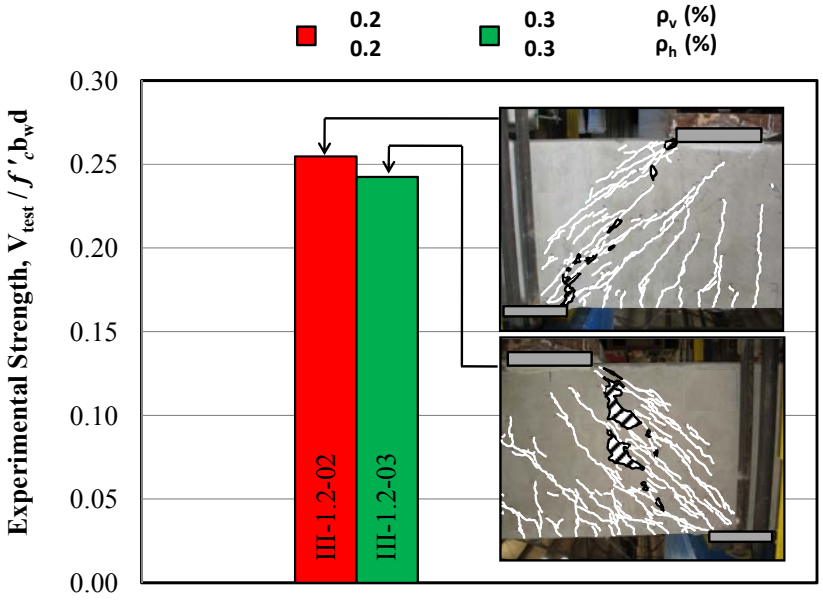

Figure 4.53: Strength results from specimens tested at a/d ratio of 1.2

Of the three specimens tested with an a/d ratio of 2.5, one did not have any web reinforcement (III-2.5-0). This test was the companion test of III-1.85-0. During the test of III-1.85-0, post-tensioned clamps were attached to the low-shear span (future region of test III-2.5-0) to prevent a premature failure. The condition of the test region for III-2.5-0 after the III-1.85-0 test is shown in Figure 4.54 (a). The condition of the test region at the maximum applied shear is provided in Figure 4.54 (b). It is evident from the failure picture that this beam failed due to sectional shear, i.e. diagonal tension. No evidence of crushing in the test region existed. The failure shear for this specimen was considerably low. In fact, it failed at $1.8\sqrt{f'_c}b_w d$, approximately 10% less than the ACI sectional shear equation for V_c ($2\sqrt{f'_c}b_w d$) (ACI, 2008). It is possible that the precracked condition of the shear span contributed to the unconservative failure load. Nevertheless, the results of III-2.5-0 supports two conclusions. First, excluding transverse reinforcement from a concrete beam can be dangerous. Second, at an a/d ratio of 2.5, a single-panel STM may not be appropriate. The behavior of III-2.5-0 was consistent with a sectional shear model, not a single-panel strut-and-tie model. This conclusion was not unexpected since both AASHTO LRFD (2008) and ACI 318-08 limit the treatment of deep beams to an a/d ratio $\leq$ 2.0. It should be noted that deep beam behavior has been reported in experiments up to an a/d ratio of 2.5 (Section 5.3).

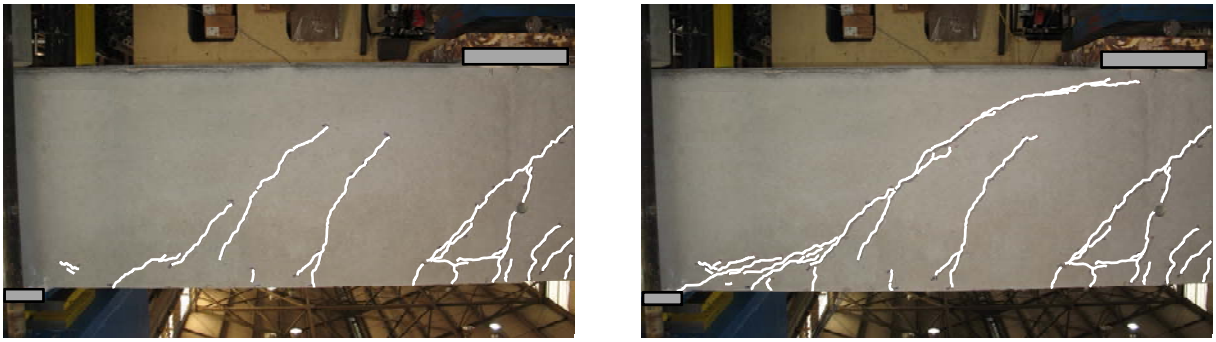

(a). V = 0 (pre-cracked) (b). V = V_{max}

Figure 4.54: Crack development in III-2.5-0

The other two specimens tested at an a/d ratio of 2.5 had 0.2% (III-2.5-02) and 0.3% (III-2.5-03) crack control reinforcement in each orthogonal direction. The strength results and failure pictures for these two tests are presented in Figure 4.55. From this figure, it is evident that an increase in strength and a change in behavior existed as the amount of web reinforcement increased from 0.2% to 0.3% in each direction. The cracking pattern and failure picture for III-2.5-02 was very consistent with the sectional shear, or diagonal tension, failure seen in III-2.5-0. A single diagonal shear crack dominated the test region up until failure. Very little parallel diagonal cracking was observed. On the contrary, III-2.5-03 behaved more like a deep beam. Extensive redistribution of diagonal cracks occurred with increasing applied load, presumably due to the additional amount of web reinforcement. Near ultimate, a parallel shear crack formed along the axis of the assumed compression strut between the load and the support as observed in tests at smaller a/d ratios. An increase in load-carrying capacity of approximately 60% accompanied the change in failure mode.

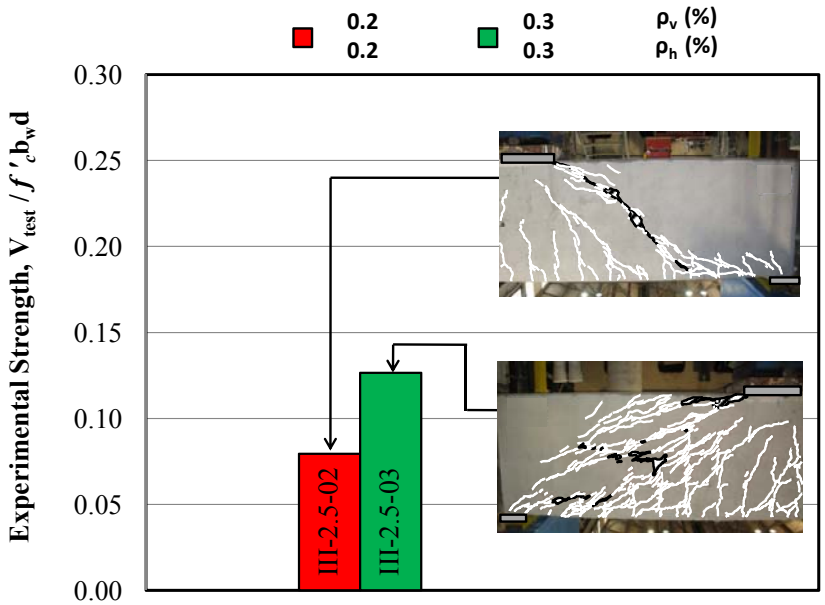

Figure 4.55: Strength results from specimens tested at an a/d ratio of 2.5

The comparison of III-2.5-02 to III-2.5-03 revealed that the quantity of web reinforcement becomes relevant at higher a/d ratios (a/d > 2). The behavior of the test region is transitioning from strut-and-tie action to sectional shear behavior. Vertical reinforcement improves the sectional shear strength of reinforced concrete beams. In test III-2.5-03, the vertical reinforcement enabled significant redistribution to occur increasing the load-carrying capacity of the member. The final failure mode of this specimen was consistent with a combination of sectional shear and strut-and-tie behavior. It should be noted that the beneficial effect of web reinforcement on the strength of beams tested at a/d ratios in excess of 2 was also observed through the analysis of the database as discussed in Section 4.5.2 (Figure 4.44). Additional information regarding the transition of deep beam behavior to sectional shear behavior is provided in Section 5.3.

4.5.3 Serviceability Results

The effect of web reinforcement on the serviceability of deep reinforced concrete beams was also investigated within this task. As previously discussed, the diagonal cracking loads and the width of diagonal cracks were used to assess the serviceability performance of deep beams.

Serviceability Results from the Evaluation Database

Very little crack width data was available in the literature. However, the load at first diagonal cracking was recorded for numerous specimens in the evaluation database (59). The diagonal cracking loads were normalized by the $\sqrt{f_c'}\, b_w d$ and were plotted versus the reinforcement ratio in each direction in Figure 4.56 and Figure 4.57. The results in these figures did not reveal any effect of the quantity of reinforcement on the normalized diagonal cracking loads. This finding was plausible since reinforced concrete members behave elastically prior to cracking. The strain in the concrete at first cracking is very small preventing any effect of the reinforcement to be observed until cracks develop.

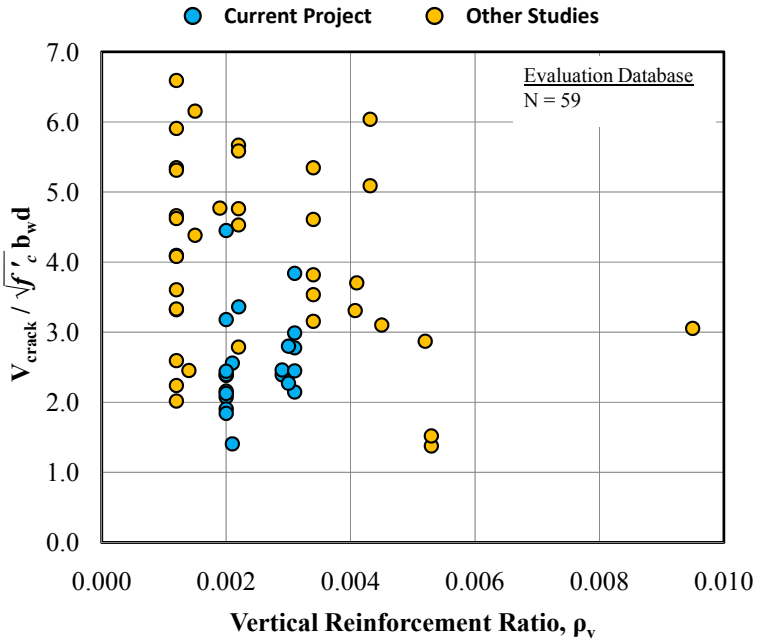

Figure 4.56: Effect of vertical reinforcement on the diagonal cracking load

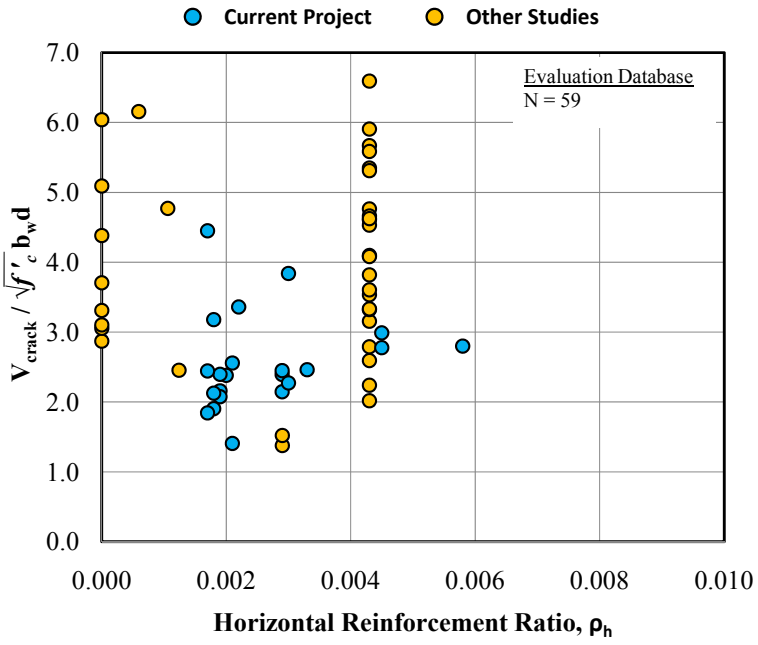

Figure 4.57: Effect of horizontal reinforcement on the diagonal cracking load

Serviceability Results from the Experimental Program

The diagonal cracking loads for each specimen relevant to the current task are provided in Table 4.9. The strength data for the same specimens in Table 4.9 were provided in Table 4.7. As noted in Section 3.6, it was only possible to obtain the cracking load for the first test on each 42-, 44-, and 48-inch specimen. The first cracking loads for both tests conducted on the 75- and 23-inch specimens were measured.

Table 4.9: Summary of serviceability results for specimens in minimum reinforcement task

Beam I.D.	b_w in.	d in.	ρ_v	Bar size	s_v in.	ρ_h	Bar size	s_h in.	a/d ratio	V_{crack} kip	$\frac{V_{crack}}{\sqrt{f_c'} \cdot b_w d}$
I-03-2	21	38.5	0.0029	#4	6.5	0.0033	#4	5.75	1.84	144	2.5
I-03-4	21	38.5	0.0030	#3	7.0	0.0033	#4	5.75	1.84	-	-
I-02-2	21	38.5	0.0020	#4	9.5	0.0020	#4	9.5	1.84	121	2.4
I-02-4	21	38.5	0.0021	#3	10	0.0020	#4	9.5	1.84	-	-
II-03-CCC2021	21	38.6	0.0031	#5	9.5	0.0045	#5	6.6	1.84	139	3.0
III-1.85-00	21	38.6	0	-	-	0	-	-	1.84	98	2.1
III-2.5-00	21	38.6	0	-	-	0	-	-	2.47	-	-
III-1.85-02	21	38.6	0.0020	#5	14.5	0.0019	#4	10.1	1.84	112	2.2
III-1.85-025	21	38.6	0.0024	#5	12	0.0014	#3	7.6	1.84	-	-
III-1.85-03	21	38.6	0.0029	#5	10	0.0029	#5	10.1	1.84	137	2.4
III-1.85-01	21	38.6	0.0011	#4	18	0.0014	#3	7.6	1.84	-	-
III-1.85-03b	21	38.6	0.0032	#4	6	0.0029	#5	10.1	1.84	114	2.4
III-1.85-02b	21	38.6	0.0020	#4	9.5	0.0019	#4	10.1	1.84	-	-
III-1.2-02	21	38.6	0.0020	#4	9.5	0.0019	#4	10.1	1.20	165	3.2
III-1.2-03	21	38.6	0.0031	#5	9.5	0.0029	#5	10.1	1.20	-	-
III-2.5-02	21	38.6	0.0020	#4	9.5	0.0019	#4	10.1	2.49	105	1.9
III-2.5-03	21	38.6	0.0031	#5	9.5	0.0029	#5	10.1	2.49	-	-
IV-2175-1.85-02	21	68.9	0.0020	#4	9.5	0.0019	#4	10.1	1.85	216	2.1
IV-2175-1.85-03	21	68.9	0.0031	#5	9.5	0.0029	#5	10.1	1.85	218	2.1
IV-2175-2.5-02	21	68.9	0.0021	#5	14.25	0.0021	#5	14.25	2.5	144	1.4
IV-2175-1.2-02	21	68.9	0.0021	#5	14.25	0.0021	#5	14.25	1.2	262	2.6
IV-2123-1.85-03	21	19.5	0.0030	#4	6.25	0.0030	#4	6.25	1.85	60	2.3
IV-2123-1.85-02	21	19.5	0.0022	#3	5.25	0.0017	#3	6.25	1.85	65	2.4
M-03-4-CCC2436	36	40	0.0031	#5	11	0.0027	#5	6.5	1.85	354	3.8
M-09-4-CCC2436	36	40	0.0086	#5	4	0.0027	#5	6.5	1.85	-	-
M-02-4-CCC2436	36	40	0.0022	#4	10	0.0022	#5	8	1.85	256	3.4

As shown in Table 4.9, the diagonal cracking loads of several specimens with different amounts of web reinforcement were measured. Information regarding the measurement of the diagonal cracking loads was provided in Section 4.2.2. The load at first diagonal cracking normalized by the $\sqrt{f_c'}\, b_w d$ for each of these specimens is plotted in Figure 4.58. The results indicated that the quantity of web reinforcement has no effect on the diagonal cracking load. This finding was in agreement with the results from the evaluation database. As previously mentioned, the amount of reinforcement does not affect the behavior of reinforcement concrete members until after the beam has cracked. It is interesting to note that the normalized diagonal cracking loads of the 36"x48" specimens were considerably greater than those of the 21"x23", 21"x42", 21"x44", and 21"x75" specimens. It is likely that the higher longitudinal reinforcement ratio in the 36"x48" specimens (2.9% vs. 2.3%) contributed to the higher normalized diagonal cracking loads. Since the first diagonal crack was generally a flexure-shear crack, the amount of reinforcement at the tip of the flexural crack affects the diagonal cracking load. Additional information regarding the factors affecting the load at first diagonal cracking is provided in Section 5.4.

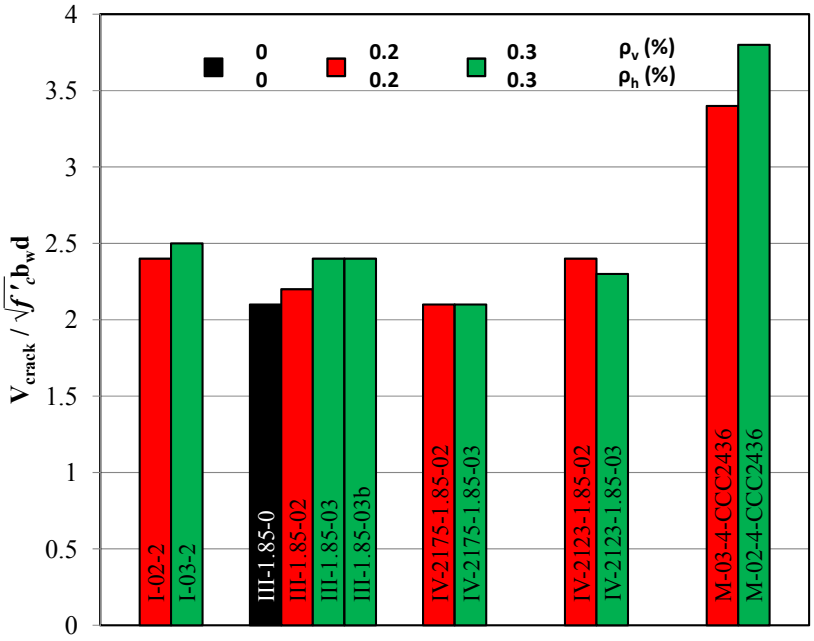

Figure 4.58: Diagonal cracking loads of specimens in current task

The serviceability performance of the test specimens was also evaluated with the maximum width of the diagonal cracks. As noted in Section 3.5.4, the crack widths were measured during each load increment with a crack comparator card. The maximum diagonal crack widths were recorded for each side of the test specimen and were plotted versus the percent of the maximum applied load. Plotting the data in this manner was appropriate to permit specimens of different sizes and with different concrete strengths to be placed on the same plot. Also, this approach was consistent with another objective of the current research study: to correlate the maximum diagonal crack width with the residual capacity of the member (Section 5.5).

Maximum diagonal crack widths for six 21"x42" specimens tested at an a/d ratio of 1.85 are presented in Figure 4.59. Several important observations can be made regarding this figure. First, it is clear that the quantity of web reinforcement directly influences the width of diagonal cracks. As the amount of reinforcement crossing the diagonal crack increases, the width of the diagonal crack decreases for a given percent of applied load. Therefore, the specimen with 0.3% reinforcement in the vertical direction and 0.45% reinforcement in the horizontal direction (II-03-CCC2021) had the narrowest diagonal cracks throughout its loading history. The effectiveness of horizontal reinforcement was evaluated with this test as well. Comparing the crack widths of specimens II-03-CCC2021 and III-1.85-03b demonstrated that additional horizontal reinforcement effectively restrained diagonal crack widths at high a/d ratios (1.85). While it was emphasized in the literature and through the use of the database (Figure 4.43) that additional horizontal reinforcement had a negligible impact on the strength of deep beams, these crack width data suggested that horizontal reinforcement may be important for serviceability. Comparing the crack widths of specimens III-1.85-02 and III-1.85-025 did not reveal significant differences. This observation was not unexpected due to minimal differences in the spacing of the reinforcement required to target the reinforcement ratio in each specimen. The spacing of the #5 stirrups for these two specimens only differed by 2.5-inches. As a result of these findings and of the format of several existing minimum reinforcement provisions, equal reinforcement in each orthogonal direction was targeted as the most effective and most practical solution for minimum web reinforcement in deep beams.

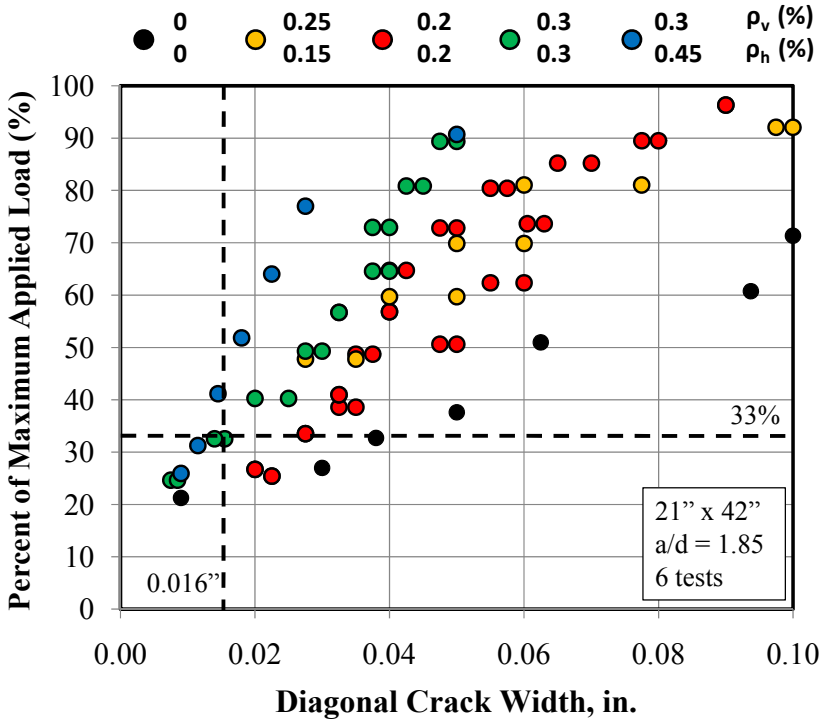

Figure 4.59: Diagonal crack widths for 6 - 21"x42" specimens tested at a/d of 1.85

The crack width data in Figure 4.59 can be compared to the crack width limit of 0.016-inches (Section 4.1.2). At first diagonal cracking, the maximum crack width for III-1.85-02 and

III-1.85-02b exceeded the 0.016-inches limit. On the contrary, at the first cracking of specimens II-03-CCC2021 and III-1.85-03b, the maximum crack width was only approximately 0.009-inches. The diagonal crack width did not reach 0.016-inches in these specimens until 30- to 40-percent of the maximum applied load was reached. For the unreinforced specimen (III-1.85-0), the maximum diagonal crack width was also less than 0.016-inches at first diagonal cracking. However, it is clear from Figure 4.59 that the crack width increased rapidly for a minimal increase in applied load. The data in Figure 4.59 can also be evaluated with respect to the estimated service load on the structure of 33% of the maximum applied load (Section 4.2.2). At this level, the specimens with 0.3% web reinforcement or greater in each direction had diagonal crack widths at or less than 0.016-inches. The specimens without any reinforcement or with 0.2% reinforcement had maximum crack widths of 0.038- and 0.028-inches respectively. It should be noted that the crack width limit of 0.016-inches and the estimated service load (33% of ultimate) should be not be treated as definite limits. They should be used as general benchmarks. Nevertheless, the data in Figure 4.59 clearly indicated that the specimens with at least 0.3% in each direction performed much better than those with less reinforcement.

The crack patterns at approximately 90% of the maximum applied load for four of the aforementioned tests are provided in Figure 4.60. In a general sense, the crack patterns of each test specimen agree favorably with the maximum diagonal crack width data presented in Figure 4.59. At a given load stage, as the distribution of diagonal cracking, i.e. the number of parallel diagonal cracks, increased, the maximum diagonal crack width decreased. Comparing the crack patterns of test III-1.85-03b and II-03-CCC2021 further illustrated the benefit of horizontal reinforcement. While horizontal reinforcement was shown in the literature and through the use of the database (Figure 4.43) to be less effective than vertical reinforcement in terms of strength, the data from these tests suggested that it is important for limiting diagonal crack widths. This finding supported keeping the quantity of minimum web reinforcement the same in each orthogonal direction.

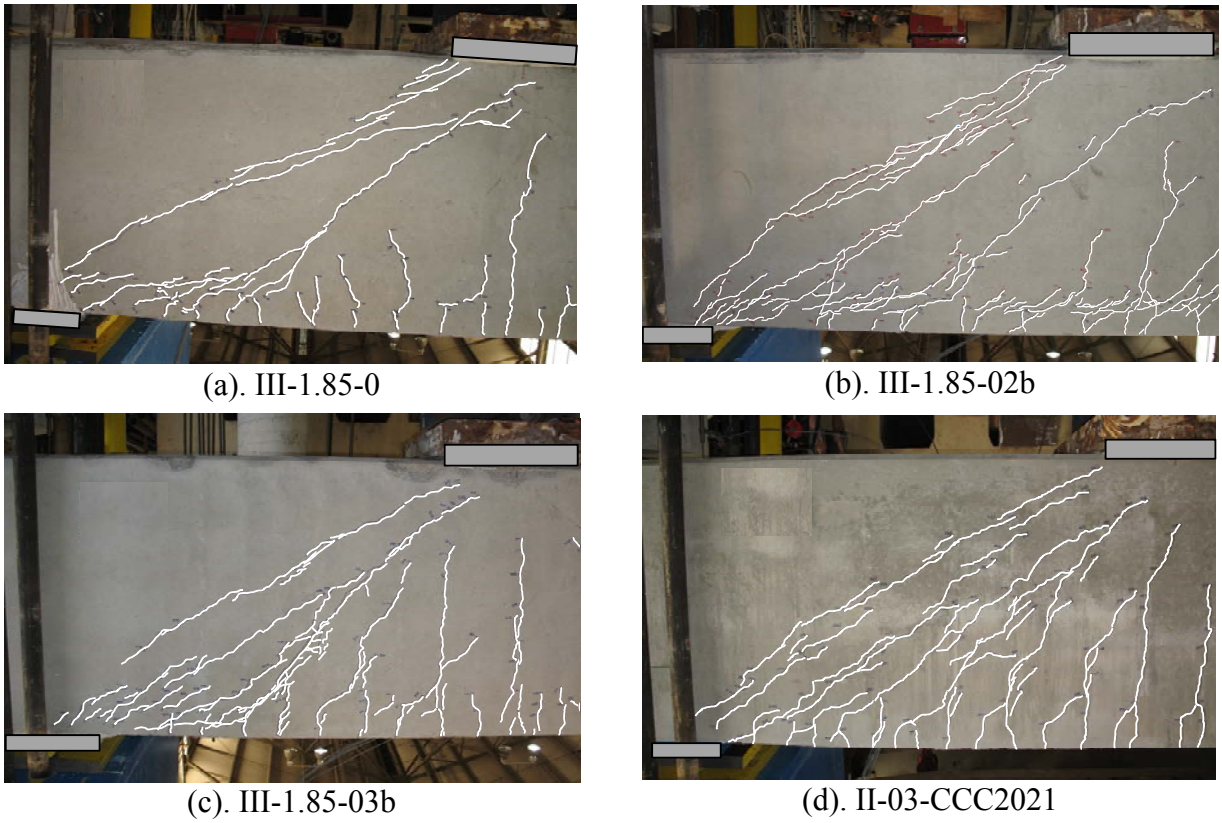

(a). III-1.85-0 (b). III-1.85-02b

(c). III-1.85-03b (d). II-03-CCC2021

Figure 4.60: Crack patterns of four specimens at approximately 90% of capacity

The crack width data from tests III-1.85-01 and III-1.85-03 are presented in Figure 4.61 with the data from Figure 4.59. The maximum diagonal crack width data from III-1.85-03 agreed favorably with the data from the other specimen with the same web reinforcement (III-1.85-03b) even though they failed at considerably different normalized shear stresses. On the other hand, the crack width data from III-1.85-01 did not match the trend with reinforcement quantity that was otherwise represented in Figure 4.61. The reason for this discrepancy was the difference in failure modes between III1.85-01 and the rest of the tests. As discussed previously (Figure 4.50), the failure mode of III-1.85-01 more closely resembled a sectional shear failure than a deep beam failure, primarily due to insufficient web reinforcement.

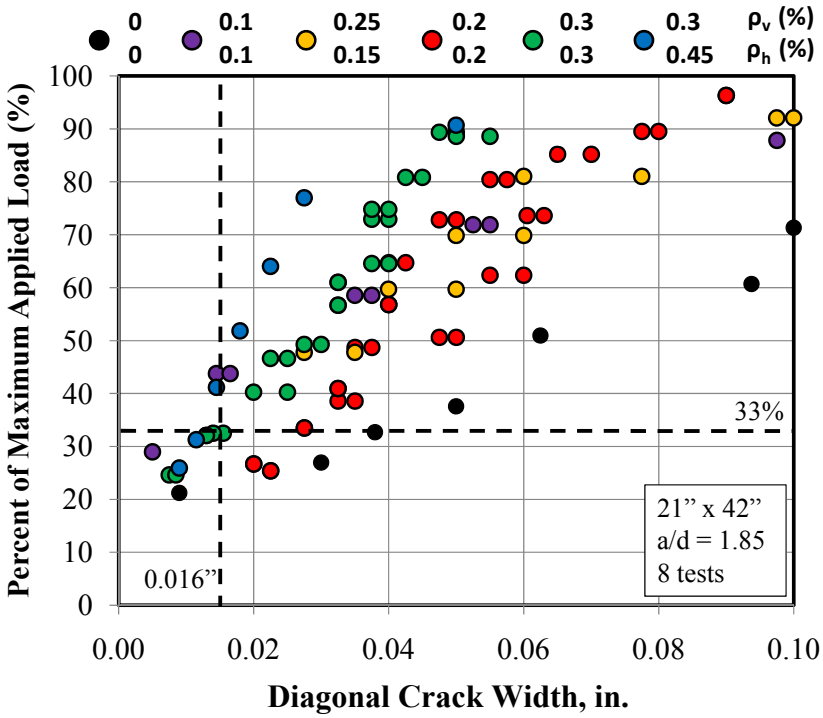

Figure 4.61: Diagonal crack widths for 8 – 21"x42" specimens tested at a/d of 1.85

Consistent load transfer mechanisms were required to compare diagonal crack width data when normalizing the applied load by the maximum applied load. If the crack width data in Figure 4.61 was plotted versus the applied shear, the trend in Figure 4.62 resulted. This trend illustrated that regardless of the load transfer mechanism, maximum diagonal crack widths are a function of the applied shear and the quantity of web reinforcement. However, as previously discussed, plotting crack width data versus the percent of maximum applied load was more useful for the current project.

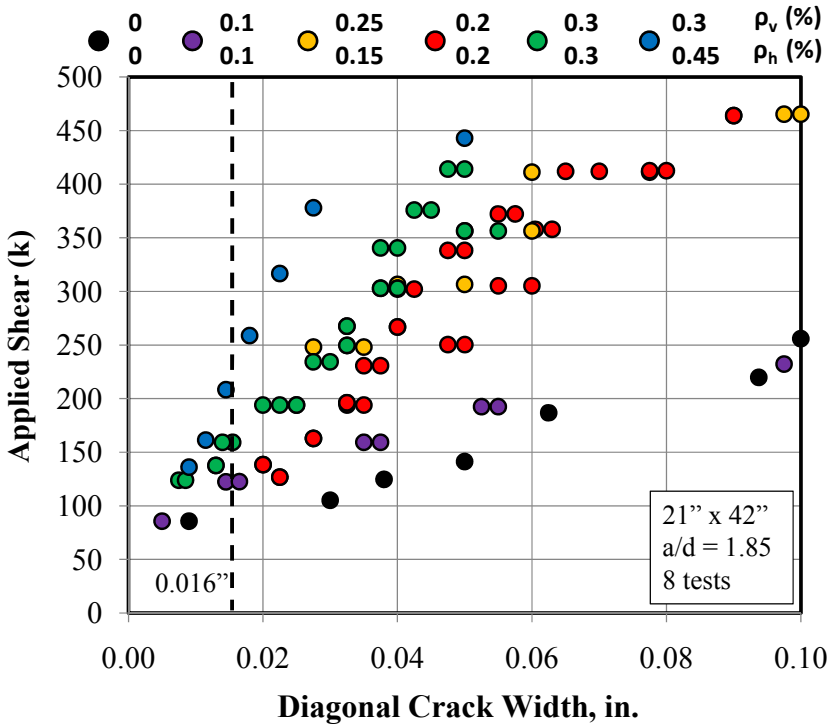

Figure 4.62: Diagonal crack widths of 8 – 21"x42" specimens versus applied shear

Several other tests were conducted at an a/d ratio of 1.85 within the experimental program to evaluate the difference between 0.2% and 0.3% web reinforcement in each orthogonal direction. The crack width data for these tests is provided in Figure 4.63 through Figure 4.66. The data in these figures can be used to compare the maximum diagonal crack widths for the 21"x75" specimens, the 36"x48" specimens, and the four 21"x44" specimens with either 2 or 4 legged stirrups. In all cases, the same general conclusions regarding the effect of web reinforcement on maximum diagonal crack widths can be reached. Providing 0.3% reinforcement in each orthogonal direction better restrained the diagonal crack widths throughout the loading history of the member and at first cracking, in general. At the estimated service load (33% of ultimate), the maximum diagonal crack widths for the specimens with 0.3% reinforcement in each direction were generally at or below the tolerable crack width limit of 0.016-inches. The crack widths for the specimens with 0.2% reinforcement were generally greater than the tolerable crack width limit.

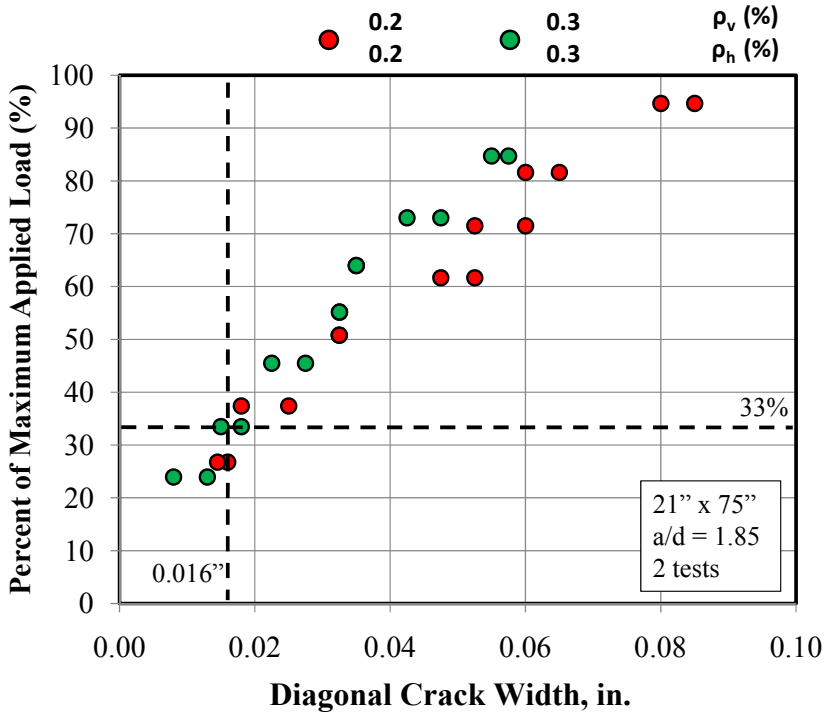

Figure 4.63: Diagonal crack widths for 21"x75" specimens with 0.2% and 0.3% reinforcement

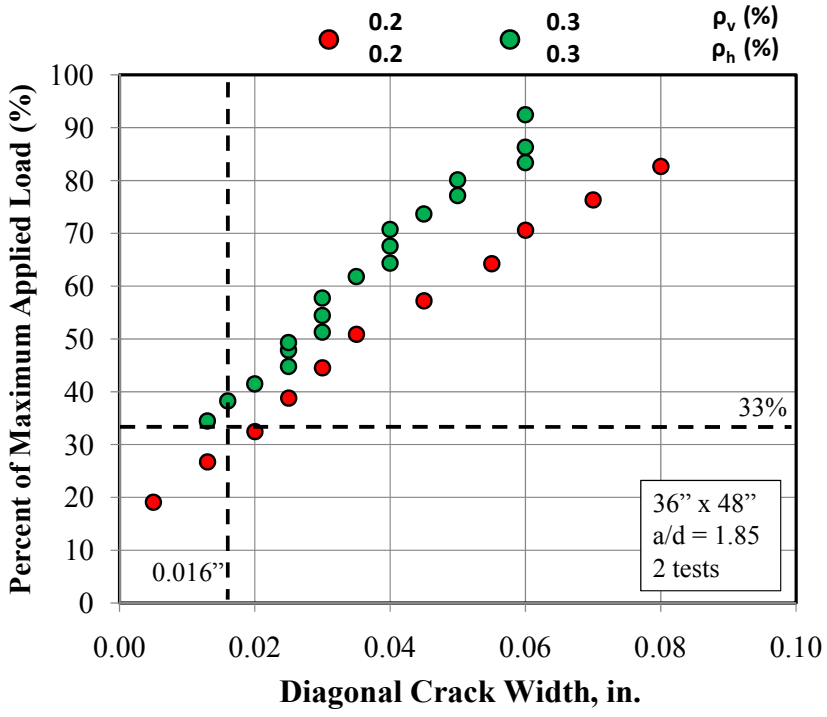

Figure 4.64: Diagonal crack widths for 36"x48" specimens with 0.2% and 0.3% reinforcement

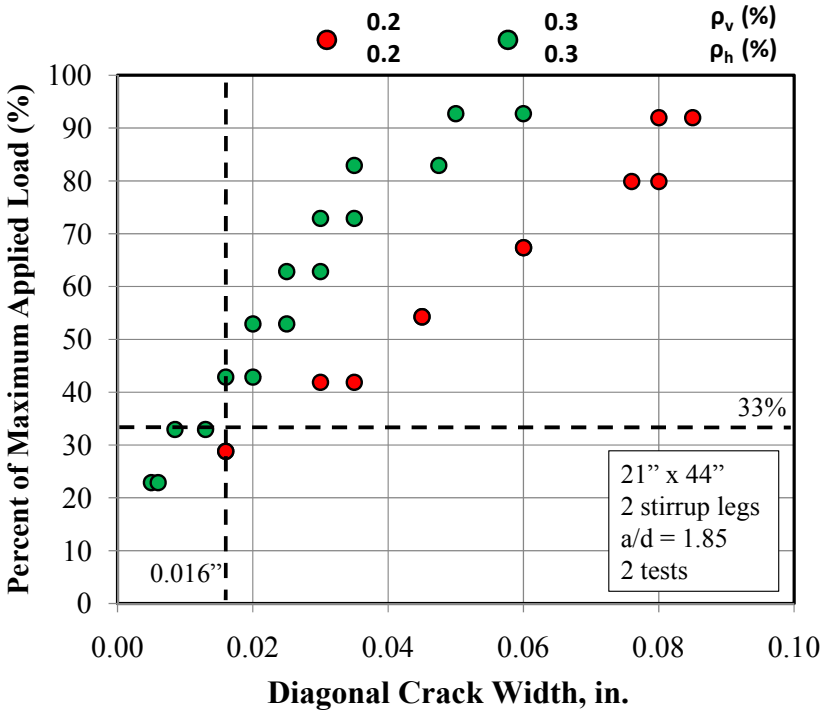

Figure 4.65: Diagonal crack widths for 21"x44" specimens with 0.2% or 0.3% 2-legged reinforcement

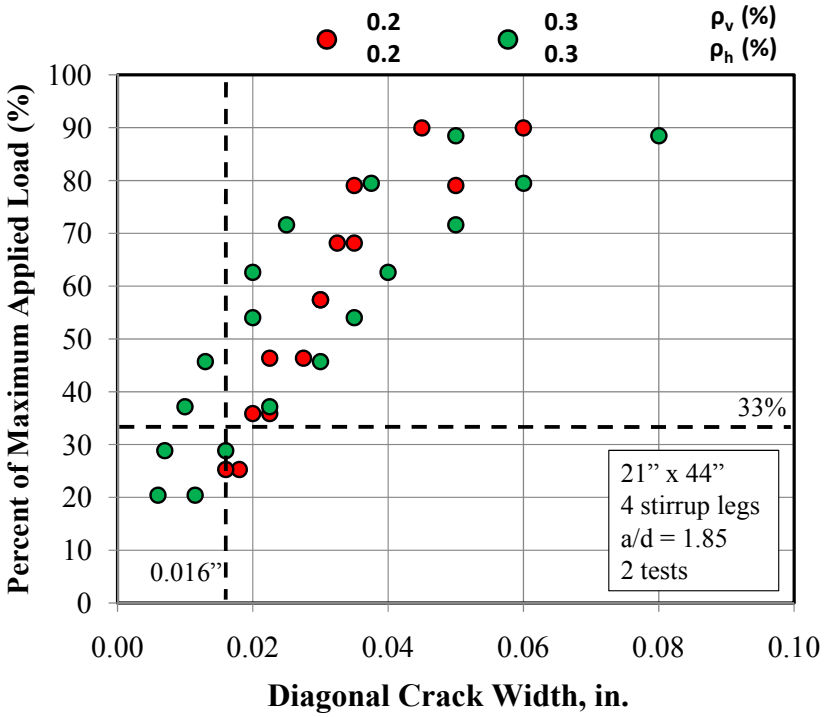

Figure 4.66: Diagonal crack widths for 21"x44" specimens with 0.2% or 0.3% 4-legged reinforcement

Due to the variable nature of crack width data, it is important to base overall conclusions on as much data as possible. The maximum crack width data for the specimens in the current task (Table 4.9) that were tested at an a/d ratio of 1.85 was plotted in Figure 4.67 with the exception of III-1.85-01. The data from this test was excluded because the load transfer mechanism was not consistent with a deep beam as noted previously. In all, the data from 16 tests were included in Figure 4.67. Among the tests were beams of several different sizes, with 2- and 4-legged stirrups, and with several different distributions of web reinforcement.

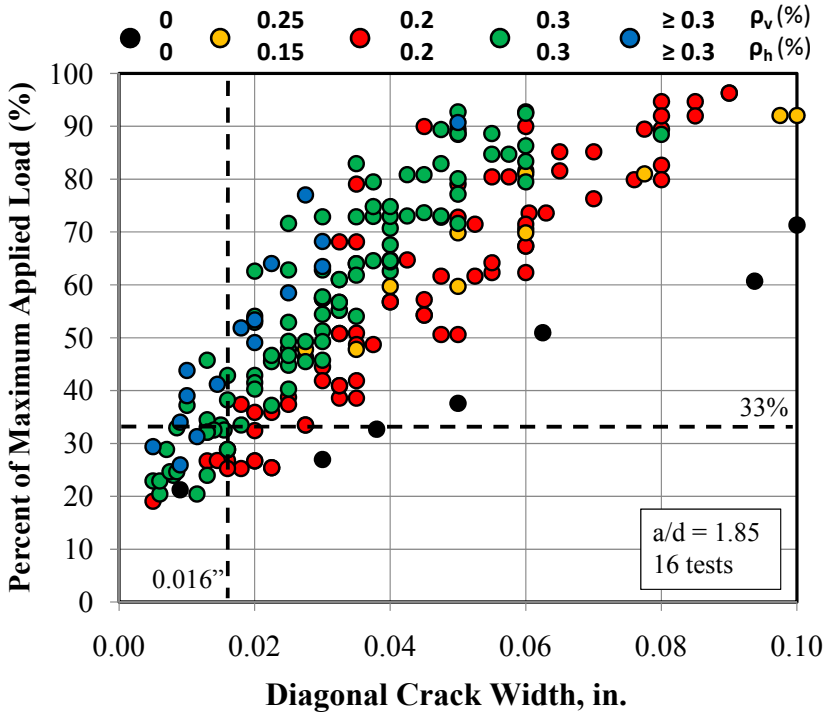

Figure 4.67: Diagonal crack width data for all comparable specimens at a/d of 1.85

In Figure 4.67, it is evident that some scatter existed with diagonal crack width data. However, in general, the trend between maximum diagonal crack width and the reinforcement ratio in the web is remarkably clear. At first diagonal cracking, the specimens with 0.2% web reinforcement in each orthogonal direction often exceeded the tolerable crack width limit of 0.016-inches. This amount of reinforcement was not sufficient to restrict the width of diagonal cracks to this general limit even at first cracking. At the estimated service load level, the maximum crack widths of all of the specimens with 0.2% reinforcement exceeded 0.016-inches. The specimens with 0.3% in each orthogonal direction, on the other hand, had crack widths narrower than 0.016-inches at first diagonal cracking. In almost all cases, the maximum crack width was less than or equal to 0.016-inches at the estimated service load of 33% of ultimate. Due to the approximate nature of the tolerable crack width limit and the service load of 33% of ultimate, the performance of the specimens with 0.3% reinforcement was considered acceptable. Providing web reinforcement in excess of 0.3% in each direction did a better job than 0.3% at restraining crack widths, but mostly at higher levels of applied load. Near first cracking and at the expected service load, there was only a moderate reduction in the maximum diagonal crack

widths. The two specimens representing the blue data points in Figure 4.67 had the following amount of web reinforcement:

- II-03-CCC2021: $\rho_v = 0.31\%$, $\rho_h = 0.45\%$
- M-09-4-CCC2436: $\rho_v = 0.86\%$, $\rho_h = 0.27\%$

Even with a large increase in the amount of vertical reinforcement in test M-09-4-CCC2436, the maximum diagonal crack widths were only slightly narrower than those in specimens with 0.3% reinforcement. This observation suggested that near service loads, there are diminishing returns regarding the effect of web reinforcement on maximum diagonal crack widths.

In addition to an a/d ratio of 1.85, a few tests were conducted at a/d ratios of 1.2 and 2.5. Crack width data for the three specimens tested at an a/d ratio of 1.2 and the three specimens tested at an a/d ratio of 2.5 are presented in Figure 4.68 and Figure 4.69, respectively.

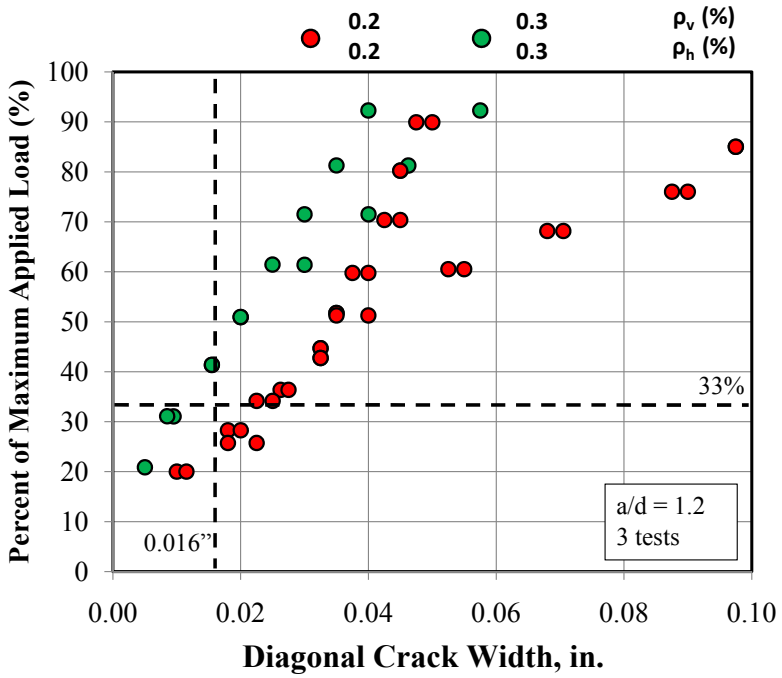

Figure 4.68: Diagonal crack widths of specimens tested at an a/d ratio of 1.2

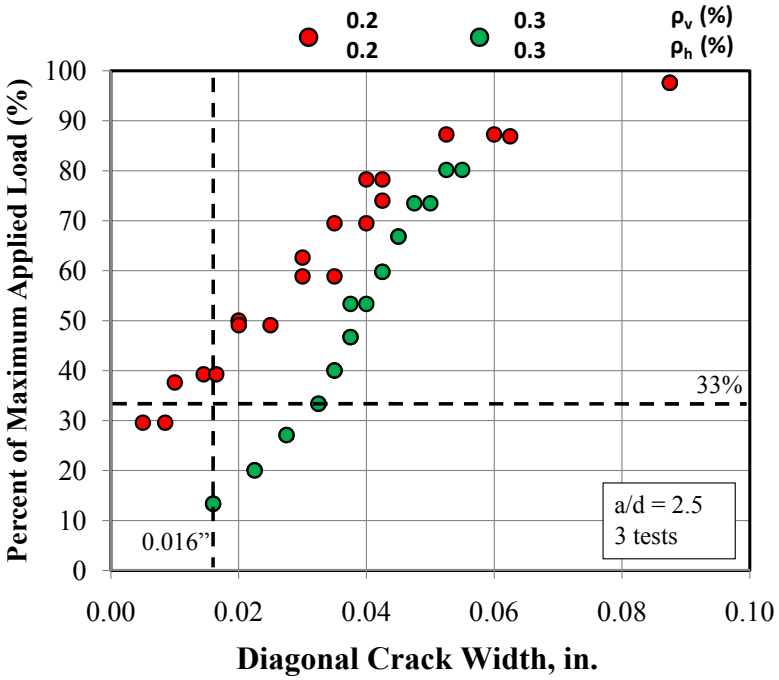

Figure 4.69: Diagonal crack widths of specimens tested at an a/d ratio of 2.5

The results presented in Figure 4.68 (a/d = 1.2) are consistent with the crack widths of beams tested at an a/d ratio of 1.85 (Figure 4.67). Web reinforcement in both directions corresponding to 0.3% better restrained the width of diagonal cracks than 0.2% in each direction. At the expected service load, the maximum width of the diagonal cracks in the specimen with 0.3% reinforcement is well below the tolerable limit of 0.016-inches. On the other hand, the maximum crack width of the specimens with 0.2% reinforcement is approximately 0.02-inches, exceeding the crack width limit slightly.

The results presented in Figure 4.69 are not in agreement with the data from the tests conducted at an a/d ratio less than 2. The reason for this discrepancy was that for the beams in Figure 4.69 with 0.2% reinforcement, the failure mode was consistent with a sectional shear or diagonal tension failure. The specimen with 0.3% reinforcement in each direction (III-2.5-03) failed in a manner consistent with a combination of deep beam and sectional shear behavior. As noted previously, the reinforcement in test III-2.5-03 provided additional redistribution capacity that increased the strength of the test specimen. As a result of this inconsistency, a direct comparison between these tests is considered to be neither practical nor valid.

The required spacing of minimum web reinforcement was not explicitly evaluated in the experimental program. However, a couple of valid comparisons were possible. Two pairs of tests were conducted at an a/d ratio of 1.85. In both cases, the difference between each test in the pair was the spacing of the stirrups (s_v). The spacing of the horizontal reinforcement was the same in all four tests (10-inches). The crack width data for the two specimens with 0.2% reinforcement (III-1.85-02 and III-1.85-02b) are plotted in Figure 4.70. The crack width data for the two specimens with 0.3% reinforcement (III-1.85-03 and III-1.85-03b) are plotted in Figure 4.71.

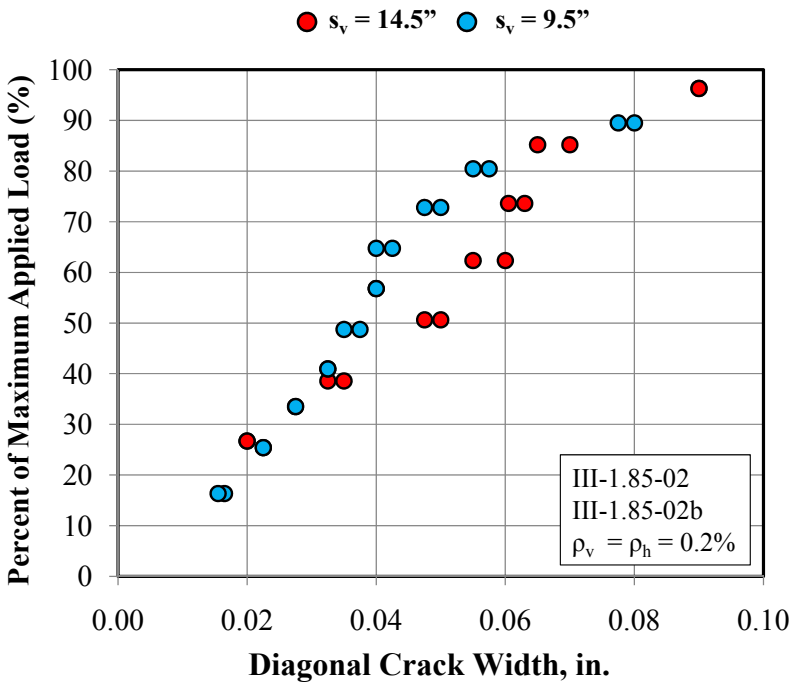

Figure 4.70: Effect of stirrup spacing on crack width for specimens with 0.2% web reinforcement

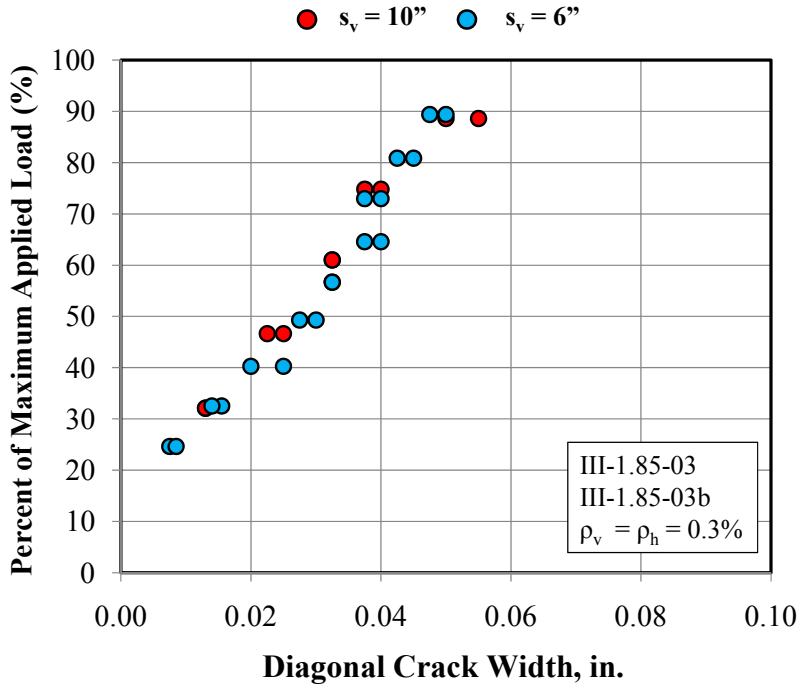

Figure 4.71: Effect of stirrup spacing on crack width for specimens with 0.3% web reinforcement

In Figure 4.70, the crack width data indicates that larger stirrup spacing may result in wider diagonal cracks. For specimen III-1.85-02, the stirrups were spaced at 14.5-inches or approximately d/2.5. This spacing is larger than that required by many of the minimum

reinforcement provisions reviewed in Section 4.5.1. In general, spacing of minimum reinforcement is limited to d/4, d/5, or 12-inches. While the effect shown in Figure 4.70 is minimal, it does show the benefits of restricting the spacing of crack control reinforcement. In Figure 4.71, the crack width data for the specimens with 0.3% reinforcement indicates that stirrup spacing smaller than 10-inches or approximately d/4 did not further reduce diagonal crack widths. Thus, there is no apparent benefit from recommending a spacing limit less than d/4. Based on the results in Figure 4.70 and Figure 4.71 and to be consistent with previous recommendations for the spacing of minimum web reinforcement, it is proposed that the spacing be limited to the smaller of d/4 or 12-inches. This limit is the same that is recommended in Article 5.13.2.3 of AASHTO LRFD (2008).

4.5.4 Design Recommendations

Based on the strength and serviceability results discussed in Section 4.5.1 through 4.5.3, minimum reinforcement of 0.3% in each orthogonal direction is recommended for use in deep beams. This amount of reinforcement adequately restrained the width of diagonal cracks at first cracking and up to an approximate service load level of 33% of ultimate. Reinforcement of 0.2% did not adequately restrain the width of diagonal cracks. It is possible that for applications in which the serviceability performance (restraint of diagonal crack widths) is not a priority, then minimum web reinforcement of 0.2% in each direction would be satisfactory.

In regards to the minimum reinforcement provisions in current design specifications, 0.3% in each orthogonal direction is similar to that required in AASHTO LRFD (2008) and CHBDC (2006). The one difference is that in AASHTO and in CHBDC the total horizontal reinforcement is based off of the gross concrete section whereas the reinforcement recommended herein is based off of the effective strut area. To resolve this difference and for clarity, new minimum reinforcement provisions are recommended for article 5.6.3.6 in AASTHO LRFD (2008) as seen in Appendix A.

It was observed that limiting the spacing of the web reinforcement was important for reaching the full design strength of the strut and for distributing the diagonal cracks. Currently, in AASHTO LRFD (2008), the spacing of crack control reinforcement is restricted to 12-inches. It is proposed that this limit be supplemented with a restriction of d/4. Thus, the spacing of the web reinforcement in each direction shall not exceed d/4 or 12-inches. This limit is consistent with the spacing limits of the other minimum reinforcement provisions reviewed in Section 4.5.1.

4.5.5 Summary

In Section 4.5, the effect of web reinforcement on the strength and serviceability performance of deep beams was addressed. The results indicated that minimum orthogonal reinforcement pertaining to 0.3% of the strut area should be provided in deep beams ($a/d < 2$). This conclusion was based on the test results of beams of various size (21”x23”, 21”x42”, 21”x44”, 36”x48”, and 21”x75”), of beams tested at a/d ratios of 1.2 and 1.85, and of beams with either 2- or 4-legged stirrups.

In general, the failure mode and overall performance of the deep beam specimens was consistent with a single-panel strut-and-tie model in which the load was transferred through the member via a direct, diagonal strut. As such, the purpose of the reinforcement in terms of strength was to resist the transverse tensile stress in the bottle-shaped strut. For this reason, companion specimens with different amounts of reinforcement in each direction had similar

shear strength as long as at least 0.2% reinforcement was provided. However, a difference in performance was observed in regards to the width of diagonal cracks. The crack data was evaluated with an approximate tolerable crack width of 0.016-inches and at a service load of 33% of ultimate. The results indicated that the width of the cracks were proportional to the amount of web reinforcement with diminishing returns near service load levels as the reinforcement greatly exceeded 0.3% in each direction. Specifically, the data suggested that 0.2% reinforcement in each orthogonal direction was insufficient to restrain the width of the cracks to 0.016-inches at service loads and often at first cracking. Specimens with 0.3% reinforcement in each direction performed significantly better, satisfying the serviceability criteria at first cracking and at service loads.

For the few members tested at an a/d ratio of 2.5, the amount of web reinforcement did affect the shear strength. The specimen with 0.3% reinforcement in each direction failed at a load 60% higher than the companion specimen with 0.2% in each direction. The failure mode of test III-2.5-02 was consistent with a sectional shear failure with minimal parallel diagonal cracking. The failure mode of test III-2.5-03 was consistent with the combination of a deep beam and sectional shear failure due to presence of the additional reinforcement.

4.6 Effect of Member Depth

The purpose of this task was to evaluate the effect of member depth on the strength and serviceability performance of reinforced concrete deep beams. A brief review of the literature associated with the effect of depth on deep beams is provided. After that, the strength and serviceability results obtained through the experimental program are presented.

4.6.1 Background

Numerous research studies have been conducted on the effect of depth on the shear strength of reinforced concrete beams. Most of the work has focused on slender beams in which the a/d ratio is greater than 2. However, several studies conducted within the last fifteen years have addressed the effect of depth on the behavior of deep beams as well (a/d < 2). In both cases, most of these investigations have concluded that a size effect exists. In this case, size effect refers to a reduction in ultimate shear strength, typically measured by a normalized shear stress at failure ($V / f_c' b_w d$ or $V / \sqrt{f_c'}\, b_w d$), as the depth of the member increases. There are numerous theories in the literature that attempt to explain size effect, but there is little consensus. Three of the most common size effect theories for shear are based upon material strength variations, diagonal crack widths, and fracture mechanics.

The oldest size effect theory, that of statistical strength variations, was based on the work of Weibull in 1939. Applied to reinforced concrete, the theory justifies the reduction in strength that exists with an increase in member size to the randomness of material strength. A reinforced concrete structure is compared to a series of chain links in which the failure of one link causes the entire chain to fail. As the depth of a beam gets larger, the number of links increases and the probability of a lower stress at failure increases due to the variability in the material strength of concrete.

Size effect has also been explained in terms of the width of diagonal cracks. According to modified compression field theory, as the depth of a beam increases, the spacing of diagonal cracks increase and thus, the width of diagonal cracks increase (Collins and Kuchma, 1999 and

Macgregor and Wight, 2005). The increase in crack width reduces the ability to transmit shear across the diagonal crack by aggregate interlock. Thus, size effect is explained by the reduced effectiveness of the interface shear transfer mechanism.

Other researchers explain size effect for shear in reinforced concrete beams with fracture mechanics (Reinhardt, 1981 and Bazant and Kazemi, 1991). It is theorized that there are differences in the rate at which stored energy is released during crack propagation for beams of different sizes. Specifically, cracks propagate faster in larger beams than in smaller beams. Several research studies have shown that the cracking pattern of a larger beam is more extensive than an otherwise identical smaller beam at the same shear stress (Walraven and Lehwalter, 1994 and Tan and Lu, 1999).

In general, these theories were originally derived for slender beams ($a/d > 2$). While they can be applied to the study of deep beams ($a/d < 2$) to some degree, another approach may be more appropriate. After strength results from the literature and from the experimental program are presented, it will be apparent that the effect of depth on the strength of deep beams can be better understood in terms of a strut-and-tie model analysis.

4.6.2 Strength Results

Strength Results from the Literature

Numerous experimental studies have been conducted on the size effect of deep beam shear. Four studies will be reviewed in this section in detail. In 1994, thirteen reinforced concrete deep beams were tested at an a/d ratio of 1.0 by Walraven and Lehwalter. All of the beams were approximately 9.8-inches wide. The effective depth ranged from 6.3- to 36.6-inches. The length of the load plate and the support plate varied with the effective depth such that the ratio between the two equaled 0.25. Each beam was simply supported and was loaded with a single concentrated load at midspan. The test specimens were divided into three groups. The first group did not have any web reinforcement. The second and third groups had vertical reinforcement corresponding to a ρ_v of approximately 0.0015 and 0.003, respectively. The experimental shear strength normalized by the shear area and the compressive strength of concrete are plotted versus the effective depth in Figure 4.72. From the test results, a size effect is apparent. As the depth of the member increases, the normalized shear stress at failure decreases. The loss in shear strength was attributed to the difference in the rate of crack propagation for the beams of different depths. Specifically, the ability to transmit tensile stress across diagonal cracks was reduced for the larger beams due to larger crack widths when compared to smaller beams at similar stress levels.

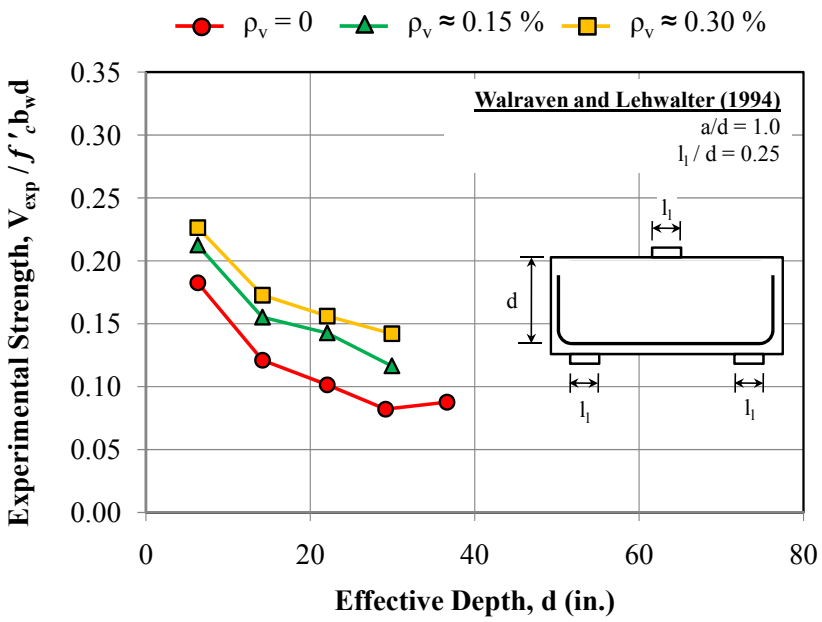

Figure 4.72: Size effect strength results from Walraven and Lehwalter (1994)

In 1999, twelve reinforced concrete deep beams were tested by Tan and Lu. Size effect in deep beam shear was studied at three different a/d ratios: 0.56, 0.84, and 1.13. All of the beams had a width of 5.8-inches. The effective depths ranged from 17.5- to 61.4-inches. The length of the bearing plates at the load and the support were kept constant at 9.8-inches for all of the specimens (Tan and Cheng, 2006). Each beam was simply supported and was loaded with two point loads at the third points. The test specimens were divided into three groups by the a/d ratio. The smallest beam in each group (d=17.5-inches) did not have any web reinforcement. The other three beams in each group had equal reinforcement in the horizontal and vertical directions satisfying a reinforcement ratio of 0.0012. The test results are plotted in Figure 4.73. These test results agree well with those in Figure 4.72. The normalized shear stress at failure decreases with the increasing depth of the member. The authors attributed the decline in strength to the difference in the rate of energy release due to crack propagation for the beams of different sizes. Specifically, they noted that the larger beams had more developed cracks than the smaller beams at a given shear stress. In addition, the authors noted that size effect was greatest when the effective depth increased from 17.5- to 34.8-inches. At depths larger than 34.8-inches, the reduction in shear stress at failure was not as high.

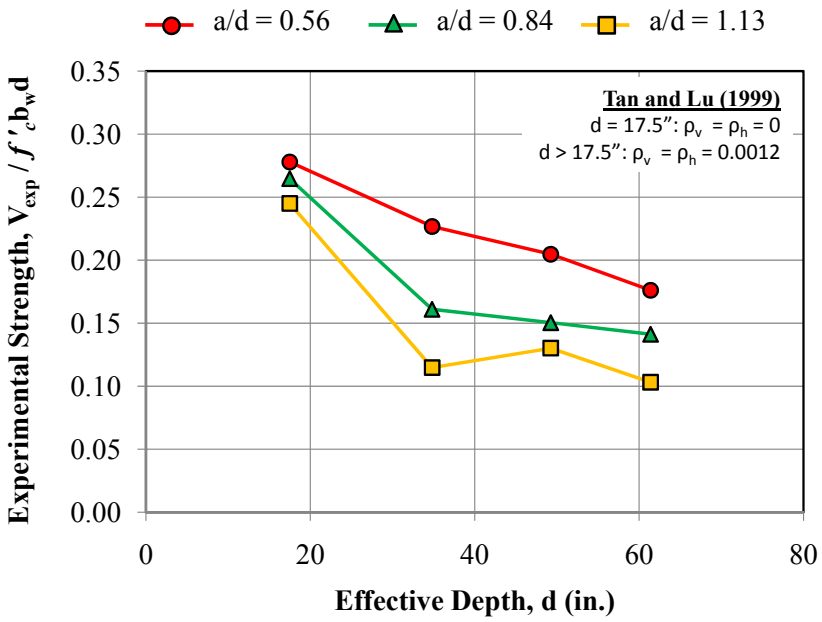

Figure 4.73: Size effect strength results from Tan and Lu (1999)

In 2001, nine reinforced concrete deep beams were tested at an a/d ratio of 1.0 by Matsuo et al. All of the beams were 5.9-inches in width. The effective depths ranged from 7.9-inches to 23.6-inches. Similar to the study by Walraven and Lehwalter, the length of the load and support plates were varied with the effective depth of the beam such that the ratio between the two was 0.25 for all of the specimens. Also, the beams were simply-supported and were tested with a single concentrated load at midspan. Three beams did not have any web reinforcement; three beams had vertical reinforcement corresponding to a ρ_v of 0.0042; three beams had vertical reinforcement corresponding to a ρ_v of 0.0084. The test results are plotted in Figure 4.74. All of the beams failed according to a shear-compression mode with a considerable amount of crushing around the loading point. For the specimens without web reinforcement, the normalized shear stress at failure decreased with increasing depth, indicating size effect. While the shear strength of the specimens with web reinforcement generally decreased with increasing depth as well, the reduction was not as consistent. It is possible that web reinforcement acted to alleviate size effect to some degree. According to the authors, the size effect was attributed to a reduction in "*the ratio of the region of compression failure to total region of the specimen*" (Matsuo et al., 2001).

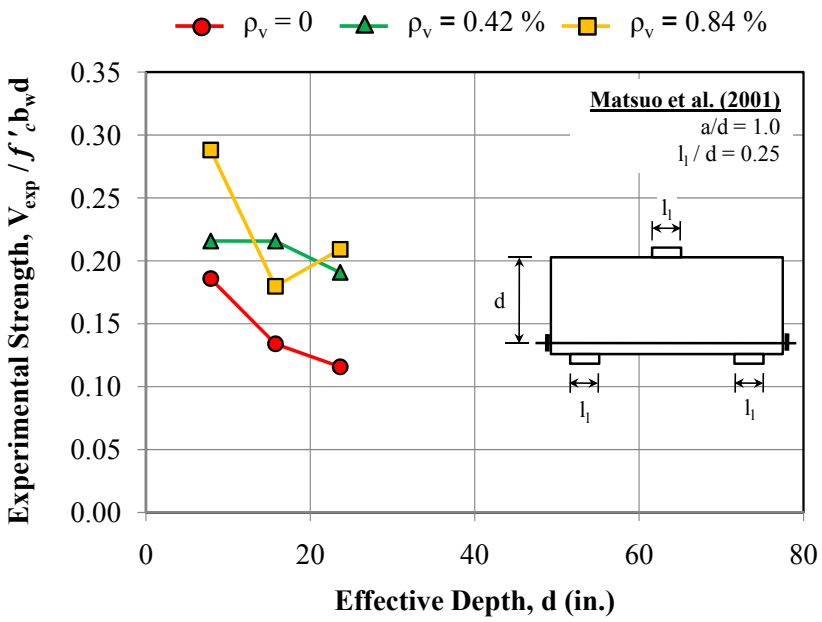

Figure 4.74: Size effect strength results from Matsuo et al. (2001)

In 2007, twelve reinforced concrete deep beams were tested at an a/d ratio of 1.1 by Zhang and Tan. The test specimens were divided into three groups of four. Within each group, the effective depth of the beam varied from 12.3- to 35.6-inches. In the first group, the beam width was constant at 3.2-inches, and there was not any web reinforcement. In the second group, there was also no web reinforcement; but the beam width varied from 3.2- to 9.8-inches. In the third group, the beam width varied as in group 2; and web reinforcement corresponding to a ρ_v of approximately 0.004 was provided ($\rho_h = 0$). For all of the specimens, the length of the load and support plates varied with the effective depth such that the ratio between the two was approximately 0.17. The beams in this study were loaded with two concentrated loads at the third points. The test results are plotted in Figure 4.75. Unlike the data plotted in Figure 4.72 through Figure 4.74, no size effect is apparent for the tests conducted by Zhang and Tan. The authors attributed the lack of size effect to the appropriate proportioning of the length of the load and support plates to the depth of the beams. "*Thus, [controlling] strut geometry plays a dominant role in mitigating the size effect in ultimate shear strength of deep beams*" (Zhang and Tan, 2007). From a strut-and-tie model perspective, where the strength of a deep beam is often governed by dimensions of the struts and nodes, these results make sense.

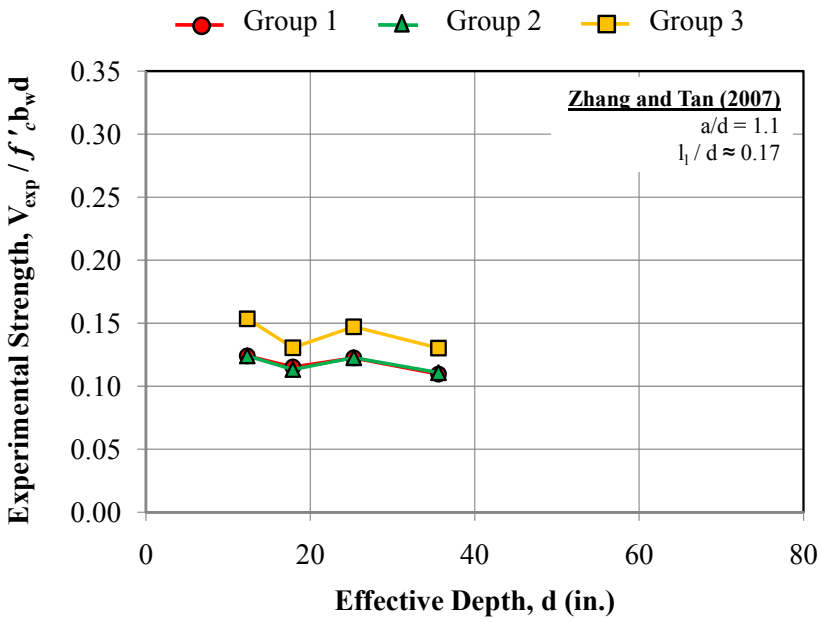

Figure 4.75: Size effect strength results from Zhang and Tan (2007)

The experimental results in Figure 4.75 were further explained with finite element models (FEM) by Zhang and Tan (2007). Two sets of analyses were conducted. In the first set, each of the twelve test specimens were analyzed with the same loading conditions as the actual tests. The FEM results agreed well with the test results. In the second set, the lengths of the support and load plates were not varied with the depth of the specimens as they were in the actual tests. Instead, a constant length of 2.1-inches was used for the length of all bearing plates in all of the beams. This length equaled the length of the plates for the smallest test specimen (d = 12.3-inches). The results of the analyses are illustrated in Figure 4.76 and Figure 4.77. When the bearing plates were varied with the depth of the member, no apparent size effect existed. Whereas, when the bearing plate sizes were kept constant as the depth of the member increased, size effect was present. These results indicate that the strut geometry dominates the ultimate shear strength of deep beams, and controlling this geometry can effectively mitigate size effect.

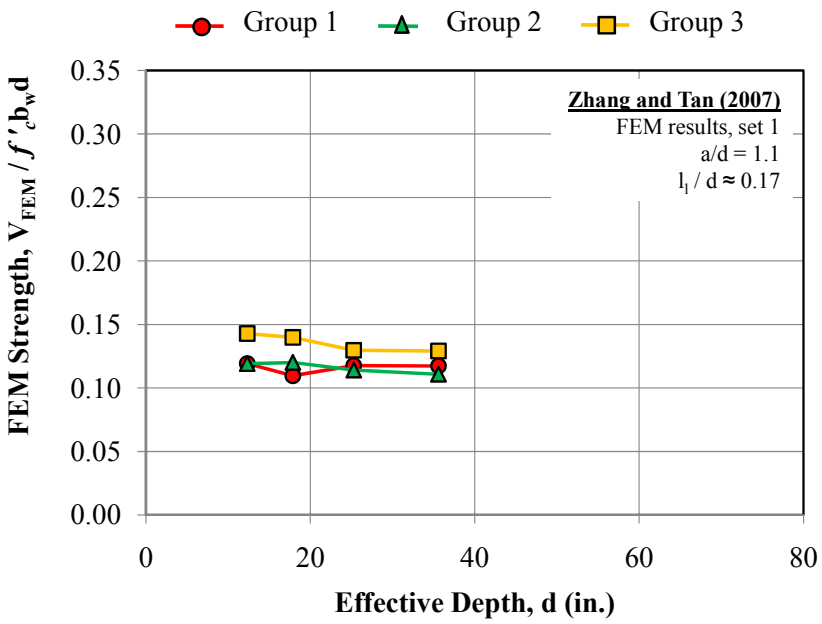

Figure 4.76: FEM results in which bearing plate sizes increased with increasing member depth (Zhang and Tan, 2007)

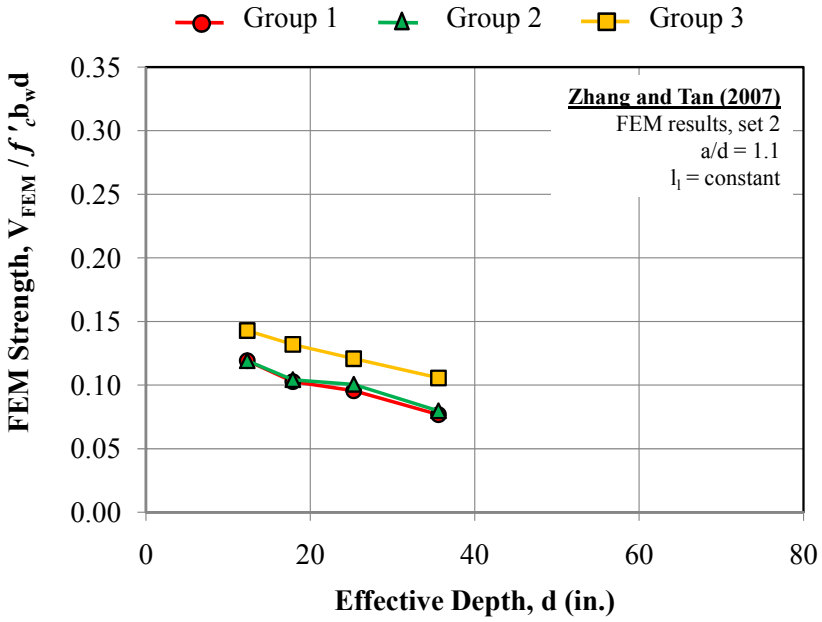

Figure 4.77: FEM results in which bearing plate sizes were constant with increasing member depth (Zhang and Tan, 2007)

There is some disagreement between the findings of Zhang and Tan (2007) and the test results of Walraven and Lehwalter (1994) and Matsuo et al. (2001). By proportioning the length of the load and support plates according to the depth of the beam, Zhang and Tan were able to mitigate size effect. However, when both Walraven and Lehwalter and Matsuo et al.

proportioned their bearing plates in the same manner, size effect was not mitigated. Zhang and Tan attributed the discrepancy between their findings and those of Walraven and Lehwalter to the "*uneven distribution of shear reinforcement*" for the different beam sizes of the latter. The spacing of the transverse reinforcement in specimens of Walraven and Lehwalter was approximately d/4 for each beam regardless of the size. However, the same numerical spacing of approximately 5.9-inches was used for all of the beams of Zhang and Tan. While the distribution of reinforcement for the larger beams may have contributed to the discrepancy between the results of these two studies, it was not solely responsible. In the study by Matsuo et al., the bearing plates were varied according to the depth of the beam and the distribution of reinforcement was consistent between each of the beams. Size effect was still apparent in these tests, albeit not as pronounced.

It is plausible that the other contributing factor to the discrepancy between the aforementioned studies is the loading configuration. Walraven and Lehwalter and Matsuo et al. tested their specimens with a single concentrated load at midspan. They proportioned the length of the load and the support plates according to the depth of the beam. However, since a single load is applied at midpsan, the bearing stresses at the load are twice as high as those at the supports. Conversely, Zhang and Tan tested their specimens with two concentrated loads applied at the third points. Due to this arrangement, the bearing stresses at the load and the support were equivalent. It is possible that the uneven proportioning of the length of the load and support plates in the tests by Walraven and Lehwalter and Matsuo et al. contributed to the difference in results with those of Zhang and Tan.

From the aforementioned studies, it was shown that a reduction in the normalized shear stress at failure ($V/f_c'b_wd$) existed when the load and support plates were not properly proportioned according to the depth of the beam. When the length of the bearing plates were increased with the depth of the member, no size effect was apparent, especially for members with web reinforcement. From a strut-and-tie model perspective, these results make sense. In STM, the strength of a deep beam is often controlled by the stress on the nodal faces. If the size of the nodes is increased proportionally to the depth of the member, then a similar normalized stress at failure should be expected. (Node size increases, V_{ult} increases, d increases, and $V/f_c'b_wd$ remains constant). Similarly, if the node size remains constant as the depth of the member increases, then a reduction in the normalized shear stress at failure should be expected. (Node size is similar, V_{ult} is similar, d increases, and $V/f_c'b_wd$ decreases). Therefore, evaluating the effect of depth on the strength of deep beams should be done from a strut-and-tie model perspective.

Strength Results from the Experimental Program

Before the tests in Series IV could be conducted, the size of the load and support plates of the different-sized specimens needed to be determined. Based on previous research studies, it was apparent that the length of the bearing plates affected the strength results of deep beams as the effective depth increased. Also, the tests in the current study on triaxially-confined nodal regions (Section 4.4) revealed that the length of the bearing plates at CCC nodes were far more important to the strength of deep beams than the width. Thus, the bearing plate dimensions used for the tests in Series IV were carefully chosen.

The dimensions for the bearing plates and the supporting columns of several TxDOT bent caps were studied (Figure 4.78). In general, the length of the bearing plates appeared to be based

off the size of the girder supported by the bent cap, rather than the depth of the bent cap itself. The length of the bearing plates used in the Greens Road bent caps and in standard Type IV bent caps were identical even though the overall depth of these members differed by nearly a factor of 2. The length of the pot bearings used in the I-345 bent cap in Dallas, however, were exceptionally large due to the size of the continuous steel plate girders resting on top of it. Therefore, notwithstanding the I-345 bent cap, the length of bearing plates were generally independent of the depth of the member.

Bent Cap	Bent Cap Size (bxh)	Girder Type	Bearing Plate Size (l x b)	Supporting Column Size
Standard Interior Bent Cap	33" x 36"	A*	12" x 7"	circular φ = 30"
		B*	14" x 7"	
		C*	16" x 7"	
	39" x 42"	IV*	22" x 7"	circular φ = 36"
	42" x 42"	Tx28 – Tx54*	21" x 8"	
Greens Road	45" x 78"	Steel Box	22" x 22"	rect. 57" x 56"
I-345	72" x 120"	Steel Plate	42" x 36"	rect. 72" x 72"

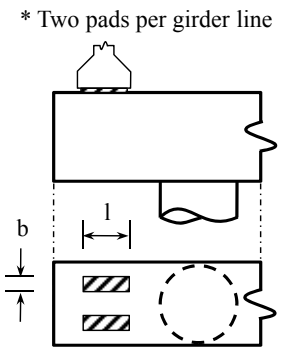

Figure 4.78: Bearing plate dimensions in several TxDOT bent caps (TxDOT, 2008)

For the Series IV specimens, the sizes of the bearing plates were not linked to the depth of the member. Instead, the bearing plate dimensions were selected to create similar size nodal regions (CCC and CCT) for each of the three sections tested within this task. The effect of increasing the member depth without increasing the size of the nodal regions on the strength of deep beams was evaluated with this choice. More importantly, it appeared to be more consistent with typical TxDOT practice. The relative sizes of the nodal regions using a single-panel STM for the three sections tested within this task are depicted in Figure 4.79 and Figure 4.80.

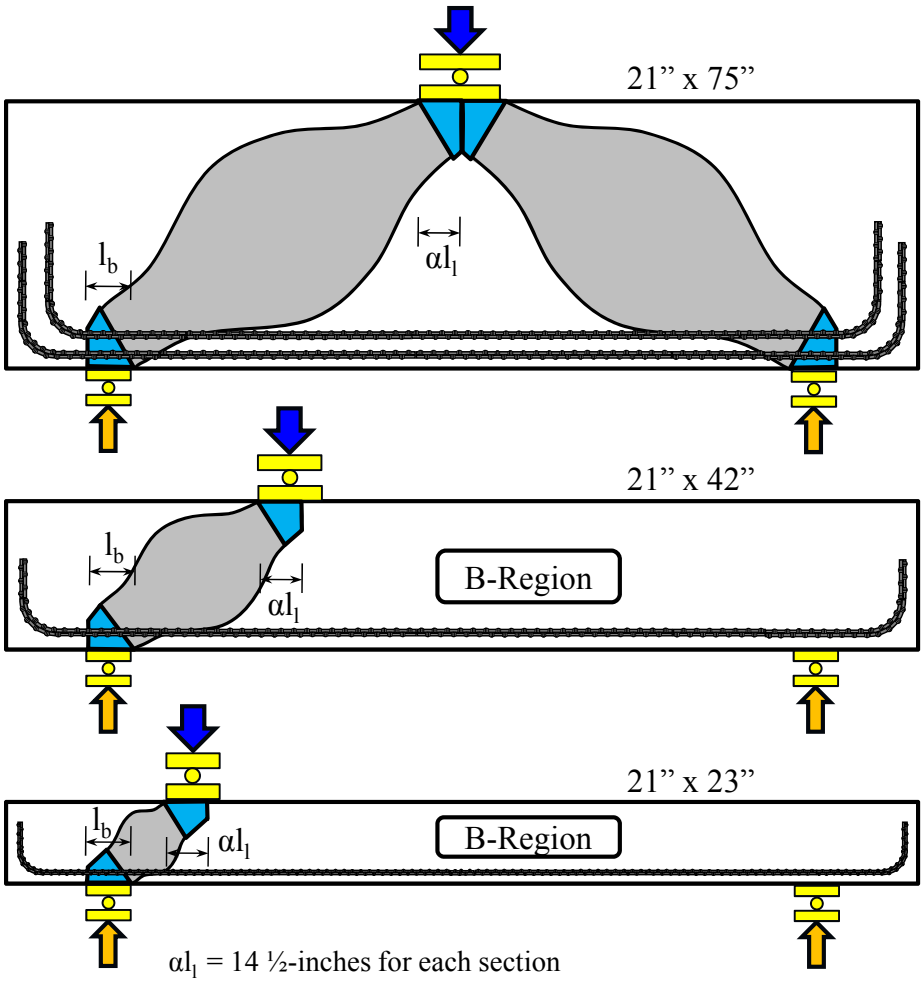

αl_l = 14 ½-inches for each section
l_b = 16-inches for each section
a/d = 1.85
*Reinforcement does not represent actual steel in specimen

Figure 4.79: Relative size of nodal regions for depth effect specimens

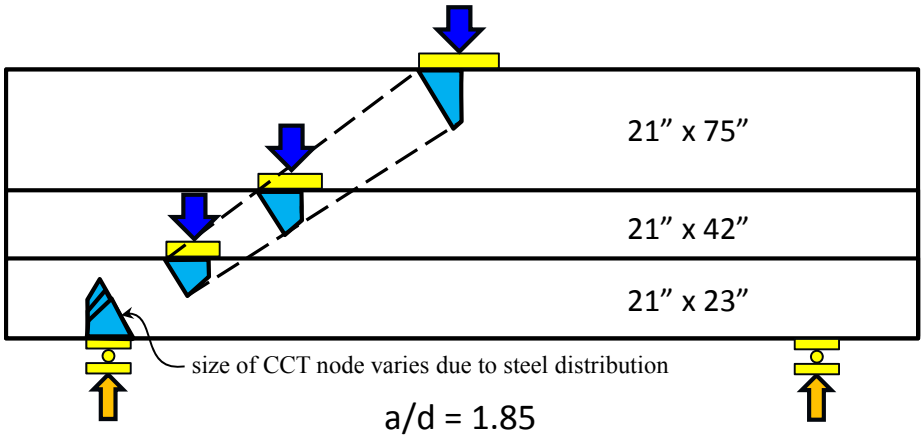

Figure 4.80: Relative size of nodal regions in depth effect specimens (2)

Since the test specimens were loaded with a single point load, the critical dimension at the load point was not the full length of the bearing plate, but rather the percentage of the bearing plate that was used in the strut-and-tie model for the test region. Therefore, this dimension, αl_l, was kept constant for the three beam sizes (14.5-inches). For reference, α equals 0.5 for the specimen loaded at midspan. The length of the support plates was constant for all of the beams (16-inches). As shown in Figure 4.80, the resulting sizes of the nodal regions were fairly equal even though the overall depth of the test specimen increased from 23- to 75-inches. The size of the node-to-strut interface increased slightly as the depth increased due to the increase in the back face dimensions of the CCC and CCT nodes. It was not possible to keep these dimensions constant for specimens of different sizes while maintaining the same longitudinal reinforcement ratio.

The test specimens from the experimental program used to evaluate the effect of depth on the strength of deep beams are listed in Table 4.10. The small (21"x23") and the large (21"x75") sections were tested in Series IV. The results of these tests were compared with similar tests conducted on the 21"x42" section in Series III. The experimental strength results and the relevant information about each specimen is listed in Table 4.10.

Table 4.10: Strength results for depth effect specimens

Beam I.D.	b_w in.	d in.	f'_c psi	Nominal ρ_v & ρ_h	Support Plate† in.	Load Plate† in.	α	a/d ratio	V_{test} kip	$\frac{V_{test}}{f_c' \cdot b_w d}$	$\frac{V_{test}}{\sqrt{f_c'} \cdot b_w d}$	V_{crack} / V_{test}
III-1.85-02	21	38.6	4100	0.002	16x21	20x21	0.72	1.84	488	0.15	9.4	0.23
III-1.85-03b	21	38.6	3300	0.003	16x21	20x21	0.72	1.84	471	0.18	10.1	0.24
III-1.85-02b	21	38.6	3300	0.002	16x21	20x21	0.72	1.84	468	0.17	10.1	-
III-1.2-02	21	38.6	4100	0.002	16x21	20x21	0.82	1.20	846	0.25	16.3	0.20
III-1.2-03	21	38.6	4220	0.003	16x21	20x21	0.82	1.20	829	0.24	15.7	-
III-2.5-02	21	38.6	4630	0.002	16x21	20x21	0.62	2.49	298	0.08	5.4	0.35
III-2.5-03	21	38.6	5030	0.003	16x21	20x21	0.62	2.49	516	0.13	9.0	-
IV-2175-1.85-02	21	68.9	4930	0.002	16x21	29x21	0.5	1.85	763	0.11	7.5	0.28
IV-2175-1.85-03	21	68.9	4930	0.003	16x21	29x21	0.5	1.85	842	0.12	8.3	0.26
IV-2175-2.5-02	21	68.9	5010	0.002	16x21	24x21	0.33	2.50	510	0.07	5.0	0.28
IV-2175-1.2-02	21	68.9	5010	0.002	16x21	24x21	0.67	1.20	1223	0.17	11.9	0.21
IV-2123-1.85-03	21	19.5	4160	0.003	16x21	16.5x21	0.86	1.85	329	0.19	12.5	0.18
IV-2123-1.85-02	21	19.5	4220	0.002	16x21	16.5x21	0.86	1.85	347	0.20	13.0	0.19
IV-2123-2.5-02	21	19.5	4570	0.002	16x21	15.5x21	0.81	2.50	161	0.09	5.8	0.32
IV-2123-1.2-02	21	19.5	4630	0.002	16x21	18x21	0.91	1.20	592(f)	0.31	21.2	0.21

† *Length along span (l) x length along width (w)*

(f) *Maximum shear carried in specimen upon the occurrence of concrete crushing at the compression face.*

The strength results for the specimens in Table 4.10 tested at an a/d ratio of 1.85 are plotted in Figure 4.81. The experimental shear strength was normalized by the shear area and the compressive strength of concrete. It is clear from the plot that with increasing depth, the normalized shear stress at failure decreases. These results are consistent with those of previous research studies (Walraven and Lewalter, 1994; Tan and Lu, 1999; and Matsuo et al., 2001). It is also clear from the plot that increasing the web reinforcement ratio in each direction from 0.2% to 0.3% did not affect the strength of the member. This finding confirms the results discussed in Section 4.5.2 regarding the effect of web reinforcement on the strength of deep beams.

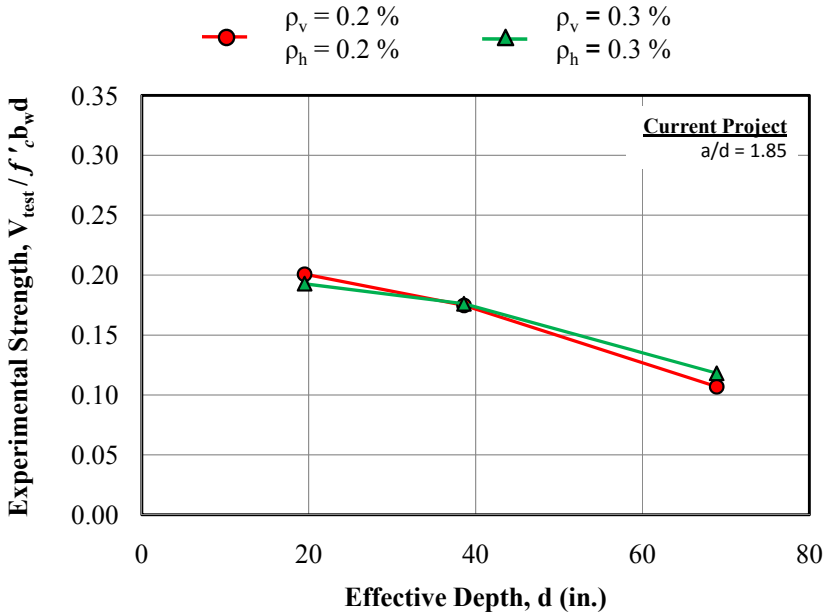

Figure 4.81: Strength results of depth effect specimens at a/d of 1.85

The test regions at failure for the three specimens representing the red line in Figure 4.81 ($\rho_v = \rho_h = 0.002$) are illustrated in Figure 4.82. The mode of failure for these tests was generally the same. Numerous parallel cracks formed along the line between the applied load and the support indicating the presence of a direct strut transfer mechanism. At the ultimate applied load, local crushing near the load point and along the strut occurred. The black lines in Figure 4.82 represent the final failure crack of each specimen. It is interesting to note that the final failure crack for the 75-inch specimen extended from the edge of the load plate at an angle of approximately 45-degrees instead of extending from the edge of both plates as in other tests.

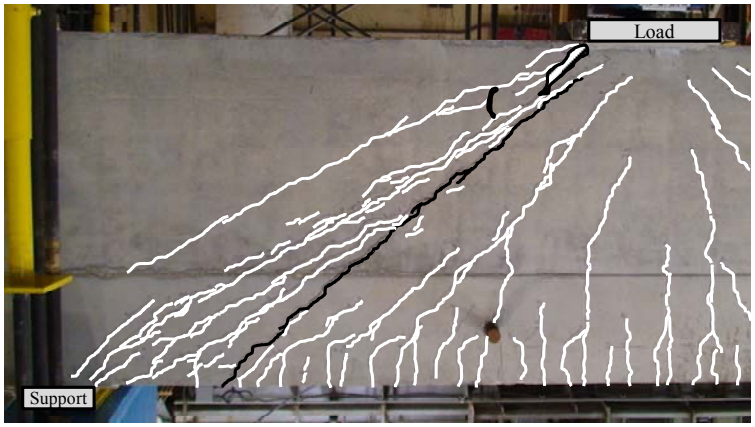

a). IV-2175-1.85-02

V_{max} = 763 kips
$7.5\sqrt{f'_c}\cdot b_w\cdot d$
$0.11 f'_c\cdot b_w\cdot d$

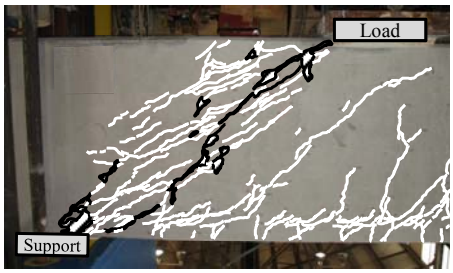

b). III-1.85-02b (pre-cracked)

V_{max} = 468 kips
$10\sqrt{f'_c}\cdot b_w\cdot d$
$0.17 f'_c\cdot b_w\cdot d$

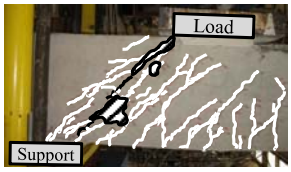

c). IV-2123-1.85-02 (pre-cracked)

V_{max} = 347 kips
$13\sqrt{f'_c}\cdot b_w\cdot d$
$0.20 f'_c\cdot b_w\cdot d$

Figure 4.82: Failure photographs for depth effect specimens with a/d of 1.85 and 0.2% reinforcement

The strength results for the specimens tested at several a/d ratios (1.2, 1.85, and 2.5) and with 0.2% web reinforcement in each direction are plotted in Figure 4.83. The normalized shear strength of the specimens decreased with increasing depth as before. It is important to note that the normalized shear strength of the 23-inch specimens at a/d ratios of 1.2 and 1.85 differ with that of the 75-inch specimens by a factor of 2. For the specimens tested at an a/d ratio of 2.5, the normalized shear strength only slightly decreased with increasing effective depth. The reduction in size effect as the a/d ratio increases was also reported by Tan et al. (2005). In their study, the strength results indicated that size effect was more dominant for beams tested at an a/d ratio of 1.69 and less as compared to similar beams tested at an a/d ratio of 3.38.

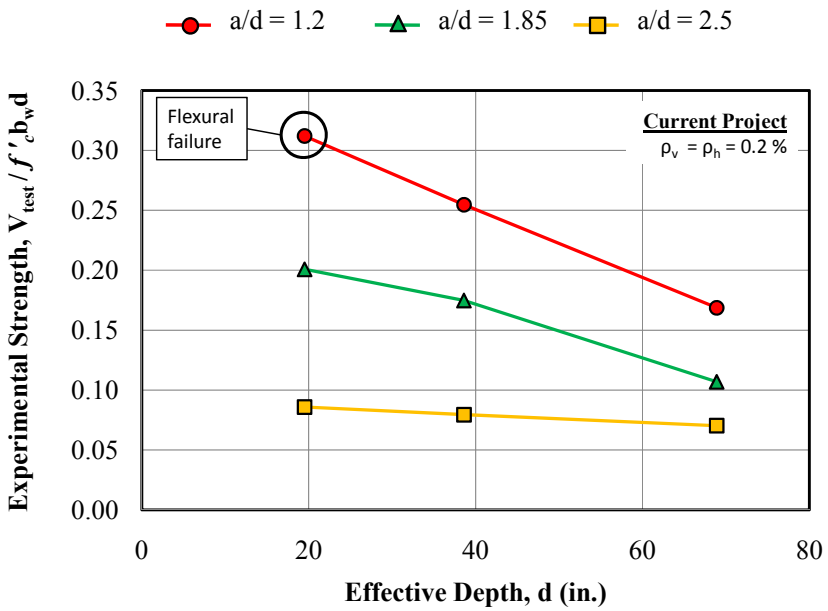

Figure 4.83: Strength results of all depth effect specimens

The test regions at failure for the three specimens representing the red line in Figure 4.83 (a/d = 1.2) are illustrated in Figure 4.84. The mode of failure for the 42- and the 75-inch specimen was the crushing of the direct strut between the load and the support. The cracking patterns and the presence of local crushing along the strut and near the applied load were similar to those of the specimens tested at an a/d ratio of 1.85 (Figure 4.82). The 23-inch specimen, however, failed in flexure. The size of the nodal regions in relation to the shear span increased the shear capacity to the point where flexure was the controlling failure mechanism. From an academic standpoint, it can be inferred that the actual shear strength of this specimen was greater than the shear that produces the flexural failure. It is important to note that the strut-and-tie procedure does account for flexural failures with the check of tensions ties and the back face of CCC nodes.

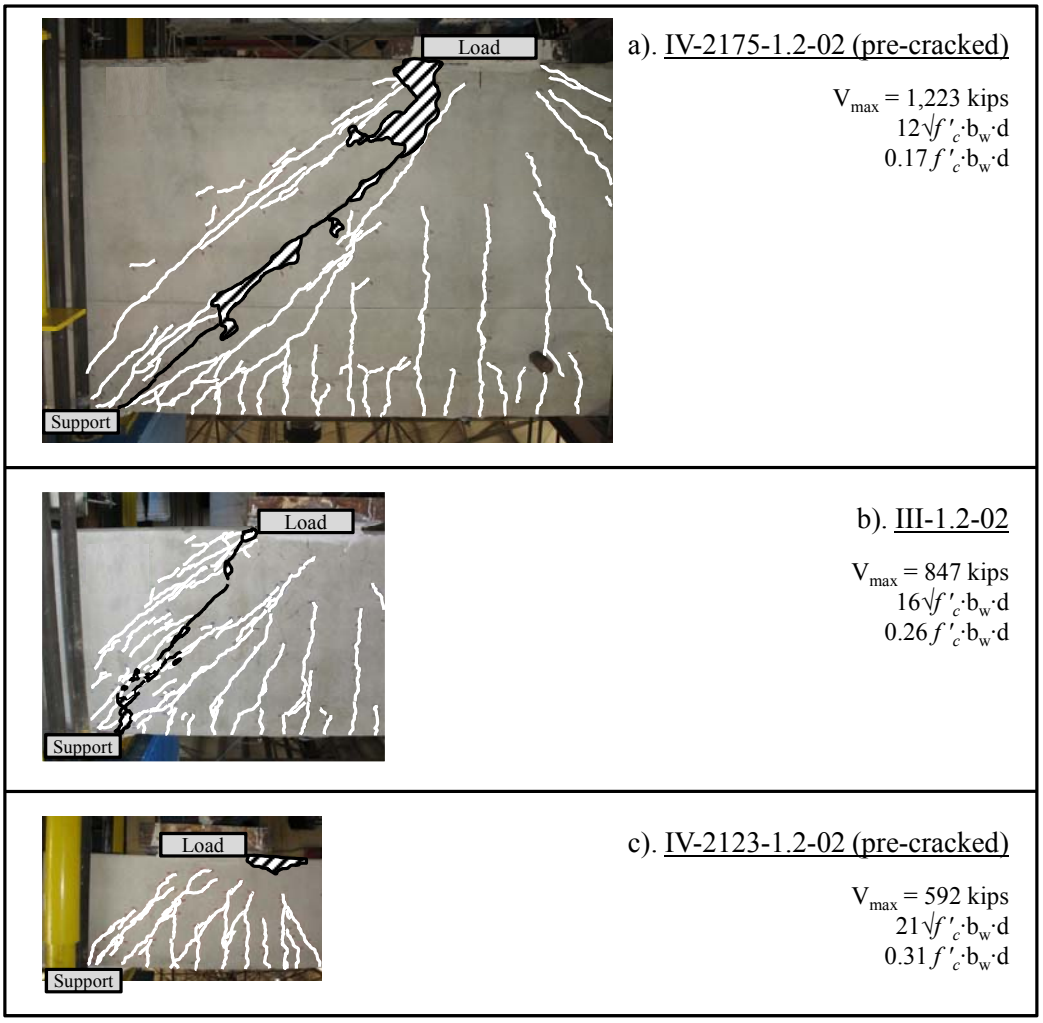

Figure 4.84: Failure photographs of depth effect specimens with a/d of 1.2

Lastly, the test regions at failure for the specimens loaded at an a/d ratio of 2.5 (orange line in Figure 4.83) are provided in Figure 4.85. For the 23- and 42-inch specimens, the mode of failure was drastically different than those at the other a/d ratios. As seen in Figure 4.85, the failure crack resembled a sectional shear, or diagonal tension, crack. Very little crushing or parallel cracking was detected in the region of a direct strut. This difference in behavior was not surprising since it is well known that as the a/d ratio approaches 2, the dominant shear transfer mechanism starts to change. At low a/d ratios (a/d < 2), an arching, direct strut mechanism is dominant. At higher a/d ratios (a/d > 2), a sectional shear mechanism in which shear resistance is provided by the concrete (V_c) and steel (V_s) is dominant. For the 75-inch specimen, the final failure crack slightly resembled a sectional shear crack, but there was a considerable amount of parallel cracking in the region of the direct strut. The behavior of this test further illustrates that the transition between deep beam behavior and sectional behavior is gradual; it does not occur at a distinct a/d ratio. The transition between deep beam behavior and sectional behavior and variables that affect it are addressed explicitly in Section 5.3. From the test results of these three beams (orange line in Figure 4.83), it is clear that the amount of size effect depends upon the dominant transfer mechanism and thus, the a/d ratio.

Figure 4.85: Failure photographs of depth effect specimens with a/d of 2.5

The reduction in the normalized shear strength with increasing depth (size effect) in Figure 4.81 and Figure 4.83 can be explained with a strut-and-tie model analysis. As discussed throughout this report (Section 5.3), the primary load carrying mechanism for deep beams (a/d < 2) is best captured with a single-panel strut-and-tie model. According to the model, the capacity of deep beams is often governed by the size of the nodal regions. The depth of the member does not directly affect the strength. Therefore, it is inappropriate to normalize the experimental strength of deep beams by the member depth. Doing so assumes that the strength of deep beams is a function of the beam depth. A similar conclusion was reached by Zhang and Tan (2007). They, too, noted that the primary cause of size effect was the inappropriate use of the "*conventional definition of shear strength of V/(bd)*" for concrete deep beams (Zhang and Tan, 2007).

From a design perspective, the most appropriate way to normalize experimental strength is with design strength. The design procedure should account for every major variable that affects the strength of the member, and therefore, should provide a consistent means of comparison between beams with any combination of these variables. The experimental strength of the specimens tested in the current task was normalized with the design strength computed

according to the strut-and-tie model provisions discussed in Section 5.2. The results are depicted in Figure 4.86. For the deep beams (a/d < 2), there was very little difference in the reserve capacity (V_{test} / $V_{calc.}$) as the depth of the member increased. A reasonably uniform level of conservatism existed as the effective depth increased. The reserve capacity of the 75-inch deep beams (a/d < 2) was approximately 15% less than that of the 23-inch deep beams. This difference is considered negligible in regards to deep beam shear strength. These results indicate that the single-panel strut-and-tie model adequately captured the experimental behavior of the specimens tested at an a/d ratio less than 2. It should be noted that similar conclusions would be reached if the STM provisions in ACI 318-08 or AASHTO LRFD (2008) were used to estimate capacity.

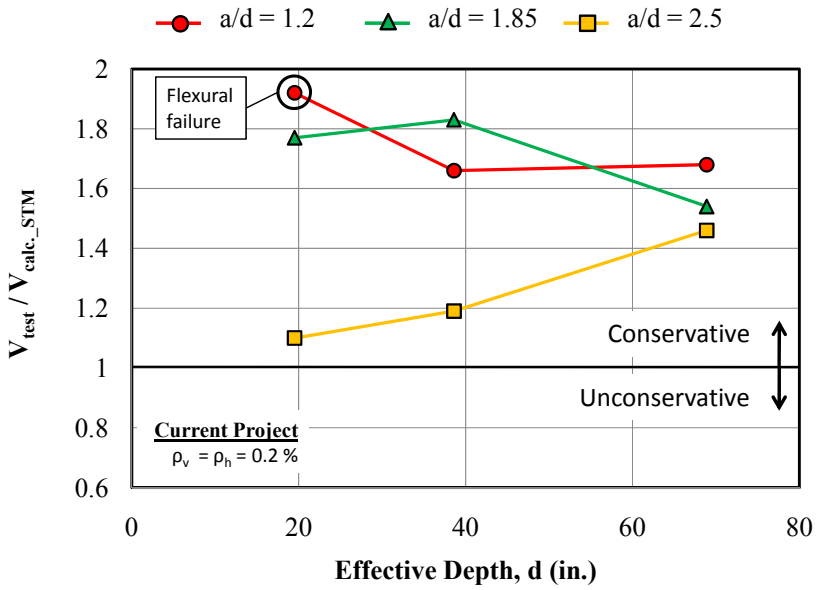

Figure 4.86: Experimental strength of depth effect specimens normalized by calculated strength

Based on the results and discussion of this task, it appears that size effect (reduction in shear strength with increasing depth) is largely eliminated when a strut-and-tie analysis is used to design deep beams (a/d < 2). The specimens tested in the current experimental program at an a/d ratio less than 2 failed in general agreement with a single-panel strut-and-tie model. The capacity of the STM was governed by the size of the nodal regions. As such, the strength of the deep beams was a function of the size and stress conditions in the nodal regions, not a function of the beam depth. The size effect of deep beams reported in the literature is largely the result of incorrectly assuming that their strength is a function of section size.

For the beams tested at an a/d ratio of 2.5, the same conclusions did not apply. As noted in Figure 4.85, the specimens tested at this a/d ratio did not fail in a consistent manner with a single-panel STM. Instead, their failure modes more closely resembled sectional shear, or diagonal tension, failures. For this reason, the reserve capacity ($V_{test.}$ / $V_{calc.}$) for these specimens was not consistent with the rest of the tests (Figure 4.86). However, in all three cases, the strength was conservatively estimated due to the inherent conservatism in the strut-and-tie modeling procedure. These results illustrate a limitation of using a single-panel STM on beams

loaded with an a/d ratio greater than 2. When the behavior of the member is not consistent with the design procedure, the chance of calculating an unconservative estimate of strength increases.

Therefore, in general, it may not be appropriate to apply a single panel STM analysis to design deep beams with a/d ratios of 2.5. The experimental behavior of these members does not match the behavior assumed in a single-panel STM. Similarly, size effect of beams loaded with an a/d ratio of 2.5 should not be evaluated by normalizing the experimental strength with calculated strength from a single panel STM. Instead, size effect of these members should be evaluated by normalizing the strength with $\sqrt{f'_c}b_w d$ since these variables are known to be linked to members governed by sectional shear.

The strength results of the specimens tested at an a/d ratio of 2.5, normalized with $\sqrt{f'_c}b_w d$, are presented in Figure 4.87. In this plot, the data indicated that with increasing depth a small decrease in the normalized shear strength existed. The normalized strength dropped by approximately 10% between each increase in section size. This amount of strength loss appears to be fairly negligible considering the range of scatter that is consistent with experimental shear tests. It should be noted that there was some difference in the maximum diagonal crack widths between the 23-inch specimens and the larger specimens that may have contributed to this slight loss in strength. However, the maximum diagonal crack widths for the 42- and 75-inch specimens were similar. The crack width data will be presented in Section 4.6.3.

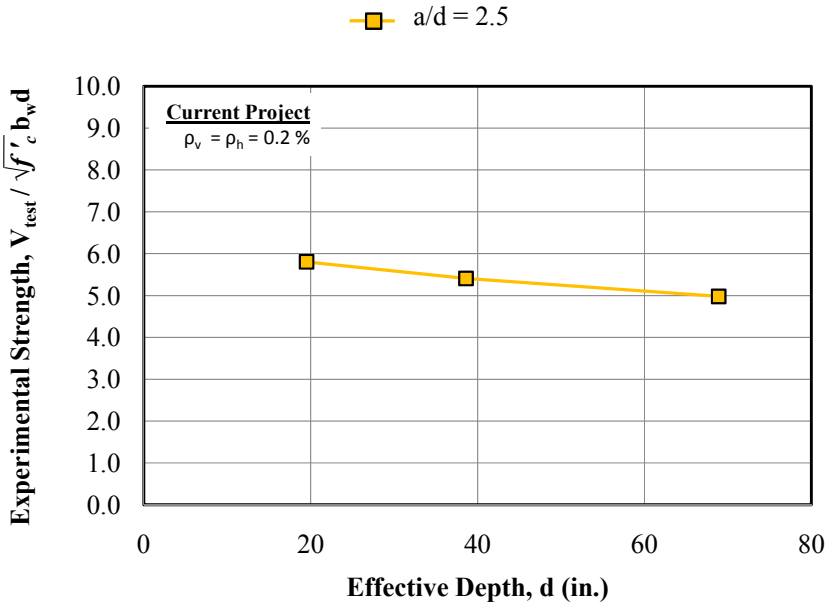

Figure 4.87: Strength results of size effect specimens with a/d of 2.5

The experimental strength of the specimens with an a/d of 2.5 is compared to the calculated strength using the sectional shear provisions ($V_c + V_s$) in AASHTO LRFD (2008) and ACI 318-08 in Figure 4.88. The results indicate that even though there was a loss in strength with increasing depth, the strength was estimated conservatively with the provisions in both specifications. Since the calculated capacity according to each provision does not account for a

size effect, there is a slightly decreasing level of conservatism (V_{test} / (V_c + V_s)) with increasing depth. For the strength estimate according to the AASHTO LRFD provisions, the approximate procedure was used since each specimen contained sufficient transverse reinforcement. The sectional shear provisions in AASHTO LRFD (2008) and ACI 318-08 are provided in Section 5.3.3 for reference.

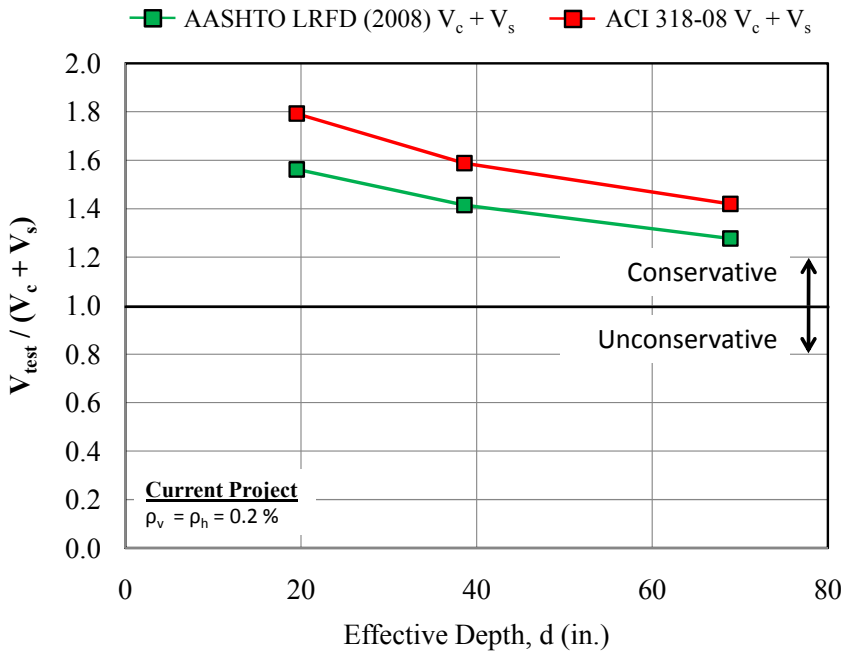

Figure 4.88: Level of conservatism in sectional shear provisions for specimens with a/d of 2.5

For the benefit of the reader, the experimental shear strength, measured in kips, of the beams tested for the depth effect task is plotted in Figure 4.89. The purpose of this plot is to illustrate that the actual load carrying capacity of all the specimens did in fact increase with increasing depth. However, the reason for the increase in strength was not the same for all of the specimens. For the specimens tested at an a/d ratio less than 2, the increase in strength with increasing depth was a result of a slight increase in the back face of the CCC and CCT nodes and the resulting increase in the size of the node-strut interface of each node (Figure 4.80). For these tests, the node-strut interface at the CCT node generally governed the design capacity computed according to Section 5.3. It is clear that the increase in load carrying capacity was not proportional to the increase in depth for the deep beams (a/d < 2) (Figure 4.83). For the specimens tested at an a/d ratio of 2.5, the increase in strength was directly related to the increase in depth, with a minimal reduction due to size effect (Figure 4.87). It is clear that section-based design approaches are more applicable to beams with a/d ratios of 2.5.

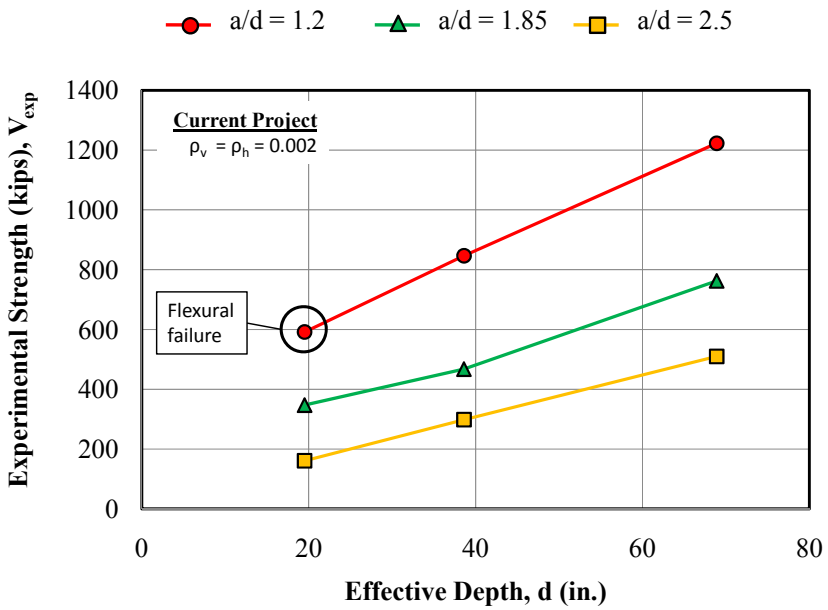

Figure 4.89: Ultimate shear capacity (kips) of size effect speicmens

In the context of strut-and-tie modeling, size effect of deep beams is negligible. Size effect needs to be evaluated in terms of the shear transfer mechanism that governs the behavior of the specimen. In previous studies, it was assumed that the strength of deep beams was a function of the shear area ($b_w d$). While this assumption does not affect the comparisons of beams with similar depths, it is inappropriate for evaluating the performance of beams of varying depth. The strength of deep beams is not a function of their shear area, but rather, a function of a single-panel strut-and-tie model.

4.6.3 Serviceability Results

Serviceability Results from the Literature

A few of the experimental studies that investigated the effect of depth on deep beam performance recorded serviceability information. Most of the researchers noted the diagonal cracking loads of their test specimens. Some studies emphasized the load at which the maximum diagonal crack width reached a limiting value (such as 0.012- or 0.016-inches). The serviceability results of test specimens with web reinforcement from three previously-reviewed studies are presented in this section.

In these projects, minimal effect of depth on the shear stress at first diagonal cracking was detected. The experimental test results are plotted in Figure 4.90. The loads at first diagonal cracking were normalized by $\sqrt{f'_c}b_w d$. In the context of a single-panel STM, the mechanism of diagonal cracking in deep beams is a function of the spreading of compressive stress in the bottle-shaped strut. For the member to crack, the transverse tensile stress in the strut must exceed the tensile capacity of the concrete. Thus, normalizing the diagonal cracking loads by the

approximate cross-sectional area of the strut, $b_w d$, and the tensile strength of concrete, $\sqrt{f'_c}$, is consistent with the mechanism of behavior.

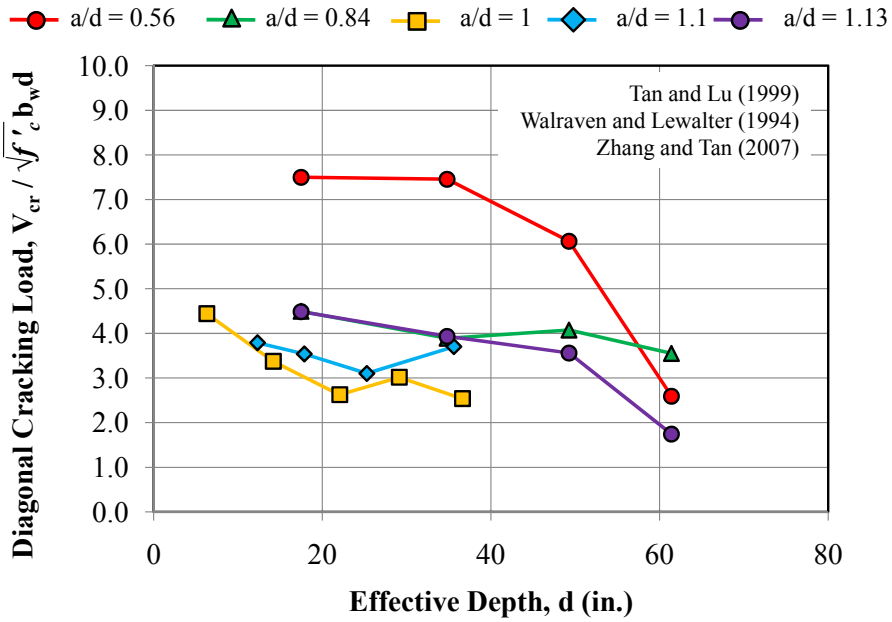

Figure 4.90: Diagonal cracking loads of size effect specimens in literature

The data in Figure 4.90 indicated that the normalized shear stress at first diagonal cracking is relatively constant with increasing depth. Two exceptions were the series of tests at a/d ratios of 0.56 and 1.13 conducted by Tan and Lu (1999). When the effective depth of the member increased from 49- to 61-inches, the stress at first diagonal cracking decreased considerably. Tan and Lu attributed the drop in stress with increasing depth to Weibull's statistical theory (Weibull, 1939). In this theory, the diagonal cracking strength of a beam is compared to a chain of links in which the strength of the chain is governed by the weakest link. As the depth of the beam increases, the number of links increases and a lower cracking strength is expected. For the other data in Figure 4.90, negligible effect of depth on the first diagonal cracking stress was apparent. This conclusion was reached by Walraven and Lehwalter and Zhang and Tan in the following statements:

> *"...the load at which inclined cracking occurs is hardly size-dependent." (Walraven and Lehwalter, 1994)*

> *"...the diagonal cracking strengths of deep beams are not size dependent." (Zhang and Tan, 2007)*

The diagonal cracking loads from these research studies can also be normalized by the load carrying capacity. The results are illustrated in Figure 4.91. The diagonal cracking loads of the test specimens represented in Figure 4.91 ranged from approximately 20% to 60% of the ultimate load-carrying capacity. There is not a distinct trend with increasing depth.

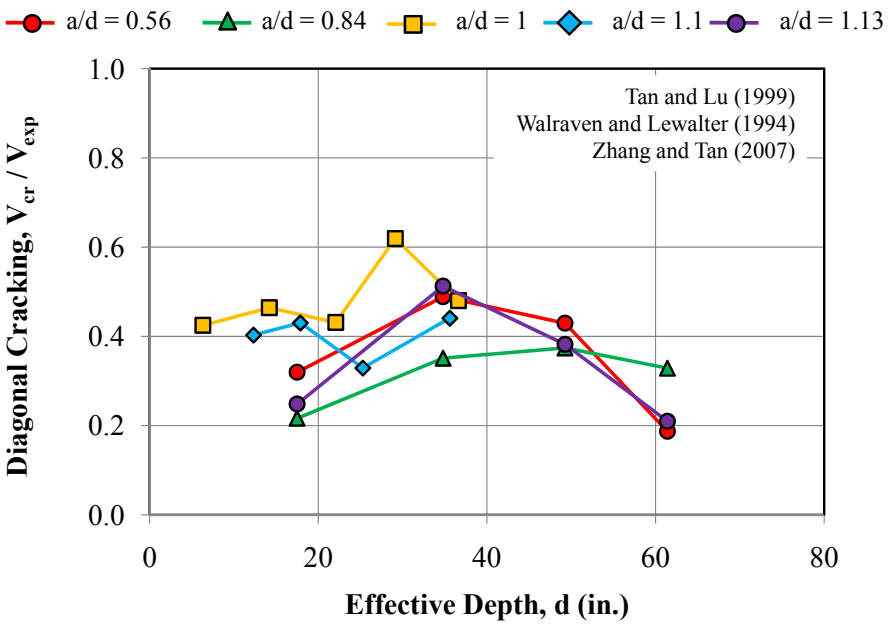

Figure 4.91: Diagonal cracking loads of size effect specimens in literature (function of ultimate)

The loads at which the width of the inclined cracks reached 0.012-inches (0.3-mm) were recorded in a couple of research studies as well. These loads were termed the serviceability loads since a crack width of 0.012-inches is generally accepted as a tolerable crack width for exterior exposure conditions (ACI 224R-01). The experimental test results are plotted in Figure 4.92. In this plot, the serviceability loads were also normalized by the ultimate load-carrying capacity. The serviceability loads as a percentage of the ultimate capacity generally decreased with increasing depth, albeit with some inconsistency. The diagonal crack widths reached the limiting width at lower percentages of their ultimate strength as the depth of the member increased. It seems plausible to extend the results in Figure 4.92 to suggest that with increasing depth, diagonal crack widths increase for a given percentage of ultimate capacity.

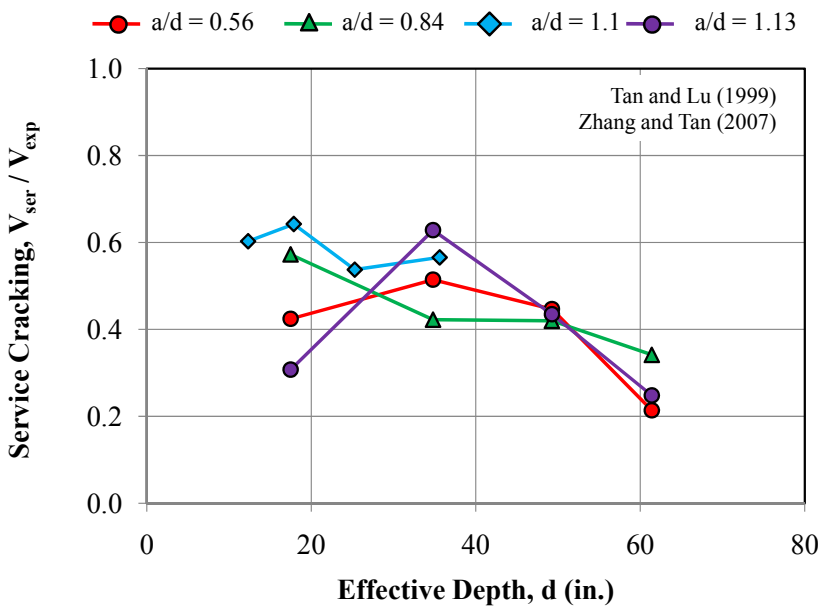

Figure 4.92: Service loads (diagonal crack width = 0.012-inches) as function of ultimate of size effect specimens in literature

Serviceability Results from the Experimental Program

In the current task, the effect of depth on the serviceability performance of deep beams was also evaluated. The first diagonal cracking load and corresponding crack width and the maximum diagonal crack width at every load stage thereafter were recorded for all of the tests in the current project. As noted in Section 4.2.2, for the test regions that were pre-cracked prior to testing, a load at first diagonal cracking was not available. This restriction did not apply for the beams in Series IV. For the 75-inch specimens, the diagonal cracking loads for each test region were obtained during the first test since the position of the ram did not change between the two tests. For the 21-inch specimens, the test region for the second test of each beam was uncracked due to the low level of load resisted by the long shear span. The diagonal cracking loads for the test specimens relevant to the current task are listed in Table 4.11.

Table 4.11: Diagonal cracking loads of depth effect specimens

Beam I.D.	b_w in.	d in.	f'_c psi	Nominal ρ_v & ρ_h	Support Plate† in.	Load Plate† in.	α	a/d ratio	V_{crack} kip	$\frac{V_{crack}}{\sqrt{f_c'} \cdot b_w d}$	V_{crack} / V_{test}
III-1.85-02	21	38.6	4100	0.002	16x21	20x21	0.72	1.84	112	2.2	0.23
III-1.85-03b	21	38.6	3300	0.003	16x21	20x21	0.72	1.84	114	2.4	0.24
III-1.85-02b	21	38.6	3300	0.002	16x21	20x21	0.72	1.84	-	-	
III-1.2-02	21	38.6	4100	0.002	16x21	20x21	0.82	1.20	165	3.2	0.20
III-1.2-03	21	38.6	4220	0.003	16x21	20x21	0.82	1.20	-	-	
III-2.5-02	21	38.6	4630	0.002	16x21	20x21	0.62	2.49	105	1.9	0.35
III-2.5-03	21	38.6	5030	0.003	16x21	20x21	0.62	2.49	-	-	
IV-2175-1.85-02	21	68.9	4930	0.002	16x21	29x21	0.5	1.85	216	2.1	0.28
IV-2175-1.85-03	21	68.9	4930	0.003	16x21	29x21	0.5	1.85	218	2.1	0.26
IV-2175-2.5-02	21	68.9	5010	0.002	16x21	24x21	0.33	2.50	144	1.4	0.28
IV-2175-1.2-02	21	68.9	5010	0.002	16x21	24x21	0.67	1.20	262	2.6	0.21
IV-2123-1.85-03	21	19.5	4160	0.003	16x21	16.5x21	0.86	1.85	60	2.3	0.18
IV-2123-1.85-02	21	19.5	4220	0.002	16x21	16.5x21	0.86	1.85	65	2.4	0.19
IV-2123-2.5-02	21	19.5	4570	0.002	16x21	15.5x21	0.81	2.50	51	1.8	0.32
IV-2123-1.2-02	21	19.5	4630	0.002	16x21	18x21	0.91	1.20	124	4.5	0.21

† *Length along span (l) x length along width (w)*

(f) *Maximum shear carried in specimen upon the occurrence of concrete crushing at the compression face.*

The experimental load at first diagonal cracking for the beams in the current task were normalized, as before, by $\sqrt{f_c'}\, b_w d$. Information regarding the measurement of the diagonal cracking loads was provided in Section 4.2.2. The results for the beams in the current task are plotted in Figure 4.93.

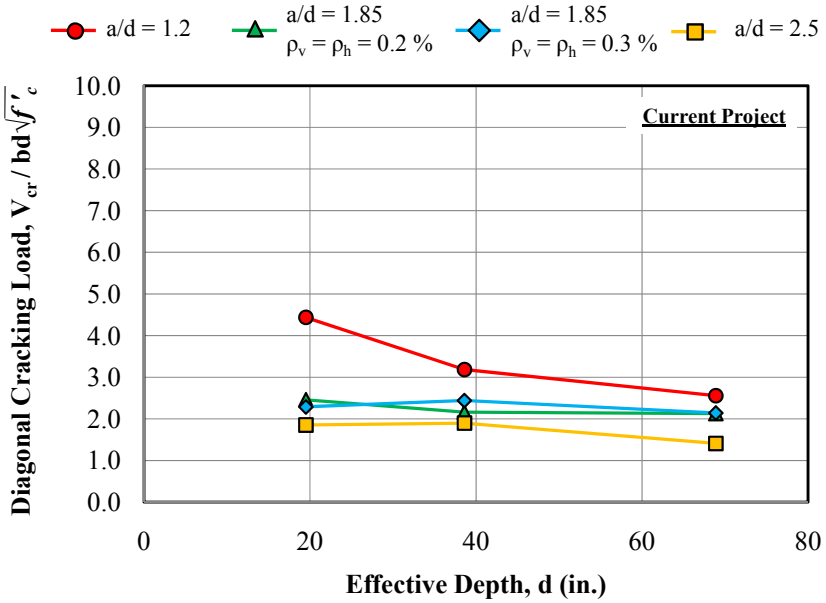

Figure 4.93: Normalized diagonal cracking loads for the depth effect specimens

The test results in Figure 4.93 agreed well with the results in the literature. For the specimens tested at a/d ratios of 1.85 or 2.5, a negligible difference in diagonal cracking strength existed as the depth of the member increased. It is interesting to note that for these members, the shear at first diagonal cracking was approximately $2\sqrt{f_c'}\, b_w d$ which is the assumed diagonal cracking strength (and concrete strength contribution) of members subjected to sectional shear. For the specimens tested at an a/d ratio of 1.2, however, the shear stress at first diagonal cracking decreased with increasing depth. The high stress at first diagonal cracking for specimen IV-2123-1.2-02 could have been due to the size of the bearing plates in relation to the shear span, effectively decreasing the a/d ratio (Figure 4.79). However, this explanation cannot be used to explain the differences in shear stress at diagonal cracking between the 42- and 75-inch specimens. It is possible that a Weibell-type statistical size effect or a variation in the tensile strength of concrete contributed to this reduction in stress at first diagonal cracking.

As with the data from the literature, the diagonal cracking shears can be normalized with the ultimate load carrying capacity. This normalization technique applied to the beams tested in the current task is provided in Figure 4.94. In this figure, the diagonal cracking strength of the specimens ranged from approximately 20% to 35% of the ultimate capacity. Also, as the depth of the specimen increased, the ratio of the cracking shear to the ultimate shear was fairly constant for the beams tested at each a/d ratio. This finding was particularly interesting for the set tested at an a/d ratio of 1.2. The results indicated that the diagonal cracking strength of deep beams

may not be just a function of the shear area and the $\sqrt{f_c'}$. Perhaps, other variables that affect the ultimate capacity, namely the size of the bearing plates, may also affect the diagonal cracking strength. More research in this area is recommended.

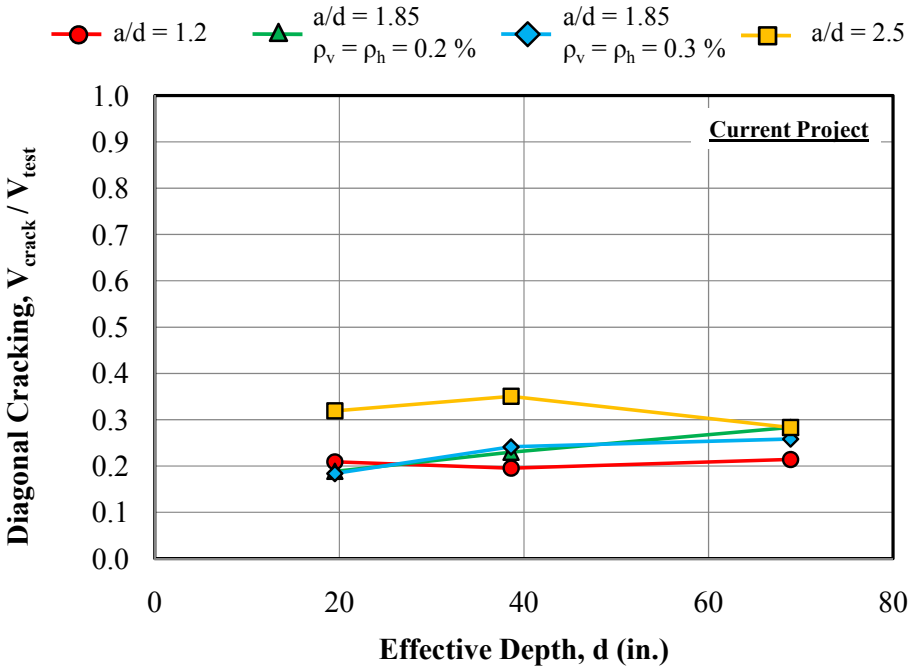

Figure 4.94: Diagonal cracking loads normalized by ultimate strength for depth effect tests

In addition to obtaining the diagonal cracking loads of the test specimens, the maximum width of the primary diagonal crack was recorded for the duration of each test. As noted in Section 3.6, the width of the diagonal cracks was measured using a crack comparator card. Measurements were taken on each side of the specimen and at each load increment. The crack width data for all of the specimens relevant to this task are provided in Figure 4.95 through Figure 4.98. Each plot contains the crack width data for a set of tests where the only difference among the specimens is their depth. As before, the maximum diagonal crack widths are plotted versus the percent of the maximum applied load for the reasons cited in Section 4.2.2.

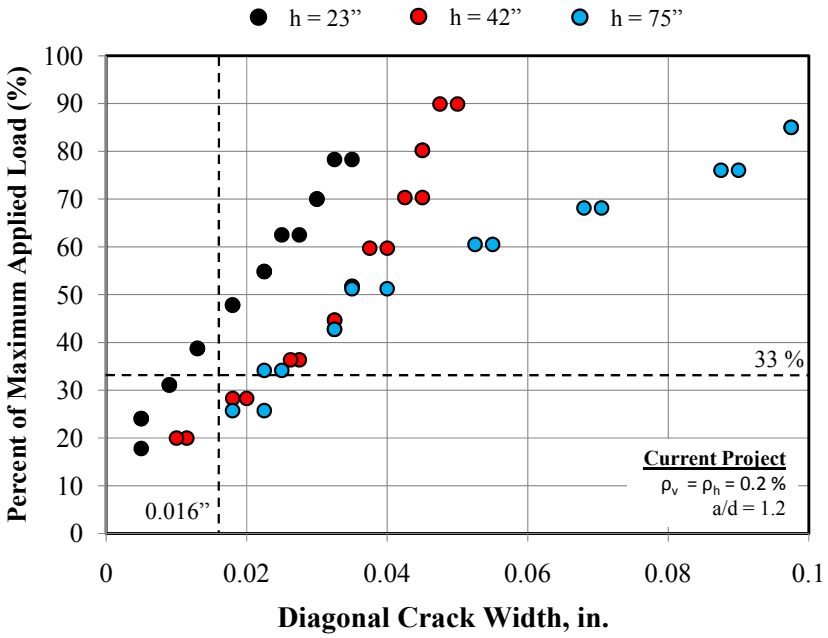

Figure 4.95: Diagonal crack widths for depth effect specimens with an a/d ratio of 1.2

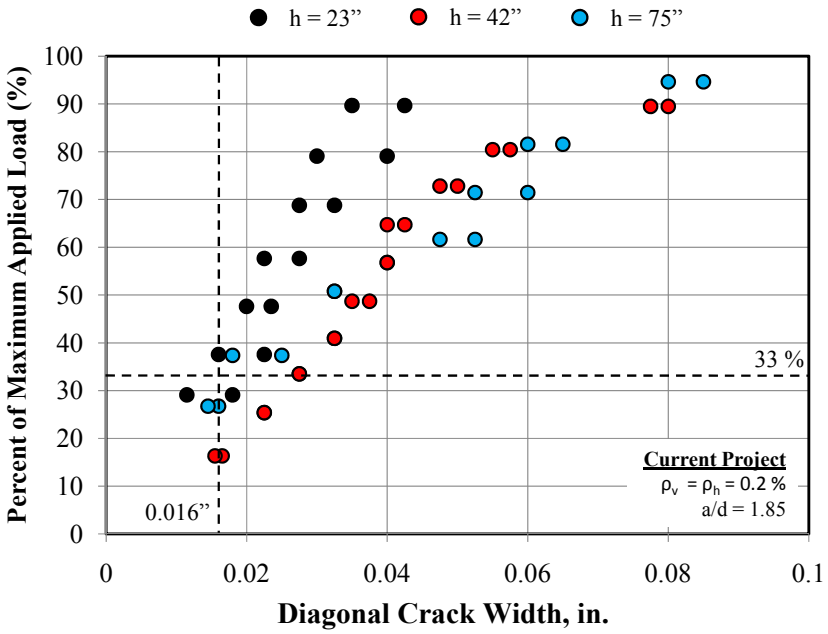

Figure 4.96: Diagonal crack widths for depth effect specimens with an a/d ratio of 1.85 and 0.2% web reinforcement

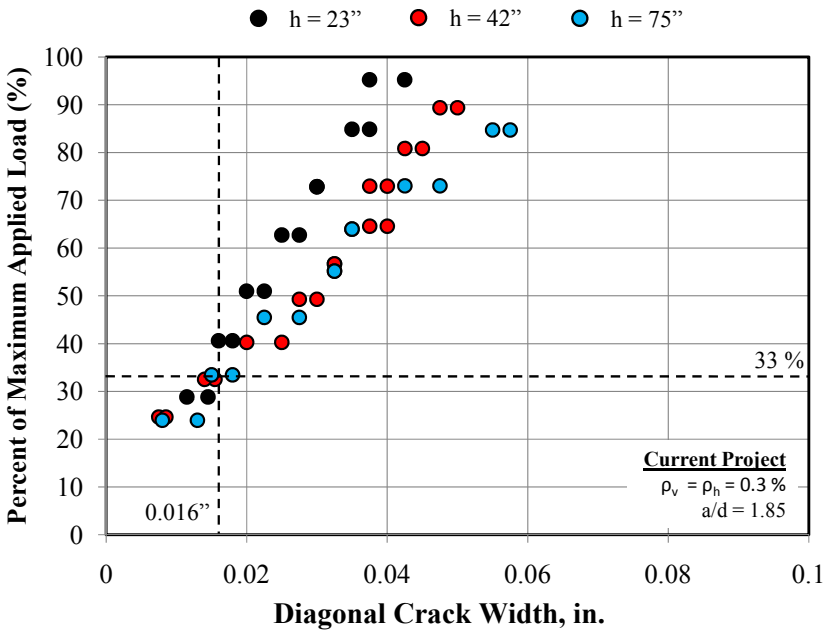

Figure 4.97: Diagonal crack widths for depth effect specimens with an a/d ratio of 1.85 and 0.3% web reinforcement

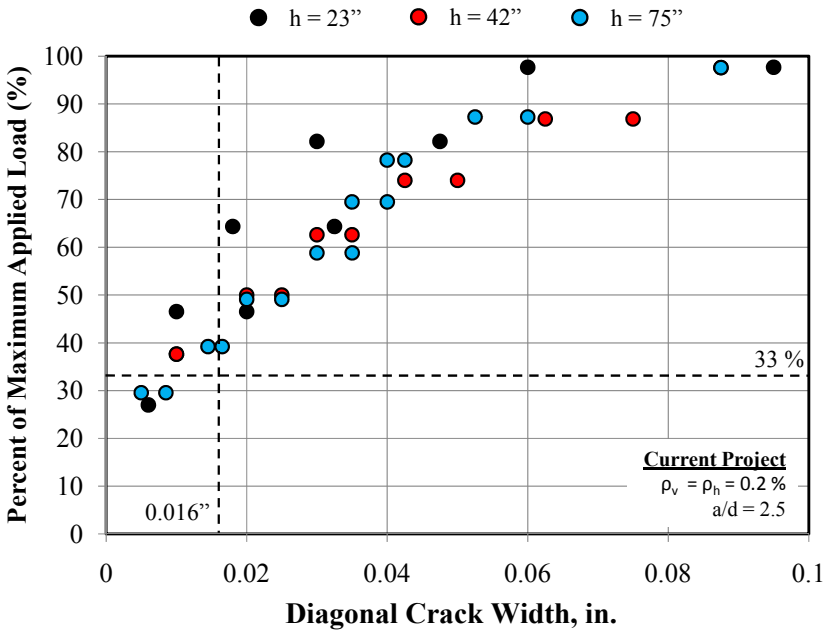

Figure 4.98: Diagonal crack widths for depth effect specimens with an a/d ratio of 2.5

In Figure 4.95 through Figure 4.98, the diagonal crack width data for the depth effect series were provided. In general, the widths of the diagonal cracks in the 42- and 75-inch specimens were fairly consistent for all three a/d ratios. An increase in depth from 42- to 75-inches did not significantly affect the maximum diagonal crack width. The widths of the

diagonal cracks in the 23-inch specimens, however, were consistently narrower than the larger specimens at a given percentage of ultimate capacity for all three a/d ratios. These data indicated that caution should be used in extrapolating crack width data from smaller members to large or full-scale members. Also, the data presented in Figure 4.95 through Figure 4.98 was fairly consistent with the results from the literature presented in Figure 4.92. Crack width data presented by Tan and Lu (1999) and Zhang and Tan (2007) indicated that the width of diagonal cracks for larger members reached the tolerable crack width limit (0.012-inches) at lower percentages of their ultimate capacity than for smaller members.

The trend of the data in Figure 4.95 through Figure 4.98 can be explained with aspects of modified compression field theory. According to this theory, as the depth of the member increases, the spacing of the diagonal cracks tends to increase (Collins and Kuchma, 1999). The diagonal crack width is a function of transverse tensile strain in the member and the spacing of the cracks. Therefore, as the depth of the member increases, the width of the diagonal cracks is expected to increase due to the increase in crack spacing. It should be noted that this theory was formulated for the use with slender beams and was based on flexural theory assumptions. However, the dependence of crack spacing on member depth and the influence of spacing on crack width seem applicable to deep beams as well. It is important to note that an appreciable difference in crack width was only observed as the overall depth increased from 23- to 42-inches. There were negligible differences in crack widths as the overall depth increased from 42- to 75-inches. Thus, it would appear that effect of size on diagonal crack width is mitigated by the time the overall depth reaches 42-inches.

4.6.4 Design Recommendations

Based on the results presented and discussed in Section 4.5, the design of reinforced concrete deep beams (a/d < 2) should be performed with a strut-and-tie analysis. The behavior of deep beams is often governed by the size and stress conditions of the nodal regions which single-panel STMs explicitly address. In this way, size effect of deep beams is negligible. Sectional design approaches are unacceptable for reinforced concrete deep beams. They inappropriately assume that the strength of deep beams increases proportionally to an increase in depth.

4.6.5 Summary

In Section 4.6, the effect of member depth on the strength and serviceability performance of reinforced concrete deep beams was investigated. Tests were conducted at an a/d ratio of 1.2, 1.85, and 2.5 on specimens with a 21”x23”, 21”x42”, and 21”x75” cross-section. With increasing depth, the normalized shear strength at failure ($V_{test}/f_c'b_wd$) decreased. The apparent reduction in strength is due to the incorrect association of deep beam capacity to the cross-sectional area (b_wd). On the contrary, the strength of deep beams is a function of a strut-and-tie analysis. Provided that the bottle-shape strut is adequately reinforced and the force in the tension tie does not control, the strength of deep beams is governed by the size and stress conditions in the nodal regions, not by the effective depth of the member. The findings in this section illustrate the importance of using a strut-and-tie model analysis to design reinforced concrete deep beams. Section-based approaches are inappropriate.

Diagonal cracking loads and maximum diagonal crack widths were recorded at load stages to evaluate the effect of depth on the serviceability performance of a deep beam. It was shown that for the beams tested at an a/d ratio of 1.85 and 2.5, the diagonal cracking load,

normalized by $\sqrt{f_c'}\, b_w d$, was not appreciably affected by an increase in depth. For an a/d ratio of 1.2, a reduction in the normalized diagonal cracking load was observed. In light of previous findings in the literature, it is likely that depth can influence the diagonal cracking load to some extent, but the effect is often negligible or erratic. With increasing overall depth from 23" to 42", an increase in the maximum diagonal crack width at a given percentage of the maximum applied load was recorded. An increase in maximum diagonal crack widths was not observed when the overall depth increased from 42" to 75" in general. As a result, the crack width data indicated that a size effect exists in terms of the crack widths of small specimens. Caution should be used in basing recommendations on full-scale structures off of crack width data of small specimens. The measured data suggested that the effect of depth on crack widths is mitigated at depths ≥ 42-inches.

4.7 Summary

In Chapter 4, the experimental results of the testing program were presented in detail. The results were separated by the first four tasks of the research study. These tasks included the (1) distribution of stirrups across the width of a beam web, (2) triaxial confinement of the load and support plates, (3) minimum web reinforcement (transverse and longitudinal), and (4) effect of member depth. The data obtained from the tests conducted for these tasks (Series I through IV and Series M) are also used with data from the evaluation database to address the remaining four tasks of the current project. The results from these tasks are presented individually in Chapter 5.

Chapter 5. Analysis of Results

5.1 Overview

In this chapter, data from the experimental program and from the evaluation database was analyzed to address the final four tasks of the current project. Tasks 5 through 8 included:

- Proposed STM design provisions
- Discrepancy in calculated shear strength at an a/d ratio of 2
- Limiting diagonal cracking under service loads
- Correlation of maximum diagonal crack width to capacity

5.2 Proposed STM Design Provisions

The theoretical background of STM is presented in Section 2.2. Specific details related to the elements that form a truss model are presented in Section 2.3. Next, a summary of current code provisions is presented in Section 5.2.1. A historical background of the current design provisions is presented in Section 5.2.2.

5.2.1 Current Code Provisions for STM

The design provisions that are examined for this research program are the Building Code Requirements for Structural Concrete per the American Concrete Institute (ACI 318-08), the Bridge Design Specifications per the American Association of State Highway and Transportation Officials (AASHTO LRFD 2008 Interim), and the updated knowledge of the CEB/FIP 1990 Model Code per the International Federation for Structural Concrete (*fib* 1999). The recommendations of *fib* (1999) have been adopted by the European design standard, Eurocode. The reason that the *fib* (1999) provisions are evaluated rather than Eurocode 2 is because the *fib* (1999) provisions provide much more detailed information in regards to the strut-and-tie modeling procedure.

The load carried by an element in an STM must be less than the capacity of the element (Equation 5.1). This is the basic premise for all STM provisions. The strength of an element in an STM is measured in terms of its *effectiveness* or *efficiency*. An efficiency factor, *v*, is the ratio of the stress applied to an element at failure and its concrete compressive strength.

$$F_n \geq F_u \tag{5.1}$$

Where,

$$F_n = A_{nz} \cdot f_{ce}$$

$$f_{ce} = \nu \cdot f'_c$$

A_{nz} = Area of the face of a nodal zone, in^2
F_n = Nominal strength of a node face, kip
F_u = Force acting on the face of a nodal zone, kip
f'_c = Specified compressive strength of concrete, psi
f_{ce} = Effective concrete strength, psi

v = Efficiency factor

Efficiency factors as specified by ACI 318-08, AASHTO LRFD (2008), and the *fib* (1999) are presented as follows. It is important to note that differences exist between load, material, and strength reduction factors for the codes mentioned. Therefore, in order to maintain clarity when evaluating efficiency factors of different code provisions; reduction factors are not considered in the comparisons.

Design of Struts

Ideally, to ensure adequate deformation capacity to develop the forces in a truss model, the orientation of a strut should not deviate excessively from 45-degrees with respect to a tie. According to ACI 318-08, the minimum strut angle should not be taken as less than 25-degrees with respect to a tie. Similarly, *fib* (1999) states that strut *angles smaller than 30-degrees are unrealistic and involve high incompatibility of strains*. AASHTO LRFD (2008) allows any strut angle but accounts for the ineffectiveness of shallow struts by reducing the efficiency factor accordingly.

ACI 318-08 and AASHTO LRFD (2008) designate a strut design separate from a node design and concurrently assign separate efficiency factors. This area of inconsistency is a source of confusion for designers when determining the capacity of the node-to-strut interface. Contrary to ACI 318-08 and AASHTO LRFD (2008), *fib* (1999) does not explicitly require the strut to be designed. *fib* (1999) recognizes the fact that the critical stress in a strut occurs at the strut-to-node interface. According to *fib* (1999):

Except for prismatic stress fields, the design strength of stress fields is, in fact, very rarely needed in practice…Critical concrete stresses in D-regions occur in the regions of concentrated nodes. These are…checked with the node design.

For the purposes of comparison, the efficiency factors are presented in the following section for the three faces of a nodal region. The efficiency factor assigned to a *strut* by ACI 318-08 and AASHTO LRFD (2008) is presented as the efficiency of the *node-to-strut interface*.

Design of Nodes: Nodal Efficiency Factors

In an STM design, the stress applied to each face of a node is kept less than its capacity; and the capacity is taken as a fraction of its material strength. CCC nodes are usually assumed to have the highest capacity because concrete is subjected to biaxial or triaxial confining stresses. CCT and CTT nodes have reduced capacities because tensile strains across the nodal region are thought to reduce the compressive strength. Allowable stresses for nodal regions are listed as follows.

CCC Nodal Zone

The three nodal faces in a CCC region are illustrated in Section 2.3. The allowable capacities of the CCC nodal faces are presented in Table 5.1.

Table 5.1: Allowable Stresses for a CCC Node.

Node Face	Design Code	Efficiency Factor	Reduction Factor, φ_c
Back Face	ACI 318	0.85·(1) = 0.85	$\varphi_c = 0.75$
	AASHTO	0.85	$\varphi_c = 0.70$
	fib (1999)†	$0.85 \cdot \left(1 - f_c'/40ksi\right)$	$\alpha_c/\gamma_c = 0.5$††
Bearing Face	ACI 318-08	0.85·(1) = 0.85	$\varphi_c = 0.75$
	AASHTO	0.85	$\varphi_c = 0.70$
	fib (1999)†	$0.85 \cdot \left(1 - f_c'/40ksi\right)$	$\alpha_c/\gamma_c = 0.5$††
Strut-Node Interface	ACI 318	0.85·(0.75) = 0.64 when $\rho > \rho_{min}$††† 0.85·(0.60) = 0.51 when $\rho < \rho_{min}$†††	$\varphi_c = 0.75$
	AASHTO	0.85	$\varphi_c = 0.70$
	fib (1999)†	$0.85 \cdot \left(1 - f_c'/40ksi\right)$	$\alpha_c/\gamma_c = 0.5$††

† *fib* (1999) includes a material variability factor, α_c, embedded within their efficiency factor expression. This factor varies depending on the strength of concrete (0.7 to 0.8 for 4000 to 7000-psi); it is not included as part of the efficiency factor for ease of comparison. An argument can be made for expressing the efficiency factor differently; however, the overall trend between code provisions will remain unchanged.

†† Concrete compressive strength assumed to be 4000-psi.

††† ρ_{min} defined in Section 5.2.3

The back face and bearing face efficiency factors are the same for ACI 318 and AASHTO LRFD (i.e. 0.85). The *fib* (1999) factor is slightly lower and is reduced as the compressive strength of concrete increases.

A stress check at the back face of a CCC node is essentially the same procedure that is performed when checking the flexural capacity of a beam. The maximum concrete compressive stress allowed for a flexural design is $0.85f_c'$. This is consistent with the efficiency factor allowed by ACI 318-08 and AASHTO LRFD (2008).

Similarly, the stress check at the bearing face of a CCC node is the same check that is conducted when determining the bearing capacity of concrete. According to ACI 318-08 and AASHTO LRFD (2008), the bearing capacity of unconfined concrete is equal to $0.85f_c'$ This is consistent with the bearing face efficiency factor.

Another trend to point out is that the efficiencies of all three faces in the CCC nodal zone are identical according to the AASHTO LRFD (2008) and *fib* (1999) provisions. The factor specified by ACI 318-08 is smaller at the node-to-strut interface. A discrepancy exists when the efficiency factor is the same at all three nodal faces: the capacity of a truss model will never be controlled by the capacity of the strut-to-node interface. Depending on the angle of the strut framing into the node, the stress at either the bearing or back face will be the most critical.

CCT Nodal Zone

The three nodal faces in a CCT region are illustrated in Section 2.3. The allowable capacities of the CCT nodal faces are presented in Table 5.2.

Table 5.2: Allowable Stresses for a CCT Node.

Node Face	Design Code	Efficiency Factor	Reduction Factor, φ_c
Back Face	ACI 318	$0.85 \cdot (0.80) = 0.68$	$\varphi_c = 0.75$
	AASHTO	0.75	$\varphi_c = 0.70$
	fib (1999)†	NA	-
Bearing Face	ACI 318-08	$0.85 \cdot (0.80) = 0.68$	$\varphi_c = 0.75$
	AASHTO	0.75	$\varphi_c = 0.70$
	fib (1999)†	$0.70 \cdot \left(1 - f_c'/40ksi\right)$	$\alpha_c/\gamma_c = 0.5$††
Strut-Node Interface	ACI 318	$0.85 \cdot (0.75) = 0.64$ when $\rho > \rho_{min}$††† $0.85 \cdot (0.60) = 0.51$ when $\rho < \rho_{min}$†††	$\varphi_c = 0.75$
	AASHTO	$\left(\frac{1}{0.8 + 170\varepsilon_1}\right) \leq 0.85$*	$\varphi_c = 0.70$
	fib (1999)†	$0.70 \cdot \left(1 - f_c'/40ksi\right)$	$\alpha_c/\gamma_c = 0.5$††

† *fib* (1999) includes a material variability factor, α_c, embedded within their efficiency factor expression. This factor varies depending on the strength of concrete (0.7 to 0.8 for 4000 to 7000-psi); it is not included as part of the efficiency factor for ease of comparison. An argument can be made for expressing the efficiency factor differently; however, the overall trend between code provisions will remain unchanged.

†† Concrete compressive strength assumed to be 4000-psi.

††† ρ_{min} defined in Section 5.2.3

* Refer to Section 5.2.3 for more details of the equation used to calculate AASHTO LRFD interface efficiency factor.

The efficiency factors in the CCT nodal region are generally less than those in the CCC region because transverse tensile stresses are present, resulting in a reduction in the effective compressive strength of concrete.ACI 318-08 specifies the same efficiency factor at the node-to-strut interface in both the CCC and CCT regions.

The stress that must be resisted by the back face of a CCT node can be attributed to anchorage of the tie reinforcement, bearing from an anchor plate or headed bar, or external indeterminacy such as that at an interior node over a continuous support (Figure 5-1).

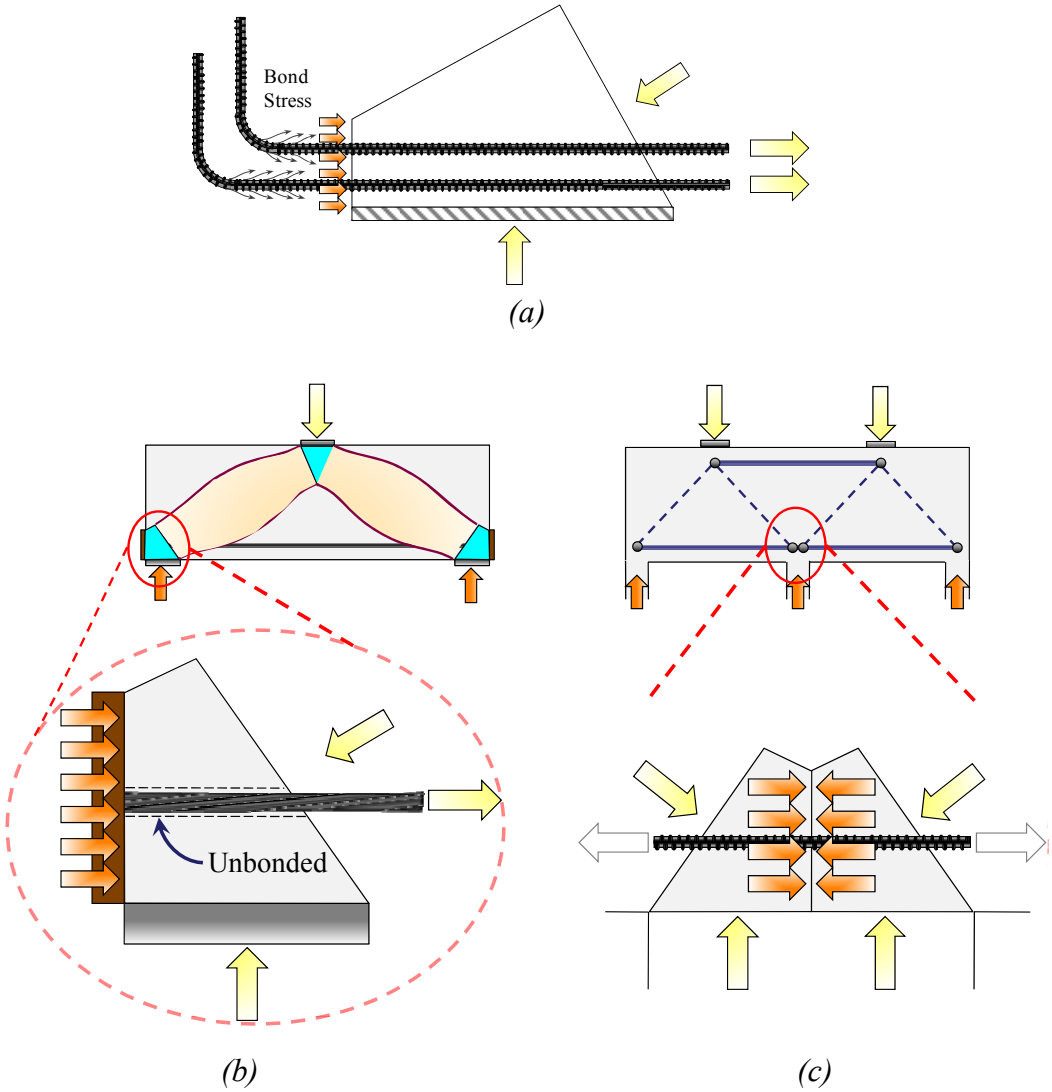

Figure 5-1. Stress condition at the back face of a CCT node: (a) bonding stress; (b) bearing of an anchor plate; (c) interior node over a continuous support.

The effectiveness of the back face of a CCT node is dependent on the stress condition. *fib* (1999) provisions recognize that the stress caused by the bonding of an anchored bar [Figure 5-1(a)] is not critical and need not be considered when evaluating the capacity of a CCT node. This fact is acknowledged by Thompson et al. (2003). According to the researchers:

The philosophy of the current code provisions for determining the capacity of CCT nodes may require reconsideration. The evidence from the tests shows that the failure of these nodes was primarily related to anchorage and that the current stress limits for nodes were unrealistic. It is possible that CCT nodes cannot fail in compression if anchorage of the tie bars is sufficient. The stress limits imposed by the code provisions may be unnecessary.

When the stress that is resisted by a CCT node is attributed to a condition other than anchorage, *fib* (1999) recommends the efficiency factor presented in Table 5.2 as follows:

In conclusion, it can be stated, that the concrete in the node [over an interior support] is under biaxial compression, but the horizontal compression is difficult to assess. On the other hand, tensile reinforcement penetrates the node region and is anchored there to some extent. Therefore, [the CCT bearing face efficiency] will again be applied here as design node strength, the [the CCC bearing efficiency] might eventually be considered.

ACI 318-08 and AASHTO LRFD (2008) provisions require that the stress attributed to the anchorage of a tie be applied to the back face of the CCT node as a concentrated force. The provisions do not distinguish between the stress conditions illustrated in Figure 5-1.

CTT Nodal Zone

The three nodal faces in a CTT region are illustrated in Section 2.4.3. The allowable capacities of the CTT nodal faces are presented in Table 5.3.

Table 5.3: Allowable Stresses for a CTT Node.

Node Face	Design Code	Efficiency Factor	Reduction Factor, φ_c
Back Face	ACI 318	$0.85 \cdot (0.60) = 0.51$	$\varphi_c = 0.75$
	AASHTO	0.65	$\varphi_c = 0.70$
	fib (1999)†	NA	-
Exterior Face	ACI 318-08	$0.85 \cdot (0.60) = 0.51$	$\varphi_c = 0.75$
	AASHTO	0.65	$\varphi_c = 0.70$
	fib (1999)†	NA	-
Strut-Node Interface	ACI 318	$0.85 \cdot (0.75) = 0.64$ when $\rho > \rho_{min}$††† $0.85 \cdot (0.60) = 0.51$ when $\rho < \rho_{min}$†††	$\varphi_c = 0.75$
	AASHTO	$\left(\frac{1}{0.8 + 170\varepsilon_1}\right) \leq 0.85$*	$\varphi_c = 0.70$
	fib (1999)†	$0.60 \cdot \left(1 - f_c'/40ksi\right)$	$\alpha_c/\gamma_c = 0.5$††

† *fib* (1999) includes a material variability factor, α_c, embedded within their efficiency factor expression. This factor varies depending on the strength of concrete (0.7 to 0.8 for 4000 to 7000-psi); it is not included as part of the efficiency factor for ease of comparison. An argument can be made for expressing the efficiency factor differently; however, the overall trend between code provisions will remain unchanged.

†† Concrete compressive strength assumed to be 4000-psi.

††† ρ_{min} defined in Section 5.2.3

* Refer to Section 5.2.3 for more details of the equation used to calculate AASHTO LRFD interface efficiency factor.

In general, the efficiency factor specified for a CTT nodal region is less than a CCT region due to the presence of additional tensile stresses. Again, ACI 318-08 specifies the same efficiency at the node-to-strut interface regardless of the type of nodal region.

Similar to the back face of a CCT node, *fib* (1999) recognizes that the back face and exterior face of a CTT node are not critical (provided bars are anchored properly). According to *fib* (1999):

If… bars are distributed over a great length of the main reinforcement, as is normally the case in beams, the node is of the "smeared" type and needs not be checked in detail.

Schlaich et al. (1987) also makes the same point:

Since D-regions usually contain both smeared and singular nodes, the latter will be critical and a check of concrete stresses in smeared nodes is unnecessary.

Design of Ties

The design strength of ties is straightforward. The maximum capacity of a tie is simply taken as the specified yield strength of the reinforcement, f_y.

The important factors to consider when detailing a tie are proper bar distribution, spacing, and development length. Ties must be anchored behind the nodal zones with a minimum amount of development length as previously illustrated in Section 2.3.

5.2.2 Historic Development of Empirical Shear Provisions

In 2002, *Strut-and-Tie Modeling* provisions were added to the ACI 318 building code in Appendix A. The chapter was introduced as a method for designing deep beams or other regions of discontinuity. Prior to 2002, deep beams were designed for shear based on an empirically derived formula. The evolution of these empirical shear provisions is presented next. The purpose of presenting the history of shear is to provide insight into current STM provisions.

Before 1963, provisions specific to the design of deep beams did not exist. Until that time, deep beams were most likely designed based on the prescriptive requirements specified for a wall design. These requirements can be traced back to the 1910 standard. In 1910, the National Association of Cement Users (NACU 1910) listed the following requirement for the design of concrete walls.

Concrete walls must be reinforced in both directions. The maximum spacing of reinforcing bars shall be 18 inches… Total reinforcement shall not be less than one-fourth of one percent [0.25%].

This provision remained essentially unchanged until 1956. In the 1956 version of ACI 318, the minimum reinforcement ratio for walls in the vertical direction was reduced from 0.25% to 0.15% (ACI 318-56). The reason for the change is most likely due to the addition of a minimum reinforcement provision for beams. Based on advancements in shear research, the minimum amount of transverse web reinforcement for typical beams resisting shear was found to be 0.15%. Subsequently, a provision limiting the minimum amount of web reinforcement to 0.15% made its first appearance in Section *807-Minimum web reinforcement*. Therefore, it can be assumed that the minimum reinforcement provision was changed in Section *1111-Reinforced concrete walls* in order to provide consistency between the two sections.

In 1963, the first provision specific to the design of deep beams appeared in the ACI 318 specifications. ACI 318-63 contains the first definition of a deep beam and explicitly requires a

minimum amount of reinforcement. According to the requirements of ACI 318-63, deep beams are to be designed as follows:

Beams with depth/span ratios greater than 2/5 for continuous spans, or 4/5 for simple spans shall be designed as deep beams taking account of nonlinear distribution of stress, lateral buckling, and other pertinent effects. The minimum horizontal and vertical reinforcement in the faces shall be the same as in 2202(f) [0.25% and 0.15% respectively].

Suggestions for the design of deep beams were based on recommendations from Chow et al. (1952). These studies determined the non-linear stress distribution in a deep beam based on a finite element analysis of a homogenous material. The researchers recognized the fact that concrete is a non-homogenous material. However, according to Chow et al. (1952), *a rigorous theoretical analysis of the stresses in such beams is hardly feasible*. As a result, Chow et al. (1952) recommended providing sufficient steel reinforcement in the tensile zones to *convert the beam, as closely as possible, to a homogenous beam*. The requirement in ACI 318-63 for the minimum amount of horizontal and vertical web reinforcement was taken to be the same as that required for walls based on the conventional construction practice at the time. According to the ACI 318-63 Commentary:

The empirical requirements [for walls] have been changed little since first presented in 1928 and have resulted in satisfactory construction.

In 1971, entirely new provisions were included in the ACI code for the design of deep beams (ACI 318-71). Similar to a sectional shear design, the nominal shear strength of a deep beam was taken as the sum of the concrete and steel contributions (Equation 5.2).

$$v_n = v_c + v_s \tag{5.2}$$

Where,

$$v_c = \left(3.5 - 2.5\frac{M_u}{V_u d}\right)\left(1.9\sqrt{f_c'} + 2500\rho_w \frac{V_u d}{M_u}\right)$$

$$v_s = \frac{A_v f_y}{b_w s_1}\left(\frac{1+\frac{l_n}{d}}{12}\right) + \frac{A_{vh} f_y}{b_w s_2}\left(\frac{11-\frac{l_n}{d}}{12}\right)$$

A_v	=	area of shear reinforcement within a distance s_1, in^2
A_{vh}	=	area of shear reinforcement within a distance s_2, in^2
ρ_w	=	ratio of main tensile reinforcement to $b_w d$
M_u	=	applied design moment at the critical section, in.-lb
V_u	=	applied design shear at the critical section, lb
f_c'	=	specified compressive strength of concrete, psi
f_y	=	specified tensile strength of reinforcement, psi
d	=	distance from extreme compression fiber to centroid of tension reinforcement, in.
b_w	=	web width, in.
s_1	=	center-to-center spacing of vertical reinforcement, in.

s_2 = center-to-center spacing of horizontal reinforcement, in.

The concrete contribution, v_c, contains two terms in parentheses. The second term is the empirical formula for the diagonal cracking strength of concrete; the same equation that is used to this day for a sectional shear design. The first term provides an increase in shear strength above the diagonal cracking strength for an a/d ratio less than 2.0 and *shall not exceed 2.5*. According to ACI-ASCE Committee 426 (1973), *this equation is based on the work by Crist (1966, 1967), and de Pavia and Siess (1965)*.

The derivation of the web reinforcement contribution, v_s, is based on the shear friction capacity of the beam along the inclined crack. The shear friction equation is not normally applied to sections where there is a significant moment; however, for deep beams, there is significant shearing action along the critical inclined crack (ACI-ASCE 426-73). Normal forces on the inclined crack are developed by tension in the web reinforcing, and the tension in the web reinforcing is developed by the slip along the crack. If all of the web reinforcement is assumed to have yielded at ultimate load conditions; then the resistance provided can be derived based on the orientation and location of the reinforcement along the crack. Crist (1966) simplified the derivation of v_s based on a lower bound of test data. He expressed the trigonometric terms associated with crack inclination and the shear span in terms of overall span, l_n, and depth, d; resulting in the expression eventually adopted by ACI 318-71 (Equation 5.2).

The minimum requirement for horizontal and vertical web reinforcement remained unchanged from previous codes (0.25% and 0.15% respectively); however a maximum spacing requirement was added (d/5 or 18-inches and d/3 or 18-inches in the horizontal and vertical directions, respectively).

The deep beam shear provisions remained essentially unchanged until the release of the 2002 version of the ACI 318 code (ACI 318-02). In 2002, the empirical deep beam shear equation (Equation 5.2) was completely removed from Chapter 11 and replaced with the following provision.

> *Deep beams shall be designed using either a nonlinear analysis… or Appendix A [Strut-and-Tie Models]*

The deep beam provisions in the current version of the ACI 318 code (ACI 318-08) have remained essentially unchanged since 2002. Next, a review of the background of STM provisions is presented.

5.2.3 Historic Development of Strut-and-Tie Model Provisions

The concept of idealizing reinforced concrete members using a truss model dates back to the end of the nineteenth century. In 1899, Wilhelm Ritter suggested a truss mechanism to explain the role of transverse reinforcement in resisting shear of a beam. Mörsch later refined Ritter's model in 1902. After 1927, truss modeling fell out of favor in the United States when Richart proposed a sectional method of shear design in which the concrete and steel contributions to shear strength were calculated independently (Brown et al. 2006).

In 1971, Lampert and Thürlimann developed a three-dimensional space truss to explain the combined actions of shear and torsion. Their torsion model was further refined by Mitchell and Collins (1971) and Ramirez and Breen (1983) so that the space truss could account for all combinations of shear, bending, torsion, and axial loadings. Vecchio and Collins (1982) took the

theory of plasticity a step further and derived the *modified compression field theory* – taking into account the deformation compatibility of the truss model. At this time, truss modeling re-emerged in American design standards. Based on the experimental program by Rogowsky et al. (1986), Rogowsky and MacGregor (1986) developed the *plastic truss theory*. This theory is an extension of the plasticity theory presented by Nielson et al. (1978) and Thürlimann (1978). At the same time, Marti (1985) and Schlaich et al. (1987) extended the truss modeling approach to overall discontinuity regions with a *strut-and-tie modeling* approach.

The STM provisions in the ACI 318-08 code are largely attributed to the work conducted by Rogowsky and MacGregor (1986), Ramirez and Breen (1991), Bergmeister et al. (1993), Schlaich et al. (1987), and Marti (1985). AASHTO LRFD (2008) provisions are based on the modified compression field theory (MCFT) proposed by Vecchio and Collins (1986). *fib* (1999) recommendations can be traced to the research conducted by Nielson et al. (1978) and Bergmeister et al. (1993). A summary of previous research findings is presented in the following sections.

Behavior of Struts (Strut-to-Node Interface)

There is a tremendous amount of research that has been conducted to determine the efficiency of concrete at the strut-to-node interface and numerous efficiency equations have been proposed. For detailed information on research programs that focused on the efficiency of a strut, refer to Brown et al (2006) and ACI 445R-99.

ACI 318-08 Strut Efficiency Factors

Derivation of the efficiency factors selected by ACI 318-08 (Table 5.1, Table 5.2, and Table 5.3) is summarized by MacGregor (2002). According to MacGregor (2002):

> *...the values of the f_{cu} [effective concrete capacity] presented in the ACI Code were chosen to satisfy four criteria: Simplicity in application; Compatibility with tests of D-regions; Compatibility with other sections of ACI 318; Compatibility with other codes or design recommendations.*
>
> *Because these four criteria lead to different values of f_{cu} for a given application, judgment was required in selecting the values of f_{cu}. The [values] are generally higher than those from other codes because more weight was given to [compatibility with the ACI Code and tests of D-regions] than was given to other codes.*

ACI 318-08 efficiency factors at the strut-to-node interface are attributed to the research conducted by Rogowsky et al. (1986), Ramirez and Breen (1991), Bergmeister et al. (1993), Schlaich et al. (1987), and Marti (1985). A summary of their findings is presented in this section.

Rogowsky and MacGregor (1986)

Rogowsky and MacGregor (1986) based their recommendations on an experimental program conducted by Rogowsky et al. (1986). The researchers tested 7 simply supported and 17 two-span continuous beams with various vertical and horizontal reinforcement ratios. They found that beams with significant amounts of vertical reinforcement were ductile and had consistent failure loads. The researchers recommended that the capacity of the stirrups crossing the diagonal of the shear span should be greater than 30% of the applied shear force.

Also, Rogowsky and MacGregor (1986) observed that the selection of the truss model was more important than the selection of an efficiency factor. If the selected truss differs excessively from the elastic distribution of stresses, full redistribution may not occur and the truss may fail prematurely, giving the appearance of a low efficiency factor. For general use, they recommended the following efficiency factor.

$$\nu = 0.6 \tag{5.3}$$

Finally, the researchers recommended a minimum strut angle relative to a tie similar to that recommended by Thürlimann (1978) and Ramirez and Breen (1991).

$$25° \le \theta \le 65°$$

Ramirez and Breen (1991)

Ramirez and Breen (1991) proposed a modified truss model that recognizes that concrete efficiency decreases as compressive strength increases. The strut efficiency factor that they recommended is expressed as follows:

$$\nu = \frac{30}{\sqrt{f'_c}} \tag{5.4}$$

Values range between 0.55 and 0.34 for 3000 to 8000-psi concrete. A comparison between the Ramirez and Breen (1991) recommendations and the current ACI 318-08 provisions is presented in Figure 5.2.

Bergmeister, Breen, Jirsa, and Kreger (1993)

Bergmeister et al. (1993) proposed the following efficiency factors. The researchers based the expression on a *large number of test results*. Also, they recognized that efficiency decreased as the compressive strength of concrete increased. The efficiency factor values range between 0.8 and 0.42 for 3000 to 8000-psi concrete (Equation 5.5 and Figure 5.2).

$$\nu = \begin{cases} 0.8\nu_{ed} \;\; if \;\; f'_c \le 4000\,psi \\ \left(0.9 - \dfrac{0.25 f'_c}{10{,}000\,psi}\right)\nu_{ed} \;\; if \;\; 4000\,psi < f'_c < 10{,}000\,psi \\ 0.65\nu_{ed} \;\; if \;\; f'_c \ge 10{,}000\,psi \end{cases} \tag{5.5}$$

Where,

ν_{ed} = 0.6 for compression diagonals (i.e. CCC and CCT strut-to-node interface)
1.0 otherwise (i.e. CCC and CCT back and bearing face)

A comparison between the Bergmeister et al. (1993) recommendations and the current ACI 318-08 provisions is presented in Figure 5.2.

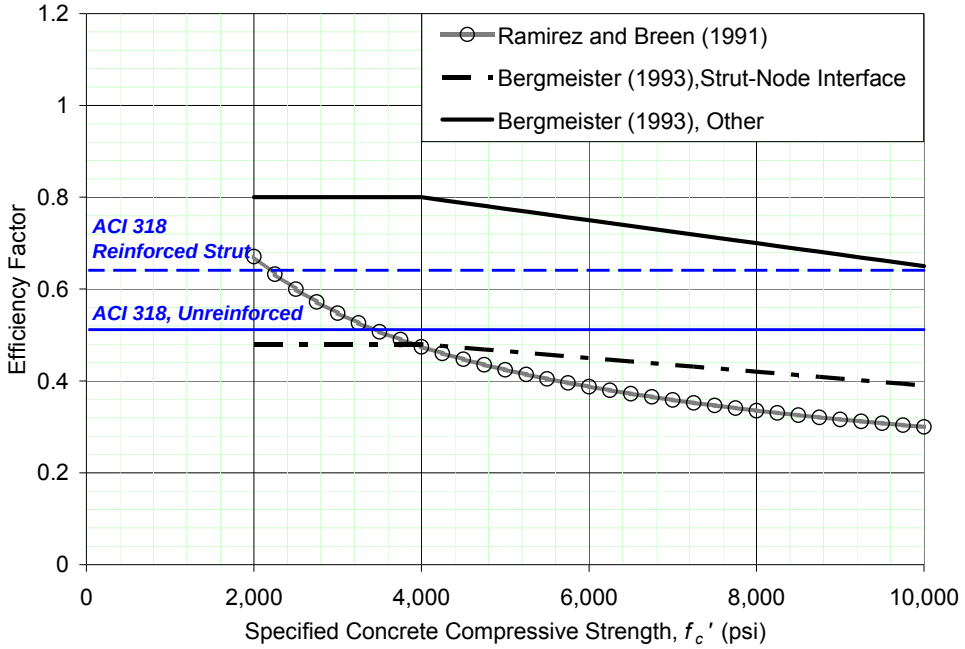

Figure 5.2: Comparison of strut efficiency factors: ACI 318-08

Marti (1986)

Based on comparisons with experimental research, Marti (1986) suggested that the following efficiency factor be used.

$$\nu = 0.6 \tag{5.6}$$

Marti suggested this value as a *first start*; the efficiency factor may then be decreased or increased depending on details such as presence of distributed reinforcement or lateral confinement. Marti (1986) also pointed out that distributed minimum transverse reinforcement contributes significantly to the ability of a deep beam to redistribute internal forces after cracking.

Schlaich, Schäfer, and Jennewein (1987)

Sclaich et al. (1987) proposed that the efficiency factor should reflect the fact that the strength of concrete is dependent on the multi-axial state of stress and on disturbances from cracks and reinforcement. The researchers stated that confinement was favorable and could be provided by transverse reinforcement or by bulk concrete surrounding a relatively small compression field. They further stated that transverse tensile stresses were detrimental to the efficiency. For reasons of *practicality*, the researchers recommended the following efficiency factors:

$$\nu = 0.85 \cdot \beta_n \tag{5.7}$$

Where,

ν = 0.85, ($\beta_n = 1.0$), for undisturbed, uniaxial state of compressive stress (CCC bearing and back face).

0.68, ($\beta_n = 0.8$), nodal regions where tension bars are anchored or crossing (CCT nodal regions).

0.51, ($\beta_n = 0.6$), if tensile strains result in cracking skewed to the strut (CTT nodal regions).

0.34, ($\beta_n = 0.4$), for skewed cracks with extraordinary crack width.

The recommendations proposed by Schlaich et al. (1987) are very similar to the efficiency factors adopted by the ACI 318-02 code.

AASHTO LRFD Strut Efficiency Factors: MCFT

The strut efficiency factors specified in the AASHTO LRFD (2008) specifications are based on the Compression Field Theory developed by Mitchell and Collins (1974) and, later, the Modified Compression Field Theory developed by Vecchio and Collins (1986). Vecchio and Collins (1986) suggested that the maximum compressive stress that the concrete can resist reduces with the increase of cracking parallel to the compressive stress field. As a result, the stress limit recommended by Vecchio and Collins (1986) accounts for the principle tensile strain perpendicular to the axis of the strut. According to AASHTO LRFD (2008), the effective compressive strength of a strut is calculated as follows.

$$f_{cu} = \frac{f'_c}{0.8 + 170 \cdot \varepsilon_1} \leq 0.85 f'_c \tag{5.8}$$

Thus, the efficiency factor,

$$\nu = \frac{1}{0.8 + 170 \cdot \varepsilon_1} \leq 0.85$$

In which,

$$\varepsilon_1 = \varepsilon_s + (\varepsilon_s + 0.002)\cot^2 \alpha_s$$

Where,

α_s = the smallest angle between the compression strut and adjoining tension tie, degrees

ε_s = the tensile strain in the concrete in the direction of the tensile tie

f_c' = specified compressive strength of concrete, psi

The tensile strain in concrete, ε_s, is attributed to the tensile strain in the adjacent tie. Thus, the efficiency factor diminishes in tension regions (CCT or CTT nodal regions). Also, due to equilibrium with the strut, the tie force increases as the strut becomes shallower. As a result, the tensile strain term increases for shallow struts, further reducing the efficiency factor.

In general, practitioners have reservations when it comes to calculating the tensile strain in concrete, ε_s, as the calculation is a somewhat tedious, iterative process. The tensile strain in concrete may be estimated by dividing the tensile stress in the tie by the modulus of elasticity of steel. However, the force in the tie depends on the compressive force in the strut. This is turn depends on the efficiency factor. Hence, the calculation for the force in the strut, efficiency factor, and force in the tie must be reiterated until the values converge at a solution.

The AASHTO LRFD (2008) expression for strut efficiency has been derived by using hydrostatic nodes. Struts that are bounded by hydrostatic nodes increase proportionally with the a/d ratio. As a result, as the a/d ratio is increased, the efficiency factor must proportionally decrease in order to counteract the increasing strut width and account for the loss in strength with increasing a/d ratio. However, AASHTO LRFD (2008) §5.6.3.3.2 recommends the use of non-hydrostatic nodes. If non-hydrostatic nodes are used – as they typically are – then the STM capacity is reduced by both the diminishing efficiency factors and the diminishing strut width. Therefore, when non-hydrostatic nodes are employed, the efficiency of the strut-to-node interface is essentially penalized twice, possibly resulting in an overly conservative estimation of capacity.

fib (1999) Strut Efficiency Factors

fib (1999) provisions do not recommend separate stress checks between nodal zones and struts. They recognize the fact that the critical stress in a strut occurs at the node-to-strut interface. *fib* (1999) recommends using the same efficiency for all faces of a nodal region. Therefore, a background to the *fib* (1999) provisions is presented with the nodal zone efficiencies as follows.

Behavior of Nodal Zones

Few researchers distinguish between the efficiency of a strut or node. Typically, concrete efficiency is specified based on the degree of cracking, state of stress, or tensile strain within a compression field. However, the efficiency factors specified in ACI 318-08, AASHTO LRFD (2008), and *fib* (1999) are specific to individual elements (i.e. nodes and struts). This is primarily due to the fact that the degree of cracking and tensile straining are difficult to quantify from the perspective of the designer.

In addition to the aforementioned design standards, it is of interest to examine the efficiency factors proposed by Brown et al. (2006) as part of TxDOT Project 4371. Project 4371 was the predecessor to the current project.

ACI 318-08 Nodal Efficiency Factors

The efficiency factors contained in ACI 318-08 are based on other sections of the ACI code, other specifications, and experimental research. The efficiency factors that were adopted by ACI 318 are similar to those suggested by Schlaich et al. (1987); thus, it can be assumed that they were selected accordingly. Also, MacGregor (2002) cites research conducted by Barton et al. (1991) as contributing to the nodal efficiency factors that were eventually selected.

Barton, Anderson, Bouadi, Jirsa, and Breen (1991)

Barton et al. (1991) conducted tests of ten isolated CCT and nine CTT nodal zones. Details of the isolated node specimens are shown in Figure 5.3.

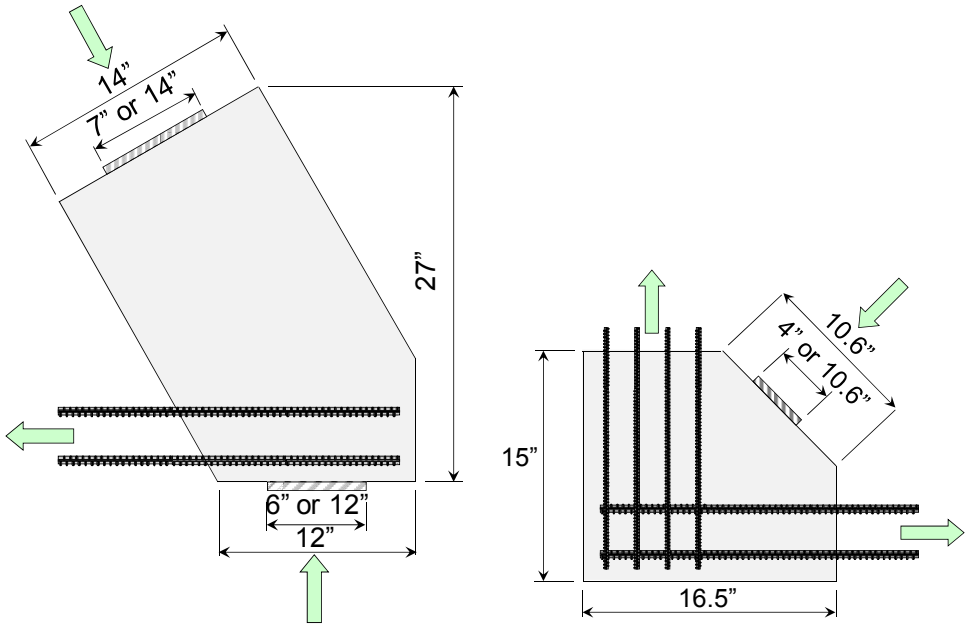

(a) CCT Node *(b) CTT Node*

Figure 5.3: Details of Isolated Node Specimens.

The researchers found that the ultimate strength of the CTT specimens was governed by yielding of the ties. Therefore, anchorage and reinforcement details had more of an impact on design strength rather than the efficiency factor.

Effective strength limits proposed by Schlaich et al. (1987) and Mitchell and Collins (1974) were found to be conservative. Six of the CCT specimens experienced anchorage failures; the others failed due to the crushing of concrete at the support plate. Research conducted by Barton et al. (1991) indicated that an efficiency factor of 0.94 could be developed if reinforcement is properly detailed (MacGregor 2002).

AASHTO LRFD (2008) Nodal Efficiency Factors

The efficiency factor at the node-to-strut interface is based on the MCFT. At the CCC and CCT bearing and back face, the AASHTO LRFD (2007) nodal efficiency factors are similar to those selected by ACI 318-08. It can be assumed that they were selected in a similar fashion [i.e. per Schlaich et al. (1987)].

fib (1999) Nodal Efficiency Factors

Nodal efficiency factors suggested by *fib* (1999) are similar to those recommended by Nielson (1978) and Bergmeister et al. (1993). Both researchers recognize the fact that the efficiency of concrete decreases as its compressive strength increases.

Nielson (1978); Bergmeister, Breen, Jirsa, and Kreger (1993)

According to Bergmeister et al. (1993), Nielson et al. (1978) developed the following empirical expression for the strength of concrete in beam webs.

$$\nu = 0.7 - \frac{f'_c}{29{,}000\,psi} \tag{5.9}$$

Bergmeister et al (1993) expanded upon Nielson's recommendation by developing efficiency factors for both undisturbed and disturbed regions (i.e. cracked and uncracked regions). The factors recommended by Bergmeister et al. (1993) for nodes are the same as those listed for struts (Equation 5.5). According to the researchers, *when compared with a large number of test results the function gave acceptable results*. The Nielson et al. (1978) and Bergmeister et al. (1993) efficiency factors are presented along with those adopted by *fib* (1999); presented in Figure 5.4.

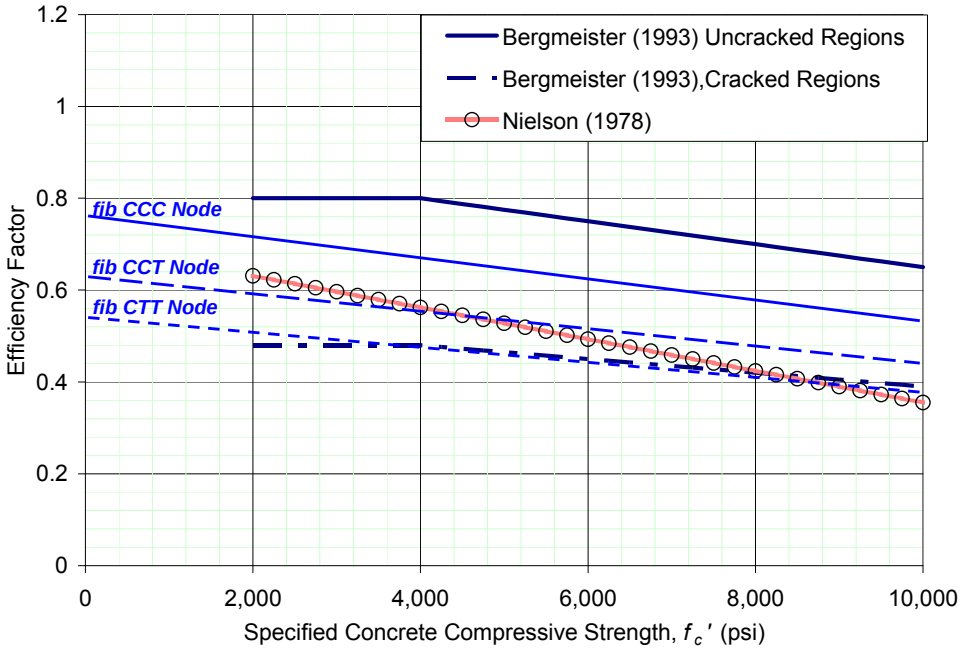

Figure 5.4: Comparison of nodal efficiency factors: fib (1999)

TxDOT Project 4371 Nodal Efficiency Factors: Brown et al. (2006)

Brown et al. (2006) examined both STM and sectional design methods for shear. As part of the experimental program, the researchers fabricated and tested a series of isolated strut specimens, and three series of deep beam specimens. Additionally, Brown et al. (2006) compiled a database of over 1200 shear tests. The database in combination with the experimental program was used to evaluate design expressions and develop a new strut-and-tie modeling procedure.

Brown et al (2006) determined that the critical location of a strut is at the strut-to-node interface. The researchers recommend limiting the strength of concrete within a nodal zone according to the following efficiency factors:

$$\nu_R = \frac{27}{a/d\sqrt{f'_c}} \le \nu_{max} \tag{5.10}$$

$$\nu_P = \frac{9}{a/d\sqrt{f'_c}} \leq \nu_{max}$$

Where,

ν_{max} = 0.85 for a CCC Node
0.75 for a CCT Node
0.65 for a CTT Node

The higher value of efficiency factor, ν_R, is to be used for struts that are sufficiently reinforced per Equation 5.11. When examining the effect of their proposed efficiency factors, the researchers found that 95% of the beams in their database carried loads in excess of the calculated values.

$$\rho_{\perp,min} \geq \frac{k_s \cdot \nu \cdot f'_c \cdot A_c \sin\theta}{f_y \cdot b \cdot d \cdot m} \tag{5.11}$$

Where,

A_c = minimum cross sectional area of the strut, in2
b = web width, in.
d = distance from extreme compression fiber to centroid of longitudinal reinforcement, in.
f_c' = specified compressive strength of concrete, psi
f_y = specified tensile strength of reinforcement, psi
k_s = non-hydrostatic node conversion factor
m = slope of the dispersion of compression
θ = angle of strut respective to horizontal, degrees
v = strut efficiency factor

Brown et al. (2006) derived the proposed efficiency factors assuming the beams in the database contain hydrostatic nodes. When non-hydrostatic nodes are used, the researchers recommended the following conversion factors:

$v_b = (1.0) \cdot v_R$, Bearing face of node

$v_t = \left(\frac{l_b}{w_t \cdot \tan\theta}\right) \cdot v_R$, Back face of node

$v_s = \left(\frac{l_b}{w_s \cdot \sin\theta}\right) \cdot v_R$, Node-to-strut interface

Where,

w_s = Width of the strut-to-node interface (Equation 2-2), in.
w_t = Height of the nodal back face, in.
θ = Angle of strut with respect to horizontal plane, degrees

Given that the method was derived using hydrostatic nodes, the Brown et al. (2006) STM procedure may be unnecessarily conservative when non-hydrostatic nodes are used. A goal of the

current project is to refine the method proposed by Brown et al. (2006) by evaluating design provisions through the use of non-hydrostatic nodes.

A background of the ACI 318-08, AASHTO LRFD (2008), *fib* (1999), and TxDOT 4371 STM provisions has been presented. Based on a review of both historical and current research, the following STM procedure is proposed.

5.2.4 Overview of Proposed STM Design Method

In a strut-and-tie model, the complex state of stress in a D-region is idealized as a series of compression and tension members within a truss. When establishing an STM design procedure, consideration is given to: simplicity; coordination with experimental data; and coordination between other design provisions.

In developing an STM procedure, it is first necessary to explicitly define the model. This step cannot be over-emphasized as the performance of a strut-and-tie model and corresponding efficiency factors are intrinsically linked to the geometry of the nodal regions. In addition, an evaluation of a STM procedure must be made in a comprehensive manner. In other words, the entire procedure must be considered as a whole. Often times, researchers in the past have made recommendations for a single aspect of strut-and-tie modeling. However, the efficiencies of each component are linked to one another.

Based on the preceding requirements, the approach taken in this study in developing a STM method is to comprehensively evaluate the STM procedures specified according to ACI 318, AASHTO LRFD, *fib* (1999), and TxDOT Project 4371. An established and consistent truss model is used in order to evaluate each provision in an unbiased manner. The selection process used to determine this standard truss model is outlined as follows.

5.2.5 Selection of Strut-and-Tie Model

One of the benefits of strut-and-tie modeling is its versatility. The method can be used for any structural configuration and results in a conservative design. However, in part, because of the flexibility of strut-and-tie modeling, current provisions lack explicit guidance and consistency. As a result, design engineers often express apprehension towards the current STM provisions. Therefore, it is a goal of the research project to clearly define a STM procedure and alleviate some of the confusion attributed to current methods.

Many types of discontinuities can be classified as D-regions. Common examples of D-regions include: deep beams (e.g. transfer girders, bridge bents), shear walls, corbels, post-tensioned anchorage zones, and pile supported footings (pile caps). Examples of a few of these D-regions are illustrated in Figure 5.5. Strut-and-tie models can be used to design any of the D-regions shown in Figure 5.5.

Strut-and-tie modeling is based on the lower bound theory of plasticity which states that if a stress distribution exists in a member in which the yield strength of the materials are not exceeded, and the stress distribution is in internal and external equilibrium, then the member will not collapse (Nielson, 1998). Based on experimental and analytical evidence, many researchers suggested that some truss models are better than others. Specifically, a good truss model reasonably follows the elastic stress distribution and does not have exceptionally large angles between the struts and the ties. To determine the appropriate values of strength for the individual

elements of a STM (efficiency factors for nodal faces, struts, etc.), experimental data was used. The efficiency factors were selected in such a way that conservative estimates for strength were obtained. Thus, the use of strut-and-tie modeling as a general procedure was validated.

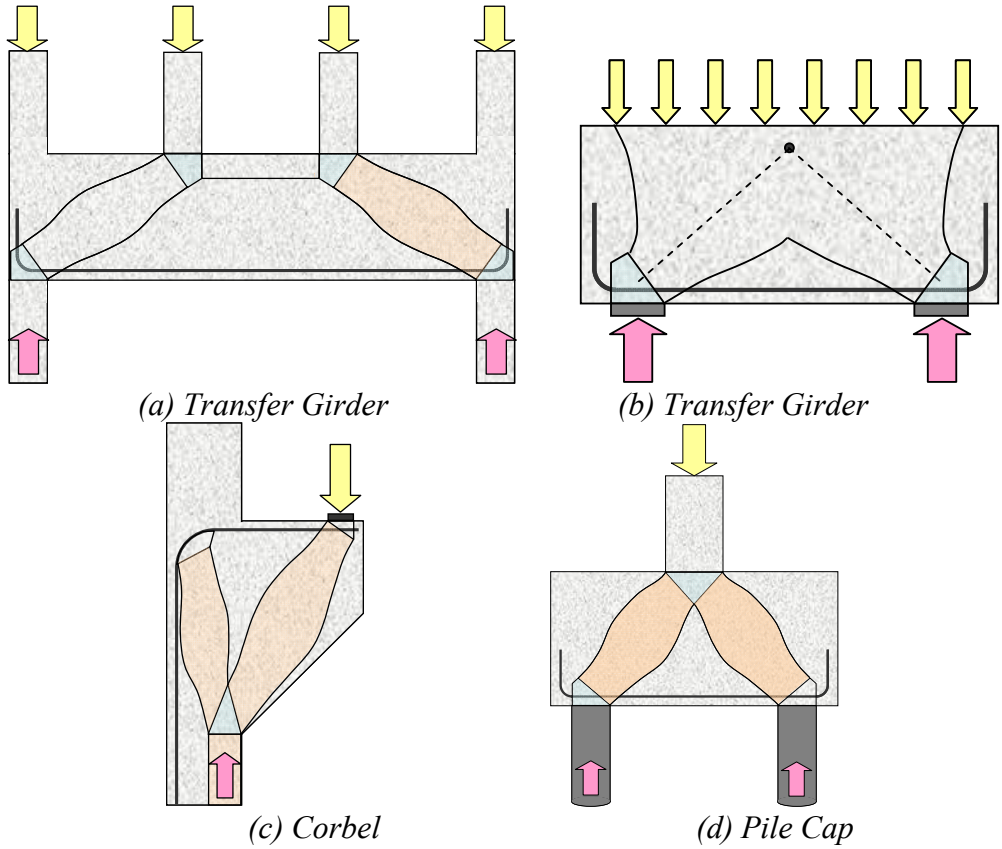

(a) Transfer Girder *(b) Transfer Girder*

(c) Corbel *(d) Pile Cap*

Figure 5.5: Examples of D-regions.

With regard to the current task, efficiency factors were determined from the experimental data of 179 deep beams in the evaluation database. These members contain the essential elements of any strut-and-tie model ((i) a direct strut, (ii) a tie, (iii) a CCC node, (iv) and a CCT node), and it is known that a single-panel STM is consistent with their behavior. This fact was validated in the current project (Section 5.3) and by numerous researchers of deep beams (Section 5.3.2). Thus, deep beam tests provide a convenient means to determine the efficiency factors at the specific nodal faces of CCC and CCT nodes. Since these nodes are generally the singular nodes (i.e. nodes with defined geometry) in a STM, the efficiency factors for them are often the most critical (Schlaich et al. 1987, fib, 1999).

It is believed that the efficiency factors and the general STM procedure derived from the use of deep beam data is applicable to other structures since the basic principles of strut-and-tie

modeling (equilibrium and yield criteria) are satisfied. In addition, the single-panel strut-and-tie model that was used in the derivation of the efficiency factors is consistent with the failure mechanism of deep beam members. Additional discussion regarding the selection of a single-panel model for deep beams is presented later in this section.

Nodal geometries of the D-regions shown in Figure 5.5 can be determined based on the techniques outlined in Section 2.3. By using these unambiguous rules for proportioning a strut-and-tie model, it is possible to comprehensively examine the resulting efficiency factors and draw conclusions based on the trends and differences. A single-panel truss with non-hydrostatic nodal zones was selected to represent all of the beams in the evaluation database for the purposes of examining current design provisions and calibrating new efficiency factors. Figure 5.6 illustrates the details of such a model.

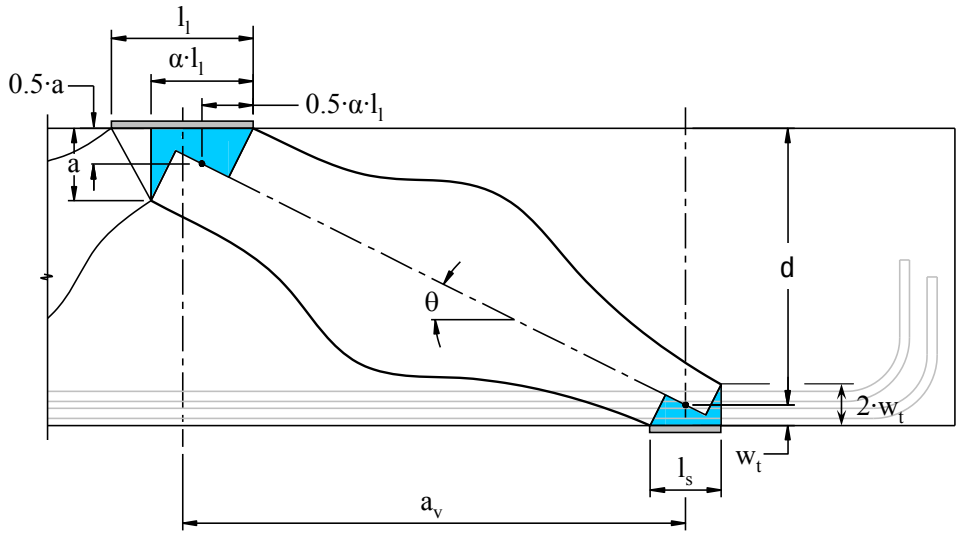

Figure 5.6: Non-hydrostatic single-panel strut-and-tie model.

The dimensioning techniques necessary to proportion this model are established in the ACI 318-08, AASHTO LRFD (2008) and *fib* (1999) provisions and have been outlined in Chapter 2. For the convenience of the reader, these techniques are summarized in Figure 5.7.

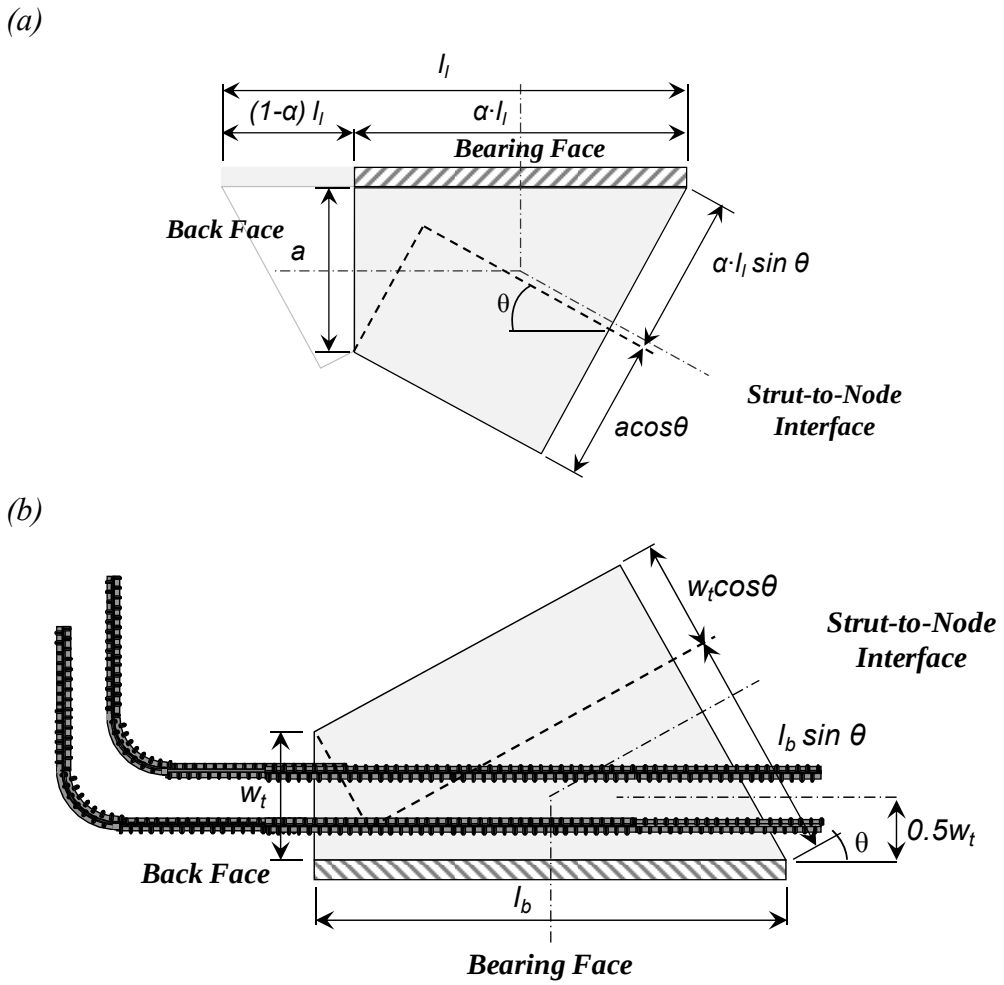

Figure 5.7: Definition of the geometry of a (a) CCC Node (b) CCT Node

Where,

a = depth of equivalent rectangular stress block (Equation 2-1)
d = distance from extreme compression fiber to centroid of longitudinal tension reinforcement
l_l = length of the bearing plate at the CCC node
l_s = length of the bearing plate at the CCT node
w_t = twice the distance from extreme tension fiber to centroid of longitudinal tension reinforcement
α = proportion of applied load that flows to near support
θ = angle of strut measured from the horizontal axis

When selecting a standard model, the two decisions affecting nodal efficiencies include: (i) whether the nodal regions are to be defined with hydrostatic or non-hydrostatic nodes; (ii) whether a one-panel or two-panel truss is to be used. A single-panel non-hydrostatic model was selected because it is simple, practical, and accurately depicts the behavior of deep beams.

Justification for using a single-panel non-hydrostatic model along with the corresponding implications is presented as follows.

Single-Panel Truss Model

It has been experimentally shown that a direct strut forms between the load and support for beams loaded with *low* a/d ratios: (i) according to Kani et al. (1979), beams with a shear span-to-depth ratio less than about 2.5 carry the load by a direct strut; (ii) research conducted as part of the current research program has shown that a direct strut is the primary shear transfer mechanism when the a/d ratio is equal to 1.85 (Section 5.3.2). Also, ACI 318-08 allows a designer to use a single-panel strut when the a/d ratio is less than or equal to 2.1 [note, this is accomplished indirectly as the strut angle is limited to 25-degrees (i.e. $a/d = 1/\tan 25^\circ = 2.1$)]. As a result, it can be concluded that using a single-panel truss to evaluate STM provisions is well founded for specimens with an a/d ratio less than or equal to two based on experimental observations, past research, and current design provisions.

As the a/d ratio exceeds 2, a single-panel STM becomes less appropriate. However, as detailed in Section 5.3.2, the reduction in the effectiveness is gradual, not immediate. Thus, a single-panel model is still appropriate at a/d ratios slightly greater than 2. In addition, due to the inherent conservatism of strut-and-tie modeling (lower bound theory of plasticity) some discrepancy between the model and the actual behavior of the member is accounted for.

Another objective of the current project was to evaluate the discrepancy between shear strength calculated using sectional shear models and STM provisions at an a/d ratio of 2. A goal was to develop STM provisions that would estimate shear capacity comparably with that of sectional shear provisions. For this reason, it was determined to include beams in the evaluation database with a/d ratios up to 2.5. While the behavior of members with a/d ratios between 2 and 2.5, may not follow a single-panel mechanism as well as members with smaller a/d ratios, this discrepancy seems small in context of the assumptions and basic principles of strut-and-tie modeling.

Non-Hydrostatic Nodal Regions

When the a/d ratio of a beam is in the range of one to two, and if a single-panel truss model is used, the strut width associated with non-hydrostatic nodes is more realistic than that obtained when using hydrostatic nodes. As an example, consider the hydrostatic and non-hydrostatic truss models illustrated in Figure 5.8.

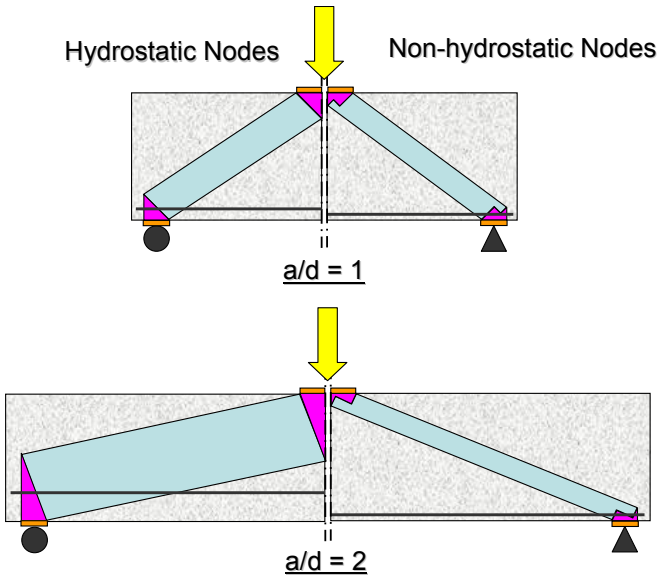

Figure 5.8: Difference between hydrostatic and non-hydrostatic nodes as a/d ratio increases.

The width of a strut abutting a hydrostatic node increases substantially as the a/d ratio increases. Whereas, the width of a strut abutting a non-hydrostatic node decreases slightly as the a/d ratio increases. If hydrostatic nodes are used, coordinating the centroid of the tie reinforcement with the centroid of a hydrostatic CCT node is illogical and unrealistic. Similarly, it is difficult to coordinate the aforementioned unrealistic placement of flexural reinforcement with the depth of a beam's flexural compression zone, i.e. the back face of a CCC node.

It is well established that the shear strength of a beam decreases as the a/d ratio increases (MacGregor and Wight, 2005; Kani et al., 1979; ACI-ASCE 1973; Section 5.3.2). The reduction in shear strength associated with an increasing a/d ratio is accounted for when non-hydrostatic nodes are used as seen by the reduction in the width of the strut in Figure 5.8. In contrast, as discussed in Section 2.2.3, when hydrostatic nodes are used, the corresponding efficiency factors must decrease in a manner that is inversely proportional to the a/d ratio to counteract the increasing size of the strut. This is why STM methods that have been derived using hydrostatic nodes – such as AASHTO LRFD (2008) – have a strut efficiency factor that decreases as the a/d ratio increases. On the other hand, when non-hydrostatic nodes are used the strut size diminishes slightly as the a/d ratio increases, thereby, accounting for the reduction in shear strength. This is why constant efficiency factors are used in several design codes. These differences in nodal dimensions are illustrated in Figure 5.9 for the example presented in Figure 5.8.

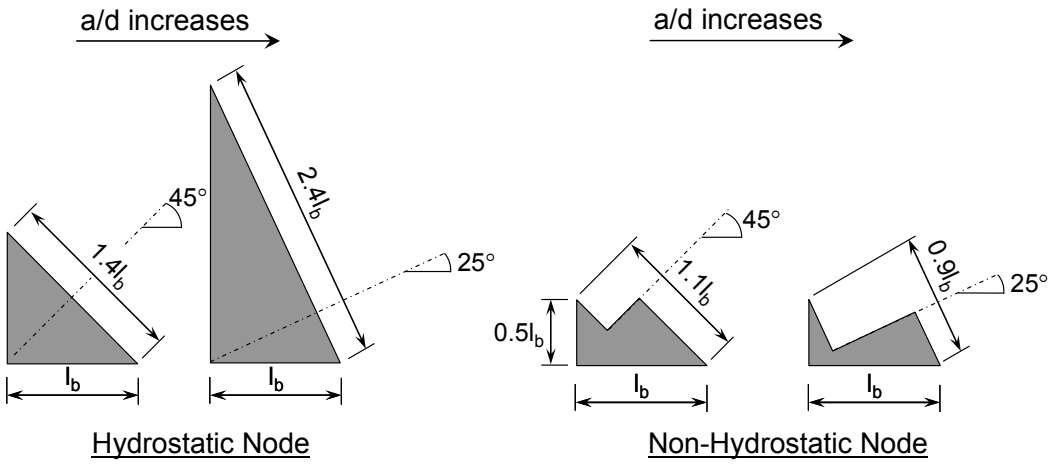

Figure 5.9: Typical difference in node dimensions between an a/d ratio of one and two.

Both ACI 318-08 and AASHTO LRFD (2008) include provisions that direct a designer towards using non-hydrostatic nodes (ACI 318-08, Figure RA.1.5; and AASHTO LRFD (2008), Figure 5.6.3.3.2-1). Additionally, most designers use non-hydrostatic nodes, as it is difficult to coordinate the dimensions of a hydrostatic node with other beam details.

In summary, the use of either hydrostatic or non-hydrostatic nodes is an assumption – a design tool intended to provide a simple method for proportioning a STM. Each nodal dimensioning technique has its theoretical strengths and weaknesses. For example, a hydrostatic state of stress is typically associated with materials that cannot resist shear; yet, concrete has the ability to resist shear stresses. As such, it is reasonable to assume that the nodal region in a concrete beam is in a non-hydrostatic state of stress. On the other hand, the dimensioning technique used to proportion a non-hydrostatic node can be overly simplified and overly conservative, as is suggested to be the case at the back face of the CCT node. Nonetheless, the benefits of using non-hydrostatic nodes are that they allow for the use of constant efficiency factors and they consider additional details such as reinforcement location and flexural capacity.

In order to directly compare STM provisions with one another, an explicitly defined truss model (Figure 5.6) is used. Using a consistent model to evaluate code provisions is essential as the resulting nodal stresses (i.e. efficiencies) are dependent on the model.

5.2.6 Evaluation of Current Design Provisions

A comparison between the ACI 318-08 STM, AASHTO LRFD (2008), *fib* (1999), ACI 318-99 [empirical provisions in lieu of STM (Equation 5.2)], and TxDOT Project 4371 (Sections 2.4 and 2.5) design provisions for deep beam shear is made. A single-panel strut-and-tie model was analyzed using the nodal geometries presented in Figure 5.7. An outline of the calculations performed for each STM procedure is located in Appendix F. In summary, the following seven stress checks are conducted for all of the beams in the database: **1)** Back face of CCC and **2)** CCT nodes; **3)** Bearing face of CCC and **4)** CCT nodes; **5)** Strut-to-node interface at the CCC and **6)** CCT nodes; and **7)** stress in the tie reinforcement. The locations of these seven stress checks are illustrated in Figure 5.10.

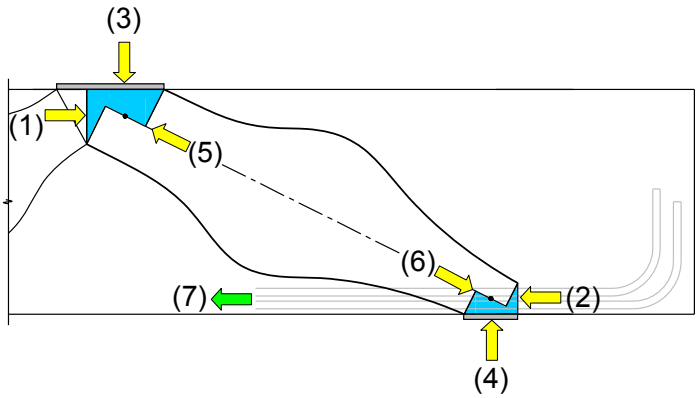

Figure 5.10: Seven stress checks used to evaluate STM procedures.

In addition to the seven stress checks shown above, failure of the D-region may be attributed to the longitudinal splitting of the strut. This failure mechanism is accounted for through the node-to-strut interface checks and through minimum transverse reinforcement. All of the beams in the evaluation database contained sufficient transverse reinforcement to resist the transverse tensile stresses in the bottle-shaped strut after the strut cracks. The minimum amount of transverse reinforcement required for a bottle-shaped strut to reach is design capacity is discussed in detail in Section 4.5.

Design provisions are compared to one another based on the experimental results of the 179 beams in the evaluation database (35 contributed from the current study). Since the aforementioned 7 stress checks are performed, it is appropriate to consider both shear and flexural failures in the database. An appropriate strut-and-tie modeling procedure should "catch" both. Furthermore, beams are often designed in practice such that flexure governs. For these reasons, specimens with flexure and shear failure modes were included in the evaluation database. A description of the filtering criteria used to form the evaluation database was presented in Section 2.5. The primary attributes of the evaluation database are summarized in Figure 5.11; details are included in Appendix D.

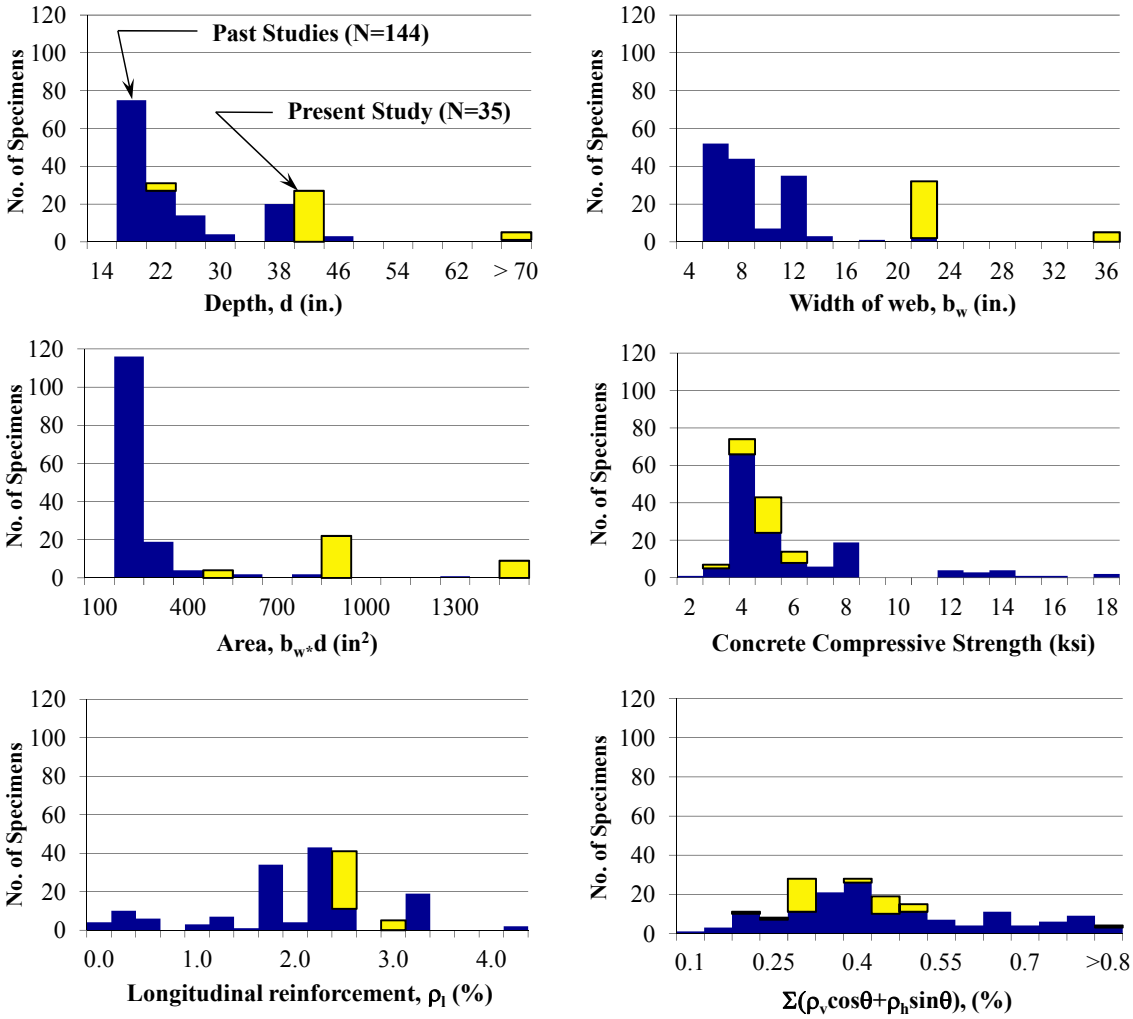

Figure 5.11: Primary attributes of the specimens in the evaluation database (N = 179).

The purpose of comparing the provisions is to establish a basis for an improved design method. Figure 5.12 and Table 5.4 present a summary of the accuracy and conservatism of the five design procedures. The ratio of experimental to calculated shear capacity was determined for the beams in the evaluation database. A histogram of the findings is presented as follows.

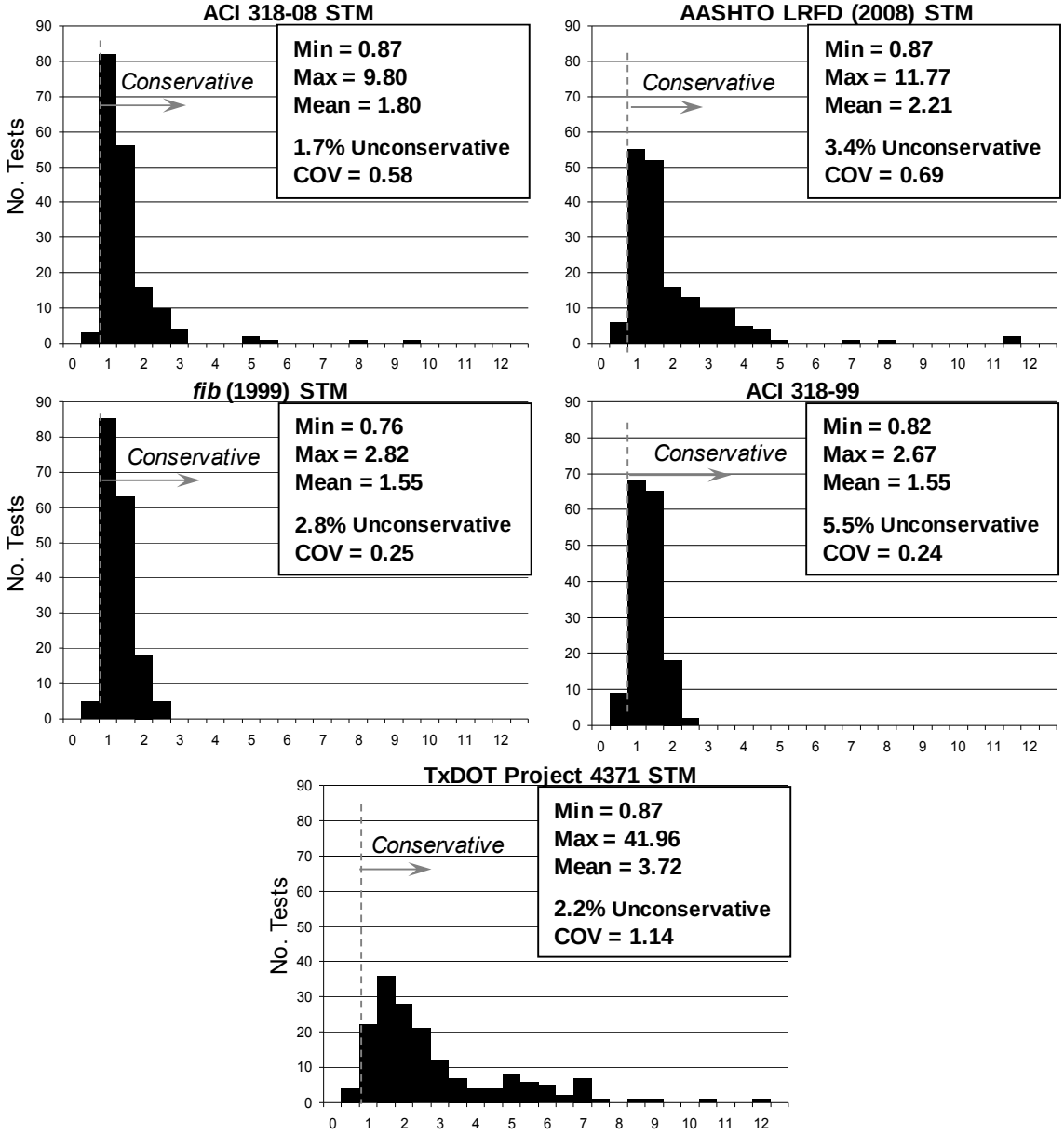

Figure 5.12: Range of experimental/calculated values determined using evaluation database (179 data points).

Table 5.4. STM Provisions: Evaluation Database

N = 179	Experimental/Calculated				
Design Provision	**Max**	**Min**	**Mean**	**% Unconservative†**	**COV††**
ACI 318 STM	9.80	0.87	1.80	1.7%	0.58
AASHTO LRFD	11.77	0.87	2.21	3.4%	0.69
***fib* (1999)**	2.82	0.76	1.55	2.8%	0.25
ACI 318-99	2.67	0.82	1.55	5.5%	0.24
Project 4371	41.96	0.87	3.72	2.2%	1.14

† Unconservative = Experimental/Predicted Value < 1.0

†† *COV* = Coefficient of Variation = Standard Deviation/Mean

Based on a comparison of the five sets of design provisions presented in Figure 5.12, the empirical equation removed from the ACI 318 provisions (Equation 5.2) in 2002 and the STM provisions recommended by *fib* (1999) are the most accurate (COV of 0.24 and 0.25 respectively).

The reason that a strut-and-tie method is preferred over an empirical equation is because a STM is more versatile and the emphasis of a truss model is on the critical details. Details that are often the cause of a deep beam shear failure include: development length, nodal bearing stresses, stresses at the back face of a CCC node and stress in the tie. If the ACI 318 empirical equation is used to design a deep beam region, the bearing stresses and flexural capacity of the beam also need to be checked. However, if a STM is used to design a deep beam region, then the model accounts for these potentially critical bearing and flexural stresses.

The AASHTO LRFD (2008) and TxDOT Project 4371 methods are sufficiently conservative. However, there is a large amount of scatter associated with the two methods. The reason for the large amount of scatter and conservatism can be attributed to the derivation of these methods. The derivation is based on using hydrostatic nodes. As a result, the efficiency factors for these methods diminish as the a/d ratio increases. As discussed previously, when non-hydrostatic nodes are used in combination with efficiency factors that diminish as the shear span increases, the result is overly conservative estimations of shear capacity.

The efficiency factors specified by ACI 318-08 and *fib* (1999) are similar in magnitude. However, the *fib* (1999) method is much more accurate [COV of 0.25 for *fib* (1999) versus 0.58 for ACI 318-08]. The difference in accuracy between the two procedures can be attributed to the following:

- *fib* (1999) explicitly allows the allowable stress at all faces of a nodal zone to be increased when triaxial confinement due to surrounding concrete is present.
- *fib* (1999) states that a stress check at the back face of a CCT due to bond stresses is not necessary – provided bars are anchored properly.
- The efficiency factors recommended by *fib* (1999) decrease as the compressive strength of concrete increases.

It is a major goal of this research study to make improvements to the ACI 318-08 and AASHTO LRFD (2008) STM procedures. According to MacGregor (2002), the selection of efficiency factors shall satisfy the following four criteria:

- Simplicity in application.
- Compatibility with tests of D-regions.
- Compatibility with other sections of ACI 318-08 and/or AASHTO LRFD (2008)
- Compatibility with other codes or design recommendations.

Based on the accuracy of the *fib* (1999) procedure, it was decided to pursue this method further. The *fib* (1999) provisions provide an engineer with an accurate and safe procedure for the design of a deep beam region. However, the *fib* (1999) provisions are not consistent with ACI 318-08 or AASHTO LRFD (2008). Therefore, minor improvements are recommended in order to make the *fib* (1999) provisions more consistent with ACI 318-08 and AASHTO LRFD (2008). An improved STM approach is presented in Section 5.2.7 and summarized in Section 5.2.9.

5.2.7 Proposed method

As detailed in Section 5.2.5, a single-panel non-hydrostatic truss model (Figure 5.6) is used to evaluate a dataset of 179 specimens and make a recommendation for an improved STM procedure. For the selected model, a STM procedure consists of the seven stress checks illustrated in Figure 5.10.

The stress at each nodal face is compared to its respective allowable efficiency factor. The face that controls the calculated capacity is the one with the largest stress to efficiency ratio. If the stress in the tie controls the beam's capacity, then that particular specimen is not used to calibrate efficiency factors. The controlling efficiency of each of the six nodal faces is examined for all beams in the database as follows. A recommendation at each face is made accordingly.

Triaxial Confinement

Based on the test results from the specimens with triaxially confined CCC and CCT nodes (i.e. Series II specimens discussed in Chapter 5), it was concluded that the effective compressive strength of all faces of a triaxially confined node can be increased by the bearing capacity modification factor specified in the ACI 318-08 and AASHTO LRFD (2008) provisions. According to ACI 318-08 §10.14 and AASHTO LRFD §5.7.5 the allowable bearing capacity of concrete can be expressed as follows.

$$P_n = m \cdot 0.85 f_c' \cdot A_1 \tag{5.12}$$

Where,

P_n = nominal bearing resistance

m = bearing capacity modification factor, $\sqrt{\frac{A_2}{A_1}} \le 2$

The definition of A_2 and A_1 is illustrated in Figure 5.13.

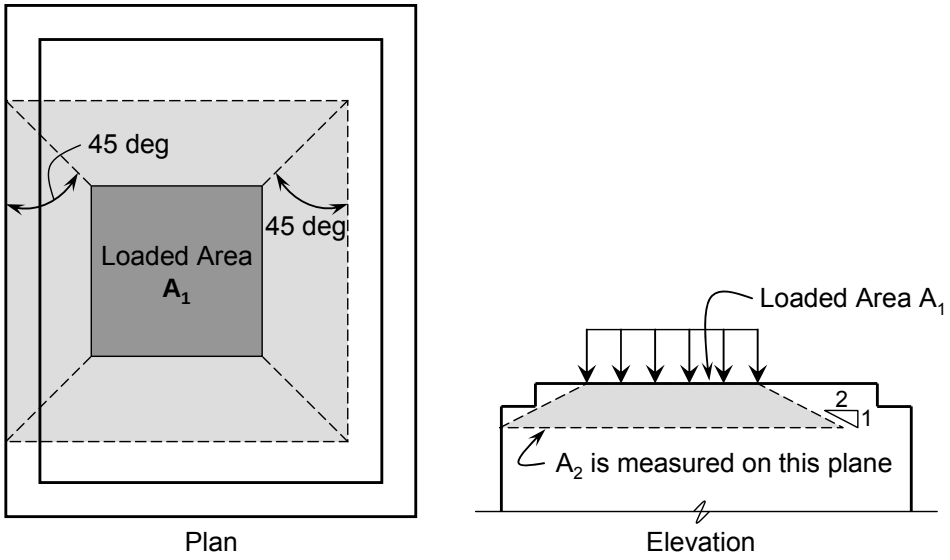

Figure 5.13: Application of frustum to find A_2 in stepped or sloped supports (ACI 318-08).

From a theoretical standpoint, when a nodal zone is triaxially confined, the compressive strength of concrete is increased in the entire region. Therefore, it is reasonable to assume that the compressive strength of all nodal faces is increased when triaxial confinement is present. This phenomenon is verified with beams fabricated and tested as part of the current study and past studies. In Figure 5.14, the ratio of experimental capacity to the calculated capacity is presented for all beams in the filtered database whose bearing plate width was smaller than the width of the beam. The capacity of the specimens is calculated with the ACI 318-08 STM provisions in which an increase in nodal capacity due to triaxial confinement is both accounted for and ignored. Although not presented, similar results exist if the AASHTO LRFD (2008) STM provisions are used to estimate capacity.

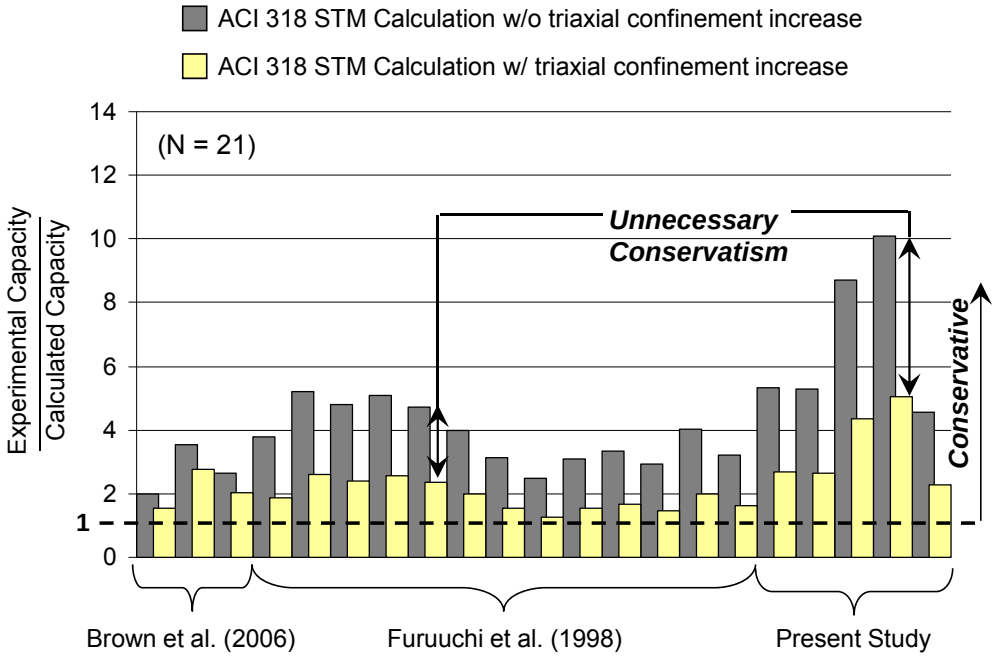

Figure 5.14: The effect of triaxial confinement: Experimental capacity/Estimated capacity (ACI 318-08).

Upon examination of Figure 5.14, it can be concluded that an increase in the capacity of all triaxially confined nodal faces improves the accuracy of a STM prediction without diminishing its conservatism. This conclusion is justified on a theoretical and experimental basis.

For reference, the data represented in Figure 5.14 is discussed. Brown et al. (2006) tested three beams whose load plates had a width less than the width of the beam (Section 4.4). Furuuchi et al. (1998) tested a series of deep slabs with varying load and support plate dimensions (Section 4.4). Specimens tested by Furuuchi et al. (1998) were 6-inch deep, 20-inch wide, and did not contain any shear reinforcement. Based on their aspect ratio and lack of stirrups, these beams are considered the worst-case scenario when evaluating triaxial confinement provisions.

Back Face of the CCT Node

In a strut-and-tie model, the height of the back face of a CCT node is taken as twice the distance from the exterior beam surface to the centroid of the reinforcement that defines the tie (Figure 5.15).

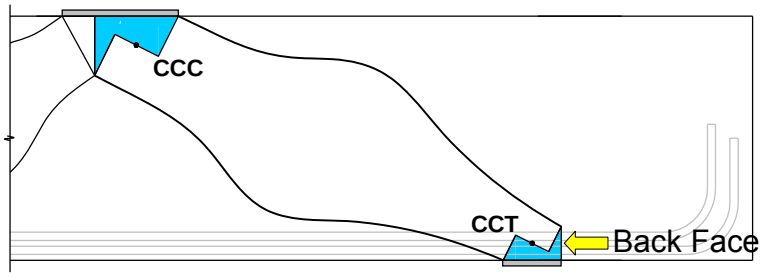

Figure 5.15: Back face of a CCT node.

As previously discussed, the efficiency of the back face of a CCT node is dependent on the stress condition. Stress at this surface can be attributed to the bond stress that results from the anchorage of a tie, bearing stress of an anchor plate or headed bar, or an external indeterminacy such as occurs at an interior node over a continuous support. An example of these configurations is illustrated in Figure 5-1.

The effectiveness of a CCT node to resist bond stress is investigated separately from the other stress conditions shown. The results of this study are presented in the next section. The effectiveness of the back face to resist bearing stresses caused by conditions other than anchorage is discussed afterwards.

Effectiveness of Back Face to Resist Bonding Stresses

According to the ACI 318-08 and AASHTO LRFD (2008) STM provisions, stresses at the back face of a CCT must always be checked. Alternatively, the *fib* (1999) provisions do not require a check at the back face of a CCT node if the applied force is the resultant of the bond stress attributed to the anchorage of a tie (provided that the tie is sufficiently developed).

In general, the technique used to proportion the back face of a CCT node typically results in an excessively small face. As a result, it often controls the nominal capacity of a truss model. If the tie is anchored properly, crushing of concrete at the back face of the support is unlikely and should not be used to determine the capacity of a CCT node. As recommended by Thompson et al. (2003) and as discussed in Section 5.2.1, *the stress limits imposed by the code provisions [at the back face of a CCT node] may be unnecessary*.

In order to investigate the criticality of stresses at the back face of the CCT node, the capacity of beams estimated per the ACI 318-08 provisions was examined in further detail. The node face that determined the capacity of each beam in the database was found according to the ACI 318-08 STM provisions. Then, the capacity of each of the beams in the database was determined per the ACI 318-08 STM provisions except that the stress at the back face of the CCT node was ignored. As a result, not considering the stress at the back face of the CCT node had an insignificant impact on the conservatism of the ACI 318-08 provisions. This point is illustrated in Figure 5.16.

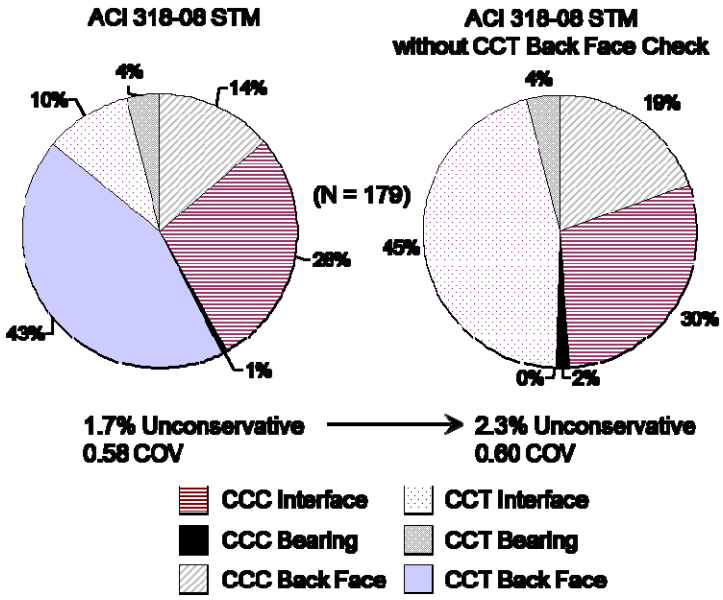

Figure 5.16: Governing node face with and without a stress check at the back face of the CCT node: ACI 318.

As can be observed in Figure 5.16, if ACI 318-08 STM provisions are used without any modifications, the stress check performed at the back face of the CCT node controls the capacity for 43% of the beams in the evaluation database. If the stress at the back face of the CCT node is not checked, the amount of unconservative predictions increases from 1.7% to 2.3% and the coefficient of variation increases from 0.58 to 0.60. This is a minor change considering that the CCT back face stress check originally controlled the design of almost half the beams in the database. Therefore, it can be concluded that checking the stresses at the back face of the CCT node minimally improves the accuracy and conservatism of the ACI 318-08 STM design provisions.

In order to gather more information on the stress distribution at the back face of the CCT nodes, concrete strain gauges were affixed behind the support plate of beams tested as part of the current experimental program, as illustrated in Section 3.5.2. The purpose of collecting strain data at the back face of the CCT node was to determine the magnitude and distribution of stresses in the region and compare these results with typical modeling assumptions.

The height of the back face of a CCT node is taken as twice the distance from the exterior face of the beam to the centroid of the longitudinal reinforcement. For the Series I and III specimens, that distance is equal to approximately 11" and 7" respectively. According to ACI 318-08 and AASHTO LRFD (2008), the limiting efficiency factor at the back face of a CCT node is 0.68 and 0.75, respectively. In other words, the allowable stress at the back face is $0.68 \cdot f_c'$ and $0.75 \cdot f_c'$. The assumed CCT nodal geometries and allowable stress at the back face are presented in Figure 5.17 for the Series I and III specimens. An allowable stress of $0.70 \cdot f_c'$ is assumed and shown for illustration purposes.

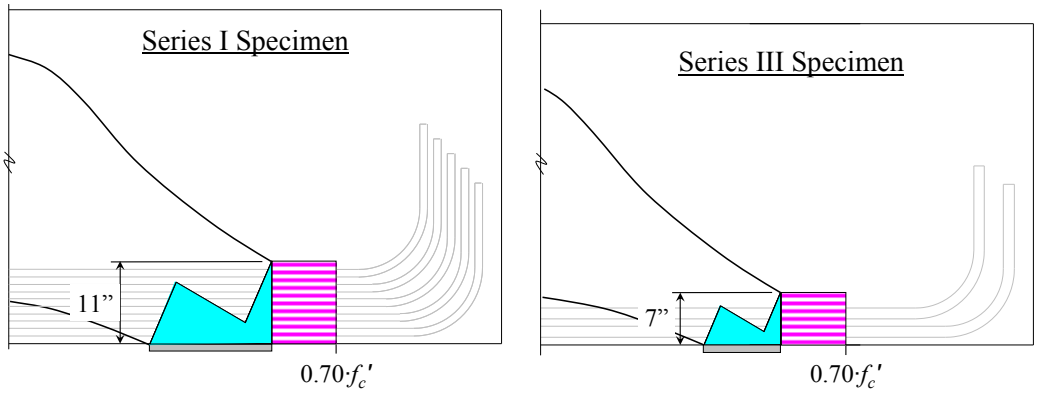

Figure 5.17: Assumed nodal dimensions and allowable stress distribution at back face of CCT node.

Strain gauges were applied behind the support plate (Section 3.5.2) for all of the Series I specimens and the following Series III specimens: III-1.85-0, III-1.85-02, and III-1.85-025. The strain distribution at 90% of ultimate capacity is presented for specimens I-02-4 and I-02-2; and for specimens III-1.85-0, III-1.85-02, and III-1.85-025 in Figure 5.18. In addition, the theoretical stress at the back face based on the assumed nodal geometry is presented.

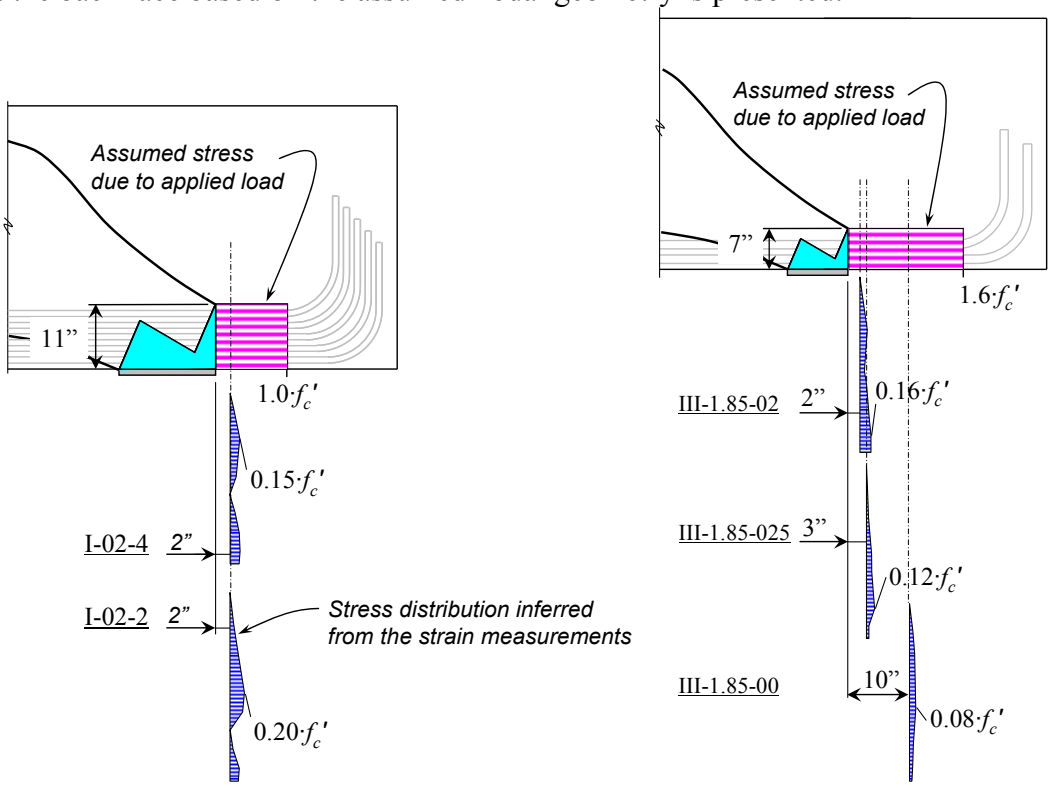

Figure 5.18: Strain distribution measured behind the support plate at 90% of ultimate capacity.

Based on the strain data measured behind the CCT nodal region, it can be concluded that the distribution of bond stresses is not concentrated at the assumed location of the back face of the CCT node. Rather, the stress is distributed throughout much of the section. Furthermore, the magnitude of the stress is so small that crushing of concrete at the back face of the CCT node due to bond stresses from an appropriately-developed tie is implausible. This type of failure mode was not observed in any of the tests conducted within this research program nor those reported in the literature. As such, applying bond stresses of developed reinforcement to the back face of CCT nodes is inappropriate.

In order to verify data obtained from concrete gauges, steel strain gauges were applied to all twelve of the main longitudinal bars for specimens III-1.85-02 and III-1.85-025 as described in Section 3.5.1. The rebar gauges were located in the same plane as the concrete surface gauges. The force in the steel reinforcement was inferred based on the experimentally measured strains, modulus of elasticity of steel, and nominal area of the reinforcing bars. The force applied to the same plane of concrete was inferred based on the area under the strain profile curve shown in Figure 5.18, the width of the beam, and the modulus of elasticity of concrete taken as $57{,}000\sqrt{f_c'}$. The resulting force measured in the reinforcement was within 10% of the value measured with the concrete surface gauges for both specimens. Thus, it can be concluded that the surface gauge data was reliable.

Effectiveness of Back Face to Resist Direct Stresses

Conditions exist where the stress applied to the back face of a CCT node is attributed to forces other than those caused by the bonding of anchored reinforcement. An example of such conditions is at the CCT node over an interior support or at a CCT node where the anchorage of the reinforcement is provided by a bearing plate or headed bar (Figure 5-1).

When the stress at the back face of a CCT node is the result of a condition other than the transfer of bonding stresses, the nodal dimension must be proportioned accordingly so that the crushing of concrete does not occur.

Based on the recommendations of *fib* (1999), Schlaich et al. (1987), and Thompson et al. (2003), the bond stresses attributed to the anchorage of a tie are not critical and need not be applied to the back face of a CCT node provided that the tie meets the necessary anchorage requirements. If the force applied to the back face of a CCT node is attributed to stresses other than those caused by anchorage, the effectiveness of the node to resist crushing must be checked. In this case, an efficiency factor consistent with the CCT bearing face should be used.

If the stress applied to the back face of a CCT node is the result of a combination of both anchorage and a discrete force from another strut framing into the node, it is only necessary to proportion the node to resist the direct compression stresses. It is believed that the small amount of stress that may indirectly occur in the nodal region due to anchorage is accounted for by the conservative dimension of the CCT node and the respective efficiency factor.

Efficiency of the Bearing and Back Face of CCC Node

The dimensions of the bearing and back face of a CCT node, as shown in Figure 5.19, is proportioned as illustrated in Figure 5.7.

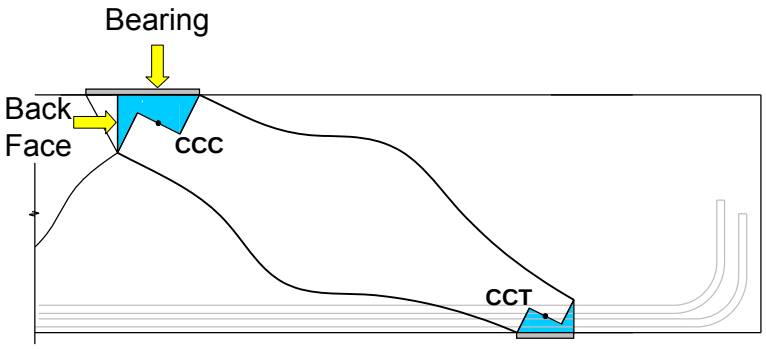

Figure 5.19: Bearing and back face of a CCC node.

The height of the back face of the CCC node is based on the depth of the equivalent compression block determined from flexural mechanics. This dimension is justified, as the crushing of the back face of a CCC node is the same failure mode observed in a flexural failure. In a flexural analysis, it is assumed that the compression block is loaded uniaxially. Similarly, it is assumed that the bearing face of the CCC node is uniaxially loaded in compression. According to both ACI 318-08 and AASHTO LRFD (2008), the efficiency of concrete in an undisturbed state of uniaxial compression is typically taken as a constant value of 0.85. Therefore, for purpose of maintaining consistency with the ACI 318-08 and AASHTO LRFD (2008) specifications, it is proposed that the efficiency of the undisturbed uniaxial compression stress field associated with the back face of the CCC node be set to a constant value of 0.85.

The efficiency of the bearing face of the CCC node is established in a similar manner. This recommendation is consistent with what is currently done in the ACI 318-08 and AASHTO LRFD (2008) specifications.

The implications of these proposals are examined within the evaluation database. The normalized stress at the back and bearing face of the CCC node is plotted for beams where said nodal boundaries control the design (Figure 5.20). Based on the results obtained from the database and illustrated in Figure 5.20, a constant efficiency of 0.85 is an appropriate value.

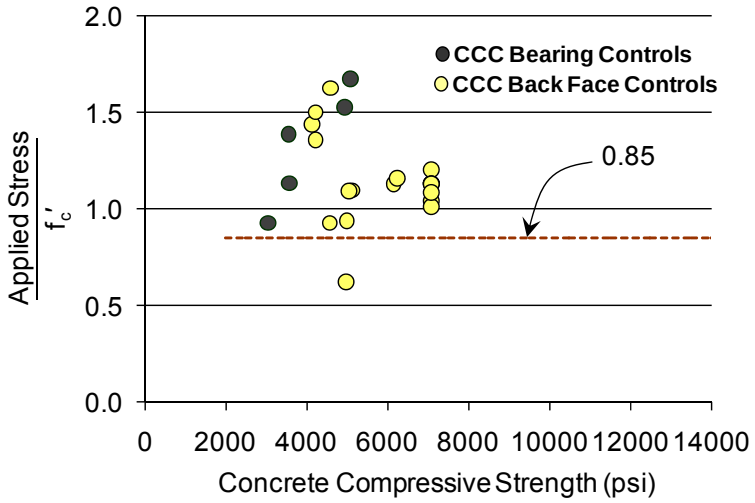

Figure 5.20: CCC back (N=19) and bearing face (N=6) efficiency factor: Proposed Method.

The efficiency factor specified by *fib* (1999) is also considered an appropriate value. However, a constant efficiency factor is recommended as opposed to variable one (Table 5.1) for the bearing and back face of the CCC node based on following: (i) in the interest of maintaining consistency with other sections of ACI 318-08 and AASHTO LRFD (2008); and (ii) in the interest of having the simplest code provision that captures the trends (or lack thereof) of the data presented in Figure 5.20.

Efficiency of the Bearing Face of CCT Node

The dimension of the bearing face of a CCT node, as shown in Figure 5.21, is proportioned as illustrated in Figure 5.7.

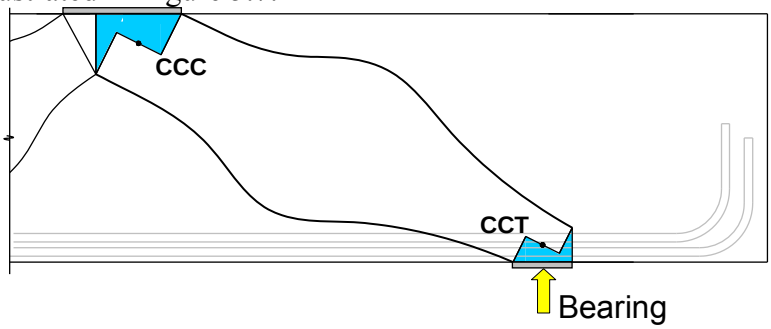

Figure 5.21: Bearing face of a CCT node.

According to Vecchio and Collins (1986), the effective compressive strength of concrete decreases with the accumulation of transverse tensile strains (i.e. a CCT nodal region). The philosophy that concrete has a reduced efficiency in the CCT nodal region has been adopted by ACI 318-08, AASHTO LRFD (2008), and *fib* (1999). In accordance with ACI 318-08, AASHTO

LRFD (2008), and *fib* (1999) it is proposed that the efficiency at the bearing face of the CCT node be set to a constant value of 0.70.

The conservativeness of this proposal is examined by using the evaluation database. The normalized stress at the bearing face of the CCT node is plotted for beams where said boundary controls the STM calculations (Figure 5.22).

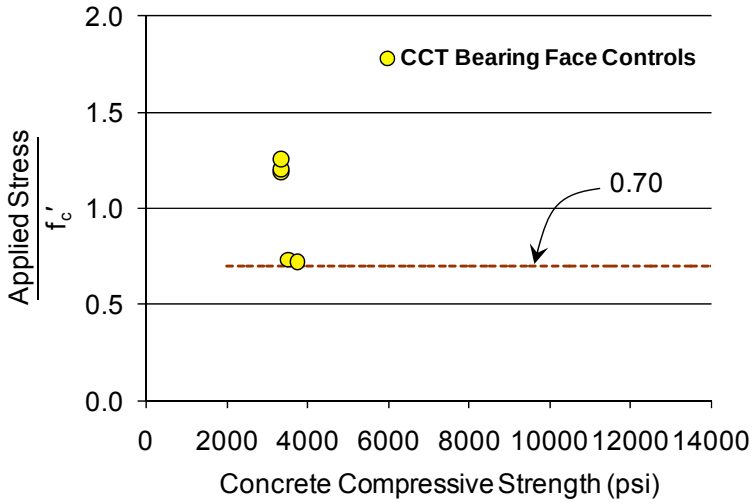

Figure 5.22: CCT bearing face efficiency factor (N = 5): Proposed Method.

Admittedly, there are a sparse number of beams in the database that are controlled by the CCT bearing face. Nevertheless, based on the results obtained from the database, and in accordance with ACI 318-08 and AASHTO LRFD (2008), a constant efficiency of 0.70 is appropriate.

Efficiency of the Strut-to-Node Interface

The dimension of the CCC and CCT strut-to-node interface, as shown in Figure 5.23, is proportioned as illustrated in Figure 5.7.

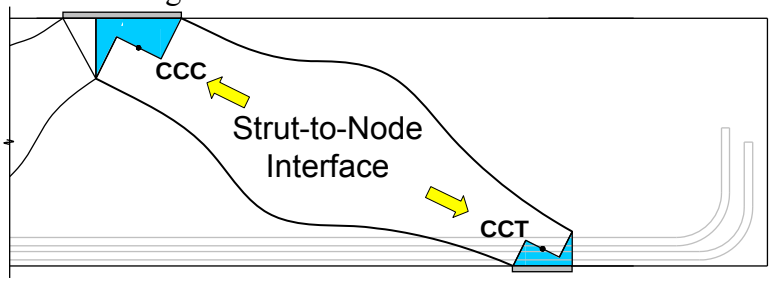

Figure 5.23: CCC and CCT strut-to-node interface.

AASHTO LRFD (2008) and *fib* (1999) specify a concrete efficiency at the CCT interface lower than at the CCC interface for the same reason cited for the bearing faces; i.e. the presence of transverse tensile stresses diminish the compressive strength of concrete. ACI 318-08, on the other hand, specifies the same efficiency at both the CCC and CCT interface.

Although the theoretical efficiency of a CCT region has been shown to be lower than that of a CCC region, the diminishing effect is not detectable due to the assumed dimensions of the node-to-strut interfaces that the efficiency factors are applied to. There is not enough accuracy in proportioning non-hydrostatic node-to-strut interface dimensions to account for a reduction in the compressive strength of concrete due to transverse tensile stresses. Consider, for example, the beams in the database whose calculated capacities are controlled by the ACI 318-08 stress checks at the CCC or CCT node-to-strut interface (Figure 5.24).

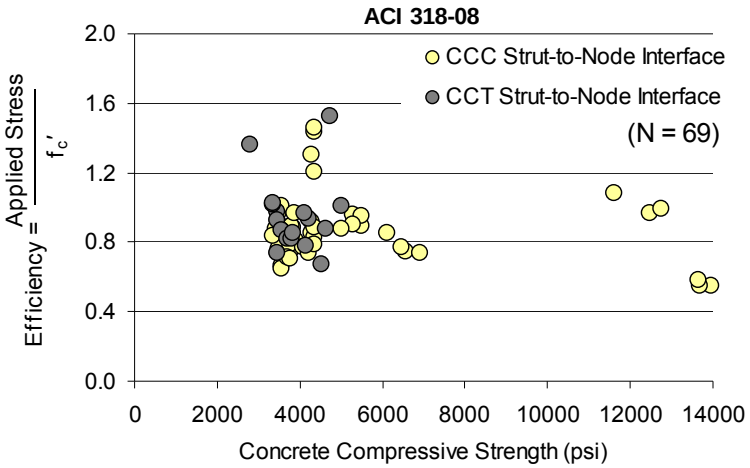

Figure 5.24: Experimental efficiency vs. ACI 318-08 at the CCC and CCT strut-to-node interface.

As seen in Figure 5.24, the efficiency at the strut-to-node interface is defined as the ratio of the applied stress at said interface to the compressive strength of concrete. Upon examination of the capacity of the beams in the database as estimated by the ACI 318-08 STM provisions, the CCC strut-to-node interface governed the capacity for 50 beams while the CCT strut-to-node interface governed for 19 beams. It is important to observe that the data for the 69 beams controlled by the CCC and CCT strut-to-node interface is equally scattered and with a similar lower bound.

Accordingly, it can be concluded that efficiency of the CCC or CCT strut-to-node interface is equivalent when those interfaces control the capacity calculations (per ACI 318-08). A similar conclusion can be reached for the calculations carried out by the AASHTO LRFD (2008) STM specifications (Figure 5.25).

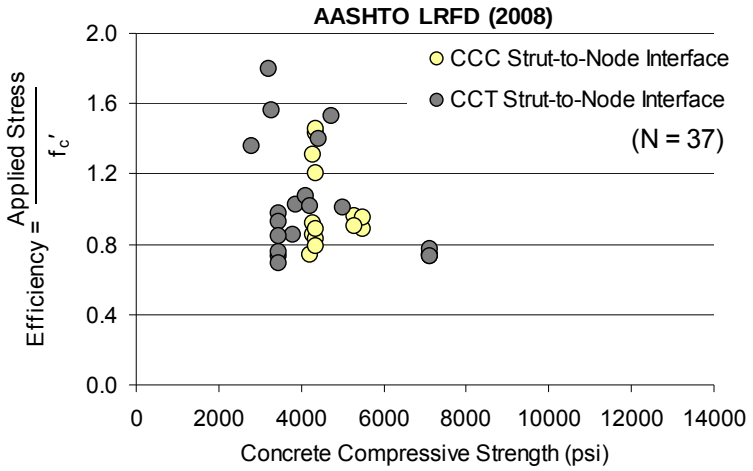

Figure 5.25: Experimental efficiency vs. AASHTO LRFD (2007) at the CCC and CCT strut-to-node interface.

In light of the data presented in Figure 5.24 and Figure 5.25, there is no reason to specify a lower efficiency factor at the CCT strut-to-node interface.

Efficiency factors recommended by *fib* (1999) are a function of concrete compressive strength. High strength concrete has a lower efficiency because of the corresponding reduction in shear transmitted along the main diagonal crack. The strength of the cement paste in high-strength concrete is more than that of the aggregate. When shear cracks form in high-strength concrete, the resulting cracks are transmitted through, rather than around the aggregate. As a result, the main inclined crack is smoother, so it has a lower interface shear capacity. Additionally, research conducted by Nielson (1978), Ramirez and Breen (1991), Bergmeister et al. (1993) Brown et al. (2006) support the use of an interface efficiency factor that diminishes as concrete compressive strength increases.

Figure 5-26 illustrates the results of the calculations performed on the specimens in the evaluation database by using the *fib* (1999) efficiency factors.

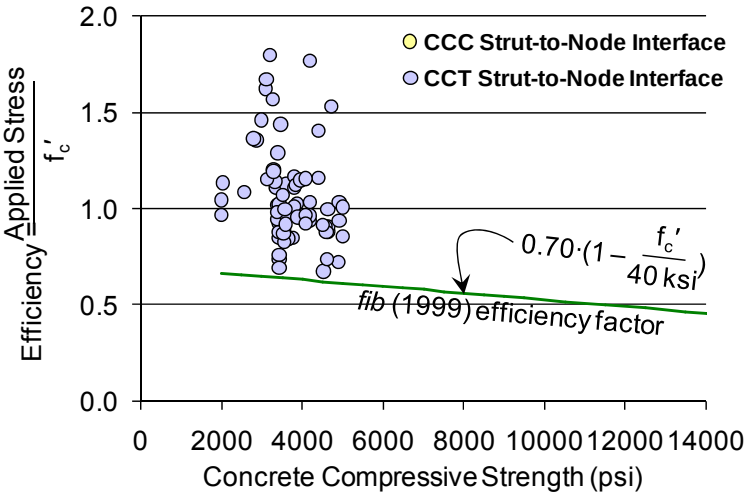

Figure 5-26. Experimental efficiency vs. fib (1999) recommendations at the CCC and CCT strut-to-node interface.

As seen in Figure 5-26, the CCC strut-to-node interface never controls the capacity of a deep beam estimated per the *fib* (1999) STM provisions. This is attributed to the geometric proportions that define the CCC nodal zone. The bearing and back face of the CCC node are always smaller than the interface and the *fib* (1999) recommended efficiency is the same at all three nodal faces. As a result, the critical stress cannot occur at the node-to-strut interface. It will always occur at either the back face or bearing face depending on the strut angle. The same phenomenon does not occur in the CCT nodal zone because a stress check is not required at the back face.

Given that the experimental stress at the CCC and CCT strut-to-node interface is equivalent when estimated per ACI 318-08 and AASHTO LRFD (2008) (Figure 5.24 and Figure 5.25); and given that the capacity of a beam estimated per *fib* (1999) STM provisions is never controlled by the stress at the CCC strut-to-node interface; it is proposed that the efficiency factor assigned to the CCC strut-to-node interface also be assigned to the CCT node-to-strut interface. This recommendation is consistent with the general philosophy of the ACI 318-08 provisions.

It has previously been determined that the nodal efficiency is independent of the a/d ratio when non-hydrostatic nodes are used and dependent on the compressive strength of concrete. Therefore, in accordance with *fib* (1999), it is proposed that the efficiency at the node-to-strut interface diminish as the compressive strength of concrete increases. Modifications to the *fib* (1999) efficiency factor are suggested as follows.

The *fib* (1999) strut-to-node efficiency factor is equal to 0.43 when the compressive strength of concrete is 14,000-psi. In general, concrete is considered *high-strength* when the compressive strength is greater than 8,000-psi. Given that there is not much data available in the high-strength range, it is proposed that the efficiency be capped at a lower value of 0.45 for compressive strengths greater than 8,000-psi. Similarly, it is proposed that the efficiency be capped at an upper value of 0.65 [the *fib* (1999) factor is equal to 0.63 when the compressive strength of concrete is 4000-psi]. Finally, it is proposed that the efficiency linearly decrease

between 4,000 and 8,000-psi. As such, the proposed CCC and CCT strut-to-node interface efficiency factor, v, is expressed as follows:

$$v = 0.45 \leq \ 0.85 - f_c'/20ksi \ \leq 0.65 \tag{5.13}$$

The conservativeness of this proposal is examined by using the evaluation database (Figure 5.27). The efficiency factors at the CCC and CCT strut-to-node interface are plotted for beams whose capacity is calculated by using the proposed method.

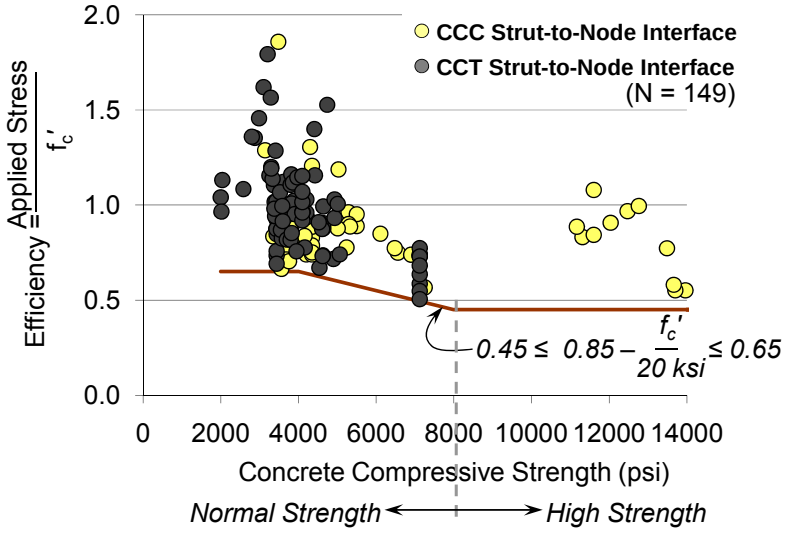

Figure 5.27: Experimental vs. proposed efficiency at the CCC and CCT strut-to-node interface.

Based on the results obtained from the evaluation database, the efficiency factor proposed for the determination of the capacity of the CCC and CCT strut-to-node interface (Equation 5.13) is an appropriate expression.

The recommendations outlined by *fib* (1999) were used to formulate a new STM design procedure. In accordance with *fib* (1999), the following attributes of the proposed STM provisions are consistent with the *fib* (1999) STM provisions:

- Disregard the stress check at the back face of the CCT node when the applied force is the resultant of bonding stresses from a sufficiently anchored tie.
- Increase the allowable stress in triaxially confined nodal regions.
- At the CCC and CCT strut-to-node interface, the efficiency of concrete decreases as the compressive strength increases.

The following attributes of the proposed STM provisions are consistent with the ACI 318-08 and AASHTO LRFD (2008) provisions:

- A triaxial confinement modification factor is used to account for the increase in nodal capacity due triaxial confinement. The modification factor is expressed the same as for bearing capacity (Equation 5.12).

- In accordance with ACI 318-08, the efficiency of the CCC and CCT node-to-strut interfaces are identical.
- At the bearing and back face of the CCC node, the efficiency of concrete is a constant value of 0.85.
- At the bearing face of the CCT node, the efficiency of concrete is a constant value of 0.70.

Based on the fundamental principles of strut-and-tie modeling given in the ACI 318-08, AASHTO LRFD (2008), and *fib* (1999) design provisions, and based on tests of the D-regions analyzed using the evaluation database, a new STM provision is proposed. The details of the proposed provision are summarized in Figure 5-28. The proposed STM procedure is compared to ACI 318-08, AASHTO LRFD (2007), and *fib* (1999) in Section 5.2.8. A complete outline of the new procedure is presented in Section 5.2.9.

$$\varphi F_n > F_u$$

$$F_n = m \cdot \nu \cdot f_c' \cdot A_{nz}$$

Where,

$$m = \sqrt{A_2 / A_1} \quad \text{(Equation 5.12)}$$

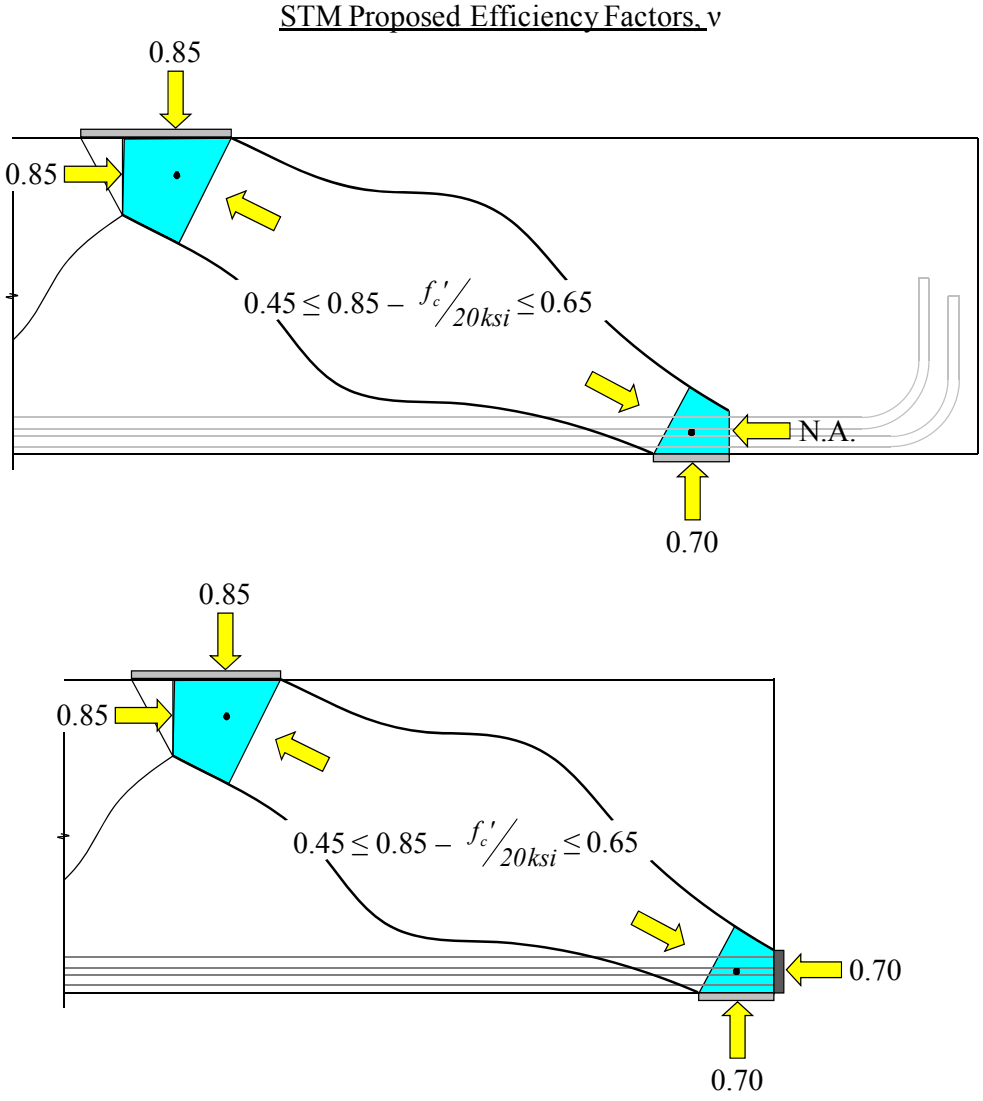

Figure 5-28. Proposed STM design provisions

5.2.8 Assessment of Proposed Method

An assessment of the proposed method based on the experimental results of the beams in the evaluation database is presented in Table 5.5 and Figure 5.29.

Table 5.5. STM Provisions: Evaluation Database

N = 179	Experimental/Calculated				
Design Provision	**Max**	**Min**	**Mean**	**% Unconservative†**	**COV††**
ACI 318	9.80	0.87	1.79	1.7%	0.58
AASHTO LRFD	11.77	0.87	2.21	3.4%	0.69
fib (1999)	2.82	0.76	1.55	2.8%	0.25
ACI 318-99*	2.67	0.82	1.56	5.5%	0.24
Project 4371	41.96	0.87	3.72	2.2%	1.14
PROPOSED	***4.14***	***0.73***	***1.54***	***0.6%***	***0.28***

† *Unconservative* = Experimental/Calculated Value < 1.0

†† *COV* = Coefficient of Variation = Standard Deviation/Mean

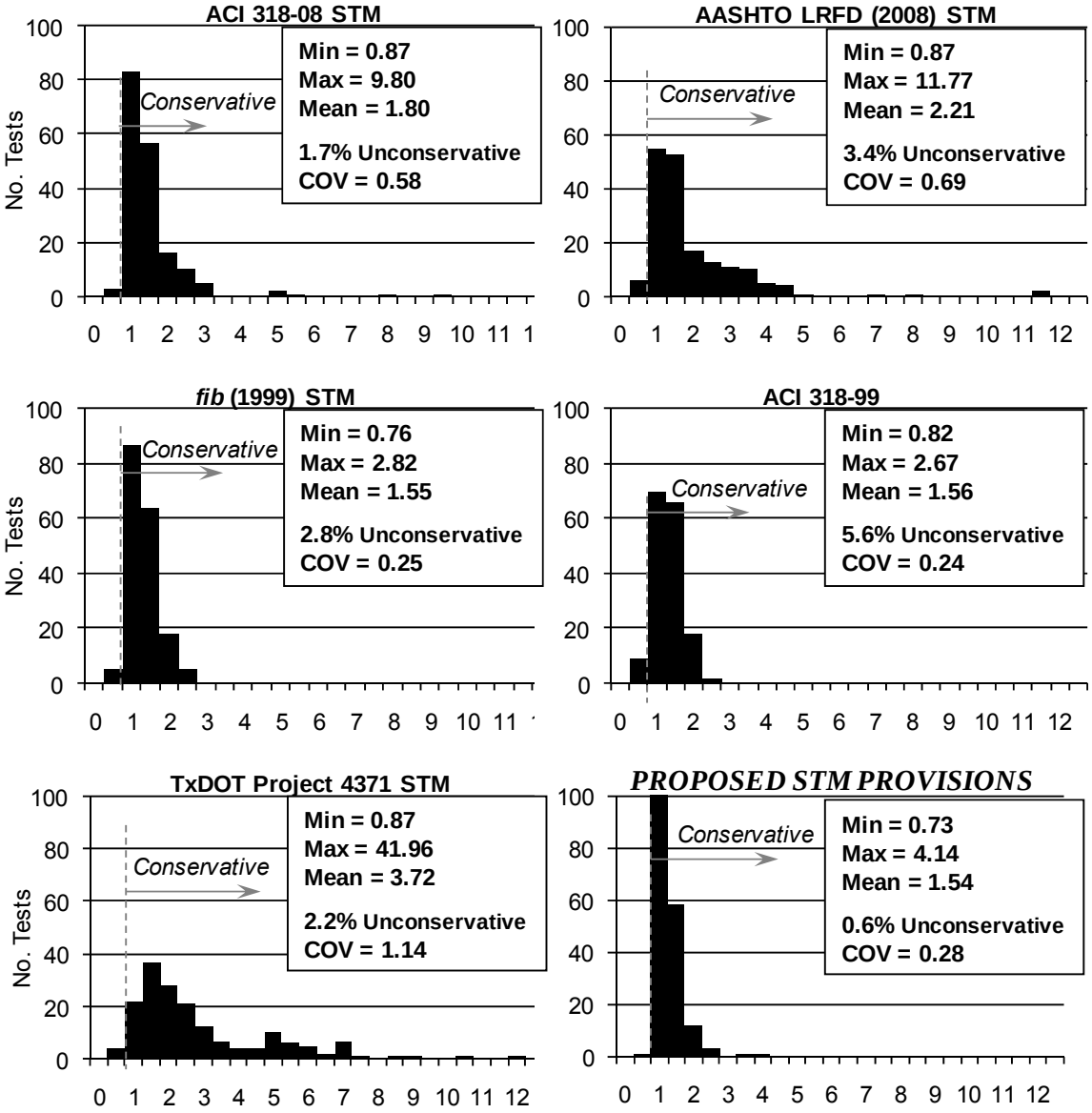

Note: In accordance with ACI 318-08 and AASHTO LRFD (2008), the proposed method contains a limit on the triaxial confinement modification factor equal to 2 (Equation 5.12); whereas, fib (1999) limits this factor to 4. The proposed method would perform slightly better than fib (1999) if the triaxial confinement modification limit were increased to 4 [Mean = 1.51, 0.6% unconservative, COV = 0.22].

Figure 5.29: Comparison of proposed STM provisions with other design provisions (Evaluation Database = 179 data points).

As shown, the proposed strut-and-tie modeling procedure is a significant improvement over the current ACI 318-08 and AASHTO LRFD (2008) procedures. The amount of unconservative estimations using the proposed provisions is slightly less than the *fib* (1999) provisions, but the *fib* (1999) methodology is slightly more accurate than the proposed procedure. However, if both methods contained the same limit on the triaxial confinement modification factor, then the proposed procedure would have a COV equal to 0.22, a slight improvement compared to the *fib* (1999) provisions. As it is, the proposed triaxial confinement factor is consistent with the ACI 318-08 and AASHTO LRFD (2008) bearing capacity provisions.

Filtered Database

The specimens in the *evaluation database* were selected from a larger dataset based on their geometry and proportions. It was the intent of the research team to formulate design recommendations based on test specimens that best represented actual structural members. As a result, the larger beams contained in the evaluation database were used to calibrate the recommended nodal efficiencies. Upon derivation of the proposed STM methodology, it is of interest to compare the performance of the procedure with a larger dataset; i.e. a dataset that contains data other than those that were used to calibrate the proposed STM procedure. Therefore, the performance of the proposed STM provisions is compared with the other design provisions for the tests that are contained in the *filtered database*.

As previously discussed, the STM model that was used to evaluate deep beam design provisions indirectly accounts for failure controlled by the longitudinal splitting of the strut by only considering beams that contain a minimum amount of reinforcement. Therefore, only those beams in the filtered database that contain a minimum amount of transverse reinforcement are evaluated. An assessment of the proposed provisions is presented in Figure 5-30. The data presented in Figure 5-30 is based on the experimental results of the beams in the filtered database with reinforcement that satisfies the minimum for reinforced struts according to ACI 318 Appendix A (Equation 4.7 in Section 4.5.1) (i.e. $\rho_{\perp} > 0.1\%$).

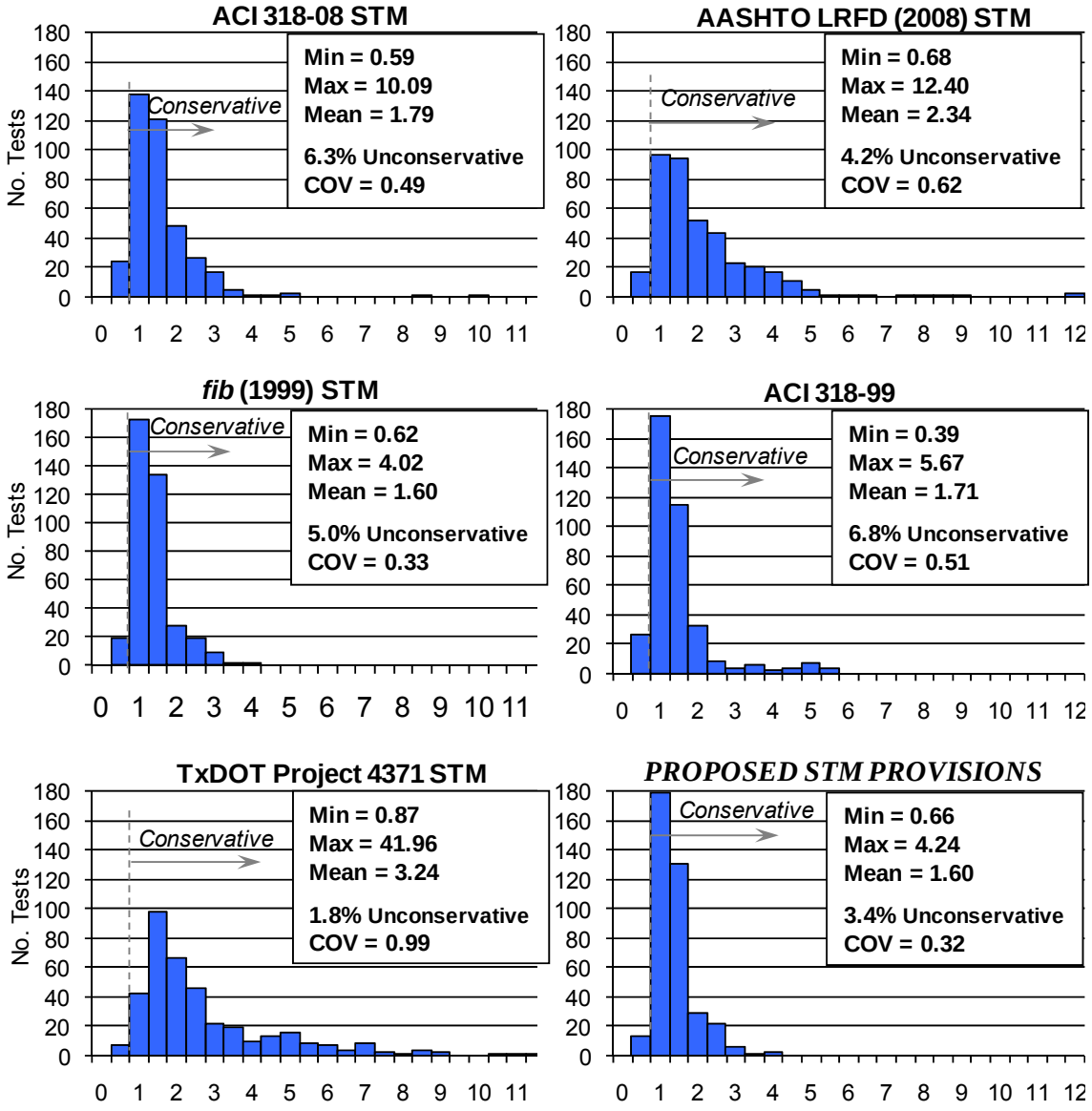

Note: If the triaxial confinement modification limit of the proposed method were increased to 4 [Mean = 1.59, 3.4% unconservative, COV = 0.31].

Figure 5-30. Comparison of proposed STM provisions with other design provisions (Filter Database with $\rho_{\perp} > 0.1\% =$ 381 data points)

Upon observation of Figure 5-30, it can be concluded that the trends between the design provisions are consistent when a similar evaluation is conducted using the beams in the filtered database. Again, the proposed STM procedure is a significant improvement over the ACI 318-08 and AASHTO LRFD (2008) provisions.

Many of the specimens in the filtered database were not used to calibrate the proposed STM provisions. However, the proposed procedure estimates the capacity of the beams in the filtered and evaluation database with an equivalent amount of accuracy. The reason that the procedure performs as well for the specimens in the filtered database can be attributed to the fact that it accounts for governing modes of failure better than other STM provisions.

Transverse Reinforcement Ratio: $\rho_{\perp} > 0.1\%$

When a deep beam is designed by using a single-panel strut-and-tie model, transverse reinforcement is required to reinforce the bottle-shape strut and to provide sufficient deformation capacity for the assumed *plastic* truss model to develop. Additionally, transverse reinforcement is also necessary to ensure adequate serviceability behavior. The quantity of reinforcement that is required for strength and serviceability is a primary research objective and was discussed in detail by Section 4.5.

According to Brown et al. (2006), the amount of transverse reinforcement necessary to maintain the equilibrium of a strut due to spreading of compression is approximately 0.15% in each direction; *fib* (1999) requires a minimum amount of 0.2% in each direction without specifying whether this amount is required for strength, serviceability, or both; and AASHTO LRFD (2008) requires 0.3% in each direction and explicitly denotes it as crack control reinforcement. ACI 318-08 allows the use of unreinforced struts. For a strut to be considered reinforced a minimum amount of 0.3% reinforcement perpendicular to the strut ($\rho_{\perp}$) must be provided.

All design provisions evaluated as part of the current research program were examined using specimens with $\rho_{\perp}$ values as low as 0.1%; i.e. much less than required by ACI 318-08, AASHTO LRFD (2007), or *fib* (1999). The proposed method summarized in Section 5.2.9 was calibrated based on the same lightly reinforced specimens. The implications of considering beams with a transverse reinforcement ratio, $\rho_{\perp}$, as low as 0.1%, are presented in Table 5.6 and Figure 5.31.

Table 5.6. Influence that Transverse Reinforcement Ratio has on Accuracy of STM Provision

	$\Sigma\rho_{\perp} \geq 0.001$ *No. = 179*		$\Sigma\rho_{\perp} \geq 0.003$ *No. = 127*		$\rho_v = \rho_h \geq 0.002$ *No. = 44*		$\rho_v = \rho_h \geq 0.003$ *No. = 25*	
	% NG†	COV	% NG†	COV	% NG†	COV	% NG†	COV
ACI 318-08	1.7%	0.58	2.4%	0.54	2.3%	0.69	4.0%	0.82
AASTHO LRFD (2007)	3.4%	0.69	1.6%	0.68	0.0%	0.76	0.0%	0.88
fib (1999)	2.8%	0.25	2.4%	0.25	0.0%	0.23	0.0%	0.24
Proposed Method	0.6%	0.28	0.0%	0.27	0.0%	0.33	0.0%	0.36

† *%NG* = percentage of beams with Experimental/Calculated ratio < 1.0.

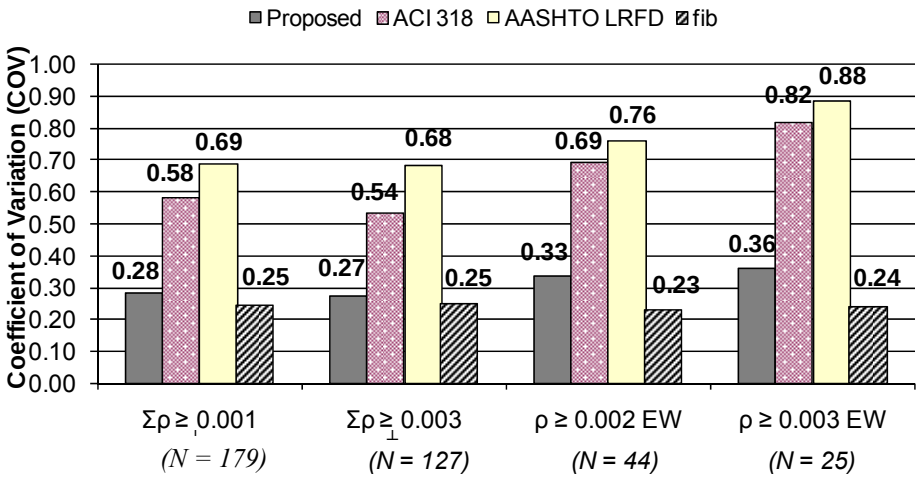

Note: In accordance with ACI 318-08 and AASHTO LRFD (2007), the proposed method contains a limit on the triaxial confinement modification factor equal to 2 (Equation 5.12); whereas, fib (1999) limits this factor to 4. The proposed method would perform slightly better than shown if the triaxial confinement limit were increased to 4 [COV = 0.22; 0.22; 0.24; and 0.24 respectively, for the reinforcement ratios presented in Table 5.6 and Figure 5.31].

Figure 5.31: Influence that transverse reinforcement ratio has on the COV of various STM provisions.

The purpose of comparing the performance of the proposed STM provisions for differing amounts of minimum transverse reinforcement is to determine whether the earlier observations in regards to conservatism and accuracy remain valid for the proposed STM methodology. The difficulty with evaluating the provisions for beams with, for example, the AASHTO minimum of 0.3% transverse reinforcement in each direction, is that only a sparse number of beams meet the criteria. More specifically, only 44 beams meet the *fib* (1999) minimum requirement (0.2% in each direction) and only 25 meet the AASHTO LRFD requirement (0.3% in each direction). Therefore, significant conclusions should not be inferred from statistical comparisons based on such small data sets. Nonetheless, upon comparison of the various STM design provisions, it can be seen that the performance of each provision (as indicated by the COV) is relatively equivalent to one another regardless of the minimum amount of reinforcement. As a result, it can be concluded that the lightly reinforced specimens in the evaluation database provide a valid basis of comparison among different STM provisions. In other words, the conclusions remain valid for beams with a higher percentage of crack control reinforcement.

Upon observation of the number of unconservative predictions for the proposed method, it could be concluded that, from a strength standpoint, a transverse reinforcement ratio of $\rho_{\perp}$ = 0.1% is adequate to ensure that the strength of more than 95% of the specimens in the dataset. However, one of the beams tested as part of the experimental program (Specimen III-1.85-01) had 0.1% vertical and 0.14% horizontal reinforcement ($\rho_{\perp}$ = 0.15%), yet the ratio of experimental to estimated capacity was 0.73 when using the proposed provisions. This low strength value should not be overlooked despite all of the statistical analyses. Therefore, based on the findings of the experimental program, a transverse reinforcement ratio of at least 0.2% in each direction is recommended in order to ensure adequate strength. If less reinforcement is provided, then the chance increases that the capacity will be unconservatively estimated. Minimum reinforcement requirements were addressed in Section 4.5. As noted in this section, more reinforcement may be needed for serviceability considerations.

5.2.9 Outline of Proposed Strut-and-Tie Modeling Procedure

A detailed examination of the ACI 318-08, AASHTO LRFD (2008), and *fib* (1999) provisions was conducted and recommendations were discussed for the newly proposed strut-and-tie modeling procedure. For the reader's convenience, the proposed STM procedure is summarized as follows.

Step 1: Define Critical Nodal Regions

Stresses in a D-region concentrate into nodal zones. Failure of a D-region is typically due to crushing of concrete in the nodal region (i.e. strut-to-node interface, bearing face) or anchorage failure. The advantage of a strut-and-tie model over a sectional model for the design of a D-region is that the focus of the design is on the critical nodal regions rather than the less relevant cross-sectional behavior (Section 4.6). Efficiency factors are directly dependent on the assumed proportions of the nodal region. The proposed strut-and-tie method is based on the non-hydrostatic node proportions outlined in Section 2.3 and illustrated in Figure 5.32.

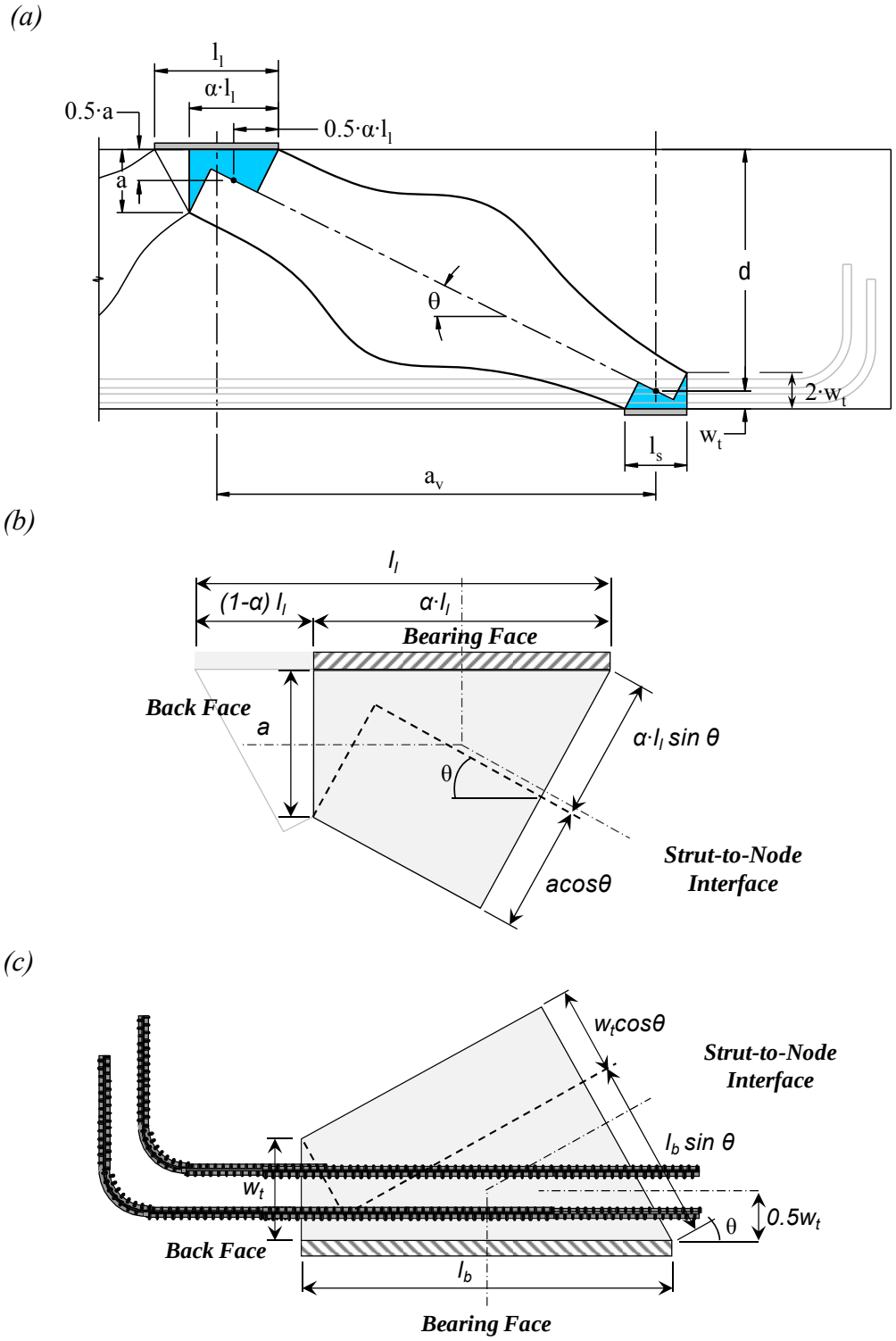

Figure 5.32: (a) Single-panel STM (b) CCC Node (c) CCT Node

Bond stresses in a smeared node region (CTT nodes) and at the back face of the CCT node are not critical if the anchorage of longitudinal bars or stirrups is adequately developed.

Step 2: Design Nodal Regions

The nominal compression strength of a nodal zone, F_n, shall be as follows.

$$F_n = f_{ce} \cdot A_{nz} \tag{5.14}$$

Where,

f_{ce} = effective compressive strength of concrete in nodal zone, psi

A_{nz} = the area of the face of the nodal zone, in^2

The effective compressive stress, f_{ce}, on the face of a nodal zone shall not exceed the following value.

$$f_{ce} = m \cdot \nu \cdot f_c' \tag{5.15}$$

Where,

f_c' = Specified compressive strength of concrete, psi

m = $\sqrt{A_2/A_1} \le 2$, Triaxial confinement modification factor

Definition of A_2 and A_1 is illustrated in Figure 5.33.

ν = 0.85, Bearing and Back Face of CCC node.

0.70, Bearing Face of CCT node.

It is not necessary to apply the resultant of bonding stresses directly to the back face of a CCT node provided that tie is adequately anchored.

$\left(0.85 - f_c'/20ksi\right)$, CCC and CCT Strut-to-Node Interface

Not to exceed 0.65 nor less than 0.45.

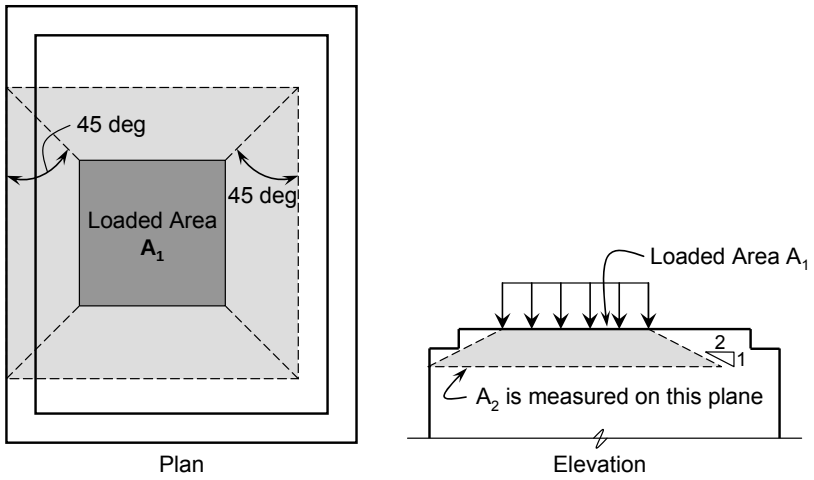

Figure 5.33: Application of frustum to find A_2 in stepped or sloped supports (ACI 318-08).

5.2.10 Proposed STM Procedure: Summary

A new STM design procedure was developed for the design of deep beams and D-regions. The efficiency factors recommended for the proposed procedure have been calibrated

using the results of experimental tests, while maintaining consistency with current design provisions. Although the efficiency factors of the proposed procedure were calibrated based on tests of deep beams, they were also calibrated based on maintaining consistency with current design provisions, and theoretical STM principles. Thus, it is strongly believed that the proposed STM method is valid for other types of structures.

The new method provides a significant improvement in accuracy over the ACI 318-08 and AASHTO LRFD (2008) procedures. Thus, based on the new STM provisions, it is proposed that the ACI 318-08 and AASHTO LRFD (2008) provisions be modified accordingly. A summary of the proposed changes to AASHTO LRFD (2008) is presented in Appendix A. An example problem that illustrates the differences between the existing and proposed provisions is presented in Appendix B.

5.3 Discrepancy in Calculated Shear Strength at a/d Ratio of 2.0

The objective of this task was to reduce the discrepancy between shear strength calculated using the STM and the sectional shear provisions in AASHTO LRFD (2008) at an a/d ratio of 2. In this section, a review of the effect of the a/d ratio on the shear behavior of reinforced concrete members is provided. Information regarding the transition from deep beam behavior to sectional shear behavior is emphasized. Based on data from the experimental program and from the literature, the use of a single-panel strut-and-tie model for a/d ratios up to 2 is justified. Lastly, the reason for the discrepancy between shear strength calculated using the STM and the sectional shear provisions at an a/d ratio of 2 is explained. With the use of the proposed STM provisions discussed in Section 5.2, the discrepancy is largely eliminated.

5.3.1 Background

In Article 5.8.1.1 of AASHTO LRFD 2008, a deep component is defined as:

> *Components in which the distance from the point of zero shear to the face of the support is less than 2d or components in which a load causing more than ½ (1/3 in case of segmental box girders) of the shear at a support is closer than 2d from the face of the support.*

In this requirement, the shear span is defined; and the limiting ratio of shear span to effective depth is set at 2. It is required in Article 5.13.2.1 that beams or components meeting the definition of a "deep component" be designed according to the strut-and-tie provisions in AASHTO LRFD (Article 5.6.3) or another recognized theory. The basis for restrictions on "deep components" is due to the nonlinear strain distribution that exists in regions near concentrated loads, supports, or abrupt changes in geometry. Conventional flexural theory, i.e. plane-sections-remain plane, is not valid in these regions. According to St. Venant's principle, the strain distribution is not affected by the disturbance at approximately a distance 'd' away from it (Schlaich et al., 1987). This principle is the basis for the limit of a/d ratio of 2. In regions where "it is reasonable to assume that plane sections remain plane after loading," the sectional model can be used for shear design (Article 5.8.1.1, AASHTO LRFD (2008)). The stress trajectories of an asymmetrically-loaded beam are shown in Figure 5.34. According to AASHTO LRFD (2008), different design models should be used in the regions to either side of the concentrated load.

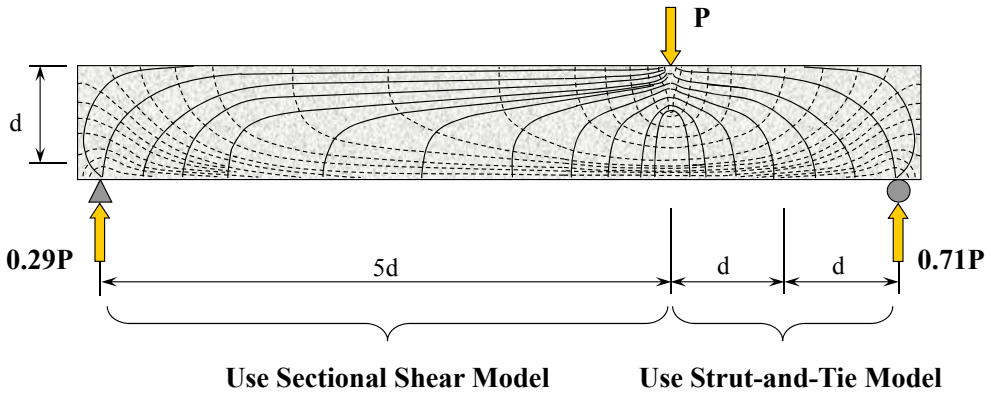

Figure 5.34: Stress trajectories in an asymmetrically-loaded beam

Therefore, at an a/d ratio of 2, there is a discrepancy in the required shear design model according to the specifications of AASHTO LRFD (2008). If a structure is loaded in such a way that an a/d ratio of 2.1 exists, then the sectional shear model applies for design. Conversely, if the structure is loaded such that an a/d ratio of 1.9 exists, then a strut-and-tie analysis is required. It is known that near an a/d ratio of 2, a gradual transition in the dominant shear transfer mechanism occurs consistent with each of the required models. The transition is not immediate and a large discrepancy in calculated capacity at an a/d ratio of 2 is not justified.

The main purpose of the current task is illustrated qualitatively in Figure 5.35. For members with an a/d ratio less than 2, shear capacity is computed according to the strut-and-tie provisions in AASHTO LRFD. It was shown in Section 5.2.5 that due to the efficiency factor at the CCT node-strut interface and the geometry of non-hydrostatic nodes, the calculated capacity decreases rapidly as the a/d ratio approaches 2. For members with an a/d ratio greater than 2, shear capacity is calculated with a sectional model consisting of $V_c + V_s$ in AASHTO LRFD (2008). The capacity computed according to the sectional model is often greater than that according to the STM at an a/d of 2, especially if there is a considerable amount of transverse reinforcement in the member. The purpose of the current task is to remove the discrepancy between the calculated shear capacities from each model at an a/d ratio of 2, thereby providing a uniform level of conservatism across the transition from deep beam to sectional shear behavior.

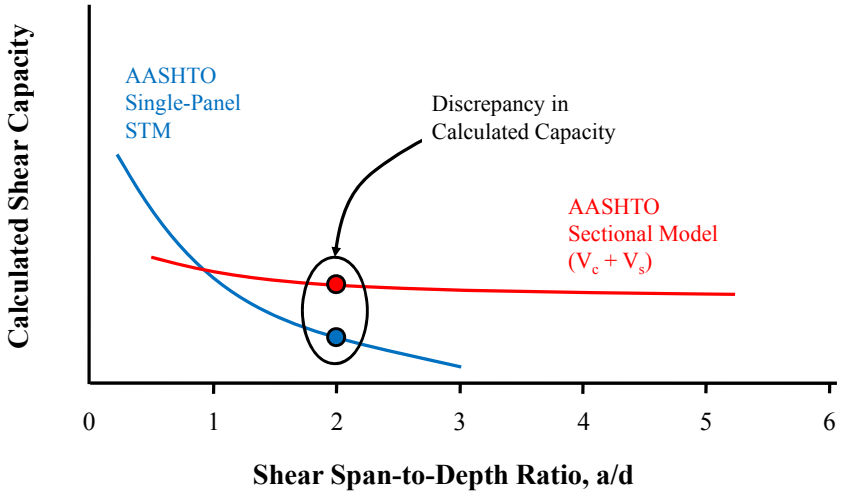

Figure 5.35: Discontinuity in calculated shear capacity in AASHTO LRFD 2008 at a/d ratio of 2

5.3.2 Effect of a/d ratio on Shear Behavior

Shear span-to-depth ratio (a/d) has been recognized as an important parameter affecting the shear strength of reinforced concrete beams since the 1950s (ACI-ASCE Committtee 326, 1962). For single or double concentrated loads acting on a beam, the shear span is clearly defined. For other types of loading, namely distributed loads, it is convenient to present the shear span-to-depth ratio as the ratio of M / Vd to aid in its application. A clear definition of the shear span-to-depth ratio is required for its proper use in empirical equations. For strut-and-tie models, the a/d ratio (and also the clear span-to-depth ratio in ACI 318-08) is used to determine if a strut-and-tie analysis is required. In calculating the strength of a member with a STM, the

path of the applied loads is traced through the structure directly, without the direct use of the a/d ratio.

Results from the Literature

Numerous researchers have shown the effect of the a/d ratio on the shear strength and overall behavior of reinforced concrete beams. A few studies are reviewed in this section with an emphasis on the effect of the a/d ratio on the dominant transfer mechanism of the member.

In 1954, forty-two reinforced concrete beams were loaded to failure by Moody et al. to evaluate their shear strength. The size and loading conditions of the test specimens were divided into three groups corresponding to three a/d ratios: approximately 1.5, 3, and 3.5. Primarily, the behavior of beams without transverse reinforcement was studied. Two specimens were tested with web reinforcement. The test results indicated that the beams with higher a/d ratios (3 and 3.5) failed soon after the load causing first diagonal cracking was reached. For the beams that were loaded with smaller a/d ratios (1.5), the beam had additional capacity after first diagonal cracking. A redistribution of internal stresses took place after the formation of diagonal cracks in which compression and shear stresses concentrated in the compression zone at the top of the inclined crack. It was observed that the stress distribution in the tension reinforcement along the shear span did not follow the distribution of external moments. The failure of the specimens loaded with an a/d ratio of 1.5 was classified as shear-compression (Moody et al., 1954).

In 1957, thirty-eight concrete beams without transverse reinforcement were tested by Morrow and Viest. The a/d ratio ranged from approximately 1 to 7.8 for the test specimens. It was observed that the a/d ratio greatly contributed to the failure mode and overall performance of the beams. At an a/d ratio less than about 3.4, the test specimens failed in shear-compression. The beams failed due to crushing of the compression zone above the diagonal crack at a higher load than the load at first diagonal cracking. With increasing a/d ratio, the ratio between the ultimate load and the first diagonal cracking load decreased. The beams loaded with an a/d ratio between 3.4 and 6.1 failed in diagonal tension in which the load at first cracking was synonymous with the ultimate load. Beams with an a/d ratio greater than 6.1 failed in flexure. The authors warned that the aforementioned limits on a/d ratio were a function of the properties of the beams that were tested and should only be used qualitatively (Morrow and Viest, 1957). It is interesting to note that the transition between shear compression and diagonal tension failure was found to be 3.4 in this study. In other studies reviewed in this section, the a/d ratio at this transition is typically around 2 or 2.5. It is possible that the difference is due to the strict definition of a diagonal-tension failure as a case in which the first diagonal cracking load and the ultimate capacity are equivalent.

Hundreds of tests on reinforced concrete beams were conducted by Kani for the purpose of understanding the mechanism of diagonal failure, also called shear failure (Kani et al., 1979). Based on the observed behavior of the test specimens, two mechanics-based models were derived to form a shear-strength envelope. The applicability of each model was a function of the a/d ratio. The shear-strength envelope is illustrated in Figure 5.36.

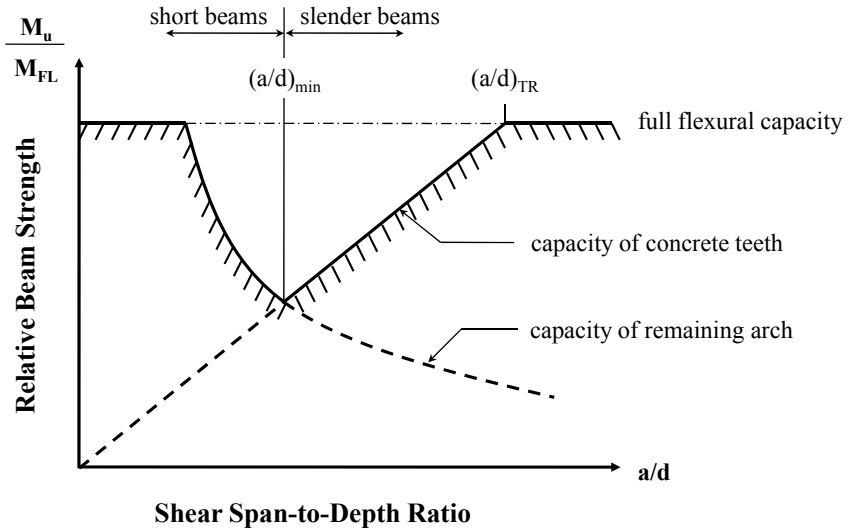

Figure 5.36: Proposed shear-strength envelope by Kani (Kani et al., 1979)

In Figure 5.36, the strength of the member is quantified as a percentage of the moment capacity. The moment capacity is not reached in a "valley of diagonal failure" bounded by two critical a/d ratios: $(a/d)_{min}$ and $(a/d)_{TR}$. $(a/d)_{min}$ is the intersection between the two models that govern diagonal failure. $(a/d)_{TR}$ is the a/d ratio at which flexural failure governs the capacity instead of diagonal, or shear, failure. At mid-range a/d ratios ($(a/d)_{min} < a/d < (a/d)_{TR}$), the shear strength of a beam is governed by the "capacity of concrete teeth." This model consists of treating a cracked, reinforced concrete beam as a "comb-like structure" with a series of "concrete teeth" cantilevered from its base (Kani et al., 1979). The diagonal failure of the beam is a result of overstressing the tooth at its base. An equation for the capacity of a tooth was developed that was a function of the a/d ratio, the flexural strength of concrete, the flexural moment arm, the cross-sectional dimensions, and the width and length of the cracks. The width and length of the cracks outlined the dimension of the tooth and were determined empirically. At low a/d ratios ($a/d < (a/d)_{min}$), the shear strength of a beam was defined as a function of the "capacity of the arch." This model treated the reinforced concrete beam as a tied arch in which the load transferred directly to the support. The equation that was developed for this model was simplified such that it was only a function of the flexural capacity of the beam and the a/d ratio. Good agreement existed between test data and the proposed models.

In his study of diagonal failure, Kani recognized the transition of the dominant mechanism of behavior as a function of the a/d ratio. At low a/d ratios ($a/d < (a/d)_{min}$), the shear strength of the beam was governed by a tied-arch failure. At higher a/d ratios ($(a/d)_{min} < a/d < (a/d)_{TR}$), the shear strength of the beam was governed by a bending failure of a "concrete tooth." The transition between these different mechanisms was labeled $(a/d)_{min}$ because it coincided with the smallest shear strength of the member. The value of $(a/d)_{min}$ was a function of the longitudinal reinforcement ratio, the yield strength of the reinforcement, the flexural strength of the concrete, and the width and length of the cracks. Even though $(a/d)_{min}$ changed based on the properties of the beam, it was usually close to 2.5. This value was supported by experiments.

The effect of transverse reinforcement on the diagonal failure of reinforced concrete beams was also investigated by Kani. The function of the reinforcement was to create internal supports for the series of concrete arches that are formed by the concrete teeth. In a sense, the

a/d ratio is essentially shortened by the internal supports created by the transverse reinforcement. In terms of the shear-strength envelope, the region governed by the "capacity of the arch" is extended due to the effective shortening of the a/d ratio.

An experimental study was conducted by Ahmad and Lue (1987) on specimens with high-strength concrete (f'c > 8,800-psi). A model similar to the one proposed by Kani was developed that was applicable to beams with both normal- and high-strength concrete. Through the experimental study, it was determined that the capacity and the failure mode of the test specimens were largely a function of the a/d ratio. Four different failure modes were evident. At an a/d > 6, the beams generally failed in flexure. At an a/d ratio between 2.5 and 6, the failure of the beams was due to a diagonal tension crack that originally propagated from a flexural crack (flexure-shear crack). At an a/d ratio between 1.5 and 2.5, the beams failed by shear compression of the web. At a/d < 1.5, the failure was by crushing of the arch rib of the beams. Thus, a similar breakdown of failure modes to that observed by Kani was also observed by Ahmad and Lue (1987). At an a/d ratio of approximately 2.5, the shear behavior of the beam transitioned from a shear-compression type failure to a diagonal-tension type failure.

The experimental shear strength of high-strength concrete beams with an a/d ratio ranging from 1.5 to 2.5 was investigated by Shin at al. (1999). It was also observed in this study that the failure mode of the test specimens was dependent on the a/d ratio. However, in this study the transition in failure mode from shear-compression to shear-tension occurred at an a/d ratio of approximately 2.

Results from the Experimental Program

In the experimental program of the current study, the effect of a/d ratio was also investigated. Tests were conducted on beams with shear-span-to-depth (a/d) ratios of 1.2, 1.85, and 2.5. The normalized shear strength of six 21"x42" specimens in which the a/d ratio varied from 1.2 to 2.5 is depicted in Figure 5.37. With increasing a/d ratio, the normalized shear strength at failure decreased; and the failure mode of the test specimens changed.

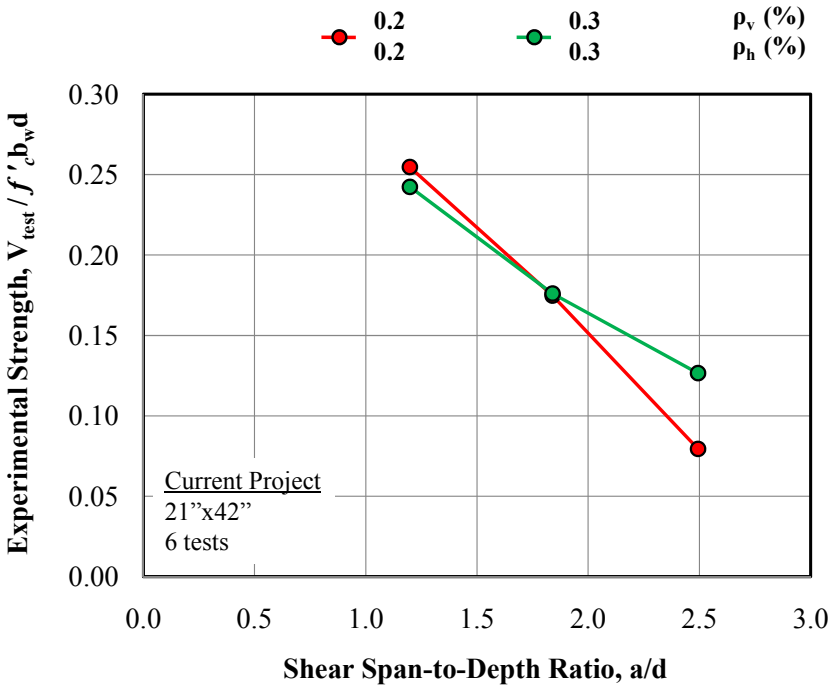

Figure 5.37: Effect of a/d ratio on experimental strength of test specimens

The pictures of the test regions at failure for the specimens represented by the red line in Figure 5.37 are displayed in Figure 5.38. It is important to emphasize that each of these specimens had identical reinforcement details (0.2% web reinforcement in each direction); the only difference between them was the a/d ratio. With increasing a/d ratio, a change in failure mode was evident. At an a/d ratio of 1.2, the failure of the specimen was the result of crushing along the diagonal strut and near the CCT nodal region. The orientation and number of the diagonal cracks was consistent with a single-panel strut-and-tie model in which the load is transferred to the support via an inclined strut. At an a/d ratio of 1.85, a similar appearance at failure existed. At failure, crushing was visible along the strut and near both the CCC and CCT nodal regions. Parallel, inclined cracks formed along the axis of a direct strut from the load to the support. The final failure crack slightly resembled the shape of an "S" which is customary to sectional shear failures. This detail may suggest that a portion of the shear is transferred by a sectional-shear mechanism at an a/d ratio of 1.85. However, it is evident from the amount of parallel cracking and local crushing in Figure 5.38 that a direct-strut mechanism still governs at this a/d ratio. At an a/d ratio of 2.5, a completely different appearance at failure was present. Virtually no parallel, diagonal cracking existed in the shear span. The behavior of the specimen was dominated by a single, diagonal tension crack that formed an S-shape between the load and the support. Some local crushing was visible along the diagonal crack, but it was not due to crushing of the concrete, but rather the shearing of the interfaces between each side of the diagonal tension crack. It is clear from the behavior of this specimen (III-2.5-02) that at an a/d ratio of 2.5, the dominant mechanism of shear transfer is consistent with a sectional-shear model.

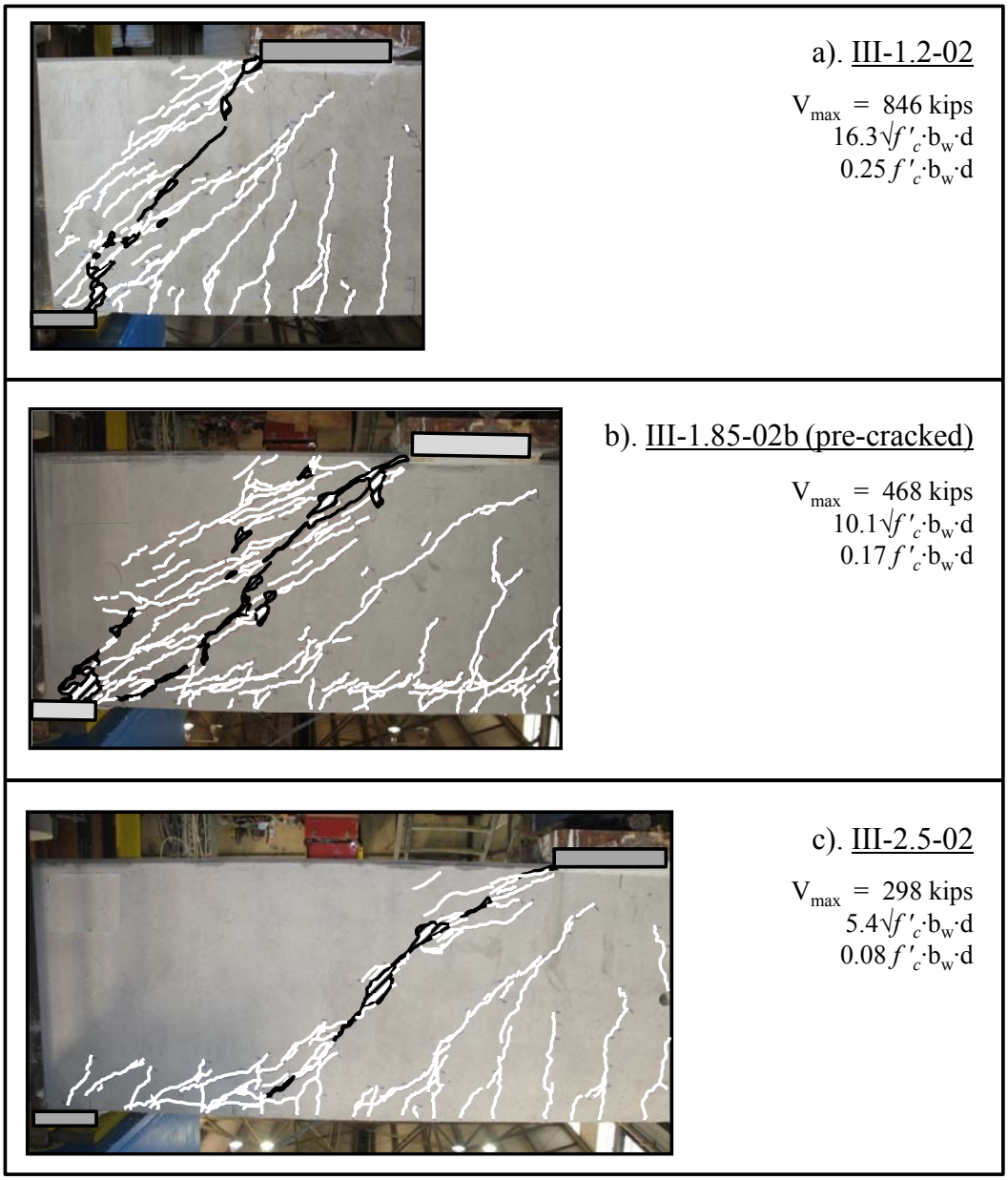

Figure 5.38: Failure pictures of test specimens with 0.2% reinforcement and variable a/d

The pictures of the test regions at failure for the specimens representing the green line in Figure 5.37 are displayed in Figure 5.39. As before, the primary difference between the specimens was the a/d ratio. Each specimen contained 0.3% web reinforcement in each direction. At an a/d ratio of 1.2, a similar appearance at failure to the specimen with 0.2% reinforcement was observed. The only difference was that the parallel cracking was better distributed, thereby reducing the width of the diagonal cracks (Section 4.5.3) and enabling more crushing to occur. At an a/d ratio of 1.85, the failure mode was consistent with the companion specimen with 0.2% reinforcement. Several parallel cracks extended from the load to the support. At the ultimate load, concrete in the CCC nodal region and within the strut crushed. The behavior of both specimens at an a/d ratio < 2 was consistent with a single-panel, direct strut

transfer mechanism. At an a/d ratio of 2.5, a remarkable difference in performance with respect to the specimen with 0.2% web reinforcement was observed. The only difference between these two specimens (III-2.5-02 and III-2.5-03) was the size of the web reinforcement (#4 versus #5 bars). The additional reinforcement in III-2.5-03 helped distribute the diagonal cracks such that the failure of the specimen was due to crushing along the diagonal strut and near the load plate. This switch in failure mode was accompanied by an increase in the shear strength by at least 60%. This performance suggests that at an a/d ratio of 2.5, a significant portion of the applied load is transferred to the support by a sectional-shear mechanism since additional reinforcement increased the capacity.

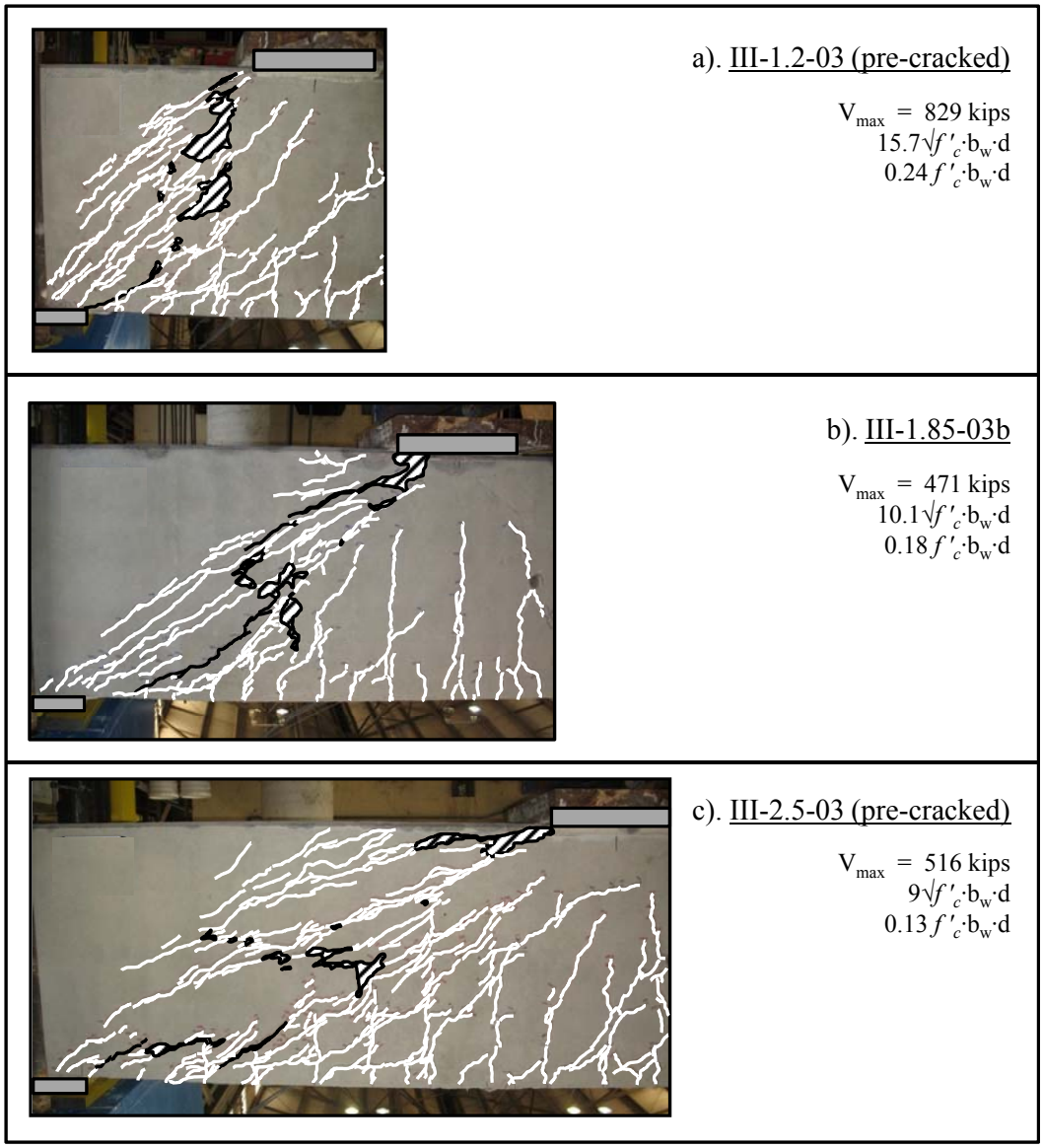

Figure 5.39: Failure pictures of test specimens with 0.3% reinforcement and variable a/d

The results of the six tests displayed in Figure 5.38 and Figure 5.39 show that the transition from deep-beam to sectional-shear behavior does not occur at a distinct a/d ratio.

Rather, it is a gradual process in which the effectiveness of one mechanism reduces with respect to the other. The results of these six tests support the idea that the quantity of web reinforcement affects the behavior as the a/d ratio exceeds 2. This finding is in agreement with results from the database presented in Section 4.5.2 that showed at a/d ratios greater than 2, the quantity of web reinforcement increases the strength of the member. Also, the results of these six tests show that at an a/d ratio less than 2, the quantity of web reinforcement does not affect the shear strength of the member provided that there is enough reinforcement to maintain equilibrium in the diagonal, bottle-shaped strut (Section 4.5.2).

The results of the 21"x75" tests provided additional data to understand the effect of a/d ratio on the shear behavior of reinforced concrete beams. In both of these members, the extreme layer of the longitudinal reinforcement was instrumented with strain gauges along the entire length of the beam (Section 3.5.1). The purpose of the instrumentation was to monitor the strain in the reinforcement at different locations along the shear span. This strain data was used to correlate the behavior of the specimen with the most appropriate type of shear model. For example, in a single-panel strut-and-tie model (STM) in which a direct strut carries the applied load to the support, the force in the tension tie is constant along the length of the shear span. Conversely, in a multiple-panel STM, the force in the tie reduces as a step function due to the intermittent compression diagonals along the shear span. In the case of a Bernoulli beam, in which a sectional shear model is used for shear design, the force in the tie varies according to the moment diagram. These distributions of tensile force are illustrated in Figure 5.40. It is clear that the change in tie-force of a multiple-panel model is an approximation of the gradual decline of the tension force consistent with a Bernoulli beam. For a slender beam with well-distributed stirrups, the change in tie force according to a Bernoulli beam analysis and a multiple-panel STM analysis should be equivalent. Therefore, the data from the strain gauges along the longitudinal reinforcement in the test specimens was used to evaluate the governing shear transfer mechanism as the a/d ratio changed from 1.2 to 1.85 to 2.5. It is important to note that several researchers have measured strain in this fashion for similar purposes (Moody et al., 1954, Watstein and Mathey, 1958, Rogowsky et al., 1986, Quintero Febres et al., 2006, and Tan et al., 2007).

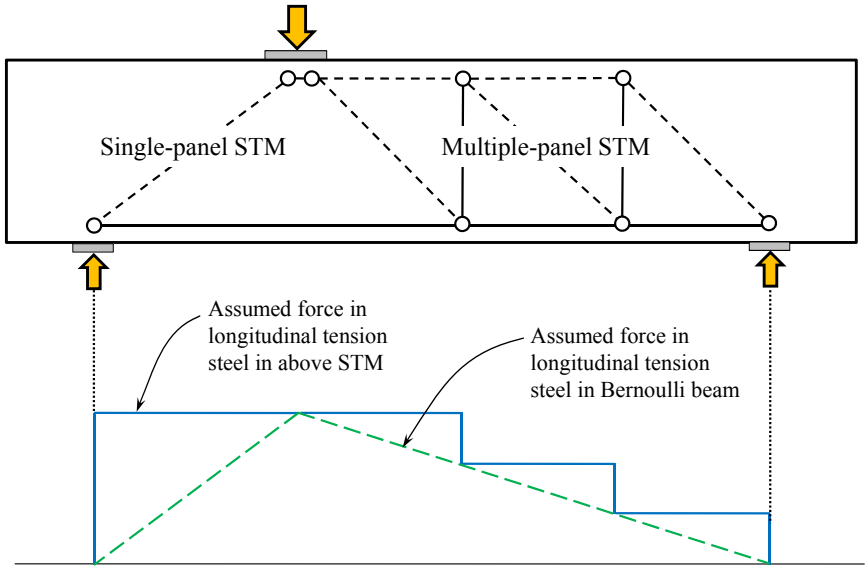

Figure 5.40: Distribution of force in longitudinal tension steel along length of beam according to different shear models

The strain measurements in the longitudinal steel for IV-2175-1.85-02 and IV-2175-1.85-03 are displayed in Figure 5.41. Recall from Section 3.6 that for the 21"x75" beams, two tests were conducted simultaneously. After one shear span failed, external, post-tensioned clamps strengthened the failed span; and the beam was re-loaded in the same arrangement. For the beam in Figure 5.41, the load was applied at midspan such that two tests were conducted at an a/d ratio of 1.85. The difference in the two tests was the quantity of web reinforcement. Strain gauges were applied on the extreme layer of tension reinforcement at midspan (at the load point) and at three locations along each shear span. The gauges closest to the support were located far enough away from the edge of the bearing plate to avoid any detection of local effects at the support, but close enough to represent the last probable location of a vertical tie in a multiple-panel STM. The gauges were placed near a stirrup since it was observed in previous tests that cracks tended to form at the location of stirrups, and strain gauge data was generally more reliable near cracks. Two of the six longitudinal bars were instrumented in this fashion. One set of results is depicted in Figure 5.41, although the data was consistent for both sets. The strain measurements are plotted along the length of the specimen at three different levels of applied load for the first test on this beam. At each load level, calculated strain values along the length of the beam are also provided. The calculated strain in the tension tie of a single-panel, strut-and-tie model is constant over the entire member. It is depicted for each load level as a dashed line in Figure 5.41 and will subsequently be referred to as ε_{l_STM}. The calculated strain in the reinforcement for a Bernoulli beam was also plotted in Figure 5.41 for each load level. This strain is identical to the strain in the tension tie of a single-panel STM at the applied load but varies approximately with the moment diagram, reaching zero at the supports. This strain will subsequently be referred to as ε_{BEAM}.

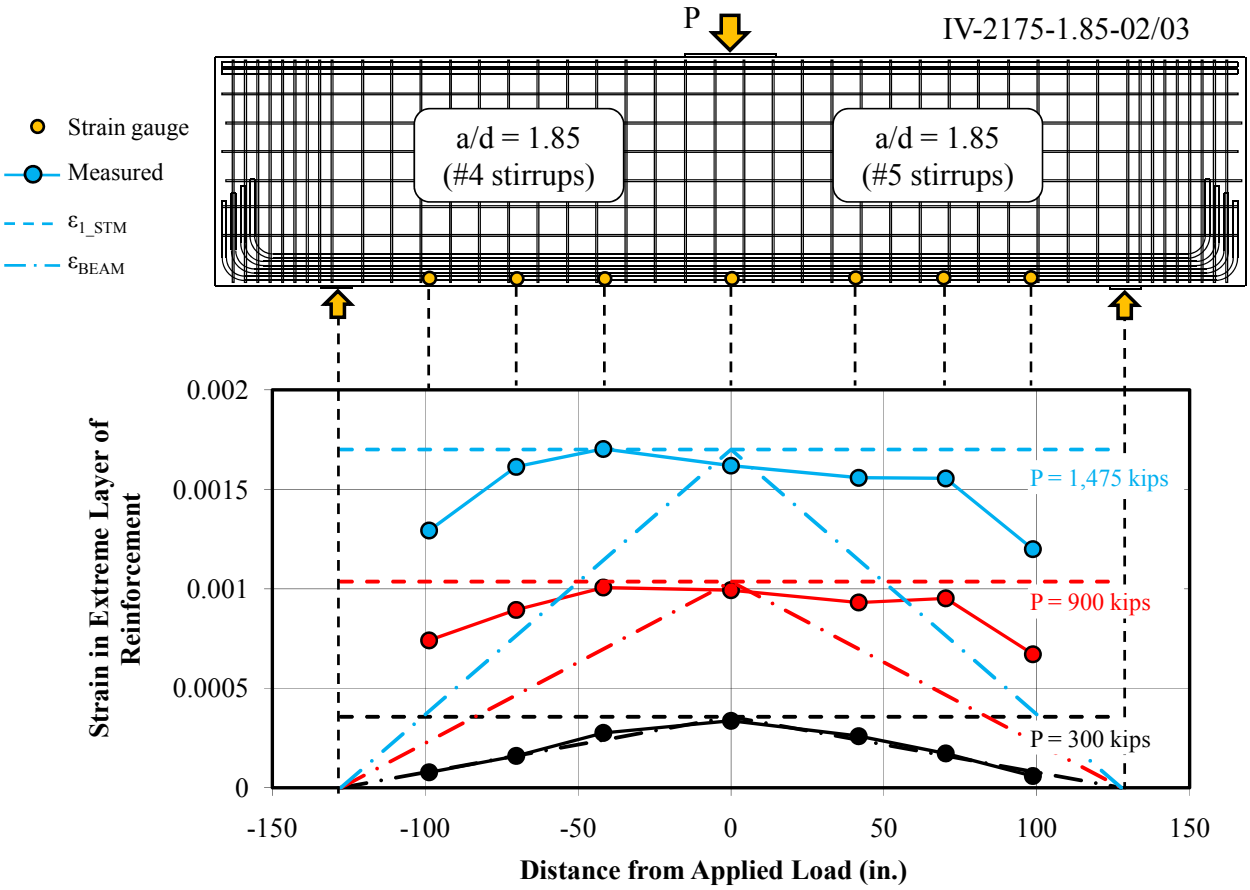

Figure 5.41: Comparison of measured and calculated strain along the length of specimen with a/d of 1.85

At an applied load of 300-kips (black lines in Figure 5.41), the beam had not diagonally cracked. The measured strain in the reinforcement matched the assumed strain from a Bernoulli beam analysis. This finding matched a previous observation by Moody, Viest, Elstner, and Hognestad (1954):

> *Until diagonal tension cracks form, the stresses in the tension steel and in the concrete are distributed along the length of the beam in the same way as the external moments so that these stresses at any section are approximately proportional to the moment at that particular section. The formation of diagonal tension cracks changes these relationships. Such changes are called the redistribution of internal stresses.*

At an applied load of 900-kips (well after diagonal cracking), the measured strains close to the load point were consistent with the calculated strain according to a single-panel, STM analysis. Further along each shear span, however, the measured strain gradually reduced. The reduction is an indication that a portion of the applied load is being transferred to the support via a multiple-panel or sectional shear model.

A similar distribution of measured strain exists along the member at an applied load of 1475-kips (ultimate for IV-2175-1.85-02 and at 90% of ultimate for IV-2175-1.85-03). The

measured strain slightly reduces along the length of the shear span suggesting that a portion of the load was being transferred to the supports via a sectional shear model. It is clear that the measured strain in the two gauges adjacent to the supports is closer to ε_{l_STM} than ε_{BEAM}. In fact, the difference between the measured strain and ε_{l_STM} is approximately 1/3 of the total difference between ε_{l_STM} and ε_{BEAM}. This reduction implies that approximately 1/3 of the load is being transferred to the support with a sectional shear model. The results presented in Figure 5.41 suggest that at an a/d ratio of 1.85, the primary shear transfer mechanism is a single-panel, direct strut mechanism. However, a portion of the load (approximately 1/3) is being transferred via a sectional shear model signifying that that the transition from deep beam behavior to sectional shear behavior has begun. If the measured strain along the length of the member was equal to the calculated Bernoulli beam strain, it would indicate that the full shear is transferred by a multiple-panel or sectional shear model.

The strain measurements in the longitudinal steel for IV-2175-1.2-02 and IV-2175-2.5-02 are displayed in Figure 5.42. As in the other 21"x75" beam, two tests were conducted simultaneously. In this case, the difference between the two tests was the a/d ratio. The depth of the beam was calibrated with the length of the test setup to achieve this arrangement. Strain gauges were applied to the extreme layer of the tension reinforcement at the location of the load point and along each shear span. As before, gauges were placed reasonably close to the supports to capture any effect of sectional shear behavior without being influenced by local stress conditions at the support.

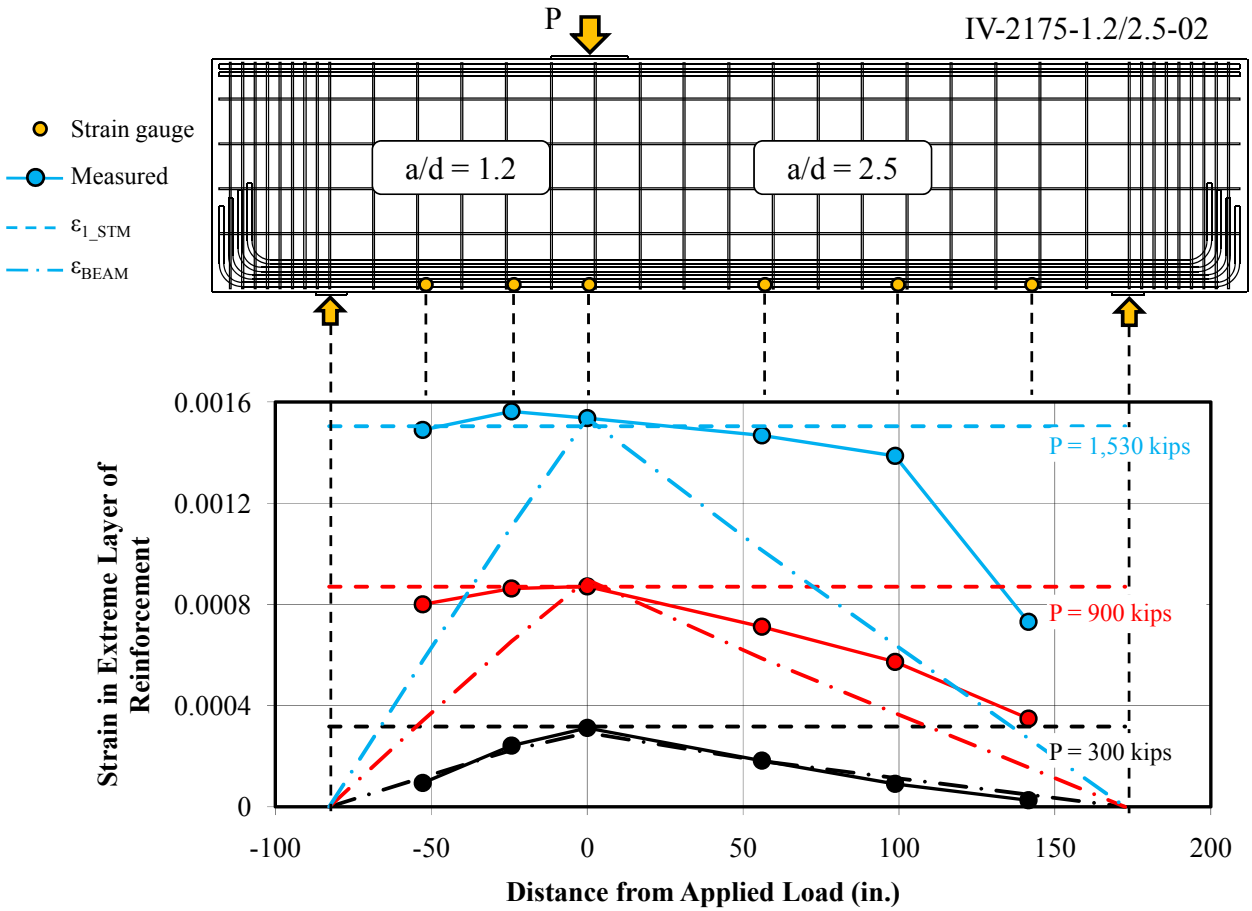

Figure 5.42: Comparison of measured and calculated strain along length of specimen with a/d of 1.2 and 2.5

At an applied load of 300-kips, the beam had not yet diagonally-cracked; and the measured strain in the longitudinal reinforcement matched ε_{BEAM} along the entire length of the member. This observation was consistent with the results of the previous 21"x75" beam.

After the redistribution of internal stresses due to diagonal cracking, the measured strains depart from ε_{BEAM} in both shear spans. At an applied load of 900- and 1,500-kips, a similar distribution of the strain in the reinforcement exists along the beam. At 1,500-kips, the shear span with an a/d ratio of 2.5 was at ultimate; whereas the shear span with an a/d ratio of 1.2 was at approximately 83% of ultimate. In the span with an a/d ratio of 1.2, the measured strains are very similar to ε_{l_STM}. This suggests that the shear in the short span was transferred to the support solely by a single-panel strut-and-tie model. On the contrary, in the span with an a/d ratio of 2.5, the measured strains are closer to ε_{BEAM} than to ε_{l_STM}. By inspection, the difference between the measured strain and ε_{l_STM} is approximately 2/3 of the total difference between ε_{l_STM} and ε_{BEAM}. These data suggest that approximately 2/3 of the shear in the long-shear span (a/d = 2.5) was transferred to the support via a sectional-shear mechanism. Approximately 1/3 of the shear was transferred to the support by a mechanism consistent with a single-panel STM. Thus, from the data in Figure 5.42, it is evident that the dominant shear transfer mechanism has transitioned to a sectional shear mechanism at an a/d ratio of 2.5.

It is clear from the results in Figure 5.41 and Figure 5.42 that the transition between the dominant shear transfer mechanisms near an a/d ratio of 2 is a gradual process. This finding is consistent with the results presented in Figure 5.38 and Figure 5.39 for the 21"x42" specimens. It was shown that at an a/d ratio of 1.2, the shear was transferred to the support solely by a single-panel, direct-strut mechanism. At an a/d ratio of 1.85, evidence of the initiation of sectional shear behavior was observed; however, the dominant transfer mechanism was still consistent with a single-panel STM. At an a/d ratio of 2.5, the dominant shear transfer mechanism was consistent with a sectional shear model; however, a portion of the applied load was transferred by a single-panel STM.

From a design standpoint, the results in this section can be used to determine the most appropriate shear design model for a given a/d ratio. Clearly, for an a/d ratio of 1.2, a single-panel strut-and-tie model is the most suitable choice. For an a/d ratio of 1.85, a single-panel model is also the most appropriate choice, but to a slightly lesser extent. It can be argued that two overlapping models should be used. A single-panel STM could be designed to carry 2/3 of the applied load, and a two-panel STM or a sectional shear model could be designed to carry 1/3 of the applied load. While this approach sounds attractive in theory, it is more difficult than using a single-panel STM for the total applied load; and it may be inappropriate. In the case of all three of these models, stresses are concentrated in the nodal regions. The capacity of the nodal regions cannot be double-counted or unchecked because different models are used. Since it is known that at an a/d ratio less than 2, the conditions in the nodal regions often govern the behavior, they should be focused on in the design. Therefore, a single-panel strut-and-tie model should be used to design beams with an a/d ratio of 1.85. It is fairly simple; it appropriately accounts for the stress concentrations in the nodal regions due to the *total* applied load; and it is consistent with the dominant shear transfer mechanism.

For an a/d ratio of 2.5, it was shown that the dominant transfer mechanism is more consistent with a sectional shear model than a single-panel STM. The implications of using a single-panel model for a beam with an a/d ratio of 2.5 were discussed in Section 4.6.2. In that section, for the specimens tested as part of the depth effect series (Series IV), the experimental strength was compared to the calculated strength with a single-panel strut-and-tie model. For the beams with an a/d ratio of 1.2 and 1.85, there was a consistent level of reserve strength (V_{test} / $V_{calc.}$) as the section size increased since the failure mode of these specimens reasonably matched the assumed behavior in the STM. For the beams with an a/d ratio of 2.5, however, there was not a uniform level of conservatism. The failure mode of these specimens was more consistent with a sectional shear model than a single-panel STM model. The results are replotted in Figure 5.43 for quick reference.

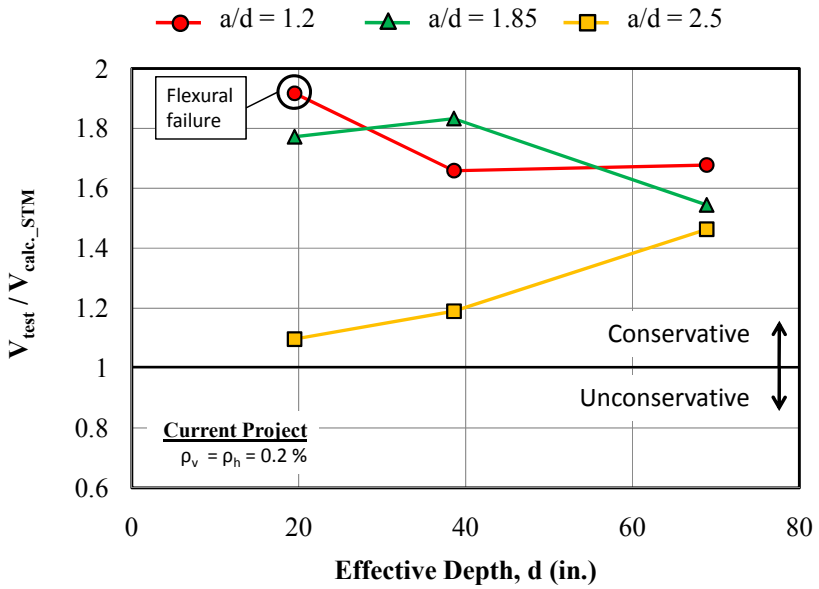

Figure 5.43: Experimental strength divided by calculated strength for depth effect specimens

As illustrated in Figure 5.43, the experimental strength of the specimens tested at an a/d ratio of 2.5 was conservatively estimated even though the failure mode of the specimens was more consistent with a sectional shear model. These results illustrate the inherent conservatism of the strut-and-tie modeling procedure. However, the difference in the level of conservatism between the beams tested at an a/d ratio of 2.5 and that of the deep beams (a/d < 2) indicates that a single-panel STM should be used with caution when the a/d ratio exceeds 2. It is likely that the size of the bearing plates relative to the section size contributed to the decline in the level of conservatism as the effective depth decreased for the specimens with an a/d ratio of 2.5.

It was shown in Section 5.2 that the proposed efficiency factors were developed using the evaluation database which consisted of beams with a/d ratios from 0 to 2.5. A single-panel strut-and-tie model was used to analyze all of the specimens. With the proposed efficiency factors and the use of non-hydrostatic nodes, conservative and reasonably accurate estimates of strength were obtained for the specimens with a range of a/d ratios from 0 to 2.5. This finding further indicates that the inherent conservatism in strut-and-tie modeling can account for some differences between the strut-and-tie model and the actual behavior of the member.

Therefore, it can be concluded that the transition from deep beam behavior to sectional shear behavior near an a/d ratio of 2 is a gradual process. The experimental results indicate that for an a/d ratio up to 1.85, the dominant shear transfer mechanism is consistent with a single panel strut-and-tie model. Due to the inherent conservatism in strut-and-tie modeling, it is appropriate to extend this finding up to an a/d ratio of 2. Thus, it is recommended that a single-panel strut-and-tie model be used to design deep beam regions with a/d ratios from 0 to 2. At a/d ratios above 2, the use of a single-panel strut-and-tie model gradually becomes less appropriate. It was shown that up to an a/d ratio of 2.5, a single-panel STM can estimate the experimental strength conservatively. However, the amount of conservatism in the strength estimate was greatly reduced with respect to that of the deep beam specimens (a/d < 2). These findings are

consistent with the current division of deep beam behavior (a/d ≤ 2) and sectional shear behavior (a/d ≥ 2) present in AASHTO LRFD (2008) and ACI 318-08.

5.3.3 Reducing Discrepancy between Shear Models at a/d ratio of 2.0

The discrepancy in the calculated strength of a member loaded near an a/d ratio of 2 using the STM and the sectional shear provisions in AASHTO LRFD (2008) is the result of a fundamental deficiency in the AASHTO LRFD STM provisions. In this section, it is shown that with the use of the proposed STM provisions presented in Section 5.2, the discrepancy in calculated strength is largely eliminated.

As discussed in the previous section (Section 5.3.2), it is known that the strength of deep beams decrease as the a/d ratio increases. This decline is due to the reduction in the effectiveness of a direct-strut mechanism as the a/d ratio increases. An appropriate model to design deep beams should account for this reduction. It was shown in Section 5.2 that as the a/d ratio increases, AASHTO LRFD accounts for the decline in strength through the use of a variable efficiency factor at the CCT node-strut interface. With increasing a/d ratio, the efficiency factor decreases. In addition, it was shown that when using non-hydrostatic nodes in a single-panel strut-and-tie model, the length of the node-strut interface also decreases. Therefore, when the AASHTO LRFD efficiency factors are used with non-hydrostatic nodes in a single-panel strut-and-tie model, the reduction in strength as the a/d ratio approaches 2 is accounted for *twice*. It is likely that the AASHTO efficiency factors were originally derived using hydrostatic nodes in which case the length of the node-strut interface increases with increasing a/d ratio. However, the use of non-hydrostatic nodes is explicitly recommended in AASHTO LRFD (Figure 5.6.3.3.2-1, 2008). Overly conservative estimates of strength are calculated with the AASHTO LRFD STM provisions near an a/d ratio of 2 due to this lack of consistency between the nodal geometry and the efficiency factors. The change in size of hydrostatic and non-hydrostatic nodes with increasing a/d ratio is illustrated for a simple case in which the back face of a CCT node is approximately half the length of the bearing pad in Figure 5.44.

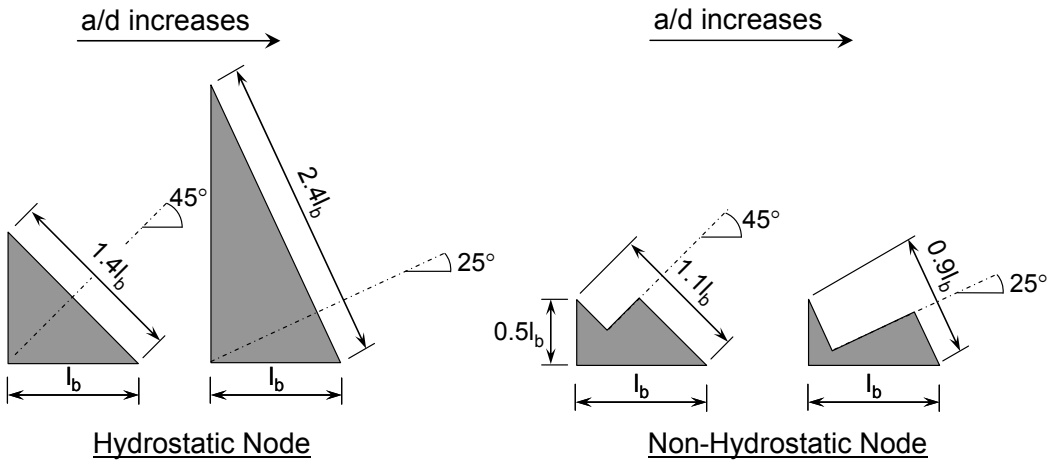

Figure 5.44: Difference in node geometry with increasing a/d ratio for single-panel STM

In the proposed STM provisions presented in Section 5.2, the reduction in shear strength with increasing a/d ratio is accounted for solely with the reduction in the length of the node-strut interfaces. None of the proposed efficiency factors vary with the a/d ratio. Thus, the reduction

in strength with increasing a/d ratio is obtained in the proposed STM provisions by applying a constant efficiency factor (in terms of the a/d ratio) on a smaller length of the node-strut interface (Figure 5.44).

A comparison between the strength estimates for the beams in the evaluation database calculated using the AASHTO LRFD STM provisions and the proposed STM provisions are depicted in Figure 5.45. For the 179 beams in the evaluation database, the experimental strength was divided by the calculated strength using a single-panel STM, non-hydrostatic nodes, and both the proposed efficiency factors and those in AASHTO LRFD (2008). The results are plotted versus the a/d ratio to illustrate how increasing the a/d ratio affects the use of each set of provisions.

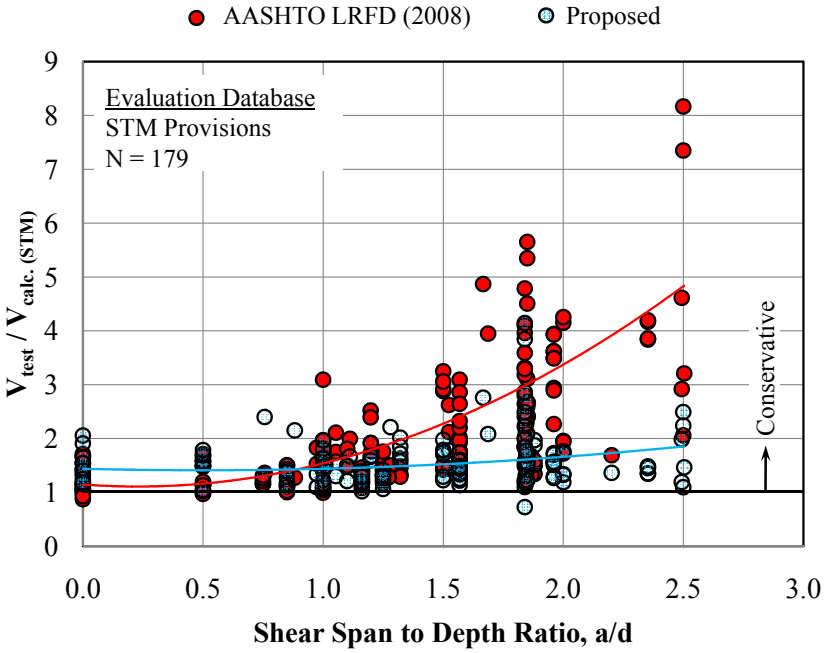

Figure 5.45: Level of conservatism in STM provisions with increasing a/d ratio

In Figure 5.45, at an a/d ratio ≤ 1, the difference in the results from the proposed STM provisions and those in AASHTO LRFD is negligible. In both procedures, a fairly uniform level of conservatism exists. However, at a/d ratios approaching and exceeding 2, the difference in the results is substantial. Whereas a reasonably consistent amount of inherent conservatism (V_{test} / $V_{calc.}$) exists with the use of the proposed STM provisions, overly conservative estimates of capacity are calculated with the AASHTO STM provisions for a/d ratios ranging from 1 to 2.5. For instance, the capacity of a specimen at an a/d ratio of 2 is conservatively calculated with the AASHTO STM provisions by a factor of 4. The experimental capacity divided by the calculated capacity according to the proposed STM provisions for the same beam is less than 2. Several examples such as these are illustrated in Figure 5.45. The consistent level of inherent conservatism provided by the proposed STM provisions indicate that the primary variables that affect the strength of deep beams are appropriately accounted for. In general, the experimental strength was approximately 1.5 times the strength calculated using the proposed provisions, which is appropriate for the scatter in deep beam shear strength. At an a/d ratio near 2, the behavior of the specimens in the database is more accurately captured with the use of the

proposed STM provisions than with those in AASHTO LRFD (2008). The unnecessary amount of conservatism that results with the use of the AASHTO LRFD (2008) STM provisions was the primary factor contributing to the large discrepancy in calculated shear capacity at the transition between deep beam and sectional shear behavior at an a/d ratio of 2.

To evaluate the difference in calculated shear strength between the proposed STM provisions and the sectional shear provisions in AASHTO LRFD (2008), the sectional shear provisions need to be presented. When "*it is reasonable to assume that plane sections remain plane*" (a/d > 2), the shear capacity of a member can be determined as the summation of a concrete component, V_c, and a stirrup component, V_s (AASHTO LRFD, 2008). This model is based on the free-body diagram presented as Figure 5.46. The shear at the diagonal tension crack is resisted by the stirrups crossing the diagonal crack and three different mechanisms of shear transfer that is lumped into the concrete contribution V_c. These mechanisms include the shear resistance of the concrete in the compression zone, aggregate interlock across the diagonal crack, and dowel action from the longitudinal reinforcement. It is important to note that this sectional shear model differs from a multiple-panel STM in that no contribution from the concrete is recognized in the latter.

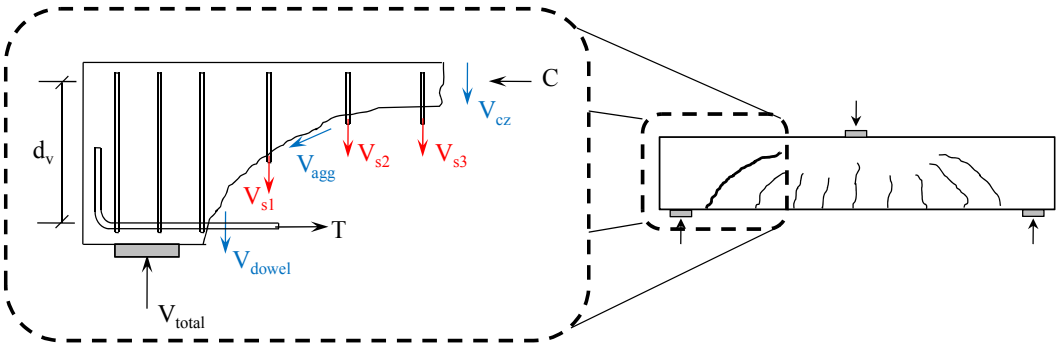

V_{total} = total shear on the member
V_{dowel} = shear resistance due to dowel action, contributes to V_c
V_{agg} = shear resistance due to aggregate interlock, contributes to V_c
V_{cz} = shear resistance of concrete in compression zone, contributes to V_c
V_{s1-3} = shear resistance provided by the stirrups, contributes to V_s
C = compression force due to flexure
T = tension force due to flexure
d_v = effective shear depth, distance from C to T

Figure 5.46: Free-body diagram used as basis for sectional shear model

The sectional shear provisions in AASHTO LRFD (2008) are presented as the following:

The nominal shear resistance, V_n, shall be determined as the lesser of:

$$V_n = V_c + V_s + V_p \tag{5.16}$$

$$V_n = 0.25 f_c' b_v d_v + V_p \tag{5.17}$$

in which:

$$V_c = 0.0316 \beta \sqrt{f_c'} b_v d_v \tag{5.18}$$

$$V_s = \frac{A_v f_y d_v \cot\theta}{s} \quad \text{(oriented 90-degrees with longitudinal axis)} \tag{5.19}$$

where f'_c = compressive strength of concrete (ksi)
b_v = effective web width within d_v (in.)
d_v = effective shear depth, taken as the distance between the resultants of the tensile and compressive forces due to flexure (in.)
V_p = component of the prestressing force in direction of applied shear (kips)
β = factor indicating the ability of diagonally-cracked concrete to transmit tension and shear, assumed equal to 2 per article 5.8.3.4.1
A_v = area of shear reinforcement within distance s (in.^{2})
f_y = yield strength of shear reinforcement (ksi)
θ = angle of inclination of diagonal compressive stresses, assumed equal to 45 degrees per article 5.8.3.4.1
s = spacing of stirrups (in.)

For comparison purposes, the equations for V_c and V_s in ACI 318-08 are presented as well:

The nominal shear resistance, V_n, shall be determined as the lesser of:

$$V_n = V_c + V_s \tag{5.20}$$

$$V_n = V_c + 8\sqrt{f'_c}\, b_w d \tag{5.21}$$

in which:

$$V_c = 2\lambda\sqrt{f'_c}\, b_w d \tag{5.22}$$

$$V_s = \frac{A_v f_{yt} d}{s} \tag{5.23}$$

where f'_c = compressive strength of concrete (psi)
b_w = effective web width within d_v (in.)
d = effective depth, taken as the distance from extreme compression fiber to centroid of longitudinal tension reinforcement (in.)
λ = modification factor for lightweight concrete
A_v = area of shear reinforcement within distance s (in.^{2})
f_{yt} = yield strength of shear reinforcement (ksi)
s = spacing of stirrups (in.)

The sectional shear provisions in AASHTO LRFD (2008) and ACI 318-08 are similar provided that the simplified procedure for nonprestressed sections (Article 5.8.3.4.1) is used. In the simplified procedure, a β of 2.0 and a θ of 45-degrees are allowed if the member has a minimum amount of transverse reinforcement according to Equation 5.24.

$$A_v \geq 0.0316\sqrt{f'_c}\,\frac{b_v s}{f_y} \tag{5.24}$$

As in Figure 5.45, the experimental strength of the beams in the database can be compared to the calculated shear strength using the AASHTO LRFD (2008) and the ACI 318-08

sectional shear provisions. The experimental strength for each specimen is divided by the calculated strength and plotted versus the a/d ratio in Figure 5.47. It is clear from the results in Figure 5.47 and from the derivation of the sectional shear provisions that using $V_c + V_s$ for beams with a/d ratios smaller than 2 is unacceptable. The model is completely inconsistent with the shear transfer mechanism. At a/d ratios between 2 and 2.5, however, there is a reasonable level of conservatism (V_{test} / ($V_c + V_s$) using both the AASHTO LRFD and the ACI 318 sectional shear provisions. It is interesting to note that the sectional shear provisions in ACI 318-08 estimate consistently higher shear capacity than those in AASHTO LRFD for the full-range of a/d ratios. Since the approximate procedure was used for the AASHTO LRFD provisions, the only difference between them and ACI 318 is the distance used for the effective depth of the section. In AASHTO LRFD, the depth is taken as the distance between the resultant of the compressive and tensile forces from a flexural analysis. In ACI 318-08, the depth is taken as the distance between the extreme compression fiber and the centroid of the longitudinal reinforcement. Thus, the depth used in the AASHTO LRFD equations is always less than that used in the ACI equations, which results in slightly more conservative estimates using AASHTO LRFD (2008).

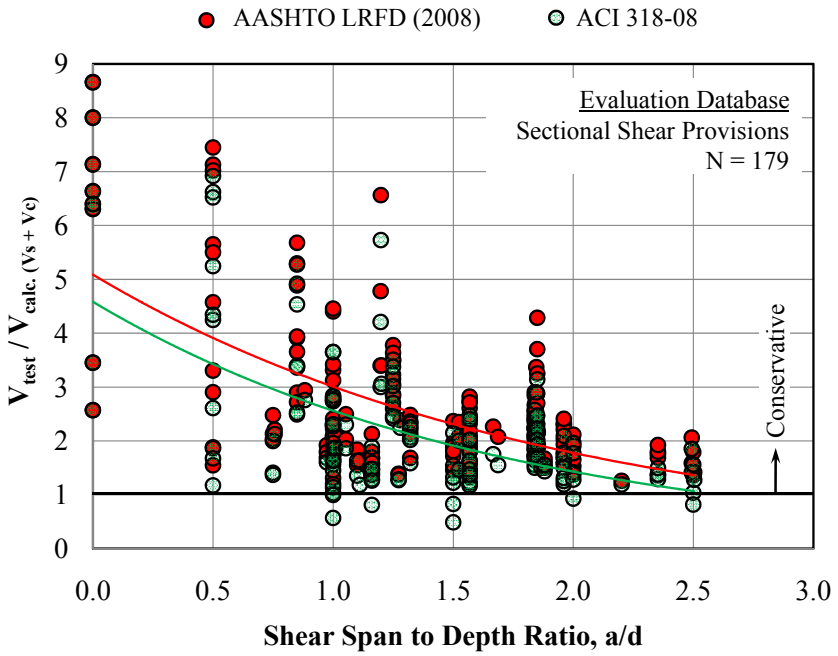

Figure 5.47: Level of conservatism in sectional shear provisions with increasing a/d ratio

From the results in Figure 5.47 and from the experimental program presented in Section 5.3.2, it is evident that only the beams with a/d ratios between 2 and 2.5 should be used to evaluate sectional shear provisions. There are 25 beams in the evaluation database that meet this criterion. Using the data from these specimens, the level of conservatism consistent with the sectional shear provisions in AASHTO LRFD (2008) and ACI 318-08 can be determined. This amount of conservatism can be compared to the amount of conservatism when using the proposed STM provisions for beams with a/d ratios between 0 and 2. In this way, the discrepancy, if any, in the amount of inherent conservatism (V_{test} / $V_{calc.}$) between the proposed

STM provisions and the sectional shear provisions in AASHTO LFRD and ACI 318 can be assessed. The experimental shear strength of the 25 beams in the evaluation database tested at a/d ratios between 2 and 2.5 are divided by the shear strength calculated with the sectional shear provisions in AASHTO LRFD and ACI 318 in Figure 5.48. The results are plotted versus the ratio of V_s/V_c to determine if this variable has any effect on the conservatism of the sectional shear provisions.

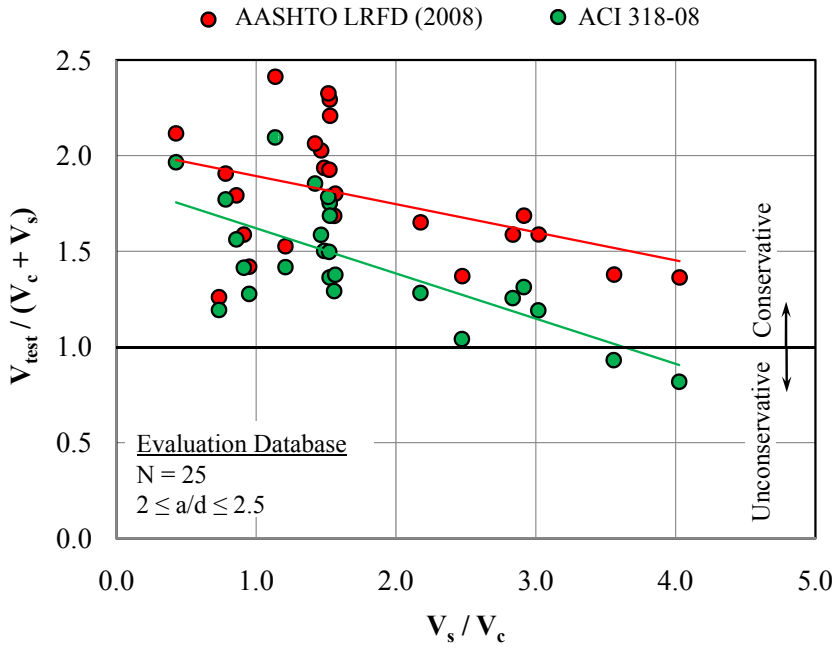

Figure 5.48: Level of conservatism in sectional shear provisions for a/d ratios between 2 and 2.5

The results in Figure 5.48 indicate that the sectional shear provisions in AASHTO LRFD conservatively estimate the strength of beams with an a/d ratio between 2 and 2.5 for a wide range of V_s/V_c ratios. While there is a downward trend in the red data in Figure 5.48, the lower bound indicates a fairly consistent level of inherent conservatism. The level of conservatism in Figure 5.48 for the AASHTO LRFD sectional shear provisions can be compared to the level of conservatism for the proposed STM provisions at an a/d ratio near 2. From the data presented in Figure 5.45 at an a/d ratio of 2, the experimental shear strength was on average approximately 1.5 times the strength calculated with the proposed STM provisions. This level of conservatism is reasonably consistent with the estimates from the AASHTO LRFD sectional shear provisions displayed in Figure 5.48, especially at V_s/V_c ratios between 2 and 4. Therefore, at an a/d ratio near 2, the proposed STM provisions and the AASHTO LRFD sectional shear provisions provide reasonably consistent levels of conservatism. In other words, there is not an inappropriate amount of discrepancy between the shear strength calculated using these two different shear models at an a/d ratio of 2.

The results in Figure 5.48 in which the ACI sectional shear provisions were used to estimate shear strength (green data points) show a downward trend with the V_s/V_c ratio. When the V_s/V_c ratio is less than 2, a comparable level of conservatism exists between the ACI sectional shear provisions and the proposed STM provisions (~1.5). At higher ratios of V_s/V_c, the level of conservatism when using the ACI sectional shear provisions decreases for beams

with an a/d ratio between 2 and 2.5. This data suggests that at an a/d ratio near 2, the stirrup contribution to the total shear capacity of the member should be limited since the member is transitioning from deep beam behavior to sectional shear behavior. It may not be prudent to rely on a large amount of shear capacity from stirrups at a/d ratios near 2.

It should be noted that the current study did not explicitly address the suitability of the sectional shear provisions in AASHTO LRFD or ACI 318-08. The sectional shear provisions in each specification were used to determine the appropriate level of conservatism that the proposed STM provisions should target at an a/d ratio near 2. The results in Figure 5.48 indicate that the AASHTO sectional shear provisions, namely the use of an effective shear depth, may capture the behavior of beams at an a/d ratio between 2 and 2.5 better than the ACI sectional shear provisions. However, more research is needed in this area to reach a firm conclusion.

The results in Figure 5.45 and Figure 5.48 show that in terms of inherent conservatism (V_{test} / $V_{calc.}$), there is a relatively smooth transition between the proposed Project 5253 STM provisions and the AASHTO LRFD (2008) sectional shear provisions. The transition is not as smooth when the ACI 318-08 sectional shear provisions are used especially at high V_s/V_c ratios. The transition between design models can also be addressed strictly from a design perspective. That is, the design strength calculated with STM and sectional shear provisions can be compared for the beams in the database as shown in Figure 5.49.

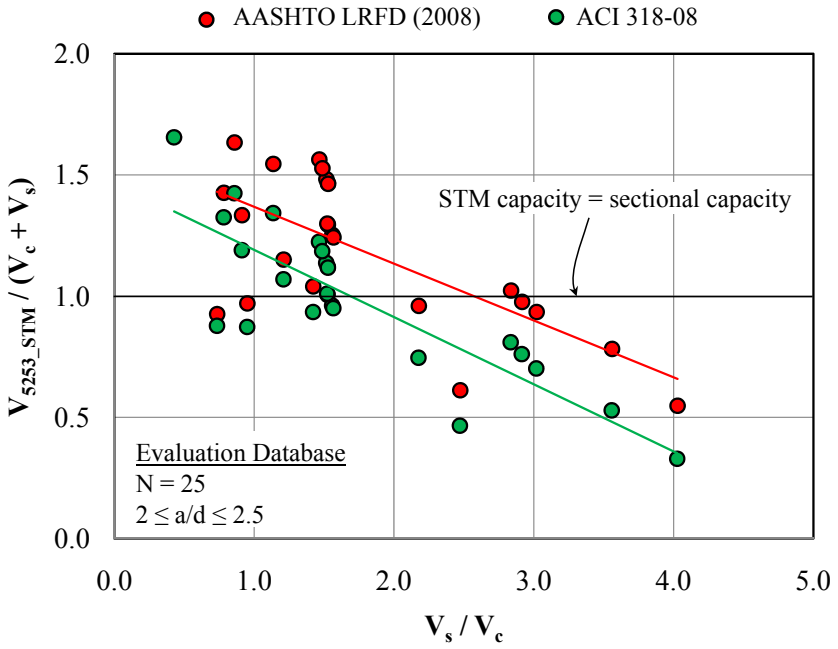

Figure 5.49: Comparison of calculated capacity: Project 5253 STM vs. sectional shear

In Figure 5.49, the Project 5253 STM calculated capacity is divided by the sectional shear capacity calculated according to AASHTO LRFD (2008) and ACI 318-08 for the 25 beams in the evaluation database with an a/d ratio between 2 and 2.5. The data are plotted versus the V_s/V_c ratio. The data indicate that with increasing V_s/V_c ratio, the calculated sectional shear capacity becomes larger than the calculated Project 5253 STM capacity. This finding is expected since the sectional shear provisions are a function of the stirrup contribution (V_s) whereas the Project 5253 STM capacity is a function of a single-panel strut-and-tie model. In

both cases, the Project 5253 STM capacity is closest to the sectional shear capacity at a V_s/V_c ratio near 2, albeit with a considerable amount of scatter. Thus, from a design perspective, limiting the ratio of V_s/V_c to a value near 2 is recommended to reduce the discrepancy between shear strength calculated with STM and sectional shear provisions near an a/d ratio of 2.

5.3.4 Design Implications

The results in this section indicate that a single-panel STM should be used with the proposed STM provisions for members with an a/d ratio less than 2. A single-panel model is consistent with the dominant shear transfer mechanism and is easy to apply. Multiple panel strut-and-tie models are not recommended for beams with a/d ratios less than 2. They are inconsistent with the dominant shear transfer mechanism and are often governed by the vertical tie force since this force is equal to the externally applied shear (Section 4.3.4). Combinations of single- and two-panel models can be applied to deep beams (a/d < 2), but the stress conditions in the nodal regions due to the total applied force must be accounted for. At a/d ratios greater than 2, multiple-panel STMs are consistent with the behavior of the member but do not account for the contribution of concrete. In addition, the required tie reinforcement may be unnecessarily large if the diagonal struts are steeper than 45-degrees with respect to the horizontal. Therefore, it is recommended that a sectional shear model is used for members with a/d ratios greater than 2.

With the use of the proposed Project 5253 STM provisions, a relatively smooth transition exists between deep beam and sectional shear capacity at an a/d ratio of 2. A similar level of inherent conservatism (V_{test} / $V_{calc.}$) of approximately 1.5 exists on average when shear strength is calculated with the proposed STM provisions and the sectional shear provisions in AASHTO LRFD (2008) and ACI 318-08. In addition, similar design capacities are calculated with these provisions when the V_s/V_c ratio in the sectional shear provisions is close to 2. The improved transition between sectional shear capacity and deep beam shear capacity with the use of the Project 5253 STM provisions is illustrated qualitatively in Figure 5.50. Some discrepancy in the strength calculated between the Project 5253 STM provisions and the sectional shear provisions in AASHTO LRFD (2008) should be expected; however, the discrepancy is drastically reduced relative to when the STM provisions in AASHTO LRFD (2008) are used to calculate deep beam shear strength. It is important to note that the proposed STM provisions were not developed solely to reduce this discrepancy. The improved transition between deep beam and sectional shear strength is the result of the careful calibration of the proposed STM provisions with data from the evaluation database, from the experimental program, and from existing STM specifications (Section 5.2).

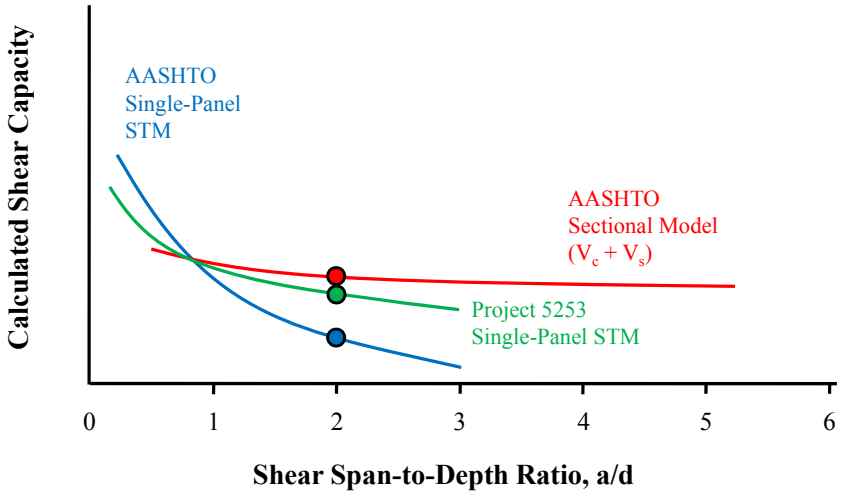

Figure 5.50: Reduction in discrepancy in shear capacity at a/d ratio of 2 with the proposed STM provisions

The transition between deep beam shear capacity and sectional shear capacity is discussed further in the design example presented in Appendix B.

5.3.5 Summary and Conclusions

The a/d ratio has a significant effect on the shear behavior of reinforced concrete beams. As the a/d ratio increases from 0, the shear strength of a member gradually declines due to the reduction in the effectiveness of a direct-strut mechanism. It was shown with results from the experimental program that the transition from deep beam behavior to sectional shear behavior was gradual. However, up to an a/d ratio of 1.85, the dominant shear transfer mechanism was consistent with a single-panel strut-and-tie model. Based on these results, it was concluded that a single-panel strut-and-tie model should be used to design regions of reinforced concrete members with a/d ratios less than 2. At a/d ratios greater than 2, the dominant shear transfer mechanism transitions to a sectional-shear mechanism. While it was shown that a single-panel strut-and-tie model can provide a conservative estimate of strength for beams with a/d ratios up to 2.5, the behavior of the member is generally not consistent with the assumed behavior in the STM. Therefore, for a/d ratios greater than 2, a sectional shear model should be used.

At a/d ratios approaching 2, overly conservative estimates of strength were calculated for the beams in the evaluation database using the AASHTO LRFD (2008) STM provisions. The excessive amount of conservatism was due to the inconsistency of the efficiency factor at the CCT node-strut interface with the geometry of non-hydrostatic nodes. Due to this excessive conservatism, a large discrepancy in calculated shear strength between the STM provisions and the sectional shear provisions in AASHTO LRFD (2008) exist at an a/d ratio of 2. With the use of the STM provisions proposed in Section 5.2 and a limit on the V_s/V_c ratio of 2, the discrepancy in calculated shear strength is largely eliminated.

5.4 Diagonal Cracking under Service Loads

The objective of this task was to assess the feasibility of limiting diagonal cracking under service loads. It was determined that the most appropriate approach to limit diagonal cracking was to perform a separate design check comparing service level shear to an estimate for the diagonal cracking load. Data from the literature and the experimental program were used to develop an empirical equation that provides a conservative estimate for the diagonal cracking load of deep beams.

5.4.1 Background

It may not be possible to completely eliminate the presence of diagonal cracking of bent caps under service loads due to a variety of inconsistencies between design assumptions and field conditions such as overloads, restrained shrinkage, temperature changes, etc. However, there are a few design considerations that can be made to restrict the width of diagonal cracks to an acceptable level or to mitigate the chance of the formation of diagonal cracks. In Section 4.5.3, the beneficial effect of web reinforcement on the width of diagonal cracks was discussed. It was shown that with minimum web reinforcement of 0.3% in each direction, the width of diagonal cracks was limited to acceptable values at first cracking and up to typical service loads. Providing additional reinforcement can further restrict the width of diagonal cracks to some degree. In this section, the task of reducing the risk of diagonal cracking under service loads is explicitly addressed.

Two types of diagonal cracks are recognized in reinforced concrete beams: flexure-shear cracks and web-shear cracks (MacGregor and Wight, 2005). Flexure-shear cracks form after or concurrently with flexural cracks. They extend from the tip of the flexural crack towards the origin of load. Web-shear cracks occur independently of flexural cracking. They form when the principal tension stress in the web of the member exceeds the tensile strength of concrete. In deep beams, web-shear cracks are also referred to as bursting or splitting cracks. Specifically, they are caused by transverse tensile stresses that exist due to the spreading of compressive stresses in bottle-shaped struts. It is apparent that the spreading of compressive stresses in deep beams contributes to the width of flexure-shear cracks as well. Both of these cracks are depicted in Figure 5.51.

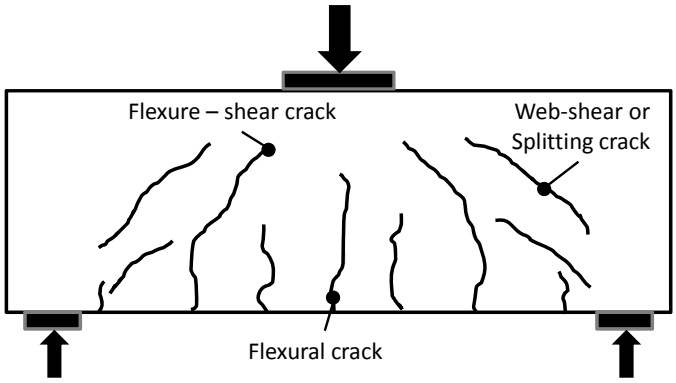

Figure 5.51: Types of cracks in reinforced concrete deep beams

With regard to this task, no distinction was made between flexure-shear or web shear cracks when evaluating the diagonal cracking load of the test specimens. Both were treated simply as inclined cracks. However, as noted in Section 4.2.2, the first diagonal crack to appear in the test specimens was generally a flexure-shear crack. The load at which it formed was determined through visual observation and with the help of electrical strain gauges attached to the web reinforcement. For example, the appearances of the test regions of several specimens after first diagonal cracking are included in Figure 5.52. It is clear that the inclined cracks in these pictures are flexure-shear cracks. Also, note that the applied shear at the time the picture was taken is slightly greater than the cracking shear determined with the strain gauge data attached to the web reinforcement.

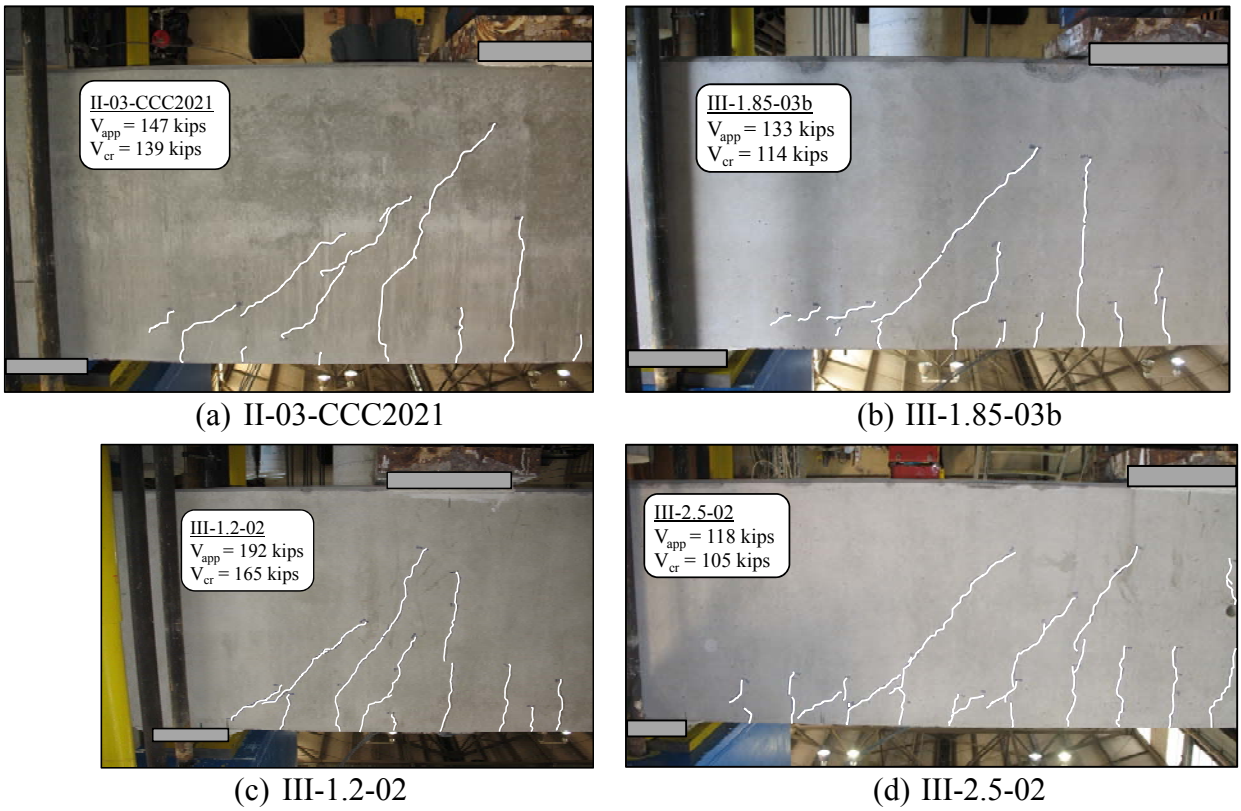

(a) II-03-CCC2021 (b) III-1.85-03b

(c) III-1.2-02 (d) III-2.5-02

Figure 5.52: First pictures taken after the formation of first diagonal crack in several tests

5.4.2 Approach

Two approaches were considered to limit diagonal cracking under service loads. The first approach was associated with a single-panel strut-and-tie model. To limit diagonal cracking, the force generated in the bottle-shaped strut due to service loads would be limited to a specified percentage of the unfactored strut capacity. In effect, this strategy consisted of performing a separate service-load strut-and-tie analysis in which a reduced efficiency factor at the node-strut interface (consistent with the diagonal cracking strength of the strut) would be compared to the stress in the strut due to unfactored service loads. The advantage of this approach was that it could be integrated fairly easily with the ultimate-strength strut-and-tie

analysis since the same model would be used. The differences would be the applied loads and the efficiency factor at the node-strut interface.

However, it was determined that this approach was flawed. The basic theory behind strut-and-tie modeling is that it is a lower-bound plasticity-based approach. It is intended to be used in design to provide a safe estimate for ultimate strength. It is not intended to accurately estimate service level stresses or to limit diagonal cracking. In fact, cracking is expected to occur for the member to reach the ultimate capacity estimated by a strut-and-tie analysis. Therefore, it was inappropriate to use a STM-based approach to limit diagonal cracking under service loads.

The second approach considered for this task consisted of a separate, service load check. The service level shear would be compared to an estimate for the diagonal cracking load of the member. This check would be done separately from the ultimate strength analysis. It was more theoretically justified than the first approach and was still very simple. To use this approach, an estimate of the diagonal cracking load of deep beams was required. In this task, a recommendation is given to estimate the diagonal cracking load of deep beams based on data from the experimental program and the literature.

5.4.3 Results

One approach to estimating the diagonal cracking load of a deep beam is to perform an elastic analysis. However, due to the proximity of the load to the support, there is a complicated state of stress in the member (Figure 5.53). Plane sections do not remain plane and general flexural theory assumptions do not apply. To address this difficulty, a finite element analysis (FEA) can be performed to determine the location and magnitude of the principal tension stress in the member. This procedure is plausible for cases in which the maximum principal stress is in the web of the member indicating that the first crack should be a web-shear crack. However, in cases where the maximum principal stress is at the extreme tension fiber of the member, the beam is expected to develop flexural cracks first. After which, shear cracks will extend from the end of the flexural cracks (flexure-shear cracks). In this case, the elastic analysis needs to be modified to account for the redistribution of stresses after flexural cracking (MacGregor and Wight, 2005). In the past, researchers have addressed the difficulty associated with an elastic analysis of a deep beam by estimating the diagonal cracking load with empirical models. This approach was taken in this project as well.

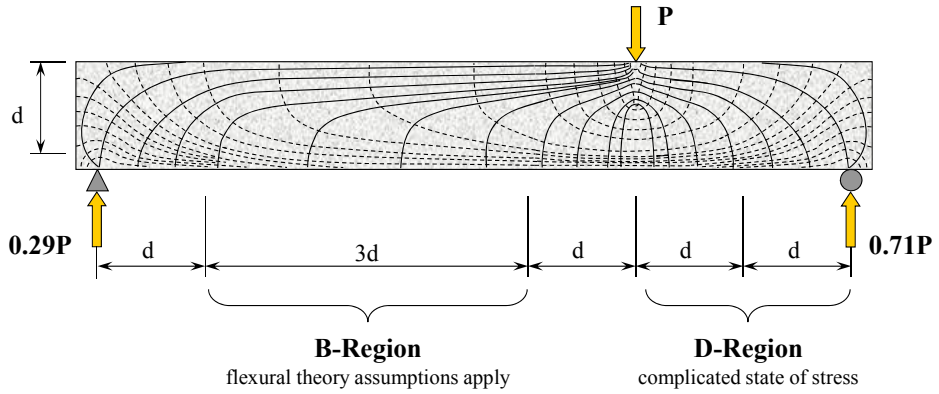

Figure 5.53: Stress trajectories in B-regions (Bernoulli) and in D-regions (discontinuity)

Variables that affect diagonal cracking loads of deep beams

In 1962, a landmark paper was published entitled "Shear and Diagonal Tension" by ACI-ASCE Committee 326. In this paper, the development of a semi-empirical equation for the diagonal tension cracking load of reinforced concrete beams was discussed. The equation was based off a principal stress analysis and was calibrated with test data from several research studies (ACI-ASCE Committee 326, 1962). The equation is presented as Equation 5.25.

$$V_{cr} = \left(1.9\sqrt{f_c'} + 2500\rho_l \frac{V\,d}{M} \right) b_w d \tag{5.25}$$

with f'_c = compressive strength of concrete (psi)
ρ_l = longitudinal reinforcement ratio (A_s / b_wd)
V = shear at critical section (kips)
M = moment at critical section (in-kips)
b_w = web width of the member (in.)
d = effective depth of the member (in.)

The equation incorporated all of the major variables that affected the diagonal cracking load of reinforced concrete beams known at the time, namely (1) the section size (b_wd), (2) the tensile strength of concrete ($\sqrt{f_c'}$), (3) the longitudinal reinforcement ratio (ρ_l), and (4) the ratio of moment to shear at the critical section (M/V). The equation could be applied to reinforced concrete beams with any a/d ratio as long as the critical section was appropriately defined. It was determined that for deep beams (a/d $\leq$ 2), the critical section is located at the middle of the shear span (a/2). This critical section produces an M/V ratio for simple beams with single or double concentrated loads of a/2. For beams with an a/d > 2, the critical section is located at a distance d from the maximum applied moment. In this case the M/V ratio is equal to a minus d. Thus, the equation was intended to be used for beams with any a/d ratio and was calibrated as such.

In ACI 318-08, Equation 5.25 is listed as Equation 11-5. In the commentary (R11.2.2.1), it is stated that the variables accounted for in Equation 5.25 are still considered the primary variables that affect diagonal cracking loads. However, some research has shown that Equation 5.25 does not appropriately weigh each of the variables. In addition, it is suggested that the overall depth of the member may influence the diagonal cracking strength as well (ACI 318-08).

In the current task, the effects of the aforementioned variables (b_wd, $\sqrt{f_c'}$, a/d, ρ_l, d) on the diagonal cracking load of deep beams were assessed with data from the experimental program and the literature through the use of the evaluation database. The purpose was to validate that these variables do affect the diagonal cracking loads of deep beams. Ultimately, this information was used to recommend an equation to estimate diagonal cracking loads for the purpose of limiting diagonal cracking in service.

The evaluation database consists of 179 specimens from the literature and the experimental program (Section 2.5.2). The diagonal cracking loads from more than half of the specimens from the literature were not reported. In addition, as noted in Section 3.6, only the cracking load of the first test of each 42"-, 44"-, and 48"-deep specimen was available due to the testing procedure. As a result, the diagonal cracking loads of 59 specimens existed in the

evaluation database. The diagonal cracking loads for all of the test specimens are listed in Table 4.1.

The effect of section size on the diagonal cracking load of the specimens in the evaluation database is shown in Figure 5.54. As expected, as the shear area ($b_w d$) of the specimen increases, the diagonal cracking load increases. Prior to diagonal cracking, the member primarily behaves elastically. The entire section contributes to the diagonal cracking strength. It is important to note that this finding is not necessarily consistent with the ultimate strength of deep beams as shown in Section 4.6.2.

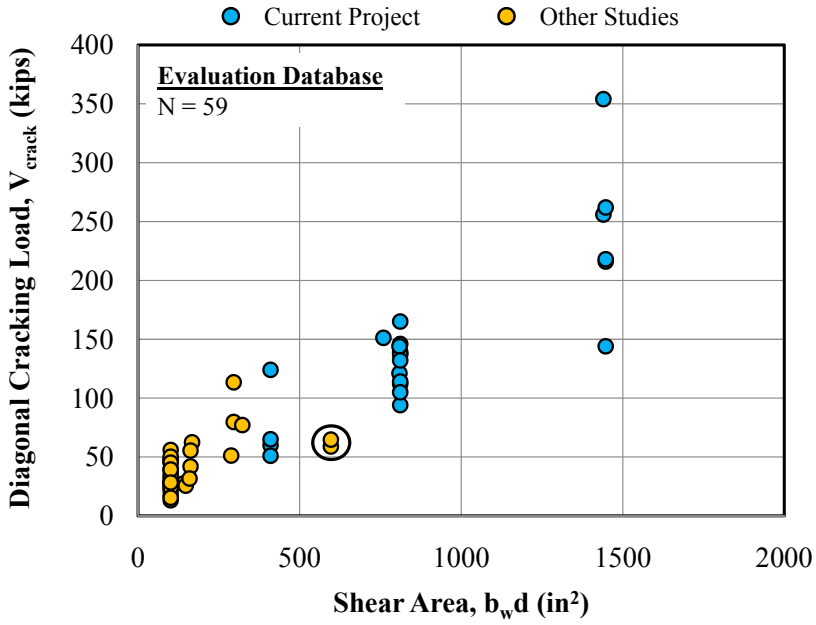

Figure 5.54: Effect of shear area on the diagonal cracking load of beams in evaluation database

The diagonal cracking loads of two specimens from the literature were circled in Figure 5.54 because longitudinal bars were cut off within the shear span (Uribe and Alcocer, 2001). To ensure that the specimens would fail in shear, additional longitudinal reinforcement at midspan was provided; but the reinforcement was terminated at two locations within the shear span. It is likely that the stress concentration that existed at the cutoff locations affected the first cracking load. These specimens were included in the evaluation database to illustrate the effect of bar cutoffs on the load at first diagonal cracking and because a similar situation could arise in practice.

It is clear from Figure 5.54 that within each group of data of the same section size there is a considerable amount of scatter. The scatter is a result of the other variables that contribute to the diagonal cracking load of deep beams. The effect of these variables ($\sqrt{f_c'}$, a/d, ρ_l, d) were assessed with the evaluation database as well. To isolate the effect of the tensile strength of concrete, the diagonal cracking load was normalized by the shear area and plotted versus $\sqrt{f_c'}$ in Figure 5.55.

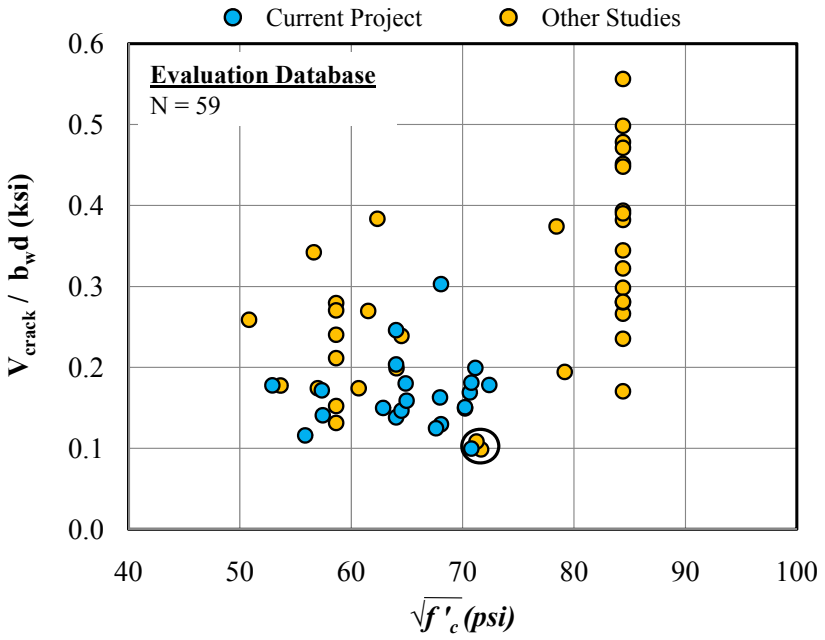

Figure 5.55: Effect of tensile strength on diagonal cracking load of deep beams in database

Since it is widely accepted that the tensile strength of concrete is a function of $\sqrt{f_c'}$ (with considerable scatter), it is appropriate to evaluate the effect of the tensile strength of concrete on the diagonal cracking load by plotting it versus the square root of the compressive strength. The results in Figure 5.55 indicate that the diagonal cracking load is a function of the square root of the compressive strength of concrete, although the trend is relatively weak. It is expected that the diagonal cracking load would increase with increasing tensile strength since a crack forms when the principal tension stress exceeds the tensile strength of concrete. However, as before there is a substantial amount of scatter in Figure 5.55 for specimens with identical values of $\sqrt{f_c'}$. This scatter is the result of the contributions of other variables to the diagonal cracking load and of the inherent scatter associated with the tensile strength of concrete in general.

In the literature and throughout this report, diagonal cracking loads are normalized by the shear area and the square root of the compressive strength of concrete. It is accepted that both of these parameters are primary variables affecting the diagonal cracking load. The results presented in Figure 5.54 and Figure 5.55 support this practice, albeit with significant amounts of scatter.

The effect of the shear-span-to-depth (a/d) ratio on the load at first diagonal cracking is illustrated in Figure 5.56. With increasing a/d ratio, the normalized diagonal cracking load decreases for the most part. This trend is associated with the change in the principle tensile stress distribution that occurs as the a/d ratio changes. At low a/d ratios, a complicated state of stress exists due to the proximity of the applied load to the support. As the a/d ratio approaches and exceeds 2, the state of stress near midheight of the member is not affected by local support or loading conditions. The state of stress is consistent with flexural theory assumptions. As a result, as the a/d ratio approaches 2 in Figure 5.56, the diagonal cracking loads approach the

diagonal cracking strength of slender beams, $2\sqrt{f_c'}\,b_w d$. For slender beams without transverse reinforcement, the diagonal cracking load of $2\sqrt{f_c'}\,b_w d$ is equivalent to the ultimate strength. It is important to note that the trend of decreasing diagonal cracking loads with increasing a/d ratio was observed previously by numerous researchers for deep beams (Smith and Vantsiotis, 1982, Tan et al., 1995, Tan and Lu, 1999, Shin et al., 1999, and Oh and Shin, 2001).

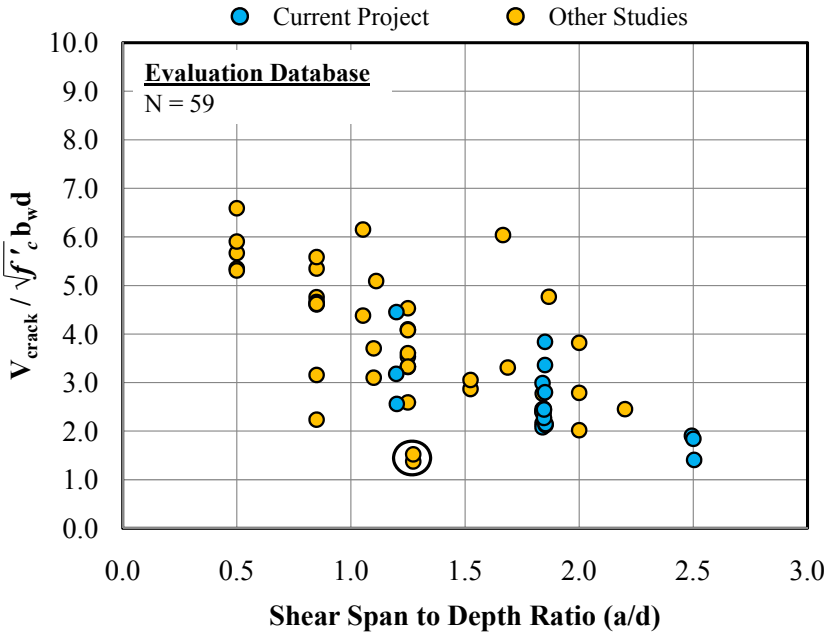

Figure 5.56: Effect of a/d ratio on diagonal cracking load of deep beams in database

The effect of the longitudinal reinforcement ratio, ρ_l, on the diagonal cracking load of the deep beams in the evaluation database is depicted in Figure 5.57. The results do not indicate a clear trend. It is likely that the lack of a significant number of specimens outside of the range of 1.5% to 2.5% reinforcement contributes to the lack of a trend. It is possible to isolate the effect of the longitudinal reinforcement ratio on the cracking load by only plotting data from similar specimens tested at similar a/d ratios. This approach was taken in Figure 5.58.

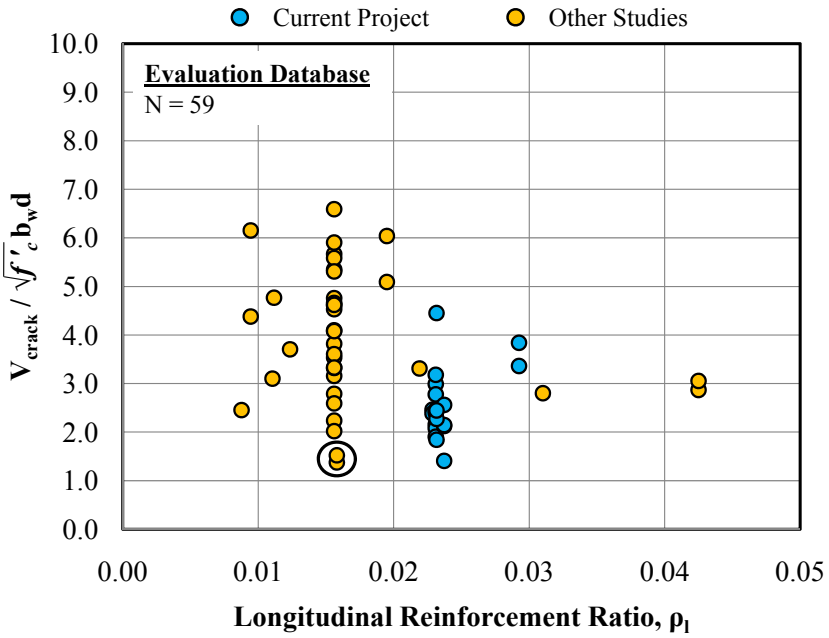

Figure 5.57: Effect of longitudinal reinforcement ratio on diagonal cracking load of beams in the database

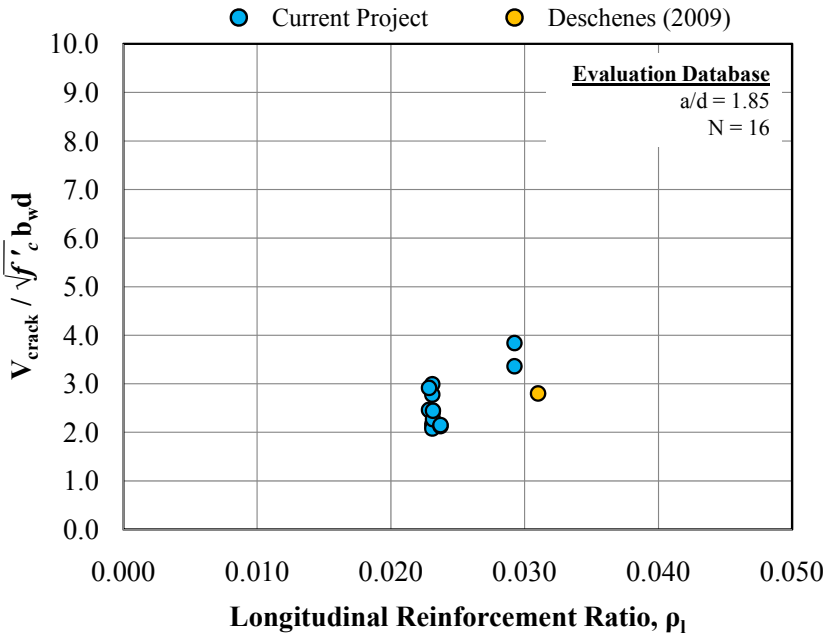

Figure 5.58: Effect of longitudinal reinforcement ratio on diagonal cracking load of beams with the same a/d ratio

The data in Figure 5.58 is from specimens tested in the experimental program and from one specimen tested by Deschenes (2009). All of the tests were conducted at an a/d ratio of 1.85. The 21-inch wide specimens in the experimental program had a longitudinal reinforcement ratio

of 2.3%; the 36"x48" specimens had a longitudinal reinforcement ratio of 2.9%. The specimen tested by Deschenes had a 21"x42" cross-section and a longitudinal reinforcement ratio of 3.1%. Since all of the specimens in Figure 5.58 were tested at the same a/d ratio and were similar in size, the effect of the longitudinal reinforcement ratio on the diagonal cracking load can be isolated from other contributing variables. The results indicate that the normalized diagonal cracking load increases with increasing longitudinal reinforcement ratio to some degree. This finding is in agreement with the results of several research studies (Moody et al., 1954, Morrow and Viest, 1957, de Paiva and Siess, 1965), most of which were used in the development of Equation 5.25. The results in Figure 5.58 are justified since the first diagonal crack is generally a flexure-shear crack. At the tip of the flexural crack, the amount of longitudinal reinforcement reduces the principal tension stress thereby delaying the load at which the flexural crack turns into a diagonal crack.

The effect of depth on the diagonal cracking load of the beams in the evaluation database is shown in Figure 5.59. The results indicate that the diagonal cracking load of deep beams decreased with increasing depth, on average. However, it is clear that the scarcity of data for beams with effective depths greater than 40-inches likely contributed to this average reduction. From a lower bound perspective, the decrease in cracking load with increasing depth is small. As before, the effect of depth on the diagonal cracking load of deep beams can be isolated by plotting the data from specimens with different depths, but identical a/d ratios and beam parameters. The diagonal cracking loads of the beams tested in the experimental program are provided in Figure 5.60.

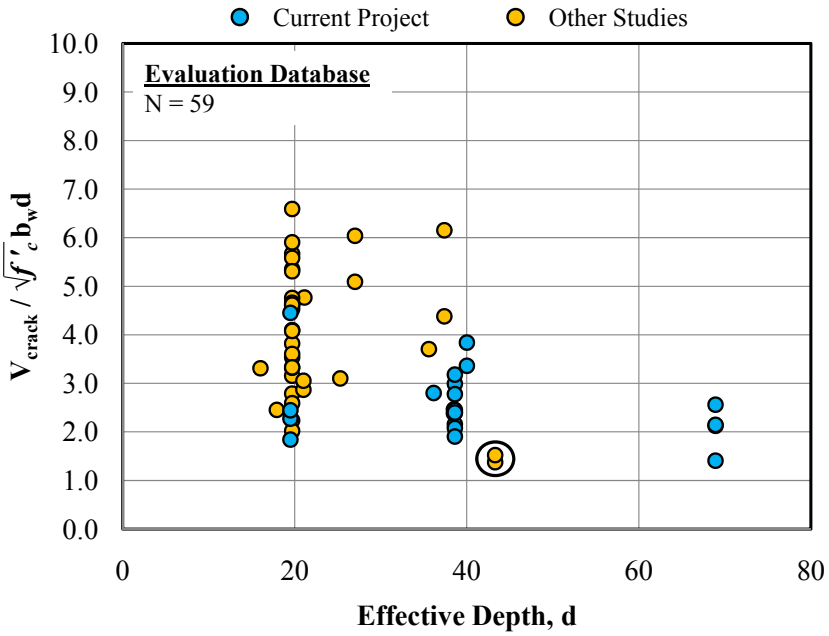

Figure 5.59: Effect of depth on the diagonal cracking load of beams in the evaluation database

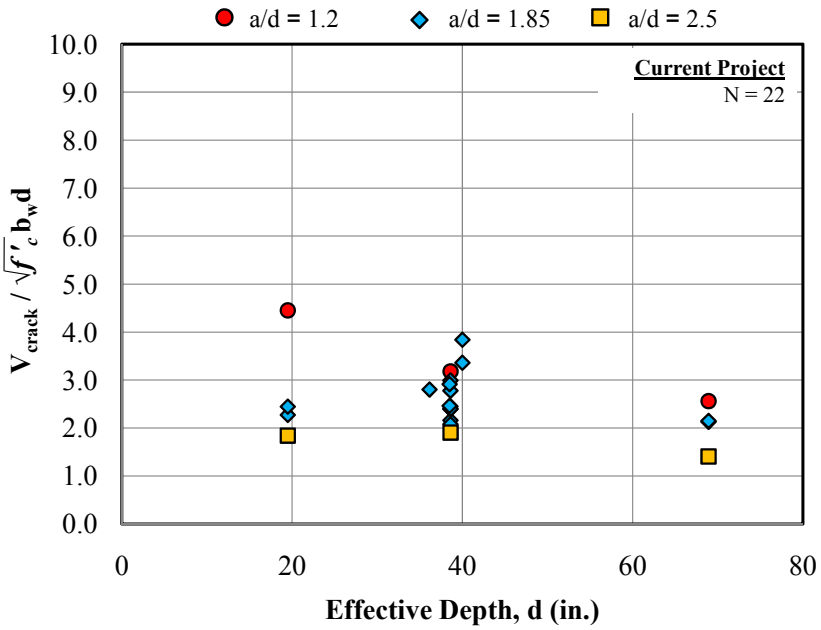

Figure 5.60: Effect of depth on the diagonal cracking load of deep beams in testing program

All of the data in Figure 5.60 is from the current experimental program. The normalized diagonal cracking loads of the specimens tested at an a/d ratio of 1.2 decreased with increasing depth. At a/d ratios of 1.85 and 2.5, little to no depth effect was apparent. As noted previously in Section 4.5.3, the reduction in diagonal cracking load for specimens with an a/d ratio of 1.2 may be due to a Weibell statistical effect. Conflicting results on this issue exist in the literature. Similar results to that in Figure 5.60 were presented by Tan and Lu (1999) for specimens tested at a/d ratios of 0.56 and 1.13, but not for specimens tested at an an a/d ratio 0.84. Conversely, in experimental studies by Walraven and Lehwalter (1994) and Zhang and Tan (2007), both researchers concluded that the diagonal cracking load of deep beams is not affected by size. The specimens in these studies were tested at an a/d ratio of approximately 1. As a result, it is possible that the effective depth of a deep beam contributes to the diagonal cracking load to some extent, but the effect is likely small and erratic, especially as the a/d ratio approaches and exceeds 2.

The effect of the quantity of web reinforcement on the diagonal cracking load of deep beams was also evaluated in the experimental program and with the evaluation database. In Section 4.5.3, it was shown that the diagonal cracking loads of deep beams were not appreciably affected by the quantity of web reinforcement, either in the horizontal or the vertical direction (Figure 4.57 and Figure 4.58). This finding is plausible since the web reinforcement should not affect the performance of the beam until diagonal cracks form. The results from the specimens in the experimental program in which web reinforcement was the primary variable are illustrated in Figure 5.61.

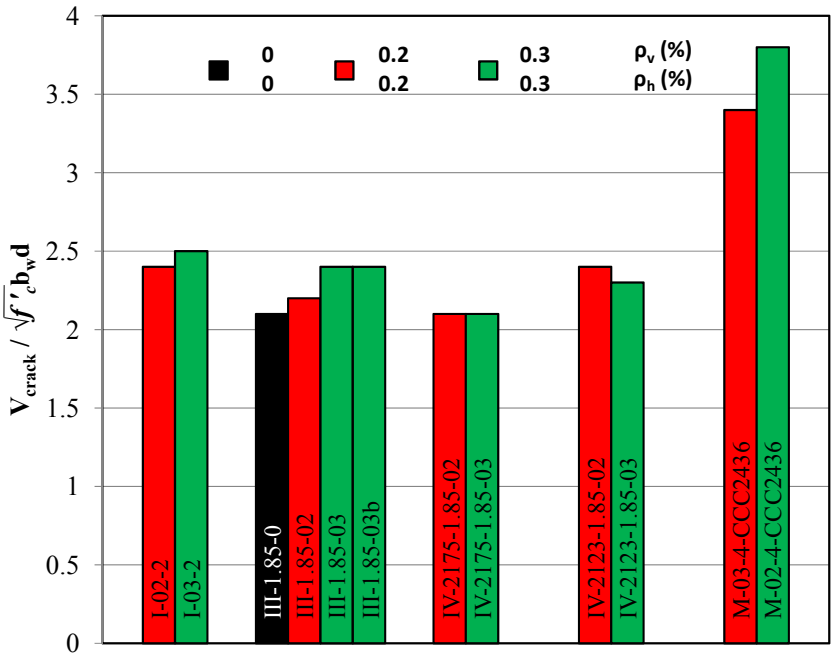

Figure 5.61: Effect of web reinforcement on the diagonal cracking load of similarly sized deep beams

In summary, based on the results presented in this section, it is apparent that a considerable amount of scatter exists in diagonal cracking loads of deep beams. One reason for the scatter is the number of variables that affect the load at first cracking. It was shown that the primary variables affecting the diagonal cracking load of deep beams are the section size ($b_w d$), the tensile strength of the concrete ($\sqrt{f_c'}$), and the a/d ratio. The longitudinal reinforcement ratio may contribute to the diagonal cracking load to some degree, although there was only a minimal amount of data available to evaluate this variable. Based on the results in Figure 5.59, Figure 5.60, and from the literature, it was shown that the effect of section depth on the diagonal cracking load is likely small and erratic. Lastly, the load at first diagonal cracking was not noticeably affected by the quantity of web reinforcement.

Estimating Diagonal Cracking Loads

For this task, an estimate for the diagonal cracking load of deep beams was required. Previous researchers have proposed empirical equations aimed at estimating the diagonal cracking load of reinforced concrete beams. In general, the equations have accounted for the primary variables that affect diagonal cracking with the exception of the effective depth. In this section, a few equations from the literature are evaluated with the data in the evaluation database.

The first equation to be evaluated is ACI-318-08 Equation 11-5, presented previously as Equation 5.25. This equation was developed in the early 1960s and accounts for the following variables: $b_w d$, $\sqrt{f_c'}$, a/d, and ρ_l. For each specimen in the database, the estimated cracking load according to Equation 5.25 was computed. For beams with an a/d $\leq$ 2, the critical section was taken as the halfway point on the shear span producing an M/V ratio equal to a/2. For beams

with an a/d > 2, the critical section was taken as d away from the location of maximum moment which slightly affected the M/V ratio for these specimens. The experimental diagonal cracking loads were divided by the estimated diagonal cracking loads. The results were plotted in Figure 5.62 versus the a/d ratio.

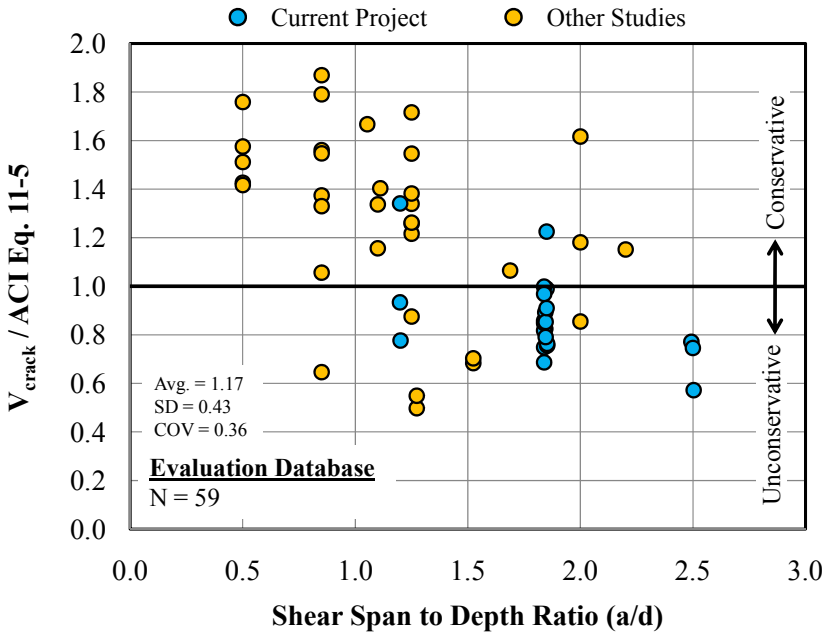

Figure 5.62: Comparison of measured and estimated diagonal cracking loads – ACI Eq. 11-5

In Figure 5.62, a value of 1.0 represents a cracking load estimate that is equal to the measured cracking load. Values below 1 represent unconservative estimates; values above 1 represent conservative estimates. It is clear from Figure 5.62 that a trend exists with a/d ratio. As the a/d ratio increases, the estimated diagonal cracking load is less conservative. This trend implies that Equation 5.25 underestimates the effect of the a/d ratio on the diagonal cracking load of deep beams. Another observation from Figure 5.62 is the large amount of scatter. On average, the diagonal cracking loads are computed conservatively (Avg. = 1.17), but with a very high standard deviation (SD = 0.43). The high standard deviation is a reflection of the inaccuracy of Equation 5.25 and the inherent scatter in the diagonal cracking loads themselves.

In 1968, an equation for the diagonal cracking load of reinforced concrete beams was developed by Zsutty. The equation was based on a linear regression analysis of data in the literature. Another equation was needed because Zsutty claimed that Equation 5.25 did not properly weigh the primary variables that affect the diagonal cracking load. The equation is presented as Equation 5.26. In the derivation of the equation, the data was split by the a/d ratio. Beams with an a/d ratio > 2.5 were considered slender. Beams with an a/d ratio < 2.5 were considered short. The cutoff at an a/d ratio of 2.5 was made because Zsutty found that above this value, the diagonal cracking load data agreed well with his empirical equation. At an a/d ratio less than 2.5, there was significantly greater errors. Based on this abrupt change in performance, the cutoff between short beams and slender beams was taken at an a/d ratio of 2.5. The reason for the additional error in the short beam data was believed to be the result of the "arch action" in short beams (Zsutty, 1968). Improvements to the equation for short beams were attempted to no

avail. In the words of the author: "several attempts to remove variables such as ρ, or add variables such as bond contact area ratio, did nothing to improve the prediction precision" (Zsutty, 1968). In a later publication, a modification to Equation 5.26 was made to estimate the ultimate strength of short beams (Zsutty, 1971). In estimating the ultimate strength of short beams, Zsutty commented that the equation "must contain an accurate representation of the top and bottom pressures due to load and support conditions" (Zsutty, 1968). No need was seen to alter the estimate for first diagonal cracking of short beams since these members carry additional load after first cracking. However, great attention was given to improving the estimated diagonal cracking load for slender beams since this value is often the ultimate strength of unreinforced specimens and is used as the concrete contribution in the sectional shear design model. The diagonal cracking loads in the evaluation database are compared to those estimated with Equation 5.26 in Figure 5.63.

$$V_{cr} = \left(59 \left(\frac{f'_c \, \rho_l d}{a} \right)^{\frac{1}{3}} \right) b_w d \tag{5.26}$$

with f'_c = compressive strength of concrete (psi)
ρ_l = longitudinal reinforcement ratio (A_s / b_wd)
d = effective depth of the member (in.)
a = shear span (in.)
b_w = web width of the member (in.)

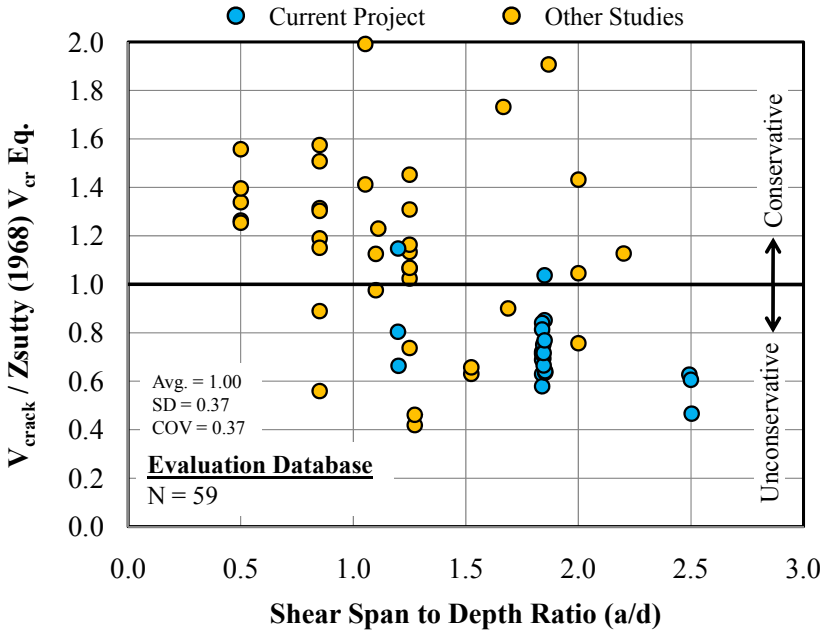

Figure 5.63: Comparison of measured and estimated diagonal cracking loads – Zsutty Equation

The results in Figure 5.63 do not show a significant improvement with respect to the results in Figure 5.62. There still appears to be a trend with increasing a/d ratio. Even though the average of the experimental diagonal cracking loads divided by the estimated diagonal

cracking loads are 1.0 with Equation 5.26, the standard deviation and the coefficient of variation are very high (SD = 0.37). The amount of error seen in Figure 5.63 is consistent with what Zsutty found. In his study, the error was attributed to "the wide dispersion of the arch action shear stress values," not the inappropriate form of the equation (Zsutty, 1968). Even though it appears that the a/d ratio is not appropriately weighed in Equation 5.26 based on the results in Figure 5.63, it is likely that the scatter in diagonal cracking loads of nominally identical specimens greatly contributes to the inability to accurately predict them.

In 1999, an experimental study was conducted by Shin et al. in which thirty high-strength concrete beams were tested at a/d ratios ranging from 1.5 to 2.5. The cross-section of the specimens was 4.9"x9.8" and the longitudinal reinforcement ratio was 3.8%. Two series of tests were conducted in which the concrete strength was either 7,600-psi or 10,600-psi. The diagonal cracking loads of the specimens were evaluated with Equations 5.25 and 5.26. The authors found that Equation 5.25 was overly conservative when used to estimate the cracking loads of their specimens. A fairly good correlation was found with the use of Equation 5.26. Based on a regression analysis of their test data, a different equation for the diagonal cracking load of deep beams was recommended. The equation is presented as Equation 5.27. The diagonal cracking loads in the evaluation database are compared to those estimated with Equation 5.27 in Figure 5.64.

$$V_{cr} = \left(72\left(f'_c\,\rho_l\right)^{\frac{1}{3}}\left(\frac{d}{a}\right)^{\frac{1}{2}} \right) b_w d \qquad (5.27)$$

with f'_c = compressive strength of concrete (psi)
ρ_l = longitudinal reinforcement ratio (A_s / b_wd)
d = effective depth of the member (in.)
a = shear span (in.)
b_w = web width of the member (in.)

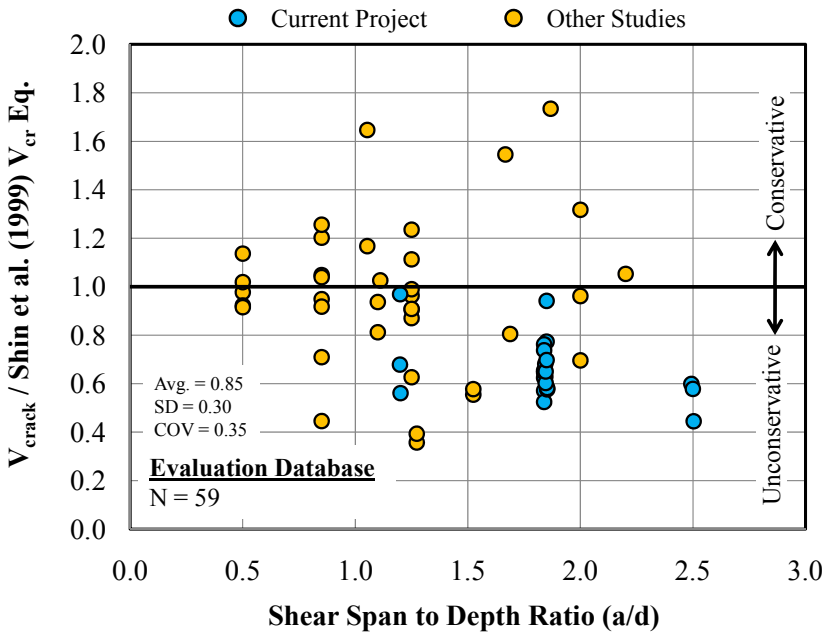

Figure 5.64: Comparison of measured and estimated cracking loads – Shin et al. Eq.

At the conclusion of the study, it was warned by Shin et al. that "Strictly speaking, the equations are valid only within the ranges of variability of the parameters studied" (Shin et al., 1999). Since high-strength concrete and a reinforcement ratio of 3.8% were used in their test specimens, the beams in the evaluation database are not similar. Furthermore, only the beams loaded at a/d ratios ranging from 1.5 to 2.5 would be applicable. Nevertheless, for comparison purposes, the estimates obtained by using Equation 5.27 are compared to the cracking loads in the evaluation database as shown in Figure 5.64. It is clear from the figure that excluding the data at a/d ratios less than 1.5 would only further penalize the accuracy of Equation 5.27. With respect to the other equations, the use of Equation 5.27 did have slightly less scatter as measured by the standard deviation and coefficient of variation. However, the standard deviation is still large (SD = 0.30) and the accuracy on average is unconservative (Avg. = 0.85). The point of comparing the data in the evaluation database with Equation 5.27 is not to assess the accuracy of the equation since it was obviously not calibrated with the range of parameters in the evaluation database. Instead, the point is to illustrate the wide range of scatter that can result when the quantities of the primary variables that affect the diagonal cracking load are altered. Whereas the data from the study by Shin et al. was predicted with their proposed equation with remarkable accuracy (Avg. = 1.0, SD = 0.06, COV = 0.06), the data in the evaluation database was not. This inconsistency suggests that while the parameters that affect diagonal cracking are correctly identified, it is difficult to weigh them appropriately for the wide range of values for each pertinent variable. In addition, there may be inconsistencies in the way with which each researcher is measuring the diagonal cracking load, although the description of first diagonal cracking in each study is similar.

Based on the results presented in this section, it is clear that it is very difficult to accurately estimate diagonal cracking loads of deep beams. It is likely that a new equation could be developed that better agrees with the data in the evaluation database than Equations 5.25,

5.26, and 5.27. However, there still will be a considerable amount of error due to the difficulty with accurately accounting for the wide range of each variable that affects diagonal cracking loads. Furthermore, a significant amount of error will result from the variability in the diagonal cracking loads themselves as pointed out by Zsutty (1968). To illustrate the variability in diagonal cracking loads of nominally-identical specimens, the cracking loads of several beams from the evaluation database in which the only variable is the quantity of web reinforcement are plotted in Figure 5.65. Fifteen specimens with an identical cross-section and longitudinal reinforcement ratio from the research study conducted by Oh and Shin (1999) are included. Eight specimens with a longitudinal reinforcement ratio and cross-section from the experimental program are included as well.

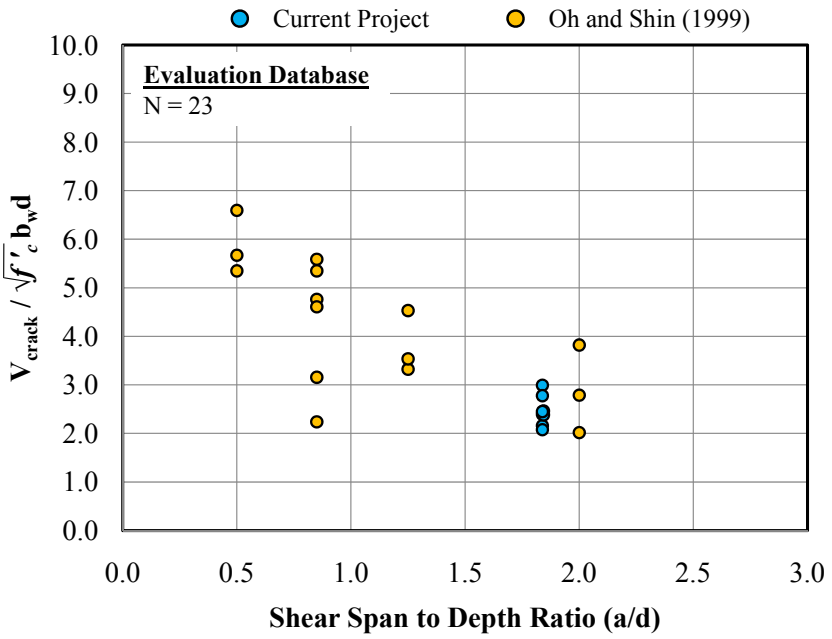

Figure 5.65: Diagonal cracking loads for nominally-identical specimens

As shown previously in Figure 5.61 and in Section 4.5.3, the quantity of web reinforcement did not have an appreciable effect on the diagonal cracking load. Therefore, the diagonal cracking loads in Figure 5.65 at each a/d ratio should be similar. Instead, a considerable amount of scatter exists. Often, the maximum diagonal cracking load in a group is 50% greater than the minimum. In a couple of cases, the maximum and minimum diagonal cracking load differ by a factor of 2. Thus, for nominally-identical specimens, the diagonal cracking loads are considerably different. The most likely reason for the scatter is the variability in the tensile strength of concrete. Improving the accuracy of diagonal cracking loads beyond the accuracy with which the tensile strength of concrete is estimated is not possible.

Due to the difficulties associated with accurately estimating diagonal cracking loads and due to the nature of the current task, it was determined that a simple and reasonably conservative estimate of the diagonal cracking load was the most appropriate approach. The equation should be simple to use, and it should be conservative since the goal of the current task is to prevent diagonal cracking in service. The proposed equation is based off of the data previously presented in Figure 5.56. The proposed equation is shown with the data in Figure 5.66.

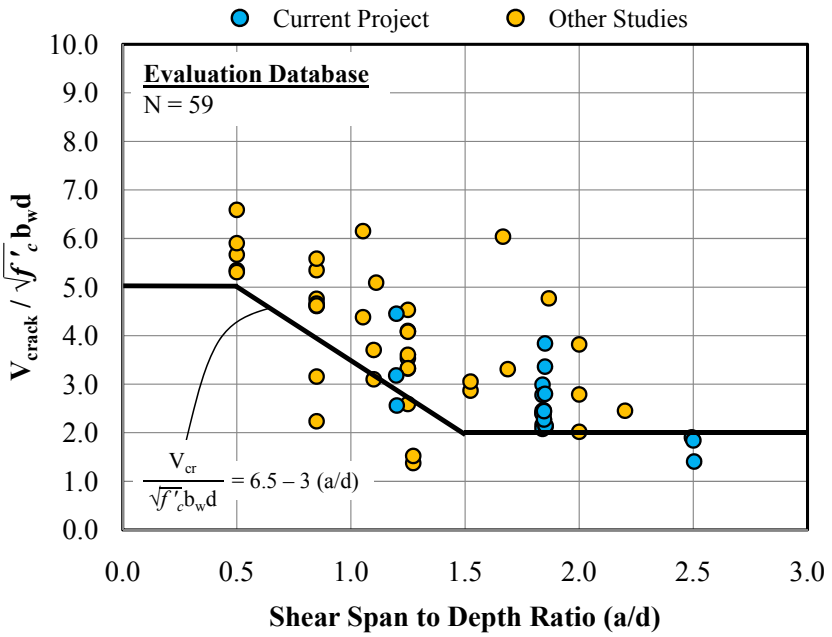

Figure 5.66: Development of proposed equation for a reasonably conservative estimate of diagonal cracking

The proposed diagonal cracking load equation is a reasonable lower bound to the data considering the primary variables that affect first cracking, namely the section size ($b_w d$), the tensile strength of concrete ($\sqrt{f_c'}$), and the a/d ratio of the member. For an a/d ratio less than 0.5, the estimated diagonal cracking load is $5\sqrt{f_c'}\, b_w d$. As the a/d ratio increases from 0.5 to 1.5, the estimated diagonal cracking load decreases from $5\sqrt{f_c'}\, b_w d$ to $2\sqrt{f_c'}\, b_w d$. For an a/d ratio > 1.5, the diagonal cracking load is $2\sqrt{f_c'}\, b_w d$. Limiting the diagonal cracking load to $2\sqrt{f_c'}\, b_w d$ at an a/d ratio of 2 is consistent with the diagonal cracking load of slender beams. Since the equation is a lower bound estimate, it inherently accounts for other variables that may contribute to the scatter in Figure 5.66 (i.e. the longitudinal reinforcement ratio or the effective depth). Furthermore, it does not seem practical to recommend an equation that varies with the longitudinal reinforcement ratio since ρ_l in TxDOT structures does not vary as much as it does for beams in the literature. In typical bent caps, the longitudinal reinforcement ratio is generally less than 1% (TxDOT, 2008). It is important to emphasize that the proposed diagonal cracking load estimate is intended to be simple and reasonably conservative.

5.4.4 Design Implications

To limit diagonal cracking under service loads, the following approach should be taken. After the completion of a strength analysis, a service load shear check should be performed. The shear in the member due to the unfactored service loads should be computed. This value should then be compared to the estimated diagonal cracking load given by the following equation:

$$V_{cr} = \left[6.5 - 3\left(\frac{a}{d} \right) \right] \sqrt{f'_c} b_w d \qquad (5.28)$$

but not greater than $5\sqrt{f_c'}\, b_w d$ nor less than $2\sqrt{f_c'}\, b_w d$

with a = shear span (in.)
d = effective depth of the member (in.)
f'_c = compressive strength of concrete (psi)
b_w = web width of the member (in.)

If the service level shear is less than the estimated diagonal cracking load, then the member is not expected to crack in service. If the service level shear is greater than the estimated diagonal cracking load, several options exist for the designer. First, the design of the member can be altered to increase the value of the diagonal cracking load. The section size ($b_w d$) of the member can be increased. If the depth is increased, the a/d ratio of the member for the typical situation in which the span length is fixed will also be reduced. Alternatively, or in conjunction with an increase in section size, a higher compressive strength of concrete can be specified. Second, if these options are not practical, the designer can provide additional web reinforcement to help restrain the diagonal crack widths under service loads. However, as noted in Section 4.5.3, there are diminishing returns in regards to the benefits of the quantity of web reinforcement for crack width control.

At the very least, the service load check outlined in this section provides an indication of the likelihood of the formation of diagonal cracks in service. If the service load shear exceeds the expected diagonal cracking load, the designer can determine at what percentage of the live load the member is expected to form a diagonal crack. In extreme cases, this check will indicate if the member is expected to crack under dead loads.

In the design example in Appendix B, this service load shear check is performed on two sections of a bent cap with a/d ratios of 0.85 and 2.0. In both cases, for the sections that were designed according to the proposed strength provisions in Section 5.2, the diagonal cracking load estimate was equal to the full dead load shear plus approximately 25% of the live load shear. Thus, for these examples, diagonal cracking would be expected under full service loads. To reduce the risk of diagonal cracking under full service loads, modifications to the cross-section will need to be made. This example indicates that it may be slightly impractical to design the cross-section to remain free of diagonal cracks under the application of the *full* service load. Instead, limiting diagonal cracking under the full dead load and a percentage of the live load may be more realistic. This adjustment can be made in the proposed service load shear check by simply computing the shear due to the dead load plus a reasonable amount of live load.

5.4.5 Summary and Conclusions

In this task, the variables that affect the diagonal cracking load of deep beams were determined with data from the experimental program and from the literature. It was verified that the cross section of the member ($b_w d$), the tensile strength of concrete ($\sqrt{f_c'}$), and the a/d ratio are primary variables. The diagonal cracking load appeared to be a function of the longitudinal reinforcement ratio to some degree, but there was not a wide enough range of data to evaluate this variable properly. It should be noted that the longitudinal reinforcement ratio does not vary

much in TxDOT bent caps in general. It was shown that the effective depth of the member may have an effect on the normalized diagonal cracking load, but it is likely small. Using empirical equations presented in the literature, it was determined that accurately estimating the diagonal cracking load is difficult. The difficulty is due to the complexity of accounting for the wide range in the values of each variable that affect diagonal cracking and due to the inherent scatter of the diagonal cracking loads of nominally-identical specimens. The latter problem is likely due to the variability in the tensile strength of concrete. As a result, a simple and conservative empirical equation was recommended to estimate the diagonal cracking load of deep beams. This estimate can be compared to service level shear to determine the likelihood of diagonal cracking in service.

Following the procedure outlined in this section will not guarantee that a reinforced concrete deep beam will remain uncracked in service, primarily due to the inconsistencies between many design assumptions and actual field conditions such as overloads, restrained shrinkage, temperature changes, etc. However, it is a simple and logical approach that can significantly reduce or limit diagonal cracking in service. Furthermore, it forces the designer to think about the serviceability performance of the structure in the design phase.

5.5 Correlation of Maximum Diagonal Crack Width to Capacity

On occasion, diagonal cracks are discovered in bent caps (deep beams) in service (Section 1.2). Upon inspection of the structures, field engineers are asked to assess the amount of distress in the cracked member. Currently, there is little information in the literature regarding a method to link the width of diagonal cracks to the amount of distress in the deep beam.

The objective of this task was to develop a means to aide field engineers in evaluating the residual capacity of a diagonally-cracked bent cap. Data from the literature and data from the current experimental program were used to identify key variables that influence the width of diagonal cracks. Accounting for these variables, a simple chart was developed that correlates the maximum width of the primary diagonal crack in a deep beam to the corresponding percent of its ultimate capacity.

5.5.1 Background

Contrary to that of diagonal cracks, the variables affecting the width of flexural cracks have been studied extensively over the last fifty years. Several empirical relationships based on experimental data exist for estimating the width of flexural cracks. A brief background on variables affecting the width of flexural cracks will be discussed in this section. Less information on the width of diagonal cracks is present in the literature, particularly for members governed by shear behavior. Of the many research projects conducted on deep beam shear, diagonal crack width information was only included in a few studies. These studies will provide some indication of the primary variables that affect diagonal crack width in shear-critical members.

Variables affecting width of flexural cracks

Based on research conducted over the last fifty years, the three primary variables affecting flexural crack width are steel stress, concrete cover, and bar spacing. Test results indicate that steel stress is the most important of the three, especially at service load levels. In ACI 318-08, crack width is limited through the maximum bar spacing of the reinforcement (ACI, 2008). The equation for bar spacing accounts for the stress in the reinforcement and concrete cover. In AASHTO LRFD 2008, crack width is also limited by restricting the spacing of mild reinforcement (AASHTO, 2008). However, the AASHTO equation for bar spacing addresses exposure condition and strain gradient in addition to concrete cover and steel stress. A distinction between exposure conditions is not made in ACI 318-08 due to "the inherent variability in cracking" and due to experimental evidence that does not support the width of cracks influencing corrosion at service-load levels (Committee Closure, 1999 and ACI 318-08, 2008). As noted in Section 4.2.2, exposure conditions were addressed in ACI-318 prior to the 1999 version of the code.

Tensile stress of the longitudinal reinforcement was confirmed as the primary variable affecting flexural crack widths in a research study conducted by Young et al. in 2002. In this project, sixteen full-scale reinforced concrete bent caps were tested at an a/d ratio of approximately 1.6. Limiting the longitudinal reinforcement stress at the face of the column to 30-ksi and 24-ksi under service load levels corresponded to maximum flexural crack widths of 0.016- and 0.013-inches, respectively. It was found that the distribution of longitudinal reinforcement through transverse spacing had little effect on flexural crack widths.

Types of diagonal cracks

As noted in Section 5.4.1, two different types of diagonal cracks exist in reinforced concrete deep beams: flexure-shear cracks and web-shear cracks. Flexure-shear cracks form after or concurrently with flexural cracks. They extend from the top of the flexural crack towards the origin of load. Web-shear cracks occur independently of flexural cracking. They form when the principal tension stress in the web of the member exceeds the tensile strength of concrete. In deep beams, web-shear cracks are also referred to as bursting or splitting cracks. Specifically, they are caused by transverse tensile stresses that exist due to the spreading of compressive stresses in bottle-shaped struts. It is apparent that the spreading of compressive stresses in deep beams contributes to the width of flexure-shear cracks as well. Both of these cracks are depicted in Figure 5.67.

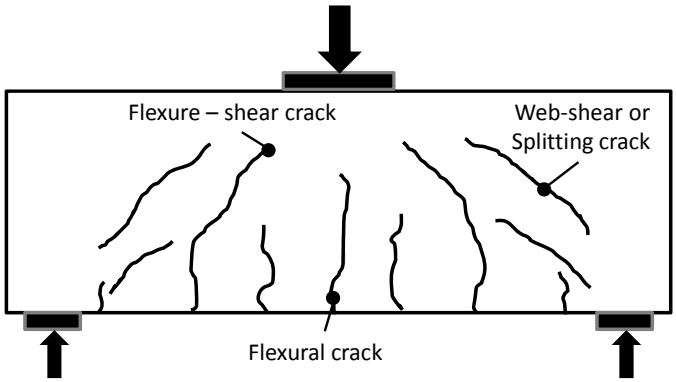

Figure 5.67: Types of cracks in reinforced concrete deep beams

The purpose of this task was to correlate maximum diagonal crack widths with the residual capacity of a deep beam bent cap. In the analysis of the crack width data from the experimental program and the literature, a distinction between web-shear cracks and flexure-shear cracks was not made. Both were treated simply as inclined cracks. The only relevant distinction between the two is related to the level of distress present in a shear-critical member. In general, the presence of web-shear cracks is a sign of impending failure (Section 4.5.2).

Effect of web reinforcement on diagonal crack widths of deep beams

In the literature, transverse reinforcement was found to be the most important variable in controlling diagonal crack widths. Unfortunately, very little diagonal crack width data was reported in the literature. A few studies in which diagonal crack widths were monitored during deep beam tests are discussed in this section. Crack width data from these studies are replotted where possible. In each case, the qualitative findings of the researchers are presented.

In a study by Smith and Vantsiotis, fifty-two deep reinforced concrete beams with a 4”x14” cross-section were tested to failure (1982). The purpose of the study was to evaluate the effect of web reinforcement on the strength and overall performance of deep beams. Specimens were tested with simple supports at a/d ratios of 0.77, 1.01, 1.34, and 2.01. During the tests, maximum crack widths were recorded at each load increment. In the paper, the maximum diagonal crack width at failure for each of the specimens was listed. However, only representative crack width data was provided from a beam at each a/d. Nevertheless, the authors

indicated that "web reinforcement was effective in reducing crack widths at all corresponding load levels and particularly in beams with a/d > 1.0" (Smith and Vantsiotis, 1982). Specifically, the researchers recommended minimum web reinforcement to restrain crack widths corresponding to 0.18% in the vertical direction and 0.23% in the horizontal direction (ρ_v = 0.0018 and ρ_h = 0.0023). It was apparent from the maximum crack width at failure data that reinforcement in addition to the minimum did little to further restrain the diagonal crack widths.

A research study conducted by Kong et al. focused on varying the amount of transverse reinforcement depending on the a/d ratio of the test specimen (1970). Kong et al. tested thirty-five reinforced concrete deep beams with a/d ratios ranging from 0.35 to 1.18. The crack width data indicated that at low a/d ratios (0.35), horizontal reinforcement placed near the tension steel was most effective at restraining crack widths. As the a/d ratio increased, the effectiveness of the vertical reinforcement at restraining diagonal cracks increased.

In an investigation by Tan et al., crack width data was recorded for eighteen deep reinforced concrete beams (1997). Six specimens each were tested at an a/d ratio of 0.85, 1.13, and 1.69. It was observed that for specimens with reinforcement in only one direction, vertical reinforcement was more effective than horizontal reinforcement at restraining crack widths. However, the most effective crack width restraint was provided by similar amounts of reinforcement in both orthogonal directions (Tan et al., 1997). These trends were evident at all three a/d ratios.

The effect of transverse reinforcement on the width of diagonal cracks was also evaluated in the full-scale study conducted by Bracci et al. (Bracci et al., 2000 and Young et al., 2002). Sixteen 33"x36" bent caps were tested to failure at an a/d ratio of approximately 1.6. The longitudinal reinforcement ratio for the specimens ranged from 0.6% to 0.8%. Three different web reinforcement arrangements were included in the test specimens. For the Group 1 and 2 specimens, the reinforcement in the horizontal direction ranged from 0.19% to 0.22%; the reinforcement in the vertical direction was 0.3%. The vertical reinforcement consisted of two-legged, #5 stirrups. In the Group 3 specimens, the horizontal reinforcement was 0.22% and the vertical reinforcement was 0.6%. The vertical reinforcement in the Group 3 specimens consisted of four-legged #5 stirrups. During the tests to failure, the maximum width of inclined cracks was recorded for each specimen. From the test results, it was observed that the additional vertical reinforcement in the Group 3 specimens promoted "a more desirable (ductile) flexural failure mechanism at ultimate loading" (Young et al., 2002). The diagonal crack width data from this study are replotted in Figure 5.68. From the data, it is evident that the additional vertical reinforcement did little to further restrain the diagonal crack widths at first cracking and in the service load range. Above 50% of the total applied load, however, the Group 3 specimens had narrower crack widths than the Group 1 or 2 specimens. These results from full-scale specimens agree well with the findings in Section 4.5.3 regarding minimum web reinforcement. Increasing the amount of vertical reinforcement from 0.3% to 0.6% did little to reduce the crack widths at first cracking or at typical service loads. These data indicate that there are diminishing returns in regards to the diagonal crack width restraint from increasing the amount of transverse reinforcement.

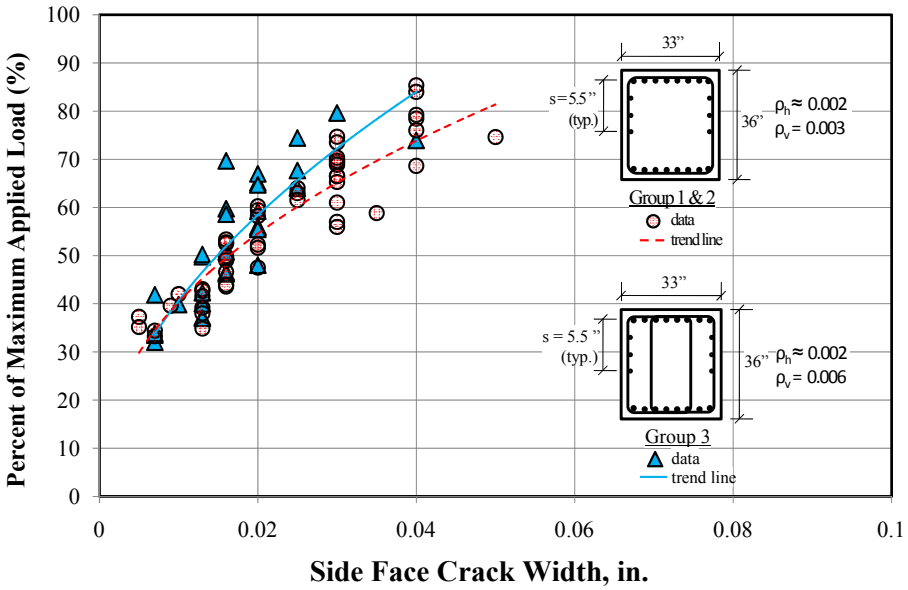

Figure 5.68: Effect of transverse reinforcement on width of diagonal cracks (Bracci et al., 2000)

Effect of a/d ratio on diagonal crack widths

In the literature, there are mixed observations regarding the effect of a/d ratio on diagonal crack width. This effect was not comprehensively studied by any previous researcher. In a few research projects, some trends between diagonal cracks widths and a/d ratio were either noted or denied. When possible, only specimens with transverse reinforcement are evaluated in this section.

In the study by Kong et al., a trend with a/d ratio was detected (1970). Thirty-five deep beams were tested at a/d ratios of 0.35, 0.54, and 1.18. As the a/d ratio increased, average and maximum diagonal crack widths increased. The maximum crack width data from the Series 4 and 5 specimens are replotted in Figure 5.69. These series had the most practical reinforcement layouts of the beams tested. From the data, a considerable difference in the diagonal crack widths was seen at 50% of the maximum applied load and greater. The first cracking load for the specimens tested at an a/d ratio of 0.35 was approximately 40% of the maximum applied load. It is important to note that different a/d ratios were obtained by changing the depth of the section. It is possible that the change in depth also influenced the crack widths based on the results that were presented in Section 4.6.3. In this case, the effect of depth would have mitigated the width of the diagonal cracks as the a/d ratio increased (and the depth of the member decreased).

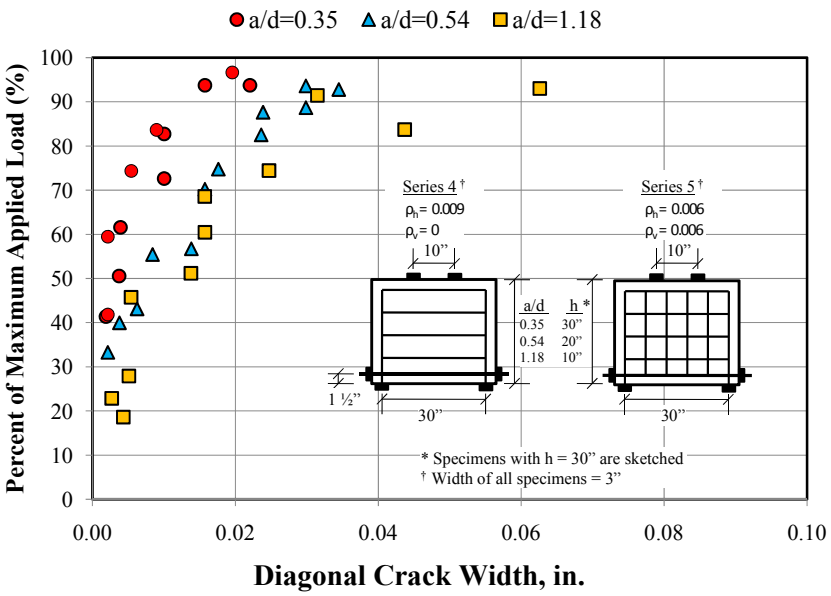

Figure 5.69: Effect of a/d ratio on width of diagonal cracks (Kong et al., 1970)

In the study by Tan et al. (1997), a slight increase in diagonal crack widths with increasing a/d ratios was noticed. Diagonal crack width plots were provided for the beams tested at each a/d ratio: 0.85, 1.13, and 1.69. Unfortunately, only the general trends in the data were visible in the original reference; it was not possible to extract the data from the plots due to their size. Nevertheless, at similar percentages of the maximum applied load, it appeared that the diagonal crack widths were greater in the specimens with an a/d ratio of 1.69 when compared to those tested at an a/d ratio of 0.85 or 1.13. However, there was not a clear difference between the data from the specimens with an a/d ratio of 0.85 and 1.13. For the specimens tested at an a/d ratio of 1.69, it was noted that "the fastest development rate of the diagonal crack occurred" (Tan et al., 1997).

In the research study conducted by Smith and Vantsiotis, however, no trend between diagonal crack widths and a/d ratio was detected (1982). Fifty reinforced concrete beams were tested at a/d ratios of 0.77, 1.01, and 1.34. Two additional beams were tested at an a/d ratio of 2.0. Maximum crack width at failure was tabulated for all of the specimens. Negligible differences in maximum crack width at failure were evident as the a/d ratio changed for the test specimens. In addition, representative load versus crack width plots were provided at each a/d ratio. From these plots, an effect of a/d ratio on the width of diagonal cracks was not apparent. The data from the representative crack width plots are replotted in Figure 5.70.

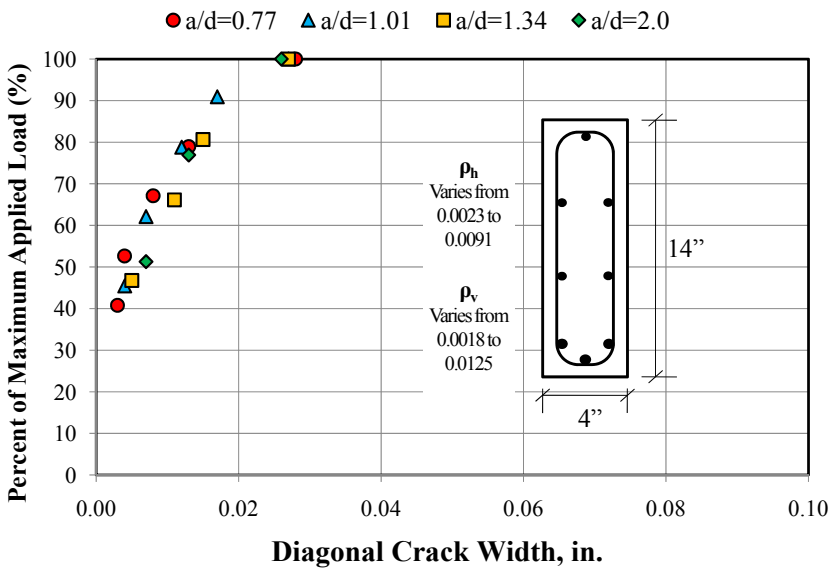

Figure 5.70: Effect of a/d ratio on diagonal crack width (Smith and Vantsiotis, 1982)

Effect of longitudinal reinforcement on diagonal crack widths

In 1971, Suter and Manuel tested twelve deep beams (6” x 13”) at an a/d ratio of 1.5 and 2.0. At each a/d ratio, the longitudinal reinforcement was either 0.96% or 2.44%. Four of the beams were unreinforced transversely; the remaining eight were reinforced with a single stirrup at the midspan of the beam. The experimental results suggested that the beams with greater longitudinal reinforcement (2.44%) were more shear critical. Specifically, the width of diagonal cracks was more dominant than the flexural cracks at service loads and near ultimate. On the contrary, the width of the diagonal cracks of the beams with a lower amount of longitudinal reinforcement (0.96%) was not as critical as the flexural cracks at service loads ($0.4M_{ultimate}$). At approximately 70% of the ultimate load, the width of the diagonal cracks exceeded that of the flexural cracks. All of the transversely reinforced beams with 0.96% longitudinal reinforcement failed in flexure; two of the four transversely reinforced beams with 2.44% longitudinal reinforcement failed in flexure; the other two in shear. This study illustrated that longitudinal reinforcement can affect the diagonal crack widths in a deep beam by affecting the governing mechanism of behavior.

Effect of concrete cover on diagonal crack widths

It is known that the width of *flexural* cracks is affected by the thickness of the concrete cover to the extreme tension face (Gergely and Lutz, 1968 and Frosch, 1999). The reason is due to the strain gradient. The crack width measured at the extreme tension face will increase as the concrete cover increases because the restraint provided by the primary tension reinforcement is further away. The situation is different for diagonal crack widths and side face cover.

An experimental study was conducted by Rahal to investigate the effect of concrete cover on shear behavior (2006). Attention was given to the effect on diagonal crack widths. Seven tests were carried out at an a/d ratio of 3. The overall depth of the test specimens was 15.7-

inches. The width of the specimens ranged from 8.3- to 13.8-inches. The side concrete cover to the stirrups increased proportionally with the width of the member. Four different covers were evaluated: 0.2-, 1-, 2-, and 3-inches. The diagonal crack widths were plotted versus the applied shear for the test specimens. A similar increase in the width of diagonal cracks with increasing applied load was observed for the specimens with 0.2-, 1-, and 2-inches of cover. When the cover was within this range, the diagonal crack widths were not affected. For the specimens with 3-inch side cover, however, "a sharp increase in crack width" occurred shortly after cracking, nearly 10-times larger than that of the specimens with smaller cover (Rahal, 2006). The same general trend was seen for specimens with 3,600- and 6,000-psi concrete. Thus, the study by Rahal suggests that concrete cover should not affect the width of diagonal cracks provided that the cover is less than 2-inches. For reference, the side face cover for most of the specimens in the experimental program was 0.75-inches.

In summary, the primary variable that affects the width of diagonal cracks is the amount of web reinforcement. While there was not much crack width data in the literature showing this relationship, numerous researchers unanimously came to this conclusion. However, it was shown that there is a limit to the reduction in diagonal crack widths that can be obtained by providing additional web reinforcement. There was not as much consensus in the literature with regards to the effect of a/d ratio on the width of diagonal cracks. Based on the available data, it is likely that the a/d ratio affects the diagonal crack widths to some degree. Perhaps, the lack of consensus is an indication that the effect is relatively minor. Also, it was shown that the longitudinal reinforcement ratio can affect the width of diagonal cracks by altering the governing behavior of the member. In the current task, the performance of shear-critical members was addressed in response to the observed cracking patterns in field specimens (Section 1.2). With knowledge of the primary variables that affect diagonal crack widths, an approach to correlate them with the residual capacity of a deep beam can be determined.

5.5.2 Approach

In this task, a technique to link the maximum width of a diagonal crack with the residual capacity of an in-service bent cap was required. Two different approaches were considered that incorporated the primary variables that affect the width of diagonal cracks in deep beams.

First, an analytical approach was taken. The steps of the approach are illustrated in Figure 5.71. A simple strut-and-tie model was used to estimate the perpendicular tensile force in a bottle-shaped strut, assuming that the diagonal crack forms along the axis of the strut. The perpendicular tensile force was calculated as a function of the angle of spreading in the bottle-shaped strut, the angle of the strut with respect to the horizontal, and the amount of shear on the section. The tensile force was converted to tensile strain assuming that all of the strain exists in the transverse steel, ignoring the strain in the concrete. Multiplying the perpendicular tensile strain by the perpendicular crack spacing provided an estimate for the average width of a diagonal crack. From the literature, a constant of 2.0 was used to convert the average width of the diagonal crack to the maximum diagonal crack width, or the 95-percentile crack width (Adebar, 2001). Several assumptions were required to estimate diagonal crack widths with this approach. They include the following:

- Strain in the concrete perpendicular to the diagonal crack was ignored
- Crack spacing perpendicular to the diagonal crack was calculated assuming that longitudinal crack spacing (s_l) was equal to stirrup spacing

- The difference between average crack widths and maximum crack widths was taken as 2.0
- An angle of spreading was assumed (α)

$$w = \varepsilon_{\perp} s_{\perp} \quad (1)$$

$$s_{\perp} = s_l \sin\theta \quad (2)$$

$$\varepsilon_{\perp} = \frac{T}{E_s A_{\perp}} \quad (3)$$

$$T = \frac{V \tan\alpha}{\sin\theta} \quad (4)$$

$$A_{\perp} = A_v \cos\theta + A_h \sin\theta \quad (5)$$

$$w = \frac{V \tan\alpha \cdot s_l}{E_s (A_v \cos\theta + A_h \sin\theta)} \quad (6)$$

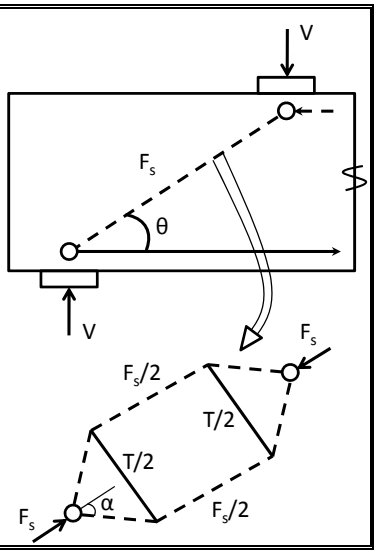

Figure 5.71: Preliminary analytical model for estimating diagonal crack widths

A few of the aforementioned assumptions are troublesome. Neglecting the contribution of the concrete in resisting the transverse tensile stresses in a bottle-shaped strut is fairly reasonable. The tensile strain in the concrete between cracks is very small in relation to the strain in the reinforcement at the cracks. Assuming that the crack spacing equaled the stirrup spacing is also a fair assumption. The basis of this assumption was the crack patterns of similar specimens in the experimental program in which the main difference between them was a stirrup spacing of 6-, 10-, or 15-inches. However, even though the crack spacing changed between these tests, the maximum diagonal crack width was not affected proportionally to the spacing. It is likely that the difference between average crack widths and maximum crack widths is not constant as the stirrup spacing changes. Lastly, and most important, it is difficult to justify an assumed angle of spreading (α). In ACI 318-08 Appendix A, the angle of spreading is assumed to be approximately 26-degrees, corresponding to a slope of 2:1 (ACI 318-08, 2008). In 1982, Schlaich and Weischede presented a model for estimating the spreading of compressive stresses in an elastic body based off of the starting width of the bottle-shaped strut and an assumed width at midheight (1982). In general, this approach yielded angles of spreading shallower than 26-degrees. It is difficult to justify either assumption.

In addition to the problems with the assumptions of this analytical approach, there are significant problems with its applicability. Crack widths are calculated as a function of the shear in the member. Since this task is aimed at correlating crack widths to residual capacity, an estimate for the load-carrying capacity of the member must be made as well. As such, a full strut-and-tie model analysis would be required. This level of calculation is inappropriate for a task conducted in the field. Lastly, conditions in the field can be very different from those in the laboratory. Some differences may include boundary conditions, axial restraint, long-term (time) effects, and the presence of repeated loads. The inherent variability of crack widths and the

differences between field and laboratory conditions negate the level of accuracy that is implied with these detailed calculations.

It should be noted that a study was conducted by Zhu et al. aimed at crack width prediction using a "compatibility-aided strut-and-tie model" (2003). This study focused specifically on the diagonal cracking of members with re-entrant corners. In this study, some of the aforementioned assumptions of the analytical approach were addressed. Strains in the concrete perpendicular to the diagonal crack were accounted for, but in conjunction with an assumed area of concrete contributing to the restraint. Instead of crack spacing, an estimate for gauge length was used that was calibrated with test data. Due to the dominance of a single crack at re-entrant corners, a difference between average and maximum crack widths was not made. Lastly, assumptions regarding the angle of spreading were not necessary due to the defined geometry of this application. While the approach by Zhu et al. (2003) is more sophisticated and more calibrated than the analytical approach discussed herein, it suffers from the same limitations in applicability in regards to the current task. The required amount of calculations is significant, an ultimate-strength estimate is required, and the level of accuracy is not justified due to inevitable differences between field and laboratory conditions.

The second approach used to address this task was empirically-based. Maximum crack width data was obtained for the specimens tested in the current study as discussed in Section 3.5.4. Each crack width measurement was plotted versus the corresponding percent of ultimate load. The data was grouped by the amount of web reinforcement in the test specimen. A strong relationship between the maximum diagonal crack width and the amount of web reinforcement crossing the crack was supported by the test data. A chart was developed with the diagonal crack width data from the experimental program that links the maximum diagonal crack width to the amount of load in the member (quantified as a percent of the ultimate capacity). Only the amount of web reinforcement in each direction is needed to use the chart.

The data used in the development of the chart is discussed in the next section. Following that, the chart is presented. Estimates from the chart are compared to crack width data from sixteen full-scale bent caps tested by Bracci et al. that were not used in the calibration of the chart (2000).

5.5.3 Results

All of the test specimens fabricated in the current project are listed in Table 5.7. Two specimens fabricated and tested by Deschenes are listed in the table as well (Deschenes, 2009). The beam details and test results for the specimens tested by Deschenes are provided in Table 5.8 and Table 5.9, respectively. The data from these specimens were included with the beams from the experimental program due to the scarcity of reliable diagonal crack width data for full-scale deep beams in the literature. In addition, the specimens contained different amounts of longitudinal and web reinforcement than those in the current study.

The shaded specimens in Table 5.7 were not used to address the current task primarily because their details did not reflect typical TxDOT practice. The data from specimens with insufficient web reinforcement, overall beam height of 23", and abnormally large bearing plates were excluded. Also, since the current project focused on deep beam behavior, specimens tested at an a/d ratio greater than 2 were not used. Lastly, the crack width data from two specimens, II-02-CCC1007 and M-03-2-CCC2436, were excluded because it was unreliable.

Therefore, the results of 24 deep beam shear tests were used in the current task (two of which were tested by Deschenes (2009)). Twenty-one specimens were tested at an a/d ratio of

1.85; three specimens were tested at an a/d ratio of 1.2. The overall height of the specimens ranged from 42- to 75-inches. The width ranged from 21- to 36-inches. The minimum amount of web reinforcement in the specimens corresponded to a reinforcement ratio of 0.002 in both orthogonal directions. The maximum amount of reinforcement in the vertical and horizontal direction corresponded to a reinforcement ratio of 0.0086 and 0.0058, respectively. Several different bearing plate sizes were used as shown in Table 5.7. Lastly, the longitudinal reinforcement ratio ranged from 2.3% to 3.1%.

The measured diagonal crack width data from the tests in the experimental program were plotted versus the percent of maximum applied load. It was determined that plotting crack widths in this manner was an appropriate way to compare data from beams with a variety of different section parameters, such as size and compressive strength. Furthermore, it was consistent with the primary goal of this task: to correlate maximum diagonal crack widths to the load on the structure, quantified as a percent of the ultimate capacity. Provided that the depth of the member was greater than or equal to 42-inches, the size of the member did not affect the diagonal crack width data when plotted in this fashion (Section 4.6.3). Also, the size of the bearing plates had no effect on the width of diagonal cracks as long as the size did not significantly alter the effective a/d ratio (Section 4.4.3).

Table 5.7: Specimens used in correlating crack width-to-capacity (shaded tests not used)

Testing Series	Beam I.D.	b in.	d in.	Support Plate†	Load Plate†	No. of Stirrup Legs	ρ_v	ρ_h	a/d ratio
I	I-03-2	21	38.5	16”x21”	20”x21”	2	0.003	0.003	1.84
	I-03-4					4			
	I-02-2					2	0.002	0.002	
	I-02-4					4			
II	II-03-CCC2021	21	38.6	10”x21”	20”x21”	2	0.003	0.0045	1.84
	II-03-CCC1007			10”x21”	10”x7”				
	II-03-CCT1021			10”x21”	36”x21”				
	II-03-CCT0507			5”x7”	36”x21”				
	II-02-CCT0507			5”x7”	36”x21”		0.002	0.002	
	II-02-CCC1007			10”x21”	10”x7”				
	II-02-CCC1021			10”x21”	10”x21”				
	II-02-CCT0521			5”x21”	20”x21”				
III	III-1.85-0	21	38.6	16”x21”	20”x21”	-	0.000	0.000	1.84
	III-2.5-0								2.47
	III-1.85-02					2	0.002	0.002	1.84
	III-1.85-025						0.0025	0.0015	
	III-1.85-03						0.003	0.003	
	III-1.85-01						0.001	0.001	
	III-1.85-03b						0.003	0.003	
	III-1.85-02b						0.002	0.002	
	III-1.2-02						0.002	0.002	1.20
	III-1.2-03						0.003	0.003	
	III-2.5-02						0.002	0.002	2.49
	III-2.5-03						0.003	0.003	
IV	IV-2175-1.85-02	21	68.9	16”x21”	29”x21”	2	0.002	0.002	1.85
	IV-2175-1.85-03						0.003	0.003	
	IV-2175-2.5-02				24”x21”		0.002	0.002	2.50
	IV-2175-1.2-02						0.002	0.002	1.20
	IV-2123-1.85-03		19.5		16.5”x 21”		0.003	0.003	1.85
	IV-2123-1.85-02						0.002	0.002	
	IV-2123-2.5-02				15.5”x21		0.002	0.002	2.50
	IV-2123-1.2-02				18”x21”		0.002	0.002	1.20
M	M-03-4-CCC2436	36	40	16”x36”	24”x36”	4	0.003	0.003	1.85
	M-03-4-CCC0812				8”x12”		0.003	0.003	
	M-09-4-CCC2436				24”x36”		0.0086	0.003	
	M-02-4-CCC2436				24”x36”		0.002	0.002	
	M-03-2-CCC2436				24”x36”	2	0.003	0.003	
Deschenes (2009)	Validation	21	42	16”x21”	20”x21”	2	0.003	0.0058	1.85
	nR1						0.003	0.0058	

† Load plate dimensions: [in direction of span] x [transverse to direction of span]

Table 5.8: Summary of beam details for two specimens tested by Deschenes (2009)

Beam I.D.	b_w (in.)	h (in.)	d (in.)	ρ_l	ρ'_l	ρ_v	ρ_v	Support Plate	Load Plate	a/d
Validation	21	42	36.1	0.031	0.01	0.003	0.0058	16"x21"	20"x21"	1.85
nR1	21	42	36.1	0.031	0.01	0.003	0.0058	16"x21"	20"x21"	1.8

Table 5.9: Summary of test results for two specimens tested by Deschenes (2009)

Beam I.D.	f'_c (psi)	f_{yl} (ksi)	f_{yv} (ksi)	V_{crack} (kips)	V_{crack} / V_{test}	V_{test} (kips)
Validation	5,060	66	65	151	0.26	571
nR1	7,250	66	65	-	-	561

Effect of web reinforcement on diagonal crack widths of deep beams

The variables that affect the width of diagonal cracks of deep beams were explicitly evaluated with the tests in the experimental program. The most important variable noted in the literature was the amount of web reinforcement crossing the diagonal crack. The same conclusion was reached in this project. The effect of the quantity of web reinforcement on the diagonal crack widths of deep beams was discussed in Section 4.5.3. Diagonal crack width data from six 21"x42" specimens tested at an a/d ratio of 1.85 are shown in Figure 5.72. In general, the amount of transverse reinforcement directly affects the maximum width of the diagonal crack at first cracking and throughout the loading history. It is interesting to note that in the case of test III-1.85-0, a narrow diagonal crack at first cracking was recorded. However, due to a lack of web reinforcement, the width of that crack increased dramatically in the next load increment. Providing web reinforcement of 0.25% in the vertical direction and 0.15% in the horizontal direction yielded similar results to providing 0.2% in each direction. For this reason, the data from these specimens were grouped together in the development of the crack-width-to-capacity chart later in this section.

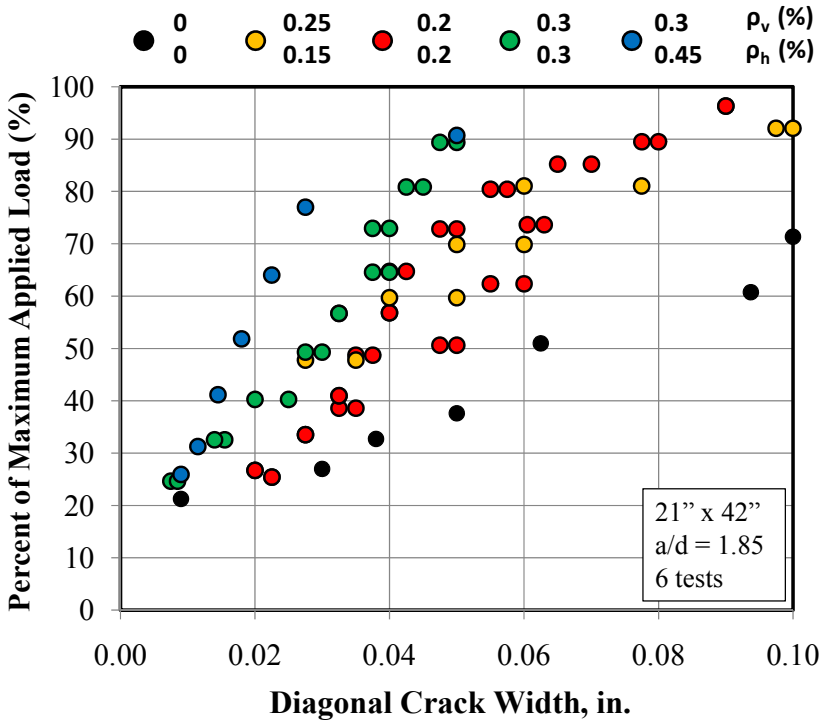

Figure 5.72: Effect of web reinforcement on diagonal crack widths of test specimens

The spacing of web reinforcement was not explicitly evaluated in the experimental program. However, a couple of valid comparisons were possible. As noted in Section 4.5.3, the spacing of the vertical reinforcement only slightly affected the width of diagonal cracks and only if the reinforcement was not adequately distributed. For one specimen, III-1.85-02, the spacing of the stirrups was 14.5-inches. The diagonal crack widths for this specimen were compared to that of a nominally-identical specimen with a stirrup spacing of 9.5-inches. The results indicated that the larger stirrup spacing in III-1.85-02 contributed to more scatter in the crack width data. However, the scatter was within the total scatter of specimens with similar section sizes and quantities of web reinforcement (Section 4.5.3). Based on this data, it was recommended that the existing spacing limit of d/4 or 12-inches in Section 5.13.2.3 of AASHTO LRFD 2008 be upheld. Thus, for the purposes of this task, the spacing of web reinforcement was not considered a primary variable that affects the width of diagonal cracks in deep beams.

Effect of a/d ratio on diagonal crack widths of deep beams

The effect of a/d ratio on the diagonal crack widths of deep beams was also evaluated through the tests in the experimental program. Little consensus exists in the literature regarding the effect of a/d ratio. In the experimental program, tests were conducted at a/d ratios of 1.2, 1.85, and 2.5. The test results of three specimens with identical beam details are presented in Figure 5.73. All three 21"x42" specimens had 0.3% web reinforcement in each direction. The only difference among the tests was the a/d ratio. Since the current task is limited to evaluating deep beams (a/d < 2), the data from specimen III-2.5-03 was not specifically needed. It is included in Figure 5.73 for comparison purposes. It is appropriate to compare the data from this

specimen with that of the other specimens because the final failure mode was reasonably consistent for all three (Section 4.5.2).

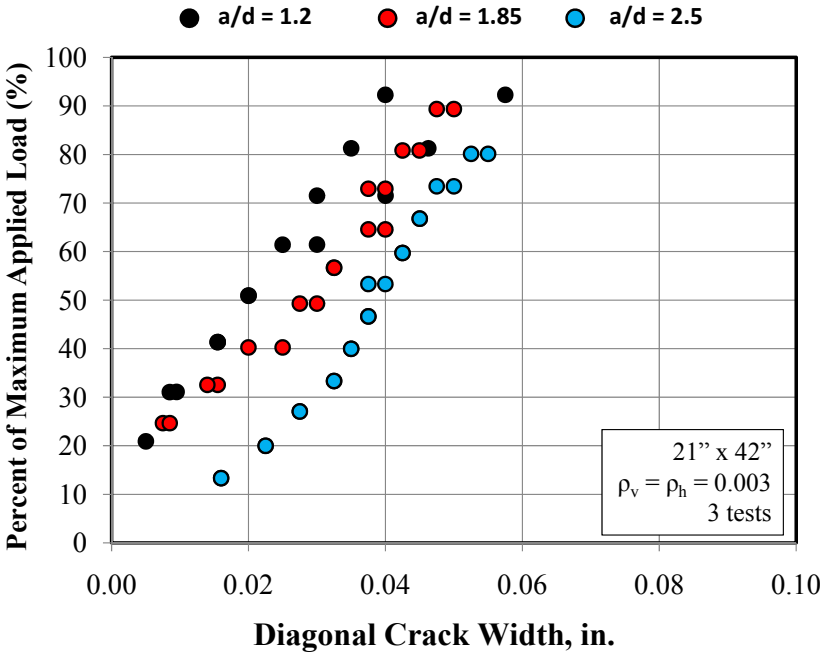

Figure 5.73: Effect of a/d ratio on diagonal cracking widths, 3 specimens, 0.3% reinf.

In Figure 5.73, a trend between the a/d ratio and the maximum width of diagonal cracks is observed. For a given percentage of maximum applied load, the diagonal crack width increases as the a/d ratio increases. The data in Figure 5.73 plotted with the diagonal crack widths of the other applicable tests in the experimental program is shown in Figure 5.74. The data in Figure 5.74 indicates that while there may be an effect with a/d ratio, the effect is relatively small in light of the scatter that exists in diagonal crack width data. The change in the maximum width of diagonal cracks from an increase in a/d ratio from 1.2 to 1.85 was not greater than the scatter associated with the crack widths of similar specimens.

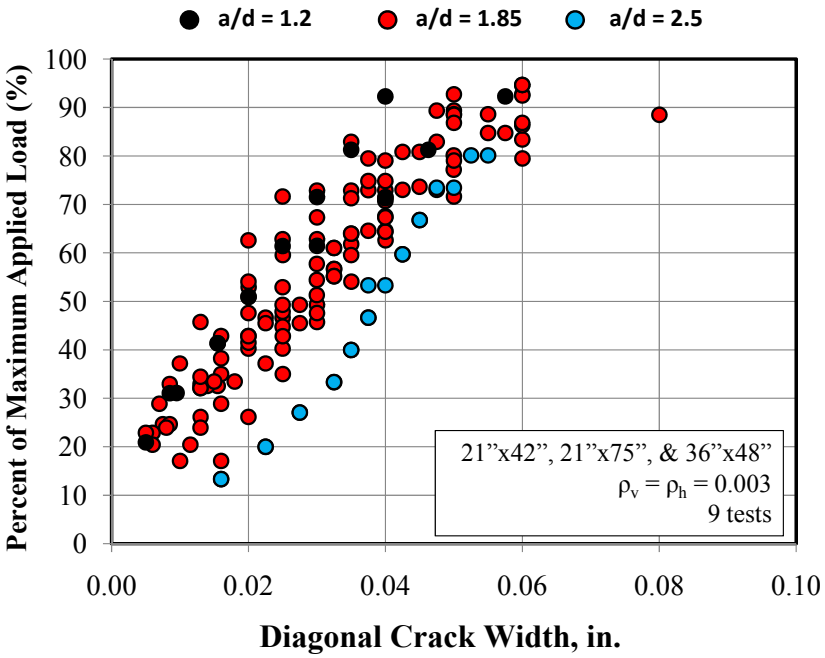

Figure 5.74: Effect of a/d ratio on diagonal crack widths, 9 specimens, 0.3% reinf.

The diagonal crack width data for two similar specimens with 0.2% web reinforcement tested at an a/d ratio of 1.2 and 1.85 are presented in Figure 5.75. The specimens have a 21"x42" cross-section. A trend with a/d ratio is not evident in this plot. It should be noted that the crack width data from a similar specimen tested at an a/d ratio of 2.5 was excluded from Figure 5.75 because this specimen failed in sectional shear whereas the other two specimens failed by crushing of the direct strut. As noted previously (Section 4.5.3), the dominant shear transfer mechanism must be similar to compare crack width data from multiple tests. The crack width data from all of the specimens with 0.2% web reinforcement is plotted in Figure 5.76. The maximum diagonal crack widths from IV-2175-1.2-02 were included in this plot as well. In Figure 5.76, it is clear that no trend with a/d ratio is evident, especially considering the scatter that exists in diagonal crack width data.

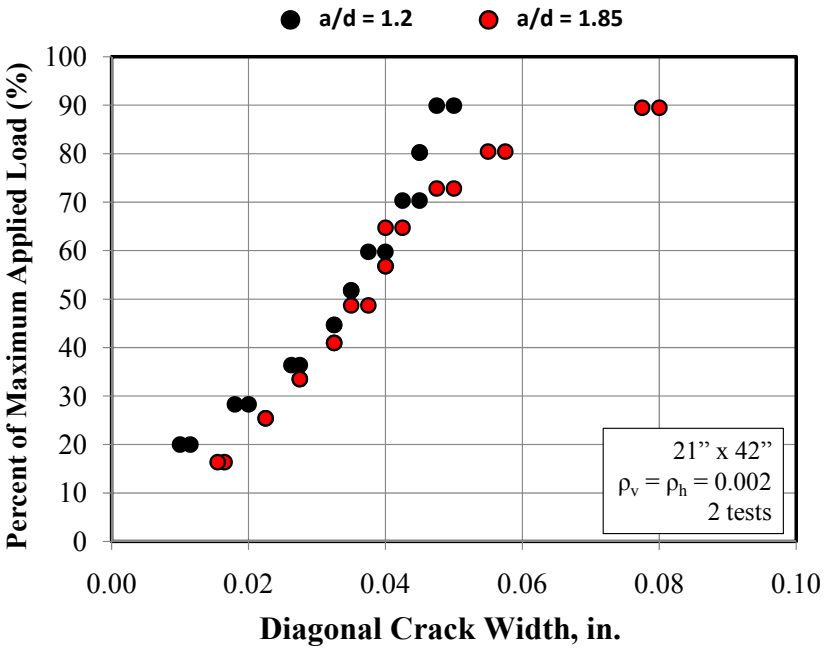

Figure 5.75: Effect of a/d ratio on diagonal crack widths, 2 specimens, 0.2% reinf.

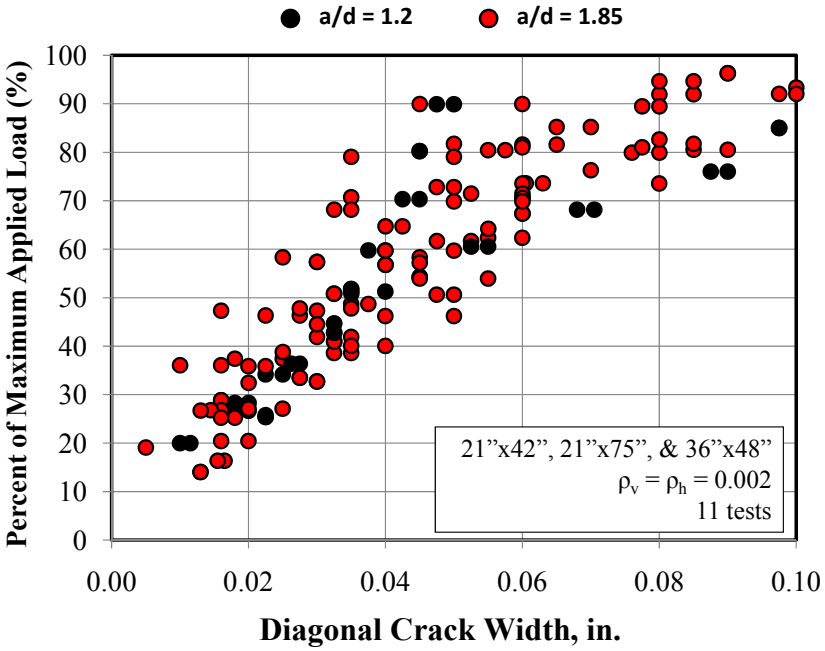

Figure 5.76: Effect of a/d ratio on diagonal crack widths, 11 specimens, 0.2% reinf.

The results presented in Figure 5.73 indicate that a trend with a/d ratio exists to some extent. However, the results presented in Figure 5.74 through Figure 5.76 suggest that the trend is relatively small considering the scatter in diagonal crack width data for deep beams. Based on these findings, it was determined that increasing the a/d ratio from 1.2 to 1.85 did not

significantly affect diagonal crack widths. Thus, it was not considered a primary variable for the purpose of this task.

Effect of longitudinal reinforcement on diagonal crack widths of deep beams

The effect of the longitudinal reinforcement ratio on the width of diagonal cracks was not explicitly studied in the experimental program. However, the crack width data from two tests with similar beam parameters but different longitudinal reinforcement can be compared to evaluate it to some degree. In Figure 5.77, the diagonal crack width data from two tests in the experimental program, II-03-CCC2021 and II-03-CCC1007, was compared to that of the two tests conducted by Deschenes (2009) that were described previously (Table 5.8 and Table 5.9). All four specimens had an identical cross-section and similar amounts of web reinforcement. The main difference between the specimens was the amount of longitudinal reinforcement. Specimens II-03-CCC2021 and II-03-CCC1007 had 2.3% longitudinal reinforcement; the beams tested by Deschenes (2009) had 3.1% reinforcement.

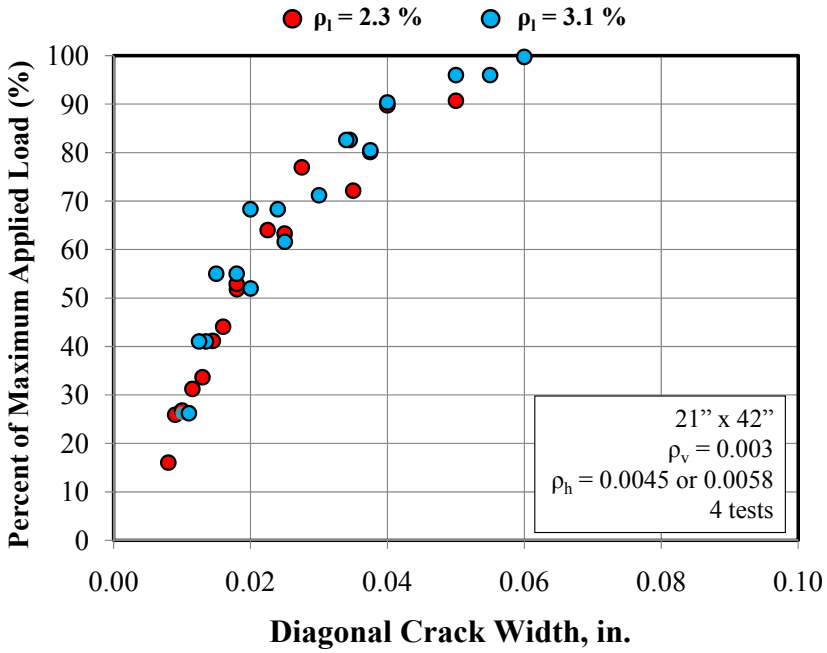

Figure 5.77: Effect of longitudinal reinforcement on diagonal cracks in shear-critical members

The results in Figure 5.77 indicate that the quantity of longitudinal reinforcement does not affect the width of diagonal cracks in deep beams in general. Since the maximum diagonal crack width was often measured near the mid-depth of the member, this finding makes sense. It should be noted, however, that the width of diagonal cracks can be affected by the longitudinal reinforcement by affecting the dominant mechanism of behavior as noted by Suter and Manuel (1971). More discussion related to the effect of longitudinal reinforcement on the width of diagonal cracks exists later in this section when the data from Bracci et al. (2000) is compared to the estimates from the proposed chart.

It was shown from the crack width data from the experimental program that the quantity of web reinforcement is the primary variable that affects the maximum width of diagonal cracks. To some extent, the a/d ratio contributed to the width of diagonal cracks. However, the effect was small in relation to the scatter associated with the crack widths of similar specimens. Also, it was shown with the data from the experimental program that the longitudinal reinforcement ratio does not affect the width of diagonal cracks for shear-critical members. Lastly, based on the conclusions of Rahal (2006) regarding the influence of concrete side cover on diagonal crack widths, this variable is also unlikely to significantly affect the width of diagonal cracks (Section 5.5.2). As a result, a method for correlating the diagonal crack width to the residual capacity of the member was developed considering the quantity of web reinforcement as the primary variable.

Correlation of Crack Width to Residual Capacity

The crack width data for the 21 specimens used in the current task are plotted in Figure 5.78. All of the beams represented in this plot were tested at an a/d ratio of 1.85. The data was separated into three groups by the quantity of web reinforcement: 0.2% reinforcement in each direction, 0.3% reinforcement in each direction, and greater than 0.3% reinforcement in each direction. The data from one specimen with 0.25% vertical reinforcement and 0.15% horizontal reinforcement was included in the 0.2% group (Figure 5.72). The data in the greater-than-0.3% group had a variety of different distributions in each direction. In general, the specimens in this group had reinforcement in one direction greater than 0.3% and reinforcement in the other direction of approximately 0.3%.

From the data in Figure 5.78, a consistent trend of the maximum diagonal crack width to the amount of web reinforcement is seen. It is clear that there is some scatter in the plot consistent with crack widths in general. A power function trend line was fitted through the data in each group. The square of the correlation coefficient (R^2) is provided next to each trend line. This value quantifies the error between the trend line and the data points. An R^2 value of 1.0 represents a perfect fit. In Figure 5.78, it is interesting to note that the R^2 value increases as the quantity of web reinforcement increases in each group. This finding indicates that with less reinforcement (0.2% in each direction), there was generally more scatter in the diagonal crack width data. As the amount of web reinforcement approached and exceeded 0.3% in each direction, the maximum width of diagonal cracks was more consistent.

In Figure 5.79, the power function trend line is replaced with straight line segments. From these straight line segments, a table was created that correlated the maximum width of diagonal cracks to the corresponding percent of the ultimate capacity. At several values for the maximum diagonal crack width, the average percent of ultimate capacity was tabulated for each data group. With each average value, a range of the scatter in terms of the percent of ultimate capacity was placed in parentheses. The chart is included as Figure 5.80.

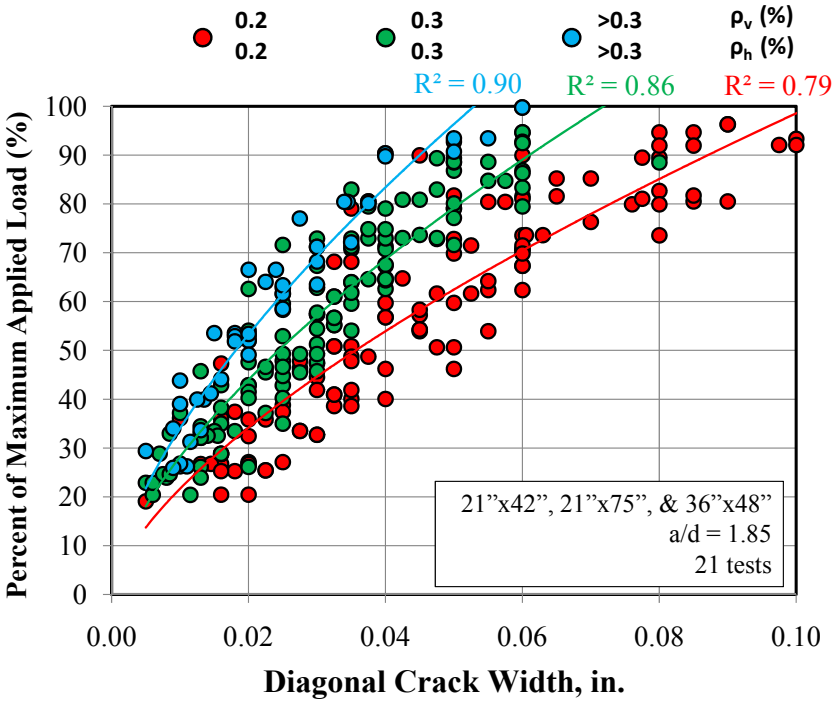

Figure 5.78: All crack width data at a/d ratio of 1.85 used in this task with trend lines

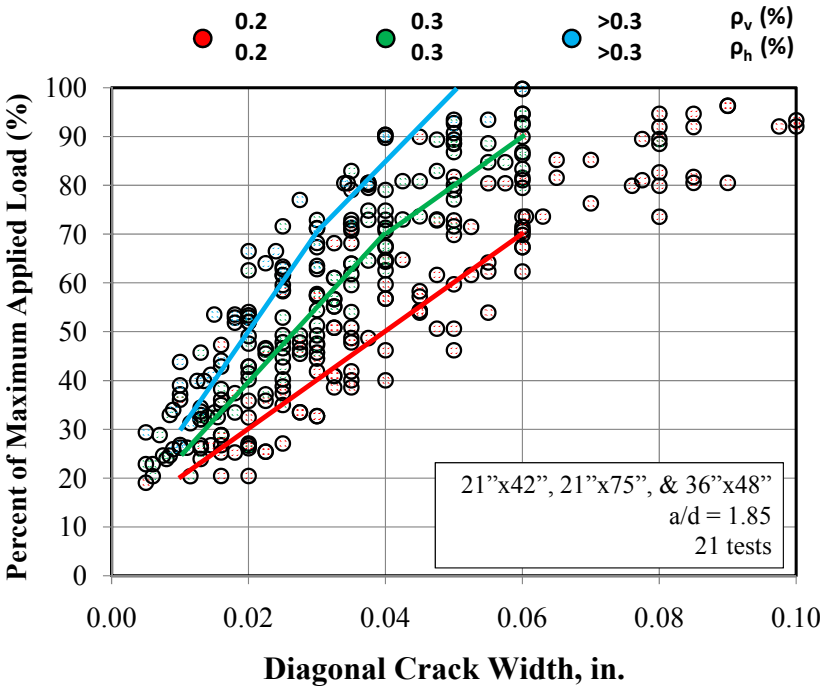

Figure 5.79: All crack width data at a/d ratio used in this task with straight line approximations

Load on the Member, Quantified as a Percent of Ultimate Capacity on Average (± scatter)						
Reinforcement \ **w_{max} (in.)**	**0.01**	**0.02**	**0.03**	**0.04**	**0.05**	**0.06**
ρ_v = 0.002 ρ_h = 0.002	20 (+10)	30 (±10)	40 (±10)	50 (±10)	60 (±15)	70 (±15)
ρ_v = 0.003 ρ_h = 0.003	25 (±10)	40 (±10)	55 (±10)	70 (±10)	80 (±10)	90 (±10)
ρ_v > 0.003 ρ_h > 0.003	30 (±10)	50 (±10)	70 (±10)	85 (±10)	~ Ultimate	~ Ultimate

Notation:

w_{max} = maximum measured diagonal crack width (in.)

ρ_v = reinforcement ratio in vertical direction ($\rho_v = A_v / bs_v$)

ρ_h = reinforcement ratio in horizontal direction ($\rho_h = A_h / bs_h$)

A_v & A_h = total area of stirrups or horizontal bars in one spacing ($in.^2$)

s_v & s_h = spacing of stirrups or horizontal bars (in.)

b = width of web (in.)

Directions:

1). Determine ρ_v and ρ_h for bent cap

2). Measure maximum diagonal crack width, w_{max}, in inches

3). Use chart with w_{max}, ρ_v, and ρ_h to estimate % of capacity

Important Notes:

In this chart, the maximum width of the primary diagonal crack in a shear-critical member is linked to the load on the member, quantified as a percent of its ultimate capacity. The intent of this chart is to aide field engineers in evaluating residual capacity in diagonally-cracked, reinforced-concrete bent caps subjected to concentrated loads at a/d ratios between 1.0 and 2.0. This chart was developed from crack width data from 21 tests of simply-supported reinforced concrete beams with overall heights between 42" and 75". The testing was conducted at an a/d ratio of 1.85. Data has shown that diagonal crack widths may slightly decrease with decreasing a/d ratio. The same crack width at a smaller a/d ratio indicates that a higher percentage of capacity from the above chart has already been reached.

This chart should be used in conjunction with sound engineering judgement with consideration of the following limitations:

-variability in crack widths in general (± scatter)

-members loaded at a/d < 1.85 may be at slightly higher % of capacity

-differences between field and laboratory conditions

-implications of an unconservative estimate of capacity

This chart is not intended to be used for inverted-tee bent caps.

Figure 5.80: Proposed chart that links diagonal crack width to percent of ultimate capacity of RC deep beams

The crack width measurements obtained by Bracci et al. were compared to the estimates from the proposed chart (2000). Two different distributions of web reinforcement were investigated by Bracci et al. Some judgment was required to group the data with the limits in the proposed chart. The specimens with 0.3% vertical reinforcement and 0.22% horizontal reinforcement were compared with the 0.3% group estimate. The specimens with 0.6% vertical reinforcement and 0.22% horizontal reinforcement were compared to the greater-than-0.3% group. The results of the comparisons are provided in Figure 5.81.

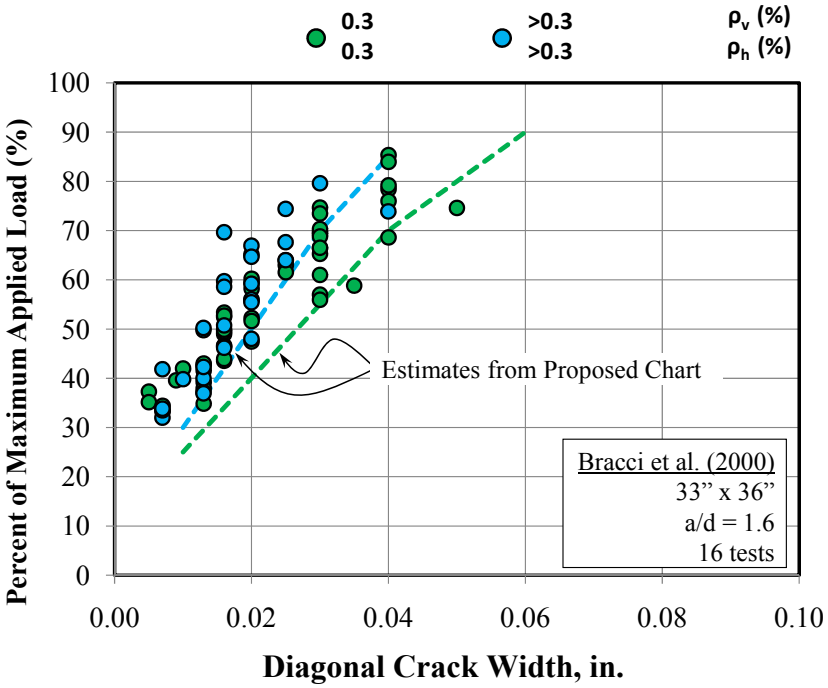

Figure 5.81: Comparison of crack width data from Bracci et al. (2000) and chart estimates

In Figure 5.81, the accuracy of the proposed chart was evaluated with independent crack width measurements of full-scale specimens. The specimens were tested at an a/d ratio of 1.6 and had longitudinal reinforcement ratios ranging from 0.6% to 0.8%. Considering the differences between the specimens tested by Bracci et al. and those used to develop the chart, the level of accuracy is reasonable. In each group, at a given crack width, the chart estimated an amount of load on the member that was within 20 percentage points of the actual capacity. For example, at a crack width of 0.02-inches, it was estimated with the chart that a member with 0.3% reinforcement in each direction was at approximately 40% (±10%) of its capacity. The specimens with a similar amount of reinforcement at the same crack width were at anywhere from 48- to 60% of their ultimate capacity. It was estimated with the chart that specimens with web reinforcement exceeding 0.3% were at 50% (±10%) of their capacity at a maximum diagonal crack width of 0.02-inches. The specimens tested by Bracci et al. (2000) with similar amounts of reinforcement and with maximum crack widths of 0.02-inches were at 48% to 68% of their ultimate capacity.

It is clear from Figure 5.81 that the data from Bracci et al. (2000) is shifted to the left with respect to the estimates from the chart. One potential reason for the shift is the longitudinal

reinforcement ratio. The smaller longitudinal reinforcement ratio in the specimens tested by Bracci et al. caused the specimens to be less shear-critical than those represented in the proposed chart. It is possible that the maximum width of the diagonal cracks reduced for this reason. Additional research is needed to improve the accuracy of the chart in relation to the effects of a/d ratio and the longitudinal reinforcement ratio.

The accuracy of the proposed chart was also compared to the specimens from the experimental program that were tested at an a/d ratio of 1.2. In this way, the implications of excluding an adjustment for the a/d ratio in the proposed chart could be evaluated. The results are presented in Figure 5.82. The results indicate that the chart does an adequate job of estimating the level of distress in each member until approximately 60% to 70% of the ultimate capacity is reached. Closer to ultimate, the crack widths for the specimens with 0.2% web reinforcement diverge from the estimated crack widths. As noted previously, changing the a/d ratio from 1.85 to 1.2 only slightly affected the maximum width of diagonal cracks.

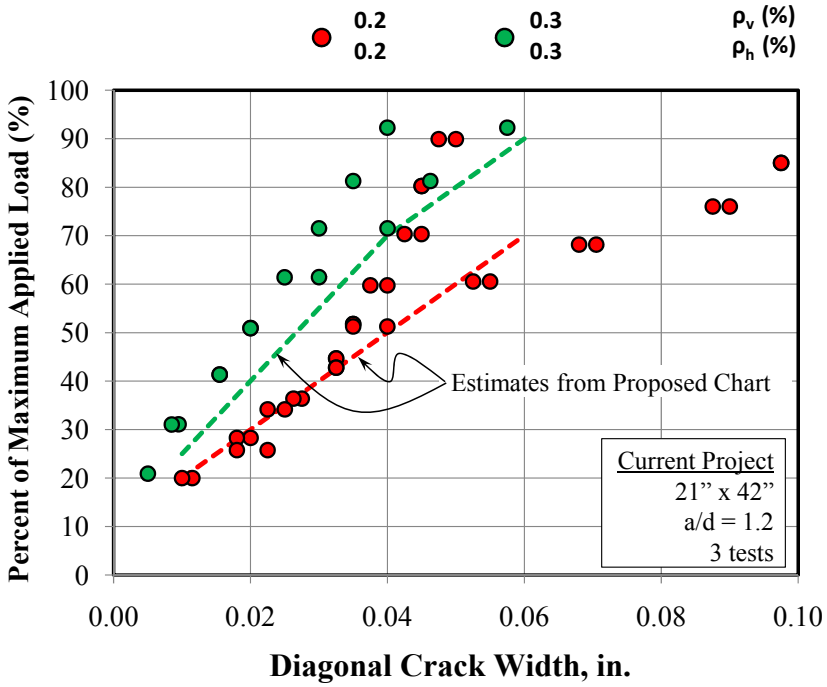

Figure 5.82: Comparison of data from specimens tested at a/d of 1.2 and chart estimates

Since the chart was developed with data from specimens tested at an a/d ratio of 1.85 and was evaluated with data from specimens at an a/d ratio of 1.2, it should not be used for cases well outside of this range. A range in a/d ratio from 1 to 2 seems appropriate due to the minor affect of a/d ratio on the width of diagonal cracks. It is not recommended to use the proposed chart for members with a/d ratios less than 1 since no data was obtained in this range. Maximum diagonal crack widths at a given percentage of capacity may slightly decrease with decreasing a/d ratio. As a result, a crack width of 0.03-inches is worse (higher percentage of capacity) for a member loaded with an a/d ratio < 1 than for a member loaded with an a/d ratio of 1.85.

The chart is not intended to be used for inverted-tee bent caps. No diagonal crack width data from inverted-tees were used in the calibration of the chart. It is possible that the presence

of tension in the web of an inverted-tee member due to load applied to the flange could significantly alter the width of diagonal cracks. Future research is required to assess the applicability of this chart to inverted-tee bent caps.

It cannot be emphasized enough that the use of this chart should be done in conjunction with sound engineering judgment. The conditions in the field can be drastically different then in the laboratory. It is clear that the chart estimate can be off by as much as 20% of the ultimate capacity due to variability in crack width data, the limited variables accounted for in the chart, and the differences between field and laboratory conditions. Thus, the chart should be viewed as an important guide to making an informed decision regarding the level of distress in a diagonally-cracked bent cap, in the absence of more sophisticated means of distress evaluation.

5.5.4 Summary and Conclusions

For the current task, information from the literature and data from the experimental program were used to determine the primary variables that affect the maximum width of diagonal cracks in shear-critical, reinforced concrete deep beams. The results indicate that the amount of web reinforcement crossing the diagonal crack is the primary variable. The effect of changing the a/d ratio from 1.2 to 1.85 did not significantly affect the maximum width of the diagonal cracks considering the inherent amount of scatter in crack widths. From the crack width data obtained in the experimental program, a chart was prepared that correlates the maximum width of the primary diagonal crack to the load acting on the member, quantified as a percent of the ultimate capacity. Experimental data from 21 full-scale tests on specimens that were 21”x42”, 21”x75”, and 36”x48” was used to develop the chart. The chart is applicable for a/d ratios between 1 and 2 and for a range of web reinforcement quantities. It is not applicable to inverted-tee bent caps. The chart should be used with sound engineering judgment considering the following limitations:

- Variability in crack widths in general
- Limited variables accounted for in the chart
- Differences between field and laboratory conditions
- Implications of an unconservative estimate of capacity

5.6 Summary

In Chapter 5, data from the experimental program and from the evaluation database was analyzed to address tasks 5 through 8 of the current project. These tasks included: (5) Proposed STM design provisions, (6) Discrepancy in calculated shear strength at an a/d ratio of 2, (7) Limiting diagonal cracking under service loads, and (8) Correlation of maximum diagonal crack width to capacity. The overall findings of the project are summarized in Chapter 6.

Chapter 6. Summary and Conclusions

6.1 Summary

Since the inclusion of Strut-and-Tie Modeling (STM) provisions in the AASHTO LRFD specifications in 1994, TxDOT engineers have been examining the impact that the provisions have on the design of their bent caps. In general, it has been difficult to implement the STM provisions due to their seemingly complicated nature. In addition, bents in the State of Texas are experiencing diagonal cracking problems with increasing frequency. These field-related issues and the difficulty in implementing the AASHTO LRFD provisions in their design practice were the impetus for TxDOT to fund the current project. The overall objective for the project was to develop safe and consistent design guidelines in regards to both strength and serviceability of bent caps and other deep beams.

In order to accomplish the aforementioned goal, the scope of the project was divided into eight tasks:

1. Determine the influence that the distribution of stirrups across the width of a beam web has on the strength and serviceability behavior of a deep beam (Section 4.3).
2. Determine the influence that triaxially confined bearing plates has on the strength and serviceability behavior of a deep beam (Section 4.4).
3. Determine the influence that the amount of web reinforcement (stirrups and longitudinal side face reinforcement) has on the strength and serviceability behavior of a deep beam (Section 4.5).
4. Determine the influence that member depth has on the strength and serviceability behavior of a deep beam (Section 4.6).
5. Propose a simple STM design methodology for the strength design of deep beams (Section 5.2).
6. Make a recommendation to reduce the discrepancy between shear strength calculated using STM and sectional shear provisions at an a/d ratio of 2 (Section 5.3).
7. Make a recommendation on the feasibility of limiting diagonal cracking under service loads (Section 5.4).
8. Make a recommendation on a methodology for relating the maximum diagonal crack width of a deep beam to its residual capacity (Section 5.5).

To achieve the primary research objectives outlined above, an exhaustive database of test results from the literature was compiled; and an experimental program was conducted. Data from approximately 250 beam tests were added to a database originally compiled by Brown et al. (2006). The total number of deep beam tests ($a/d \leq 2.5$) in the database, including the specimens of the current project, was 905. The data from the literature was generally insufficient to address the objectives of the current project for two reasons. First, very little serviceability information, primarily diagonal crack width data, exists in the literature. Second, the cross-sectional dimensions of deep beams, particularly the beam width, tested in the past are drastically smaller

than those of members in service. It was determined that the best means to improve the design and performance of actual bent caps was to examine specimens that were as representative as possible. As a result, filtering criteria were established based primarily off of cross-sectional dimensions, quantity of web reinforcement, and sufficient bearing plate details to remove specimens from the database that were exceptionally un-representative of actual members. After filtering, a statistically-significant number of tests (179), including those from the current project, remained in the *evaluation* database.

In addition, an experimental program was conducted consisting of 37 tests on some of the largest reinforced concrete deep beams ever tested in the history of shear research. The cross-sectional dimensions of the test specimens included the following sizes: 21"x23", 21"x42", 21"x44", 21"x75", and 36"x48". During the tests, measurements of the applied load, the deflection along the beam, the strain at various locations throughout the section and along the member, and the maximum diagonal crack width in the test span at each load increment were recorded. With the data from these tests and from the database, the eight primary objectives of the current project were addressed.

6.2 Conclusions

The conclusions of the current study are presented in this section. The following conclusions are based on information from the literature, data from the experimental program, and the analysis of the evaluation database.

6.2.1 Distribution of Stirrups across the Width of a Beam Web

The purpose of this task was to investigate the AASHTO LRFD (2008) STM provision that limits the width of a strut framing into a CTT node (AASHTO Article 5.6.3.3.2 and Figure 5.6.3.3.2-1 (a)). Four tests were conducted on beams with a 21"x44" cross-section, and two tests were conducted on beams with a 36"x48" cross-section. Both sets of tests had a shear span-to-depth ratio of 1.85. Transverse reinforcement ratios of 0.2% and 0.3% in each direction were investigated. In companion tests, the difference in strength and serviceability between concentrating stirrups near the member side face (2 legs) and distributing them across the web (4 legs), without changing the reinforcement ratio, was evaluated.

- **The AASHTO LRFD (2008) provision requiring designers to limit the strut width framing into a CTT node within a D-region is unnecessary (AASHTO Figure 5.6.3.3.2-1 (a)).** Singular node regions are more critical than smeared node regions [*fib* (1999); Schlaich et al. (1987)]. Thus, the focus of a STM design should be placed on the more critical singular node regions. The AASHTO LRFD (2008) CTT node limitation rarely is applicable for the design of a beam region with an a/d ratio less than two. This fact has been validated by experimental tests conducted as part of the current research program for beams as wide as 36-inches. It is proposed that the provision be removed from AASHTO LRFD (2008).
- **Distributing stirrup legs across the width of the web (while maintaining the same reinforcement ratio) did not influence the width of diagonal cracks of beams up to 36-inches wide when 0.3% web reinforcement was provided. However, distributing stirrup legs across the web width did reduce the crack widths of beams with 0.2% web reinforcement.** At loads greater than estimated service loads (>40% of capacity), distributing the stirrups across the width of the web reduced the width of diagonal cracks. At first

cracking and near estimated service loads, however, the width of diagonal cracks was similar for beams with 0.2% web reinforcement distributed in 2 or 4 legs.

6.2.2 Triaxial Confinement of Load and Support Plates (CCC and CCT Nodes)

The purpose of this task was to investigate the influence that triaxial confinement of the load or support plate (CCC or CCT node) has on the shear strength and serviceability behavior of a deep beam. Eight tests were conducted on beams with a 21"x42" cross-section, and two were conducted on beams with a 36"x48" cross-section. The shear span-to-depth ratio of all specimens was 1.85. Triaxial confinement of the load and support plates (CCC and CCT nodes) was investigated in members with 0.2% and 0.3% web reinforcement in each direction. The relative serviceability performances between confined and unconfined bearing plates were compared to one another.

- **The capacity of all faces of the CCC and CCT nodal region can be increased by the bearing capacity factor, $\sqrt{A_2/A_1}$, included in the AASHTO LRFD (2008) and ACI 318-08 provisions.** ACI 318-08 §10.14 and AASHTO LRFD (2008) Article 5.7.5 allow for an increase in the bearing capacity of concrete when triaxial confinement is present. Based on the experimental and analytical results of this research program, it was found that an increase in the capacity of the CCC and CCT nodal region by a similar factor provided for more accurate STM estimations with less unnecessary conservatism.
- **For specimens that contained a ratio of 0.2% web reinforcement in each direction, the serviceability behavior was more sensitive to the bearing plate configuration and reinforcement details.** In general, the crack widths and crack distribution for beams with 0.2% web reinforcement in each direction were wider and more erratic than beams reinforced with 0.3% web reinforcement in each direction.

6.2.3 Minimum Web Reinforcement

The purpose of this task was to recommend an appropriate amount of minimum web reinforcement to ensure adequate strength and serviceability performance in deep beams. Numerous tests in the experimental program were used to evaluate the effect of the quantity of web reinforcement on the performance of the member. At an a/d ratio of 1.85, tests were conducted on beams with a 21"x23", 21"x42", 21"x44", 21"x75", and 36"x48" cross-section. At a/d ratios of 1.2 and 2.5, two tests were conducted on beams with a 21"x42" cross-section. Several different distributions of web reinforcement were investigated. The majority of the test specimens had either 0.2% or 0.3% reinforcement in each direction. Stirrups with 2 and 4 legs were used. Two tests were conducted on specimens without web reinforcement.

- **For beams tested at an a/d ratio of 1.2 and 1.85, providing either 0.2% or 0.3% reinforcement did not affect the shear strength of the member. A specimen tested at an a/d ratio of 2.5 with 0.3% reinforcement in each direction failed at a substantially higher load than a companion specimen with 0.2% reinforcement.** The specimens tested at an a/d ratio less than 2 failed in a manner consistent with a single-panel, direct-strut mechanism. Thus, any reinforcement greater than that which is required to maintain equilibrium in the

bottle-shaped strut is unnecessary for strength. The specimens tested at an a/d ratio of 2.5 generally failed in a manner that was consistent with a sectional-shear model, or a multiple-panel STM. At this a/d ratio, increasing the amount of vertical reinforcement increases the shear strength of the member.

- **To adequately restrain maximum diagonal crack widths at first cracking and at estimated service loads, 0.3% reinforcement in each orthogonal direction should be provided and spaced evenly within the effective strut area.** The maximum diagonal crack width of specimens with 0.2% reinforcement in each direction often exceeded 0.016-inches at first cracking or at estimated service loads, whereas those with 0.3% reinforcement satisfied this limit in general. 0.3% reinforcement is consistent with the current AASHTO LRFD provision (Article 5.6.3.6, 2008) except it is proposed that the amount of reinforcement need not be based on the gross concrete section. A revised definition is provided, for adoption into the AASHTO LRFD specifications, in Appendix A.

6.2.4 Effect of Member Depth

The purpose of this task was to evaluate the effect of member depth on the strength and serviceability performance of reinforced concrete deep beams. Tests were conducted at a/d ratios of 1.2, 1.85, and 2.5 on specimens with 21"x23", 21"x42", and 21"x75" cross-sections and with 0.2% web reinforcement in each direction. The size of the nodal regions was kept as constant as possible for the tests conducted at each a/d ratio. In this way, the effect of changing the depth of a deep beam without proportionally changing the size of the nodal regions was assessed.

- **Provided that the bottle-shaped strut is adequately reinforced and the force in the tension tie does not control, the strength of deep beams (a/d ≤ 2) is governed by the size and stress conditions in the nodal regions, not by the effective depth of the member.** The results in this task highlighted the importance of using a strut-and-tie analysis to design reinforced concrete deep beams in order to explicitly address the stress conditions in the nodal regions. Using section-based approaches to design deep beams is unacceptable and inappropriately suggests that a large size effect exists.
- **The maximum diagonal crack width at a given percentage of the maximum applied load tended to increase as the overall depth of the member increased from 23" to 42" but not from 42" to 75".** The results in this task suggested that diagonal crack width data from small specimens should be used with caution in forming recommendations for full-scale structures. However, at a depth of 42-inches and greater, it appeared that the effect of depth on the width of diagonal cracks is mitigated.

6.2.5 Proposed STM Design Provisions

A new STM design procedure was developed for the design of deep beams. The new method was formulated based on the methodology used in *fib* (1999) while maintaining consistency with ACI 318-08 and AASHTO LRFD (2008). In addition, the proposed method was calibrated based on beams that were considered more representative of beams designed in practice – in terms of their size and reinforcement details.

In developing an STM procedure, it was necessary to explicitly define the truss geometries. This step cannot be over-emphasized as the performance of an STM methodology and its efficiency factors are intrinsically linked to the geometry of the nodal regions. Thus, the new STM provisions are based on an explicitly defined single-panel truss model with non-hydrostatic nodes. This model was used to define all of the beams in the evaluation database.

Another important aspect of the new STM design methodology is that it was comprehensively derived based on all the stress checks that constitute an STM design. Stress checks at all six nodal faces (three faces at CCC and three faces at CCT nodes) and in the longitudinal tie were performed for all of the beams in the evaluation database. The splitting of the strut was indirectly accounted for by only considering those beams that contained a minimum amount of transverse reinforcement. The results of the stress checks were used to formulate the new STM design provisions. Thus, the newly proposed design procedure considers every facet of an STM design. Accordingly, the following conclusion can be made:

- **The newly proposed STM procedure is: (i) simpler and (ii) more accurate than the ACI 318-08 and AASHTO LRFD (2008) STM design provisions.** The procedure is based on the fundamental principles of STM and on the procedures established in ACI 318-08, AASHTO LRFD (2008), and *fib* 1999. Thus, it has been derived based on theoretical principles, tests of D-regions, and by maintaining consistency with current design provisions. The procedure is practical, yields conservative strength estimates, and has been derived in a comprehensive and transparent manner. Implementation of the new design provisions into AASHTO LRFD (2008) is recommended as presented in Appendix A.

6.2.6 Discrepancy in Calculated Shear Strength at a/d Ratio of 2

The objective of this task was to improve the discrepancy in shear strength calculated using the STM and the sectional shear provisions in AASHTO LRFD (2008) at an a/d ratio of 2. It is well known that as the a/d ratio approaches and exceeds 2, the dominant shear transfer mechanism transitions from a deep beam mechanism to a sectional shear mechanism. However, the transition in behavior is gradual, not immediate; and therefore, a large discrepancy between the shear strength calculated at an a/d ratio of 2 according to each design model is not justified. The level of conservatism consistent with the sectional shear provisions in AASHTO LRFD was compared to that of the AASHTO LRFD and the proposed STM provisions for specimens in the database with a/d ratios up to 2.5. Also, shear capacity calculated with the proposed STM provisions was compared to capacity calculated with sectional shear provisions in AASHTO LRFD (2008) and ACI 318-08 for specimens in the database with a/d ratios between 2 and 2.5.

- **With the use of the proposed Project 5253 STM provisions and a limit on the ratio of V_s/V_c in sectional shear provisions, a reasonably smooth transition exists as the shear design model changes at an a/d ratio of 2.** The proposed STM provisions more appropriately account for the reduction in shear strength with increasing a/d ratio than the AASHTO LRFD STM provisions. As a result, excessive conservatism concurrent with the use of the AASHTO LRFD STM provisions near an a/d ratio of 2 has been largely eliminated. In terms of calculated design strength, limiting the ratio of V_s/V_c to 2 for sectional shear reduces the difference in capacity of the two design models near an a/d ratio of 2.
- **Data from the experimental program suggested that a single-panel strut-and-tie model is suitable for the design of deep beams with a/d ratios ≤ 2.** The observed failure modes of

the test specimens and measured strain data from specimens with a/d ratios of 1.2, 1.85, and 2.5 suggest that the dominant transfer mechanism for beams with an a/d ratio ≤ 2 is consistent with a single-panel STM. The use of a multiple-panel model at an a/d ratio less than 2 is not recommended since it is not consistent with the dominant load transfer mechanism and thus, often results in a overly conservative estimate of strength.

6.2.7 Limiting Diagonal Cracking under Service Loads

The purpose of this task was to assess the feasibility of limiting diagonal cracking under service loads. In addition to providing minimum web reinforcement, it was determined that a service-load shear check was a simple way to limit diagonal cracking under service loads. Measured diagonal cracking loads from the experimental program and from the database were used to determine the primary variables that affect the diagonal cracking load of deep beams.

- **A simple and reasonably conservative equation to estimate the diagonal cracking load of deep beams was developed that was a function of the shear area, the square root of the compressive strength of concrete, and the a/d ratio.** With this equation, the service level shear in the member (full dead load + live load) can be checked with the estimated diagonal cracking load. If the service level shear exceeds the estimated diagonal cracking load, the design of the section can be modified. At the very least, this check encourages the designer to consider the likelihood of diagonal cracking in service.

6.2.8 Correlation of Maximum Diagonal Crack Width to Capacity

The purpose of this task was to develop a means to help field engineers in evaluating the residual capacity of a diagonally-cracked bent cap. On occasion, diagonal cracks are discovered in bent caps in service. Currently, there is little information in the literature regarding a method to link the width of diagonal cracks to the amount of distress in the member. Data from the literature and the current experimental program were used to identify primary variables that influence the width of diagonal cracks in deep beams. All of the crack width data was from specimens with a minimum overall depth of 42-inches.

- **A simple chart was developed to correlate the maximum diagonal crack width in a deep beam to the load acting on the member, quantified as a percent of its ultimate capacity.** The chart applies to beams with an a/d ratio between 1 and 2 and is only a function of the amount of web reinforcement in the member. It was determined that the effect of a/d ratio within this range on diagonal crack widths was minimal relative to the amount of scatter inherent in diagonal crack width data. This chart is viewed as a simple means to make an informed decision regarding the amount of distress in a diagonally-cracked bent cap in the absence of a more sophisticated means of distress evaluation.

6.3 Concluding Remarks

In this research project, deep beam behavior was extensively studied. Thirty-seven tests were conducted on some of the largest deep beams ever tested in the history of shear research. In addition, an extensive database was compiled of previous shear tests in the literature. From the analysis of all of these data, the effect of the following factors on the strength and

serviceability performance of deep beams was determined: the distribution of stirrup legs across the width of the member, triaxial confinement at CCC and CCT nodes, the quantity of web reinforcement, the depth of the member, and the shear-span-to-depth ratio. With the knowledge obtained from investigating the effect of these factors, new strut-and-tie model provisions for strength were developed that are simpler and more accurate than those in AASHTO LRFD (2008) and ACI 318-08, and yet are just as conservative. In addition, design provisions aimed at improving the serviceability performance of deep beams were proposed. Minimum web reinforcement was recommended to control the width of diagonal cracks, and a service-load check was suggested to limit the formation of cracks in service. The knowledge obtained from this study was also used to improve the evaluation of bent caps in the field. A comprehensive understanding of the factors affecting the behavior of deep beams is vital to properly assessing the condition of a bent cap in service.

References

AASHTO LRFD, *2008 Interim Revisions, Bridge Design Specifications, 4th Edition, 2007*, American Association of State Highway and Transportation Officials, Washington, D.C., 2008.

AASHTO, *Standard Specifications for Highway Bridges, 17th Edition*, American Association of State Highway and Transportation Officials, Washington, D. C., 2002.

ACI Committee 224, "Control of Cracking in Concrete Structures" (ACI 224R-01), *ACI Manual of Concrete Practice*, American Concrete Institute, Farmington Hills, MI, 2002.

ACI Committee 318, "Closure to Public Comments on ACI 318-99," *Concrete International*, May 1999, pp. 318-1 to 318-50.

ACI Committee 318-02, *Building Code Requirements for Reinforced Concrete (ACI 318-02*), American Concrete Institute, Farmington Hills, MI, 2002.

ACI Committee 318-08, *Building Code Requirements for Reinforced Concrete (ACI 318-08*), American Concrete Institute, Farmington Hills, MI, 2008.

ACI Committee 318-56, *Building Code Requirements for Reinforced Concrete (ACI 318-56*), American Concrete Institute, Detroit, MI, 1956.

ACI Committee 318-63, *Building Code Requirements for Reinforced Concrete (ACI 318-63*), American Concrete Institute, Detroit, MI, 1963.

ACI Committee 318-71, *Building Code Requirements for Reinforced Concrete (ACI 318-71*), American Concrete Institute, Detroit, MI, 1971.

ACI Committee 318-95, *Building Code Requirements for Reinforced Concrete (ACI 318-95*), American Concrete Institute, Detroit, MI, 1995.

ACI-ASCE Committee 326, "Shear and Diagonal Tension," American Concrete Institute, Farmington Hills, MI, 1962.

ACI-ASCE Joint Committee 426-73, *The Shear Strength of Reinforced Concrete Members (ACI-ASCE 426-72)*, American Concrete Institute, Detroit, MI, 1973.

ACI-ASCE Joint Committee 445, *Recent Approaches to Shear Design of Structural Concrete (ACI 445R-99)*, American Concrete Institute, Farmington Hills, MI, 1999.

Adebar, P. and Zhou, Z., "Bearing Strength of Compressive Struts Confined by Plain Concrete," *ACI Structural Journal*, Vol. 90, No. 5, September-October 1993, pp. 534-541.

Adebar, P., "Diagonal Cracking and Diagonal Crack Control in Structural Concrete," SP 204-4, American Concrete Institute, Farmington Hills, Michigan, 2001, pp. 85-116.

Ahmad, S. A., and Lue, D. M., "Flexure-Shear Interaction of Reinforced High-Strength Concrete Beams," *ACI Structural Journal*, V. 84, No. 4, 1987, pp. 330 – 341.

Anderson, N. S. and Ramirez, J. A., "Detailing of Stirrup Reinforcement," *ACI Structural Journal*, Vol. 86, No. 5, September-October, 1989, pp. 507-515.

ASTM A 370 – 08a, *Standard Test Methods and Definitions for Mechanical Testing of Steel Products*, American Society for Testing and Materials, West Conshohocken, PA, May 2008.

ASTM A 615/A 615M – 08, *Standard Specification for Deformed and Plain Carbon-Steel Bars for Concrete Reinforcement*, American Society for Testing and Materials, West Conshohocken, PA, March 2008.

ASTM C 143/C 143M – 08, *Standard Test Method for the Slump of Hydraulic-Cement Concrete*, American Society for Testing and Materials, West Conshohocken, PA, March 2008.

ASTM C 31/C 31M – 08a, *Standard Practice for Making and Curing Concrete Test Specimens in the Field*, American Society for Testing and Materials, West Conshohocken, PA, April 2008.

ASTM C 39/C 39M – 05, *Standard Test Method for Compressive Strength of Cylindrical Concrete Specimens*, American Society for Testing and Materials, West Conshohocken, PA, November 2005.

Barton, D. L.; Anderson, R. B.; Bouadi, A.; Jirsa, J. O.; and Breen, J. E., *An Investigation of Strut-and-Tie Models for Dapped Beam Details*, Report No. 1127-1, Center for Transportation Research, University of Texas at Austin, Austin, Texas, May 1991.

Bažant, Z. P. and Kazemi, M. T., "Size Effect on Diagonal Shear Failure of Beams without Stirrups," *ACI Structural Journal*, Vol. 88, No. 3, May-June 1991, pp. 268-276.

Bergmeister, K.; Breen, J. E.; Jirsa, J. O.; and Kreger, M. E., *Detailing for Structural Concrete*, Report No. 1127-3F, Center for Transportation Research, University of Texas at Austin, Austin, Texas, May 1993.

Bracci, J. M., Keating, P. B., and Hueste, M. B. D., *Cracking in RC Bent Caps*, Research Report 1851-1, Texas Transportation Institute, The Texas A&M University System, College Station, Texas, Oct. 2000, 257 pp.

Brown, M. D.; Sankovich, C. L.; Bayrak, O.; Jirsa, J. O.; Breen, J. E.; and Wood, S. L., *Design for Shear in Reinforced Concrete Using Strut-and-Tie Models*, Report No. 0-4371-2, Center for Transportation Research, University of Texas at Austin, Austin, Texas, Apr. 2006.

Canadian Standards Association, *Canadian Highway Bridge Design Code* CSA-S6-06, Canadian Standards Association, Mississauga, Ontario, Canada, 2006.

Canadian Standards Association, *Design of Concrete Structures* CSA-A23.3-04, Canadian Standards Association, Mississauga, Ontario, Canada, 2004.

Chemrouk, M. and Kong, F. K., "Diagonal Cracking and Ultimate Shear Strength of Slender High Strength Concrete Deep Beams," *Advances in Structural Engineering*, Vol. 7, No. 3, 2004, pp. 217-228.

Chow, L.; Conway, H. D.; and Winter, G., "Stresses in Deep Beams," *ASCE Proceedings*, Paper No. 2557, May 1952, pp. 686-702.

Clark, A. P., "Diagonal Tension in Reinforced Concrete Beams," *ACI Journal*, V. 48, No. 10, 1951, pp. 145 – 156.

Collins, M. P. and Kuchma, D., "How Safe Are Our Large, Lightly Reinforced Concrete Beams, Slabs, and Footings?," *ACI Structural Journal*, Vol. 96, No. 4, July-August 1999, pp. 482-490.

Crist, R. A., "Shear Behavior of Deep Reinforced Concrete Beams," *Proceedings*, Symposium on the Effects of Repeated Loading of Materials and Structural Elements (Mexico City, 1966), Vol. 4, RILEM, Paris, 31 pp.

de Paiva, H. A. R., and Siess, C. P., "Strength and Behavior of Deep Beams," *ASCE Structural Journal*, V. 91, No. 10, 1965, pp. 19-41.

Deschenes, D., *M. S. Thesis in Progress*, University of Texas at Austin, May 2009.

edited by Kani, M. W.; Huggins, M. W.; and Wittkopp, R. R., *Kani on Shear in Reinforced Concrete*, University of Toronto Press, Toronto, 1979, 225 pp.

FIB, *Structural Concrete, Textbook on Behaviour, Design, and Performance*, Volume 3, International Federation for Structural Concrete, Lausanne, Switzerland, 1999, 269 pp.

Frosch, R. J., "Another Look at Cracking and Crack Control in Reinforced Concrete," *ACI Structural Journal*, Vol. 96, No. 3, May-June 1999, pp. 437-442.

Furuuchi, H.; Takahashi, Y.; Ueda, T.; and Kakuta, Y., "Effective Width for Shear Failure of RC Deep Slabs," *Transaction of the Japan Concrete Institute*, Vol. 20, 1998, pp. 209-216.

Gergely, P. and Lutz, L. A., "Maximum Crack Width in Reinforced Concrete Flexural Members," *Causes, Mechanism, and Control of Cracking in Concrete*, SP-20, American Concrete Institute, Farmington Hills, Mich., 1968, pp. 87-117.

Grob, J. and Thürlimann, B., "Ultimate Strength and Design of Reinforced Concrete Beams under Bending and Shear," IABSE Periodica, Zurich, 36, September 1976, pp. 105-120.

Hawkins, N. M., "The Bearing Strength of Concrete Loaded through Rigid Plates," *Magazine of Concrete Research*, Vol. 20, No. 62, Cement and Concrete Association, March 1968.

Hsuing, W. and Frantz, G. C., "Transverse Stirrup Spacing in R/C Beam," *ASCE Journal of Structural Engineering*, Vol. 11, No. 2, February 1985, pp. 353-362.

Huizinga, M. R., *Strength and Serviceability Performance of Large-Scale Deep Beams: Effect of Transverse Reinforcement*, Master's Thesis, University of Texas at Austin, August 2007, 232 pp.

Kong, F. K., Robins, P. J., and Cole, D. F., "Web Reinforcement Effects on Deep Beams," *ACI Journal*, V. 67, No. 12, 1970, pp. 1010-1016.

Lampert, P. and Thürlimann, B., "Ultimate Strength and Design of Reinforced Concrete Beams in Torsion and Bending," *IABSE Publications*, No 31-1, Zurich, Switzerland, p. 107-131, 1971.

Leonhardt, F. and Walther, R., translation by Amerongen, C. V., "The Stuttgardt Shear Tests, 1961", from *Beton und Stahlbeton, Vol. 56, No. 12, 1961 and Vol. 57, No. 2, 3, 6, 7, and 8, 1962*, Translation No. 111, Cement and Concrete Association, London, 1964, 138 pp.

MacGregor, J. G. and Wight, J. K., *Reinforced Concrete, Mechanics and Design*, 4th Edition, Pearson Prentice Hall, New Jersey, 2005, 1132 pp.

MacGregor, J. G., "Derivation of Strut and Tie Models for the 2002 ACI Code," *ACI SP-208 Examples for the Design of Structural Concrete with Strut-and-Tie Models*, American Concrete Institute, Michigan, 2002, 242 pp.

Marti, P., "Basic Tools of Reinforced Concrete Beam Design," *ACI Journal*, Vol. 82, No. 1, January-February 1985, pp. 46-56.

Matsuo, M., Lertsrisakulrat, T., Yanagawa, A., and Niwa, J., "Shear Behavior in RC Deep Beams with Stirrups," *Transactions of the Japan Concrete Institute*, Vol. 23, 2002, pp.385-390.

Mitchell, D., and Collins, M.P., "Diagonal Compression Field Theory – A Rational Model for Structural Concrete in Pure Torsion," *ACI Journal*, Vol. 71, No. 8, August 1974, pp. 396-408.

Moody, K. G., Viest, I. M., Elstner, R. C., and Hognestad, E., "Shear Strength of Reinforced Concrete Beams Part 1 – Tests of Simple Beams," *ACI Journal*, V. 51, No. 12, 1954, pp. 317-32.

Moody, K. G., Viest, I. M., Elstner, R. C., and Hognestad, E., "Shear Strength of Reinforced Concrete Beams Part 2 – Tests of Restrained beams Without Web Reinforcement, 1954.

Morrow, J., and Viest, I. M., "Shear Strength of Reinforced Concrete Frame Members Without Web Reinforcement," *ACI Journal*, V. 53, No. 9, 1957, pp. 833-869.

Mörsch, E., "Der Eisenbetonbau, seine Theorie und Anwendung (Reinforced Concrete, Theory and Application)," Stuggart, Germany, 1902.

NACU Standard No. 4, "Standard Building Regulations for the Use of Reinforced Concrete," *National Association of Cement Users*, Philadelphia, Pennsylvania, 1920, 20 pp.

Nielson, M. P.; Braestrup, M. W.; Jensen, B. C.; and Bach, F., *Concrete Plasticity, Beam Shear – Shear in Joints – Punching Shear*, Special Publication, Danish Society for Structural Science and Engineering, Technical University of Denmark, Lyngby, 1978, 129 pp.

Nielson, M.P., 1998, "Limit Analysis and Concrete Plasticity, 2nd Edition," CRC Press.

Oh, J. K., and Shin, S. W., "Shear Strength of Reinforced High-Strength Concrete Deep Beams," *ACI Structural Journal*, V. 98, No. 2, 2001, pp. 164-173.

Quintero-Febres, C. G., Parra-Montesinos, G., and Wight, J. K., "Strength of Struts in Deep Concrete Members Designed Using Strut-and-Tie Method," *ACI Structural Journal*, Vo. 103, No. 4, July-August 2006, pp.577-586.

Rahal, K. N., "Shear Behavior of Reinforced Concrete Beams with Variable Thickness of Concrete Side Cover," *ACI Structural Journal*, Vol. 103, No. 2, March-April 2006, pp. 171-177.

Ramirez, J.A., and Breen, J.E., "Evaluation of Modified Truss-Model Approach for Beams in Shear," *ACI Structural Journal*, Vol. 88, No. 5, September-October 1991, pp. 562-571.

Ramirez, J.A., and Breen, J.E., *Proposed Design Procedures for Shear and Torsion in Reinforced and Prestressed Concrete*, Report No. 248-4F, Center for Transportation Research, University of Texas at Austin, Austin, Texas, 1983.

Reinhardt, H. W., "Similitude of Brittle Fracture of Structural Concrete," *Advanced Mechanics of Reinforced Concrete*, IABSE Colloquium, Delft, 1981, pp. 175-184.

Ritter, W., "Die Bauweise Hennebique (The Hennebique System)," Schweizerische Bauzeitung, Bd. XXXIII, No. 7, Zurich, Switzerland, 1899.

Rogowsky, D. M. and MacGregor, J. G., "Design of Reinforced Concrete Deep Beams," *Concrete International*, Vol 8, August 1986, pp. 49-58.

Rogowsky, D. M.; MacGregor, J. G.; and Ong, S. Y., "Tests of Reinforced Concrete Deep Beams," *ACI Journal*, Vol. 83, No. 4, July-August 1986, pp. 614-623.

Schlaich, J. and Weischede, D.,"Detailing of Concrete Structures (in German)," Bulletin d'Information 150, Comité Euro-International du Béton., Paris, 1982, 163 pp.

Schlaich, J., Schäfer, K. and Jennewein, M., "Toward a Consistent Design of Structural Concrete," *PCI Journal*, Vol. 32, No. 3, May-June 1987, pp.74-150.

Shin, S., Lee, K., Moon, J., and Ghosh, S. K., "Shear Strength of Reinforced High-Strength Concrete Beams with Shear Span-to-Depth Ratios between 1.5 and 2.5," *ACI Structural Journal*, V. 96, No. 4, 1999, pp. 549-556.

Smith, K. N., and Vantsiotis, A. S., "Shear Strength of Deep Beams," *ACI Journal*, V. 79, No. 3, 1982 pp. 201-213.

Subedi, N. K., Vardy, A. E., and Kubota, N., "Reinforced Concrete Deep Beams – Some Test Results," *Magazine of Concrete Research*, V. 38, No. 137, 1986, pp. 206-219.

Suter, G. T. and Manuel, R. F., "Diagonal Crack Width Control in Short Beams," *ACI Journal*, Title No. 68-41, June 1971, pp. 451-455.

Tan, H. K., Teng, S., Kong, F., and Lu, H., "Main Tension Steel in High-Strength Concrete Deep and Short Beams," *ACI Structural Journal*, V. 94, No. 6, 1997, pp. 752-768.

Tan, K. H. and Cheng, G. H., "Size Effect on Shear Strength of Deep Beams: Insetigating with Strut-and-Tie Model," *Journal of Structural Engineering ASCE*, Vol. 132, No. 5, May 2006, pp. 673-685.

Tan, K. H., and Lu, H. Y., "Shear behavior of Large Reinforced Concrete Deep Beams and Code Comparisons," *ACI Structural Journal*, V. 96, No, 5, 1999, pp. 836-845.

Tan, K. H., Cheng, G. H., and Cheong, H. K., "Size effect in shear strength of large beams – behavior and finite element modeling," *Magazine of Concrete Research*, Vol. 57, No. 8, October 2005, pp. 497-509.

Tan, K. H., Kong, F. K., Teng, S., and Weng, L. W., "Effect of Web Reinforcement on High-Strength Concrete Deep Beams," *ACI Structural Journal*, Vol. 94, No. 5, Sept. – Oct. 1997, pp. 572-582.

Tan, K., Kong, F., Teng, S., and Guan, L., "High-Strength Concrete Deep Beams with Effective Span and Shear Span Variations," *ACI Structural Journal*, V. 92, No. 4, 1995, pp. 1-11.

Tan, K.H., Cheng, G. H., and Zhang, N., "Experiment to mitigate size effect on deep beams," *Magazine of Concrete Research*, Online, August 2007, 15 pp.

Thompson, M. K.; Young, M. J.; Jirsa, J. O., Breen, J. E., and Klingner, R. E., *Anchorage of Headed Reinforcement in CCT Nodes*, Research Report 1855-2, Center for Transportation Research, University of Texas at Austin, Austin, Texas, 2003.

TxDOT, Texas Department of Transportation Standard Bridge Drawings, 2008.

Uribe, C. M., and Alcocer, S. M., "Behavior of Deep Beams Designed with Strut-and-Tie Models," Centro Nacional de Prevención de Disastres, 2001, 247 pp. (In Spanish)

Van Landuyt, D., Personal communication, 2006.

Vecchio, F. J. and Collins, M. J., "The Modified Compression Field Theory for Reinforced Concrete Element Subjected to Shear," *ACI Structural Journal*, Vol. 83, No. 2, March-April 1986, pp.219-231.

Vogel, K., Personal Communication, 2008.

Walraven, J., and Lehwalter, N, "Size Effects in Short Beams Loaded in Shear," *ACI Structural Journal*, Vol. 91, No. 5, 1994, pp. 585-593.

Watstein, D., and Mathey, R. G., "Strains in Beams Having Diagonal Cracks," *ACI Journal*, V. 55, No. 12, 1958, pp. 717-728.

Weibull, W., "Phenomenon of rupture in solids," Ingenioersveten.-skapsakad. Handl., Vol. 153, 1939, pp. 1-55.

Wight, J.K., and Parra-Montesinos, G., "Use of Strut-and-Tie Model for Deep Beam Design as per ACI 318 Code," *ACI Concrete International*, Vol. 25, No. 5, May 2003, pp. 63-70

Yang, K. H., Chung, H. S., Lee, E. T., and Eun, H. C., "Shear characteristics of high-strength concrete deep beams without shear reinforcements," *Engineering Structures*, Vol. 25, 2003, pp. 1343-1352.

Young, B. S., Bracci, J. M., Keating, P. B., and Hueste, M. B., "Cracking in Reinforced Concrete Bent Caps," *ACI Structural Journal*, Vol. 99, No. 4, July-August 2002, pp. 488-498.

Zhang, N. and Tan, K. H., "Size effect in RC deep beams: Experimental investigation and STM verification," *Engineering Structures*, Vol. 29, 2007, pp. 3241-3254.

Zhu, R. R. H, Wanichakorn, W., Hsu, T. T. C., and Vogel, J., "Crack Width Prediction Using Compatibility-Aided Strut-and-Tie Model," *ACI Structural Journal*, Vol. 100, No. 4, July-August 2003, pp. 413-421.

Zsutty, T. C., "Beam Shear Strength Prediction by Analysis of Existing Data," *ACI Journal*, Title No. 65-71, November 1968, pp. 943-951.

Zsutty, T., "Shear Strength Prediction for Separate Categories of Simple Beam Tests," *ACI Journal*, Vol. 68, No. 2, 1971, pp. 138-143.

APPENDIX A. Proposed Changes to the AASHTO LRFD (2008) Bridge Design Specifications

A.1.1 Introduction

The proposed revisions to the strut-and-tie model specifications in AASHTO LRFD (2008), based on the results of the current project, are presented in this appendix. The proposed efficiency factors and STM methodology that were discussed in Section 5.2 are incorporated into the AASHTO LRFD (2008) strut-and-tie provisions. The proposed provisions are based on the STM recommendations in *fib* (1999) while maintaining consistency between other aspects of AASHTO LRFD (2008). They are significantly simpler than the current AASHTO LRFD (2008) STM provisions. The calculation of the tensile strain transverse to the CCT node is no longer required and stress checks on internal, or smeared, nodes are no longer recommended. The proposed procedure is significantly more accurate than the current AASHTO LRFD method, as illustrated in Section 5.2. In addition, it removes unnecessary conservatism of the AASHTO LRFD (2008) provisions at high shear span-to-depth ratios ($1.5 \leq a/d \leq 2$) such that a relatively smooth transition exists between the proposed STM provisions and current sectional shear provisions in AASHTO LRFD (2008). Based on the results discussed in Section 4.5, the proposed clarification to the crack control, or minimum reinforcement, provisions in AASHTO LRFD (2008) are also presented. The proposed changes are denoted with bold text. A brief explanation of the changes is presented in Section A.1.3.

A.1.2 Proposed Changes to AASHTO LRFD Bridge Design Specifications

5.6.3 Strut-and-Tie Model

5.6.3.1 General

Strut-and-tie models may be used to determine internal force effects near supports and the points of application of concentrated loads at strength and extreme event limit states.

The strut-and-tie model should be considered for the design of deep footings and pile caps or other situations in which the distance between the centers of applied load and the supporting reactions is less than about twice the member **depth**.

The angle between the axes of any strut and any tie entering a single node shall not be taken as less than 25 degrees.

If the strut-and-tie model is selected for structural analysis, Articles 5.6.3.2 through 5.6.3.6 shall apply.

C5.6.3.1

Where the conventional methods of strength of materials are not applicable because of nonlinear strain distribution, strut-and-tie modeling may provide a convenient way of approximating load paths and force effects in the structure. The load paths may be visualized and the geometry of concrete and steel **reinforcement** selected to implement the load path.

The strut-and-tie model is new to these Specifications. More detailed information on this method is given by Schlaich et al. (1987) and Collins and Mitchell (1991).

Traditional section-by-section design is based on the assumption that the reinforcement required at a particular section depends only on the separated values of the factored section force effects V_u, M_u, and T_u and does not consider the mechanical interaction among these force effects as the strut-and-tie model does. The traditional method further assumes that shear distribution will vary linearly over the depth of the beam.

For members such as the deep beam shown in Figure C5.6.3.2-1, these assumptions are not valid. The behavior of a component, such as a deep beam, can be predicted more accurately if the flow of forces through the complete structure is studied. Instead of determining V_u and M_u at different sections along the span, the flow of compressive stresses going from the loads, P, to the supports and the required tension force to be developed between the supports should be established.

The angle between the axes of a strut and tie should be limited between 25 to 65 degrees in order to mitigate wide crack openings and excessive strain in the reinforcement at failure.

For additional applications of the strut-and-tie model, see Articles 5.10.9.4, 5.13.2.3, and 5.13.2.4.1.

5.6.3.2 Structural Modeling

The structure and a component or region, thereof, may be modeled as an assembly of steel tension ties and concrete compressive struts interconnected at nodes to form a truss capable of carrying all applied loads to the supports. The determination of a truss is dependent on the geometry of the CCC and CCT nodal regions as defined in Figure 1. The geometry of these singular nodal regions shall be detailed as shown in Figures 1 and 2. Proportions of nodal regions are dependent on the bearing dimensions, reinforcement location, and depth of the compression zone as illustrated in Figure 2.

Interior nodes that are not bounded by a bearing plate are referred to as smeared nodes. Since D-regions contain both smeared and singular nodes, the latter will be critical and a check of concrete stresses in smeared nodes is unnecessary (Schlaich et al. 1987)

The nominal resistance of each face of a nodal region and of a tie, φP_n , shall be proportioned to be greater than the factored force acting on the node face or in the tie, P_u :

$$\varphi P_n \geq P_u \qquad (5.6.3.2\text{-}1)$$

where:

P_n = nominal resistance of **a node face** or tie (kip)

P_u = factored force acting on the face of a node or in a tie (kip)

φ = resistance factor for tension or compression specified in Article 5.5.4.2, as appropriate

C5.6.3.2

Cracked reinforced concrete carries load principally by compressive stresses in the concrete and tensile stresses in the reinforcement. The principle compressive stress trajectories in the concrete can be approximated by compressive struts. Tension ties are used to model the principal reinforcement.

A strut-and-tie model is shown in **Figure 1 for a simply supported deep beam**. The zone of high unidirectional compressive stress in the concrete is represented by a compressive strut. The regions of the concrete subjected to multidirectional stresses, where the struts and ties meet the joints of the truss, are represented by nodal zones.

Research has shown that a direct strut is the primary mechanism for transferring shear within a D-region. Therefore, a single-panel truss model is illustrated in Figure 1 and may be used in common D-regions such as: transfer girders, bents, pile caps, or corbels.

Stresses in a strut-and-tie model concentrate at the nodal zones. Failure of the structure may be attributed to the crushing of concrete in these critical nodal regions. For this reason, the capacity of a truss model may be directly related to the geometry of the nodal regions. Conventional techniques to be used for proportioning nodes are illustrated in Figure 2.

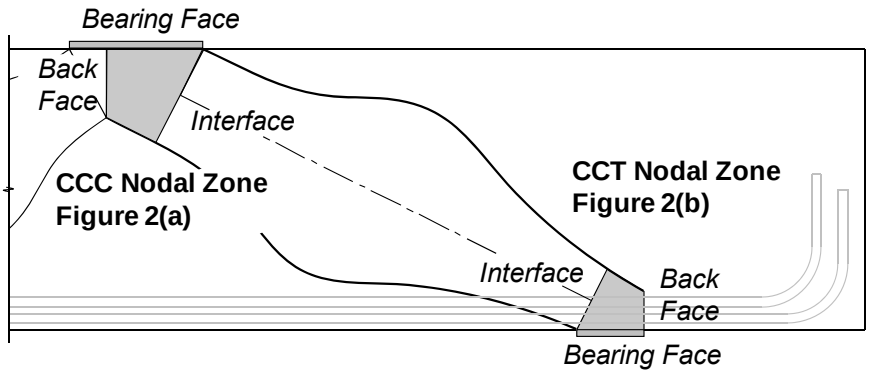

Figure 5.6.3.2-1 Strut-and-Tie Model for a Deep Beam

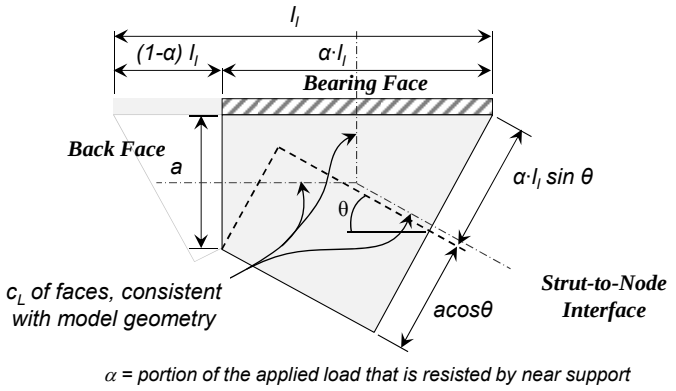

(a) CCC Node

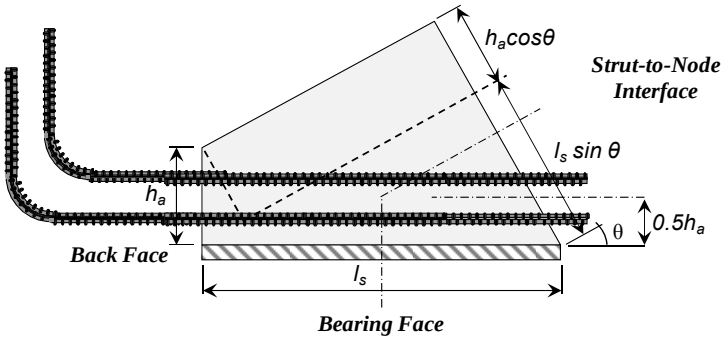

(b) CCT Node

Figure 5.6.3.2-2. Nodal Geometries.

5.6.3.3 Proportioning of Nodal Regions

*5.6.3.3.1 Strength of **the Face of a Node***

The nominal resistance of **the face of a node** shall be taken as:

$$P_n = f_{cu} \cdot \mathbf{A_{cn}} \qquad (5.6.3.3.1\text{-}1)$$

where:

P_n = nominal resistance of a **the face of a node** (kip)

f_{cu} = limiting compressive stress as specified in Article 5.6.3.3.3 (ksi)

$\mathbf{A_{cn}}$ = effective cross-sectional area of **the face of a node** as specified in Article 5.6.3.3.2 (in^2)

5.6.3.3.2 Effective Cross-Sectional Area of the Face of a Node

The value of $\mathbf{A_{cn}}$ shall be determined by considering the **details of the nodal region as illustrated in Figure 2**.

When a strut is anchored by reinforcement, **the back face of the CCT node, h_a,** may be considered to extend **twice the** distance **from the exterior surface of the beam to the centroid of the longitudinal tensile reinforcement**, as shown in **Figure 2(b).**

The depth of the back face of the CCC node, h_s , as shown in Figure 2(a), may be taken as the effective depth of the compression stress block determined from a conventional flexural analysis.

C5.6.3.3.2

A direct strut is the primary shear carrying mechanism for a deep beam. Therefore, previous reference to CTT nodal regions has been removed from the Specifications in order to place the emphasis of a deep beam design on the more critical CCC and CCT nodal regions.

Research has shown that the shear behavior of conventionally reinforced deep beams, as wide as 36 inches, are not significantly influenced by the distribution of stirrups across the section. Beams wider than 36 inches, or beams with a width to height aspect ratio greater than one may benefit from distributing stirrup legs across the width of the cross-section.

5.6.3.3.3 Limiting Compressive Stress at the Face of a Node

Unless confining reinforcement is provided and its effect is supported by analysis or experimentation, the limiting compressive stress at the face of a node, f_{cu}, shall be taken as:

$$f_{cu} = m \cdot \nu \cdot f_c' \qquad (5.6.3.3.3\text{-}1)$$

where:

f_c' = specified compressive strength of concrete (psi)

m = confinement modification factor, taken as $\sqrt{A_2/A_1}$ but not more than 2 as defined in Article 5.7.5

ν = concrete efficiency factor:

0.85, bearing and back face of CCC node

0.70, bearing and back face of CCT node

The stress applied to the back face of CCT node may be reduced as permitted in 5.6.3.3.3-1.

$0.85 - f_c'/20ksi$, CCC and CCT strut-to-node interface

Not to exceed 0.65 nor less than 0.45

0.45, CCC and CCT strut-to-node interface: *Structures that do not contain crack control reinforcement (Article 5.6.3.5)*

In addition to satisfying strength criteria, the node regions shall be designed to comply with the stress and anchorage limits specified in Article 5.6.3.4.1 and 5.6.3.4.2.

5.6.3.3.3-1 Back Face of CCT Node

Bond stresses resulting from the force in a developed tension tie need not be applied to the back face of the CCT node.

C5.6.3.3.3

Concrete efficiency factors have been selected based on simplicity in application, compatibility with other sections of the Specifications, compatibility with tests of D-regions, and compatibility with other provisions.

C5.6.3.3.3-1

The stress that must be resisted by the back face of a CCT node can be attributed to the anchorage of the tie, bearing from an anchor plate or headed bar, or an external indeterminacy such as that which occurs at a node over a continuous support (Figure C1).

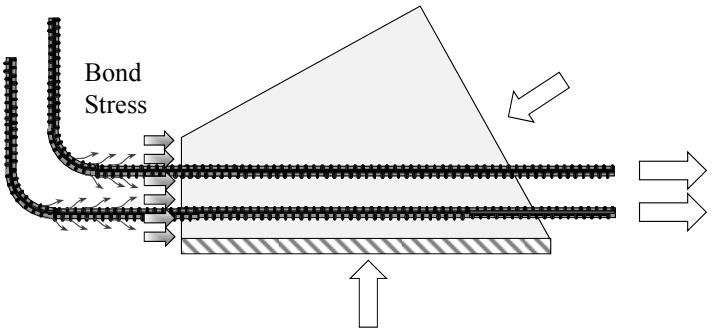

(a) Bond stress resulting from the anchorage of a developed tie.

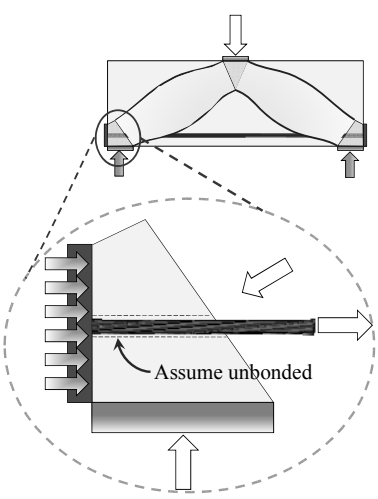

(b) Bearing stress applied from an anchor plate or headed bar.

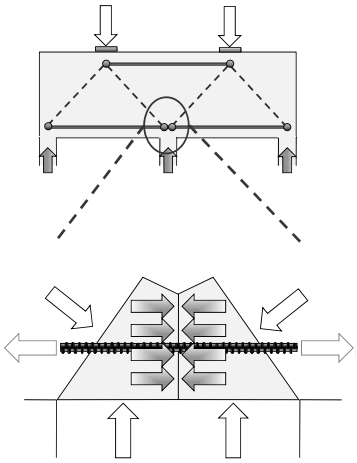

(c) Interior node over a continuous support.

Figure C5.6.3.3.3-1. Stress condition at the back face of a CCT node

If the tie is adequately developed, the bonding stresses are not critical and need not be applied as a direct force to the back face of a CCT node.

If the stress applied to the back face of a CCT node is from an anchor plate or headed bar, a check of the back face stresses should be made assuming that the bar is unbonded and all of the tie force is transferred to the anchor plate or bar head.

If the stress applied to the back face of a CCT node is the result of a combination of both anchorage and a discrete force from another strut, it is only necessary to proportion the node to resist the direct compression stresses. It is not necessary

to apply the bonding stresses to the back face, provided the tie is adequately anchored.

5.6.3.4 Proportioning of Tension Ties

5.6.3.4.1 Strength of Tie

Tension tie reinforcement shall be anchored to the nodal zones by specified embedment lengths, hooks, or mechanical anchorages. The tension tie force shall be developed at the inner face of the nodal zone.

The nominal resistance of a tension tie in kips shall be taken as:

$$P_n = f_y A_{st} + A_{ps}[f_{pe} + f_y] \qquad (5.6.3.4\text{-}1)$$

where:

A_{st} = total area of longitudinal mild steel reinforcement in the tie (in^2)
A_{ps} = area of prestressing steel (in^2)
f_y = yield strength of mild steel longitudinal reinforcement (ksi)
f_{pe} = stress in prestressing steel due to prestress after losses (ksi)

5.6.3.4.2 Anchorage of Tie

The tension tie reinforcement shall be anchored to transfer the tension force therein to the node regions of the truss in accordance with the requirements for development of reinforcement as specified in Article 5.11.

C.5.6.3.4.1

The second term of the equation for P_n is intended to ensure that the prestressing steel does not reach its yield point, thus a measure of control over unlimited cracking is maintained. It does, however, acknowledge that the stress in the prestressing elements will be increased due to the strain that will cause the concrete to crack. The increase in stress corresponding to this action is arbitrarily limited to the same increase in stress that the mild steel will undergo. If there is no mild steel, f_y may be taken as 60.0 ksi for the second term of the equation.

5.6.3.5 Crack Control Reinforcement

Structures and components or regions thereof, except for slabs and footings, which have been designed in accordance with the provisions of Article 5.6.3, shall contain an orthogonal grid of reinforcing bars near each face. The spacing of the bars in these grids shall not exceed **the smaller of d/4 and 12.0 in.**

The reinforcement in the vertical and horizontal direction shall satisfy the following:

$$\frac{A_v}{b_w s_v} \geq 0.003 \qquad \textbf{(5.6.3.5 – 1)}$$

$$\frac{A_h}{b_w s_h} \geq 0.003 \qquad \textbf{(5.6.3.5 – 2)}$$

where:

A_v, A_h = total area of vertical and horizontal crack control reinforcement within spacing s_v and s_h, respectively (in.^{2})

b_w = width of member web (in.)

s_v, s_h= spacing of vertical and horizontal crack control reinforcement, respectively (in.)

Crack control reinforcement shall be distributed evenly near the side faces of the strut. Where necessary, interior layers of crack control reinforcement may be used.

C5.6.3.5

This reinforcement is intended to control the width of cracks and to ensure a minimum ductility for the member so that, if required, significant redistribution of internal stresses is possible.

The total horizontal reinforcement can be calculated as 0.003 times the effective area of the strut denoted by the shaded region in Figure C-1. For thinner members, this crack control reinforcement will consist of two grids of reinforcing bars, one near each face. For thicker members, multiple grids of reinforcement through the thickness may be required in order to achieve a practical layout.

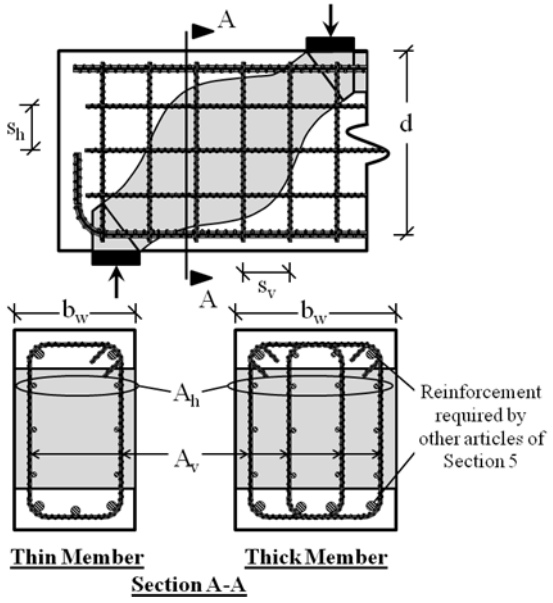

Figure C5.6.3.5-1: Distribution of crack control reinforcement in compression strut

A.1.3 Explanation for Proposed Changes

Currently, AASHTO LRFD (2008) is organized such that a STM is separated into its primary elements: struts, ties, and nodes and designed accordingly. The philosophy of the proposed method is slightly different in that the design of a strut and node-to-strut interface is not distinguished from one another. Stresses concentrate within the nodal regions, so the design of the node-to-strut interface indirectly accounts for the design of a strut. Also, a premature strut failure (strut-splitting) is prevented by providing the required crack control reinforcement. As a result, with the proposed changes to AASHTO LRFD (2008), strut-and-tie model design consists of the design of the nodal regions and the ties. Reference to the *design of a strut* and *design of a reinforced strut* has been removed to place the emphasis of a deep beam design on the critical nodal regions. A detailed explanation of the proposed limiting compressive stress (Equation 5.6.3.3.3-1) is presented in Section 5.2.

The truss model used to derive the newly proposed efficiency factors is presented in Figures 1 and 2. The purpose for including this model in the code is to provide explicit guidance for designers so that consistency can be achieved between their model and the model used to derive the new efficiency factors. As noted in Section 5.3, the dominant shear transfer mechanism for members loaded with an a/d ratio < 2 is consistent with a single-panel strut-and-tie model. It is not appropriate to use a multiple-panel model for beams with an a/d ratio < 2. This model does not capture the dominant shear transfer mechanism (Section 5.3).

It is proposed that reference to CTT nodal regions be removed from the AASHTO LRFD deep beam provisions. A CTT node is typically a smeared node and is not as critical as a singular node. The purpose for removing the provision is to place the emphasis of a deep beam design on the critical stresses in the singular, CCC and CCT nodal regions.

A.1.4 Summary

Proposed changes to the AASHTO LRFD Bridge Design Specifications are summarized in this Appendix. These changes are based on the findings of the current project. The primary changes to AASHTO LRFD are: (i) the new efficiency factors, (ii) the reorganization of the provisions to focus the design of a truss model on the nodal regions rather than the struts, and (iii) the clarified of the crack control reinforcement provision.

A design example of a multiple column bent is presented in Appendix B in order to illustrate the differences between the proposed provisions and the current AASHTO LRFD (2008) Bridge Design Specifications.

APPENDIX B. Design Example

B.1 Overview

The purpose of this case study is to compare the AASHTO LRFD (2007) and ACI 318-08 deep beam shear design provisions with the newly proposed deep beam design provisions presented in this report. One of several multiple-column bent caps that has experienced shear cracking problems in service (Section 1.2 and Figure B.1) was examined. The cracking was so extensive that a costly retrofit project was undertaken in order to strengthen all of the bent caps in the interchange. It is interesting to note that the bent caps were designed according to sectional shear provisions. No strut-and-tie modeling was performed for the original structure. The bent cap examined in this example contains several shear regions of interest, including: a D-region with an a/d ratio of 0.85; and a region with an a/d ratio of 2.05. As a result, this example can be viewed as multiple examples within one structure in which the design of D-regions with relatively low and high a/d ratios can be evaluated. In addition, the capacity of the portion with an a/d ratio of 2.05 can be analyzed according to sectional shear or strut-and-tie modeling provisions. Thus, the example problem also provides an opportunity to examine the discrepancy between sectional shear and STM provisions. In the example problem, strength and serviceability design provisions will be used.

Figure B.1: I-45 over Greens Road Bent Cap

The multiple-column bent cap to be investigated is used to support an 86-foot wide portion of a 180-foot wide roadway, comprised of nine 12-foot wide traffic lanes and one 25-foot wide *high occupancy vehicle* (HOV) lane. A layout of the bent cap is illustrated in Figure B.2. Cross-sectional details are presented for the two critical regions under investigation (a/d equal to 0.85 and 2.05).

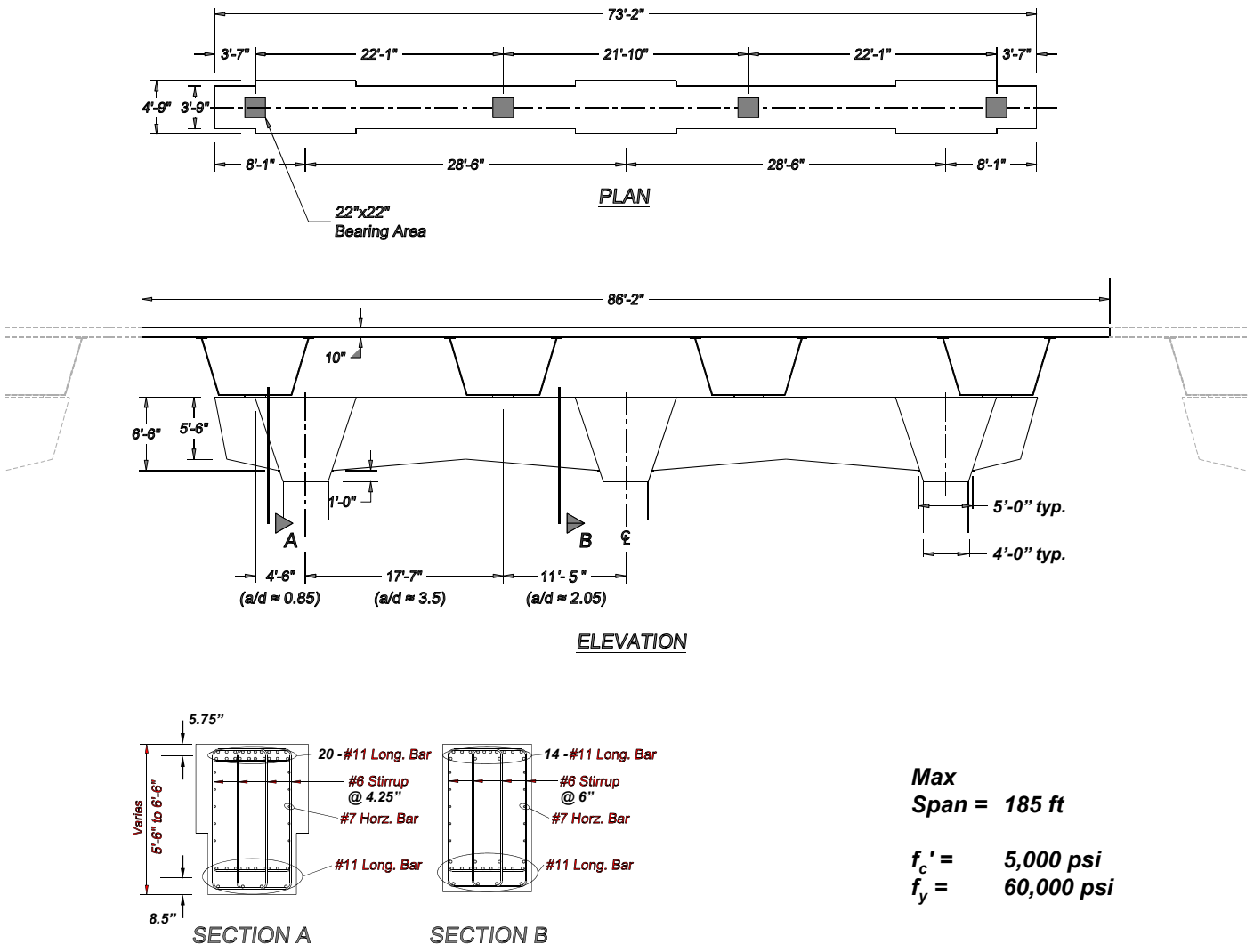

Figure B.2: Preliminary plan; elevation; and cross-sectional details at critical shear regions.

As mentioned, this cap exists in the field. The details of the original cross-section at the critical shear regions will be evaluated. Where necessary, the cross-section will be modified to meet the requirements of AASHTO LRFD (2008), ACI 318-08, and the proposed provisions. Afterwards, the cross-sections proportioned to satisfy the three sets of STM provisions are compared for both shear regions.

The design dead and live loadings applied to the bent cap from each steel box girder are presented as follows.

Dead Loads

The dead load includes the weight of the steel box girder, the concrete deck, and the self-weight of the bent cap. For simplicity, the self weight of the bent is distributed to the four girder locations in order to easily apply it to a truss model.

$P_{DL} = 792\ kip$

Live Loads + Impact

The live load includes lane load and truck load plus impact.

$P_{LL} = 280\ kip$

Service Load

The load case that is used to examine the amount of service load applied to the structure is the SERVICE I load case specified in AASHTO LRFD (2008).

$P_s = 792\ kip\ (DL) + 280\ kip\ (LL + Impact)$ $\quad \boldsymbol{P_s = 1072\ kip}$

Factored Load

Load factors specified by AASHTO LRFD (2008) and ACI 318-08 are slightly different from one another. For the purpose of comparison, the proposed methodology will use the same load factors as AASHTO LRFD (2008).

AASHTO LRFD: STRENGTH I

$P_u = 1.25 \cdot (792\ kip) + 1.75 \cdot (280\ kip)$ $\quad \boldsymbol{P_{u\_AASHTO} = 1480\ kip}$

ACI 318-08

$P_u = 1.2 \cdot (792\ kip) + 1.6 \cdot (280\ kip$ $\quad \boldsymbol{P_{u\_ACI} = 1398\ kip}$

Resistance Factors

Resistance factors specified by AASHTO LRFD (2007) and ACI 318-08 are slightly different from one another. For the purpose of comparison, the proposed methodology will use the same resistance factors as AASHTO LRFD.

AASHTO LRFD

Struts and Nodal Regions, $\boldsymbol{\varphi = 0.70}$

Steel Tie, $\boldsymbol{\varphi = 0.90}$

ACI 318-08

Struts and Nodal Regions, $\boldsymbol{\varphi = 0.75}$

Steel Tie, $\boldsymbol{\varphi = 0.90}$

B.2 Deep Beam Design

This bent example problem has three distinct shear regions. The first D-region has an a/d ratio of 0.85; this portion is designed using strut-and-tie provisions; as presented in Section B.2.2. The next shear region has an a/d ratio greater than 3.5 and would be designed using typical sectional shear provisions. Finally, the third region has an a/d ratio of approximately 2.05 (the a/d ratio varies between 1.9 and 2.1 depending where the depth is measured). This portion of the beam is considered to be in the transition zone where the shear behavior of a beam converts from sectional to deep beam shear. Therefore, this portion of the structure could be designed using either a strut-and-tie model or typical sectional shear provisions. The STM design for this region is presented in Section B.2.3 and the sectional shear design for this region is presented in Section B.3.

When designing a D-region using a strut-and-tie model, the first step is to determine the configuration of the truss model and resulting forces in the truss elements. A preliminary truss model is determined as follows.

B.2.1 Determination of Preliminary Truss Model

The structure illustrated in Figure B.2 is modeled as a truss with compressive struts and tensile ties and presented in Figure B.3. The AASHTO LRFD (2007) factored load, P_{u_AASHTO}, is applied to the structure at each girder support. Only one half of the structure is presented; the bent is symmetric about its centerline, therefore, the loading and proportions of the other half are identical.

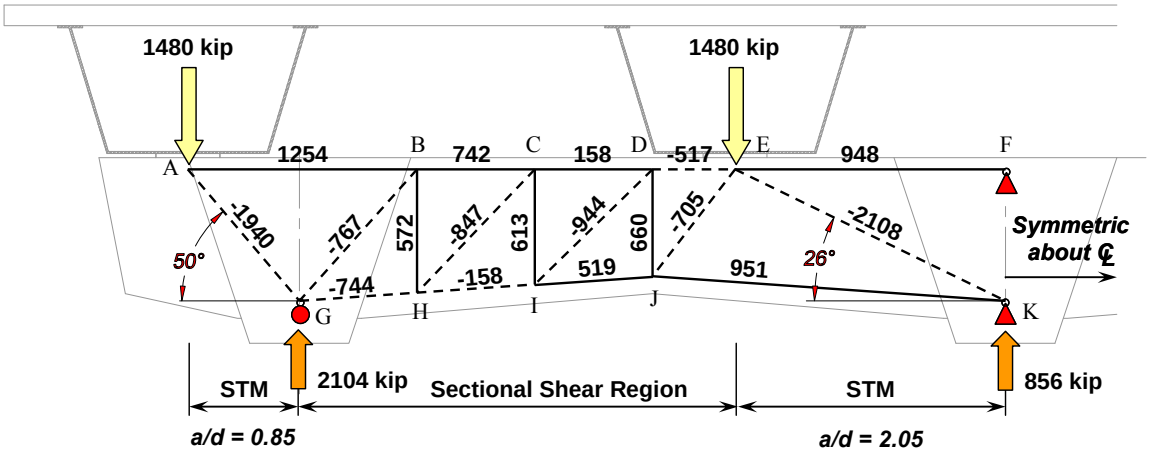

Figure B.3: Strut-and-tie model with AASHTO LRFD (2008) factored loads.

According to the proposed provisions (Appendix A), a deep beam region can be modeled with a single panel strut provided the a/d ratio is less than 2. Similarly, according to ACI 318-08, a single-panel strut may be used provided the angle of inclination is greater than 25-degrees; AASHTO LRFD (2008) does not limit a strut's angle of inclination. As a result, both D-regions are shown in Figure B.3 as single compression struts. While the a/d ratio of the interior D-region slightly exceeds 2, it is close enough to use either sectional shear or STM provisions. Also, it is

necessary to model the sectional shear portion of the bent as part of the overall truss in order to adequately represent the entire structure. Even though this portion of the structure is designed using sectional shear provisions, it is necessary to model the entire bent so that the correct quantity of shear is transferred to Strut EK.

Typically, the top and bottom chord of a STM is positioned based on the location of the centroid of the longitudinal reinforcement or the depth of compression zone depending on whether the chord resists tension or compression, respectively. In a continuous element, the top and bottom chord resist both tension and compression. For the sake of simplicity, both of their locations are based on the centroid of the longitudinal reinforcement. For this example problem, the centroid of the longitudinal reinforcement is, on average, taken to be 5.75-inches below the top surface and 8.5-inches above the bottom surface. These dimensions result in heights of the back face of the nodes of 11.5" and 17," respectively.

B.2.2 Shear Region with an a/d Ratio Equal to 0.85

A close-up of the critical Strut AG and respective nodal zones is presented to scale in Figure B.4. The dimensions of the node-to-strut interfaces (24.6" and 41.9" in Figure B.4) were calculated using the definition provided in Figure 5.6.3.2-2 in Appendix A.

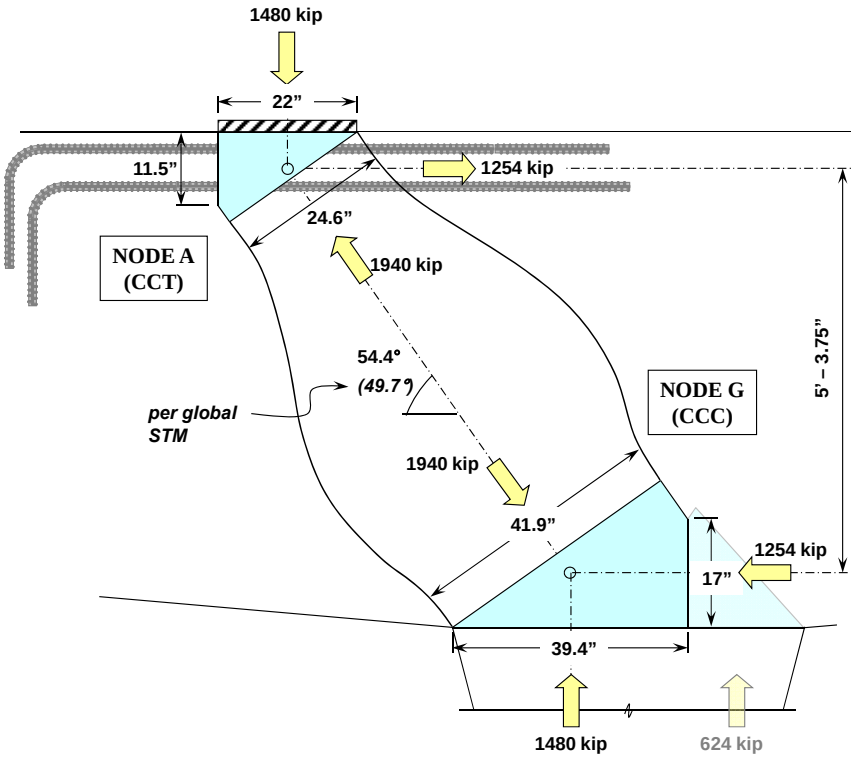

Figure B.4: Critical strut in region with a/d equal to 0.85 (AASHTO LRFD factored loads).

The length of Node G is proportioned based on the amount of force that is transferred to the near support. As a result, the angle of inclination of Strut AG shown in Figure B.4 is slightly

different from the angle in the global model shown in Figure B.3 (54.4 versus 49.7-degrees, respectively). If the global truss model were to be updated with this new angle, then the forces in the elements would change slightly. However, it is common practice to ignore this slight discrepancy. Therefore, the truss elements shown in Figure B.4 are designed for the forces presented in Figure B.3.

In order to design Strut AG, the allowable capacity of each nodal face (i.e. bearing face, back face, and strut-to-node interface) must be greater than the force applied to the boundary. This procedure is presented for the proposed method, ACI 318-08, and AASHTO LRFD (2008) provisions in the following sections.

Design of Region with a/d = 0.85: Proposed Method

Node A (CCT Node)

The back face of node A must resist the bonding stresses developed by the anchorage of the tie. For this type of condition, stresses at the back face of a CCT node are not critical. The first step of the proposed method is to determine the triaxial confinement factor, *m*, as illustrated in Figure B.5.

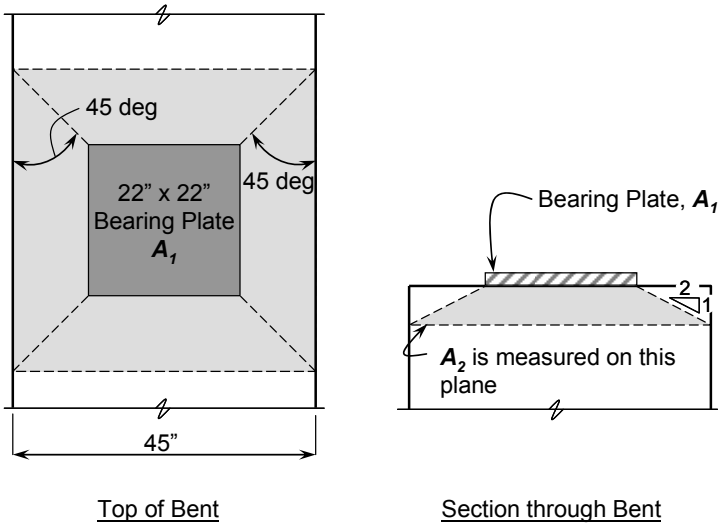

Figure B.5: Determination of Triaxial Confinement Factor

Triaxial Confinement Factor: $m = \sqrt{(45in)^2 / (22in)^2} = 2.04 \le 2$

BEARING FACE

Factored Load: $F_u = 1480\ kip$

Efficiency: $v = 0.70$

Concrete Capacity: $f_{cu} = m \cdot v \cdot f_c' = (2) \cdot (0.7) \cdot (5\ ksi) = 7.0\ ksi$

$\varphi \cdot F_n = (0.7) \cdot (7.0\ ksi) \cdot (22\ in.) \cdot (22\ in.)$

$= 2372\ kip > 1480\ kip$ ***OK***

STRUT-TO-NODE INTERFACE

Factored Load: $F_u = 1940\ kip$

Efficiency: $0.65 \le \left(0.85 - {5ksi}/{20ksi}\right) \le 0.45 = 0.60$

Concrete Capacity: $f_{cu} = m \cdot v \cdot f_c' = (2) \cdot (0.60) \cdot (5\ ksi) = 6.0\ ksi$

$\varphi \cdot F_n = (0.7) \cdot (6.0\ ksi) \cdot (24.6\ in.) \cdot (22\ in.)$

$= 2273\ kip > 1940\ kip$ ***OK***

Thus, according to the proposed procedure, the strength of Node A is sufficient to resist the applied forces. The capacity of Node G is determined as follows. Node G is not triaxially confined, so the confinement factor, *m*, is equal to one.

Node G (CCC Node)

Triaxial Confinement Factor: $m = 1.0$

BEARING FACE

Factored Load: $F_u = 1480\ kip$

Efficiency: $v = 0.85$

Concrete Capacity: $f_{cu} = m \cdot v \cdot f_c' = (1) \cdot (0.85) \cdot (5\ ksi) = 4.3\ ksi$

$\varphi \cdot F_n = (0.7) \cdot (4.3\ ksi) \cdot (39.4\ in.) \cdot (45\ in.)$

$= 5337\ kip > 1480\ kip$ ***OK***

BACK FACE

Factored Load: $F_u = 1254\ kip$

Efficiency: $v = 0.85$

Concrete Capacity: $f_{cu} = m \cdot v \cdot f_c' = (1) \cdot (0.85) \cdot (5\ ksi) = 4.3\ ksi$

$\varphi \cdot F_n = (0.7) \cdot (4.3\ ksi) \cdot (17\ in.) \cdot (45\ in.)$

$= 2303\ kip > 1254\ kip$ ***OK***

STRUT-TO-NODE INTERFACE

Factored Load: $F_u = 1940\ kip$

Efficiency: $0.65 \le \left(0.85 - {5ksi}/{20ksi}\right) \le 0.45 = 0.60$

Concrete Capacity: $f_{cu} = m \cdot v \cdot f_c' = (1) \cdot (0.6) \cdot (5\ ksi) = 3.0\ ksi$

$\varphi \cdot F_n = (0.7) \cdot (3.0\ ksi) \cdot (41.9\ in.) \cdot (45\ in.)$

$= 3960\ kip > 1940$ ***OK***

Thus, according to the proposed procedure, the strength of Node G is sufficient to resist the applied forces. The capacity of Tie AB must also be evaluated.

TIE AB

Factored Load: $F_u = 1254\ kip$

Efficiency: $v = 1.0$

Tie Capacity: $(1.0) \cdot (60ksi) \cdot (20) \cdot (1.56\ in^2) = 1872\ kip$

$\varphi \cdot F_n = (0.9) \cdot (1872\ kip)$

$= 1685\ kip > 1254\ kip$ ***OK***

Thus, the capacity of Tie AB is adequate. Verifying the tie capacity is essentially the same procedure for all three provisions. Therefore, this check is not repeated for other provisions.

Minimum Transverse Reinforcement

The original cross-section (a/d = 0.85) had #6 4-legged stirrups at 4¼" and #7 horizontal bars at approximately 9" for web reinforcement. The corresponding reinforcement ratios in each direction are calculated as follows:

$$\rho_v = \frac{A_v}{b_w s_v} \quad \rightarrow \quad 4\cdot(0.44\ in^2)/\ (45\ in\cdot 4¼\ in) = 0.0092$$

$$\rho_h = \frac{A_h}{b_w s_h} \quad \rightarrow \quad 2\cdot(0.60\ in^2)/\ (45\ in\cdot 9\ in) = 0.0029$$

The original cross-section essentially meets the minimum web reinforcement requirements of the proposed provisions (5.6.3.5 in Appendix A). The amount of stirrups exceeds the minimum by a factor of 3. The quantity of horizontal reinforcement is slightly less than the required 0.3%. If only the minimum amount of web reinforcement was provided, the web reinforcement would be as follows:

$$A_v = 0.003 \cdot b_w \cdot s_1 \quad \rightarrow \quad 2\cdot(0.44\ in^2) = 0.003\cdot(45in)\cdot s_1$$
$$s_1 = 6.5in$$
$$A_{vh} = 0.003 \cdot b_w \cdot s_2 \quad \rightarrow \quad 2\cdot(0.60\ in^2) = 0.003\cdot(45in)\cdot s_2$$
$$s_2 = 8.9in$$

This reinforcement equates to #6 vertical stirrups at 6.5-inches and #7 horizontal bars at 8.5-inches on center. The minimum web reinforcement will be shown in the cross-section designed with the proposed STM provisions for comparison with the cross-sections designed according to the other specifications. However, it is important to note that providing web reinforcement in excess of the minimum (as done in the original cross-section) is encouraged, albeit not required. Additional web reinforcement will reduce the width of diagonal cracks (with diminishing returns) and will provide additional redistribution capacity to the member.

A summary of the preceding design is presented in Figure B.7 along with the other provisions. Next, Strut AG and respective nodal regions are designed according to ACI 318-08.

Design of Region with a/d = 0.85: ACI 318-08

Check the ACI 318-08, §A.3.3.1 requirement for an adequately reinforced strut (discussed in Chapter 2, Equation 2-4).

$$\sum \frac{A_{si}}{b_s \cdot s_i} \sin\alpha_i = \left(\frac{4\cdot 0.44in^2}{45in\cdot 4.25in}\right)\sin 35.6° + \left(\frac{2\cdot 0.60in^2}{45in\cdot 8.6in}\right)\sin 54.4°$$
$$= 0.008 > 0.003\ \textbf{\textit{OK}}$$

Thus, according to ACI 318-08 §A3.2.2, the strut is adequately reinforced. As a result, a higher strut efficiency factor of 0.75 may be used.

Refer to Figure B.4 for preliminary strut proportions and applied loads. The ACI 318-08 load factors are lower than those applied to the STM presented in Figure B.3; as a result, the loads shown are multiplied by a factor of 0.945 (i.e. $P_{u\_ACI}/P_{u\_AASHTO} = 1398/1480 = 0.945$).

Node A (CCT Node)

BEARING FACE

Factored Load: $F_u = 1398$ kip

Efficiency: $\beta = 0.80$

Concrete Capacity: $f_{cu} = 0.85 \cdot \beta \cdot f_c' = (0.85) \cdot (0.8) \cdot (5 \text{ ksi}) = 3.4 \text{ ksi}$

$\varphi \cdot F_n = (0.75) \cdot (3.4 \text{ ksi}) \cdot (22 \text{ in.}) \cdot (22 \text{ in.})$

$= 1234 \text{ kip} < 1398 \text{ kip}$ ***NG!***

BACK FACE

Factored Load: $F_u = 1185$ kip

Efficiency: $\beta = 0.80$

Concrete Capacity: $f_{cu} = 0.85 \cdot \beta \cdot f_c' = (0.85) \cdot (0.8) \cdot (5 \text{ ksi}) = 3.4 \text{ ksi}$

$\varphi \cdot F_n = (0.75) \cdot (3.4 \text{ ksi}) \cdot (11.5 \text{ in.}) \cdot (22 \text{ in.})$

$= 645 \text{ kip} < 1185 \text{ kip}$ ***NG!***

STRUT-TO-NODE INTERFACE

Factored Load: $F_u = 1833$ kip

Efficiency: $\beta = 0.75$

Concrete Capacity: $f_{cu} = 0.85 \cdot \beta \cdot f_c' = (0.85) \cdot (0.75) \cdot (5 \text{ ksi}) = 3.2 \text{ ksi}$

$\varphi \cdot F_n = (0.75) \cdot (3.2 \text{ ksi}) \cdot (24.6 \text{ in.}) \cdot (22 \text{ in.})$

$= 1299 \text{ kip} < 1833 \text{ kip}$ ***NG!***

Thus, the capacity of Node A does not meet the requirements of ACI 318-08. By inspection, Node A is more critical than Node G. The most critical location of Node A is its back face. Therefore, the bearing plates and beam must be resized in order to provide the back face of Node A with sufficient capacity.

Typically, if a designer wishes to increase the capacity of a truss element, the simplest way is to increase the size of the bearing plate. However, there are realistic limits to the maximum size of a plate that can be provided. For this example, a 30"x30" bearing plate is considered to be a reasonable maximum size. It follows that increasing the size of the bearing plate to 30"x30" does not sufficiently increase the capacity of Strut AG in order for it to meet the requirements of ACI 318-08.

Based on the ACI 318-08 STM provisions, additional shear capacity can be attained by increasing the depth of the bent; increasing the compressive strength of concrete; providing supplementary longitudinal reinforcement in order to increase the assumed height of the back face of a CCT node; or by a combination of all three of these methods.

Increasing the compressive strength of concrete can be a very simple way to increase the capacity of a structure. However, TxDOT has expressed concern about maximum curing temperature in regard to concrete durability. Thus, it is believed to be impractical to exceed 5,000-psi compressive strength while complying with the maximum temperature limits of the TxDOT 2004 Specifications. Also, for the purpose of comparison among different design provisions, the compressive strength of concrete is constantly maintained to be 5,000-psi.

For the purpose of this example problem, additional capacity is acquired by increasing the depth of the bent and/or nodal region. Most likely, the solutions determined in this example would vary from those selected in a design office given the many external factors involved such as: site restrictions, construction costs, and personal preferences. Nonetheless, the conclusions formed from comparing the provisions to one another will remain valid regardless of differences in optimization preferences.

In order for Strut AG (Figure B.4) to meet the requirements of ACI 318-08, its overall depth must be increased by 18-inches and the depth of the back face of Node A must be increased by 2.5-inches. As a result, the depth of the global model shown in Figure B.3 is increased by 16.75-inches (18" – $2.5"/2$ = 16.75") and the forces in the truss members are recalculated accordingly. The strut proportions and loads associated with these increases are illustrated in Figure B-6.

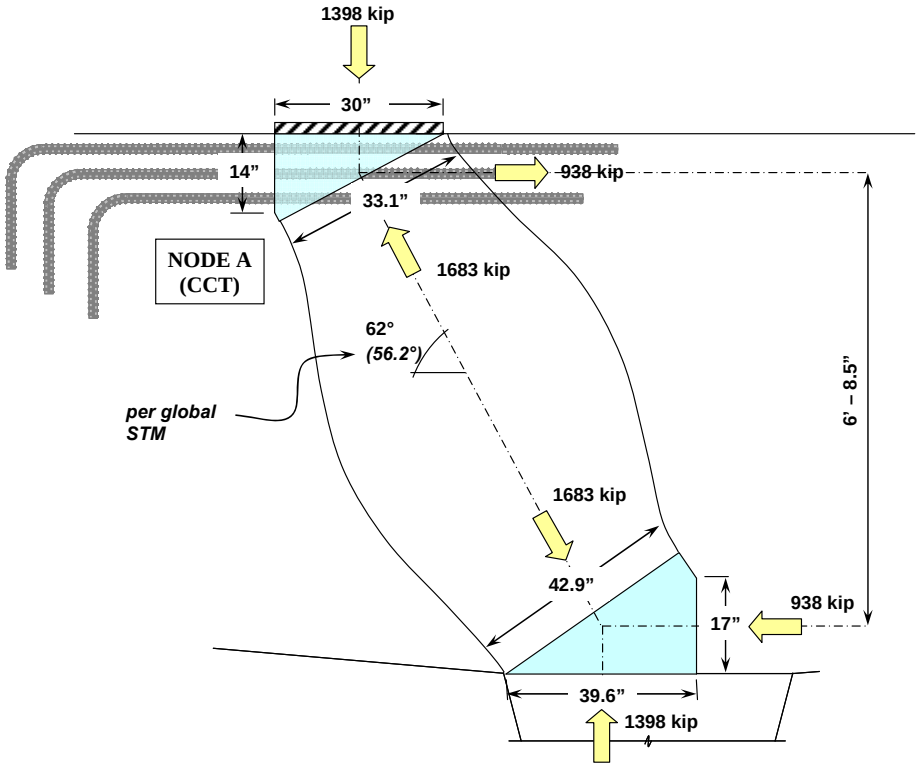

Figure B-6. Strut proportions associated with an increase in overall depth of 18-inches and increase in back face of Node A of 2.5-inches (ACI 318-08 load factors)

The capacity of the critical back face of Node A is calculated as follows according to ACI 318-08.

BACK FACE OF NODE A, PER FIGURE B-6

Factored Load: $F_u = 938\ kip$

Efficiency: $\beta = 0.80$

Concrete Capacity: $f_{cu} = 0.85 \cdot \beta \cdot f_c' = (0.85) \cdot (0.8) \cdot (5\ ksi) = 3.4\ ksi$

$\varphi \cdot F_n = (0.75) \cdot (3.4\ ksi) \cdot (14\ in.) \cdot (30\ in.)$

$= 1071\ kip > 938\ kip$ ***OK***

Thus, the capacity of the bent illustrated in Figure B-6 meets the requirements of ACI 318-08.

Minimum Transverse Reinforcement

ACI 318-08 does not require a minimum amount of transverse reinforcement. However, in order to use the higher strut efficiency factor, the following minimum amount of reinforcement must be provided:

$$\sum \frac{A_{si}}{b_s \cdot s_i} \sin \alpha_i > 0.003$$

If it is assumed that the vertical and horizontal reinforcement ratios are identical,

$$\rho \cdot \sin 28° + \rho \cdot \sin 62° > 0.003$$

Thus,

$$\rho_v = \rho_{vh} > 0.0022$$

Provide #5 vertical stirrups at 6-inches and #6 horizontal bars at 8.5-inches on center.

A summary of the preceding ACI 318-08 design is presented in Figure B.7 along with the other provisions. Next, Strut AG and respective nodal regions are designed according to AASHTO LRFD (2008).

Design of Region with a/d = 0.85: AASHTO LRFD

Refer to Figure B.4 for preliminary strut and nodal proportions, and respective applied loads.

Node A (CCT Node)

BEARING FACE

Factored Load: $F_u = 1480\ kip$

Efficiency: $v = 0.75$

Concrete Capacity: $f_{cu} = v \cdot f_c' = (0.75) \cdot (5\ ksi) = 3.8\ ksi$

$\varphi \cdot F_n = (0.7) \cdot (3.8\ ksi) \cdot (22\ in.) \cdot (22\ in.)$

$= 1287\ kip < 1480\ kip$ ***NG!***

BACK FACE

Factored Load: $F_u = 1254\ kip$

Efficiency: $v = 0.75$

Concrete Capacity: $f_{cu} = v \cdot f_c' = (0.75) \cdot (5\ ksi) = 3.8\ ksi$

$\varphi \cdot F_n = (0.7) \cdot (3.8\ ksi) \cdot (11.5\ in.) \cdot (22\ in.)$

$= 673\ kip < 1254\ kip$ ***NG!***

STRUT-TO-NODE INTERFACE

Factored Load: $F_u = 1940\ kip$

Solve set of four equations simultaneously:

Concrete Efficiency: $\nu = \frac{1}{0.8 + 170 \cdot \varepsilon_1} \le 0.85 \;=\; 0.76$

Tensile Strain Term: $\varepsilon_1 = \varepsilon_s + (\varepsilon_s + 0.002)\cot^2 54.4° \;=\; 0.0030$

Tie Tensile Strain: $\varepsilon_s = \frac{F_n \cdot \cos 54.4°}{(20 \cdot 1.56 in^2) \cdot (29{,}000 ksi)} \;= 0.0013$

Strength of Nodal Face: $F_n = \nu \cdot (5\ ksi)(24.6\ in.)(22\ in.) = 2058\ kip$

$\varphi \cdot F_n = (0.7)(2058\ kip)$

$= 1441\ kip < 1940\ kip$ ***NG!***

By inspection, Node A is more critical than Node G. The most critical location of Node A is its back face. Therefore, the bearing plates and beam are proportioned such that Node A meets the requirements of AASHTO LRFD (2008). For the purpose of comparison, the nominal capacity of Node A is determined for the same strut proportions required by ACI 318-08 (Figure B-6).

BACK FACE OF NODE A, PER FIGURE B-6

Factored Load: $F_u = 993\ kip$

Efficiency: $\nu = 0.75$

Concrete Capacity: $f_{cu} = \nu \cdot f_c' = (0.75) \cdot (5\ ksi) = 3.8\ ksi$

$\varphi \cdot F_n = (0.7) \cdot (3.8\ ksi) \cdot (14\ in.) \cdot (30\ in.)$

$= 1117\ kip > 993\ kip$ ***OK***

Thus, for an a/d ratio of 0.85, the requirements of AASHTO LRFD (2008) are similar to ACI 318-08.

Minimum Transverse Reinforcement

AASHTO LRFD requires a vertical and horizontal reinforcement ratio of 0.3% of the gross area for the purpose of controlling crack widths. So, based on this requirement, provide #6 vertical stirrups at 6.5-inches and eighteen #7 horizontal bars distributed evenly across the height of the section (resulting spacing is 5.75-inches).

Comparison of Design Provisions for Shear Region with a/d = 0.85

A comparison between the results obtained from the three design methodologies for the D-region with an a/d ratio equal to 0.85 (Figure B.2, Cross-Section A) is presented in Figure B.7.

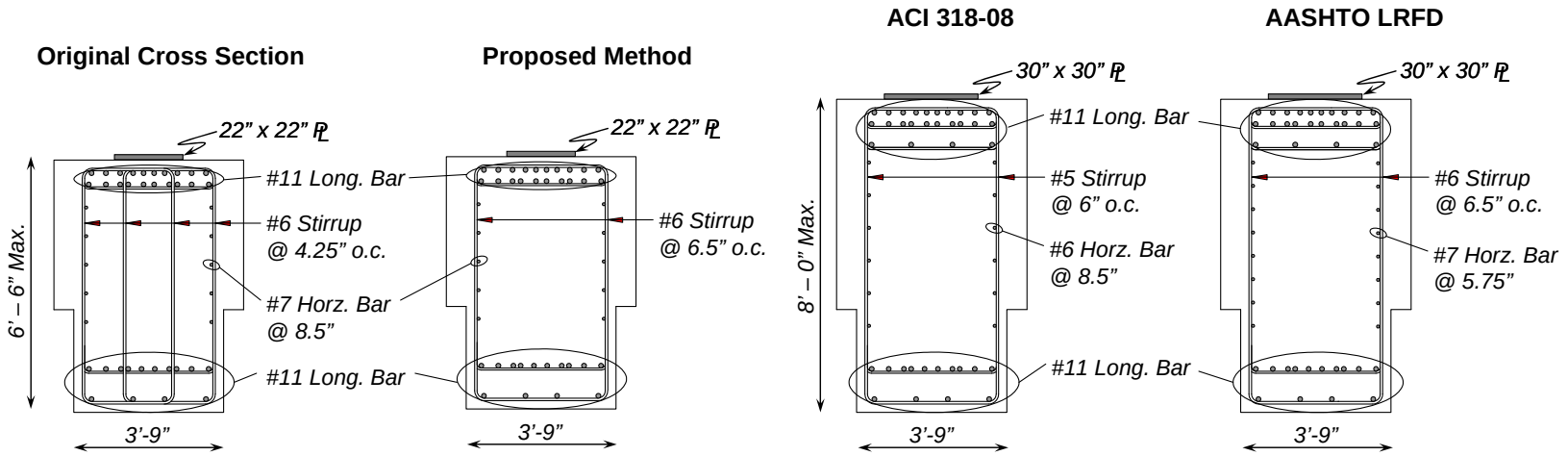

Increase Plate to 30"; Height by 18"; Depth of Node by 2.5"

Ratio of Capacity over Applied Load, $\phi V_n / V_u$

Proposed = 1.17	**<u>Proposed = 1.17</u>**	**<u>ACI 318 = 1.14</u>**	**<u>AASHTO = 1.12</u>**
ACI 318 = 0.54	**ACI 318 = 0.54**	**Proposed = 1.86**	**Proposed = 1.86**
AASHTO = 0.54	**AASHTO = 0.54**	**AASHTO = 1.12**	**ACI 318 = 1.14**

Figure B.7: Comparison of required cross-section per the proposed method, ACI 318-08, and AASHTO LRFD: a/d ratio = 0.85.

Based on a comparison of the three provisions, the following observations can be made:

The proposed method results in a much higher nominal capacity than those obtained by using the ACI 318-08 and AASHTO LRFD (2008) provisions. As a result, the required cross-section is significantly smaller. This is primarily attributed to the fact that the proposed provisions recognize that the back face check is overly conservative when the applied stress is attributed to bond of the anchored reinforcement. The capacity of the structure as determined by the ACI 318-08 and AASHTO LRFD (2008) provisions is controlled by the capacity at the back face of the CCT node. According to the proposed provisions, provided the tie is properly anchored behind the node, the stress check at this nodal face is not critical.

Also, the smaller bearing plate (22"x22") did not adversely affect the nominal capacity of the structure. The proposed method considers the increase in concrete compressive strength provided by triaxial confinement. Alternatively, the ACI 318-08 and AASHTO LRFD (2008) provisions do not consider the increase provided by triaxial confinement, so the bearing plate dimensions had to be increased to the maximum possible size (i.e. 30"x30").

Finally, the minimum amount of transverse reinforcement required by the proposed method, ACI 318-08 and the AASHTO LRFD (2008) specifications is significantly less than the amount contained in the existing bent. However, the fact that the structure contains an amount in excess of the minimum is not a deficiency. On the contrary, additional transverse reinforcement will provide for narrower crack widths and better distribution of cracks upon diagonal cracking with some diminishing returns. Next, the bent proportions and reinforcement ratio are discussed with regard to its anticipated serviceability performance.

Serviceability Behavior for Region with a/d = 0.85

By comparing the amount of shear due to service loads to the cracking strength of concrete, it is possible to estimate the likelihood that the structure will crack under service loads. The shear due to service loads for the portion of the bent with an a/d ratio of 0.85 is as follows:

V_{srv} ***= 1072 kip***

As presented in Section 5.4.4, for an a/d ratio of 0.85, the shear at which the first diagonal crack will form can estimated as the following:

$$V_{cr} = (6.5 - 3a/d)\sqrt{f_c'} \cdot b_w \cdot d = 3.95\sqrt{5000}(45in)(69.5in) \quad \textbf{= 874 kip}$$

As a result, with the original cross-section, it is likely that diagonal cracks will form under the application of the full service loads. Specifically, the first diagonal crack is expected to form under the full DL and 29-percent of the LL (792 + 0.29*280 = 874 kips). To reduce the likelihood of diagonal cracking under full service loads, the size of the cross-section can be increased (increasing 'd' will also reduce the a/d ratio) or a higher strength concrete can be specified. Minor diagonal cracking (single, narrow crack) was detected in this region of the original structure.

B.2.3 Shear Region with an a/d Ratio Equal to 2.05

Next, the nominal capacity determined by the proposed provisions is investigated for the deep beam portion of the bent with an a/d ratio equal to 2.05. Since the a/d ratio for this portion

of the structure slightly exceeds 2, a sectional analysis would be recommended according to ACI 318-08 and AASTHO LRFD 2007. However, as shown in Section 5.3, the transition between deep beam and sectional beam behavior is gradual. Thus, a STM analysis at this a/d ratio should be performed and compared with a sectional analysis. A close-up of the critical strut proportions and respective nodal zones is presented to scale in Figure B-8. Note, the vertical reactions are slightly different from one another due to the inclined tie at Node K.

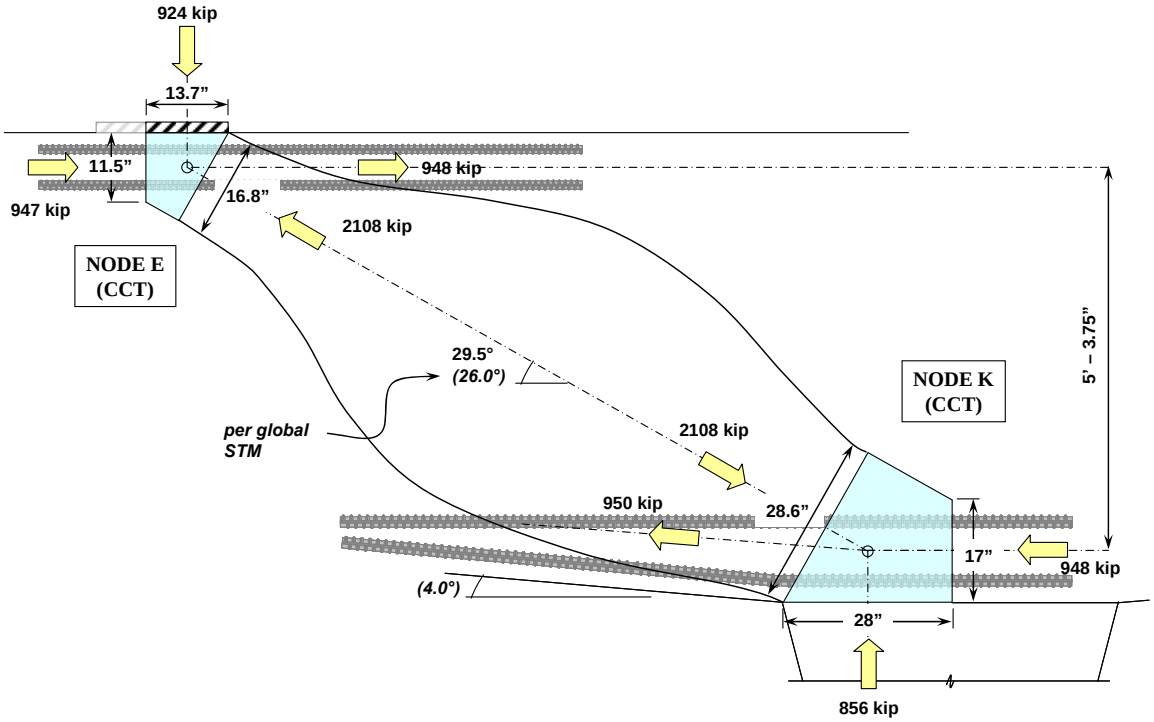

Figure B-8. Critical strut in region with a/d = 2.05.

The length of Nodes E and K are proportioned based on the amount of force that is transferred to the near support. As a result, the angle of inclination of the strut is slightly changed from the global model shown in Figure B.3. However, forces from the global model are not updated to account for the slight change in strut angle. This method is consistent with standard design practice.

Nodes E and K are classified as CCT nodes because of the presence of a horizontal tie to the right of Node E and to the left of Node K. Tensile stresses in the tie must be developed in the nodal region to some degree. However, the stress condition at the back face of Nodes E and K is much more complicated because of the compressive force that is applied from an additional strut framing into each node. These compressive stresses are not attributed to the bonding stress of an anchored tie; therefore, they must be applied to the back face and the nodes must be designed accordingly. As a result, the allowable capacity of Nodes E and K are verified as follows.

In order to design this portion of the structure, the allowable capacity of each nodal face (i.e. bearing face, back face, and strut-to-node interface) must be greater than the applied force.

This procedure is presented for the proposed method, ACI 318-08 and the AASHTO LRFD (2008) provisions as follows.

Design of Region with a/d Ratio Equal to 2.05: Proposed Method

Node E (CCT Node)

Triaxial Confinement Factor: $m = \sqrt{(45in)^2 / (22in)^2} = 2.04 \le 2$

BEARING FACE

Factored Load: 924 kip

Efficiency: $v = 0.70$

Concrete Capacity: $f_{cu} = m \cdot v \cdot f_c' = (2) \cdot (0.7) \cdot (5\ ksi) = 7.0\ ksi$

$\varphi \cdot F_n = (0.7) \cdot (7.0\ ksi) \cdot (13.7\ in.) \cdot (22\ in.)$

$= 1477\ kip > 924\ kip$ ***OK***

STRUT-TO-NODE INTERFACE

Factored Load: 2108 kip

Efficiency: $0.65 \le \left(0.85 - 5ksi / 20ksi\right) \le 0.45 = 0.60$

Concrete Capacity: $f_{cu} = m \cdot v \cdot f_c' = (2) \cdot (0.60) \cdot (5\ ksi) = 6.0\ ksi$

$\varphi \cdot F_n = (0.7) \cdot (6.0\ ksi) \cdot (16.8\ in.) \cdot (22\ in.)$

$= 1552\ kip < 2108\ kip$ ***NG!***

BACK FACE

Factored Load: 947 kip

Efficiency: $v = 0.70$

Concrete Capacity: $f_{cu} = mvf_c' = (2)(0.70)(5\ ksi) = 7.0\ ksi$

$\varphi F_n = (0.7)(7.0\ ksi)(11.5\ in.)(22\ in.)$

$= 1240\ kip > 947\ kip$ ***OK***

Node K (CCT Node)

Triaxial Confinement Factor: $m = 1.0$

BEARING FACE

Factored Load: 857 kip

Efficiency: $v = 0.70$

Concrete Capacity: $f_{cu} = m \cdot v \cdot f_c' = (1) \cdot (0.70) \cdot (5\ ksi) = 3.5\ ksi$

$\varphi \cdot F_n = (0.7) \cdot (3.5\ ksi) \cdot (28\ in.) \cdot (45\ in.)$

$= 3087\ kip > 857\ kip$ ***OK***

STRUT-TO-NODE INTERFACE

Factored Load: 2108 kip

Efficiency: $0.65 \le \left(0.85 - 5ksi / 20ksi\right) \le 0.45 = 0.60$

Concrete Capacity: $f_{cu} = m \cdot v \cdot f_c' = (1) \cdot (0.6) \cdot (5\ ksi) = 3.0\ ksi$

$\varphi \cdot F_n = (0.7) \cdot (3.0\ ksi) \cdot (28.6\ in.) \cdot (45\ in.)$

$= 2703\ kip > 2108$ ***OK***

BACK FACE

Factored Load: 948 kip

Efficiency: $v = 0.70$

Concrete Capacity: $f_{cu} = mvf_c' = (1)(0.70)(5\ ksi) = 3.5\ ksi$

$\varphi F_n = (0.7)(3.5\ ksi)(17\ in.)(45\ in.)$

$= 1874\ kip > 948\ kip$ ***OK***

Tie EF

Factored Load: $F_u = 948\ kip$

Efficiency: $v = 1.0$

Tie Capacity: $(1.0)\cdot(60ksi)\cdot(14)\cdot(1.56\ in^2) = 1310\ kip$

$\varphi\cdot F_n = (0.9)\cdot(1310\ kip)$

$= 1179\ kip > 948\ kip$ ***OK***

Thus, according to the proposed procedure, the stress check at the strut-to-node interface at Node E is not satisfied. To increase the capacity, the beam width and the size of the bearing pad can be increased. Also, the depth of the member can be increased which will decrease the force in the inclined strut. All three of these options were used. The size of the bearing plate was increased to 30"x30." This was considered to be a reasonable maximum for the size of the bearing plate. Also, the beam width and beam depth were increased by 6-inches. With these changes, the node-to-strut interface at Node E has sufficient capacity. The updated strut proportions and forces are illustrated in Figure B-9.

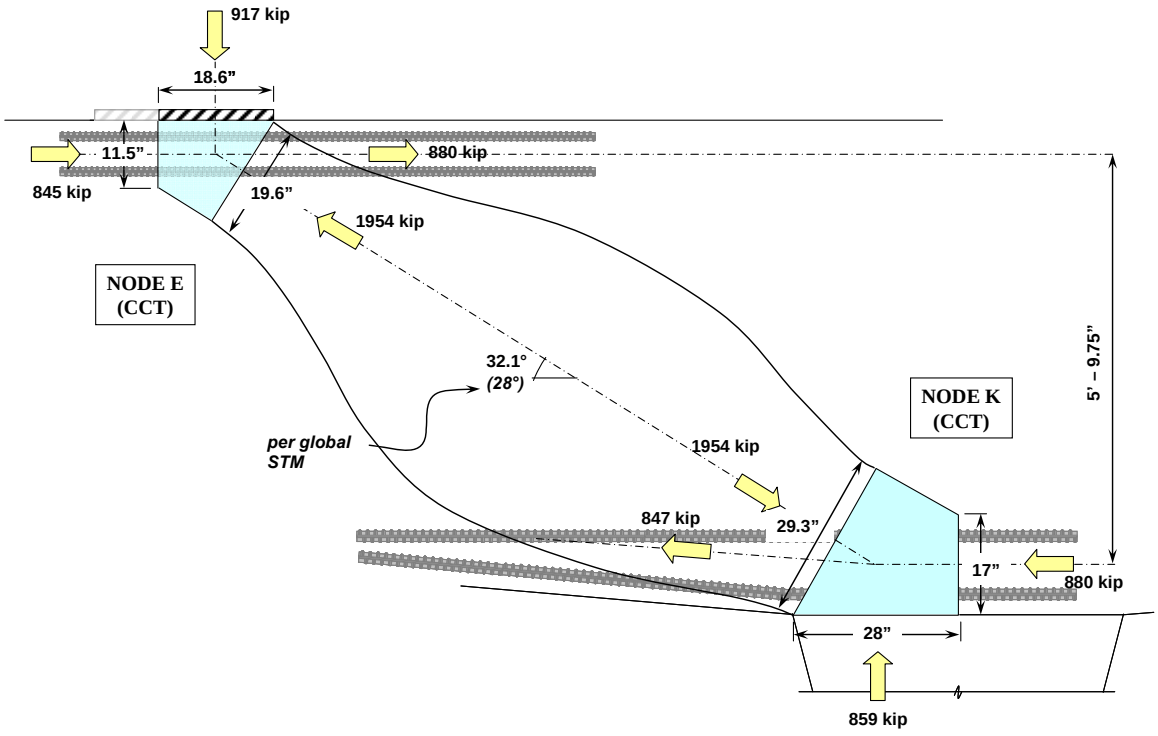

Figure B-9: Strut proportions and forces associated with a 6-inch increase in depth of bent.

NODE E STRUT-TO-NODE INTERFACE, PER FIGURE B-9

Factored Load: 1954 kip

Confinement Factor: $m = \sqrt{(51in)^2 / (30in)^2} = 1.7$

Efficiency: $0.65 \le \left(0.85 - 5ksi/20ksi\right) \le 0.45 = 0.60$

Concrete Capacity: $f_{cu} = m \cdot v \cdot f_c' = (1.7) \cdot (0.60) \cdot (5\ ksi) = 5.1\ ksi$

$\varphi \cdot F_n = (0.7) \cdot (5.1\ ksi) \cdot (19.6\ in.) \cdot (30\ in.)$

$= 2099\ kip > 1954\ kip$ ***OK***

Thus, the capacity of strut illustrated in Figure B-9 meets the requirements of the proposed method.

Minimum Transverse Reinforcement

As shown in the previous section, the size of the original cross-section (a/d = 2.05) was not sufficient according to the proposed STM provisions. The minimum reinforcement required to ensure the satisfactory serviceability performance of the new section would be as follows:

$A_v = 0.003 \cdot b_w \cdot s_1 \quad \rightarrow \quad 2 \cdot (0.44\ in^2) = 0.003 \cdot (51in) \cdot s_1$

$s_1 = 5.75in$

$A_{vh} = 0.003 \cdot b_w \cdot s_2 \quad \rightarrow \quad 2 \cdot (0.60\ in^2) = 0.003 \cdot (51in) \cdot s_2$

$s_2 = 7.8in$

This reinforcement equates #6 vertical stirrups at 5.5-inches and #7 horizontal bars at 7.5-inches on center. The reinforcement should be distributed as shown in Article 5.6.3.5 of Appendix A.

A summary of the preceding design is presented in Figure B.12 along with the other provisions. Next, Strut EK and respective nodal regions are designed according to ACI 318-08.

Design of Region with a/d Ratio Equal to 2.05: ACI 318-08

Refer to Figure B-8 for preliminary forces, strut, and nodal dimensions. By inspection, Node E is the most critical nodal zone. Therefore, the design of Strut EK is based on the design of Node E. Recall, that the ACI 318-08 load factors are less than those presented in Figure B-8. Therefore, all of the load values are multiplied by a factor of 0.945 (i.e. $P_{u\_ACI}/P_{u\_AASHTO} = 1398/1480 = 0.945$).

Node E (CCT Node)

BEARING FACE

Factored Load: $F_u = 873\ kip$

Efficiency: $\beta = 0.80$

Concrete Capacity: $f_{cu} = 0.85 \cdot \beta \cdot f_c' = (0.85) \cdot (0.8) \cdot (5\ ksi) = 3.4\ ksi$

$\varphi \cdot F_n = (0.75) \cdot (3.4\ ksi) \cdot (13.7\ in.) \cdot (22\ in.)$

$= 769\ kip < 739\ kip$ ***NG!***

BACK FACE

Factored Load: $F_u = 895\ kip + 896\ kip = 1791\ kip$

Efficiency: $\beta = 0.80$

Concrete Capacity: $f_{cu} = 0.85 \cdot \beta \cdot f_c' = (0.85) \cdot (0.8) \cdot (5\ ksi) = 3.4\ ksi$

$\varphi \cdot F_n = (0.75) \cdot (3.4\ ksi) \cdot (11.5\ in.) \cdot (22\ in.)$

$= 645\ kip < 1791\ kip$ ***NG!***

STRUT-TO-NODE INTERFACE

Factored Load: $F_u = 1992\ kip$

Efficiency: $\beta = 0.75$

Concrete Capacity: $f_{cu} = 0.85 \cdot \beta \cdot f_c' = (0.85) \cdot (0.75) \cdot (5\ ksi) = 3.2\ ksi$

$\varphi \cdot F_n = (0.75) \cdot (3.2\ ksi) \cdot (16.8\ in.) \cdot (22\ in.)$

$= 887\ kip < 1992\ kip$ ***NG!***

According to ACI 318-08, the back face of Node E is the most critical location. In order to properly design this region, the bent is proportioned such that the back face of Node E has adequate capacity. In addition to providing the maximum 30-inch bearing plate, the depth of the bent must be increased by 25-inches and the depth of the back face of Node E must be increased by 6-inches. The width of the beam was not increased because triaxial confinement is not permitted in the ACI 318-08 specifications. Since the bearing plate is still less than the width of the member, an increase in beam width does not increase the width of the nodes. Strut proportions and forces associated with these changes are illustrated in Figure B.10.

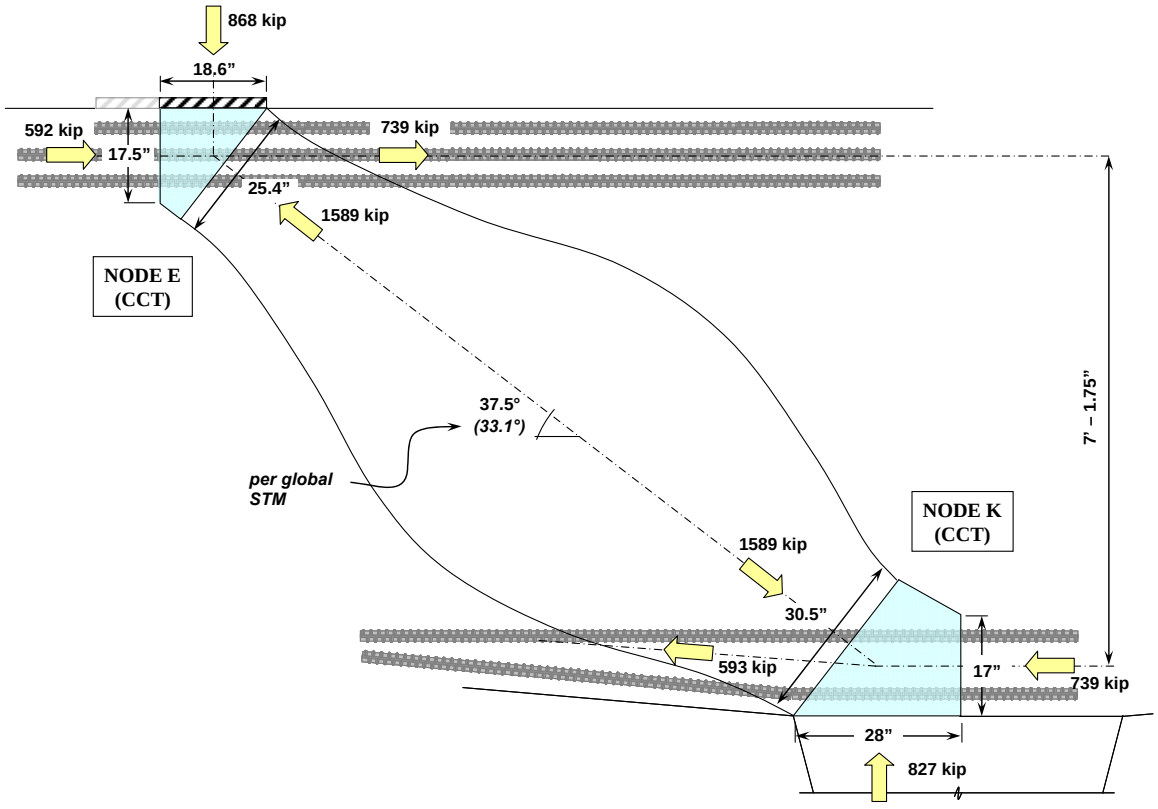

Figure B.10: Strut proportions and forces associated with a 25-inch increase in bent height and 6-inch increase in depth of Node E (ACI 318 factored loads)

BACK FACE OF NODE E: PER FIGURE B.10

Factored Load: $F_u = 739\ kip + 592\ kip = 1331\ kip$

Efficiency: $\beta = 0.80$

Concrete Capacity: $f_{cu} = 0.85 \cdot \beta \cdot f_c' = (0.85) \cdot (0.8) \cdot (5\ ksi) = 3.4\ ksi$

$\varphi \cdot F_n = (0.75) \cdot (3.4\ ksi) \cdot (17.5\ in.) \cdot (30\ in.)$

$= 1339\ kip > 1331\ kip$ ***OK***

Thus, the capacity of the bent illustrated in Figure B.10 meets the requirements of ACI 318-08.

Minimum Transverse Reinforcement

ACI 318-08 does not stipulate a minimum amount of transverse reinforcement. However, in order to use the higher strut efficiency factor, the following minimum amount of reinforcement must be provided:

$$\sum \frac{A_{si}}{b_s \cdot s_i} \sin \alpha_i > 0.003$$

If it is assumed that the vertical and horizontal reinforcement ratios are identical,

$$\rho \cdot \sin 38° + \rho \cdot \sin 52° > 0.003$$

Thus,

$$\rho_v = \rho_{vh} > 0.0021$$

Provide #5 vertical stirrups at 6-inches and #6 horizontal bars at 8.5-inches on center.

A summary of the preceding ACI 318-08 results is presented in Figure B.12 along with the other provisions. Next, Strut EK and respective nodal regions are designed according to AASHTO LRFD.

Design of Region with a/d Ratio Equal to 2.05: AASHTO LRFD

Refer to Figure B-8 for preliminary forces, strut and nodal proportions. By inspection, Node E is the most critical nodal zone. Therefore, design of Strut EK is based on the design of Node E.

Node E (CCT Node)

BEARING FACE

Factored Load: $F_u = 924\ kip$

Efficiency: $v = 0.75$

Concrete Capacity: $f_{cu} = v \cdot f_c' = (0.75) \cdot (5\ ksi) = 3.8\ ksi$

$\varphi \cdot F_n = (0.7) \cdot (3.8\ ksi) \cdot (13.7\ in.) \cdot (22\ in.)$

$= 802\ kip < 924\ kip$ ***NG!***

BACK FACE

Factored Load: $F_u = 947\ kip + 948\ kip = 1895\ kip$

Efficiency: $v = 0.75$

Concrete Capacity: $f_{cu} = v \cdot f_c' = (0.75) \cdot (5\ ksi) = 3.8\ ksi$

$\varphi \cdot F_n = (0.7) \cdot (3.8\ ksi) \cdot (11.5\ in.) \cdot (22\ in.)$

$= 673\ kip < 1895\ kip$ ***NG!***

STRUT-TO-NODE INTERFACE

Factored Load: $F_u = 2108\ kip$

Solve set of four equations simultaneously:

Concrete Efficiency: $$\nu = \frac{1}{0.8 - 170 \cdot \varepsilon_1} \le 0.85 \ = \ 0.39$$

Tensile Strain Term: $$\varepsilon_1 = \varepsilon_s + (\varepsilon_s + 0.002)\cot^2 29.5° \ = \ 0.0103$$

Tie Tensile Strain: $$\varepsilon_s = \frac{F_n \cdot \cos 29.5°}{(21.8in^2)\cdot(29{,}000ksi)} \ = 0.0010$$

Strength of Nodal Face: $F_n = \nu \cdot (5\ ksi)(16.3\ in.)(22\ in.) = 705\ kip$

$\varphi \cdot F_n = (0.7)(705\ kip)$

$= 722\ kip < 2108\ kip$ ***NG!***

The strut-to-node interface at Node E is the most critical location. Therefore, the size of the bent is increased in order to provide Node E with adequate capacity. As a preliminary check, evaluate whether or not the bent dimensions required per ACI 318-08 (Figure B.10) meet the requirements of AASHTO LRFD (2008). Recall, the loads illustrated in Figure B.10 are ACI 318-08 factored loads. AASHTO LRFD (2008) load factors are slightly higher, so the loads are multiplied by a factor of 1.059 (i.e. $P_{u\_AASHTO}/P_{u\_ACI} = 1480/1398 = 1.059$).

NODE E STRUT-TO-NODE INTERFACE, PER FIGURE B.10

Factored Load: $F_u = 1683\ kip$

Solve set of four equations simultaneously:

Concrete Efficiency: $$\nu = \frac{1}{0.8 - 170 \cdot \varepsilon_1} \le 0.85 \ = \ 0.46$$

Tensile Strain Term: $$\varepsilon_1 = \varepsilon_s + (\varepsilon_s + 0.002)\cot^2 37.5° \ = \ 0.0080$$

Tie Tensile Strain: $$\varepsilon_s = \frac{F_n \cdot \cos 37.5°}{(28.1in^2)\cdot(29{,}000ksi)} \ = 0.0017$$

Strength of Nodal Face: $F_n = \nu \cdot (5\ ksi)(25.4\ in.)(30\ in.) = 1761\ kip$

$\varphi \cdot F_n = (0.7)(1761\ kip)$

$= 1233\ kip < 1683\ kip$ ***NG!***

In order for the bent to meet the requirements of AASHTO LRFD, the bent depth must be increased by 35-inches and the depth of Node E must be increased by 10.5-inches. The width of the beam was not increased because triaxial confinement is not permitted in the AASHTO LRFD STM specifications. Since the bearing plate (30") is still less than the width of the member (45"), an increase in beam width does not increase the width of the nodes. Strut proportions associated with this increase and applied loads are illustrated in Figure B.11.

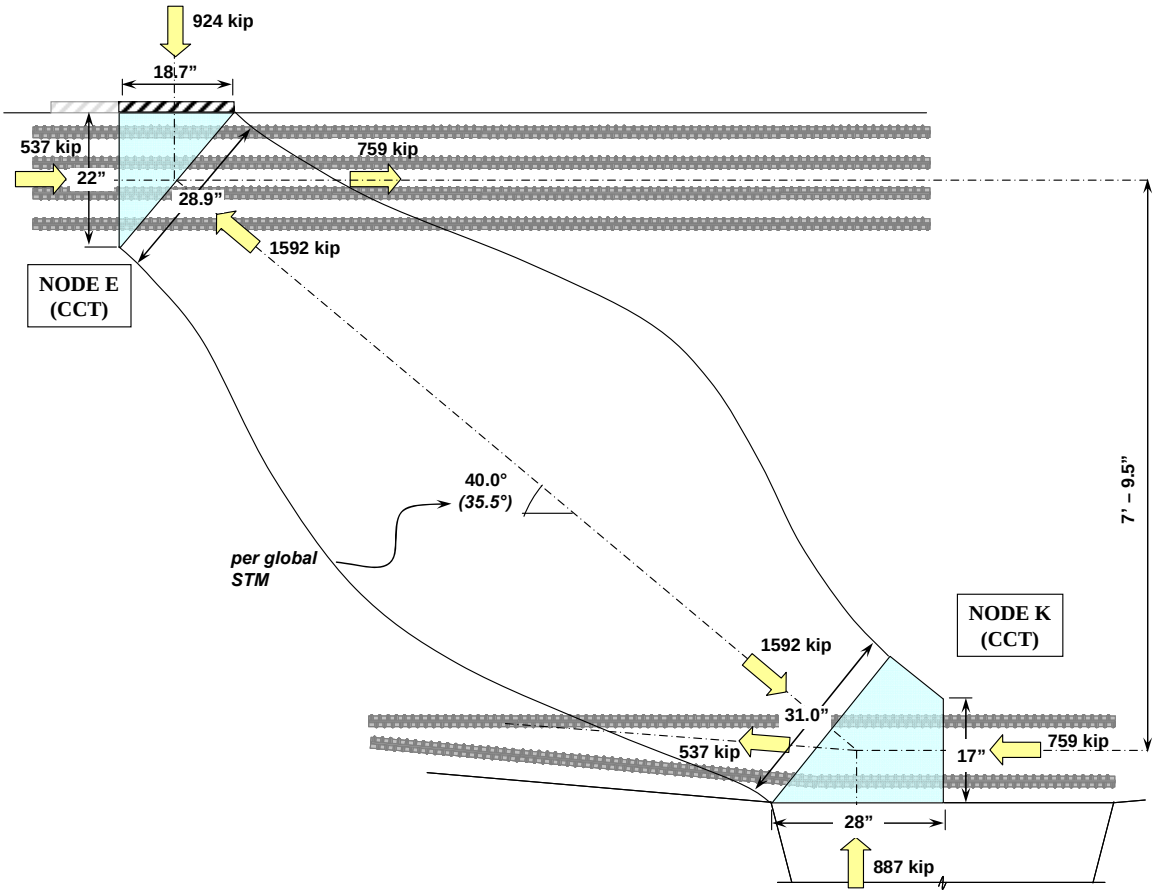

Figure B.11: Strut proportions and forces associated with a 35-inch increase in bent depth and 10.5-inch increase in depth of Node E (AASHTO LRFD factored loads).

NODE E STRUT-TO-NODE INTERFACE, PER FIGURE B.11

Factored Load: 1592 kip

Solve set of four equations simultaneously:

Concrete Efficiency: $$\nu = \frac{1}{0.8 - 170 \cdot \varepsilon_1} \le 0.85 \;=\; 0.53$$

Tensile Strain Term: $$\varepsilon_1 = \varepsilon_s + (\varepsilon_s + 0.002)\cot^2 40.0° \;=\; 0.0064$$

Tie Tensile Strain: $$\varepsilon_s = \frac{F_n \cdot \cos 40.0°}{(40.6 in^2)\cdot(29{,}000 ksi)} \;=\; 0.0015$$

Strength of Nodal Face: $F_n = \nu \cdot (5\ ksi)(28.9\ in.)(30\ in.) = 2287\ kip$

$\varphi \cdot F_n = (0.7)(2287\ kip)$

$= 1601\ kip > 1592\ kip$ ***OK***

Thus, the capacity of the bent illustrated in Figure B.11 meets the requirements of AASHTO LRFD (2007).

Minimum Transverse Reinforcement

AASHTO LRFD requires a vertical and horizontal reinforcement ratio of 0.3% of the gross area for the purpose of controlling cracking. So, based on this requirement, provide #6 vertical stirrups at 6.5-inches and twenty #8 horizontal bars distributed evenly across the height of the section (resulting in a spacing of 7-inches).

A summary of the preceding AASHTO LRFD results is presented along with the other provisions in the following section.

Comparison of Design Provisions for Shear Region with a/d = 2.05

A comparison between the results obtained from the three design methodologies (i.e. proposed method, ACI 318-08, and AASHTO LRFD) for the portion of the bent with an a/d ratio equal to 2.05 (Figure B.2, Cross-Section B) is presented in Figure B.12.

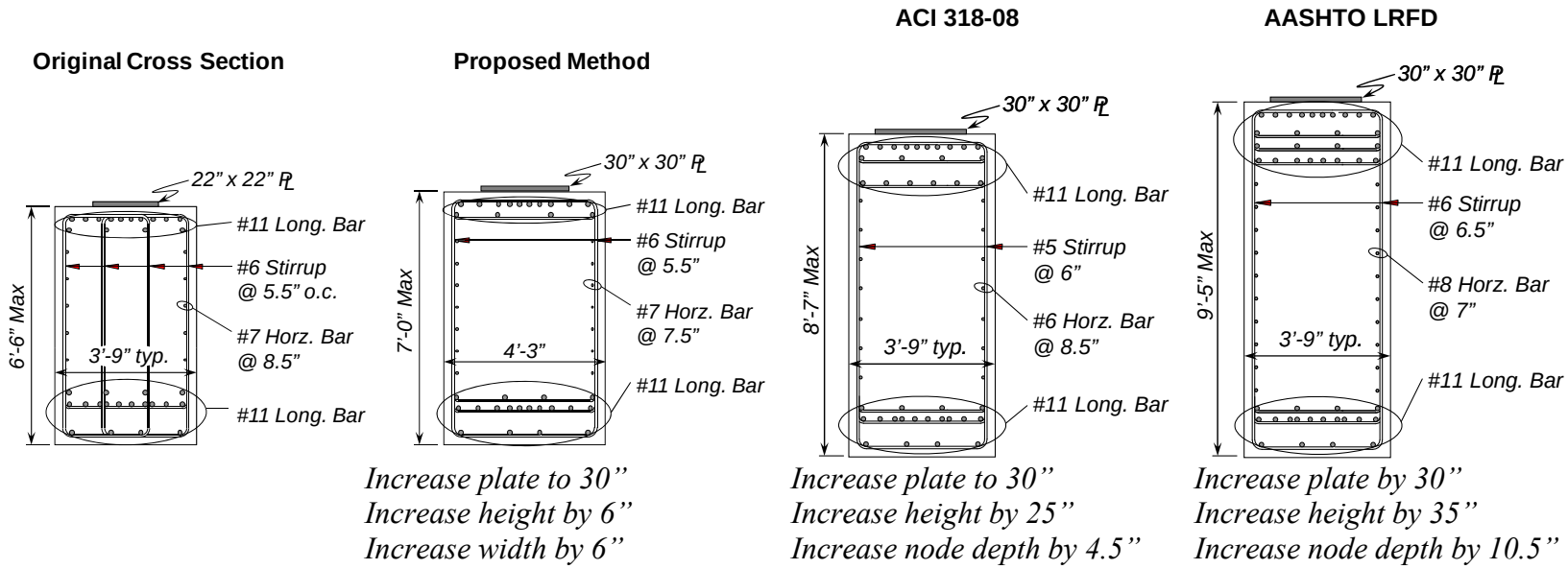

Figure B.12: Comparison of required cross-section per the proposed method, ACI 318-08, and AASHTO LRFD (2007): a/d ratio = 2.05.

Based on a comparison of the three provisions, the following observations can be made:

The proposed method results in a much higher capacity than the ACI 318-08 and AASHTO LRFD (2008) provisions. As a result, the cross-section required by the proposed procedure is significantly smaller. One reason for the difference can be attributed to the fact that the proposed procedure considers the increase in concrete compressive strength provided by triaxial confinement of the bearing plate. Neither the ACI 318-08 nor the AASHTO LRFD (2008) provisions consider the beneficial effects of triaxial confinement. In addition, according to the AASHTO LRFD (2008) provisions, the efficiency of the node-to-strut interface decreases as the shear span-to-depth ratio increases. It follows that excessively conservative results can be expected when using AASHTO LRFD (2008) for D-regions with an a/d ratio in the range of two. Despite the differences in the results of the three methods, they are similar in the fact that the results suggest that the dimensions of the original cross-section are inadequate to resist the application of the factored loads.

Since this portion of the bent has an a/d ratio slightly greater than 2.0, the capacity of this region may be determined according to sectional shear provisions. The sectional shear strength of this region is determined according to ACI 318-08 and AASHTO LRFD (2008). A discussion on the implications of using a sectional analysis rather than a deep beam analysis is presented in Section B.3.

In addition to the sectional shear strength, it is also of interest to examine the ratio of service load to cracking strength applied to this portion of the bent. The service loading is compared with the cracking strength of concrete in the following section.

Serviceability Behavior for Region with a/d = 2.05

By comparing the amount of service shear to the diagonal cracking strength of concrete, it is possible to estimate the likelihood that the structure will crack while in service. The shear force due to service loads for the portion of the bent with an a/d ratio of 2.05 is as follows:

$V_{srv} = (856\ kip) \cdot (1072kip/1480kip)$ ***= 620 kip***

According to Section 5.4.4, for an a/d ratio of 2.05, the shear at which the first diagonal crack will form with the original section dimensions can be estimated as the following:

$$V_{cr} = 2\sqrt{f_c'} \cdot b_w \cdot d = 2\sqrt{5000}(45in)(63in) \quad \textbf{= 401 kip}$$

The cracking capacity of this portion of the structure is less than the full service level loading. As a result, it is expected that diagonal cracks will exist under full service loads. In fact, diagonal cracks are expected to form under the application of 65% of the service-level loading (i.e. *401/620 = 0.65*) or 88% of the DL (i.e. (856/1480)*792 = 458 kips DL; 401/458 = 0.88). In the actual structure, a number of parallel, diagonal cracks existed in this portion of the structure (a/d = 2.05). The significant amount of cracking agrees with the above calculation regarding the expectancy of the member to crack under only 88% of the DL.

In order to prevent cracking from occurring under the application of service loads, bent dimensions or the compressive strength of concrete must be increased such that $V_{cr} \geq V_{srv}$. For the proposed section, the diagonal cracking load can be estimated as:

$$V_{cr} = 2\sqrt{f_c'} \cdot b_w \cdot d = 2\sqrt{5000}(51in)(69in) \quad \textbf{= 498 kip}$$

The cracking capacity of this portion of the structure is less than the full service level loading. However, diagonal cracks are not expected to form until the full dead load and approximately 25-percent of the live load is on the structure (i.e. 498-458 = 40 kips of LL;

40/(856/1480*280) = 0.25). To further reduce the likelihood of diagonal cracking under service, the design of the cross-section can be altered as before.

B.3 Sectional Shear Design

The purpose of calculating the sectional shear capacity for the portion of the beam with an a/d ratio of 2.05 (Figure B.2, Section A) is to compare the results to those determined from a strut-and-tie model. The discrepancy in the shear capacity at an a/d ratio near 2 determined by deep beam and sectional shear provisions is a topic of interest to the current project.

The ACI 318-08 and AASHTO LRFD (2008) provisions require that a designer use deep beam provisions for structures with a shear span-to-depth ratio less than or equal to two. For structures whose a/d ratio is near two, it is logical to expect that the capacity determined from a strut-and-tie model to be similar to that determined from a sectional model. In other words, the calculated capacity of a member should not significantly vary for an a/d ratio of 2.1 or 1.9. However, the difference in the allowable shear capacity according to sectional shear or a STM is often quite drastic (Section 5.3).

B.3.1 Shear Region with a/d Ratio Equal to 2.05

Refer to Figure B.3 for the critical shear force in Section A. The AASHTO LRFD (2008) factored shear is 856-kip; the ACI 318-08 factored shear is 809-kip. The ACI 318-08 and AASHTO LRFD (2008) reduction factors for sectional shear are 0.75 and 0.9, respectively. The nominal shear capacity according to ACI 318-08 and AASHTO LRFD (2008) is presented as follows.

ACI 318-08 §11.1, Shear Strength

Factored Load: $V_u = 809\ kip$

Sectional Capacity: $V_n = V_c + V_s$

Where,

$$V_c = 2\sqrt{f_c'} \cdot b_w \cdot d = 2\sqrt{5000\,psi} \cdot (45in) \cdot (63in) = 401\ kip$$

$$V_s = A_v \cdot f_v \cdot d / s = 4 \cdot (0.44in^2) \cdot (60ksi) \cdot (63in) / 5.5in = 1210\ kip$$

$$\varphi V_n = (0.75) \cdot (1611\ kip) = 1208\ kip > 809\ kip\ \textbf{OK}$$

According to ACI 318-08, the strength of the bent is adequate. However, recall that according to the STM design previously presented, the depth of the bent had to be considerably increased in order to meet the requirements of ACI 318-08. The degree of discontinuity between sectional shear and STM provisions is discussed in Section B.3.2. Next, the sectional shear capacity according to the AASHTO LRFD (2008) provisions is presented.

AASHTO LRFD§5.8.3, Sectional Design Model (General Procedure)

Factored Load: $V_u = 856\ kip$

Sectional Capacity: $V_n = V_c + V_s$

Where,

$$V_c = 0.0316\beta\sqrt{f_c'}\,b_v d_v$$

$$V_s = A_v f_y d_v \Big/ s \cdot \tan\theta$$

and,

$\beta =$ factor indicating the ability of diagonally cracked concrete to transmit tension and shear.

According to AASHTO LRFD (2008), the factor, β, is determined based on the longitudinal strain, shear stress, spacing and inclination of cracking across the web. For non-prestressed beams, sufficiently reinforced, the factor, β, may be determined according to Equation B.1:

$$\beta_s = \frac{4.8}{(1+750\varepsilon_s)} \tag{B.1}$$

And the angle of inclination of the cracking, θ, is determined according to Equation B.2:

$$\theta = 29 + 3500\varepsilon_s \tag{B.2}$$

Where the longitudinal strain, ε_s, in the web is determined according to Equation B.3.

$$\varepsilon_s = \frac{\left(\frac{|M_u|}{d_v} + 0.5N_u + 0.5|V_u|\cot\theta\right)}{2(E_s A_s)} \tag{B.3}$$

Where,

M_u = Factored moment at critical section, kip-in.
V_u = Factored shear at critical section, kip
N_u = Factor axial force at critical section, kip
θ = Angle of inclination of diagonal cracking, radian
d_v = distance between longitudinal top and bottom reinforcement, in.
E_s = Modulus of elasticity of steel reinforcement
A_s = Area of flexural tension reinforcement, in^2

Based on a linear analysis of the multiple-column bent, the factored moment at the critical section is 51,750-kip·inches and the factored shear force is 856-kip. The longitudinal strain and angle of inclination terms are simultaneously calculated as follows:

$$\varepsilon_s = \frac{\left(\frac{|51{,}750kip\cdot in|}{57in} + 0.5(0kip) + 0.5|856kip|\cot 32.4°\right)}{2(29{,}000ksi\cdot 28.1in^2)} = 0.00097$$

$$\theta = 29 + 3500\cdot(0.00097) = 32.4°$$

Thus,

$$\beta_s = \frac{4.8}{(1+750\cdot 0.00097)} = 2.78$$

Therefore, the nominal shear capacity can be calculated as follows:

$$V_c = 0.0316\cdot 2.7\sqrt{5ksi}\cdot(45in.)(57in.) = 489\ kip$$

$$V_s = 4(0.44in^2)\cdot(60ksi)\cdot(57in) \Big/ (5.5in.)\tan 32.4° = 1724\ kip$$

$\varphi V_n = (0.90)\cdot(2214\ kip) = 1992\ kip > 856\ kip$ **OK**

According to AASHTO LRFD (2008), the strength of the bent is adequate. Yet, recall that the depth of the bent had to be considerably increased in order to meet the requirements of the strut-and-tie provisions of AASHTO LRFD (2008). The discontinuity between sectional shear and deep beam provisions is discussed in the following section.

B.3.2 Comparison of Deep Beam and Sectional Shear Provisions

The capacity of the bent at Section B (Figure B.2) has been determined according to the proposed, ACI 318-08, and AASHTO LRFD (2008) STM provisions; and the ACI 318-08 and AASHTO LRFD (2008) section-based provisions. A comparison between the results of these analyses is presented in Table B.1.

Table B.1. Shear Capacity of Original Cross-Section B (a/d = 2.05)

Design Procedure	Capacity / Factored Load		$\frac{\phi V_n \ Sectional}{\phi V_n \ STM}$
	STM, $\frac{\phi \cdot V_n}{V_u}$	Sectional, $\frac{\phi \cdot V_n}{V_u}$	
Proposed Method	0.74	1.49†	2.01
ACI 318	0.36	1.49	4.14
AASHTO LRFD	0.34	2.33	6.85

† ACI 318-08 sectional shear capacity

The information presented in Table B.1 illustrates the relative discontinuity in nominal capacity as determined by sectional shear and deep beam provisions. This phenomenon is especially apparent for a structure with an a/d ratio equal to 2.05. As an example, according to the AASHTO LRFD (2008) sectional shear provisions, the capacity of the structure under investigation is estimated to be 6.85 times greater than the capacity as determined per the deep beam provisions. The implication of such a discrepancy is that a bent over nine feet deep is required per AASHTO LRFD (2008) for an a/d ratio of 1.9 (Figure B.12), yet a 6.5-foot deep bent is sufficient if the a/d ratio is slightly greater than two.

The proposed strut-and-tie modeling procedure addresses this discontinuity to a large extent. The ratio of the capacity according to a sectional shear model and that of the proposed STM provisions is 2.01. That is, the sectional shear strength is 1.92 times the STM strength. While this amount of discrepancy is still large, it is a substantial improvement relative to the factors of 4.14 and 6.85 that result with the use of the STM provisions in ACI 318-08 and AASHTO LRFD (2008), respectively (Table B.1).

It is important to note that the discrepancy is increased by the large ratio of V_s/V_c. As noted in Section 5.3.3, the V_s/V_c ratio should be limited to a value near 2 to help reduce the discrepancy between sectional shear and deep beam shear capacity. For the AASHTO LRFD (2008) and the ACI 318-08 sectional shear provisions, the ratio of V_s/V_c was 3.5 and 3.0, respectively. It is not recommended to rely on such a large percentage of shear capacity from stirrup contribution for members with an a/d ratio near 2.

Completely eliminating the discrepancy between shear strength calculated with sectional shear and STM provisions in general is unlikely. The models are completely different and a

function of many variables. However, it was shown through this example and in Section 5.3.3 that with the use of the proposed STM provisions, the discrepancy is largely reduced relative to the STM provisions in AASHTO LRFD (2008) and ACI 318-08. Also, limiting the V_s/V_c ratio to a value near 2 may help reduce the discrepancy in shear strength at an a/d ratio near 2.

B.4 Summary

In this section, a multiple-column bent cap was evaluated. Several findings of the current project were specifically implemented in the re-design or analysis of the structure. First and foremost, the proposed STM provisions were used to check the capacity of the original cross-section. While the shear span with an a/d ratio of 0.85 was found to be satisfactory from a strength point of view, the shear span with an a/d ratio of 2.05 was not. Using the proposed STM provisions, it was determined that one of the node-to-strut interfaces was overstressed by approximately 36% (2108/1552). The amount of distress present in the bent cap in service (Figure B.1) seems to be fairly consistent with the level of distress implied by the strut-and-tie analysis of the original cross-section. From a strength perspective, the use of the proposed STM provisions would suggest an increase in the cross-section (6-inches in depth and width) and an increase in the size of the bearing plate. In the experimental program of the current study, the importance of bearing plate dimensions and triaxial confinement in regards to the strength of deep beams was illustrated definitively (Section 4.6 and 4.4).

When the original bent cap was checked with the STM provisions in AASHTO LRFD (2008) and ACI 318-08, it was found to be drastically too small. In fact, the use of the AASHTO LRFD (2008) and ACI 318-08 provisions recommended substantially larger cross-sections (Figure B.7 and Figure B.12). From a strength standpoint, it is unlikely that such a dramatic change is warranted. The reason for the reduction in unnecessary conservatism between the use of the proposed STM provisions and the AASHTO LRFD (2008) and ACI 318-08 provisions was the allowance for triaxial confinement and the treatment of the bond stresses at the back face of the CCT node in the case of the former.

To limit the width of diagonal cracks at service loads, minimum reinforcement can be provided. In addition, a simple serviceability check may be used to reduce the likelihood of diagonal cracking under service loads. In the example problem, it was shown that the recommended minimum reinforcement was actually less than that provided in the original cross-section. When practical, providing additional reinforcement in excess of the minimum is satisfactory and will reduce the width of diagonal cracks (with diminishing returns) should they form. When service load shear checks were performed on the original cross-section, it was found that the member was expected to crack under service loads. For the span with an a/d ratio of 0.85, the load at first diagonal cracking was estimated to occur under full service load and approximately 29-percent of the live-load. For the span with an a/d ratio of 2.05, the load at first diagonal cracking was estimated to occur at only 88-percent of the dead load. From this check, it is clear that the original section was expected to crack in service. After performing these checks on the proposed section, it was found that diagonal cracking was expected to occur under full dead loads and approximately 25-percent of the live load for both shear spans. From a strength perspective, this amount of distress seems satisfactory since the diagonal cracking load was generally only 30-percent of the ultimate capacity of the structure. However, it may not be satisfactory from a serviceability perspective. The designer has the option to increase the size of the section and specify higher concrete strength to reduce the risk of diagonal cracking in service.

Since one portion of the structure was loaded at an a/d ratio of 2.05, it can be designed with a sectional shear model. In the example problem, it was illustrated that due to the unnecessary conservatism of the STM provisions in ACI 318-08 and AASHTO LRFD (2008) and the relatively high ratios of V_s/V_c, there was a large discrepancy between the sectional capacity and the STM capacity according to these provisions. When the capacity according to the proposed STM provisions was compared to the sectional shear capacity, a more reasonable discrepancy was observed. This discrepancy can likely be further reduced by limiting the V_s/V_c ratio to a value near 2.

In short, the example problem presented in this section was a unique case study in which several of the findings of the current project could be applied directly. It is believed that the results of this example problem further support the recommendations of the current study.

APPENDIX C. Collection Database

C.1 References

Ahmad, S. H., and Lue, D. M., "Flexure-Shear Interaction of Reinforced High-Strength Concrete Beams," *ACI Journal*, No. 84, July-August 1987, pp. 330-341.

Alcocer, S. M., and Uribe, C. M., "Monolithic and Cyclic Behavior of Deep Beams Designed Using Strut-and-Tie Models," *ACI Journal*, No. 105, May-June 2008, pp. 327-337.

Angelakos, D., The Influence of Concrete Strength and Longitudinal Reinforcement Ratio on the Shear Strength of Large-Size Reinforced Concrete Beams With, and Without, Transverse Reinforcement, Master's Thesis, 1999, Department of Civil Engineering, University of Toronto, 195 pp.

Angelakos, D.; Bentz, E. C; and Collins, M. P., "Effect of Concrete Strength and Minimum Stirrups on Shear Strength of Large Members," *ACI Journal*, No. 98, May-June 2001, pp. 290-300.

Bažant, Z. P., and Kazemi, M. T., "Size Effect of Diagonal Shear Failure of Beams without Stirrups," *ACI Journal*, No. 88, May-June 1991, pp. 268-276.

Bresler, B., and Scordelis, A. C., "Shear Strength of Reinforced Concrete Beams," *ACI Journal*, No. 60, January 1963, pp. 51-74.

Brown, M. D.; Sankovich, C. L.; Bayrak, O.; Jirsa, J. O.; Breen, J. E.; and Wood, S. L., *Design for Shear in Reinforced Concrete Using Strut-and-Tie Models*, Report No. 0-4371-2, Center for Transportation Research, University of Texas at Austin, Austin, Texas, Apr. 2006.

Brown, M. D.; Sankovich, C. L.; Bayrak, O.; Jirsa, J. O., "Behavior and Efficiency of Bottle-Shaped Struts," *ACI Journal*, No. 103, May-June 2006, pp. 348-355.

Cao, S., Size Effect and the Influence of Longitudinal Reinforcement on the Shear Response of Large Reinforced Concrete Members, Master's Thesis, University of Toronto, Toronto, Ontario, Canada, 2001, 195 pp.

Chang, T. S., and Kesler, C. E., "Static and Fatigue Strength in Shear of Beams with Tensile Reinforcement," *ACI Journal*, No. 54, June 1958, pp. 1033-1057.

Clark, A. P., "Diagonal Tension in Reinforced Concrete Beams," *ACI Journal*, No. 48, October 1951, pp. 145-156.

de Cossio, R. D., and Siess, C. P., “Behavior and Strength in Shear of Beams and Frames without Web Reinforcement,” *ACI Journal*, No. 56, February 1960, pp. 695-735.

de Paiva, H. A. R., and Siess, C. P., ”Strength and Behavior of Deep Beams in Shear,” Journal of the Structural Division, ASCE Proceedings, ST 5, October 1965, pp. 19-41.

Ferguson, P. M., “Some Implications of Recent Diagonal Tension Tests,” *ACI Journal*, No. 53, August 1956, pp. 157-172.

Foster, S. J., and Gilbert, R. I., “Experimental Studies on High-Strength Concrete Deep Beams,” *ACI Journal*, No. 95, July-August 1998, pp. 382-390.

Furuuchi, H.; Takahashi, Y.; Ueda, T.; and Kakuta, Y., “Effective Width for Shear Failure of RC Deep Slabs,” *Transaction of the Japan Concrete Institute*, Vol. 20, 1998, pp. 209-216.

Ghoneim, M., “Shear Strength of High-Strength Concrete Deep Beams,” *Journal of Engineering and Applied Science*, Vol. 48, No. 4, August 2001, pp. 675-693.

Hara, T., The Shear Strength of Reinforced Concrete Deep Beams, *Transaction of the Japan Concrete Institute*, Vol. 6, 1985, pp. 395-402.

Hassan, T. K.; Seliem, H. M; Dwairi, H.; Rizkalla, S. H.; Zia, P., “Shear Behavior of Large Concrete Beams Reinforced with High-Strength Steel,” *ACI Journal*, No. 105, March-April 2008, pp. 173-179.

Hsuing, W. and Frantz, G. C., “Transverse Stirrup Spacing in R/C Beam,” *ASCE Journal of Structural Engineering*, Vol. 11, No. 2, February 1985, pp. 353-362

Johnson, M. K., and Ramirez, J. A., “Minimum Shear Reinforcement in Beams with Higher Strength Concrete,” *ACI Journal*, No. 86, July-August 1989, pp. 376-382.

edited by Kani, M. W.; Huggins, M. W.; and Wittkopp, R. R., *Kani on Shear in Reinforced Concrete*, University of Toronto Press, Toronto, 1979, 225 pp.

Kong, P. Y. L., and Rangan, B. V., “Shear Strength of High-Performance Concrete Beams,” *ACI Journal*, No. 95, November-December 1998, pp. 677-688.

Kong, F.; Robins, P. J.; and Cole D. F., “Web Reinforcement Effects on Deep Beams,” *ACI Journal*, No. 67, December 1970, pp. 1010-1018.

Krefeld, W. J., and Thurston, C. W., “Studies of the Shear and Diagonal Tension Strength of Simply Supported Reinforced Concrete Beams,” *ACI Journal*, No. 63, April 1966, pp. 451-476.

Krefeld, W. J., and Thurston, C. W., "Contribution of Longitudinal Steel to Shear Resistance of Reinforced Concrete Beams," *ACI Journal*, No. 63, March 1966, pp. 325-344.

Leonhardt, F. and Walther, R., translation by Amerongen, C. V., "The Stuttgardt Shear Tests, 1961", from *Beton und Stahlbeton, Vol. 56, No. 12, 1961 and Vol. 57, No. 2, 3, 6, 7, and 8, 1962*, Translation No. 111, Cement and Concrete Association, London, 1964, 138 pp.

Manuel, R. F.; Slight, B. W.; and Suter, G. T., "Deep Beam Behavior Affected by Length and Shear Span Variables," *ACI Journal*, No. 68, December 1971, pp. 954-958.

Matsuo, M.; Lertsrisakulrat, T.; Yanagawa, A.; and Niwa, J., "Shear Behavior of RC Deep Beams with Stirrups," *Transaction of the Japan Concrete Institute*, Vol. 23, 2002, pp. 385-390.

Moody, K. G.; Viest, I. M.; Elstner, R. C.; and Hognestad, E., "Shear Strength of Reinforced Concrete Beams, Part 1 – Tests of Simple Beams," *ACI Journal*, No. 51, December 1954, pp. 317-332.

Morrow, J., and Viest, I. M., "Shear Strength of Reinforced Concrete Frame Members without Web Reinforcement," *ACI Journal*, No. 53, March 1957, pp. 833-869.

Oh, J., and Shin, S., "Shear Strength of Reinforced High-Strength Concrete Deep Beams," *ACI Journal*, No. 98, March-April 2001, pp. 164-173.

Ozcebe, G.; Ersoy, U.; and Tankut, T., "Evaluation of Minimum Shear Reinforcement Requirements for Higher Strength Concrete," *ACI Journal*, No. 95, May-June 1999, pp. 361-369.

Quintero-Febres, C. G.; Montesinos, G. P.; and Wight, J. K., "Strength of Struts in Deep Concrete Members Designed Using Strut-and-Tie Method," *ACI Journal*, No. 103, July-August 2006, pp. 577-586.

Rajagopalan, K. S., and Ferguson, P. M., "Exploratory Shear Tests Emphasizing Percentage of Longitudinal Steel," *ACI Journal*, No. 65, August 1968, pp. 634-638.

Ramakrishnan, V. and Ananthanarayana, Y., "Ultimate Strength of Deep Beams in Shear," *ACI Journal*, No. 65, February 1968, pp. 87-98.

Rigotti, M., *Diagonal Cracking in Reinforced Concrete Deep Beams – An Experimental Investigation*, PhD Dissertation, Concordia University, Montreal, Quebec, Canada, November 2002, 235 pp.

Rogowsky, D. M.; MacGregor, J. G.; and Ong, S. Y., "Tests of Reinforced Concrete Deep Beams," *ACI Journal*, No. 83, July-August 1986, pp. 614-623.

Roller, J. J., and Russell, H. G., "Shear Strength of High-Strength Concrete Beams with Web Reinforcement," *ACI Journal*, No. 87, March-April 1990, pp. 191-198.

Sarsam, K. F., and Al-Musawi, J. M. S., "Shear Design of High and Normal Strength Concrete Beams with Web Reinforcement," *ACI Journal*, No. 89, November-December 1992, pp. 658-664.

Shin, S.; Lee, K.; Moon, J.; and Ghosh, S. K., "Shear Strength of Reinforced High-Strength Concrete Beams with Shear Span-to-Depth Ratios between 1.5 and 2.5," *ACI Journal*, No. 96, July-August 1999, pp. 549-557.

Shioya, T. S., *Shear Properties of Large Reinforced Concrete Member*, Special Report of Institute of Technology, Shimizu Corporation, No. 25, February 1989, 213 pp.

Smith, K. N. and Vantsiotis, A. S., "Shear Strength of Deep Beams," *ACI Journal*, No. 79, May-June 1982, pp. 201-213.

Stanik, B. A. P., The Influence of Concrete Strength, Distribution of Longitudinal Reinforcement, Amount of Transverse Reinforcement and Member Size on Shear Strength of Reinforced Concrete Members, Master's Thesis, 1998, Department of Civil Engineering, University of Toronto, 369 pp.

Subedi, N. K.; Vardy, A. E.; and Kubota, N., "Reinforced Concrete Deep Beams – Some Test Results," *Magazine of Concrete Research*, Vol. 38, No. 137, December 1986, pp. 206-219.

Tan, K.; Kong, F.; Teng, S.; and Guan, L.,"High-Strength Concrete Deep Beams with Effective Span and Shear Span Variations," *ACI Journal*, No. 92, July-August 1995, pp. 1-11.

Tan, K.; Kong, F.; Teng, S.; and Weng, L., "Effect of Web Reinforcement on High-Strength Concrete Deep Beams," *ACI Journal*, No. 94, September-October 1997, pp. 572-582.

Tan, K. H., and Lu, H. Y., "Shear Behavior of Large Reinforced Concrete Deep Beams and Code Comparisons," *ACI Journal*, No. 96, September-October 1999, pp. 836-846.

Tan, K.; Teng, S.; Kong, F.; Lu, H., "Main Tension Steel in High Strength Concrete Deep and Short Beams," *ACI Journal*, No. 94, November-December 1997, pp. 752-768.

Tanimura, Y., and Sato, T., "Evaluation of Shear Strength of Deep Beams with Stirrups," *Quarterly Report of the Railway Technical Research Institute*, Vol. 46, No. 1, February 2005, pp. 53-58.

Uzel, A., *Shear Design of Large Footings*, Ph. D. Dissertation, University of Toronto, Toronto, Ontario, Canada, 2003, 404 pp.

Van Den Berg, F. J., ”Shear Strength of Reinforced Concrete Beams without Web Reinforcement,” *ACI Journal*, No. 59, November 1962, pp. 1587-1600.

Vecchio, F. J., “Analysis of Shear-Critical Reinforced Concrete Beams,” *ACI Journal*, No. 97, January-February 2000, pp. 102-110.

Walraven, J., and Lehwalter, N., “Size Effects in Short Beams Loaded in Shear,” *ACI Journal*, No. 91, September-October 1994, pp. 585-593.

Watstein, D., and Mathey, R. G., “Strains in Beams having Diagonal Cracks,” *ACI Journal*, No. 55, December 1958, pp. 717-728.

Xie, Y.; Ahmad, S. H.; Yu, T.; Hino, S.; and Chung, W., “Shear Ductility of Reinforced Concrete Beams of Normal and High-Strength Concrete,” *ACI Journal*, No. 91, March-April 1954, pp. 140-149.

Yang, K.; Chung, H.; Lee, E.; and Eun, H., “Shear Characteristics of High-Strength Concrete Deep Beams without Shear Reinforcements,” *Engineering Structures*, No. 25, April 2003, pp. 1343-1352.

Yoon, Y.; Cool, W. D.; and Mitchell, D., “Minimum Shear Reinforcement in Normal, Medium, and High-Strength Concrete Beams,” *ACI Journal*, No. 93, September-October 1996, pp. 1-9.

Yoshida, Y., *Shear Reinforcement for large Lightly Reinforced Concrete Members*, Master’s Thesis, University of Toronto, Toronto, Ontario, Canada, 2000, 162 pp.

Zhang, N., and Tan, K., “Size Effect in RC Deep Beams: Experimental Investigation and STM Verification,” *Engineering Structures*, No. 29, October 2007, pp. 3241-3254.

APPENDIX D. Evaluation Database

D.1 Overview

The following details are presented in Table D.1 for the specimens in the Evaluation Database:

b = beam width, in.

h = beam height, in.

d = distance form extreme compression fiber to centroid of tensile reinforcement, in.

$\mathbf{f_c'}$ = compressive strength of concrete at the time of testing, psi.

Note: if the compressive strength was measured based on the test of a standard 100 or 150-mm cube, then it was converted to the equivalent 6-inch cylinder strength according to fib (1999).

$\mathbf{f_y}$ = yield strength of tensile reinforcement, ksi.

$\mathbf{f_{yv}}$ = yield strength of vertical transverse reinforcement, ksi.

$\boldsymbol{\rho_l}$ = ratio of longitudinal tensile reinforcement to effective area, $A_s / b \cdot d$

$\boldsymbol{\rho_l'}$ = ratio of longitudinal compression reinforcement to effective area, $A_s' / b \cdot d$

$\boldsymbol{\rho_v}$ = ratio of vertical transverse reinforcement to effective area, $A_v / b \cdot s_1$

$\boldsymbol{\rho_h}$ = ratio of horizontal transverse reinforcement to effective area, $A_{vh} / b \cdot s_2$

s = spacing of vertical ties, in.

Load Plate = dimensions of the load bearing plate measured in the longitudinal and transverse direction (*l* x *w*), in.

Support Plate = dimensions of the support bearing plate measured in the longitudinal and transverse direction (*l* x *w*), in.

a/d ratio = shear span-to-depth ratio

$\mathbf{V_{test}}$ = maximum shear carried in test region, including the estimated self weight of the specimen and transfer girders, kip

Table D.1: Evaluation Database (1 of 10)

Beam I.D.	**b** in.	**h** in.	**d** in.	**f'_c** psi	**f_y** ksi	**f_{yv}** ksi	**ρ_l'**	**ρ_l**	**ρ_v**	**ρ_h**	**s** in.	**Load Plate** *l* x *w* in.	**Support Plate** *l* x *w* in.	**a/d ratio**	**V_{test}** kip
Current Study (2008)															
M-03-4-CCC2436	36	48	40	4100	67	61	0.0043	0.0293	0.0031	0.0030	11	24x36	16x36	1.85	1128.3
M-09-4-CCC2436	36	48	40	4100	67	61	0.0043	0.0293	0.0086	0.0030	4	24x36	16x36	1.85	1426.0
M-02-4-CCC2436	36	48	40	2800	65	63	0.0043	0.0293	0.0022	0.0022	10	24x36	16x36	1.85	1102.0
M-03-4-CCC0812	36	48	40	3000	65	63	0.0043	0.0293	0.0031	0.0030	11	8x12	16x36	1.85	930.0
M-03-2-CCC2436	36	48	40	4900	68	62	0.0022	0.0293	0.0031	0.0027	11	24x36	16x36	1.85	1096
I-03-2	21	44	38.5	5240	73	67	0.0116	0.0229	0.0029	0.0033	6.5	20x21	16x21	1.84	569.2
I-03-4	21	44	38.5	5330	73	73	0.0116	0.0229	0.0030	0.0033	7	20x21	16x21	1.84	657.4
I-02-2	21	44	38.5	3950	73	67	0.0116	0.0229	0.0020	0.0020	9.5	20x21	16x21	1.84	453.7
I-02-4	21	44	38.5	4160	73	73	0.0116	0.0229	0.0021	0.0020	10	20x21	16x21	1.84	528.1
II-03-CCC2021	21	42	38.6	3290	64	65	0.0115	0.0231	0.0031	0.0045	9.5	20x21	10x21	1.84	499.5
II-03-CCC1007	21	42	38.6	3480	64	65	0.0115	0.0231	0.0031	0.0045	9.5	10x7	10x21	1.84	477.4
II-03-CCT1021	21	42	38.6	4410	66	71	0.0115	0.0231	0.0031	0.0045	9.5	36x21	10x21	1.84	635.4
II-03-CCT0507	21	42	38.6	4210	66	71	0.0115	0.0231	0.0031	0.0045	9.5	36x21	5x7	1.84	597.4
II-02-CCT0507	21	42	38.6	3120	69	64	0.0115	0.0231	0.0020	0.0019	15	36x21	5x7	1.84	401.4
II-02-CCC1007	21	42	38.6	3140	69	64	0.0115	0.0231	0.0020	0.0019	15	10x7	10x21	1.84	334.8
II-02-CCC1021	21	42	38.6	4620	69	67	0.0115	0.0231	0.0020	0.0019	15	10x21	10x21	1.84	329.0
II-02-CCT0521	21	42	38.6	4740	69	67	0.0115	0.0231	0.0020	0.0019	15	20x21	5x21	1.84	567.4
III-1.85-02	21	42	38.6	4100	66	64	0.0115	0.0231	0.0020	0.0019	14.5	20x21	16x21	1.84	487.8
III-1.85-025	21	42	38.6	4100	66	64	0.0115	0.0231	0.0024	0.0014	12	20x21	16x21	1.84	515.6
III-1.85-03	21	42	38.6	4990	69	64	0.0115	0.0231	0.0029	0.0029	10	20x21	16x21	1.84	412.3
III-1.85-01	21	42	38.6	5010	69	63	0.0115	0.0231	0.0010	0.0014	18	20x21	16x21	1.84	272.6

Table D.1: Evaluation Database (2 of 10)

Beam I.D.	**b** in.	**h** in.	**d** in.	**f'_c** psi	**f_y** ksi	**f_{yv}** ksi	**ρ_l'**	**ρ_l**	**ρ_v**	**ρ_h**	**s** in.	**Load Plate** *l* x *w* in.	**Support Plate** *l* x *w* in.	**a/d ratio**	**V_{test}** kip
Current Study (2008), continued…															
III-1.85-03b	21	42	38.6	3300	69	62	0.0115	0.0231	0.0031	0.0029	6	20x21	16x21	1.84	471.1
III-1.85-02b	21	42	38.6	3300	69	62	0.0115	0.0231	0.0020	0.0018	9.5	20x21	16x21	1.84	467.6
III-1.2-02	21	42	38.6	4100	66	60	0.0115	0.0231	0.0020	0.0018	9.5	20x21	16x21	1.84	846.5
III-1.2-03	21	42	38.6	4220	66	68	0.0115	0.0231	0.0031	0.0029	9.5	20x21	16x21	1.84	829.2
III-2.5-02	21	42	38.6	4630	66	62	0.0115	0.0231	0.0020	0.0018	9.5	20x21	16x21	1.84	298.3
III-2.5-03	21	42	38.6	5030	66	65	0.0115	0.0231	0.0031	0.0029	9.5	20x21	16x21	1.84	516.0
IV-2175-1.85-02	21	74.5	68.9	4930	68	66	0.0129	0.0237	0.0020	0.0018	9.5	29x21	16x21	1.85	762.7
IV-2175-1.85-03	21	74.5	68.9	4930	68	66	0.0129	0.0237	0.0031	0.0029	9.5	29x21	16x21	1.85	842.4
IV-2175-2.5-02	21	74.5	68.9	5010	68	64	0.0129	0.0237	0.0021	0.0021	14.3	24x21	16x21	2.50	509.9
IV-2175-1.2-02	21	74.5	68.9	5010	68	64	0.0129	0.0237	0.0021	0.0021	14.3	24x21	16x21	1.2	1222.8
IV-2123-1.85-03	21	22.5	19.5	4160	66	66	0.0232	0.0232	0.0030	0.0030	6.3	16.5x21	16x21	1.85	328.5
IV-2123-1.85-02	21	22.5	19.5	4220	66	81	0.0232	0.0232	0.0020	0.0017	5.3	16.5x21	16x21	1.85	347.0
IV-2123-2.5-02	21	22.5	19.5	4570	65	58	0.0232	0.0232	0.0020	0.0017	5.3	15.5x21	16x21	2.50	160.7
IV-2123-1.2-02	21	22.5	19.5	4630	65	58	0.0232	0.0232	0.0020	0.0017	5.3	18x21	16x21	1.20	591.6
Rogowsky, MacGregor, and Ong (1986)															
1/1.0N	7.9	39.4	37.4	3785	55	83	0.0000	0.0094	0.0015	0.0000	7.4	11.8x7.9	7.9x7.9	1.05	136.3
2/1.0N	7.9	39.4	37.4	3887	55	83	0.0003	0.0094	0.0015	0.0006	7.4	11.8x7.9	7.9x7.9	1.05	169.6
2/1.5N	7.9	23.6	21.1	6150	66	83	0.0005	0.0112	0.0019	0.0011	5.9	11.8x7.9	7.9x7.9	1.87	78.8
2/2.0N	7.9	19.7	17.9	6266	66	83	0.0006	0.0088	0.0014	0.0012	7.9	7.9x7.9	7.9x7.9	2.20	46.3

Table D.1: Evaluation Database **(3 of 10)**

Beam I.D.	**b** in.	**h** in.	**d** in.	**f′$_c$** psi	**f$_y$** ksi	**f$_{yv}$** ksi	**ρ$_l$′**	**ρ$_l$**	**ρ$_v$**	**ρ$_h$**	**s** in.	**Load Plate** *l* x *w* in.	**Support Plate** *l* x *w* in.	**a/d ratio**	**V$_{test}$** kip
Brown, Sankovich, Bayrak, Jirsa, Breen, and Wood (2006)															
I-CL-8.5-0	6	30	27	2584	68	73	0.0195	0.0014	0.0043	0.0000	8.5	6x6	6x6	1.11	79.9
I-2C-8.5-0	6	30	27	3208	68	73	0.0195	0.0014	0.0043	0.0000	8.5	12x6	6x6	1.67	121.6
II-N-F-5.8-3	18	18	16	2880	68	73	0.0219	0.0008	0.0041	0.0000	3	10x18	6x18	1.69	180.8
Moody, Viest, Elstner, and Hognestad (1954)															
III-30	7	24	21	3680	44	47	0.0425	0.0213	0.0052	0.0000	6	8x7	8x7	1.52	108.1
III-31	7	24	21	3250	44	44	0.0425	0.0213	0.0095	0.0000	6	8x7	8x7	1.52	114.6
Oh and Shin (2001)															
N42A2	5.1	22.1	19.7	3440	60	60	0.0156	0.0022	0.0012	0.0043	16	7.1x5.1	5.1x5.1	0.85	64.1
N42B2	5.1	22.1	19.7	3440	60	60	0.0156	0.0022	0.0022	0.0043	8.7	7.1x5.1	5.1x5.1	0.85	84.9
N42C2	5.1	22.1	19.7	3440	60	60	0.0156	0.0022	0.0034	0.0043	5.7	7.1x5.1	5.1x5.1	0.85	80.6
H41A2(1)	5.1	22.1	19.7	7121	60	60	0.0156	0.0022	0.0012	0.0043	16	7.1x5.1	5.1x5.1	0.50	160.3
H41B2	5.1	22.1	19.7	7121	60	60	0.0156	0.0022	0.0022	0.0043	8.7	7.1x5.1	5.1x5.1	0.50	158.7
H41C2	5.1	22.1	19.7	7121	60	60	0.0156	0.0022	0.0034	0.0043	5.7	7.1x5.1	5.1x5.1	0.50	159.3
H42A2(1)	5.1	22.1	19.7	7121	60	60	0.0156	0.0022	0.0012	0.0043	16	7.1x5.1	5.1x5.1	0.85	109.9
H42B2(1)	5.1	22.1	19.7	7121	60	60	0.0156	0.0022	0.0022	0.0043	8.7	7.1x5.1	5.1x5.1	0.85	102.7
H42C2(1)	5.1	22.1	19.7	7121	60	60	0.0156	0.0022	0.0034	0.0043	5.7	7.1x5.1	5.1x5.1	0.85	94.7
H43A2(1)	5.1	22.1	19.7	7121	60	60	0.0156	0.0022	0.0012	0.0043	16	7.1x5.1	5.1x5.1	1.25	78.2
H43B2	5.1	22.1	19.7	7121	60	60	0.0156	0.0022	0.0022	0.0043	8.7	7.1x5.1	5.1x5.1	1.25	85.8
H43C2	5.1	22.1	19.7	7121	60	60	0.0156	0.0022	0.0034	0.0043	5.7	7.1x5.1	5.1x5.1	1.25	90.6
H45A2	5.1	22.1	19.7	7121	60	60	0.0156	0.0022	0.0012	0.0043	16	7.1x5.1	5.1x5.1	2.00	47.6
H45B2	5.1	22.1	19.7	7121	60	60	0.0156	0.0022	0.0022	0.0043	8.7	7.1x5.1	5.1x5.1	2.00	53.6

Table D.1: Evaluation Database **(4 of 10)**

Beam I.D.	**b** in.	**h** in.	**d** in.	**f′$_c$** psi	**f$_y$** ksi	**f$_{yv}$** ksi	**ρ$_l$′**	**ρ$_l$**	**ρ$_v$**	**ρ$_h$**	**s** in.	**Load Plate** *l* x *w* in.	**Support Plate** *l* x *w* in.	**a/d ratio**	**V$_{test}$** kip
Oh and Shin (2001), continued…															
H45C2	5.1	22.1	19.7	7121	60	60	0.0156	0.0022	0.0034	0.0043	5.7	7.1x5.1	5.1x5.1	2.00	53.1
N33A2	5.1	22.1	19.7	3440	60	60	0.0156	0.0022	0.0012	0.0043	16	7.1x5.1	5.1x5.1	1.25	51.5
N43A2	5.1	22.1	19.7	3440	60	60	0.0156	0.0022	0.0012	0.0043	16	7.1x5.1	5.1x5.1	1.25	57.5
N53A2	5.1	22.1	19.7	3440	60	60	0.0156	0.0022	0.0012	0.0043	16	7.1x5.1	5.1x5.1	1.25	46.9
H31A2	5.1	22.1	19.7	7121	60	60	0.0156	0.0022	0.0012	0.0043	16	7.1x5.1	5.1x5.1	0.50	167.6
H32A2	5.1	22.1	19.7	7121	60	60	0.0156	0.0022	0.0012	0.0043	16	7.1x5.1	5.1x5.1	0.85	119.1
H33A2	5.1	22.1	19.7	7121	60	60	0.0156	0.0022	0.0012	0.0043	16	7.1x5.1	5.1x5.1	1.25	85.0
H51A2	5.1	22.1	19.7	7121	60	60	0.0156	0.0022	0.0012	0.0043	16	7.1x5.1	5.1x5.1	0.50	157.9
H52A2	5.1	22.1	19.7	7121	60	60	0.0156	0.0022	0.0012	0.0043	16	7.1x5.1	5.1x5.1	0.85	127.8
H53A2	5.1	22.1	19.7	7121	60	60	0.0156	0.0022	0.0012	0.0043	16	7.1x5.1	5.1x5.1	1.25	81.8
Foster and Gilbert (1998)															
B1.2-3	4.9	47.2	44.2	11603	58	62	0.0134	0.0017	0.0067	0.0028	3	9.8x4.9	9.8x4.9	0.76	292.9
B2.0-1	4.9	27.6	24.6	12038	58	62	0.0241	0.0030	0.0067	0.0037	3	9.8x4.9	9.8x4.9	1.32	179.0
B2.0-2	4.9	27.6	24.6	17404	58	62	0.0241	0.0030	0.0067	0.0037	3	9.8x4.9	9.8x4.9	1.32	185.8
B2.0-3	4.9	27.6	24.6	11313	58	62	0.0241	0.0030	0.0067	0.0037	3	9.8x4.9	9.8x4.9	1.32	157.7
B2.0A-4	4.9	27.6	24.6	12473	58	62	0.0241	0.0030	0.0067	0.0037	3	3.9x4.9	9.8x4.9	0.88	213.9
B2.0C-6	4.9	27.6	24.6	13489	58	62	0.0241	0.0030	0.0100	0.0000	2	9.8x4.9	9.8x4.9	1.32	164.4
B2.0D-7	4.9	27.6	24.6	15084	58	62	0.0241	0.0030	0.0067	0.0000	3	9.8x4.9	9.8x4.9	1.32	162.2
B3.0-1	4.9	27.6	24.6	11603	58	62	0.0241	0.0030	0.0067	0.0037	3	9.8x4.9	9.8x4.9	1.88	115.2
B3.0-2	4.9	27.6	24.6	17404	58	62	0.0241	0.0030	0.0067	0.0037	3	9.8x4.9	9.8x4.9	1.88	118.5

Table D.1: Evaluation Database **(5 of 10)**

Beam I.D.	**b** in.	**h** in.	**d** in.	**f′$_c$** psi	**f$_y$** ksi	**f$_{yv}$** ksi	**ρ$_l$′**	**ρ$_l$**	**ρ$_v$**	**ρ$_h$**	**s** in.	**Load Plate** *l* x *w* in.	**Support Plate** *l* x *w* in.	**a/d ratio**	**V$_{test}$** kip
Foster and Gilbert (1998), continued…															
B3.0-3	4.9	27.6	24.6	11168	58	62	0.0241	0.0030	0.0067	0.0037	3	9.8x4.9	9.8x4.9	1.88	118.5
B3.0A-4	4.9	27.6	24.6	12763	58	62	0.0241	0.0030	0.0067	0.0037	3	3.9x4.9	9.8x4.9	1.28	174.7
Clark (1951)															
A1-1	8	18	15.3	3575	47	48	0.0310	0.0018	0.0038	0.0000	7.2	3.5x8	3.5x8	2.35	50.4
A1-2	8	18	15.3	3430	47	48	0.0310	0.0018	0.0038	0.0000	7.2	3.5x8	3.5x8	2.35	47.4
A1-3	8	18	15.3	3395	47	48	0.0310	0.0018	0.0038	0.0000	7.2	3.5x8	3.5x8	2.35	50.4
A1-4	8	18	15.3	3590	47	48	0.0310	0.0018	0.0038	0.0000	7.2	3.5x8	3.5x8	2.35	55.4
B1-1	8	18	15.3	3388	47	48	0.0310	0.0018	0.0037	0.0000	7.5	3.5x8	3.5x8	1.96	63.1
B1-2	8	18	15.3	3680	47	48	0.0310	0.0018	0.0037	0.0000	7.5	3.5x8	3.5x8	1.96	58.1
B1-3	8	18	15.3	3435	47	48	0.0310	0.0018	0.0037	0.0000	7.5	3.5x8	3.5x8	1.96	64.4
B1-4	8	18	15.3	3380	47	48	0.0310	0.0018	0.0037	0.0000	7.5	3.5x8	3.5x8	1.96	60.7
B1-5	8	18	15.3	3570	47	48	0.0310	0.0018	0.0037	0.0000	7.5	3.5x8	3.5x8	1.96	54.7
B2-1	8	18	15.3	3370	47	48	0.0310	0.0018	0.0073	0.0000	3.8	3.5x8	3.5x8	1.96	68.1
B2-2	8	18	15.3	3820	47	48	0.0310	0.0018	0.0073	0.0000	3.8	3.5x8	3.5x8	1.96	72.8
B2-3	8	18	15.3	3615	47	48	0.0310	0.0018	0.0073	0.0000	3.8	3.5x8	3.5x8	1.96	75.7
B6-1	8	18	15.3	6110	47	48	0.0310	0.0018	0.0037	0.0000	7.5	3.5x8	3.5x8	1.96	85.7

Table D.1: Evaluation Database **(6 of 10)**

Beam I.D.	**b** in.	**h** in.	**d** in.	**f′$_c$** psi	**f$_y$** ksi	**f$_{yv}$** ksi	**ρ$_l$′**	**ρ$_l$**	**ρ$_v$**	**ρ$_h$**	**s** in.	**Load Plate** *l* x *w* in.	**Support Plate** *l* x *w* in.	**a/d ratio**	**V$_{test}$** kip
Clark (1951) continued…															
C1-1	8	18	15.3	3720	47	48	0.0207	0.0018	0.0034	0.0000	8	3.5x8	3.5x8	1.57	62.8
C1-2	8	18	15.3	3820	47	48	0.0207	0.0018	0.0034	0.0000	8	3.5x8	3.5x8	1.57	70.3
C1-3	8	18	15.3	3475	47	48	0.0207	0.0018	0.0034	0.0000	8	3.5x8	3.5x8	1.57	55.7
C1-4	8	18	15.3	4210	47	48	0.0207	0.0018	0.0034	0.0000	8	3.5x8	3.5x8	1.57	64.7
C2-1	8	18	15.3	3430	47	48	0.0207	0.0018	0.0069	0.0000	4	3.5x8	3.5x8	1.57	65.6
C2-2	8	18	15.3	3625	47	48	0.0207	0.0018	0.0069	0.0000	4	3.5x8	3.5x8	1.57	68.1
C2-3	8	18	15.3	3500	47	48	0.0207	0.0018	0.0069	0.0000	4	3.5x8	3.5x8	1.57	73.2
C2-4	8	18	15.3	3910	47	48	0.0207	0.0018	0.0069	0.0000	4	3.5x8	3.5x8	1.57	65.2
C3-1	8	18	15.3	2040	47	48	0.0207	0.0018	0.0034	0.0000	8	3.5x8	3.5x8	1.57	50.7
C3-2	8	18	15.3	2000	47	48	0.0207	0.0018	0.0034	0.0000	8	3.5x8	3.5x8	1.57	45.4
C3-3	8	18	15.3	2020	47	48	0.0207	0.0018	0.0034	0.0000	8	3.5x8	3.5x8	1.57	42.7
C4-1	8	18	15.3	3550	47	48	0.0310	0.0018	0.0034	0.0000	8	3.5x8	3.5x8	1.57	69.9
C6-2	8	18	15.3	6560	47	48	0.0310	0.0018	0.0034	0.0000	8	3.5x8	3.5x8	1.57	95.7
C6-3	8	18	15.3	6480	47	48	0.0310	0.0018	0.0034	0.0000	8	3.5x8	3.5x8	1.57	98.2
C6-4	8	18	15.3	6900	47	48	0.0310	0.0018	0.0034	0.0000	8	3.5x8	3.5x8	1.57	96.7
D1-1	8	18	15.5	3800	49	48	0.0163	0.0018	0.0046	0.0000	6	3.5x8	3.5x8	1.16	68.1
D1-2	8	18	15.5	3790	49	48	0.0163	0.0018	0.0046	0.0000	6	3.5x8	3.5x8	1.16	80.6
D1-3	8	18	15.5	3560	49	48	0.0163	0.0018	0.0046	0.0000	6	3.5x8	3.5x8	1.16	58.1
D2-1	8	18	15.5	3480	49	48	0.0163	0.0018	0.0061	0.0000	4.5	3.5x8	3.5x8	1.16	65.6
D2-2	8	18	15.5	3755	49	48	0.0163	0.0018	0.0061	0.0000	4.5	3.5x8	3.5x8	1.16	70.6

Table D.1: Evaluation Database **(7 of 10)**

Beam I.D.	**b** in.	**h** in.	**d** in.	**f′$_c$** psi	**f$_y$** ksi	**f$_{yv}$** ksi	**ρ$_l$′**	**ρ$_l$**	**ρ$_v$**	**ρ$_h$**	**s** in.	**Load Plate** *l* x *w* in.	**Support Plate** *l* x *w* in.	**a/d ratio**	**V$_{test}$** kip
Clark (1951) continued…															
D2-3	8	18	15.5	3595	49	48	0.0163	0.0018	0.0061	0.0000	4.5	3.5x8	3.5x8	1.16	75.6
D2-4	8	18	15.5	3550	49	48	0.0163	0.0018	0.0061	0.0000	4.5	3.5x8	3.5x8	1.16	75.7
D3-1	8	18	15.5	4090	49	48	0.0244	0.0018	0.0092	0.0000	3	3.5x8	3.5x8	1.16	89.2
D4-1	8	18	15.5	3350	49	48	0.0163	0.0018	0.0122	0.0000	2.3	3.5x8	3.5x8	1.16	70.6
Alcocer and Uribe (2008)															
MR	13.8	47	43.3	5134	65	62	0.0158	0.0079	0.0053	0.0029	6	15.8x13.8	15.8x13.8	1.27	363.4
MT	13.8	47	43.3	5076	65	62	0.0158	0.0079	0.0053	0.029	6	15.8x13.8	15.8x13.8	1.27	363.4
Tanimura and Sato (2005)															
2A	11.8	17.7	15.8	3365	66	54	0.0214	0.0033	0.0021	0.0000	3.9	3.9x11.8	3.9x11.8	0.50	184.9
3A	11.8	17.7	15.8	3365	66	56	0.0214	0.0033	0.0048	0.0000	3.9	3.9x11.8	3.9x11.8	0.50	187.6
4A	11.8	17.7	15.8	3365	66	53	0.0214	0.0033	0.0084	0.0000	3.9	3.9x11.8	3.9x11.8	0.50	195.7
6A	11.8	17.7	15.8	4206	66	54	0.0214	0.0033	0.0021	0.0000	3.9	3.9x11.8	3.9x11.8	1.00	164.7
7A	11.8	17.7	15.8	4206	66	56	0.0214	0.0033	0.0048	0.0000	3.9	3.9x11.8	3.9x11.8	1.00	169.0
8A	11.8	17.7	15.8	4206	66	53	0.0214	0.0033	0.0084	0.0000	3.9	3.9x11.8	3.9x11.8	1.00	181.1
11A	11.8	17.7	15.8	3336	66	56	0.0214	0.0033	0.0048	0.0000	3.9	3.9x11.8	3.9x11.8	1.50	110.9
12A	11.8	17.7	15.8	3408	66	53	0.0214	0.0033	0.0084	0.0000	3.9	3.9x11.8	3.9x11.8	1.50	128.6
14B	11.8	17.7	15.8	4641	66	54	0.0214	0.0000	0.0021	0.0000	3.9	3.9x11.8	3.9x11.8	1.00	169.2
15B	11.8	17.7	15.8	4641	66	56	0.0214	0.0000	0.0048	0.0000	3.9	3.9x11.8	3.9x11.8	1.00	174.4
16B	11.8	17.7	15.8	4641	66	53	0.0214	0.0000	0.0084	0.0000	3.9	3.9x11.8	3.9x11.8	1.00	191.3
17C	11.8	17.7	15.8	4540	66	54	0.0214	0.0033	0.0021	0.0000	3.9	3.9x11.8	3.9x11.8	1.00	128.5
18C	11.8	17.7	15.8	4569	66	56	0.0214	0.0033	0.0048	0.0000	3.9	3.9x11.8	3.9x11.8	1.00	174.2

Table D.1: Evaluation Database **(8 of 10)**

Beam I.D.	**b** in.	**h** in.	**d** in.	**f′$_c$** psi	**f$_y$** ksi	**f$_{yv}$** ksi	**ρ$_l$′**	**ρ$_l$**	**ρ$_v$**	**ρ$_h$**	**s** in.	**Load Plate** *l* x *w* in.	**Support Plate** *l* x *w* in.	**a/d ratio**	**V$_{test}$** kip
Tanimura and Sato (2005), continued															
19C	11.8	17.7	15.8	4612	66	53	0.0214	0.0033	0.0084	0.0000	3.9	3.9x11.8	3.9x11.8	1.00	170.4
20D	11.8	17.7	15.8	3524	102	138	0.0214	0.0033	0.0048	0.0000	3.9	3.9x11.8	3.9x11.8	1.00	149.9
21D	11.8	17.7	15.8	3902	102	152	0.0214	0.0033	0.0084	0.0000	3.9	3.9x11.8	3.9x11.8	1.00	149.0
22D	11.8	17.7	15.8	3800	102	138	0.0214	0.0033	0.0048	0.0000	3.9	3.9x11.8	3.9x11.8	1.50	121.2
23D	11.8	17.7	15.8	3814	102	152	0.0214	0.0033	0.0084	0.0000	3.9	3.9x11.8	3.9x11.8	1.50	127.7
28A	11.8	17.7	15.8	3698	66	56	0.0214	0.0033	0.0048	0.0000	3.9	3.9x11.8	3.9x11.8	0.75	145.8
29A	11.8	17.7	15.8	3800	66	53	0.0214	0.0033	0.0084	0.0000	3.9	3.9x11.8	3.9x11.8	0.75	150.0
30A	11.8	17.7	15.8	3829	66	56	0.0214	0.0033	0.0088	0.0000	5.9	3.9x11.8	3.9x11.8	0.75	157.9
31A	11.8	17.7	15.8	3858	102	56	0.0214	0.0033	0.0048	0.0000	3.9	3.9x11.8	3.9x11.8	2.00	94.1
32A	11.8	17.7	15.8	3974	102	53	0.0214	0.0033	0.0084	0.0000	3.9	3.9x11.8	3.9x11.8	2.00	99.5
33A	11.8	17.7	15.8	3582	66	56	0.0214	0.0033	0.0095	0.0000	2.0	3.9x11.8	3.9x11.8	1.00	145.9
34A	11.8	17.7	15.8	3597	66	54	0.0214	0.0033	0.0095	0.0000	7.9	3.9x11.8	3.9x11.8	1.00	134.8
36E	11.8	17.7	15.8	3553	193	56	0.0042	0.0033	0.0048	0.0000	3.9	3.9x11.8	3.9x11.8	0.50	121.5
37E	11.8	17.7	15.8	3742	193	53	0.0042	0.0033	0.0084	0.0000	3.9	3.9x11.8	3.9x11.8	0.50	124.8
39E	11.8	17.7	15.8	3684	193	56	0.0042	0.0033	0.0048	0.0000	3.9	3.9x11.8	3.9x11.8	1.00	106.1
40E	11.8	17.7	15.8	3756	193	53	0.0042	0.0033	0.0084	0.0000	3.9	3.9x11.8	3.9x11.8	1.00	106.1
41A	11.8	17.7	15.8	2988	109	56	0.0214	0.0033	0.0048	0.0000	3.9	3.9x11.8	3.9x11.8	2.50	73.5
42A	11.8	17.7	15.8	3104	109	53	0.0214	0.0033	0.0084	0.0000	3.9	3.9x11.8	3.9x11.8	2.50	85.2
46F	11.8	17.7	15.8	14141	109	139	0.0214	0.0033	0.0021	0.0000	3.9	3.9x11.8	3.9x11.8	1.00	279.8
47F	11.8	17.7	15.8	13967	109	138	0.0214	0.0033	0.0048	0.0000	3.9	3.9x11.8	3.9x11.8	1.00	292.7

Table D.1: Evaluation Database **(9 of 10)**

Beam I.D.	**b** in.	**h** in.	**d** in.	**f'_c** psi	**f_y** ksi	**f_{yv}** ksi	**ρ_l'**	**ρ_l**	**ρ_v**	**ρ_h**	**s** in.	**Load Plate** *l* x *w* in.	**Support Plate** *l* x *w* in.	**a/d ratio**	**V_{test}** kip
Tanimura and Sato (2005), continued…															
48F	11.8	17.7	15.8	13706	109	139	0.0214	0.0033	0.0021	0.000	3.9	3.9x11.8	3.9x11.8	1.50	210.0
49F	11.8	17.7	15.8	13663	109	138	0.0214	0.0033	0.0048	0.000	3.9	3.9x11.8	3.9x11.8	1.50	220.8
L6	7.9	41.3	39.4	4525	147	56	0.002	0.004	0.0029	0.000	9.8	5.9x7.9	5.9x7.9	1.00	150.7
L7	15.8	80.7	78.7	4424	147	54	0.0005	0.004	0.0029	0.000	19.7	11.8x15.8	11.8x15.8	1.00	589.9
Matsuo, Lertsrisakulrat, Yanagawa, and Niwa (2002)															
D604	5.9	25.6	23.6	4960	146	48	0.0176	0.0006	0.0042	0.0000	3.9	5.9x5.9	5.9x5.9	1.00	132.1
D608	5.9	25.6	23.6	5120	146	48	0.0176	0.0006	0.0084	0.0000	2.0	5.9x5.9	5.9x5.9	1.00	149.5
Brown, Sankovich, Bayrak, and Jirsa (2006)															
G	6	36	36	4300	0	73	0.0005	0.0000	0.0031	0.0031	6	12x6	12x6	0.00	264.5
L	6	36	36	5290	0	73	0.0005	0.0000	0.0000	0.0031	0	12x6	12x6	0.00	366.8
M	6	36	36	4300	0	73	0.0005	0.0000	0.0000	0.0031	0	12x6	12x6	0.00	283.2
N	6	36	36	4300	0	73	0.0005	0.0000	0.0000	0.0031	0	6x6	6x6	0.00	202.1
O	6	36	36	5500	0	73	0.0002	0.0000	0.0000	0.0027	0	12x6	12x6	0.00	352.4
P	6	36	36	5500	0	73	0.0005	0.0000	0.0000	0.0061	0	12x6	12x6	0.00	377.0
Q	6	36	36	4200	0	73	0.0000	0.0000	0.0000	0.0010	0	12x6	12x6	0.00	224.0
T	6	36	36	5290	0	73	0.0000	0.0000	0.0000	0.0046	0	12x6	12x6	0.00	343.1
U	6	36	36	4350	0	73	0.0000	0.0000	0.0000	0.0023	0	6x6	6x6	0.00	189.0
V	6	36	36	4350	0	73	0.0000	0.0000	0.0046	0.0015	4	12x6	12x6	0.00	259.7
W	6	36	36	4350	0	73	0.0005	0.0000	0.0000	0.0031	0	16x6	16x6	0.00	370.1

Table D.1: Evaluation Database **(10 of 10)**

Beam I.D.	**b** in.	**h** in.	**d** in.	**f'_c** psi	**f_y** ksi	**f_{yv}** ksi	**ρ_l'**	**ρ_l**	**ρ_v**	**ρ_h**	**s** in.	**Load Plate** *l* x *w* in.	**Support Plate** *l* x *w* in.	**a/d ratio**	**V_{test}** kip
Brown, Sankovich, Bayrak, and Jirsa (2006), continued															
X	6	36	36	4350	0	73	0.0005	0.0000	0.0000	0.0031	0	12x6	12x6	0.00	246.7
Y	10	36	36	4350	0	73	0.0010	0.0000	0.0000	0.0037	0	12x4	12x4	0.00	299.5
Z	10	36	36	4350	0	73	0.0010	0.0000	0.0000	0.0037	0	12x4	12x4	0.00	303.8
Walraven and Lehwalter (1994)															
V411/4	9.8	31.5	29.9	3083	60	60	0.0107	0.0000	0.0017	0.0000	7.5	7.5x9.8	7.5x9.8	0.97	105.7
V022/3	9.8	15.8	14.2	3554	60	60	0.0113	0.0000	0.0035	0.0000	3.9	3.5x9.8	3.5x9.8	1.00	85.6
V511/3	9.8	23.6	22.1	3861	60	60	0.0112	0.0000	0.0033	0.0000	5.9	5.5x9.8	5.5x9.8	1.01	130.8
V411/3	9.8	31.5	29.9	3590	60	60	0.0107	0.0000	0.0033	0.0000	7.5	7.5x9.8	7.5x9.8	0.97	150.2
Zhang and Tan (2007)															
1DB70bw	6.3	27.6	25.3	4104	76	54	0.0111	0.0010	0.0021	0.0000	5.9	4.1x6.3	4.1x6.3	1.10	96.2
1DB100bw	9.1	39.4	35.6	4162	75	66	0.0123	0.0007	0.0021	0.0000	5.9	5.9x9.1	5.9x9.1	1.10	174.9
Deschenes and Bayrak (2008)															
VALID	21	42	36.1	5061	66	65	0.0310	0.0100	0.0030	0.0058	9.5	20x21	16x21	1.85	576.6
NR1	21	42	36.1	7250	66	65	0.0310	0.0100	0.0030	0.0058	9.5	20x21	16x21	1.85	560.8

APPENDIX E. Outline of STM Calculations

E.1 Overview

The overall capacity of all of the beams in the evaluation database was estimated according to the following deep beam design provisions: ACI 318-08; AASHTO LRFD (2008); *fib* (1999); ACI 318-99 Chapter 11; and the newly proposed STM method. The purpose of this Appendix is to present the details for these calculations.

E.1.1 Known STM Truss Geometries

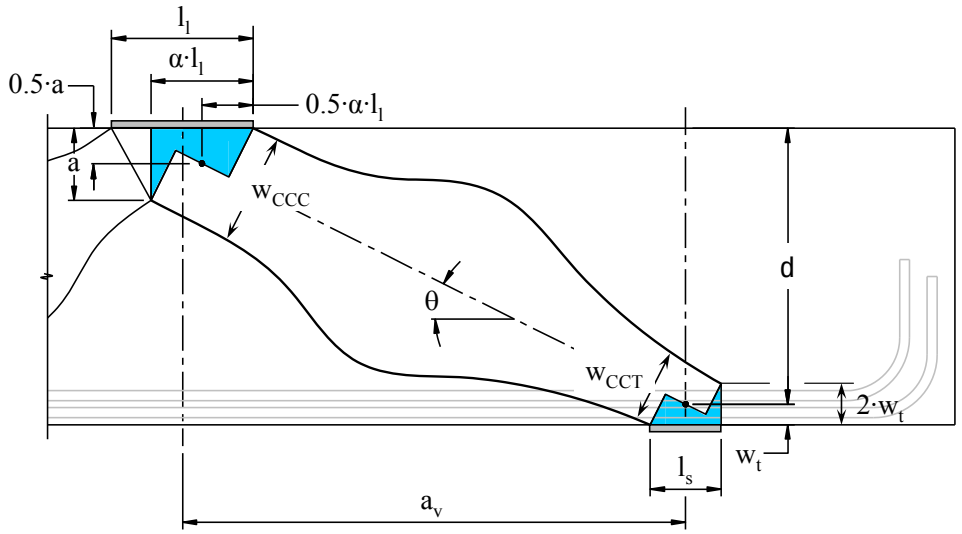

Figure E.1: Truss model.

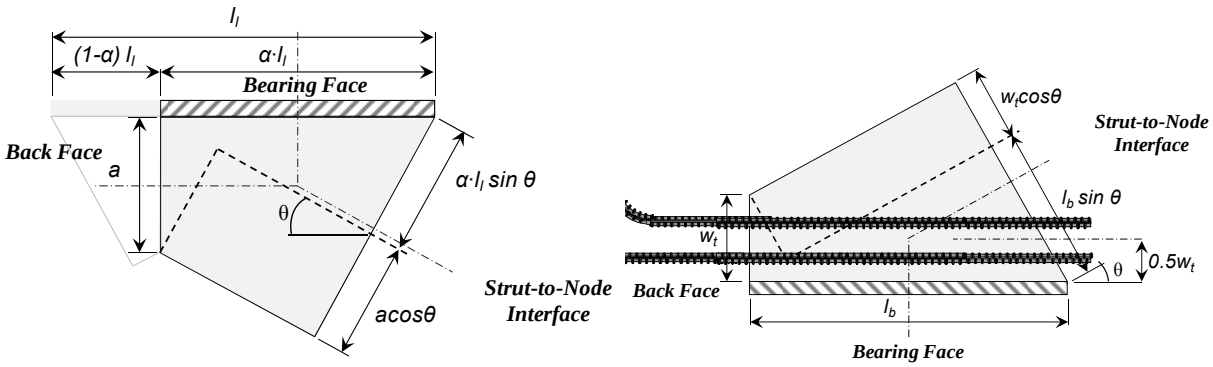

Figure E.2: CCC and CCT nodes.

Where,

1) α = portion of load that is resisted by near support.
2) θ $= tan^{-1}\left(\frac{d - a/2}{a_v}\right)$
3) w_t $= 2\cdot(h-d)$
4) W_{CCC} $= \alpha\cdot l_l\cdot sin\theta + a\cdot cos\theta$
5) W_{CCT} $= l_s\cdot sin\theta + w_t\cdot cos\theta$
6) a $= \frac{\left(A_s\cdot f_s - A_s'\cdot f_s'\right)}{0.85 f_c'\cdot b_w}$
7) $\rho_\perp$ $= \rho_v\, cos\,\theta + \rho_{vh}\, sin\,\theta$
8) b_l = width of the load plate (CCC)
9) b_s = width of the support plate (CCT)

In the calculation of the depth of the compression block, a, checks were used to ensure the appropriate strain was in the compression steel and tension steel such that compatibility, the material properties of the steel, and equilibrium were satisfied.

Stresses at each nodal face and in the tie are determined based on the experimental measured capacity, V_{test}, for each beam in the database.

CCC NODE: Experimental Stress

10) Bearing Face; $f_{cb} = \frac{V_{test}}{\alpha\cdot l_l\cdot b_l}$
11) Back Face; $f_{ck} = \frac{\left(V_{test}/tan\,\theta\right)}{a\cdot b_l}$
12) Strut-Node Interface; $f_{cs} = \frac{\left(V_{test}/sin\,\theta\right)}{W_{CCC}\cdot b_l}$

CCT NODE: Experimental Stress

13) Bearing Face; $f_{tb} = \frac{V_{test}}{l_b\cdot b_b}$
14) Back Face; $f_{tk} = \frac{\left(V_{test}/tan\,\theta\right)}{2(h-d)\cdot b_s}$
15) Strut-Node Interface; $f_{ts} = \frac{\left(V_{test}/sin\,\theta\right)}{W_{CCT}\cdot b_s}$

TIE: Experimental Stress

16) $f_{tie} = \left(V_{test} / \tan\theta \right) / A_s$

E.2 Determination of Experimental/Calculated Ratio

The capacity at each nodal face is determined according to the respective STM design provision. Once the capacity of each part of a STM is estimated (i.e. bearing face, back face, strut to node interface, and tie), the region that has the highest ratio of experimental to calculated capacity is the region that determines the overall STM design capacity.

ACI 318-08, Appendix A

CCC NODE: Design Strength

17) Bearing Face; $f_{n\_cb} = 0.85 \cdot 1 \cdot f_c' = 0.85 f_c'$
Experimental/Calculated = (10)/(17)

18) Back Face; $f_{n\_ck} = 0.85 \cdot 1 \cdot f_c' = 0.85 f_c'$
Experimental/Calculated = (11)/(18)

19) Strut-Node Interface; $f_{n\_cs} = \begin{cases} 0.85 \cdot 0.75 = 0.64 f_c' & \text{if } \rho_\perp \geq 0.003 \\ 0.85 \cdot 0.60 = 0.51 f_c' & \text{if } \rho_\perp < 0.003 \end{cases}$

Experimental/Calculated = (12)/(19)

CCT NODE: Design Strength

20) Bearing Face; $f_{n\_tb} = 0.85 \cdot 0.8 \cdot f_c' = 0.68 f_c'$
Experimental/Calculated = (13)/(20)

21) Back Face; $f_{n\_tk} = 0.85 \cdot 0.8 \cdot f_c' = 0.68 f_c'$
Experimental/Calculated = (14)/(21)

22) Strut-Node Interface; $f_{n\_ts} = \begin{cases} 0.85 \cdot 0.75 = 0.64 f_c' & \text{if } \rho_\perp \geq 0.003 \\ 0.85 \cdot 0.60 = 0.51 f_c' & \text{if } \rho_\perp < 0.003 \end{cases}$

Experimental/Calculated = (15)/(22)

TIE: Design Strength

23) $f_{n\_tie} = 1.0 f_y$
Experimental/Calculated = (16)/(23)

The maximum Experimental/Calculated ratio for each node face and tie [i.e. the maximum presented in (17) through (23)] is used to determine the Experimental/Calculated ratio for each beam in the database according to the ACI 318-08 design provisions.

AASHTO LRFD (2008)

CCC NODE: Design Strength

24) Bearing Face; $f_{n\_cb} = 0.85 f_c'$
Experimental/Calculated = (10)/(24)

25) Back Face; $f_{n\_ck} = 0.85 f_c'$
Experimental/Calculated = (11)/(25)

26) Strut-Node Interface; $f_{n\_cs} = 0.85 f_c'$
Experimental/Calculated = (12)/(26)

CCT NODE: Design Strength

27) Bearing Face; $f_{n\_tb} = 0.75 f_c'$
Experimental/Calculated = (13)/(27)

28) Back Face; $f_{n\_tk} = 0.75 f_c'$
Experimental/Calculated = (14)/(28)

29) Strut-Node Interface. Solve the following set of equations simultaneously:

$$\varepsilon_s = \frac{F_{strut} \cos\theta}{A_s E_s}$$

$$\varepsilon_1 = \varepsilon_s + (\varepsilon_s + 0.002)\cot^2\theta$$

$$f_{cu} = \min\begin{cases} \dfrac{f_c'}{0.8 + 170\varepsilon_1} \\ 0.85 f_c' \end{cases}$$

$$F_{strut} = \begin{cases} \dfrac{f_{n\_cb} \cdot \alpha \cdot l_l \cdot b_l}{\sin\theta} & \text{if (24) controls} \\ \dfrac{f_{n\_ck} \cdot a \cdot b_l}{\cos\theta} & \text{if (25) controls} \\ f_{n\_cs} \cdot W_{CCC} \cdot b_l & \text{if (26) controls} \\ \dfrac{f_{n\_tb} \cdot l_b \cdot b_s}{\sin\theta} & \text{if (27) controls} \\ \dfrac{f_{n\_tk} \cdot 2(h-d) \cdot b_s}{\cos\theta} & \text{if (28) controls} \\ f_{cu} \cdot W_{CCT} \cdot b_s & \text{if (29) controls} \\ \dfrac{A_s \cdot f_y}{\cos\theta} & \text{if (30) controls} \end{cases}$$

$f_{n\_ts} = f_{cu}$

Experimental/Calculated = (15)/(29)

TIE: Design Strength

30) $f_{n\_tie} = 1.0 f_y$

Experimental/Calculated = (16)/(30)

The maximum Experimental/Calculated ratio for each node face and tie [i.e. the maximum presented in (24) through (30)] is used to determine the Experimental/Calculated ratio for each beam in the database according to the AASHTO LRFD (2007) design provisions.

fib (1999)

CCC NODE: Design Strength

Triaxial Confinement Modification Factor, M_{CCC}

31) $M_{CCC} = \min \begin{cases} b_w / b_l \\ 4 \end{cases}$

32) Bearing Face; $f_{n\_cb} = 0.85\left(1 - \dfrac{f_c'}{40ksi}\right) \cdot M_{CCC} \cdot f_c'$

Experimental/Calculated = (10)/(32)

33) Back Face; $f_{n\_ck} = 0.85\left(1 - \frac{f_c'}{40ksi}\right) \cdot M_{CCC} \cdot f_c'$

Experimental/Calculated = (11)/(33)

34) Strut-Node Interface; $f_{n\_cs} = 0.85\left(1 - \frac{f_c'}{40ksi}\right) \cdot M_{CCC} \cdot f_c'$

Experimental/Calculated = (12)/(34)

CCT NODE: Design Strength

Triaxial Confinement Modification Factor, M_{CCT}

35) $M_{CCT} = min\left\{ \begin{array}{l} b_w / b_b \\ \\ 4 \end{array} \right.$

36) Bearing Face; $f_{n\_tb} = 0.7\left(1 - \frac{f_c'}{40ksi}\right) \cdot M_{CCT} \cdot f_c'$

Experimental/Calculated = (13)/(36)

37) Back Face; $f_{n\_tk} =$ [Not Applicable]

38) Strut-Node Interface; $f_{n\_ts} = 0.7\left(1 - \frac{f_c'}{40ksi}\right) \cdot M_{CCT} \cdot f_c'$

Experimental/Calculated = (15)/(38)

TIE: Design Strength

39) $f_{n\_tie} = 1.0 f_y$

Experimental/Calculated = (16)/(39)

The maximum Experimental/Calculated ratio for each node face and tie [i.e. the maximum presented in (32) through (34) and (36) through (39)] is used to determine the Experimental/Calculated ratio for each beam in the database according to the *fib* (1999) design provisions.

ACI 318-99, § 11.8

40) $k = min\left\{ \begin{array}{l} 3.5 - 2.5\left(a / 2d\right) \\ \\ 2.5 \end{array} \right.$

41) $V_c = \min \begin{cases} k\left(1.9\sqrt{f_c'} + 2500 \cdot \rho_l \cdot \left(2d/a\right)\right) \cdot b_w \cdot d \\ 6\sqrt{f_c'} \cdot b_w \cdot d \end{cases}$

42) $V_s = \left[\rho_v \cdot b_w \left(\frac{1 + l_n/d}{12} \right) + \rho_{vh} \cdot b_w \left(\frac{11 - l_n/d}{12} \right) \right] \cdot f_y \cdot d$

43) $V_n = \min \begin{cases} V_c + V_s \\ 10\sqrt{f_c'} \cdot b_w \cdot d \end{cases}$

Experimental/Calculated = V_{test}/(43)

Proposed STM Procedure

CCC NODE: Design Strength

Triaxial Confinement Modification Factor, M_{CCC}

44) $M_{CCC} = \min \begin{cases} \sqrt{A_2/A_1} \\ 2 \end{cases}$

Strut-to-Node Interface Efficiency Factor, v

45) $v = 0.45 \le 0.85 - \frac{f_c'}{20ksi} \le 0.65$

46) Bearing Face; $f_{n\_cb} = 0.85 \cdot M_{CCC} \cdot f_c'$
Experimental/Calculated = (10)/(46)

47) Back Face; $f_{n\_ck} = 0.85 \cdot M_{CCC} \cdot f_c'$
Experimental/Calculated = (11)/(47)

48) Strut-Node Interface; $f_{n\_cs} = v \cdot M_{CCC} \cdot f_c'$
Experimental/Calculated = (12)/(48)

CCT NODE: Design Strength

Triaxial Confinement Modification Factor, M_{CCT}

49) $M_{CCT} = \min \begin{cases} \sqrt{A_2 / A_1} \\ 2 \end{cases}$

50) Bearing Face; $f_{n\_tb} = 0.70 \cdot M_{CCT} \cdot f_c'$
Experimental/Calculated = (13)/(50)

51) Back Face; $f_{n\_tk} =$ [Not Applicable]

52) Strut-Node Interface; $f_{n\_ts} = \nu \cdot M_{CCT} \cdot f_c'$
Experimental/Calculated = (15)/(52)

TIE: Design Strength

53) $f_{n\_tie} = 1.0 f_y$
Experimental/Calculated = (16)/(53)

The maximum Experimental/Calculated ratio for each node face and tie [i.e. the maximum presented in (46) through (48) and (50) through (53)] is used to determine the Experimental/Calculated ratio for each beam in the database according to the Proposed design provisions.